SUPRAMOLECULAR CATALYSIS: HALOGEN BONDING AND REGULATION STRATEGIES APPLIED TO HYDROBORATION AND C-H FUNCTIONALIZATION REACTIONS

Lucas Carreras Vinent

UNIVERSITAT ROVIRA i VIRGILI

Supramolecular Catalysis: Halogen Bonding and Regulation Strategies Applied to Hydroboration and C–H Functionalization Reactions

Lucas Carreras Vinent

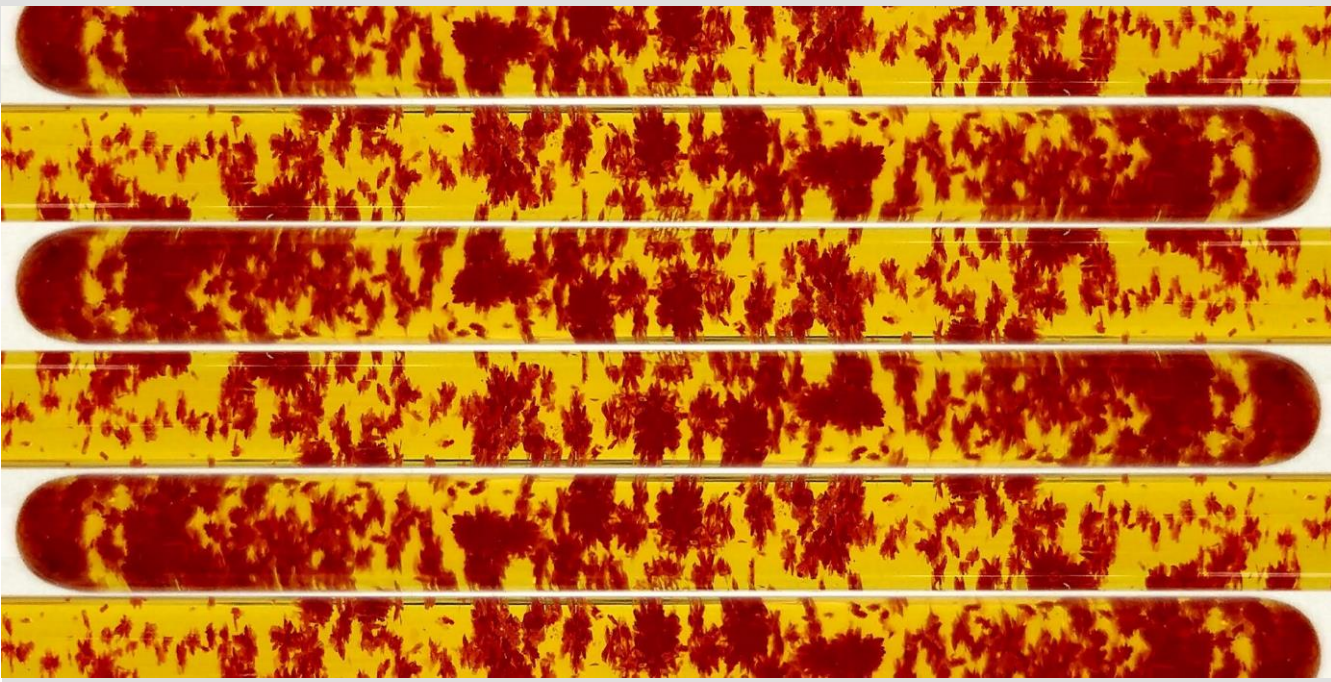

DOCTORAL THESIS

2019

Lucas Carreras Vinent

Supramolecular Catalysis: Halogen Bonding and Regulation Strategies Applied to Hydroboration and C–H Functionalization Reactions

Doctoral Thesis

Supervised by Prof. Dr. Anton Vidal i Ferran

Institute of Chemical Research of Catalonia (ICIQ)

Tarragona 2019

ICIQ
Institut Català d'Investigació Química

UNIVERSITAT ROVIRA I VIRGILI
DEPARTAMENT DE QUIMICA ANALITICA I QUIMICA ORGANICA
C/ Marcel.lí Domingo s/n
Campus Sescelades
43007 Tarragona

Prof. Dr. Anton Vidal Ferran, Group Leader of the Institute of Chemical Research of Catalonia (ICIQ) and Research Professor of the Catalan Institution for Research and Advanced Studies (ICREA),

CERTIFIES that the present Doctoral Thesis entitled: "*Supramolecular Catalysis: Halogen Bonding and Regulation Strategies Applied to Hydroboration and C–H Functionalization Reactions*" that Lucas Carreras Vinent presents to obtain the PhD degree in chemistry, has been carried out under my supervision, in the corresponding research group at the Institute of Chemical Research of Catalonia (ICIQ).

Tarragona, July 2019

PhD Thesis Supervisor

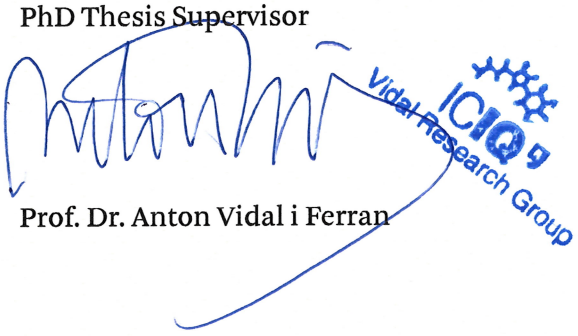

Prof. Dr. Anton Vidal i Ferran

ACKNOWLEDGEMENTS

I would like to thank Prof. Anton Vidal for letting me carry my PhD studies in his research group at the Institute of Chemical Research of Catalonia (ICIQ). With his guidance I have been constantly learning and growing both personally and scientifically. I would like to express my gratitude to Prof. Christopher Hunter for giving me the opportunity to join his research group at the University of Cambridge for three months. I would like to thank as well all the members of his group for making me feel comfortable during the stay. I am thankful to Prof. Piet van Leeuwen and Prof. Antonio Frontera for their contribution to the work presented in this doctoral thesis. I would like to thank Dr. José Luis Núñez for his help in some of the artwork of this thesis, including the cover of the thesis. I am also very grateful to the research support units at ICIQ for all the help provided during these years: X-Ray (especially to the manager, Dr. Jordi Benet), Nuclear Magnetic Resonance, Mass Spectrometry, Chemical Reaction Technologies, Chromatography (especially to Ms. Marta Serrano), Spectroscopic and Kinetics, Glass Blowing, Mechanical Workshop and IT Units. I would like to express my gratitude to all the members of Prof. Vidal's group, current (Héctor, José Luis, Alicia, Nuria, Ester, Andrés, Alba and Juanjo) and former (Nacho, Laura, Mónica, Balakrishna, Joan and Rajesh) for all their help, support and good moments during my time at the Institute. I would also like to thank Paula Segovia for the administrative support given. Altogether, thank you to all the people involved directly or indirectly in the genesis of this thesis, and all the people who contributed in having an enjoyable stay in Tarragona.

En un plànol més personal, voldria agrair a totes aquelles persones del meu entorn, amics i família, que durant aquests més de 4 anys m'han animat, ajudat i recolzat per assolir finalment aquesta fita. Específicament voldria agrair el seu suport a la Isabel Baixeras, la primera persona en acollir-me a Tarragona. A la meva família: el meus pares Pili i Llorenç, els meus avis Sito i Margarita, el meu germà Loren, la meva cunyada Marta i el meu nebot, el nouvingut Sito. També a la meva família política. Els meus sogres Jaume i Pepa, i les meves cunyades Maria i Raquel, que també han tingut cura de mi durant tot aquest temps. Finalment, i molt en especial, a la meva parella Sofia, que ha fet aquest mateix camí al meu costat. Gràcies per la teva ajuda i paciència, sobretot en aquests darrers moments.

The research work developed in the present PhD thesis has been possible thanks to the MCIU for a FPI-SO predoctoral fellowship (BES-2015-071872), and the financial support provided by the ICIQ Foundation, MCIU (CTQ2014-60256-P and CTQ2017-89814-P) and Severo Ochoa Excellence Accreditation (SEV-2013-0319).

A sa meva família i a na Sofia

"Ex nihilo nihil fit"

- Parmenides

LIST OF PUBLICATIONS

When this dissertation was submitted, the results contained herein have so far resulted in the following publications:

- "XBphos-Rh: a halogen-bond assembled supramolecular catalyst" Carreras, L.; Serrano-Torné, M.; van Leeuwen, P. W. N. M.; Vidal-Ferran, A., *Chem. Sci.* **2018**, *9*, 3644-3648. Highlighted in *ChemistryViews* (23rd February 2018).

- "Halogen bonding effects on the outcome of reactions at metal centres" Carreras, L.; Benet-Buchholz, J.; Franconetti, A.; Frontera, A.; van Leeuwen, P. W. N. M.; Vidal-Ferran, A., *Chem. Commun.* **2019**, *55*, 2380-2383.

- "Efficient modular phosphorus-containing ligands for stereoselective catalysis" (review) Llorente, N.; Fernández-Pérez, H.; Núñez-Rico, J. L.; Carreras, L.; Martínez-Carrión, A.; Iniesta, E.; Romero-Navarro, A.; Martínez-Bascuñana, A. Vidal-Ferran, A. *Pure Appl. Chem.* **2019**, *91*, 3-15.

Other publications not related to the topic covered in the present dissertation are presented below:

- "Syntheses, characterisation and solid-state study of alkali and ammonium BArF salts" Carreras, L.; Rovira, L.; Vaquero, M.; Mon, I.; Martin, E.; Benet-Buchholz, J.; Vidal-Ferran, A., *RSC Adv.* **2017**, *7*, 32833-32841.

TABLE OF CONTENTS

LIST OF ACRONYMS AND ABBREVIATIONS

The acronyms and abbreviations used in this manuscript have been used following the recommendations given by the American Chemical Society: [http://pubs.acs.org/paragonplus/submission/joceah/joceah_abbreviations.pdf, ACS guidelines for authors (accessed April 2019)]. Additional abbreviations and acronyms used in this manuscript are referenced in the list below:

Å	angstrom(s)
Ac	acetyl
acac	acetylacetonate
aq	aqueous
Ar	aryl
BArF	tetrakis[3,5-bis(trifluoromethyl)phenylborate]
br	broad (spectral)
°C	degrees, Celsius
calcd	calculated
cat.	catalytic, catalyst
CIF	Crystallographic Information Framework
cm	centimeter(s)
cod	1,5-cyclooctadiene
Cy	cyclohexyl (group), cyclohexane (solvent)
δ	chemical shift in ppm

ΔG	Gibbs free energy
EI	Electron Impact
equiv.	equivalent(s)
ESI	electrospray ionization
Et	ethyl
FID	Flame Ionization Detector
g	gram(s)
GC	Gas Chromatography
h	hour(s)
HRMS	High Resolution Mass Spectrometry
Hz	herz
IGD	Inverse Gated Decoupling
INT	intermediate
IR	infrared
J	coupling constant [expressed in Hz]
L	liter(s)
μ	micro (prefix)
m	multiplet (spectral), milli- (prefix)
M	molar (moles per liter), parent molecular ion
max.	maximum
Me	methyl
MHz	megahertz

min.	minute(s); minimum
mol	mole(s), molecular
MS	Mass Spectrometry
m/z	mass-to-charge ratio
nbd	norbornadiene
nm	nanometer(s)
NMR	Nuclear Magnetic Resonance
ORTEP	Oak Ridge Thermal Ellipsoid Plot Program
Ph	phenyl
ppm	part(s) per million
q	quartet (spectral)
rt	room temperature
s	singlet (spectra), second(s)
t	triplet (spectral), time
T	temperature
THF	tetrahydrofuran
TLC	Thin Layer Chromatography
TMS	tetramethylsilane, tetramethylsilyl
TS	Transition State
UV	ultraviolet
vis	visible
XB	halogen bond

PROLOGUE

The present dissertation has been divided into four main parts: a general introduction on recent advances in supramolecular catalysis using halogen bonding and regulation strategies, and three chapters on the research activities performed. Each chapter has been divided into the following sections: (1) abstract, (2) introduction, (3) results and discussion, (4) conclusions and (5) experimental section. Compounds have been numbered independently in each of the chapters. References have been included as footnotes and numbered jointly.

The general introduction provides an overview of the basic principles in homogeneous supramolecular catalysis and significant developments achieved using halogen bonding and regulation strategies.

Chapter I presents the first report on the use of halogen bonding to build the skeleton of a rhodium(I) catalyst and to its application to the hydroboration of terminal alkynes. The manuscript summarizing the results was published in *Chem. Sci.* **2018**, *9*, 3644-3648.

Chapter II discloses the selective preparation of new Rh(I) and cyclometallated Rh(III) complexes arising from the use of halogen bonding interactions to control the inner coordination sphere at the metal. This work has been published in *Chem. Commun.* **2019**, *55*, 2380-2383. Computational studies have been performed in collaboration with the group of Prof. Frontera (*Universitat de les Illes Balears*).

Chapter III includes an experimental and computational study (performed in collaboration with the group of Prof. Frontera, *Universitat de les Illes Balears*) on supramolecularly regulated gold(I) catalysts and their application to the selective functionalization of phenols and related derivatives. The use of appropriate regulation agents resulted in an increase of both activity and selectivity. The manuscript corresponding to the contents described in Chapter III is under preparation, and will be submitted in due time:

- "Supramolecularly regulated gold(I) catalysts for the selective functionalization of aromatic alcohols" Carreras, L.; Franconetti, A.; Hunter, C. A.; Frontera, A.; Vidal-Ferran, A.

INTRODUCTION

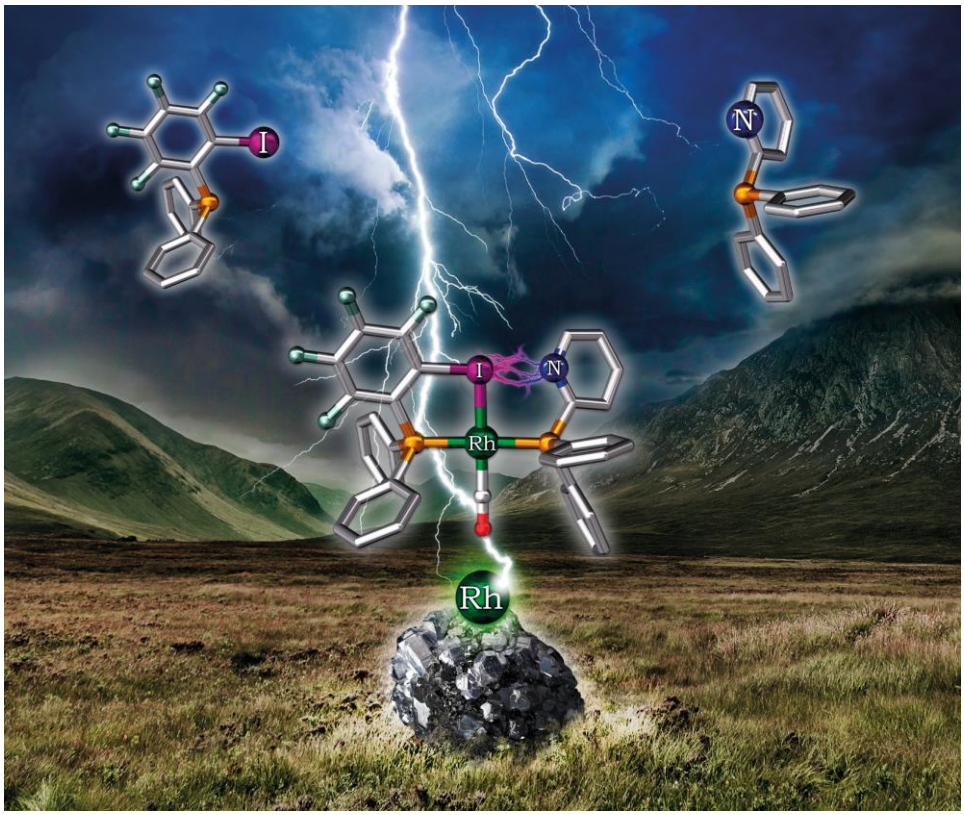

INTRODUCTION

Since the conception of supramolecular chemistry as a discipline by Jean-Marie Lehn,[1] this area of research is increasingly expanding in applications and importance. One of the most fruitful topics is the use of supramolecular interactions in catalysis, often referred to as Supramolecular Catalysis. This area of research can be defined as the use of systems involving reversible interactions,[2] aimed to increase the rate of a reaction without modifying the overall standard Gibbs energy change in the transformation.[3] After the pioneering work by Ronald Breslow, who designed a selective aromatic substitution using cycloamylose as supramolecular catalyst (Figure 1),[4] many scientists grasped the potential that arises from the merging of catalysis and supramolecular chemistry and contributed to the discipline with innumerable approaches, designs and ideas.

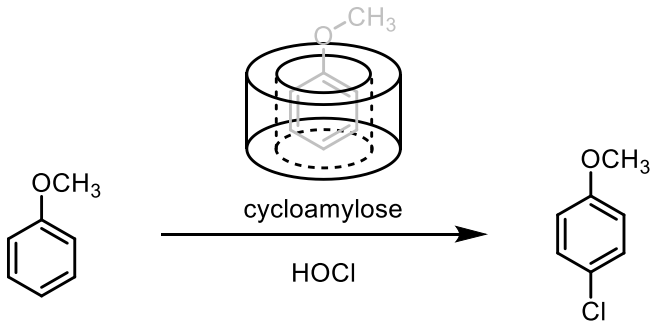

Figure 1. Selective functionalization of anisole using hypochlorous acid to afford 1-chloro-4-methoxybenzene. The use of cycloamylose blocks the functionalization at the *ortho* and *meta* positions and exposes the *para* position of anisole.[4]

(1) Lehn, J. M. *Acc. Chem. Res.* **1978**, *11*, 49-57.
(2) In this processes, the supramolecular interactions referred to are not taking part of the basic catalytic reaction.
(3) Catalysis: A process in which the rate of a reaction is increased without modifying the overall standard Gibbs energy change in the reaction. Adapted from: IUPAC, *Compendium of Chemical Terminology*, 2nd Ed. (the"Gold Book"), Blackwell Science, Oxford, **1997**.
(4) Breslow, R.; Campbell, P. *J. Am. Chem. Soc.* **1969**, *91*, 3085-3085.

Focusing on supramolecular homogeneous catalysis, abundant literature has been devoted to highlight the advances in this field, with comprehensive reviews and books dealing with the topic, given the flourishment and progress that supramolecular catalysis has experienced in the last decades.[5] Within the core concepts related to supramolecular catalysis, *the development of systems using non-conventional interactions* and *the use of regulation strategies in supramolecular catalysis* deserve mention.

Non-conventional reversible interactions have been gradually attracting interest since their discovery and description, because of a better understanding of their nature. They represent an innovative and promising tool to incorporate to the standard toolbox in supramolecular chemistry (*i.e.*, hydrogen bond, metal-ligand, π-stacking and electrostatic interactions). Non-conventional interactions, also referred to as unconventional, unorthodox or novel interactions by some authors,[6] comprise recently described interactions such as halogen bonding,[7] chalcogen bonding,[8] pnictogen bonding[9] or tetrel bonding.[10] Cation-π[11] and anion-π[12] interactions have been also classified as non-conventional interactions given that their use in catalysis is quite recent.

---

(5) For comprehensive reviews see, for example: (a) Raynal, M.; Ballester, P.; Vidal-Ferran, A.; van Leeuwen, P. W. N. M. *Chem. Soc. Rev.* **2014**, *43*, 1660-1733. (b) Raynal, M.; Ballester, P.; Vidal-Ferran, A.; van Leeuwen, P. W. N. M. *Chem. Soc. Rev.* **2014**, *43*, 1734-1787.

(6) (a) Bauzá, A.; Mooibroek, T. J.; Frontera, A. *ChemPhysChem* **2015**, *16*, 2496-2517. (b) Zhao, Y.; Cotelle, Y.; Sakai, N.; Matile, S. *J. Am. Chem. Soc.* **2016**, *138*, 4270-4277. (c) Breugst, M.; von der Heiden, D.; Schmauck, J. *Synthesis* **2017**, *49*, 3224-3236.

(7) Cavallo, G.; Metrangolo, P.; Milani, R.; Pilati, T.; Priimagi, A.; Resnati, G.; Terraneo, G. *Chem. Rev.* **2016**, *116*, 2478-2601.

(8) Vogel, L.; Wonner, P.; Huber, S. M. A*ngew. Chem., Int. Ed.* **2019**, *58*, 1880-1891.

(9) Sánchez-Sanz, G.; Trujillo, C.; Solimannejad, M.; Alkorta, I.; Elguero, J. *Phys. Chem. Chem. Phys.* **2013**, *15*, 14310-14318.

(10) Bauzá, A.; Mooibroek, T. J.; Frontera, A. *Angew. Chem., Int. Ed.* **2013**, *52*, 12317-12321.

(11) Kennedy, C. R.; Lin, S.; Jacobsen, E. N. *Angew. Chem., Int. Ed.* **2016**, *55*, 12596-12624.

(12) Zhao, Y.; Cotelle, Y.; Liu, L.; López-Andarias, J.; Bornhof, A.-B.; Akamatsu, M.; Sakai, N.; Matile, S. *Acc. Chem. Res.* **2018**, *51*, 2255-2263.

The supramolecular regulation strategy has recently come into play as an efficient approach to accelerate the discovery of new or improved homogeneous catalysts,[13] by reducing the synthetic effort to generate libraries of catalysts for a given transformation.[14] The regulation strategy is based on the modification of the catalytic site when an effector molecule binds at a distinct site on the same system (known as the regulation site) (Figure 2). This approach is inspired in the allosteric modulation mechanism from enzyme catalysis.[15]

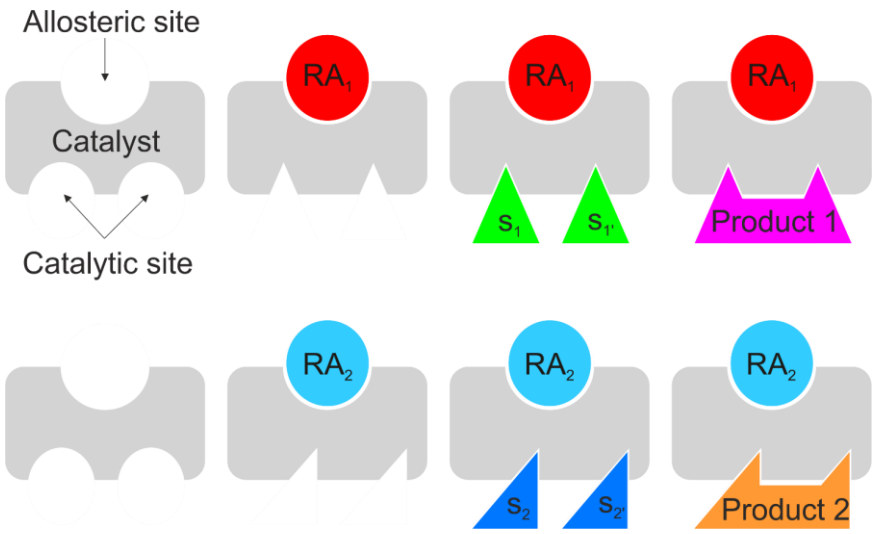

Figure 2. Schematic representation of positive regulation in catalysis. A catalyst incorporating a regulation site, upon binding of a regulation agent (RA), modifies its catalytic site to best fit the substrates(s) of interest according to the RA used, maximizing the output of the reaction.

The discussion that follows aims at providing an overview of a selection of representative examples of supramolecular catalysts using halogen bonding interactions and regulation strategies.

Since its serendipitous discovery in 1814 by J.-J. Colin when mixing ammonia with iodine,[16] halogen bonding (XB) has attracted lots of

(13) Renom-Carrasco, M.; Lefort, L. *Chem. Soc. Rev.* **2018**, *47*, 5038-5060.
(14) Vaquero, M.; Rovira, L.; Vidal-Ferran, A. *Chem. Commun.* **2016**, *52*, 11038-11051.
(15) Perutz, M. F. Q. *Rev. Biophys.* **1989**, *22*, 139-237.
(16) Colin, J.-J. *Ann. Chim.* **1814**, *91*, 252-272.

attention, mainly from the mid-90s in the areas of crystal engineering,[17] polymer science,[18] and medicinal chemistry.[19] Regarding its chemistry in solution, halogen bonding has been principally studied in molecular recognition and self-assembly processes,[20] although in the last years catalysis has been under the spotlight.[6b-c,21] Halogen bond involves the interaction of the lower electron density area, or σ-hole, of an electron-poor halogen atom and an electron-rich region of another atom or group of atoms (Figure 3).[22] This interaction is highly directional and less affected by solvents compared to hydrogen bond,[23] although solvent effects are still far from being predictable.[24] In addition, halogen bonding is a tunable interaction, more sensitive to steric effects given the participation of bulky iodine atoms.[7] Besides, the halogen bonding motifs are generally regarded as hydrophobic.[7] These properties have made halogen bonding an attractive non-conventional reversible interaction to be used in catalysis, with comparable features to hydrogen bonding processes.

Representative examples in supramolecular catalysis using halogen bonding rely on the activation of reactants containing a halogen bond acceptor (a Lewis base) with an organocatalyst containing one or multiple halogen bond donors, namely iodo groups. The halogen bond interaction activates the substrate, lowering the energy barrier of the reaction, whilst in the absence of the catalyst there is no reaction or proceeds with a very low rate. The first example using this approach was described in 2008,

(17) Christopherson, J. C.; Topić, F.; Barrett, C. J.; Friščić, T. *Cryst. Growth Des.* **2018**, *18*, 1245-1259.
(18) Berger, G.; Soubhye, J.; Meyer, F. *Polym. Chem.* **2015**, *6*, 3559-3580.
(19) Mendez, L.; Henriquez, G.; Sirimulla, S.; Narayan, M. *Molecules* **2017**, *22*, 1397/1391-1397/1315.
(20) Gilday, L. C.; Robinson, S. W.; Barendt, T. A.; Langton, M. J.; Mullaney, B. R.; Beer, P. D. *Chem. Rev.* **2015**, *115*, 7118-7195.
(21) Bulfield, D.; Huber, S. M. *Chem. - Eur. J.* **2016**, *22*, 14434-14450.
(22) Desiraju, G. R.; Ho, P. S.; Kloo, L.; Legon, A. C.; Marquardt, R.; Metrangolo, P.; Politzer, P.; Resnati, G.; Rissanen, K. *Pure Appl. Chem.* **2013**, *85*, 1711-1713.
(23) Sarwar, M. G.; Dragisic, B.; Salsberg, L. J.; Gouliaras, C.; Taylor, M. S. *J. Am. Chem. Soc.* **2010**, *132*, 1646-1653.
(24) Robertson, C. C.; Wright, J. S.; Carrington, E. J.; Perutz, R. N.; Hunter, C. A.; Brammer, L. *Chem. Sci.* **2017**, *8*, 5392-5398.

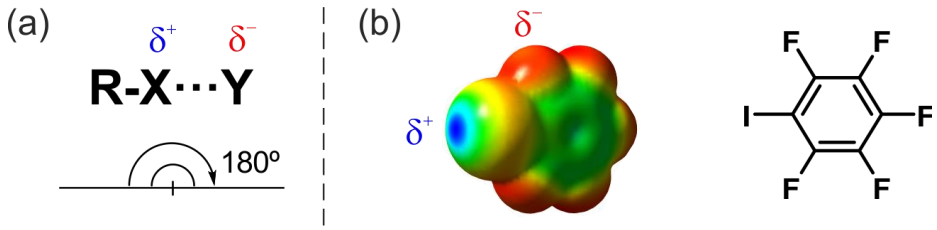

Figure 3. (a) Schematic representation of a halogen bond. The halogen bond donor (R–X, where X is a halogen atom) interacts in a directional manner (180° or aligned with the R–X bond) with the halogen bond acceptor (Y, nucleophile). (b) Electrostatic potential surface of iodopentafluorobenzene, with the σ-hole or positive electrostatic potential region at the iodine atom being indicated in blue.

when Bolm and co-workers reported the catalytic reduction of quinolines **1** in the presence of Hantzsch's ester **2** *via* a halogen-bond-induced hydrogen transfer to the C=N bond (Scheme 1).[25] This example is regarded as the first example of halogen bonding in catalysis. The effect of halogen bonding was supported by ^{13}C and ^{19}F NMR analyses, providing an indication that there was an interaction between the quinolinic nitrogen and the organocatalyst **4**.

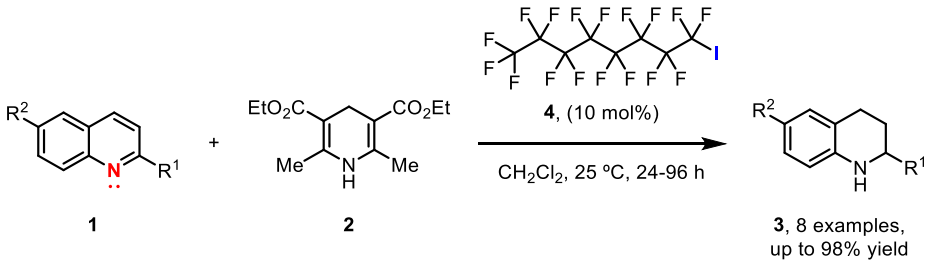

Scheme 1. Halogen-bond-induced reduction of quinolines **1** with Hantzsch's ester **2**.[25]

A variation of the previous strategy relies on the halogen-bond-mediated activation of reagents rather than reactants, in order to promote the catalytic transformation. For instance, Takemoto and co-workers described in 2015 the combined use of a halogen bond donor (**8**) with an *in situ* generated trimethylsilyl iodide for the catalytic dehydroxylative

(25) Bruckmann, A.; Pena, M. A.; Bolm, C. *Synlett* **2008**, 900-902.

coupling of an array of alcohols **5** with various nucleophiles (Scheme 2).[26] According to their work, monodentate dihydroimidazoline halogen bonding catalyst **8** activates the *in situ* generated trimethylsilyl iodide arising from the reaction between iodine **9** and allyltrimethylsilane **6**. In this sense, halogen atoms can act as halogen bond acceptors in the presence of halogen bond donors. The halogen bonding interaction increases the Lewis acidity of silicon in trimethylsilyl iodide favoring the activation of alcohols **5** that react with **6** to give the products and trimethylsilanol as the leaving group. ^{13}C NMR spectroscopy pointed to a halogen bonding interaction, which was deemed crucial for the transformation. The reaction proceeded with 15 mol% amount of catalyst under mild conditions and rendered a structurally diverse array of functionalized products in good to excellent yields. Furthermore, the utility of this approach was validated with the synthesis of antipsychotic drug pimozide.[27]

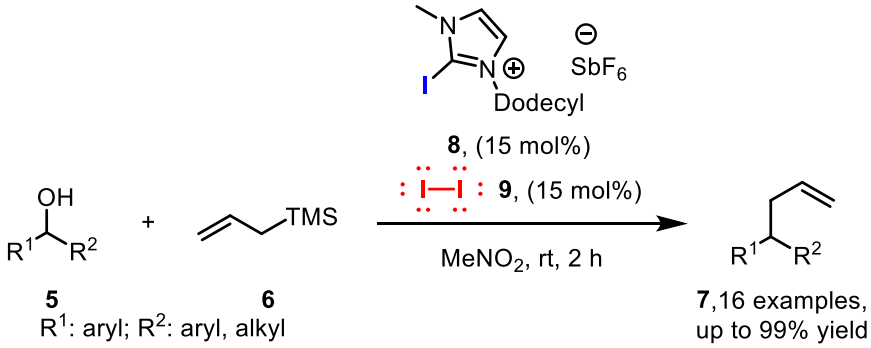

Scheme 2. Halogen-bond-catalyzed reaction of alcohols **5** with TMS-nucleophiles **6**.[26]

The use of halogen bond catalysts incorporating a halogen bond acceptor to activate reactants or reagents containing a halogen bond donor motif remains a less common approach compared to the abovementioned strategies. Generally, these examples refer to halogenation reactions, in which the halogenating agent is activated *via* the halogen bonding interaction. An example was recently published by McKenzie and co-workers, who described a halogen-bond-assisted

(26) Saito, M.; Tsuji, N.; Kobayashi, Y.; Takemoto, Y. *Org. Lett.* **2015**, *17*, 3000-3003.
(27) Colvin, C. L.; Tankanow, R. M. *Drug Intell. Clin. Pharm.* **1985**, *19*, 421-424.

sulfoxidation and epoxidation reactions using iodosylbenzene **11** as the oxo-transfer reagent with an iron(III) complex as catalyst (Scheme 3).[28] This example remains remarkable as it involves a transition-metal-catalyzed transformation, not organocatalytic, and the halogen bond donor is a hypervalent iodine(III) species, not a standard iodide derivative. The authors presented evidences to support that halogen bonding influences the reactivity observed in the transformation, by solubilizing iodosylbenzene **11**. The isolation and crystallization of the 1:1 complex between **11** and **13** was crucial to observe halogen bonding between the iodine and oxygen atoms, ultimately confirming the observations gathered in solution and in the gas phase. The authors suggested that, unlike other more soluble oxo-transfer reagents, the oxidant was incorporated as needed during the reaction, preventing the formation of oxidation by-products and increasing the selectivity of the reaction with this protocol.

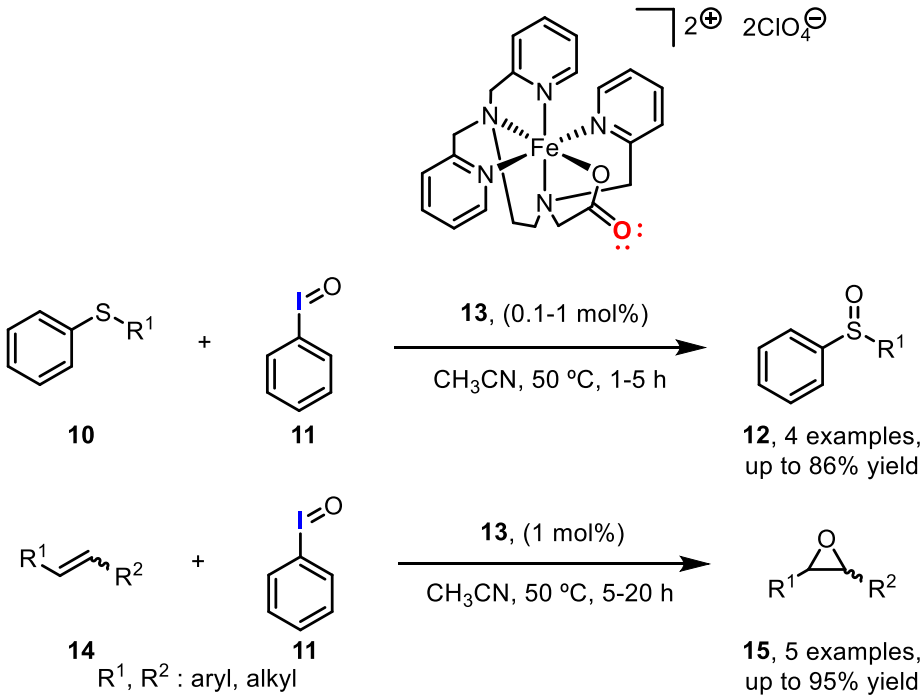

Scheme 3. Fe(III)-catalyzed sulfoxidation and epoxidation using iodosylbenzene **11** *via* halogen bond assistance.[28]

(28) de Sousa, D. P.; Wegeberg, C.; Vad, M. S.; Mørup, S.; Frandsen, C.; Donald, W. A.; McKenzie, C. J. *Chem. - Eur. J.* **2016**, *22*, 3810-3820.

Although most of the halogen bond donor motifs used in catalysis derive from iodide groups, other elements have been explored. Early in 2017, Sekar and co-workers developed a methodology for the halogen-bond-catalyzed aldol condensation between acetophenone derivatives **16** and aryl aldehydes **17** (Scheme 4) using CBr_4 **19** as organocatalyst.[29] With an excellent activity, the authors emphasized the applicability of the reaction with a broad substrate scope, including the synthesis of the active pharmaceutical ingredient (API) licochalcone A.[30] After ruling out activation by traces of *in situ* generated HBr, the authors suggested a halogen bond interaction as the underlying driving force for the reactivity observed. The researchers demonstrated that this methodology could also be extended to Knoevenagel condensations.[29]

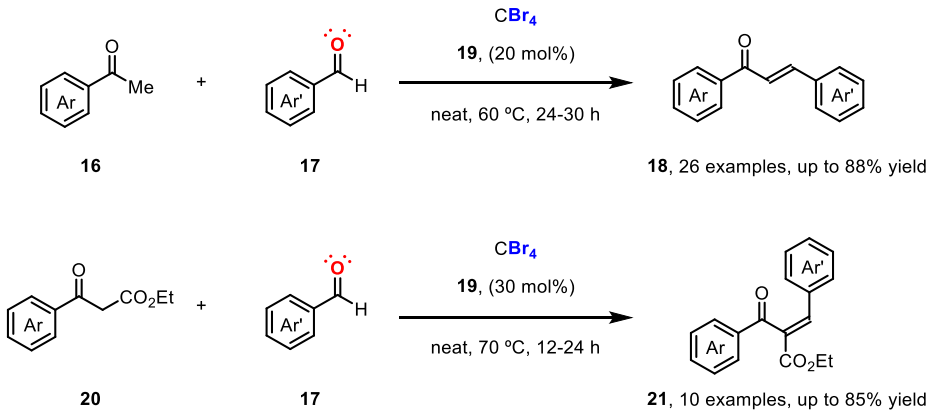

Scheme 4. Halogen-bond-catalyzed aldol condensation and Knoevenagel condensation by Sekar and co-workers.[29]

Alternative designs based on hypervalent iodine catalysts have been reported by Huber and co-workers. His group recently described hypervalent iodine(III) organocatalyst **25** for the Diels-Alder reaction between cyclopentadiene **22** and methyl vinyl ketone **23** (Scheme 5).[31] The activity of organocatalyst **25** was comparable to those of the bidentate iodoimidazolium catalysts previously developed by the same group,

(29) Kazi, I.; Guha, S.; Sekar, G. *Org. Lett.* **2017**, *19*, 1244-1247.
(30) Chen, M.; Theander, T. G.; Christensen, S. B.; Hviid, L.; Zhai, L.; Kharazmi, A. *Antimicrob. Agents Chemother.* **1994**, *38*, 1470-1475.
(31) Heinen, F.; Engelage, E.; Dreger, A.; Weiss, R.; Huber, S. M. *Angew. Chem., Int. Ed.* **2018**, *57*, 3830-3833.

demonstrating that hypervalent iodine(III) species were also suitable activators for halogen bond acceptors.

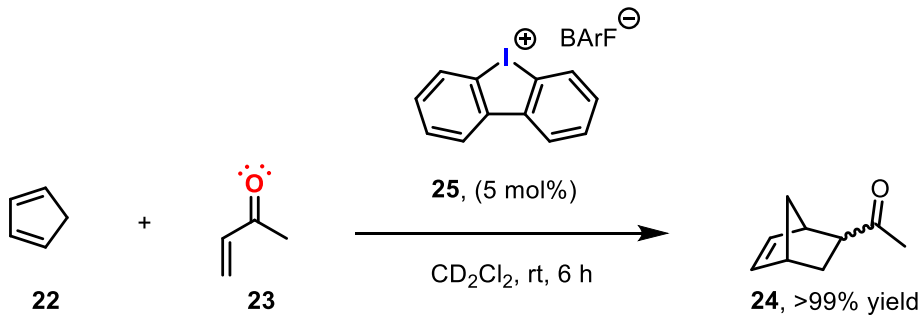

Scheme 5. Halogen-bond-catalyzed Diels-Alder reaction between cyclopenta-1,3-diene **22** and methyl vinyl ketone **23**.[31]

Efforts in halogen-bond-catalyzed reactions have also been directed to the design of systems for enantioselective transformations, although this area of research still remains underexplored. Arai and co-workers recently reported an enantiopure halogen-bond-containing catalyst **29**, which was then applied to the enantioselective Mannich reaction of malonitrile **27** with *N*-Boc imines **26** and **30**. Excellent activities and enantioselectivities were observed for a wide substrate scope (Scheme 6).[32] The catalyst design was based on the quinidine structure, which was modified by attachment of a perfluorinated iodophenyl substituent. The catalyst efficiently mediated enantioselective Mannich transformations of imine derivatives, which also incorporated an additional C=O group as halogen bond acceptor, with enantioselectivities up to 98%. The authors demonstrated that the presence of the iodo group as halogen bond donor was crucial for achieving high enantioselectivities. Moreover, the efficiency of the catalyst was demonstrated by reducing the catalyst loading down to 0.5 mol% for acyclic substrates **30**. It is interesting to highlight that the analogous hydrogen-bond-based systems tested were not efficient in this transformation.

(32) (a) Kuwano, S.; Suzuki, T.; Hosaka, Y.; Arai, T. *Chem. Commun.* **2018**, *54*, 3847-3850. (b) Arai, T.; Kuwano, A., JP2019034908A, **2019**.

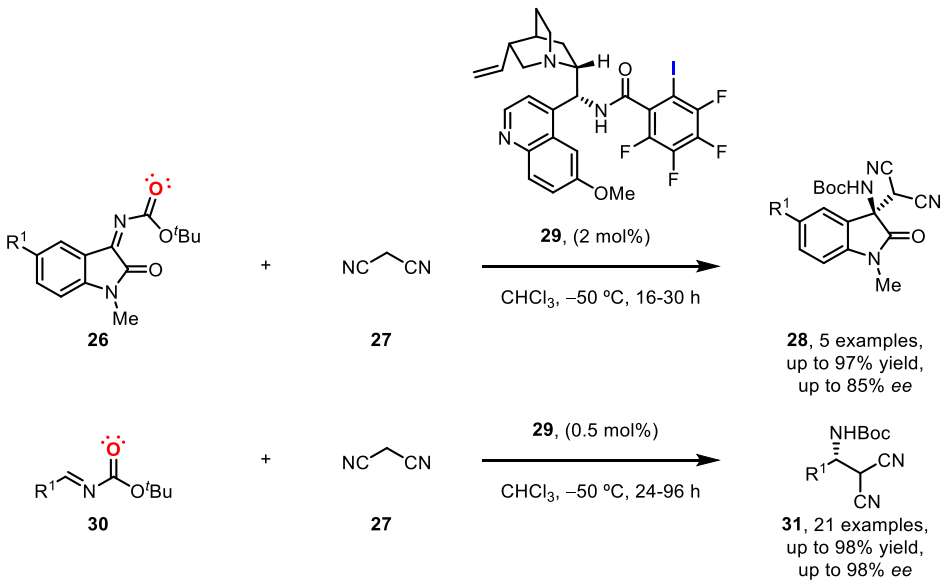

Scheme 6. Halogen-bond-mediated asymmetric Mannich reactions of malonitrile **27** with *N*-Boc substrates **26** and **30**.[32]

This brief overview on supramolecular catalysis using halogen bonding aims to provide a general picture of the current status of the field. There are more contributions, which were not summarized in this section.[6c,21] The state-of-the-art in the use of halogen bonding interactions in catalysis can be summarized as follows:

- Activation effects in most of the catalysts are based on halogen bonding interactions between reactants (containing a halogen bond acceptor) and the organocatalyst (containing one or multiple halogen bond donors, generally iodide groups).
- The application of halogen bonding to transition metal catalysis and enantioselective processes remains underexplored.
- To date, the use of alternative catalytic strategies not involving substrate activation *via* halogen bonding remains unexplored.

Allosterism, which can be defined as "the change in the affinity for binding (or another biological function) of a ligand or substrate that is caused by the binding of another ligand away from the active site",[33] was a phenomenon observed and described for enzymes.[15] Inspired by nature, catalysis practitioners have developed non-natural allosteric catalysts,[34] also known as supramolecularly regulated catalysts.[14] The first synthetic approach in regulating catalysis could be traced back to 1977, when Shinkai and co-workers reported the catalytic hydrolysis of carboxylic esters **32** by functionalized polymers **34** (Scheme 7).[35] The addition of tetraalkylammonium salts **35** (regulation agent) enhanced the reaction rate, according to kinetic experiments. The authors suggested that the regulation agents enhanced the substrate binding to the polymer, although the exact mechanism for the regulation remained still unclear.

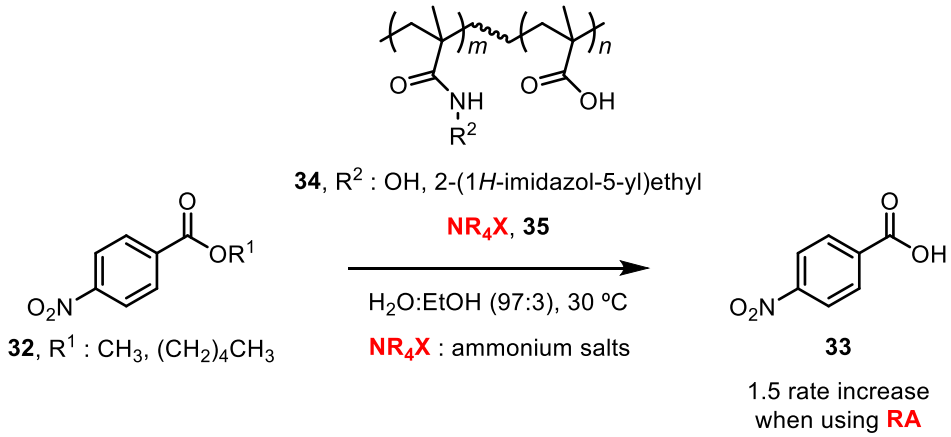

Scheme 7. Hydrolysis of carboxylic esters **32** by methacrylic polymers **34** in the presence of ammonium salts as regulation agents **35**.[35]

Rebek and co-workers also contributed to set the basis of non-natural allosteric regulation in molecular recognition, developing a supramolecularly regulated receptor for alkali metal salts (Figure 4).[36] Rebek's receptor incorporates a 2,2'-bipyridine motif as allosteric site,

(33) Pelley, J. W. *Protein Structure and Function.* In *Elsevier's Integrated Biochemistry*, Pelley, J. W., Ed. Mosby, Philadelphia, **2007**; pp 19-28.
(34) Kovbasyuk, L.; Krämer, R. *Chem. Rev.* **2004**, *104*, 3161-3188.
(35) Shinkai, S.; Tou, K.; Kunitake, T. *Polymer J.* **1977**, *9*, 381-389.
(36) Rebek, J.; Trend, J. E.; Wattley, R. V.; Chakravorti, S. *J. Am. Chem. Soc.* **1979**, *101*, 4333-4337.

which upon chelation with a transition metal, influenced the binding ability of the crown-ether motif towards alkali metal salts.

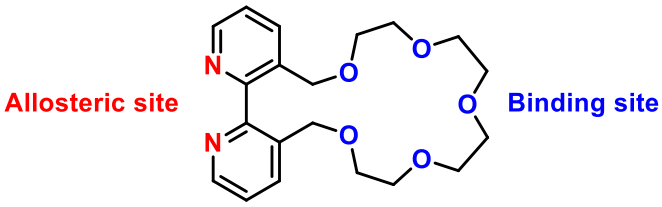

36

Figure 4. Rebek's allosteric receptor **36**, regarded as the first synthetically prepared.[36]

Since then, relevant contributions from Mirkin,[37] Reek[38] and others,[5,14,39] including us,[40] have contributed to this field of research. In the following pages, recent relevant advances (from *ca.* 2014 to the date) in supramolecular regulation catalysis will be summarized, with particular emphasis on approaches (mostly from our group) that have inspired some of the work of the present thesis.

Contributions from our research group have been based on a modular design of the catalytic system, which contains a polyether chain as the regulation site linked to metal ligating groups (G) for catalysis. Addition of an array of structurally diverse regulation agents (RA) and a transition metal ([M]), have led to a library of catalytic systems with common structural characteristics that incorporate structural peculiarities that depend on the size of the regulation agent (Figure 5). As regards to the ligating groups (G), the group has mainly focused on phosphorus-based motifs, although oxazolinyl groups have recently been used as ligating groups for catalysis.[41] Regarding the regulation agents, several polyether

(37) For a selected example, see: Gianneschi, N. C.; Bertin, P. A.; Nguyen, S. T.; Mirkin, C. A.; Zakharov, L. N.; Rheingold, A. L. *J. Am. Chem. Soc.* **2003**, *125*, 10508-10509.
(38) For a selected example, see: Dydio, P.; Rubay, C.; Gadzikwa, T.; Lutz, M.; Reek, J. N. H. *J. Am. Chem. Soc.* **2011**, *133*, 17176-17179.
(39) Yoo, C.; Dodge, H. M.; Miller, A. J. M. *Chem. Commun.* **2019**, *55*, 5047-5059.
(40) For a selected example, see: Mon, I.; Jose, D. A.; Vidal-Ferran, A. *Chem. - Eur. J.* **2013**, *19*, 2720-2725.
(41) Iniesta, E.; Vidal-Ferran, A. *Unpublished results.*

binders have been tested, particularly alkali metal, alkali earth metal, lanthanide and ammonium salts.[14,42] Concerning the metal source, rhodium(I)-, palladium(II)- and copper(I)-catalyzed transformations have been explored, the latter very recently.[41] In a number of catalyst designs, a linking group (X) was incorporated to the regulation site in order to introduce additional stereogenic elements or to restrain the flexibility of the polyether motif.[14]

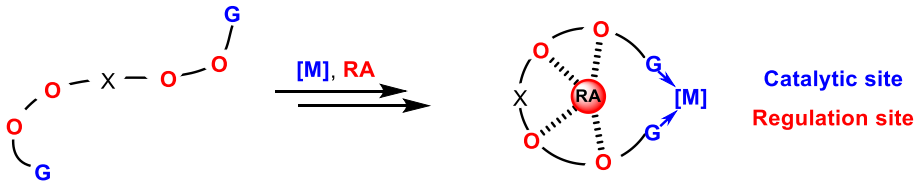

Figure 5. Schematic representation of the supramolecular regulation strategy from our research group.

Our regulation strategy has been satisfactorily demonstrated in the asymmetric hydroformylation (AHF) of olefins. The variation of the structure of the ligand, binding studies with several regulation agents, study of counterion effects, analysis of the turnover frequency (TOF) of the reaction, studies on the structure of the active catalytic species, catalyst loading assays, DFT calculations and kinetic studies were carried out to provide insight into the catalytic results observed.[40,43] Noteworthy, the addition of RbBArF as regulation agent yielded the highest positive regulation effect on the enantioselectivity of the AHF of vinyl acetate (increment of 64% *ee*) and very high conversion, regioselectivity and enantioselectivity for this substrate employing supramolecularly regulated ligand **39**. Based on computational studies, the authors postulated that the significant increase in enantiomeric excess provided by RbBArF for vinyl acetate might be result from adaption of the P–Rh–P bond angle of the catalytic rhodium species to that required for high enantioselectivity. The regulation principle was also extended to other substrates. Moreover,

(42) Carreras, L.; Rovira, L.; Vaquero, M.; Mon, I.; Martin, E.; Benet-Buchholz, J.; Vidal-Ferran, A. *RSC Adv.* **2017**, *7*, 32833-32841.
(43) (a) Vidal-Ferran, A.; Mon, I.; Bauzá, A.; Frontera, A.; Rovira, L. *Chem. - Eur. J.* **2015**, *21*, 11417-11426. (b) Martínez-Carrión, A.; Howlett, M. G.; Alamillo-Ferrer, C.; Clayton, A. D.; Bourne, R. A.; Codina, A.; Vidal-Ferran, A.; Adams, R. W.; Burés, J. *Angew. Chem., Int. Ed.* **2019**, DOI: 10.1002/anie.201903878.

the high activity of the supramolecularly regulated catalytic system derived from **39** and RbBArF was demonstrated by reducing the catalyst amount to a 0.1 mol% with no loss in catalytic activity. This supramolecularly regulated system was also successfully applied to the asymmetric hydrogenation of olefins employing ammonium salts as regulation agents (Scheme 8).[43a]

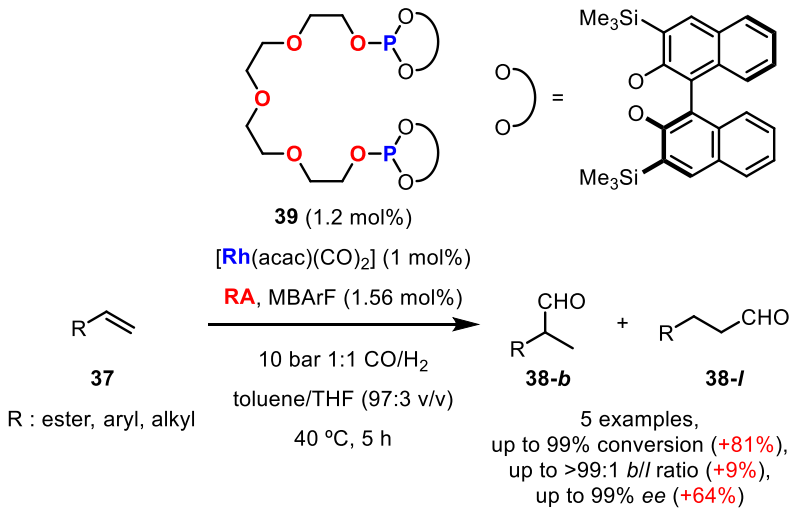

Scheme 8. Supramolecularly regulated AHF of olefins with rhodium(I) complexes derived from bisphosphite **39**. Enhancements when comparing results using the highest performing regulation agent and no RA are indicated in red.[43a]

Our group also reported a "second generation" of supramolecularly regulated ligands, which incorporated a stereogenic element in the regulation site. Catalytic systems derived from these new ligands resulted in a better enantiodiscrimination with overall high regulation effects and enantioselectivities in the AHF of heterocyclic olefins (Scheme 9).[44]

Supramolecular regulation of palladium-catalyzed asymmetric allylic substitutions was also achieved using our approach. In this case, moderate increases in the selectivity (regio- and enantioselectivity) were observed upon using metal acetates and trifluoroacetates as RAs. Interestingly, the influence of the coordination geometry of the ligand in the catalytic activity was demonstrated by proving that *trans*-chelating

(44) Rovira, L.; Vaquero, M.; Vidal-Ferran, A. *J. Org. Chem.* **2015**, *80*, 10397-10403.

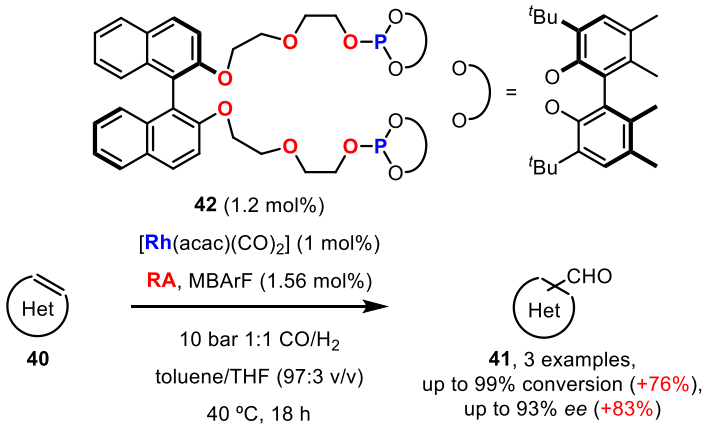

Scheme 9. Supramolecularly regulated AHF of heterocyclic olefins with Rh(I) complexes derived from bisphosphite **42**. Enhancements when comparing results using the highest performing regulation agent and no RA are indicated in red.[44]

ligands in square-planar palladium complexes were inactive (Scheme 10).[45]

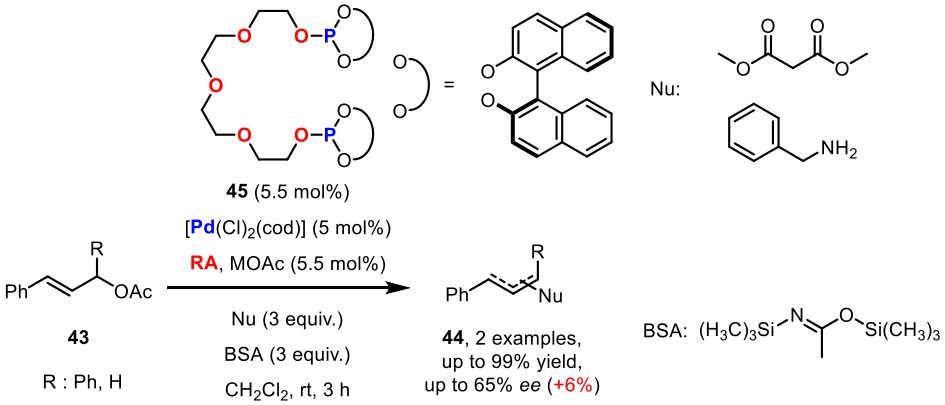

Scheme 10. Supramolecularly regulated asymmetric allylic substitutions with Pd(II)-complexes derived from bisphosphite **45**. Enhancements when comparing results using the highest performing regulation agent and no RA are indicated in red.[45]

(45) Rovira, L.; Fernández-Pérez, H.; Vidal-Ferran, A. *Organometallics* **2016**, *35*, 528-533.

These examples prompted us to design and develop other regulation mechanisms in catalysis. Homogenous gold(I) catalysis has been flourishing in the last two decades[46] with variable degrees of success limited only by the intrinsic linearity of Au(I) complexes: In gold(I) catalysis, substrates to be activated are normally placed away from the ligand aimed to affect the reactivity between the metal and the substrate. Catalysis practitioners have designed catalyst architectures that facilitate the proximity of the substrate and the catalytic center.[47] Nevertheless, this approach normally leads to synthetically challenging catalyst's designs.

Supramolecular chemistry has been used to construct the backbone of gold(I) catalysts with unprecedented ease. In 2015, Goldup and co-workers published an elegant approach to supramolecularly regulated gold catalysts.[48,49] The authors designed a switchable rotaxane **49** as catalyst, which was then applied to the cyclopropanation of alkenes (Scheme 11). Their design incorporated a 2,2'-bipyridine-containing macrocyclic motif as allosteric site and a chlorogold(I) phosphine capped thread as the catalytic site. The authors observed that, after halide abstraction, the supposedly active cationic gold(I) complex derived from **49** was inactive in the cyclopropanation of propargylic ester **46** with styrene **47**. In contrast, the use of the molecular thread (without the macrocycle) catalyzed the transformation of **46** and **47** into cyclopropane **48** in good yields. The authors reasoned that the absence of reactivity was due to the interaction of the gold with the 2,2'-bipyridine motif, therefore being inactive in the transformation. Interestingly, the addition of 4-methylbenzenesulfonic acid, copper, zinc or cadmium salts enhanced the activity and selectivity of catalyst **49** upon coordination to the regulation site. Noteworthy, the 'activated' rotaxane with copper salts outperformed the bare molecular thread in terms of activity and *cis*/*trans* selectivity. The activity and selectivity of the catalytic system for a particular substrate was maximized

(46) Hashmi, A. S. K.; Toste, F. D.; Eds. *Modern Gold Catalyzed Synthesis*; Wiley-VCH, Weinheim, **2012**.
(47) Wang, Y.-M.; Lackner, A. D.; Toste, F. D. *Acc. Chem. Res.* **2014**, *47*, 889-901.
(48) When the experimental work of this PhD thesis started, there were no known examples of supramolecularly regulated gold catalysts. Most of supramolecular approaches to gold catalysis relied on metal encapsulation, see: Jans, A. C. H.; Caumes, X.; Reek, J. N. H. *ChemCatChem* **2019**, *11*, 287-297.
(49) Galli, M.; Lewis, J. E. M.; Goldup, S. M. *Angew. Chem., Int. Ed.* **2015**, *54*, 13545-13549.

by the choice of the suitable regulation agent. Therefore, these results constitute an exquisite example of supramolecular regulation.

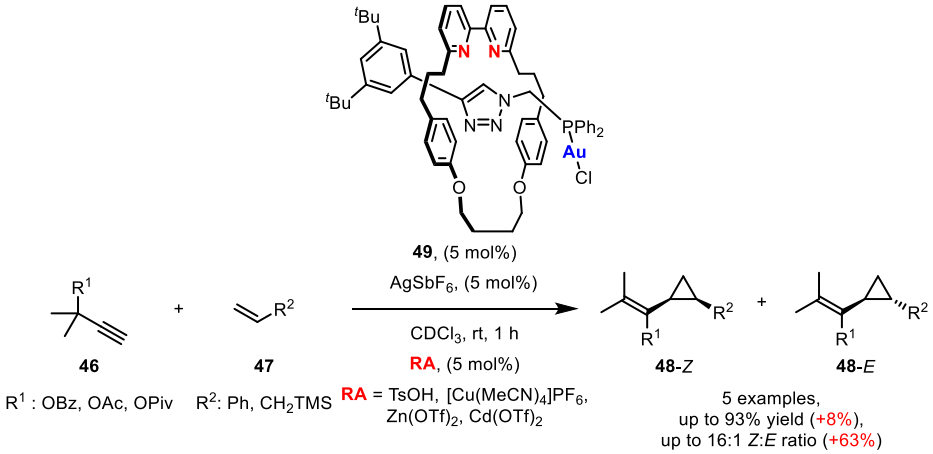

Scheme 11. Supramolecularly regulated Au-mediated cyclopropanation of propargylic esters **46** with alkenes **47**. Enhancements when comparing results using the highest performing regulation agent and the solely use of the molecular thread are indicated in red.[49]

In 2017, Peris and co-workers reported the use of supramolecularly regulated gold(I)-NHC (*N*-heterocyclic carbene) complexes as catalysts in the hydroamination of phenylacetylene (Scheme 12).[50] According to the authors, an increase in the activity (up to a 15%) and the reaction rate was observed in the presence of the regulation agent (a polycyclic aromatic hydrocarbon, PAH), with the highest regulation effects being observed for pyrene. The polycyclic aromatic hydrocarbon appears to disrupt the self-aggregation processes in catalyst **53**, thus releasing active gold(I) complexes for this chemistry.[51]

(50) Ibáñez, S.; Poyatos, M.; Peris, E. *Organometallics* **2017**, *36*, 1447-1451.
(51) Nuevo, D.; Poyatos, M.; Peris, E. *Organometallics* **2018**, *37*, 3407-3411.

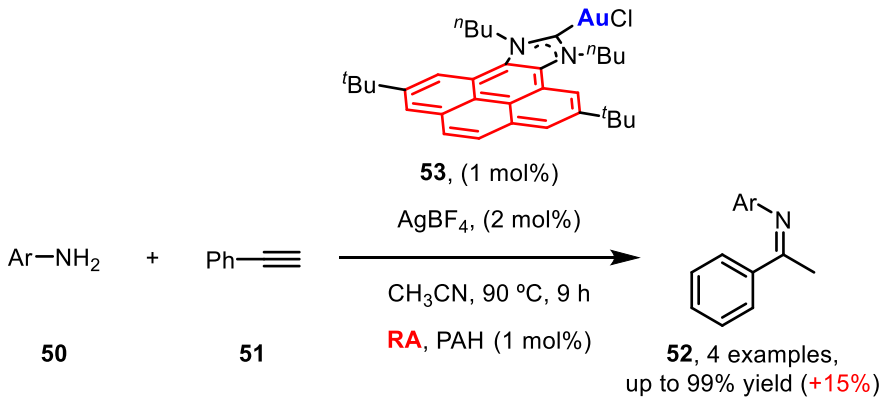

Scheme 12. Supramolecularly regulated Au-mediated hydroamination of phenylacetylene **51** with anilines **50**. Enhancements when comparing results using the highest performing regulation agent and no RA are indicated in red.[50]

OBJECTIVES

As previously summarized in this section, there were no published studies on the use of halogen bonding for the construction of the catalyst's backbone at the time that the experimental work of this thesis started. Moreover, past studies of our group demonstrated that conformationally transformable bisphosphite ligands were efficient supramolecularly regulated catalytic systems in Rh(I)- and Pd(II)-mediated asymmetric hydrogenations, hydroformylations and allylic substitution reactions.[40,43,44,45] Inspired by these positive regulation effects, we envisaged that a related regulated strategy could be devised for regulating the steric congestion around the catalytic site in gold(I)-mediated processes.

Therefore, the objectives of the present thesis are as follows:

1. Design and development of efficient synthetic methodologies for the preparation of halogen-bonded supramolecular rhodium(I) catalysts based on phosphorus(III) ligands and assessment of the catalytic performance of the resulting Rh-catalysts in the hydroboration of terminal alkynes.

2. Study and rationalization of the influence of the halogen bonding event in the outcome of the complexation processes on several rhodium(I) precursors.

3. Design and preparation of a set of diverse phosphite ligands with a distal regulation site and a steric effector capable of modifying the steric congestion around the catalytic site together with studies of the catalytic properties of these ligands in the Au(I)-catalyzed carbene insertion reaction in phenols and related derivatives.

CHAPTER I

XBphos-Rh: a Halogen-Bond-Assembled Supramolecular Catalyst for the Hydroboration of Terminal Alkynes

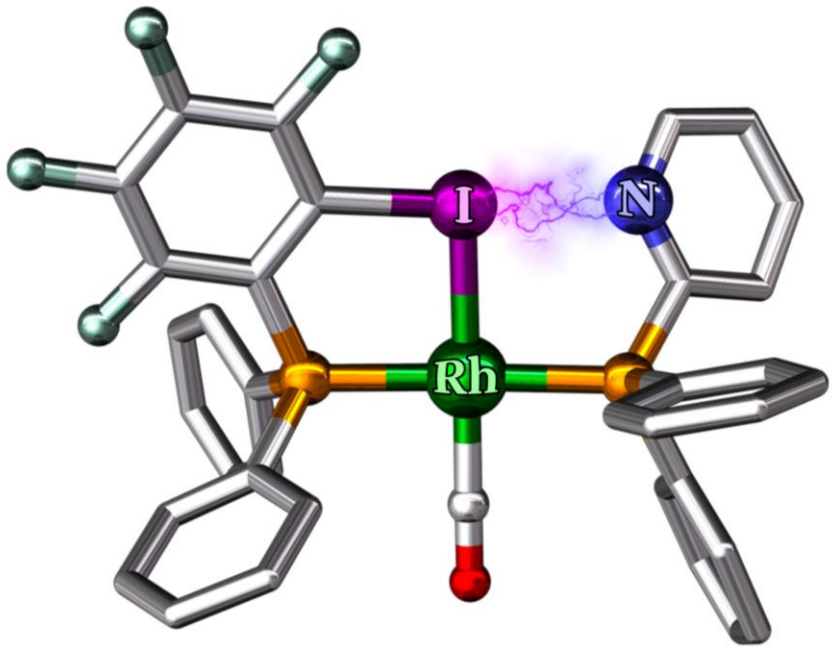

XBphos-Rh: a Halogen-Bond-Assembled Supramolecular Catalyst for the Hydroboration of Terminal Alkynes

Chem. Sci. **2018**, *9*, 3644-3648

Lucas Carreras,[a,b] Marta Serrano-Torné,[b] Piet W. N. M. van Leeuwen,[c]* and Anton Vidal-Ferran[b,d]*

a Universitat Rovira i Virgili, Departament de Química Analítica i Química Orgànica, C. Marcel·lí Domingo 1, 43007, Tarragona, Spain.
b Institut Català d'Investigació Química (ICIQ) & Barcelona Institute of Science and Technology (BIST), Av. Països Catalans 16, 43007, Tarragona, Spain.
c Laboratoire de Physique et Chimie des Nano-Objets (LPCNO), Institut National des Sciences Appliquées (INSA), Av. De Rangueil, F-31077, Toulouse, France.
d Institució Catalana de Recerca i Estudis Avançats (ICREA), Pg. Lluís Companys 23, 08010, Barcelona, Spain.

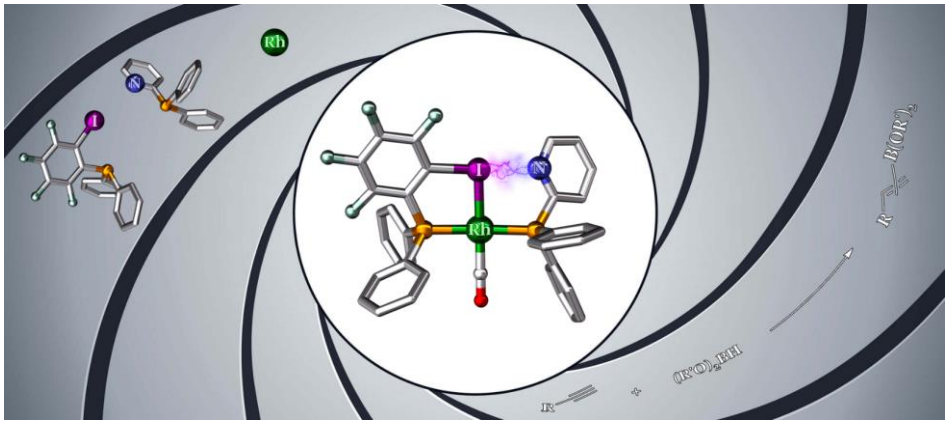

1.1. ABSTRACT

The use of halogen bonding as a tool to construct the catalyst backbone is reported. Specifically, pyridyl- and iodotetrafluoroaryl-substituted phosphines were assembled in the presence of a rhodium(I) precursor to form the corresponding halogen-bonded complex **XBphos-Rh**. The presence of fluorine substituents at the iodo-containing supramolecular motif was not necessary for halogen bonding to occur due to the template effect exerted by the rhodium center during formation of the halogen-

bonded complex. The halogen-bonded supramolecular complexes were successfully tested in the catalytic hydroboration of terminal alkynes.

1.2. INTRODUCTION

The evolution of metal-based homogeneous catalysis has run in parallel with the development of structurally diverse ligands. Ligand design allows the behavior of the metal center to be influenced and its catalytic activity and selectivity to be modified.[52]

Supramolecular chemistry has emerged as a more efficient tool for the construction of (enantiopure) ligand backbones of metal complexes when compared with standard covalent chemistry. Supramolecular strategies mainly rely on the self-assembly of building blocks that contain both the complementary motifs required for the assembly, and the binding groups necessary for the desired catalysis event. This approach has been successfully employed for the preparation of catalysts by assembling supramolecularly complementary building blocks through hydrogen bonding, metal-ligand, or ionic interactions.[53] However, the use of halogen bonding for constructing the backbone of a catalyst remains, to the best of our knowledge, unexplored.

The directionality and strength of halogen bonding,[20] together with a greater tolerance to solvent polarity changes,[23] prompted us to design and develop new halogen-bonded metal catalysts (Scheme 13). We speculated that the halogen-bond-mediated assembly of two appropriate building blocks, each bearing a ligating group, could lead to the formation of a metal complex due to the chelation effect that should be exhibited in the presence of the metal center. With regard to the ligating groups, we focused our attention on phosphino groups due to their pre-eminence in

(52) van Leeuwen, P. W. N. M., Ed. *Homogeneous Catalysis: Understanding the Art.* Kluwer Academic Publishers, Dordrecht, **2004**.

(53) For selected reviews see ref. 5 and the following references: (a) Breit, B. *Angew. Chem., Int. Ed.* **2005**, *44*, 6816-6825. (b) Sandee, A. J.; Reek, J. N. H. *Dalton Trans.* **2006**, 3385-3391. (c) Carboni, S.; Gennari, C.; Pignataro, L.; Piarulli, U. *Dalton Trans.* **2011**, *40*, 4355-4373. (d) Bellini, R.; van der Vlugt, J. I.; Reek, J. N. H. *Isr. J. Chem.* **2012**, *52*, 613-629.

homogeneous catalysis[54] and their tolerance to functionalization.[55] With respect to the halogen bonding motifs, we envisaged that the use of a fluorinated iodoarene and a pyridine group could be suitable due to the reported complementarity of both supramolecular motifs.[56] Concerning the metal center, we focused on rhodium as its complexes are catalytically active in pivotal organic transformations.[57] In the discussion that follows, we report our results in the preparation and full characterization of the first examples of halogen-bonded rhodium(I) complexes and their catalytic performance in alkyne hydroborations.

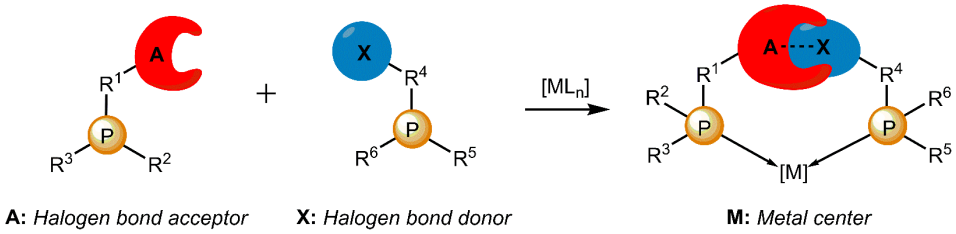

Scheme 13. Supramolecular halogen-bonded catalysts.

1.3. RESULTS AND DISCUSSION

Examination of space-filling models revealed that the relative arrangements of the phosphorus ligating groups and the halogen bond acceptor and donor motifs in 2-pyridyldiphenylphosphine (**1**) and 2-iodo-3,4,5,6-tetrafluorophenyldiphenylphosphine (**2**), respectively, were adequate for the formation of the target halogen-bonded Rh(I) complex (Scheme 14). Building blocks **1** and **2** were successfully prepared in good yields in a multigram scale by slight modification of well-established

(54) Kamer, P. C. J.; van Leeuwen, P. W. N. M.; Eds. *Phosphorus(III) Ligands in Homogeneous Catalysis: Design and Synthesis*. John Wiley & Sons Ltd., United Kingdom, **2012**.
(55) For examples on the design and use of functionalized phosphorus-based catalysts, see for instance: Fernández-Pérez, H.; Etayo, P.; Panossian, A.; Vidal-Ferran, A. *Chem. Rev.* **2011**, *111*, 2119-2176.
(56) Tsuzuki, S.; Wakisaka, A.; Ono, T.; Sonoda, T. *Chem. - Eur. J.* **2012**, *18*, 951-960.
(57) For an example of supramolecular catalysis using a rhodium(I) bisphosphite applied to the asymmetric hydroboration of alkenes, see: Moteki, S. A.; Takacs, J. M. *Angew. Chem., Int. Ed.* **2008**, *47*, 894-897.

synthetic protocols.[58] We envisaged that the use of $[Rh(Cl)(CO)_2]_2$ along with a halide scavenger would render a putative $[Rh(CO)_2]X$ intermediate that should react with phosphines **1** and **2**. After some experimentation, halogen-bonded rhodium(I) complexes were obtained by first reacting $[Rh(Cl)(CO)_2]_2$ and NaBArF,[59] and then adding ligands **1** and **2** as indicated in Scheme 14.[60] The structure of the complex was confirmed by standard spectroscopic studies. The $^{31}P\{^1H\}$ NMR spectrum showed two complex multiplets, from which a high value $^2J_{P-P}$ coupling constant (*i.e.* 276 Hz; unequivocally assigned by two-dimensional $^{31}P\{^1H\}$ *J*-resolved spectroscopy; Figure 59 in section 1.5.7) was calculated. According to the literature reviewed, this high value $^2J_{P-P}$ coupling constant indicates a *trans*-spanning bisphosphine coordinated to the rhodium center.[61] We initially expected a dicarbonyl complex, but ESI-MS analysis identified the monocarbonyl complex [Rh(CO)(**1**)(**2**)]BArF (**4**), referred to as **XBphos-Rh**[62] in the discussion that follows.

X-ray analysis confirmed the proposed halogen-bonded structure of the rhodium complex derived from **1** and **2** (see Scheme 14 for the structure of **XBphos-Rh** and Figure 6 for the crystal structure). The nitrogen and iodine atoms are aligned with a N···I distance of 2.757(8) Å and with a N···I–C

(58) For the preparation of **1**, see: (a) Klusener, P. A. A.; Suykerbuyk, J. C. L.; Verbrugge, P. A. Shell Internationale Research Maatschappij B. V., Eur. Pat. Appl. EP499328A2, **1992**. During the present thesis, phosphine **1** became commercially available by Merck. For the preparation of **2** and **3**, see: (b) Eller, P. G.; Meek, D. W. *J. Organometal. Chem.* **1970**, *22*, 631-636.

(59) The tetrakis[3,5-bis(trifluoromethyl)phenyl]borate counterion enhances the solubility and crystallinity of the resulting derivatives, which we deemed as useful for further catalytic studies. See ref. 42.

(60) Attempts to prepare homocomplexes $[Rh(CO)(\mathbf{1})_2]BArF$ or $[Rh(CO)(\mathbf{2})_2]BArF$ following an analogous strategy to that used for **XBphos-Rh** failed, as complex mixtures of rhodium derivatives were obtained in all cases. Experimental reaction conditions for the selective preparation of rhodium complexes arising from C–I oxidative addition processes in **2** have been also developed (see section 2.5.4 in Chapter II). It is interesting to note that ^{31}P NMR signals that could correspond to the above mentioned homocomplexes, or complexes arising from C–I oxidative additions in **2**, were not found in any spectra of the crude reaction mixtures.

(61) Freixa, Z.; van Leeuwen, P. W. N. M. *Coord. Chem. Rev.* **2008**, *252*, 1755-1786.

(62) XB in **XBphos-Rh** stands for halogen (X) bonding (B).

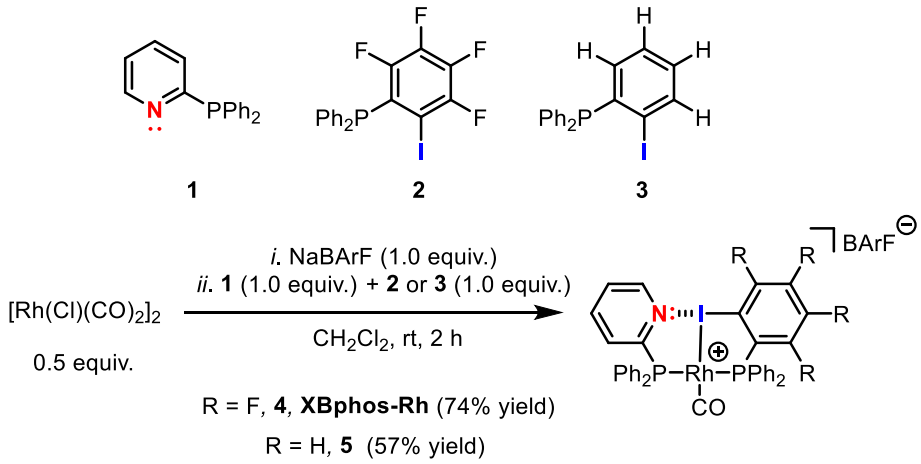

Scheme 14. Synthesis of halogen-bonded rhodium(I) chelates.

bond angle of 169.4(5)°. These structural parameters are in agreement with those reported for halogen-bonded complexes involving pyridine and fluorinated iodoaryl moieties.[63] Interestingly, the iodine appears to be coordinated to the rhodium center (Rh–I distance = 2.5535(7) Å). Thus, the tridentate coordination of the halogen-bonded ligands in square planar **XBphos-Rh** resembles that observed in pincer-type complexes,[64] and therefore this complex can be formally considered as the first reported P–I–P pincer-type complex.

Given the favorable template effect exerted by the rhodium center on the coordinated atoms in **XBphos-Rh**, we envisaged that fluorine-free compound **3** could also be used as the halogen bond donor. Thus, complex **5** could be prepared in good yields following a synthetic protocol analogous to that employed for **XBphos-Rh** (Scheme 14). Crystals from **5** suitable for X-ray analysis confirmed the proposed structure for the rhodium complex derived from **1** and **3** (Scheme 14 and Figure 6). The analysis of the solid-state structures revealed a longer N···I distance for **5** than for **XBphos-Rh** (2.84(1) Å for **5** and 2.757(8) Å for **4**), which indicates a stronger halogen bond interaction in the fluorine-containing complex.

(63) Vasylyeva, V.; Catalano, L.; Nervi, C.; Gobetto, R.; Metrangolo, P.; Resnati, G. *CrystEngComm* **2016**, *18*, 2247-2250.
(64) For representative literature reports on pincer-type metal complexes, see: Szabó, K. J.; Wendt, O. F.; Eds. *Pincer and Pincer-Type Complexes: Applications in Organic Synthesis and Catalysis*. Wiley-VCH, Weinheim, **2014**.

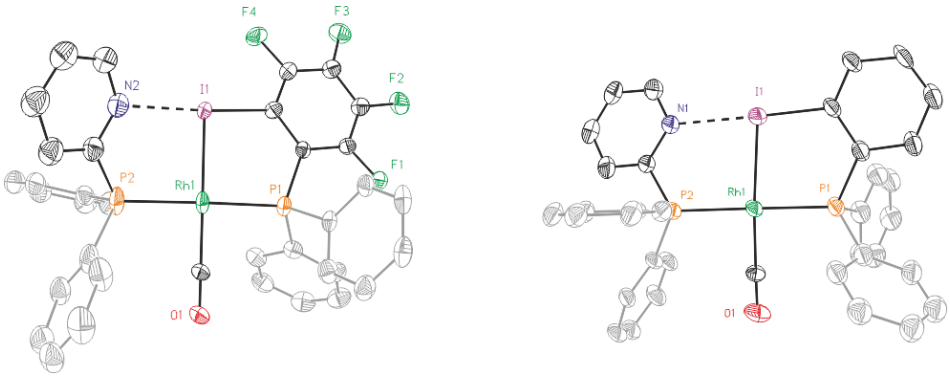

Figure 6. Crystal structures of **XBphos-Rh**, **4** (*left*) and **5** (right). Hydrogen atoms and the BArF unit have been omitted for the sake of clarity. Color scheme: C: black, P: orange, Rh: green, F: green, N: blue, I: purple, O: red. Atomic displacement ellipsoids are drawn at a 50% probability. For crystallographic data in CIF or other electronic format see CCDC 1815870 for **4** and 1815871 for **5**.

The formation of a halogen bonding interaction between the pyridine and iodoarene motifs is driven by an enthalpy gain but penalized by an entropic unfavorable contribution arising from the geometry constraints for effective bonding (*i.e.* linear arrangement of the N···I–C atoms). Overall, the free energy associated with a single interaction is low.[24] In order to gain a deeper insight into the halogen bonding event, full level DFT calculations were carried out. Geometries and stabilities of [Rh(CO)(**1**)(**2**)]$^+$ and [Rh(CO)(**1**)(**3**)]$^+$ and those of the starting building blocks were computed with Gaussian 09[65] with the TPSS[66]-D3[67] density functional employing a medium-sized triple-zeta (def2-TZVP[68]) basis set, which is a good compromise between the computational cost and the reliability in describing halogen bonding.[69] Selected geometrical

(65) Gaussian 09, Revision D.01, Frisch, M. J. *et al.* Gaussian, Inc., Wallingford CT, **2013**.
(66) Tao, J.; Perdew, J. P.; Staroverov, V. N.; Scuseria, G. E. *Phys. Rev. Lett.* **2003**, *91*, 146401/146401-146401/146404.
(67) (a) Grimme, S.; Antony, J.; Ehrlich, S.; Krieg, H. *J. Chem. Phys.* **2010**, *132*, 154104/154101-154104/154119. (b) Grimme, S.; Ehrlich, S.; Goerigk, L. *J. Comput. Chem.* **2011**, *32*, 1456-1465.
(68) (a) Weigend, F.; Ahlrichs, R. *Phys. Chem. Chem. Phys.* **2005**, *7*, 3297-3305. (b) Weigend, F. *Phys. Chem. Chem. Phys.* **2006**, *8*, 1057-1065.
(69) Sure, R.; Grimme, S. *Chem. Commun.* **2016**, *52*, 9893-9896.

parameters and computed binding free energies are summarized in Table 1. To aid comparison, the supramolecular interaction between 4-methylpyridine (4MePy) and iodopentafluorobenzene (IPFB) was also computed and was found to be a slightly endergonic process with a calculated binding constant value being in agreement with that experimentally measured (*i.e.*; $K_{exp} = 1 \pm 1\ M^{-1}$ in toluene in ref. 24 and $K_{calc} = 0.03\ M^{-1}$ from the predicted $\Delta\Delta G$ value in entry 1 in Table 1).

The computed N···I distances were in agreement with the experimental values and their formations were calculated to be highly exergonic processes. Computational studies confirmed a slightly higher stability for [Rh(CO)(**1**)(**2**)]$^+$ than for [Rh(CO)(**1**)(**3**)]$^+$ (entries 2 and 3, Table 1). Electrostatic potential surfaces were calculated at the level of theory abovementioned (see Figure 7 for **2** and [Rh(CO)(**1**)(**2**)]$^+$ and section 1.5.6 in the experimental part for all information). The maximum values of the σ-hole in **2** (Figure 7) and fluorine-free derivative **3** (section 1.5.6 in the experimental part) are 25.1 and 12.5 kcal·mol^{-1}, respectively. A lower σ-hole value indicates a lower donor character of the halogen atom to the supramolecular bond. This observation derived from electrostatic potentials is in agreement with previously discussed X-ray data (*i.e.* a longer N···I bond for **5** than for **XBphos-Rh**).

Table 1. Selected geometrical parameters for halogen-bonded complexes (TPSS-D3/def2-TZVP, 25 °C, toluene) and computed binding free energies

Entry	Complex	$d_{N\cdots I}$ (Å)	N···I–C bond angle (°)	ΔΔG (kcal·mol^{-1})
1	4MePy·IPFB[a]	2.714	179.4	+2.03[b]
2[c]	[Rh(CO)(**1**)(**2**)]$^+$	2.709 (2.757(8))	175.2 (169.4(5))	−112.83[d]
3[c]	[Rh(CO)(**1**)(**3**)]$^+$	2.827 (2.84(1))	176.2 (171.2(7))	−111.97[d]

[a] 4MePy·IPFB = complex between 4-methylpyridine and iodopentafluorobenzene. [b] ΔΔG = ΔG4MePy·IPFB − ΔG4MePy − ΔGIPFB. [c] X-ray values in parentheses. [d] ΔΔG = ΔG[Rh(CO)(**1**)(**2** or **3**)]$^+$ + ΔGCO − ΔG[Rh(CO)$_2$]$^+$ − ΔG**1** − ΔG**2** or **3**.

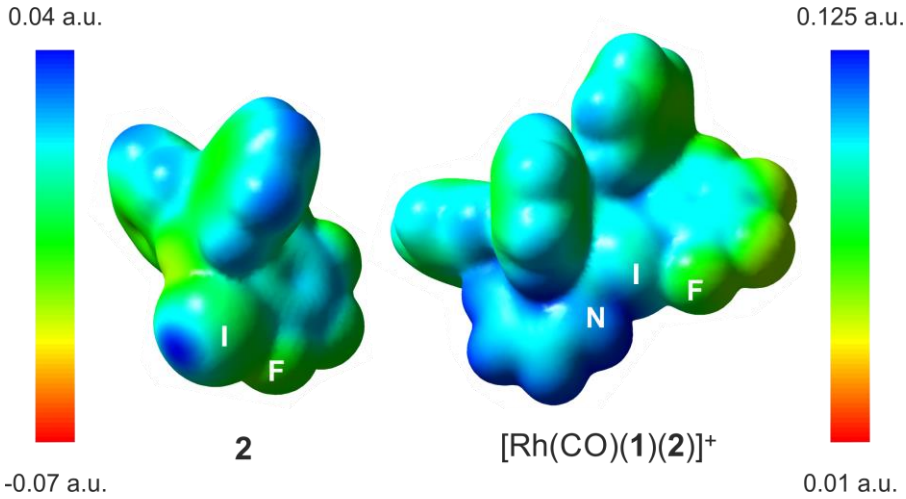

Figure 7. Electrostatic potential surfaces of ligand **2** and complex [Rh(CO)(**1**)(**2**)]$^+$ at an isovalue of 0.001 a.u.

The interesting structural features of **XBphos-Rh** and **5** (Table 2),[70] prompted us to investigate reactivity features as catalysts that could complement existing catalytic tools.

Table 2. Selected bond distances (Å) and angles (°)[a]

Entry	Complex	P1–P2	Rh–CO	P1–Rh–P2
1[b]	[Rh(CO)(xant)]BF_4	4.506(2)	1.798(5)	164.42(4)
2	**XBphos-Rh**	4.618(2)	1.872(8)	177.09(7)
3	**5**	4.632(9)	1.848(9)	178.6(3)

[a] X-ray values. [b] xant = Xantphos; see ref. 70a.

These complexes were tested in the hydroboration of terminal alkynes towards vinylboronic acid derivatives, as the outcome of these reactions is heavily influenced by the electronic and steric properties of the ligand.[71] Methods for synthesizing vinylboronic acid derivatives, which are important synthetic intermediates, by an atom-economical hydroboration reaction[72] are scarce in the literature.[71,73]

(70) Examples of ligands with a bite angle close to 180° are scarce in the literature. See, for instance: (a) Sandee, A. J.; Van der Veen, L. A.; Reek, J. N. H.; Kamer, P. C. J.; Lutz, M.; Spek, A. L.; Van Leeuwen, P. W. N. M. *Angew. Chem., Int. Ed.* **1999**, *38*, 3231-3235. (b) Kamer, P. C. J.; van Leeuwen, P. W. N. M.; Reek, J. N. H. *Acc. Chem. Res.* **2001**, *34*, 895-904.

(71) See, for example: (a) Ohmura, T.; Yamamoto, Y.; Miyaura, N. *J. Am. Chem. Soc.* **2000**, *122*, 4990-4991. (b) Cid, J.; Carbó, J. J.; Fernández, E. *Chem. - Eur. J.* **2012**, *18*, 1512-1521.

(72) These compounds can also be synthesized by hydroboration of alkynes with diboron derivatives. For selected examples, see the following references and those cited therein: (a) Jang, H.; Zhugralin, A. R.; Lee, Y.; Hoveyda, A. H. *J. Am. Chem. Soc.* **2011**, *133*, 7859-7871. (b) Ojha, D. P.; Prabhu, K. R. *Org. Lett.* **2016**, *18*, 432-435. (c) Trost, B. M.; Cregg, J. J.; Quach, N. *J. Am. Chem. Soc.* **2017**, *139*, 5133-5139.

(73) For selected examples, see the following references and those cited therein: (a) Gridnev, I. D.; Miyaura, N.; Suzuki, A. *Organometallics* **1993**, *12*, 589-592. (b) Pereira, S.; Srebnik, M. *Tetrahedron Lett.* **1996**, *37*, 3283-3286. (c) Khramov, D. M.; Rosen, E. L.; Er, J. A. V.; Vu, P. D.; Lynch, V. M.; Bielawski, C. W. *Tetrahedron* **2008**, *64*, 6853-6862. (d) Iwadate, N.; Suginome, M. *Org. Lett.* **2009**, *11*, 1899-1902.

To aid comparison of the results obtained with **XBphos-Rh** and **5**, we included the monodentate [Rh(CO)(PPh_3)$_3$]BArF (**6**) complex in our catalytic studies.[74] A summary of the results obtained is shown in Table 3. Both **XBphos-Rh** and **5** were active hydroboration catalysts, and *E*-isomers **8** were preferentially formed in all cases. Although **XBphos-Rh** is the most selective hydroboration catalyst for phenylacetylene **7a** (88% overall yield for HBpin and 51% for HBcat; entries 1 and 4 in Table 3), hydroboration selectivities for 1-octyne **7b** using **XBphos-Rh** are slightly lower than those with **6** (entries 7-12, Table 3). It is important to mention that in all cases selectivity towards branched derivatives is higher with the halogen-bonded catalysts than with the background catalyst **6**.[74] For example, a ten-fold increase in yield was obtained for the branched product **10a,pin** when **XBphos-Rh** was used (entries 1 and 3, Table 3). It is also noteworthy that, as far as we are aware, **XBphos-Rh** provides the highest reported yield for the branched derivative **10b,cat** (44% branched product with respect to all hydroboration products, entry 10, Table 3). Regarding electronic effects of the product distribution in the hydroboration of aryl-substituted acetylenes, higher ratios of the branched product were obtained for electron-deficient arene **7c** than for electron rich derivative **7d** (entries 13 and 14, Table 3).

(74) The bidentate rhodium complex [Rh(CO)(Xantphos)]BArF **11** was also considered a background catalyst in this transformation and incorporated to catalytic hydroboration studies of alkyne **7a** (see footnote *d* in Table 3). [Rh(CO)(Xantphos)]BArF displayed a lower performance than **XBphos-Rh** in terms of overall yield of hydroboration products of **7a** with HBpin.

Table 3. Rh(I)-Catalyzed Hydroboration of Terminal Alkynes[a]

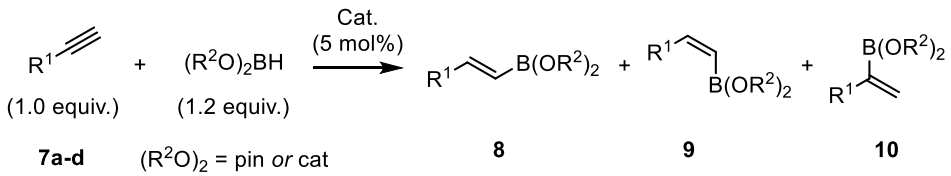

(R^1 = Ph for **7a**, $^nC_6H_{13}$ for **7b**, 4-CF_3-C_6H_4 for **7c** and 4-MeO-C_6H_4 for **7d**)

Entry	Alkyne, $(R^2O)_2BH$[b]	Cat.	8+9+10 Yield (%)	Ratio 8 : 9 : 10
1[c]	**7a**, HBpin	**XBphos-Rh**	88	78 : 2 : 20[d]
2	**7a**, HBpin	**5**	36	72 : 5 : 23
3	**7a**, HBpin	**6**	54	94 : 3 : 3
4	**7a**, HBcat	**XBphos-Rh**	51	82 : 2 : 16
5	**7a**, HBcat	**5**	49	82 : 2 : 16
6	**7a**, HBcat	**6**	50	86 : 9 : 5
7	**7b**, HBpin	**XBphos-Rh**	49	79 : 4 : 17
8	**7b**, HBpin	**5**	50	79 : 4 : 17
9	**7b**, HBpin	**6**	59	93 : 2 : 5
10	**7b**, HBcat	**XBphos-Rh**	50	52 : 4 : 44
11	**7b**, HBcat	**5**	51	66 : 4 : 30
12	**7b**, HBcat	**6**	58	86 : 4 : 10
13[c]	**7c**, HBpin	**XBphos-Rh**	58	71 : 2 : 27
14[c]	**7d**, HBpin	**XBphos-Rh**	74	83 : 3 : 14

[a] Reactions were performed in CD_2Cl_2 (0.5 M) under N_2 and reacted for 24 h at room temperature. Yields were determined by ^1H NMR using 1,2,4,5-tetramethylbenzene as the internal standard. See the experimental section for details. [b] $(R^2O)_2BH$: HBpin = pinacolborane, HBcat = catecholborane. [c] 2.0 equiv. of $(R^2O)_2BH$. [d] Results obtained with bidentate complex [Rh(CO)(Xantphos)]BArF **11** as catalyst in the reaction of **7a** and HBpin are as follows: 69% overall yield (ratio **8** : **9** : **10** = 97 : 2 : 1).

1.4. CONCLUSIONS

In summary, we have successfully prepared and fully characterized the first halogen-bonded supramolecular rhodium(I) complexes. To the best of our knowledge, these are the first examples where halogen bonding is the driving force for the assembly of the catalyst backbone. Furthermore, we have demonstrated that the presence of fluorine groups at the iodo-containing supramolecular motif is not necessary for efficient halogen bonding due to the favorable template effect exerted by the rhodium center. The two new catalysts are active in the hydroboration of terminal alkynes, with the catalytic activity of **XBphos-Rh** rivalling that of the highest performing catalysts. Moreover, this catalyst favors enhanced ratios of the branched alkenyl boronic acid products. Ongoing investigations in our group include mechanistic studies on the outcome of the reaction,[75] application of this system to other catalytically relevant transformations, extension of the application of this halogen bonding approach to other transition metals, and studies into alternative ligand designs.

(75) As a detailed mechanism on Rh-catalyzed hydroboration of terminal alkynes has still to be established (see: Trost, B. M.; Ball, Z. T. *Synthesis* **2005**, 853-887), elementary mechanistic steps involving **XBphos-Rh** cannot be unequivocally proposed.

1.5. EXPERIMENTAL SECTION

1.5.1 General considerations

All syntheses were carried out using chemicals as purchased from commercial sources unless otherwise stated. Air- and moisture-sensitive manipulations or reactions were performed under inert atmosphere, either in a glove box or with standard Schlenk techniques. Glassware was dried under vacuum before use with a hot air gun. All solvents were dried and deoxygenated by using a solvent purification system (SPS). Silica gel 60 (230-400 mesh) was used for column chromatography. NMR spectra were recorded in 400 MHz or 500 MHz spectrometers in $CDCl_3$ or CD_2Cl_2 unless otherwise cited. ^{1}H and $^{13}C\{^{1}H\}$ NMR chemical shifts are quoted in ppm relative to residual solvent peaks. $^{11}B\{^{1}H\}$ NMR chemical shifts are quoted in ppm relative to $BF_3{\cdot}Et_2O$ in $CDCl_3$. $^{19}F\{^{1}H\}$ NMR chemical shifts are quoted in ppm relative to $CFCl_3$ in $CDCl_3$. $^{31}P\{^{1}H\}$ NMR chemical shifts are quoted in ppm relative to 85% phosphoric acid in water. HRMS spectra were recorded using ESI ionization method in positive mode. GC-MS analyses were performed using EI as ionization method. GC analyses were performed with a flame ionization detector. IR spectra were recorded using Attenuated Total Reflection (ATR) technique unless otherwise cited.

1.5.2. General structural comments on X-ray crystals

Crystals suitable for X-ray measurements for complex **4** (**XBphos-Rh**) and complex **5** were obtained by solvent diffusion in the gas phase, using CH_2Cl_2 and *n*-pentane at 20 °C under inert atmosphere. The measured crystals were prepared under inert conditions immersed in perfluoropolyether as protecting oil for manipulation.

Crystal structure determination for compounds **4** and **5** were carried out using a diffractometer equipped with an area detector and MoKα radiation at −173 °C. Full-sphere data collection was used with ω and φ scans. Programs used: Data collection CrystalClear,[76] data reduction with CrysAlisPro[77] V/.60A and absorption correction with Scale3 Abspack

(76) Data collection with CrystalClear-SM Expert 2.1 b29 (Rigaku, 2013).
(77) Data reduction with CrysAlisPro 1.171.38.37f (Rigaku OD, 2015).

scaling algorithm.[78] Structure Solution and Refinement: Crystal structure solution was achieved using the computer program SHELXT.[79] Visualization was performed with the program SHELXle.[80] Missing atoms were subsequently located from difference Fourier synthesis and added to the atom list. Least-squares refinement on F^2 using all measured intensities was carried out using the program SHELXL 2015.[81] All non-hydrogen atoms were refined including anisotropic displacement parameters.

Comments to **4** (**XBphos-Rh**): The asymmetric unit contains one cationic rhodium metal complex molecule, one BArF anion and 1.17 molecules of dichloromethane. The cationic metal complex is partially disordered in two orientations (ratio 77:33) showing always the iodine and the CO-groups in a *trans*-arrangement in the square planar metal complex. The main part of the CF_3-groups in the BArF anion is showing rotational disorder. The dichloromethane molecules are involved in the disorder of the cationic metal complex and are showing occupations of 0.40 and 0.77.

Comments to **5**: The asymmetric unit contains one molecule of the metal complex, one BArF anion and a half pentane molecule. The complex is disordered in three orientations maintaining the rhodium atom always in the same position. The occupancy of this disorder is of 75:15:10. In the BArF anion most of the CF_3-groups are showing rotational disorder. The structure refines as a two-component crystal with a ratio of 84:16.

(78) Empirical absorption correction using spherical harmonics implemented in Scale3 Abspack scaling algorithm, CrysAlisPro 1.171.38.37f (Rigaku OD, 2015).
(79) SHELXT; Sheldrick, G. M. *Acta Cryst.* **2015**, *A71*, 3-8.
(80) SHELXle; Huebschle, C. B.; Sheldrick, G. M.; Dittrich, B. *J. Appl. Cryst.*, **2011**, *44*, 1281-1284.
(81) SHELXL; Sheldrick, G. M. *Acta Cryst.*, **2015**, *C71*, 3-8.

1.5.3. Syntheses of ligands 1, 2 and 3

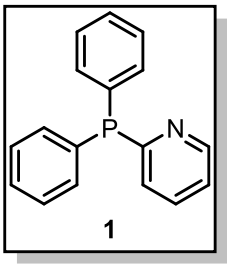

2-pyridyldiphenylphosphine (**1**): Ligand **1** was prepared according to a known procedure,[58a] with the following modifications: 1.2 g (52 mmol) of metal Na and 6 g (46 mmol) of naphthalene in 75 mL of dry tetrahydrofuran were sonicated in an ultrasound bath for 30 minutes. This solution was cannulated to an effectively stirred solution of 6 g of triphenylphosphine (23 mmol) in 75 mL of dry tetrahydrofuran under an argon atmosphere. This mixture was stirred for 12 h at 60 °C and then the temperature was decreased to room temperature. From this point, the described protocol was followed. Subsequently, 2.6 g of 2-chloropyridine (23 mmol) were added. The mixture obtained was worked up by distilling tetrahydrofuran off at reflux and atmospheric pressure, vacuum drying, addition of 50 mL of 3 M aqueous ammonium chloride solution and 50 mL of dichloromethane, phase separation, washing (3 x 50 mL H_2O), drying over $MgSO_4$, filtration of the combined organic phases, concentration under vacuum, and recrystallization from boiling hexanes. After cooling to ambient temperature, 5.0 g of white crystalline 2-pyridyldiphenylphosphine (82% yield) were collected by filtration. ^{1}H NMR, $^{13}C\{^{1}H\}$ NMR and $^{31}P\{^{1}H\}$ NMR data were in agreement with those previously reported.[82] ^{1}H NMR (400 MHz, $CDCl_3$) δ: 8.63 (dm, J = 4.8 Hz, 1 H), 7.45 (tt, J = 7.7, 2.4 Hz, 1 H), 7.35-7.20 (m, 10 H), 7.07 (ddm, J = 7.6, 4.8 Hz, 1 H), 6.99 (dm, J = 7.8 Hz, 1 H) ppm. $^{13}C\{^{1}H\}$ NMR (100 MHz, $CDCl_3$) δ: 164.1 (d, J_{C-P} = 4.2 Hz), 150.4 (d, J_{C-P} = 12.6 Hz), 136.3 (d, J_{C-P} = 10.7 Hz), 135.8 (d, J_{C-P} = 2.1 Hz), 134.3 (d, J_{C-P} = 19.8 Hz), 129.2, 128.7 (d, J_{C-P} = 7.1 Hz), 127.9 (d, J_{C-P} = 15.5 Hz), 122.3 ppm. $^{31}P\{^{1}H\}$ NMR (162 MHz, $CDCl_3$) δ: −0.8 ppm. ESI-MS: $[M+H]^+$, 264.2.

(82) Mehta, M.; García de la Arada, I.; Pérez, M.; Porwal, D.; Oestreich, M.; Stephan, D. W. *Organometallics* **2016**, *35*, 1030-1035.

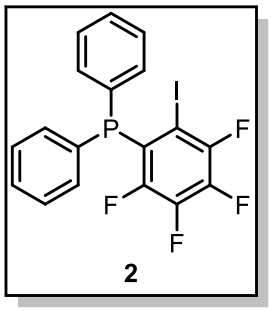

2

Ligand **2**: **2** was prepared adapting the procedure from Meek *et al.* for the preparation of 2-bromo-3,4,5,6-tetrafluorophenyldiphenylphosphine.[58b] A solution of 2.3 g (5.74 mmol) of 1,2-diiodotetrafluorobenzene in 20 mL of anhydrous tetrahydrofuran was cooled to −78 °C. 1.53 mL (3.83 mmol) of a 2.5 M solution of *n*-butyllithium in *n*-hexane were added dropwise to the cold and stirred solution of the iodo derivative. After stirring the reaction mixture for 30 minutes, 0.72 mL (3.83 mmol) of diphenylchlorophosphine were added slowly. The pale yellow solution was stirred for an additional 45 minutes and then removed from the low temperature bath and allowed to warm to room temperature. After stirring for 1 h at room temperature, the reaction mixture was quenched with 10 mL of deionized water. The aqueous phase was extracted with dichloromethane (3 x 25 mL) and then the organic phases were combined, dried over $MgSO_4$ and the volatiles were removed. The residue was purified by column chromatography (SiO_2, hexanes) to give the 2-iodo-3,4,5,6-tetrafluorophenyldiphenylphosphine **2** as a thick yellow oil (1.23 g, 70% yield) that after some time evolved to a colorless solid. ^{1}H NMR (400 MHz, $CDCl_3$) δ: 7.43-7.34 (m, 10 H) ppm. $^{13}C\{^{1}H\}$ NMR (126 MHz, $CDCl_3$) δ: 148.9 (ddm, J_{C-F} = 252.7 Hz; J_{C-P} = 9.8 Hz), 147.6 (dtd, J_{C-F} = 245.1 Hz; J_{C-P} = 10.3 Hz; J = 0.3 Hz), 141.0 (dm, J_{C-F} = 259.4 Hz), 134.3 (dd, J_{C-P} = 12.0 Hz; J = 3.5 Hz), 132.9 (dd, J_{C-P} = 20.9 Hz; J = 1.3 Hz), 131.7 (tm, J_{C-P} = 9.4 Hz), 129.4, 128.9 (d, J_{C-P} = 6.6 Hz), 125.5-125.2 (m), 90.0 (ddt, J_{C-F} = 52.0 Hz; J_{C-P} = 22.7 Hz; J = 3.9 Hz) ppm. $^{19}F\{^{1}H\}$ NMR (376 MHz, $CDCl_3$) δ: −110.2 - −110.4 (m, 1 F), −118.8 - −119.0 (m, 1 F), −148.9 - −149.0 (m, 1 F); −151.9 - −152.1 (m, 1 F) ppm. $^{31}P\{^{1}H\}$ NMR (162 MHz, $CDCl_3$) δ: 20.1 (ddd, J_{P-F} = 24.3, 10.5, 3.9 Hz) ppm. IR (neat): 3066, 3011, 2923, 1612, 1597, 1582, 1487, 1429, 1363, 1330, 1297, 1275, 1261, 1244, 1183, 1158, 1100, 1024, 835, 778, 744, 709, 692, 641, 606, 493 cm^{-1}. HRMS ESI-MS (m/z): $[M+H]^+$ calcd. for $C_{18}H_{11}F_4IP^+$ 460.9574, found 460.9578. Melting point: 67 °C.

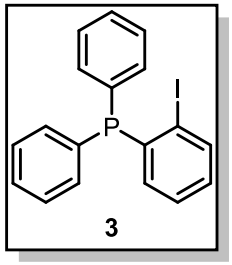

3

2-iodophenyldiphenylphosphine (**3**): A solution of diphenylphosphine (0.96 g, 5.05 mmol) in 20 mL of anhydrous tetrahydrofuran was cooled to −78 °C. 2 mL (5.05 mmol) of a 2.5 M solution of *n*-butyllithium in *n*-hexane were syringed into the cold and stirred solution of the iodo derivative using a syringe pump. The color of the solution turned intense orange. After stirring the reaction mixture for 30 minutes, 2.5 g (7.58 mmol) of 1,2-diiodobenzene dissolved in 10 mL of anhydrous tetrahydrofuran were added slowly for 30 minutes. The resulting brownish solution was stirred for an additional 45 minutes at −78 °C and then warmed up to room temperature. After 60 minutes at room temperature, 10 mL of water were added to quench the mixture. The organic phase was extracted with CH_2Cl_2 (3 x 25 mL), and then the organic fraction was evaporated. The crude mixture was purified by column chromatography using SiO_2 and cyclohexane as the eluent, to afford the 2-iodophenyldiphenylphosphine as a white solid (0.23 g, 12% yield). ^{1}H NMR, $^{13}C\{^{1}H\}$ NMR and $^{31}P\{^{1}H\}$ NMR data were in agreement with those previously reported.[83] ^{1}H NMR (400 MHz, $CDCl_3$) δ: 7.80 (ddd, J = 7.8, 3.1, 1.7 Hz, 1 H), 7.30-7.10 (m, 11 H), 6.90 (td, J = 7.6, 3.4 Hz, 1 H), 6.70 (dt, J = 7.6, 2.0 Hz, 1 H) ppm. $^{13}C\{^{1}H\}$ NMR (100 MHz, $CDCl_3$) δ: 142.4 (d, J_{C-P} = 9.4 Hz), 139.9 (d, J_{C-P} = 3.7 Hz), 136.4 (d, J_{C-P} = 11.0 Hz), 134.5, 134.1 (d, J_{C-P} = 20.4 Hz), 130.2, 129.1, 128.8 (d, J_{C-P} = 7.2 Hz), 128.4, 107.2 (d, J_{C-P} = 40.0 Hz) ppm. $^{31}P\{^{1}H\}$ NMR (162 MHz, $CDCl_3$) δ: 11.2 ppm. EI-MS: [M], 387.0.

(83) Bayardon, J.; Laureano, H.; Diemer, V.; Dutartre, M.; Das, U.; Rousselin, Y.; Henry, J.-C.; Colobert, F.; Leroux, F. R.; Jugé, S. *J. Org. Chem.* **2012**, *77*, 5759-5769.

1.5.4. Syntheses of complexes 4, 5, 6 and 11

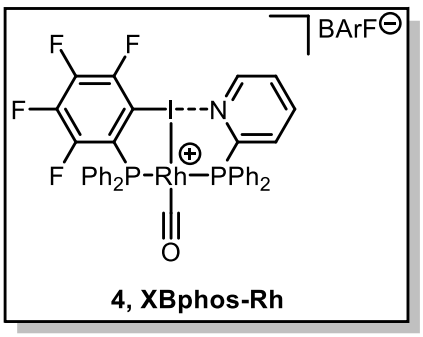

4, XBphos-Rh

XBphos-Rh, (**4**): In a glove box filled with N_2, 58.0 mg (0.15 mmol) of $[Rh(Cl)(CO)_2]_2$ were weighted in an amberized glass vial provided with a magnetic stirrer and were dissolved with 1 mL of CH_2Cl_2. Then, 274.0 mg of NaBArF (0.30 mmol) were added to the rhodium solution together with 1 mL of dichloromethane. The mixture was stirred for 1 hour at room temperature. In parallel, a solution of 2-$PyPPh_2$, **1** (78.6 mg, 0.30 mmol) and 2-iodo-3,4,5,6-tetrafluorophenyl-diphenylphosphine, **2** (137.0 mg, 0.30 mmol) in 2 mL of dichloromethane was prepared in a vial provided with a magnetic stirrer. The mixture was stirred at room temperature for 1 hour. The ligands' solution was added dropwise to the rhodium solution, observing some bubbling. This mixture was stirred for 1 hour at room temperature and then filtered with a nylon filter to remove the NaCl precipitate. The resulting red solution was partially evaporated (to *ca.* 1 mL volume), and then mixed with 5 mL of *n*-pentane, with which a precipitate was formed. This precipitate was washed with cold diethyl ether (3 x 1 mL) and *n*-pentane (3 x 2 mL) and dried under vacuum to afford 380.3 mg of **4**, **XBphos-Rh** as a pale yellow solid in 74% yield. ^{1}H NMR (500 MHz, CD_2Cl_2) δ: 8.88 (dm, J = 5.0 Hz, 1 H), 7.91 (tm, J = 7.8 Hz, 1 H), 7.75-7.40 (m, 33 H), 7.34 (ddm, J = 7.8, 3.0 Hz, 1 H) ppm. $^{13}C\{^1H\}$ NMR (126 MHz, CD_2Cl_2) δ:[84] 185.1 (br s, C_{CO}), 162.2 (q, J_{C-B} = 49.8 Hz, C_{BArF}), 152.0 (dd, J_{C-P} = 67.0 Hz, J_{C-Rh} = 4.2 Hz, C_{Py}), 150.9 (ddm, J_{C-F} = 258.1 Hz, J = 11.4 Hz, C_I), 149.5 (d, J_{C-P} = 19.1 Hz, C_{Py}), 147.7 (dm, J_{C-F} = 250.5 Hz, C_I), 143.2 (dm, J_{C-F} = 267.5 Hz, C_I), 142.5 (dm, J_{C-F} = 263.7 Hz, C_I), 139.0 (d, J_{C-P} = 4.8 Hz, C_{Py}), 135.2 (C_{BArF}), 134.0 (d, J_{C-P} = 12.6 Hz, C_{Ph}), 133.0

(84) A heavily overlapped $^{13}C\{^1H\}$ NMR spectrum was observed due to multiple couplings of the carbons with other NMR active heteronuclei present in the molecule. Whenever possible the carbons where assigned with the help of other NMR experiments as follows: C_{CO} (carbonyl carbon), C_{BArF} (BArF carbons), C_{Ph} (phenyl ring carbons), C_{Py} (pyridyl ring carbons), C_I (iodine-containing ring carbons). These abbreviations also apply for complexes **5**, **6** and **11**.

(dd, J_{C-P} = 27.1 Hz, J_{C-Rh} = 2.2 Hz, C_{Ph}), 132.9 (d, J_{C-P} = 13.7 Hz, C_{Ph}), 130.1 (dd, J_{C-P} = 11.3 Hz, J_{C-Rh} = 1.7 Hz, C_{Ph}), 129.5 (C_{Py}), 127.3 (d, J_{C-P} = 1.5 Hz, C_{Py}), 129.3 (qm, J_{C-F} = 31.5 Hz, C_{BArF}), 125.0 (q, J_{C-F} = 272.4 Hz, C_{BArF}), 117.9-117.8 (m, C_{BArF}) ppm. $^{11}B\{^1H\}$ NMR (CD_2Cl_2, 160 MHz) δ: –6.8 ppm. $^{19}F\{^1H\}$ NMR (471 MHz, CD_2Cl_2) δ: –62.9 (s, 24 F), –116.9 - –117.0 (m, 1F), –117.8 - –117.9 (m, 1F), –142.7 - –142.8 (m, 1F); –147.6 - –147.8 (m, 1F) ppm. $^{31}P\{^1H\}$ NMR (202 MHz, CD_2Cl_2) δ: 79.4 (ddd, J_{P-P} = 276.0 Hz, J_{P-Rh} = 110.9 Hz, J_{P-F} = 14.2 Hz), 50.4 (dd, J_{P-P} = 275.6 Hz, J_{P-Rh} = 115.9 Hz) ppm. IR (neat): 2039 (CO), 1613, 1576, 1500, 1440, 1353, 1308, 1274, 1155, 1120, 1029, 999, 926, 886, 839, 767, 743, 713, 692, 681, 669, 547, 534, 510, 495, 467 cm^{-1}. HRMS ESI-MS (m/z): $[M–BArF]^+$ calcd. for $C_{36}H_{24}F_4INOP_2Rh^+$ 853.9363, found 853.9348.

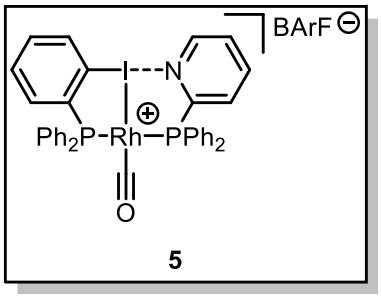

5

Complex **5**: Complex **5** was prepared identically to **XBphos-Rh**, but using 2-iodophenyldiphenylphosphine (**3**) as a ligand instead of **2**. Complex **5** was obtained as a yellow solid in 57% yield (113.1 mg, 0.07 mmol). ^1H NMR (400 MHz, CD_2Cl_2) δ: 8.77 (d, J = 4.6 Hz, 1 H), 7.95 (d, J = 7.7 Hz, 1 H), 7.81 (tm, J = 7.8 Hz, 1 H), 7.73 (br s, 8 H), 7.65-7.40 (27 H), 7.29 (qd, J = 7.5, 1.4 Hz, 2 H) ppm. $^{13}C\{^1H\}$ NMR (126 MHz, CD_2Cl_2) δ:[84] 186.1 (br s, C_{CO}), 162.2 (q, J_{C-B} = 49.8 Hz, C_{BArF}), 153.7 (dd, J_{C-P} = 68.2 Hz, J_{C-Rh} = 3.5 Hz, C_{Py}), 149.9 (d, J_{C-P} = 19.4 Hz, C_{Py}), 138.3 (d, J_{C-P} = 5.1 Hz, C_{Py}), 136.6 (s, C_I), 135.5 (d, J_{C-P} = 13.9 Hz, C_I), 135.2 (s, C_{BArF}), 134.6 (s, C_I), 134.2 (d, J_{C-P} = 13.5 Hz, C_{Ph}), 133.5 (d, J_{C-P} = 12.6 Hz, C_{Ph}), 132.5 (t, J_{C-P} = 2.5 Hz, C_{Ph}), 130.8 (s, C_I), 130.4 (d, J_{C-P} = 10.8 Hz, C_I), 129.9 (dd, J_{C-P} = 10.8 Hz, J_{C-Rh} = 6.9 Hz, C_{Ph}), 129.3 (qm, J_{C-F} = 31.2 Hz, C_{BArF}), 126.6 (d, J_{C-P} = 1.2 Hz, C_{Py}), 125.0 (q, J_{C-F} = 272.4 Hz, C_{BArF}), 117.9-117.8 (m, C_{BArF}), 110.3 (dd, J_{C-P} = 34.9 Hz, J_{C-Rh} = 4.0 Hz, C_I) ppm. $^{11}B\{^1H\}$ NMR (CD_2Cl_2, 128 MHz) δ: –6.7 ppm. $^{19}F\{^1H\}$ NMR (376 MHz, CD_2Cl_2) δ: –62.9 (s, 24F) ppm. $^{31}P\{^1H\}$ NMR (162 MHz, CD_2Cl_2) δ: 72.2 (dd, J_{P-P} = 270.7 Hz, J_{P-Rh} = 108.4 Hz), 45.5 (dd, J_{P-P} = 270.7 Hz, J_{P-Rh} = 118.7 Hz) ppm. IR (neat): 2029 (CO), 1352, 1274, 1118, 886, 838, 743, 713, 681, 544,

514 cm^{-1}. HRMS ESI-MS (m/z): $[M–BArF]^+$ calcd. for $C_{36}H_{28}INOP_2Rh^+$ 781.9740, found 781.9703.

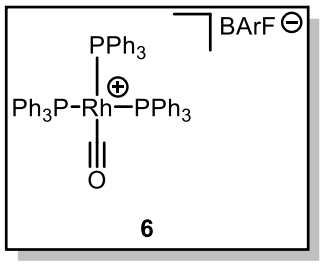

6

Tris(triphenylphosphine)rhodium carbonyl tetrakis[3,5-bis(trifluoromethyl)phenyl] borate, $[Rh(CO)(PPh_3)_3]BArF$ (**6**): Compound **6** was synthesized by slightly modifying the synthesis reported by Hope *et al.*[85] A 25 mL Schlenk tube was filled with 54.8 mg of tris(triphenylphosphine)rhodium carbonyl hydride $[Rh(H)(CO)(PPh_3)_3]$ (0.06 mmol) and 5 mL of dichloromethane. Then, a solution of 60.3 mg of $HBArF{\cdot}2Et_2O$[86] (0.06 mmol) in 1 mL of dichloromethane was added slowly to the previous solution, observing some bubbling. The reaction mixture was stirred at room temperature for 2 h before the volatile materials were removed under vacuum. The residue was washed with *n*-pentane (3 x 2 mL) and dried under vacuum to afford 67.2 mg of **6** (0.04 mmol) as a yellow solid in 63% yield. $^{31}P\{^1H\}$ NMR data were in agreement with those reported by Hope.[85] ^1H NMR (500 MHz, CD_2Cl_2) δ: 7.74 (br s, 8 H), 7.56 (br s, 4 H), 7.50-7.35 (m, 17 H), 7.33-7.20 (m, 13 H), 7.10-6.90 (m, 15 H) ppm. $^{13}C\{^1H\}$ NMR (126 MHz, CD_2Cl_2) δ:[84] 187.8-186.3 (m, C_{CO}), 162.2 (q, $J_{C–B}$ = 49.8 Hz, C_{BArF}), 135.2 (s, C_{BArF}), 134.7 (d, $J_{C–P}$ = 12.2 Hz, C_{Ph}), 134.3 (t, $J_{C–P}$ = 6.2 Hz, C_{Ph}), 131.6 (s, C_{Ph}), 131.3 (d, $J_{C–P}$ = 2.0 Hz, C_{Ph}), 129.3 (qm, $J_{C–F}$ = 31.2 Hz, C_{BArF}), 129.2 (t, $J_{C–P}$ = 5.1 Hz, C_{Ph}), 128.7 (d, $J_{C–P}$ = 10.2 Hz, C_{Ph}), 125.0 (q, $J_{C–F}$ = 272.4 Hz, C_{BArF}), 117.9-117.8 (m, C_{BArF}) ppm. $^{11}B\{^1H\}$ NMR (CD_2Cl_2, 128 MHz) δ: –6.6 ppm. $^{19}F\{^1H\}$ NMR (376 MHz, CD_2Cl_2) δ: –62.9 (s, 24 F) ppm. $^{31}P\{^1H\}$ NMR (162 MHz, CD_2Cl_2) δ: 31.0-28.0 (m) ppm. IR (neat): 3064, 2036 (CO), 1611, 1481, 1437, 1353, 1274, 1119, 1000, 885, 838, 742, 692, 681, 668, 542, 509 cm^{-1}. HRMS ESI-MS (m/z): $[M–BArF]^+$ calcd. for $C_{55}H_{45}OP_3Rh^+$ 917.1733, found 917.1709.

(85) Clark, H. C. S.; Coleman, K. S.; Fawcett, J.; Holloway, J. H.; Hope, E. G.; Langer, J.; Smith, I. M. *J. Fluorine Chem.* **1998**, *91*, 207-211.
(86) Brookhart, M.; Grant, B.; Volpe, A. F., Jr. *Organometallics* **1992**, *11*, 3920-3922.

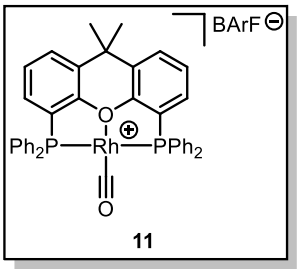

11

[Rh(CO)(Xantphos)]BArF (**11**): Compound **11** was prepared identically to complexes **4** and **5**, but using 1.0 equiv. of 9,9-dimethyl-4,5-bis(diphenylphosphino)xanthene as the ligand. Complex **11** was obtained as a yellow solid in 69% yield (293.0 mg, 0.19 mmol). $^{31}P\{^{1}H\}$ NMR Data were in agreement with the related [Rh(CO)(Xantphos)]BF_4 derivative reported by van Leeuwen *et al.*[87] ^{1}H NMR (400 MHz, CD_2Cl_2) δ: 7.80 (dd, J = 7.6, 1.6 Hz, 2 H), 7.76-7.44 (m, 36 H), 1.75 (s, 6 H) ppm. $^{13}C\{^{1}H\}$ NMR (126 MHz, CD_2Cl_2) δ:[84] 188.5 (br s, C_{CO}), 162.2 (q, J_{C-B} = 49.8 Hz, C_{BArF}), 154.7 (t, J_{C-P} = 9.2 Hz, C_{Ph}), 135.2 (s, C_{BArF}), 134.7 (s, C_{Ph}), 133.8 (t, J_{C-P} = 7.4 Hz, C_{Ph}), 133.3 (s, C_{Ph}), 132.8 (s, C_{Ph}), 132.3 (t, J_{C-P} = 3.4 Hz, C_{Ph}), 130.1 (t, J_{C-P} = 5.6 Hz, C_{Ph}), 129.3 (qm, J_{C-F} = 31.3 Hz, C_{BArF}), 129.2 (t, J_{C-P} = 27.7 Hz, C_{Ph}), 128.2 (t, J_{C-P} = 3.7 Hz, C_{Ph}), 125.0 (q, J_{C-F} = 272.3 Hz, C_{BArF}), 119.5 (t, J_{C-P} = 18.5 Hz, C_{Ph}), 117.9-117.8 (m, C_{BArF}), 34.8, 33.9 ppm. $^{11}B\{^{1}H\}$ NMR (CD_2Cl_2, 128 MHz) δ: −6.6 ppm. $^{19}F\{^{1}H\}$ NMR (376 MHz, CD_2Cl_2) δ: −62.6 (s, 24 F) ppm. $^{31}P\{^{1}H\}$ NMR (162 MHz, CD_2Cl_2) δ: 39.9 (d, J_{P-Rh} = 122.4 Hz) ppm. IR (neat): 2012 (CO), 1611, 1438, 1401, 1353, 1273, 1116, 886, 839, 738, 712, 681, 600, 559, 517, 469 cm^{-1}. HRMS ESI-MS (m/z): $[M-BArF]^+$ calcd. for $C_{40}H_{32}O_2P_2Rh^+$ 709.0927, found 709.0943.

(87) Sandee, A. J.; Reek, J. N. H.; Kamer, P. C. J.; van Leeuwen, P. W. N. M. *J. Am. Chem. Soc.* **2001**, *123*, 8468-8476.

1.5.5. General procedure for the Rh-mediated hydroboration of alkynes

1.5.5.1. Optimization of the reaction conditions

Table 4. Hydroboration of phenylacetylene with pinacolborane[a]

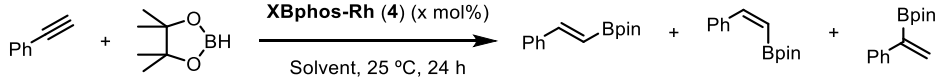

7a (1.0 equiv.) HBpin **8a,pin** **9a,pin** **10a,pin**

Entry	HBpin (equiv.)	4 (mol%)	Solvent	8+9+10 Yield (%)	Ratio 8 : 9 : 10
1	1.2	1	THF-d8	21.1	77:10:13
2	1.2	1	C_6D_6	14.3	77:13:10
3	1.2	1	CD_2Cl_2	29.2	61:10:29
4	1.2	5	CD_2Cl_2	68.1	78:4:18
5	2.0	5	CD_2Cl_2	87.6	78:2:20
6[b]	2.0	5	CD_2Cl_2	64.3	83:2:15

[a] Reactions were performed in deuterated solvent (0.5 M) in a N_2-filled glove box. Yields were determined by ^1H NMR using 1,2,4,5-tetramethylbenzene as the internal standard. HBpin = pinacolborane. [b] Experiment performed at 40 °C.

1.5.5.2. General procedure for Rh-catalyzed hydroborations

In a N_2-filled glove box, the catalyst (**4**, **5**, **6** or **11**; 5 mol%), a known amount (from 0.1 to 0.5 equiv., 5 to 20 mg) of the internal standard (1,2,4,5-tetramethylbenzene), along with 600 μL of CD_2Cl_2 were added to a 10 mL screw-capped tube provided with a stirrer . Then, 0.3 mmol of the alkyne were added followed by 0.4 mmol of borane. The mixture was stirred at 25 °C for 24 h and then analyzed by quantitative NMR and GC-FID analyses (Scheme 15).

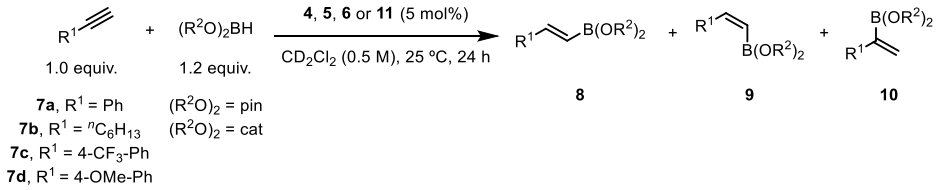

Scheme 15. General procedure for the hydroboration of alkynes; pin: pinacol, cat: catechol.

1.5.5.3. NMR and GC-FID analyses for the Rh-catalyzed hydroboration reactions

The yield towards hydroboration products was calculated using ^{1}H qNMR, employing 1,2,4,5-tetramethylbenzene as internal standard (Sigma-Aldrich TraceCERT®). The major hydroboration isomers (*E* and branched) were identified in the ^{1}H NMR spectra of the reaction mixture by comparison with data from previous reports in the literature and additionally by isolating them from the reaction mixture by flash chromatography (see section 1.5.5.4.). The minor *Z* isomer was directly identified in the ^{1}H NMR spectra of the reaction mixture by comparison with data from previous reports in the literature.[88] Finally, the catecholborane derivatives were not isolated and directly identified in the

(88) *Z* isomers were formed in low amounts, which made isolation not possible. See ref. 71 for the ^{1}H NMR spectroscopic data.

NMR spectra of the reaction mixture by comparison with data from previous reports in the literature.[89]

The reactions were also analyzed by GC-FID analysis (5% phenyl methyl siloxane; 30 m x 320 μm x 0.25 μm). Carrier gas: He; pressure: 7.5 psi; split ratio: 50:1; injector temperature: 280 °C; detector temperature: 250 °C; flow rate: 1.5 mL/min; temperature program: 50 °C, 20 °C/min to 325 °C (5 min).[90]

(89) Catecholborane is sensitive to air and decomposes in the presence of transition metal complexes, phosphines, and other nucleophiles. It also applies to catecholborane derivatives. See: Burgess, K.; Van der Donk, W. A.; Westcott, S. A.; Marder, T. B.; Baker, R. T.; Calabrese, J. C. *J. Am. Chem. Soc.* **1992**, *114*, 9350-9359. For this reason, catechol vinyl boronates could not be isolated and were identified in the NMR spectra of the reaction mixture by comparison with data from previous reports in the literature. See: (a) Brown, H. C.; Gupta, S. K. *J. Am. Chem. Soc.* **1975**, *97*, 5249-5255. (b) Khalimon, A. Y.; Farha, P. M.; Nikonov, G. I. *Dalton Trans.* **2015**, *44*, 18945-18956.

(90) The reactions employing catecholborane were not analyzed by GC-FID.

1.5.5.3.1 Hydroboration of 7a with HBpin using complex 4 as catalyst

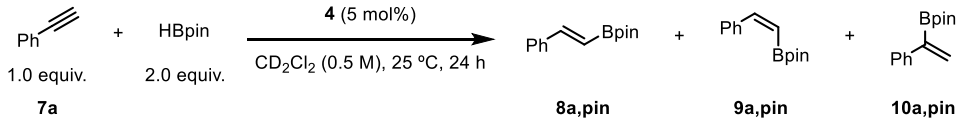

Scheme 16. Hydroboration of **7a** with pinacolborane (HBpin, 2.0 equiv.) using complex **4** as catalyst.

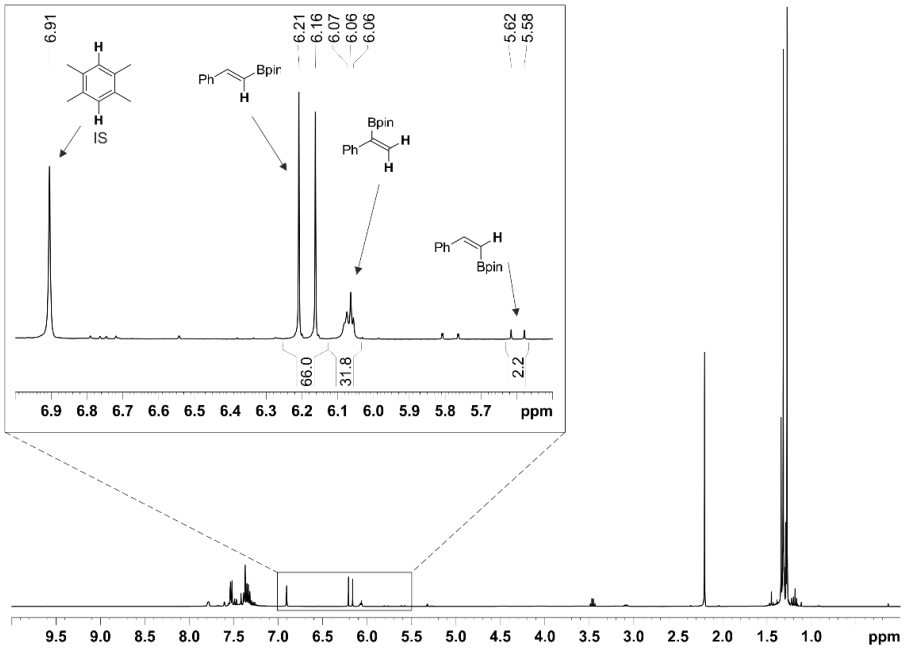

Figure 8. Reaction mixture ^{1}H NMR (400 MHz, CD_2Cl_2) of the hydroboration of **7a** and HBpin using complex **4** as catalyst.

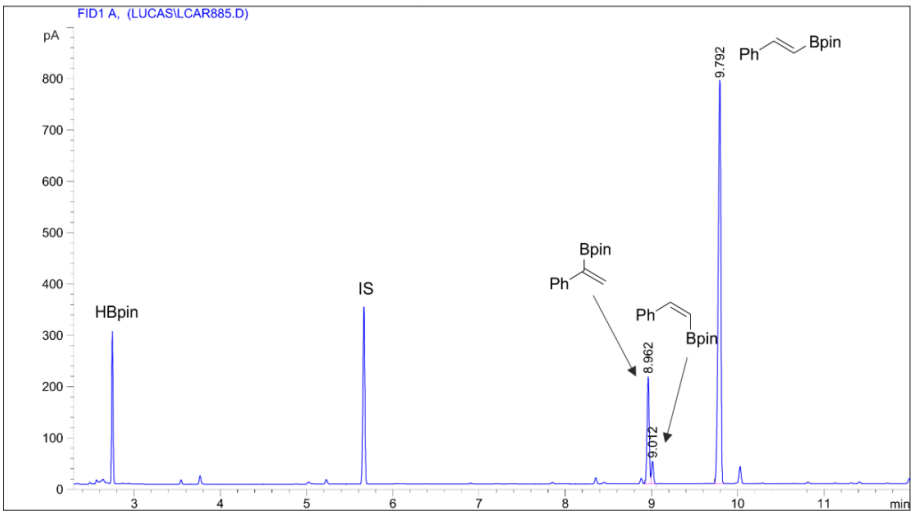

Figure 9. Reaction mixture GC-FID of the hydroboration of **7a** and HBpin using complex **4** as catalyst. Peak 1 (rt = 8.962): Area%: 16.9. Peak 2 (rt = 9.012): Area%: 3.3. Peak 3 (rt = 9.792): Area%: 79.8.

1.5.5.3.2 Hydroboration of 7c with HBpin using complex 4 as catalyst

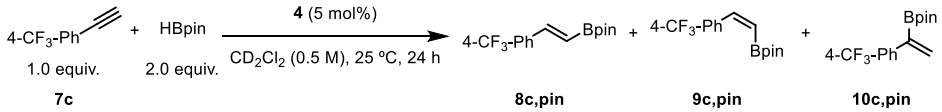

Scheme 17. Hydroboration of **7c** with pinacolborane (HBpin, 2.0 equiv.) using complex **4** as catalyst.

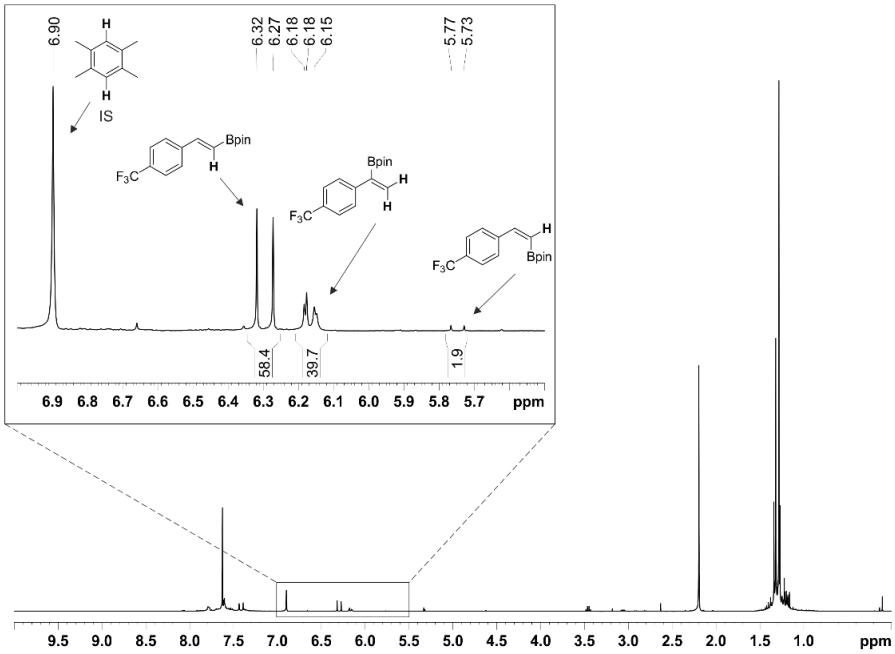

Figure 10. Reaction mixture ^{1}H NMR (400 MHz, CD_2Cl_2) of the hydroboration of **7c** and HBpin using complex **4** as catalyst.

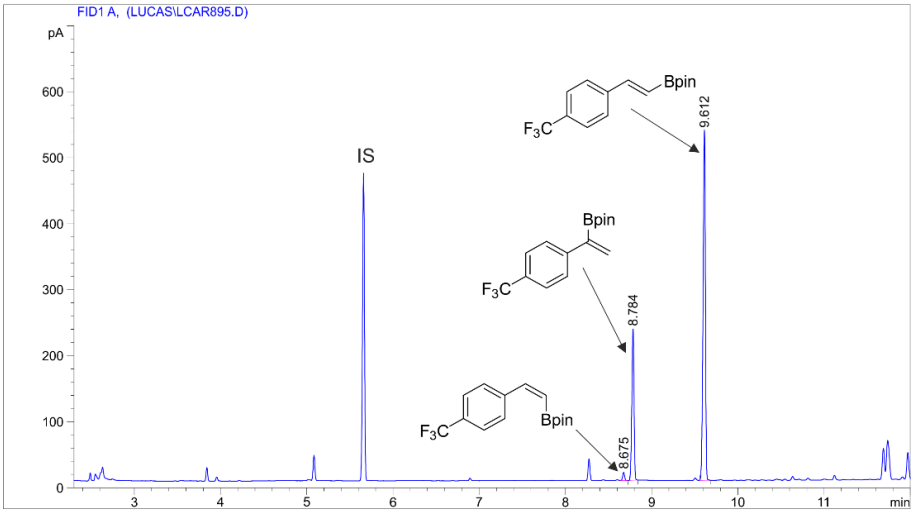

Figure 11. Reaction mixture GC-FID of the hydroboration of **7c** and HBpin using complex **4** as catalyst. Peak 1 (rt = 8.675): Area%: 1.4. Peak 2 (rt = 8.784): Area%: 28.3. Peak 3 (rt = 9.612): Area%: 70.3.

1.5.5.3.3 Hydroboration of 7d with HBpin using complex 4 as catalyst

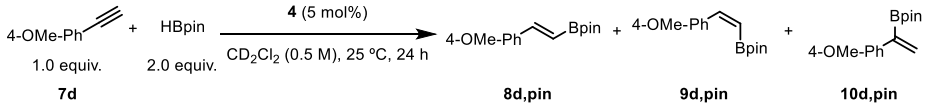

Scheme 18. Hydroboration of **7d** with pinacolborane (HBpin, 2.0 equiv.) using complex **4** as catalyst.

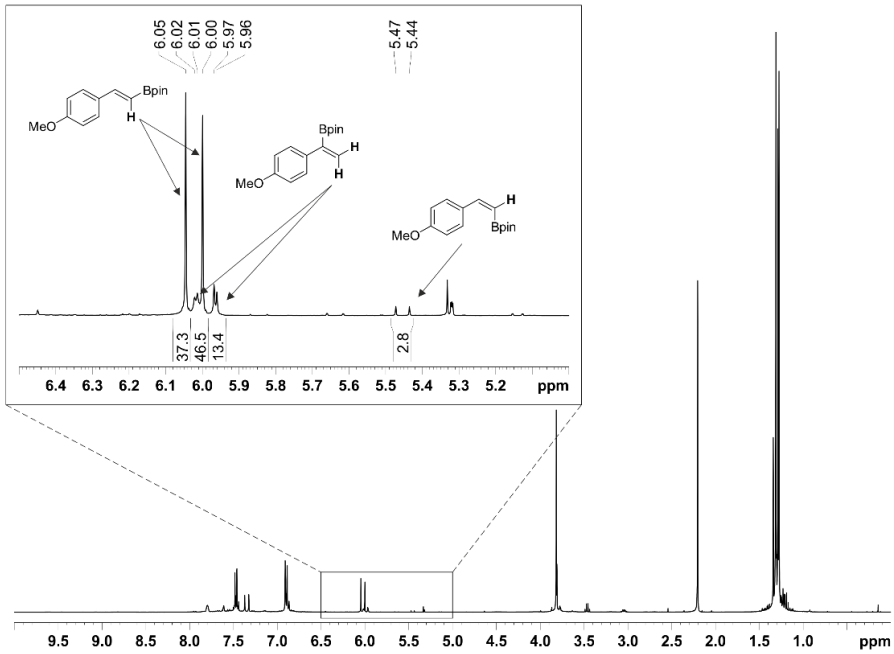

Figure 12. Reaction mixture ^{1}H NMR (400 MHz, CD_2Cl_2) of the hydroboration of **7d** and HBpin using complex **4** as catalyst.

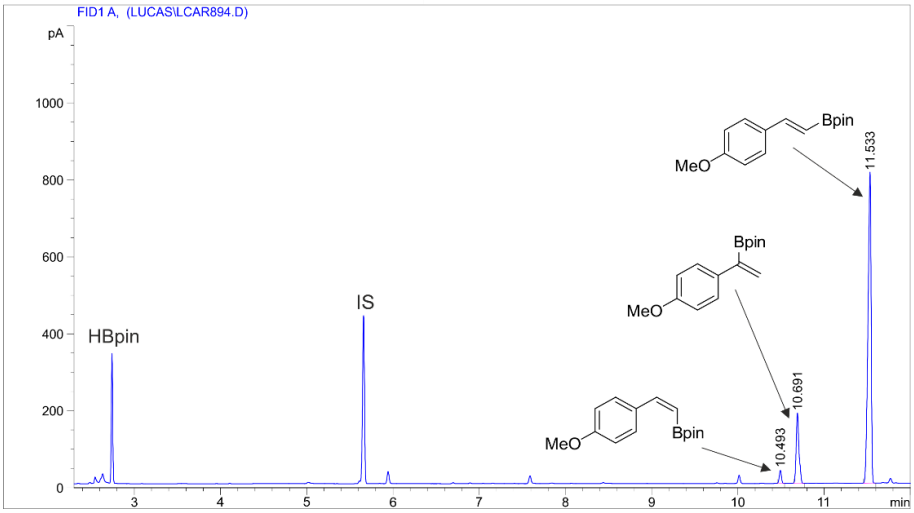

Figure 13. Reaction mixture GC-FID of the hydroboration of **7d** and HBpin using complex **4** as catalyst. Peak 1 (rt = 10.493): Area%: 2.3. Peak 2 (rt = 10.691): Area%: 16.5. Peak 3 (rt = 11.533): Area%: 81.2.

1.5.5.3.4 Hydroboration of 7a with HBpin using complex 4 as catalyst

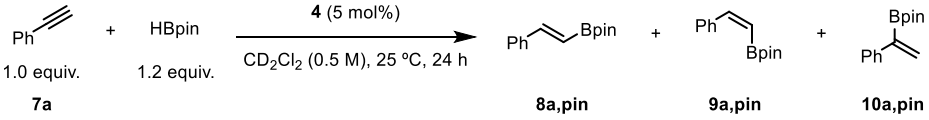

Scheme 19. Hydroboration of **7a** with pinacolborane (HBpin, 1.2 equiv.) using complex **4** as catalyst.

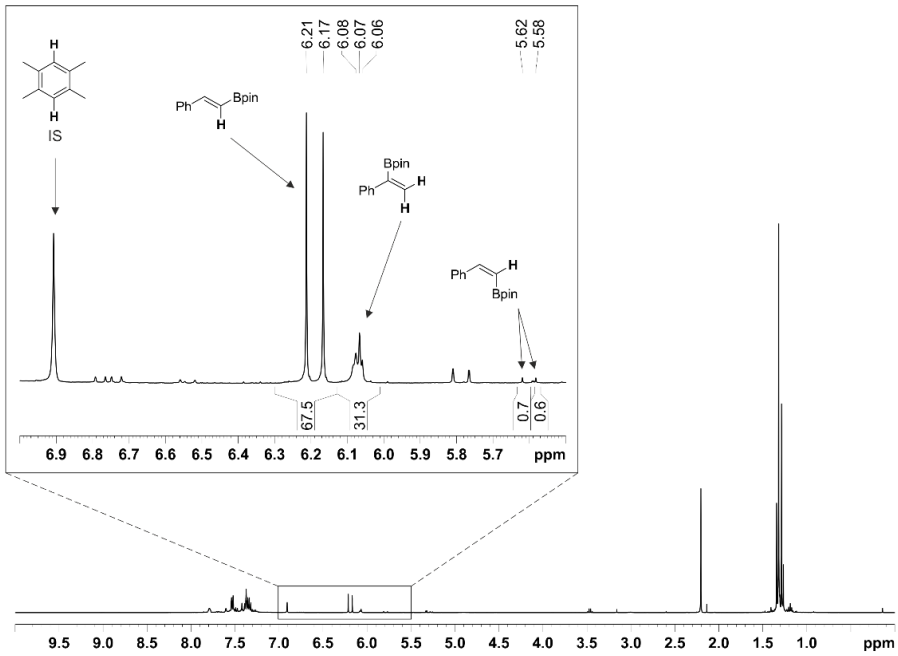

Figure 14. Reaction mixture ^{1}H NMR (400 MHz, CD_2Cl_2) of the hydroboration of **7a** and HBpin using complex **4** as catalyst.

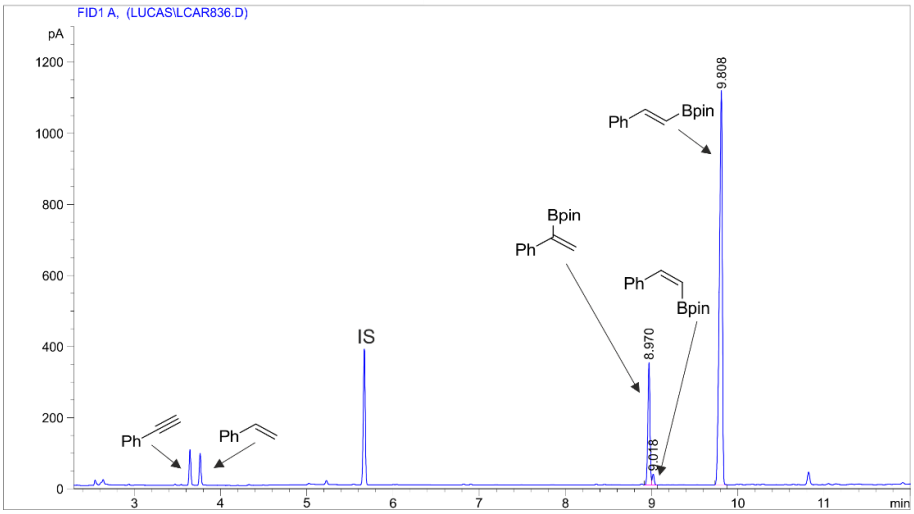

Figure 15. Reaction mixture GC-FID of the hydroboration of **7a** and HBpin using complex **4** as catalyst. Peak 1 (rt = 8.970): Area%: 18.1. Peak 2 (rt = 9.018): Area%: 1.4. Peak 3 (rt = 9.808): Area%: 80.5.

1.5.5.3.5 Hydroboration of 7a with HBpin using complex 5 as catalyst

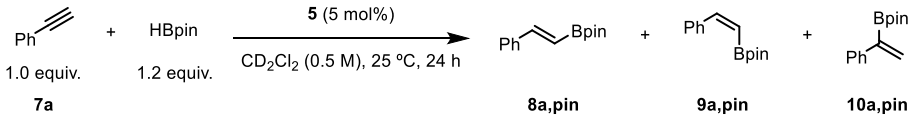

Scheme 20. Hydroboration of **7a** with pinacolborane (HBpin. 1.2 equiv.) using complex **5** as catalyst.

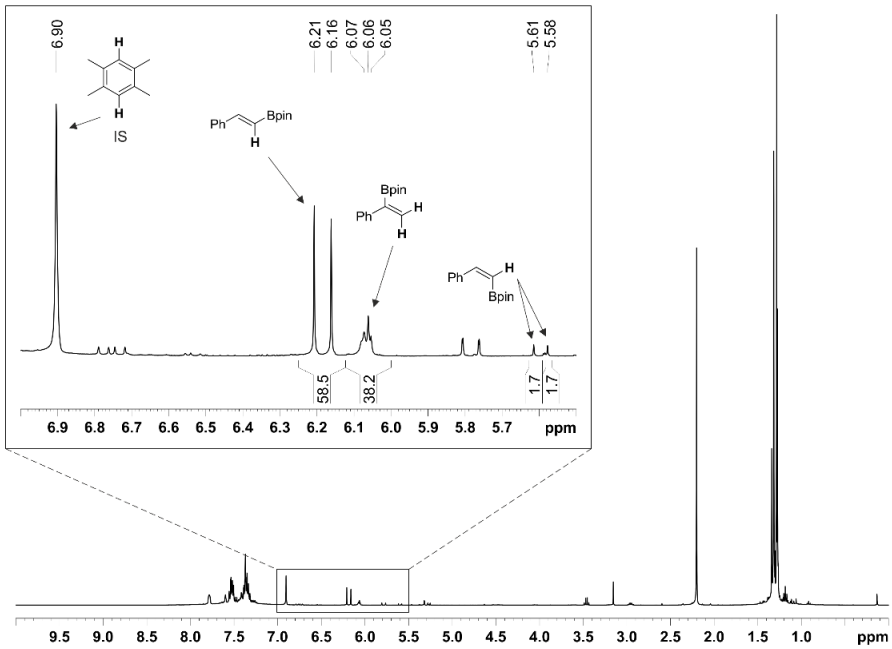

Figure 16. Reaction mixture ^{1}H NMR (400 MHz, CD_2Cl_2) of the hydroboration of **7a** and HBpin using complex **5** as catalyst.

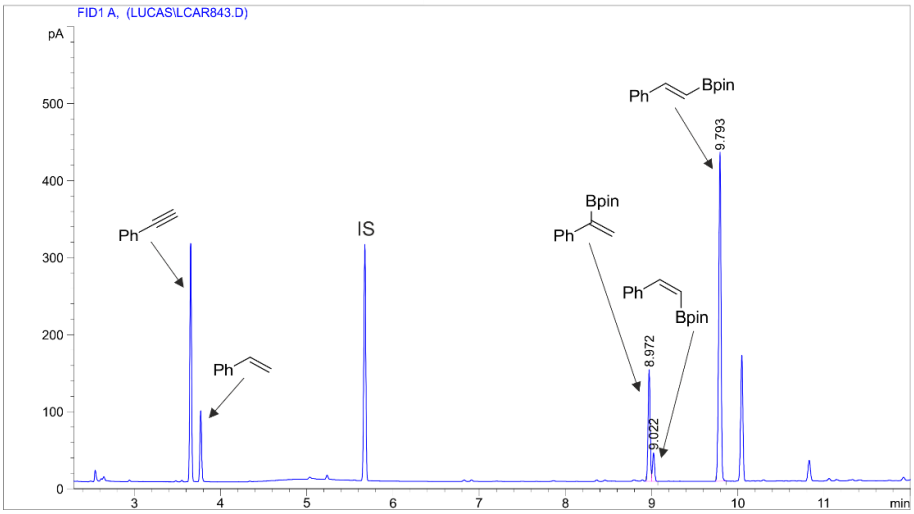

Figure 17. Reaction mixture GC-FID of the hydroboration of **7a** and HBpin using complex **5** as catalyst. Peak 1 (rt = 8.972): Area%: 21.7. Peak 2 (rt = 9.022): Area%: 5.5. Peak 3 (rt = 9.793): Area%: 72.8.

1.5.5.3.6 Hydroboration of 7a with HBpin using complex 6 as catalyst

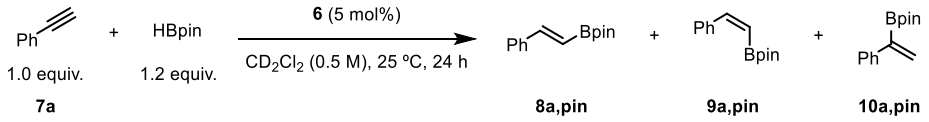

Scheme 21. Hydroboration of **7a** with pinacolborane (HBpin, 1.2 equiv.) using complex **6** as catalyst.

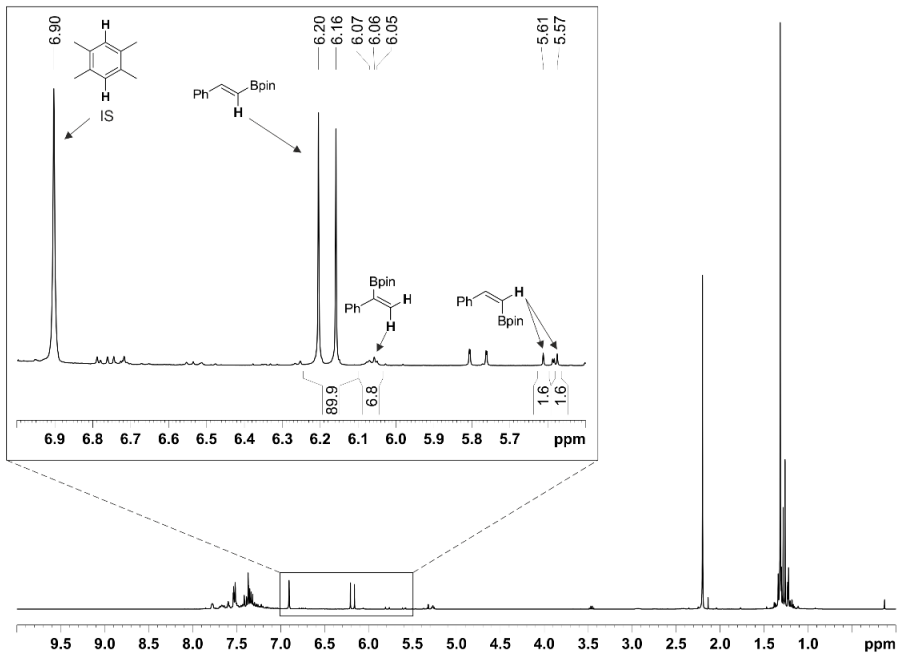

Figure 18. Reaction mixture ^{1}H NMR (400 MHz, CD_2Cl_2) of the hydroboration of **7a** and HBpin using complex **6** as catalyst.

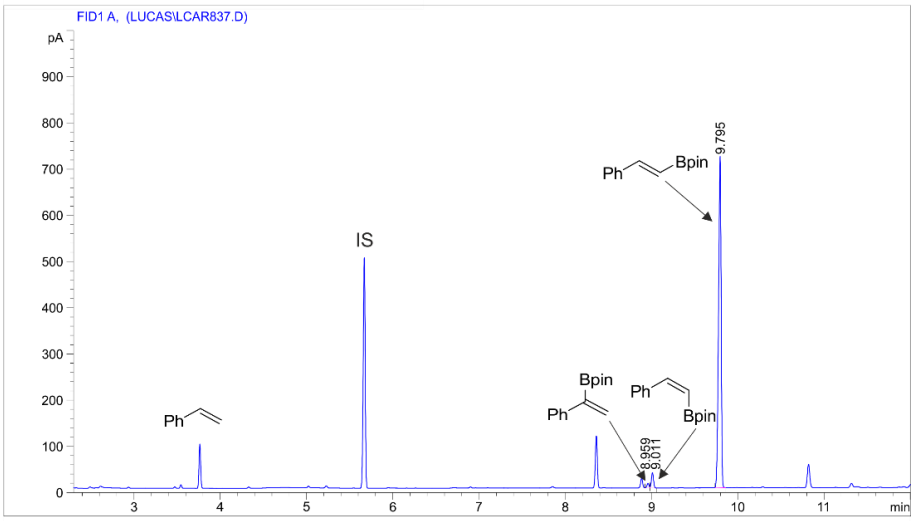

Figure 19. Reaction mixture GC-FID of the hydroboration of **7a** and HBpin using complex **6** as catalyst. Peak 1 (rt = 8.959): Area%: 1.1. Peak 2 (rt = 9.011): Area%: 3.5. Peak 3 (rt = 9.795): Area%: 95.4.

1.5.5.3.7 Hydroboration of 7b with HBpin using complex 4 as catalyst

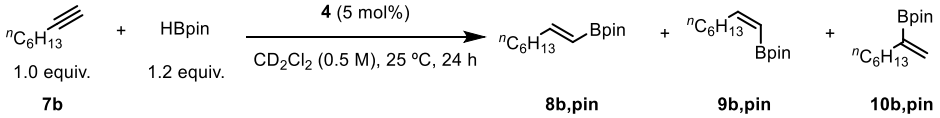

Scheme 22. Hydroboration of **7b** with pinacolborane (HBpin, 1.2 equiv.) using complex **4** as catalyst.

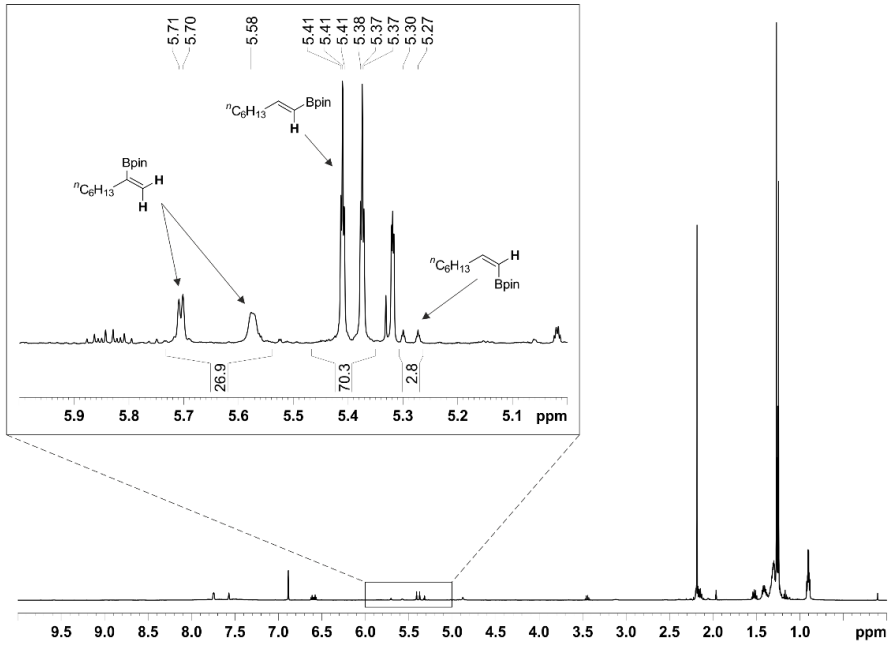

Figure 20. Reaction mixture ^{1}H NMR (400 MHz, CD_2Cl_2) of the hydroboration of **7b** and HBpin using complex **4** as catalyst.

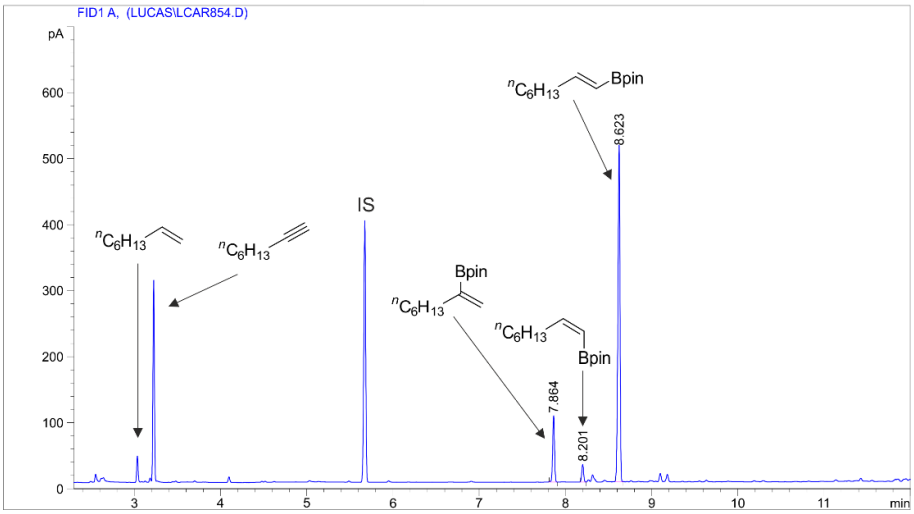

Figure 21. Reaction mixture GC-FID of the hydroboration of **7b** and HBpin using complex **4** as catalyst. Peak 1 (rt = 7.864): Area%: 14.4. Peak 2 (rt = 8.201): Area%: 3.8. Peak 3 (rt = 8.623): Area%: 81.8.

1.5.5.3.8 Hydroboration of 7b with HBpin using complex 5 as catalyst

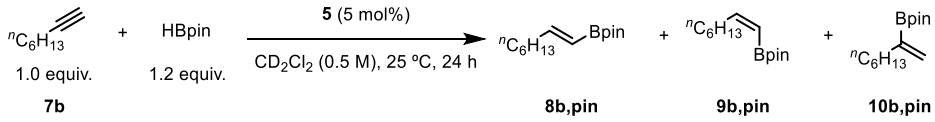

Scheme 23. Hydroboration of **7b** with pinacolborane (HBpin, 1.2 equiv.) using complex **5** as catalyst.

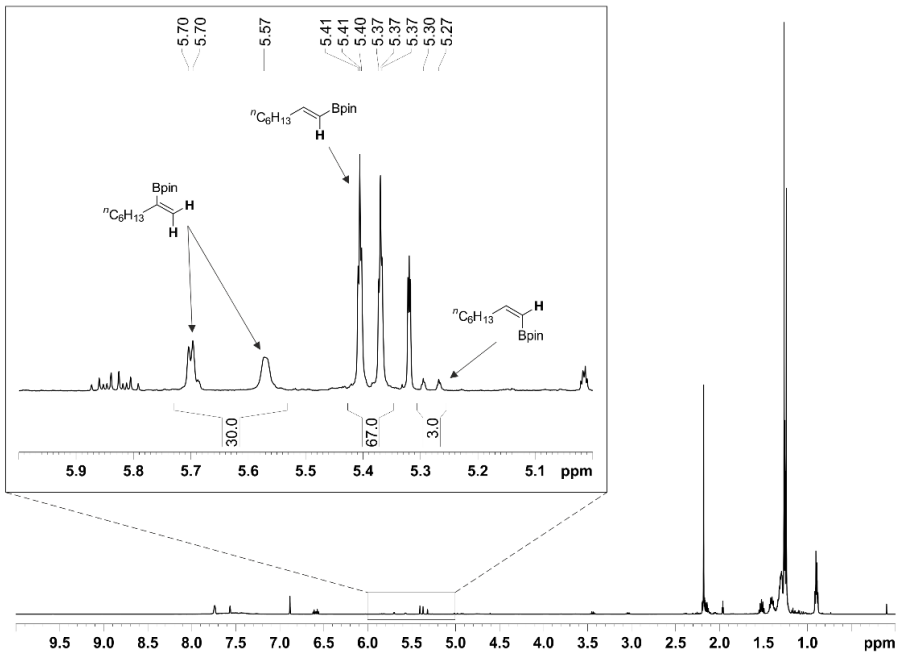

Figure 22. Reaction mixture ^{1}H NMR (400 MHz, CD_2Cl_2) of the hydroboration of **7b** and HBpin using complex **5** as catalyst.

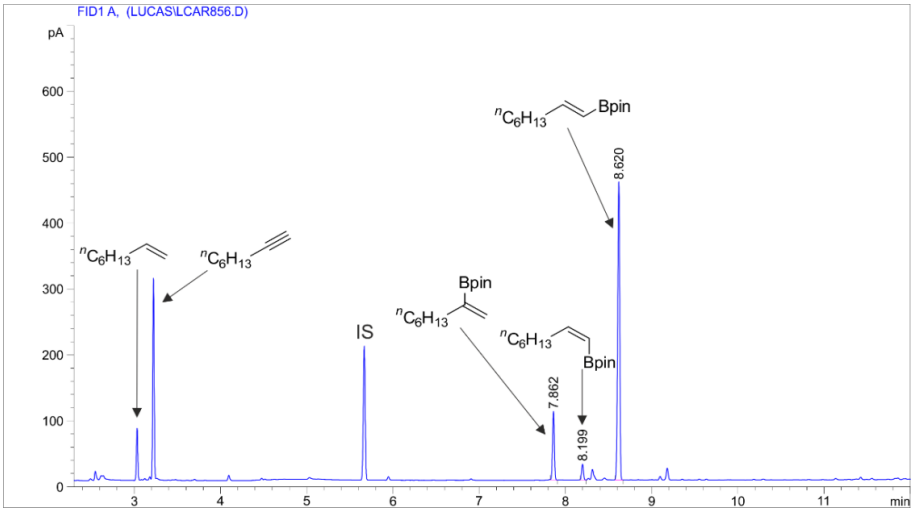

Figure 23. Reaction mixture GC-FID of the hydroboration of **7b** and HBpin using complex **5** as catalyst. Peak 1 (rt = 7.862): Area%: 16.2. Peak 2 (rt = 8.199): Area%: 3.8. Peak 3 (rt = 8.620): Area%: 80.0.

1.5.5.3.9 Hydroboration of 7b with HBpin using complex 6 as catalyst

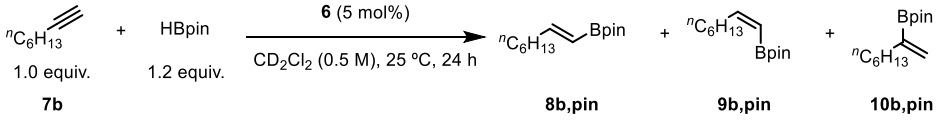

Scheme 24. Hydroboration of **7b** with pinacolborane (HBpin, 1.2 equiv.) using complex **6** as catalyst.

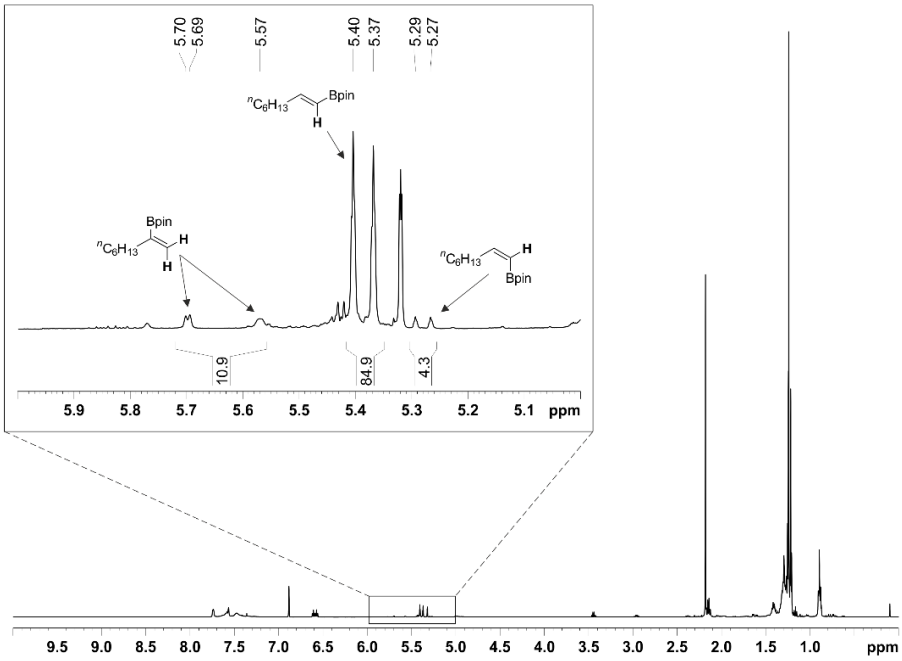

Figure 24. Reaction mixture ^{1}H NMR (400 MHz, CD_2Cl_2) of the hydroboration of **7b** and HBpin using complex **6** as catalyst.

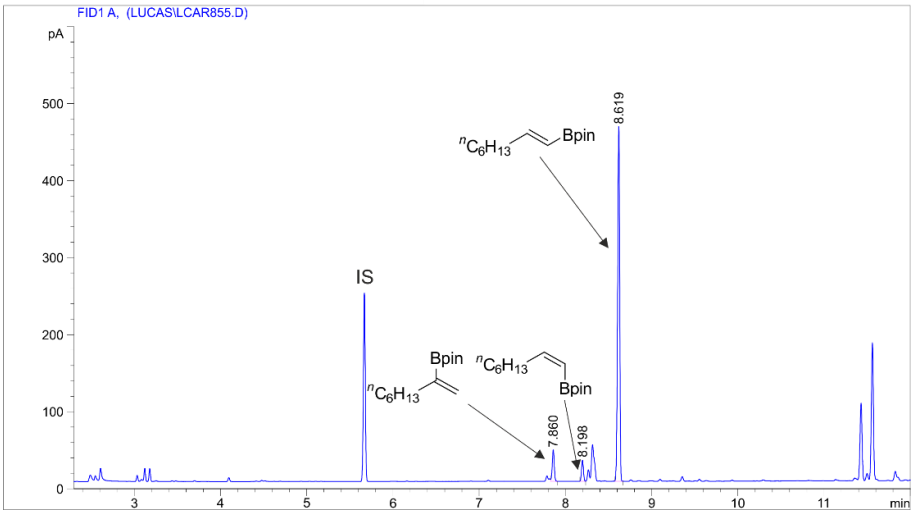

Figure 25. Reaction mixture GC-FID of the hydroboration of **7b** and HBpin using complex **6** as catalyst. Peak 1 (rt = 7.860): Area%: 7.5. Peak 2 (rt = 8.198): Area%: 4.7. Peak 3 (rt = 8.619): Area%: 87.8.

1.5.5.3.10 Hydroboration of 7a with HBcat using complex 4 as catalyst

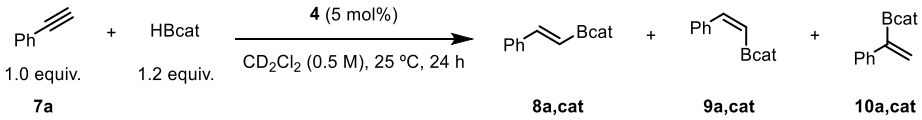

Scheme 25. Hydroboration of **7a** with catecholborane (HBcat, 1.2 equiv.) using complex **4** as catalyst.

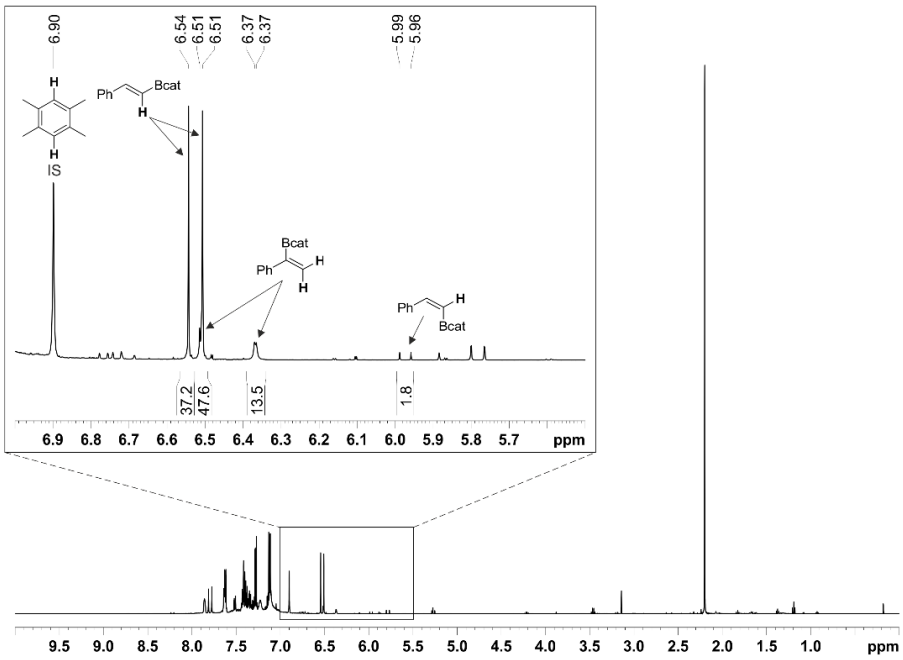

Figure 26. Reaction mixture ^{1}H NMR (400 MHz, CD_2Cl_2) of the hydroboration of **7a** and HBcat using complex **4** as catalyst.

1.5.5.3.11 Hydroboration of 7a with HBcat using complex 5 as catalyst

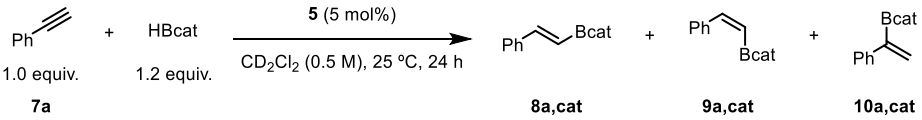

Scheme 26. Hydroboration of **7a** with catecholborane (HBcat, 1.2 equiv.) using complex **5** as catalyst.

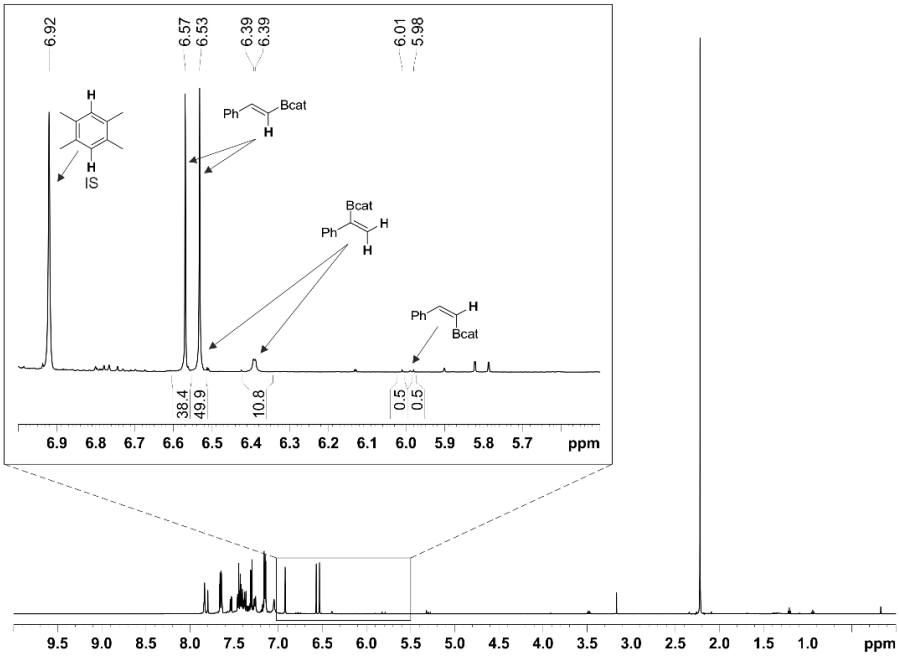

Figure 27. Reaction mixture ^{1}H NMR (400 MHz, CD_2Cl_2) of the hydroboration of **7a** and HBcat using complex **5** as catalyst.

1.5.5.3.12 Hydroboration of 7a with HBcat using complex 6 as catalyst

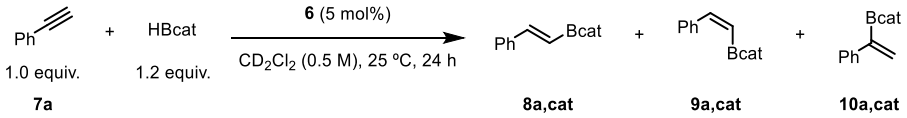

Scheme 27. Hydroboration of **7a** with catecholborane (HBcat, 1.2 equiv.) using complex **6** as catalyst.

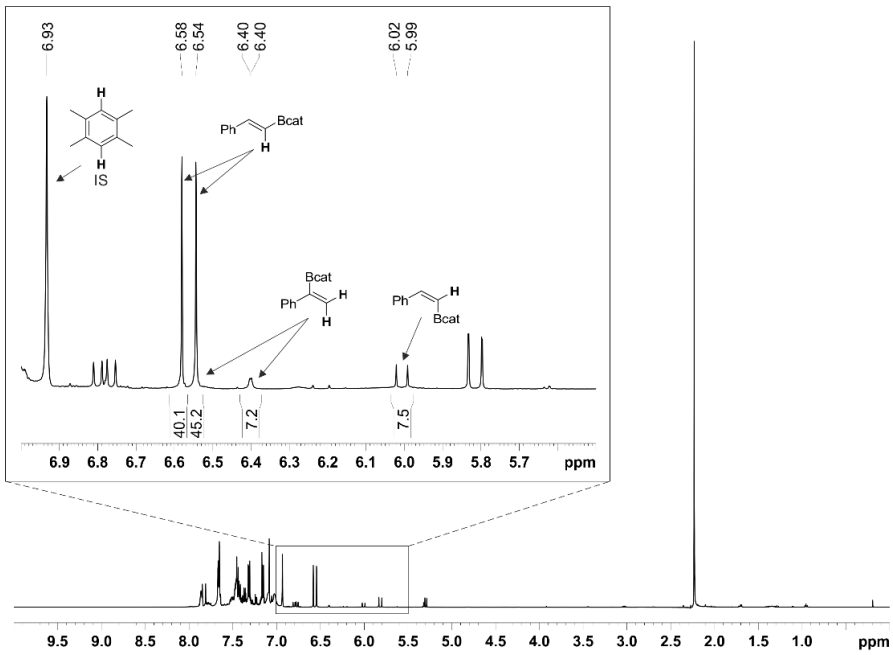

Figure 28. Reaction mixture ^{1}H NMR (400 MHz, CD_2Cl_2) of the hydroboration of **7a** and HBcat using complex **6** as catalyst.

1.5.5.3.13 Hydroboration of 7b with HBcat using complex 4 as catalyst

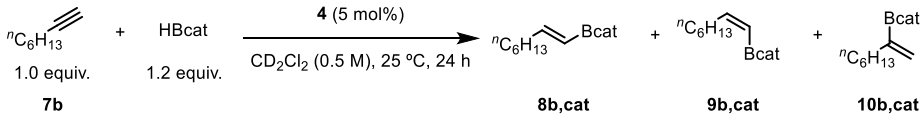

Scheme 28. Hydroboration of **7b** with catecholborane (HBcat, 1.2 equiv.) using complex **4** as catalyst.

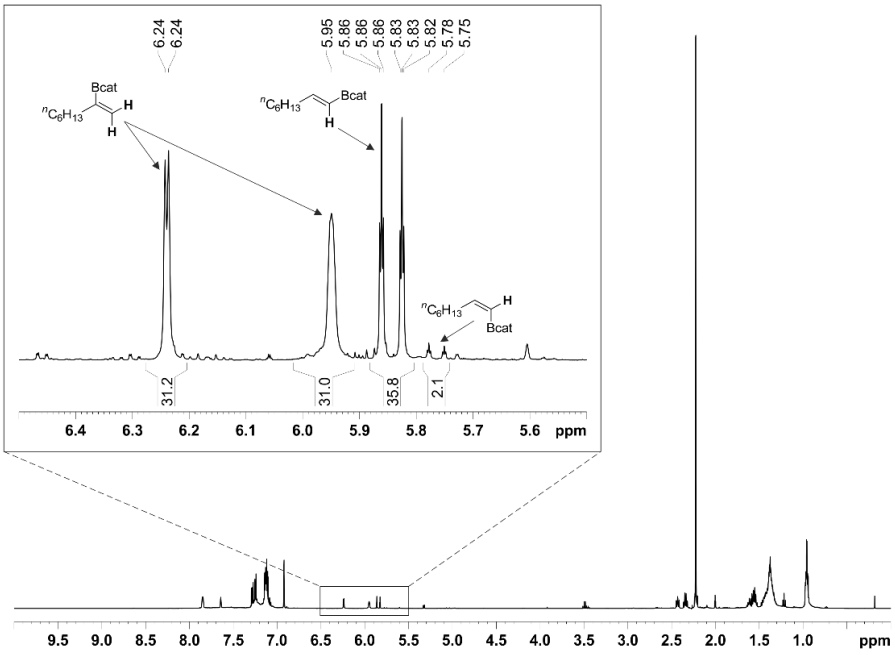

Figure 29. Reaction mixture ^{1}H NMR (400 MHz, CD_2Cl_2) of the hydroboration of **7b** and HBcat using complex **4** as catalyst.

1.5.5.3.14 Hydroboration of 7b with HBcat using complex 5 as catalyst

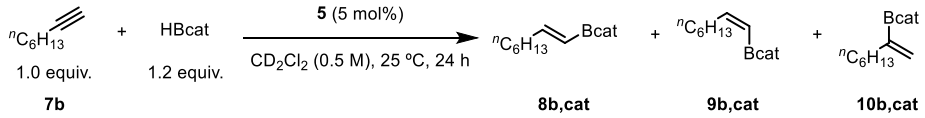

Scheme 29. Hydroboration of **7b** with catecholborane (HBcat, 1.2 equiv.) using complex **5** as catalyst.

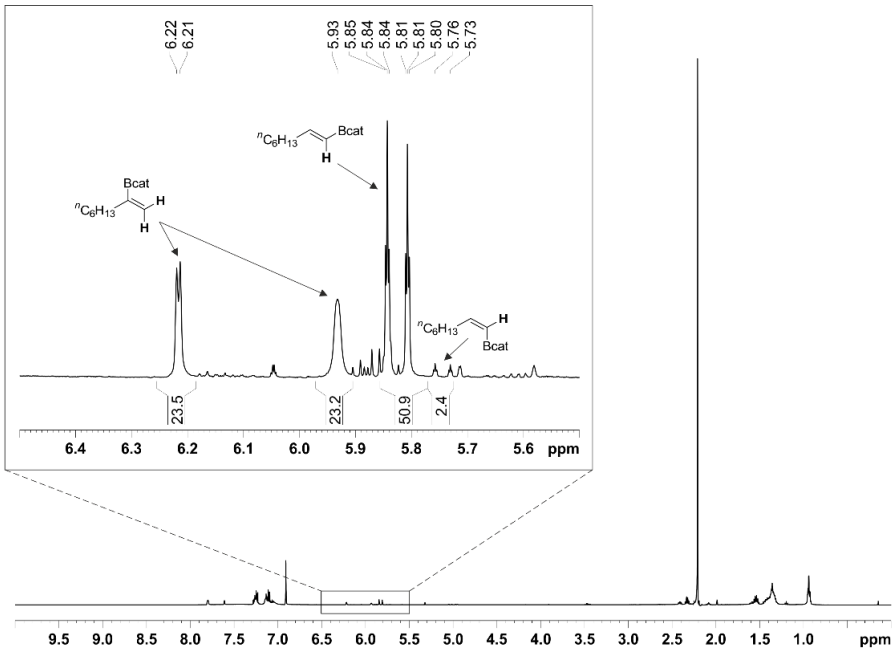

Figure 30. Reaction mixture ^{1}H NMR (400 MHz, CD_2Cl_2) of the hydroboration of **7b** and HBcat using complex **5** as catalyst.

1.5.5.3.15 Hydroboration of 7b with HBcat using complex 6 as catalyst

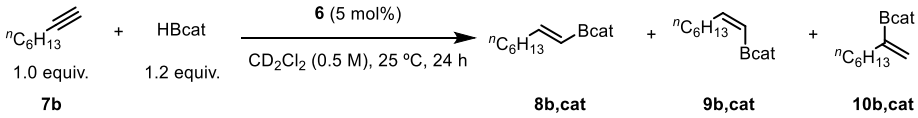

Scheme 30. Hydroboration of **7b** with catecholborane (HBcat, 1.2 equiv.) using complex **6** catalyst.

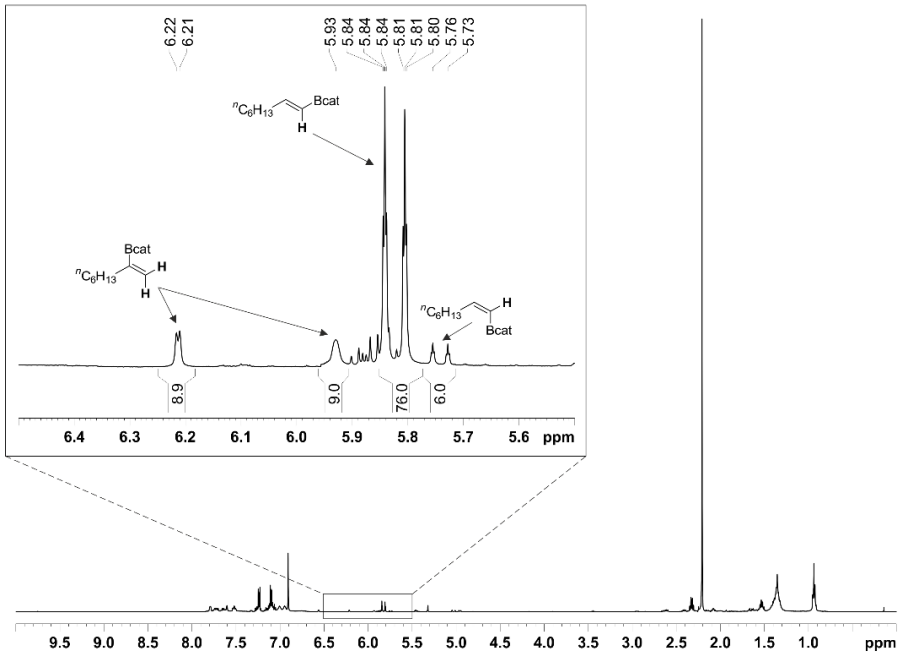

Figure 31. Reaction mixture ^{1}H NMR (400 MHz, CD_2Cl_2) of the hydroboration of **7b** and HBcat using complex **6** as catalyst.

1.5.5.3.16 Hydroboration of 7a with HBpin using complex 11 as catalyst

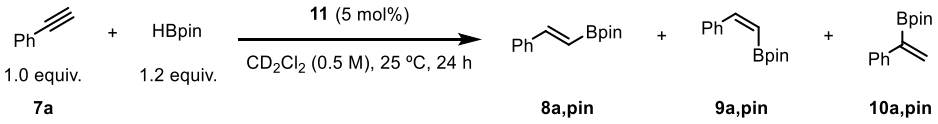

Scheme 31. Hydroboration of **7a** with pinacolborane (HBpin, 1.2 equiv.) using complex **11** as catalyst.

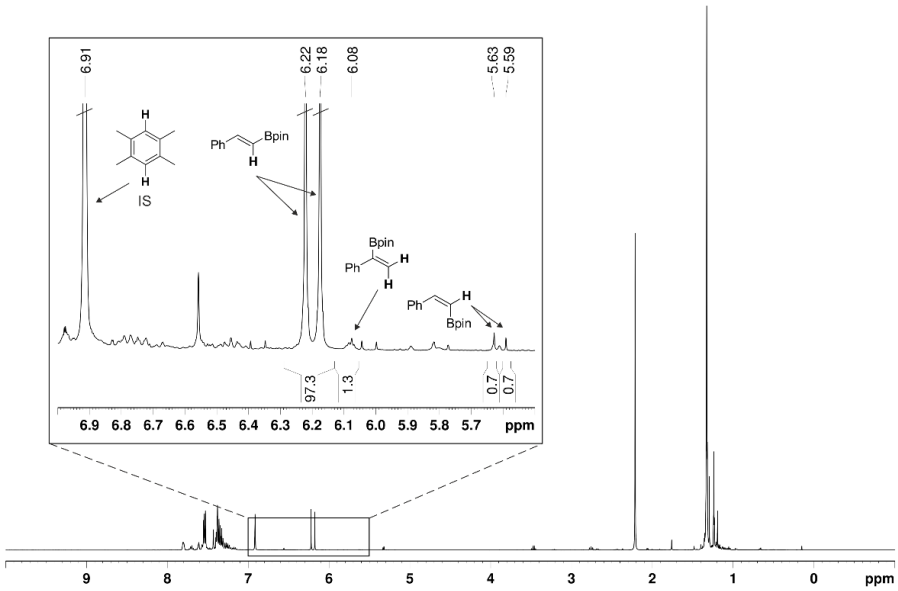

Figure 32. Reaction mixture ^{1}H NMR (400 MHz, CD_2Cl_2) of the hydroboration of **7a** and HBpin using complex **11** as catalyst.

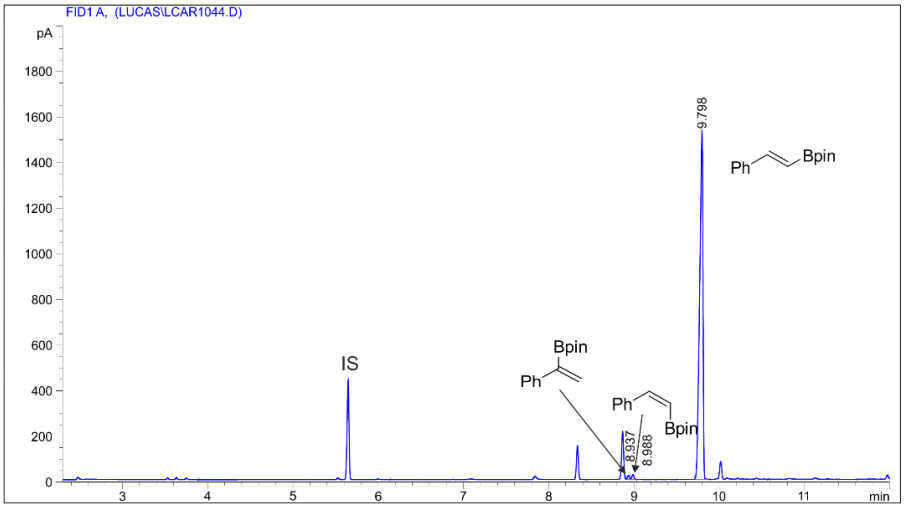

Figure 33. Reaction mixture GC-FID of the hydroboration of **7a** and HBpin using complex **11** as catalyst. Peak 1 (rt = 8.937): Area%: 0.7. Peak 2 (rt = 8.988): Area%: 0.9. Peak 3 (rt = 9.798): Area%: 98.4.

1.5.5.4. Characterization of the *E*/ branched hydroboration products

Vinylboronic esters were isolated from the crude reactions using boric acid impregnated silica gel.[91] As mentioned in section 1.5.5.3, catechol boronic esters were not isolated,[89] but directly identified in the NMR spectra of the reaction mixture by comparison with data from previous reports in the literature. ^{1}H NMR and ^{13}C{^{1}H} NMR spectra and GC-FID chromatograms of the isolated products can be found in section 1.5.7.

Boric acid impregnated silica gel: A 1 L round bottom flask equipped with a stir bar was filled under air with silica gel (300 mL), boric acid (28 g) and ethanol (550 mL). The suspension was stirred at rt for 2 h. The suspension was filtered and the ethanolic solution of boric acid was disregarded. The solid was washed with ethanol (3 x 200 mL) and dried in a vacuum oven at 140 °C for 48 h. Once dried, the boric acid impregnated silica gel was stored in a desiccator until used.

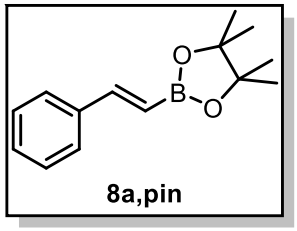

E-2-(4,4,5,5-Tetramethyl-1,3,2-dioxaborolan-2-yl) styrene (**8a,pin**): The reaction crude mixture was purified by column chromatography using $B(OH)_3$ impregnated SiO_2 and hexanes and AcOEt as the eluents (30:1→10:1, hexanes:AcOEt), to afford the compound as a yellow oil. ^{1}H NMR (400 MHz, CD_2Cl_2) δ: 7.55-7.48 (m, 2 H), 7.43-7.27 (m, 4 H), 6.17 (d, J = 18.4 Hz, 1 H), 1.30 (s, 12 H) ppm. ^{13}C{^{1}H} NMR (100 MHz, CD_2Cl_2) δ:[92] 149.6, 138.0, 129.3, 129.0, 127.4, 83.7, 25.1 ppm. GC-FID: rt = 9.783 min. ^{1}H NMR and ^{13}C{^{1}H} NMR data were in agreement with those previously reported.[93]

---

(91) Boronic esters are known to partially decompose with SiO_2. The stability of boronic esters in boric acid impregnated silica is known to be much higher. See: Hitosugi, S.; Tanimoto, D.; Nakanishi, W.; Isobe, H. *Chem. Lett.* **2012**, *41*, 972-973.
(92) The C–B signal in ^{13}C{^{1}H} NMR was not observed in the spectra. For an explanation to this observation, see: Wrackmeyer, B. *Prog. Nucl. Magn. Reson. Spectrosc.* **1979**, *12*, 227-259. This observation also applies to the rest of vinyl boronic esters.
(93) Grirrane, A.; Corma, A.; García, H. *Chem. - Eur. J.* **2011**, *17*, 2467-2478.

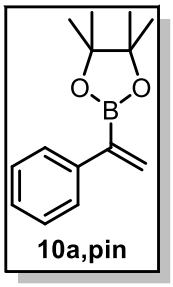

4,4,5,5-Tetramethyl-2-(1-phenylvinyl)-1,3,2-dioxaborolane (**10a,pin**): The reaction crude mixture was purified by column chromatography using $B(OH)_3$ impregnated SiO_2 and hexanes and AcOEt as the eluents (30:1→10:1, hexanes:AcOEt), to afford the compound as a yellow oil. ^1H NMR (400 MHz, CD_2Cl_2) δ: 7.50-7.45 (m, 2 H), 7.37-7.27 (m, 3 H), 6.07-6.05 (m, 2H), 1.34 (s, 12 H) ppm. $^{13}C\{^1H\}$ NMR (100 MHz, CD_2Cl_2) δ: 142.0, 131.1, 128.5, 127.6, 127.4, 84.2, 25.0 ppm. GC-FID: rt = 8.977 min. ^1H NMR and $^{13}C\{^1H\}$ NMR data were in agreement with those previously reported.[72a]

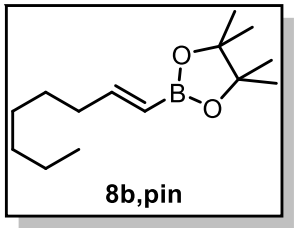

E-4,4,5,5-tetramethyl-2-(oct-1-en-1-yl)-1,3,2-dioxaborolane (**8b,pin**): The reaction crude mixture was purified by column chromatography using $B(OH)_3$ impregnated SiO_2 and hexanes and AcOEt as the eluents (30:1, hexanes:AcOEt), to afford the compound as a colorless oil. ^1H NMR (400 MHz, CD_2Cl_2) δ: 6.57 (dt, J = 17.9, 6.5 Hz, 1 H), 5.37 (dt, J = 17.9, 1.5 Hz, 1 H), 2.16-2.11 (m, 2 H), 1.46-1.19 (m, 20 H), 0.88-0.86 (m, 3 H) ppm. $^{13}C\{^1H\}$ NMR (100 MHz, CD_2Cl_2) δ: 155.0, 83.3, 36.2, 32.2, 29.4, 28.8, 25.0, 23.0, 14.3 ppm. GC-FID: rt = 8.605 min. ^1H NMR and $^{13}C\{^1H\}$ NMR data were in agreement with those previously reported.[93]

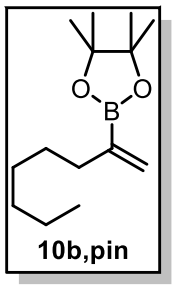

4,4,5,5-tetramethyl-2-(oct-1-en-2-yl)-1,3,2-dioxaborolane (**10b,pin**): The reaction crude mixture was purified by column chromatography using $B(OH)_3$ impregnated SiO_2 and hexanes and AcOEt as the eluents (30:1, hexanes:AcOEt), to afford the compound as a colorless oil. ^1H NMR (500 MHz, CD_2Cl_2) δ: 5.68 (d, J = 3.7 Hz, 1 H), 5.56 (br s, 1 H), 2.12-2.09 (m, 2 H), 1.46-1.22 (m, 20 H), 0.89-0.87 (m, 3 H) ppm. $^{13}C\{^1H\}$ NMR (126 MHz, CD_2Cl_2) δ: 128.6, 83.6, 35.8, 32.2, 29.7, 29.4, 24.9, 23.1, 14.3 ppm. GC-FID: rt = 7.855 min. ^1H NMR and $^{13}C\{^1H\}$ NMR data were in agreement with those previously reported.[72b]

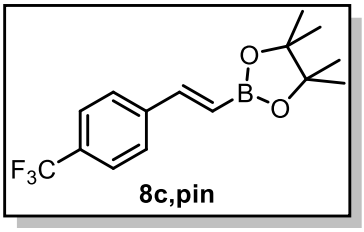

8c,pin

E-4,4,5,5-tetramethyl-2-(4-(trifluoromethyl) styryl)-1,3,2 dioxaborolane (**8c,pin**): The reaction crude mixture was purified by column chromatography using $B(OH)_3$ impregnated SiO_2 and hexanes and AcOEt as the eluents (30:1→10:1, hexanes:AcOEt), to afford the compound as a yellow oil. ^{1}H NMR (400 MHz, CD_2Cl_2) δ: 7.61 (s, 4 H), 7.38 (d, J = 18.4 Hz, 1 H), 6.26 (d, J = 18.4 Hz, 1 H), 1.29 (s, 12 H) ppm. $^{13}C\{^1H\}$ NMR (126 MHz, CD_2Cl_2) δ: 147.7, 141.4, 130.5 (q, J_{C-F} = 32.3 Hz), 127.6, 125.9 (q, J_{C-F} = 3.9 Hz), 124.6 (q, J_{C-F} = 272.1 Hz), 83.9, 25.0 ppm. GC-FID: rt = 9.603 min. ^{1}H NMR and $^{13}C\{^1H\}$ NMR data were in agreement with those previously reported.[72a]

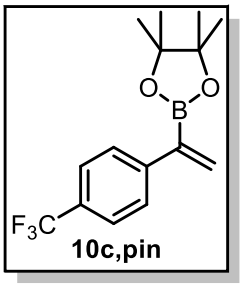

10c,pin

4,4,5,5-tetramethyl-2-(1-(4-(trifluoromethyl)phenyl) vinyl)-1,3,2 dioxaborolane (**10c,pin**): The reaction crude mixture was purified by column chromatography using $B(OH)_3$ impregnated SiO_2 and hexanes and AcOEt as the eluents (30:1→10:1, hexanes:AcOEt), to afford the compound as a yellow oil. ^{1}H NMR (400 MHz, CD_2Cl_2) δ: 7.58 (s, 4 H), 6.14 (br s, 2 H), 1.31 (s, 12 H) ppm. $^{13}C\{^1H\}$ NMR (126 MHz, CD_2Cl_2) δ: 145.8, 133.2, 129.0 (q, J_{C-F} = 32.2 Hz), 128.0, 125.3 (q, J_{C-F} = 3.7 Hz), 124.9 (q, J_{C-F} = 271.6 Hz), 84.6, 25.0 ppm. GC-FID: rt = 8.784 min. ^{1}H NMR and $^{13}C\{^1H\}$ NMR data were in agreement with those previously reported.[72a]

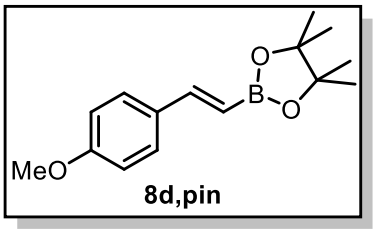

8d,pin

E-2-(4-methoxystyryl)-4,4,5,5-tetramethyl-1,3,2 dioxaborolane (**8d,pin**): The reaction crude mixture was purified by column chromatography using $B(OH)_3$ impregnated SiO_2 and hexanes and AcOEt as the eluents (30:1→10:1, hexanes:AcOEt), to afford the compound as a yellow oil. ^{1}H NMR (400 MHz, CD_2Cl_2) δ: 7.45 (dm, J = 8.8 Hz, 2 H), 7.30 (d, J = 18.4 Hz, 1 H), 6.88 (dm, J = 8.8 Hz, 2 H), 5.98 (d, J = 18.3 Hz, 1 H), 3.81 (s, 3 H), 1.28 (s, 12 H) ppm. $^{13}C\{^1H\}$ NMR (100 MHz, CD_2Cl_2) δ: 160.8, 149.2, 130.8, 128.9, 114.3,

83.5, 55.7, 25.0 ppm. GC-FID: rt = 11.530 min. ^{1}H NMR and ^{13}C{^{1}H} NMR data were in agreement with those previously reported.[94]

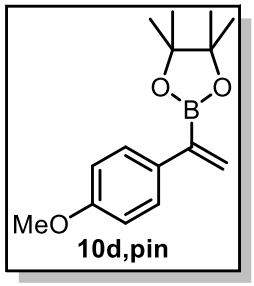

2-(1-(4-methoxyphenyl)vinyl)-4,4,5,5-tetramethyl-1,3,2 dioxaborolane (**10d,pin**): The reaction crude mixture was purified by column chromatography using $B(OH)_3$ impregnated SiO_2 and hexanes and AcOEt as the eluents (30:1→10:1, hexanes:AcOEt), to afford the compound as a yellow oil. ^{1}H NMR (400 MHz, CD_2Cl_2) δ: 7.41 (dm, *J* = 8.8 Hz, 2 H), 6.84 (dm, *J* = 8.8 Hz, 2 H), 5.98 (d, *J* = 2.8 Hz, 1 H), 5.91 (d, *J* = 3.0 Hz, 1 H), 3.79 (s, 3 H), 1.31 (s, 12 H) ppm. ^{13}C{^{1}H} NMR (100 MHz, CD_2Cl_2) δ: 159.4, 134.4, 129.1, 128.8, 113.9, 84.1, 55.6, 25.0 ppm. GC-FID: rt = 10.679 min. ^{1}H NMR and ^{13}C{^{1}H} NMR data were in agreement with those previously reported.[95]

(94) Reid, W. B.; Spillane, J. J.; Krause, S. B.; Watson, D. A. *J. Am. Chem. Soc.* **2016**, *138*, 5539-5542.
(95) Guan, W.; Michael, A. K.; McIntosh, M. L.; Koren-Selfridge, L.; Scott, J. P.; Clark, T. B. *J. Org. Chem.* **2014**, *79*, 7199-7204.

1.5.6. Computational methods

Geometry optimizations of compounds 4MePy (4-methylpyridine), IPFB (iodopentafluorobenzene), 4MePy·IPFB, **1**, **2**, **3**, $Rh[(CO)_2]^+$, CO, $Rh[(CO)(\mathbf{1})(\mathbf{2})]^+$ and $Rh[(CO)(\mathbf{1})(\mathbf{3})]^+$ were carried out using the TPSS[66]-D3[67] functional and the def2-TZVP basis set[68] as implemented in Gaussian 09, Revision D.01.[65] The TPSS-D3/def2-TZVP level of theory offers a good compromise between the size of the system (up to 70 atoms for $Rh[(CO)(\mathbf{1})(\mathbf{2})]^+$ and $Rh[(CO)(\mathbf{1})(\mathbf{3})]^+$), the computational cost and the accuracy in describing halogen bonding.[69] Solvent effects (toluene) were incorporated employing the Polarizable Continuum Model (PCM) with the integral equation formalism (IEFPCM calculations)[96] with radii and non-electrostatic terms[97] as implemented in Gaussian 09, Revision D.01. Energies in solution (toluene) include corrections for zero-point energy and free energy (incorporating temperature and entropic effects corrected to 298.15 K). Electrostatic potential surfaces were calculated with Gaussian 09 at the TPSS-D3/def2-TZVP level of theory considering the effects of toluene as the solvent and have been plotted with GaussView 5.0 using an isovalue of 0.001 a.u.

(96) Scalmani, G.; Frisch, M. J. *J. Chem. Phys.* **2010**, *132*, 114110/114111-114110/114115.
(97) Marenich, A. V.; Cramer, C. J.; Truhlar, D. G. *J. Phys. Chem. B* **2009**, *113*, 6378-6396.

Cartesian coordinates:

4MePy, 4-methylpyridine:

N	5.34583000	−0.17944600	0.01358300
C	6.06506500	0.95331300	−0.00650600
C	7.45857100	0.98703300	−0.02169700
C	8.17849700	−0.21299300	−0.01508900
C	7.43006400	−1.39630300	0.00295200
C	6.03855300	−1.32963100	0.01757800
H	5.49456900	1.88098700	−0.01361800
H	7.97755500	1.94254300	−0.04180600
H	7.92622500	−2.36410700	0.00346500
H	5.44607300	−2.24334900	0.03023600
C	9.68422500	−0.23310500	−0.00219200
H	10.05566300	−0.32122900	1.02711700
H	10.07523500	−1.08690100	−0.56500400
H	10.09951800	0.68621800	−0.42636900

IPFB, iodopentafluorobenzene:

C	−2.37992600	−0.13924200	−0.00019100
C	−1.67803600	1.06396800	−0.00075200
C	−0.28547200	1.05163300	−0.00077500
C	0.42695100	−0.14798100	−0.00025700
C	−0.29285100	−1.34320900	0.00029000
C	−1.68549100	−1.34679300	0.00033700
F	−3.72033100	−0.13513100	−0.00015900
F	−2.34709200	2.22865100	−0.00126200
F	0.35759600	2.23230500	−0.00130400
I	2.51485200	−0.15393400	−0.00029500
F	0.34291200	−2.52785300	0.00078300
F	−2.36190700	−2.50721700	0.00088000

4MePy·IPFB:

C	−2.33943400	−0.14874300	−0.00355200
C	−1.64310300	1.05731200	−0.00711500
C	−0.25058500	1.04642900	−0.00230900
C	0.47652700	−0.14164500	0.00565800
C	−0.24479200	−1.33335400	0.00911600
C	−1.63717800	−1.35131100	0.00454200
F	−3.68286500	−0.15208200	−0.00795300
F	−2.32213300	2.22017400	−0.01508300
F	0.38366000	2.23882100	−0.00598900
I	2.61293200	−0.13900500	0.01058400
F	0.39515100	−2.52271100	0.01678700
F	−2.31026100	−2.51765400	0.00796800
N	5.32654500	−0.16137100	0.01099400
C	6.03872400	0.97535500	−0.00849000
C	7.42986500	0.99347100	−0.02271500
C	8.13937600	−0.21352100	−0.01594800
C	7.38524600	−1.39403000	0.00214900
C	5.99660400	−1.32438500	0.01591500
H	5.46457300	1.89894900	−0.01591200
H	7.95567000	1.94441200	−0.04252000
H	7.87534500	−2.36407600	0.00296700
H	5.38762100	−2.22540500	0.02819400
C	9.64375500	−0.24393700	−0.00349300
H	10.01191200	−0.33133300	1.02698200
H	10.02803000	−1.10297800	−0.56237000
H	10.06522300	0.67119900	−0.42975000

Ligand **1**:

P	6.97005454	3.29558891	13.40575589
C	5.24920690	2.70249267	13.13830743
C	4.56869794	3.22901623	12.02882245
C	3.26920694	2.82035621	11.73065917
H	2.75772556	3.23546465	10.86606943
C	2.62340813	1.89271533	12.55009205
H	1.60652428	1.58151607	12.32565559
C	3.28573753	1.37354334	13.66421320
H	2.78618466	0.65426346	14.30848841
C	4.59081790	1.77186282	13.95609827
C	7.28530215	2.74955448	15.14265294
C	8.22935600	1.78732710	15.52227263
C	8.41009088	1.52451038	16.87973648
H	9.13561188	0.78189033	17.20184688
C	7.64253113	2.21925351	17.81183378
C	6.72321986	3.15908233	17.34130451
H	6.10224676	3.72352012	18.03528046
N	6.54719466	3.43322903	16.04328807
C	7.96471567	2.08033292	12.44048108
C	7.48791829	0.83528335	12.00395573
H	6.46643999	0.53877487	12.22570063
C	8.31530444	−0.02576197	11.28198095
C	9.63110769	0.34060907	10.99111365
H	10.27313924	−0.33227998	10.42869338
C	10.11520221	1.57899345	11.41690739
H	11.13540271	1.87528691	11.18655135
C	9.28420507	2.44605362	12.12652096
H	5.06203706	3.96475614	11.39722189
H	5.09434986	1.35866496	14.82519559
H	8.80311934	1.25230382	14.77210329
H	7.75106496	2.04316631	18.87803820
H	7.93130850	−0.98625547	10.94719262

H	9.66010232	3.41704979	12.44259509

Ligand **2**:

P	6.79655400	7.72906500	12.36275900
I	5.84793500	6.15913700	15.34126200
C	5.95897300	8.76475800	13.65445500
C	5.68702200	10.12292100	13.46335500
C	5.02830000	10.89918600	14.41187300
C	4.61871500	10.31133500	15.60318800
C	4.87467800	8.96069100	15.82670400
C	5.53485600	8.19184700	14.87079600
F	6.06928100	10.74997600	12.33289800
F	4.78864400	12.20233100	14.19017500
F	3.98276200	11.04430700	16.52911500
F	4.45904100	8.43617700	16.99618000
C	5.69255500	8.01014800	10.91383200
C	5.86763500	8.99009100	9.92641800
C	4.96872300	9.08558000	8.86441900
H	5.11426600	9.84914400	8.10458800
C	3.87986500	8.21485700	8.78114300
C	3.69741100	7.23598600	9.75948500
H	2.85705900	6.54967900	9.69714500
C	4.60566300	7.12594300	10.81159800
H	4.47452600	6.34932100	11.56232300
C	8.32034000	8.68273200	12.00102700
C	8.90830300	9.54917600	12.93444500
C	10.14459400	10.14042600	12.67517000
H	10.57985300	10.81512000	13.40779600
C	10.81588000	9.87428600	11.48133400
H	11.77610500	10.34035800	11.27782400
C	10.24657600	9.00173400	10.55115300
H	10.76383500	8.78348000	9.62039600
C	9.01545600	8.40234300	10.81111200
H	6.70123300	9.68213800	9.99053100
H	3.17936000	8.29599600	7.95424300
H	8.39962800	9.77000300	13.86898600
H	8.58878600	7.71767600	10.08177000

Ligand **3**:

P	6.59965900	7.60239000	12.31505400
I	7.83686700	7.13237500	15.47306300
C	5.85280500	8.63792200	13.64882300
C	4.81834100	9.55944400	13.40824200
C	4.23073200	10.28363400	14.44396800
C	4.67043300	10.10796200	15.75540200
C	5.69943500	9.20560300	16.02744400
C	6.27054700	8.48021000	14.98186600
C	5.63002400	8.14064100	10.84089000
C	5.99962300	9.20034000	10.00008500
C	5.21629800	9.53322200	8.89415600
H	5.51700900	10.35539000	8.24955700
C	4.05070800	8.81673000	8.61717100
C	3.67473800	7.75711100	9.44574200
H	2.77228300	7.19019700	9.23166700
C	4.46452100	7.41501400	10.54307100
H	4.17615800	6.57996700	11.17828000
C	8.21115300	8.45294900	12.04283500
C	8.49513100	9.75498700	12.47958100
C	9.74234500	10.32838500	12.22962400
H	9.95030900	11.33775200	12.57556300
C	10.71890300	9.61124900	11.53611600
H	11.68981900	10.05951900	11.34237400
C	10.44636300	8.31329000	11.09910200
H	11.20484700	7.74682000	10.56491900
C	9.20425100	7.73499700	11.35891300
H	6.90245300	9.76648900	10.21026700
H	3.44194500	9.07710500	7.75523100
H	7.74044900	10.32190800	13.01778900
H	9.00099700	6.71725700	11.03296100
H	4.47448900	9.71016800	12.38923800
H	3.43301200	10.98749000	14.22251200
H	4.21866900	10.66614700	16.57094100
H	6.05090500	9.06435200	17.04436500

$Rh[(CO)_2]^+$:

Rh	6.93262700	5.64698000	13.00866000
C	7.65138400	5.22630200	11.24288900
O	8.06938200	4.98165400	10.21413700
C	6.21285500	6.07133900	14.77392300
O	5.79292400	6.32120400	15.80071100

CO:

C	7.63602800	5.23213500	11.30104400
O	8.03195300	5.03147900	10.25733400

$Rh[(CO)(\mathbf{1})(\mathbf{2})]^+$:

Rh	7.00081100	5.56019400	12.97277400
P	6.74771300	7.78423100	12.35878100
P	6.93987300	3.26863200	13.39878700
I	6.07404500	6.15567100	15.39088700
C	5.96528700	8.78653200	13.69046500
C	5.67557200	10.14182000	13.50548900
C	5.04998500	10.90339200	14.48913000
C	4.70683300	10.30707100	15.70066700
C	4.99925500	8.95991500	15.90438600
C	5.61830700	8.20770200	14.91730300
F	6.00512000	10.76465600	12.35908000
F	4.78086400	12.19788000	14.28088100
F	4.11047700	11.02778800	16.65534600

F	4.67187000	8.40887500	17.09254600
C	5.63275300	7.95285400	10.92200000
C	5.74541400	8.98156200	9.97667700
C	4.85084700	9.04244800	8.90902500
H	4.94630000	9.83742200	8.17485200
C	3.83715100	8.09078100	8.78348500
C	3.71749100	7.06826500	9.72705800
H	2.93184900	6.32375700	9.63208100
C	4.61577500	6.99364500	10.78889400
H	4.54216200	6.18661500	11.51553000
C	5.23309100	2.69836700	13.08541500
C	4.67927500	2.95167800	11.81787100
C	3.36856800	2.57475400	11.53885800
H	2.95152300	2.76798700	10.55448900
C	2.59229400	1.95600800	12.52266400
H	1.56697300	1.67002900	12.30617800
C	3.13540600	1.70726500	13.78257500
H	2.53620500	1.22508300	14.54981000
C	4.45232700	2.07347400	14.06667600
C	7.26272500	2.76903200	15.14574100
C	7.86662300	1.55923900	15.49422300
C	8.02750200	1.25887700	16.84723600
H	8.49757900	0.32688300	17.14695900
C	7.57847900	2.16671300	17.80288200
C	6.99290300	3.35540700	17.36997800
H	6.63810800	4.10298700	18.07516600
N	6.84519000	3.64972900	16.07196400
C	7.61139000	5.22010900	11.27734500
O	7.97399400	5.01595700	10.19794400
C	8.30084900	8.65338000	11.97076600
C	8.94311500	9.43156400	12.94412100
C	10.17916700	10.01491100	12.67061700
H	10.66390200	10.62444100	13.42788800
C	10.78674500	9.82086400	11.42958900
H	11.74739300	10.28078600	11.21611300
C	10.15688900	9.03582100	10.46162500
H	10.62633200	8.88078500	9.49432700
C	8.92242000	8.44759100	10.72847900
C	8.03387300	2.18207400	12.43293700
C	7.59537800	0.95765400	11.91042600
H	6.56474900	0.64314600	12.04578400
C	8.48572700	0.14424700	11.20910700
C	9.81113600	0.54422800	11.03256300
H	10.50056800	−0.09094200	10.48356700
C	10.25098300	1.76395700	11.55280000
H	11.28029700	2.07957300	11.40864000
C	9.36545700	2.58466300	12.24736200
H	6.52649400	9.72867700	10.06848200
H	3.14285000	8.14452400	7.94958100
H	5.27430500	3.43881600	11.04982700
H	4.86120200	1.87081900	15.05172400
H	8.20140900	0.87099200	14.72555200
H	7.68614000	1.96912900	18.86449700
H	8.48093400	9.58866900	13.91453600
H	8.44415600	7.83948400	9.96635500
H	8.14133500	−0.80101000	10.79923600
H	9.69971900	3.54349800	12.63806900

Rh[(CO)(**1**)(**3**)]$^{+}$:

Rh	7.03660200	5.53823500	12.98755300
P	6.75228700	7.75857100	12.38063800
P	6.97245900	3.24827700	13.42851500
I	6.09141700	6.18689800	15.39008500
C	5.90083100	8.75643300	13.66195500
C	5.54639100	10.09113100	13.39916200
C	4.88760100	10.85165400	14.36026600
C	4.56911400	10.28937600	15.59827700
C	4.91064700	8.96611600	15.87782300
C	5.57273900	8.21641400	14.90552200
C	5.69458500	7.94046600	10.90302400
C	5.81480400	9.00789100	10.00216500
C	4.93789200	9.10743900	8.92187400
H	5.03947700	9.93150600	8.22125800
C	3.93657100	8.15199400	8.73813900
C	3.81174500	7.08927300	9.63534200
H	3.03611200	6.34157600	9.49458800
C	4.68991700	6.98004200	10.71070800
H	4.60840500	6.14624500	11.40509900
C	5.24445300	2.72475800	13.14912200
C	4.71483200	2.89516500	11.85786500
C	3.38842300	2.56438000	11.59640700
H	2.98995200	2.69082700	10.59360000
C	2.57251300	2.07679000	12.62143200
H	1.53547200	1.82544900	12.41778800
C	3.09202400	1.91278900	13.90504600
H	2.46176900	1.53245000	14.70409400
C	4.42477000	2.23269300	14.17233600
C	7.33775600	2.72036700	15.15888300
C	7.97380600	1.51683600	15.47170700
C	8.17954700	1.20180500	16.81512800
H	8.67576500	0.27503600	17.08814800
C	7.74229400	2.08916200	17.79505700
C	7.12107700	3.27145800	17.39334100
H	6.77166900	4.00129700	18.11983900
N	6.92942400	3.58327300	16.10548500
C	7.63191000	5.19701300	11.28996400
O	7.98192500	4.99351300	10.20508200
C	8.29895800	8.66170200	12.03445800
C	8.87301800	9.50006900	13.00054700
C	10.10398600	10.10907500	12.75628800
H	10.53822300	10.76222000	13.50802300
C	10.77161200	9.88337000	11.55237400
H	11.72824000	10.36204400	11.36259500

C	10.20757400	9.04212800	10.58997100
H	10.72391800	8.86349900	9.65092400
C	8.98052200	8.42774800	10.82865800
C	8.00238200	2.14288100	12.41238800
C	7.53364700	0.90563000	11.94804900
H	6.51561000	0.59205400	12.15949500
C	8.37605500	0.07786300	11.20595800
C	9.68551600	0.47501500	10.92983400
H	10.33697900	−0.17095800	10.34798800
C	10.15639700	1.70565900	11.39294500
H	11.17269600	2.01956300	11.17261500
C	9.31757200	2.54026700	12.12823700
H	6.59419600	9.75276100	10.13543000
H	3.25759300	8.23309900	7.89396400
H	5.34354000	3.27966300	11.05895700
H	4.81598400	2.10022100	15.17605100
H	8.30050700	0.84467400	14.68575300
H	7.88526400	1.88007100	18.85044200
H	8.35989500	9.68273600	13.94009500
H	8.54981500	7.77701800	10.07292200
H	8.00675600	−0.87652600	10.84118100
H	9.67576700	3.50742400	12.47492300
H	4.66067000	8.52918600	16.84014500
H	4.05133600	10.87818800	16.35014000
H	4.61920400	11.88094700	14.14216700
H	5.78883300	10.53080900	12.43614700

Plots of electrostatic potential surfaces (EPS):

Electrostatic potential surfaces were calculated with Gaussian 09 at the TPSS-D3/def2-TZVP level of theory considering the effects of toluene as the solvent and have been plotted with GaussView 5.0 using an isovalue of 0.001 a.u. (in each case, dark blue indicates the highest positive electrostatic potential value for the corresponding molecule and dark red indicates the highest negative electrostatic potential value for the corresponding molecule).

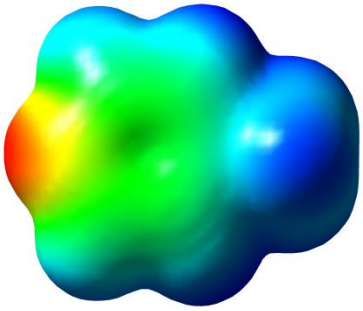

Figure 34. EPS plot for 4MePy.

Max. EPS value = 0.032 a.u.

Min. EPS value = –0.066 a.u.

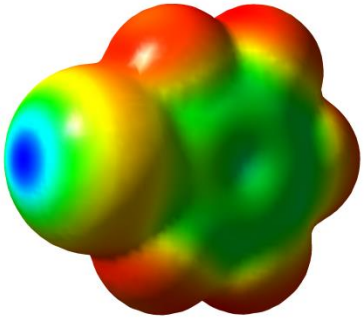

Figure 35. EPS plot for IPFB.

Max. EPS value = 0.056 a.u.

Min. EPS value = –0.013 a.u.

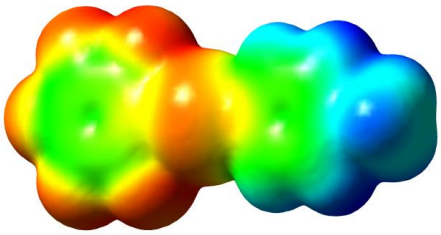

Figure 36. EPS plot for 4MePy·IPFB.

Max. EPS value = 0.046 a.u.

Min. EPS value = −0.029 a.u.

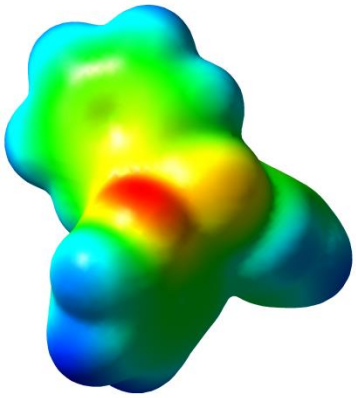

Figure 37. EPS plot for compound **1**.

Max. EPS value = 0.035 a.u.

Min. EPS value = −0.067 a.u.

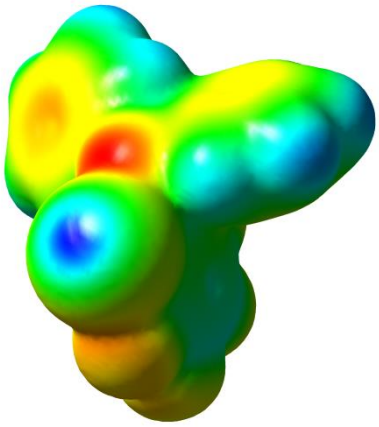

Figure 38. EPS plot for compound **2**.

Max. EPS value = 0.040 a.u.

Min. EPS value = −0.032 a.u.

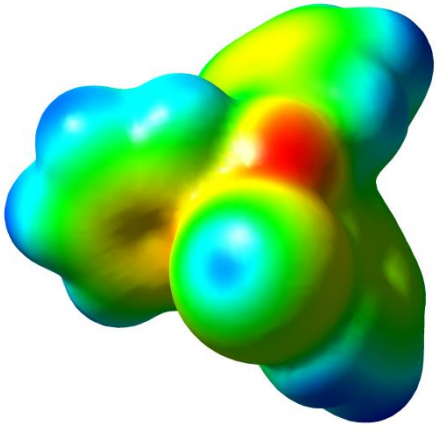

Figure 39. EPS plot for compound **3**.

Max. EPS value = 0.031 a.u.

Min. EPS value = −0.046 a.u.

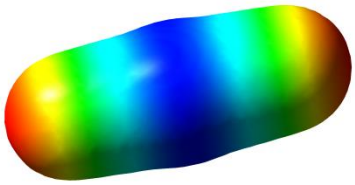

Figure 40. EPS plot for $Rh[(CO)_2]^+$.

Max. EPS value = 0.252 a.u.

Min. EPS value = 0.111 a.u.

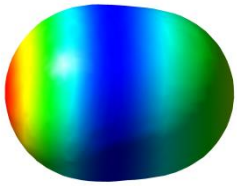

Figure 41. EPS plot for CO.

Max. EPS value = 0.018 a.u.

Min. EPS value = –0.023 a.u.

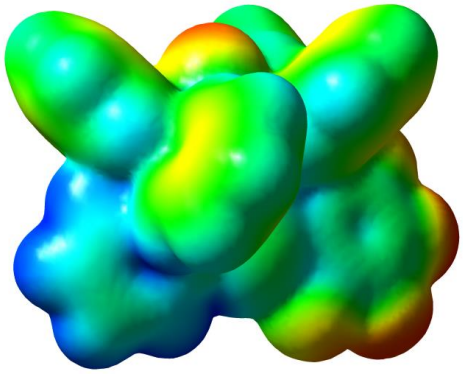

Figure 42. EPS plot for Rh[(CO)(**1**)(**2**)]$^+$.

Max. EPS value = 0.125 a.u.

Min. EPS value = 0.046 a.u.

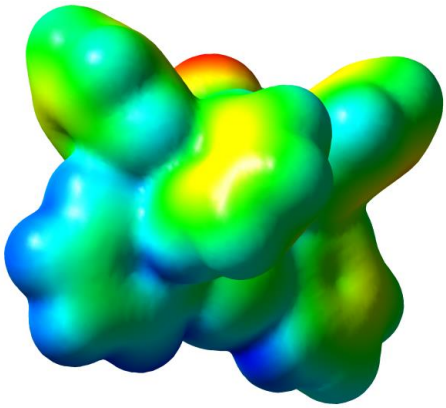

Figure 43. EPS plot for Rh[(CO)(**1**)(**3**)]$^+$.

Max. EPS value = 0.119 a.u.

Min. EPS value = 0.045 a.u.

1.5.7. Collection of spectra and chromatograms

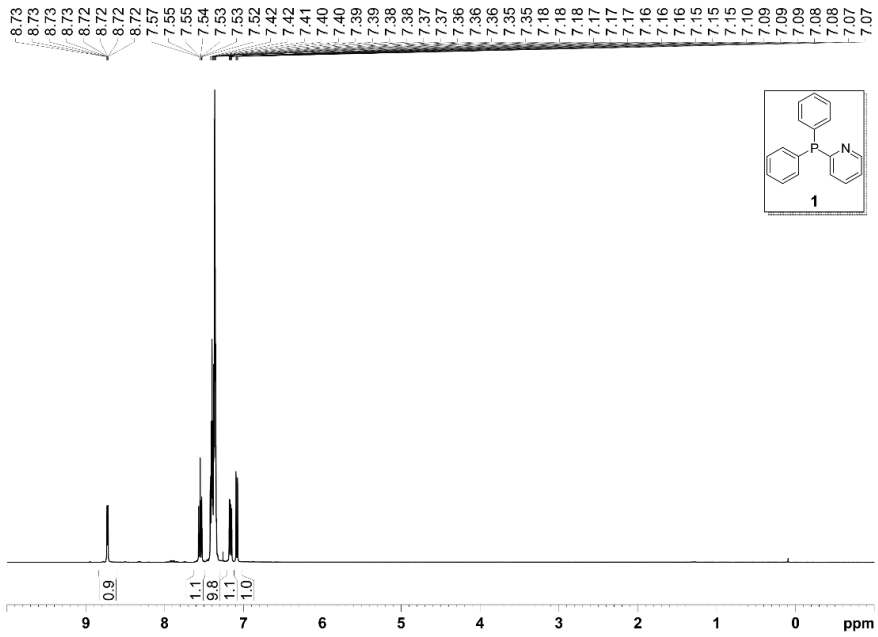

Figure 44. ^{1}H NMR spectrum (400 MHz, $CDCl_3$) for ligand **1**.

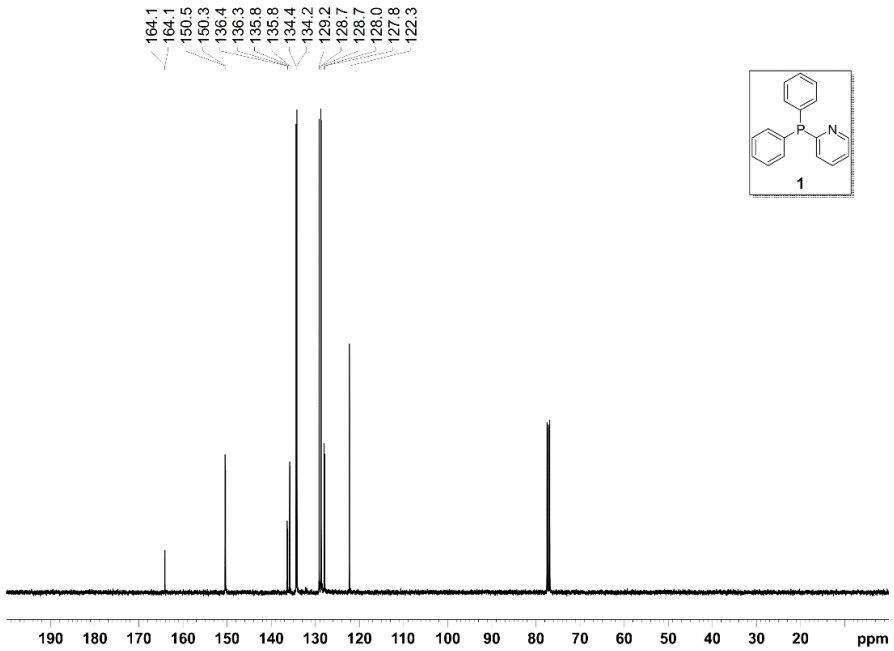

Figure 45. $^{13}C\{^{1}H\}$ NMR spectrum (100 MHz, $CDCl_3$) for ligand **1**.

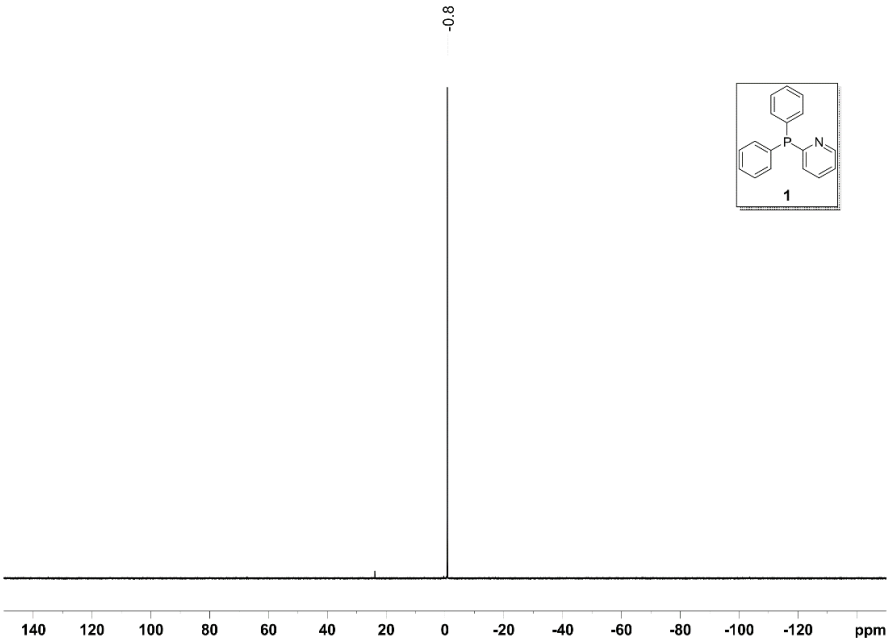

Figure 46. $^{31}P\{^{1}H\}$ NMR spectrum (162 MHz, $CDCl_3$) for ligand **1**.

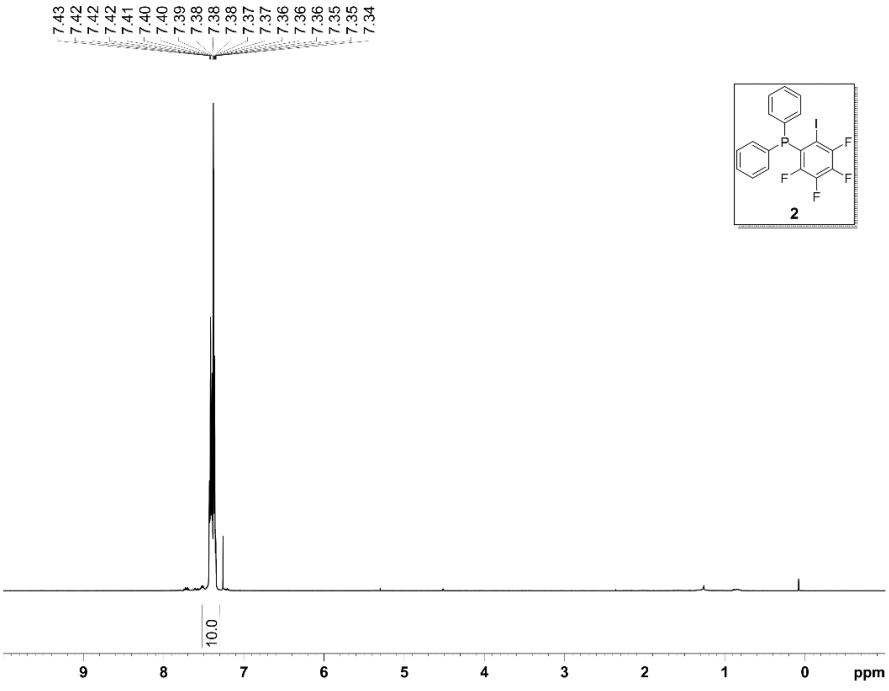

Figure 47. ^{1}H NMR spectrum (500 MHz, $CDCl_3$) for ligand **2**.

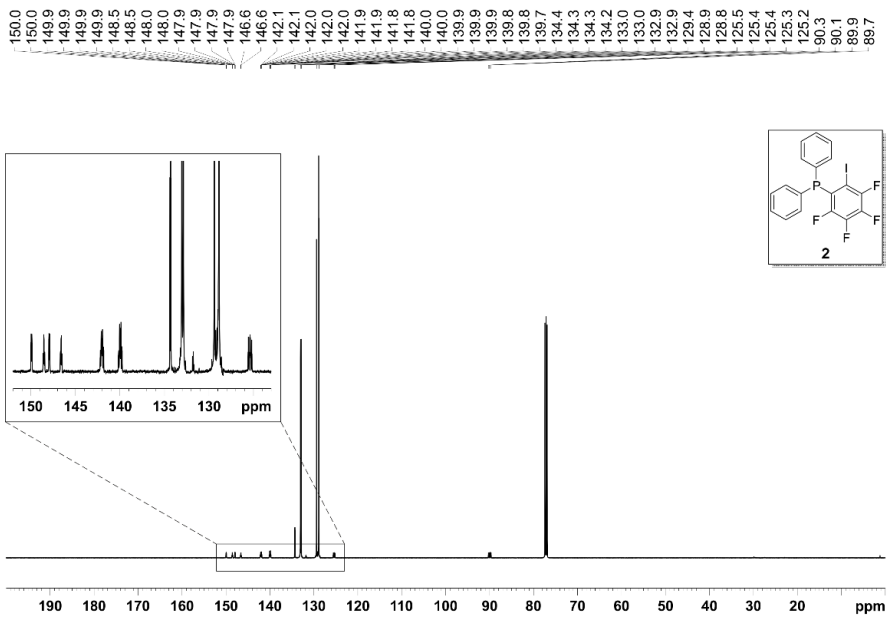

Figure 48. $^{13}C\{^{1}H\}$ NMR spectrum (126 MHz, $CDCl_3$) for ligand **2**.

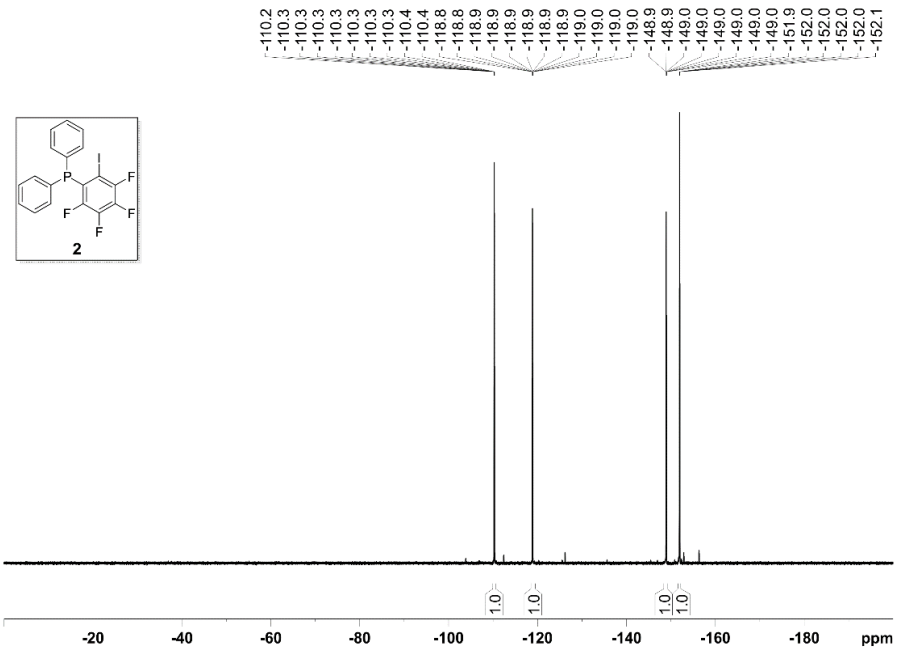

Figure 49. $^{19}F\{^{1}H\}$ NMR spectrum (376 MHz, $CDCl_3$) for ligand **2**.

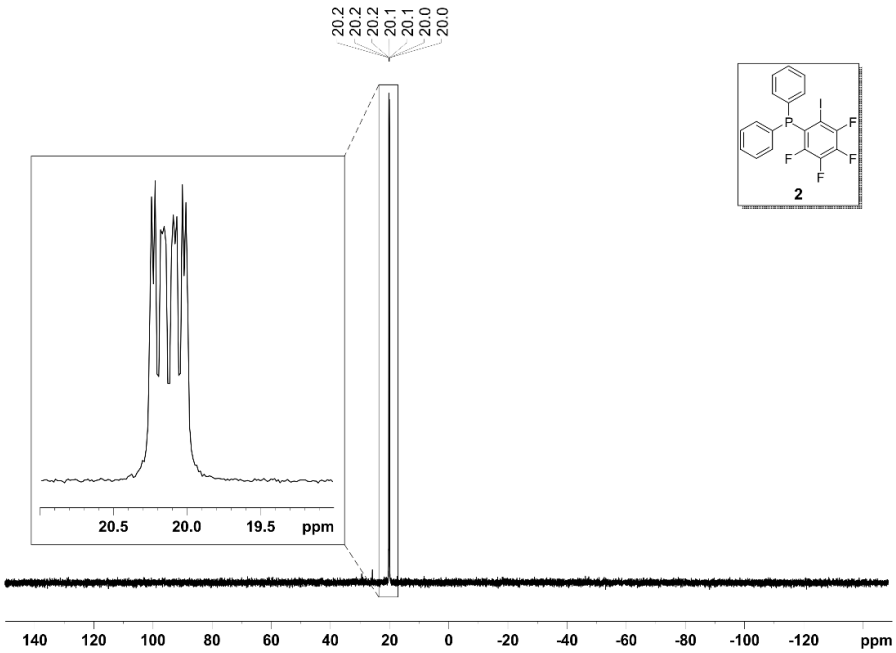

Figure 50. $^{31}P\{^{1}H\}$ NMR spectrum (162 MHz, $CDCl_3$) for ligand **2**.

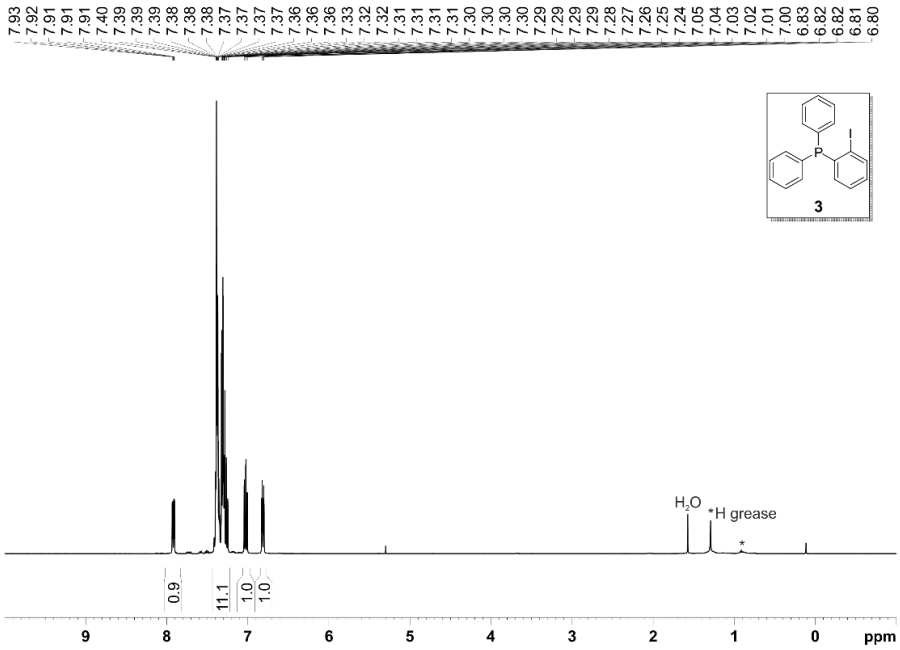

Figure 51. ^{1}H NMR spectrum (400 MHz, $CDCl_3$) for ligand **3**.

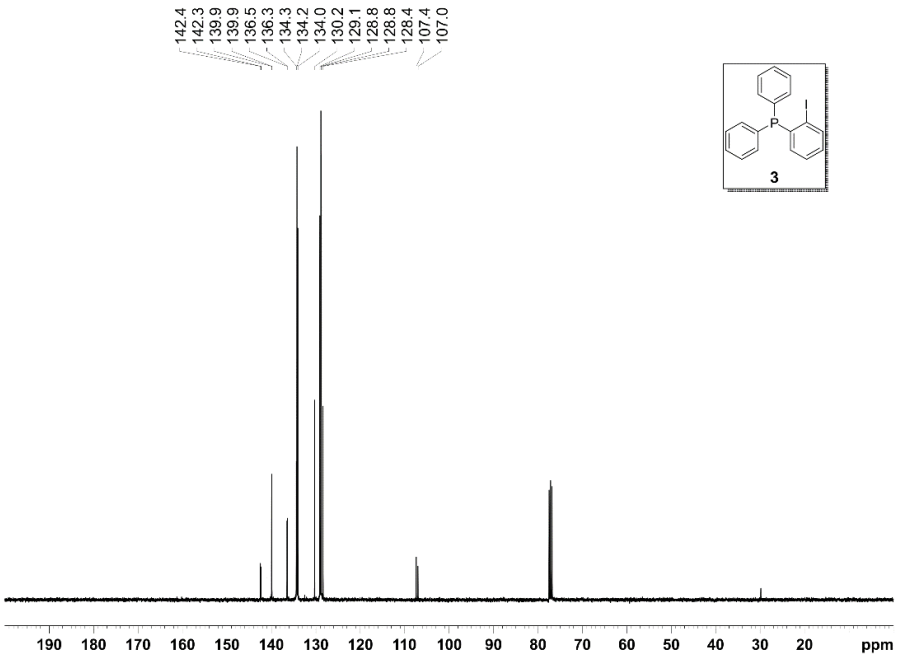

Figure 52. $^{13}C\{^{1}H\}$ NMR spectrum (100 MHz, $CDCl_3$) for ligand **3**.

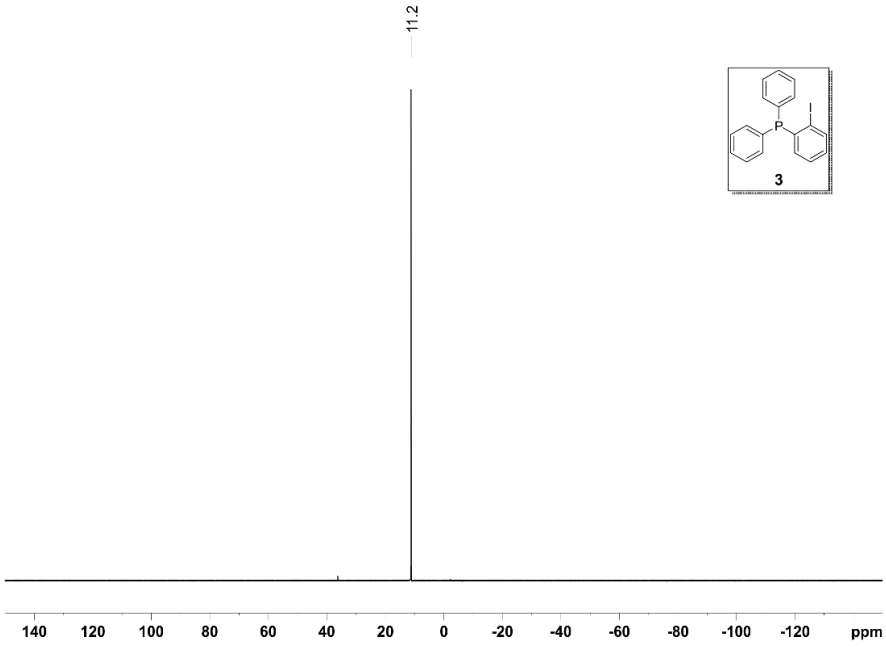

Figure 53. $^{31}P\{^{1}H\}$ NMR spectrum (162 MHz, $CDCl_3$) for ligand **3**.

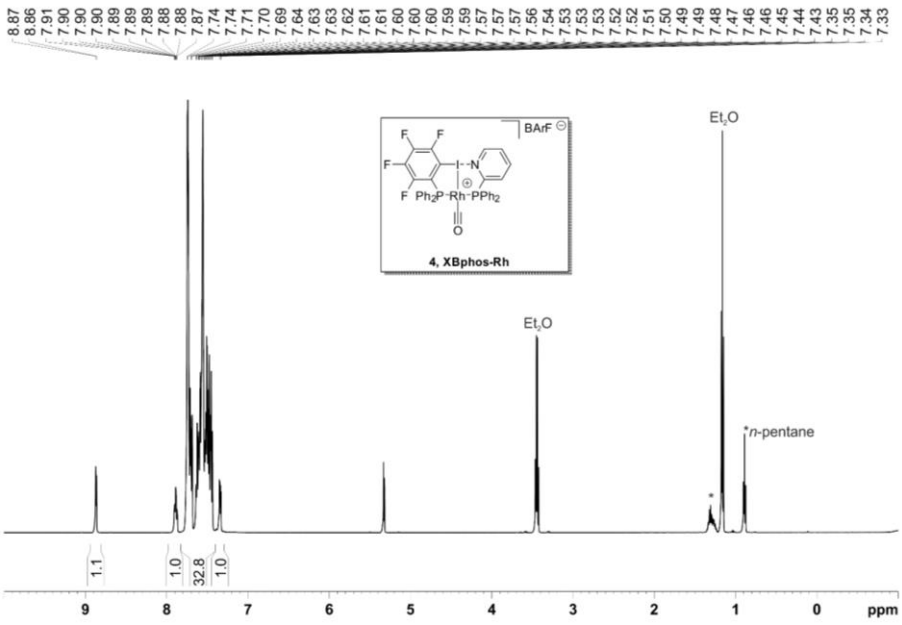

Figure 54. ^{1}H NMR spectrum (500 MHz, CD_2Cl_2) for complex **4**.

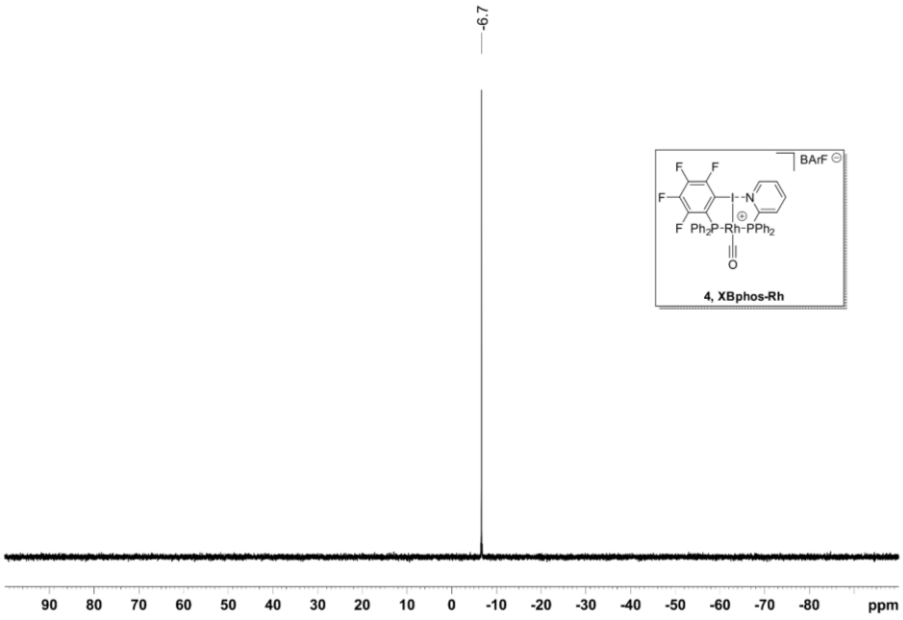

Figure 55. $^{11}B\{^{1}H\}$ NMR spectrum (160 MHz, CD_2Cl_2) for complex **4**.

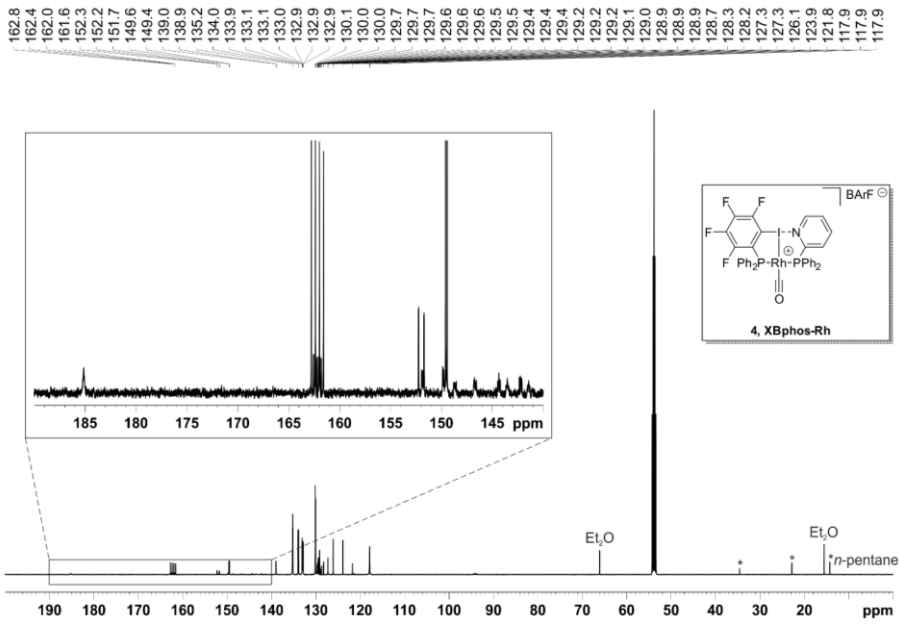

Figure 56. $^{13}C\{^{1}H\}$ NMR spectrum (126 MHz, CD_2Cl_2) for complex **4**.

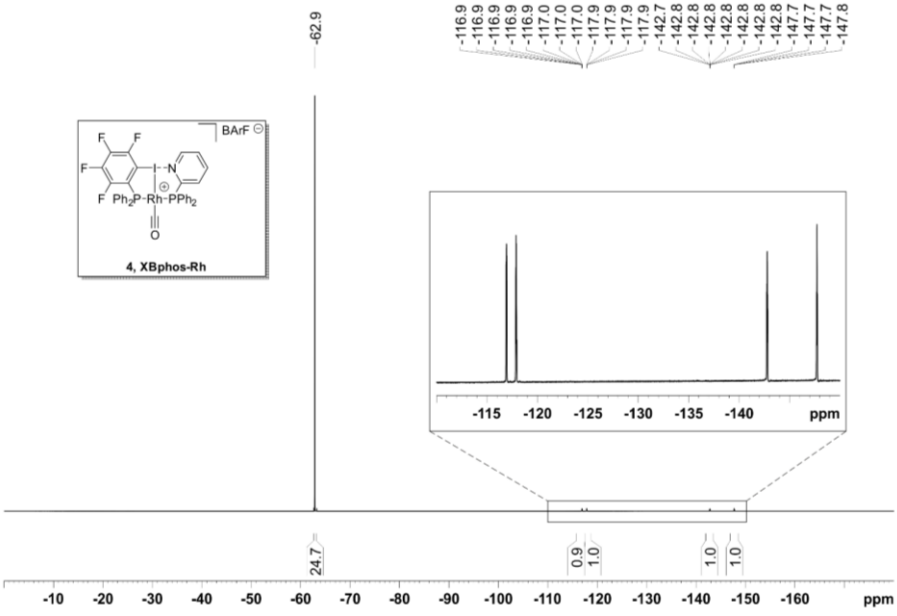

Figure 57. $^{19}F\{^{1}H\}$ NMR spectrum (471 MHz, CD_2Cl_2) for complex **4**.

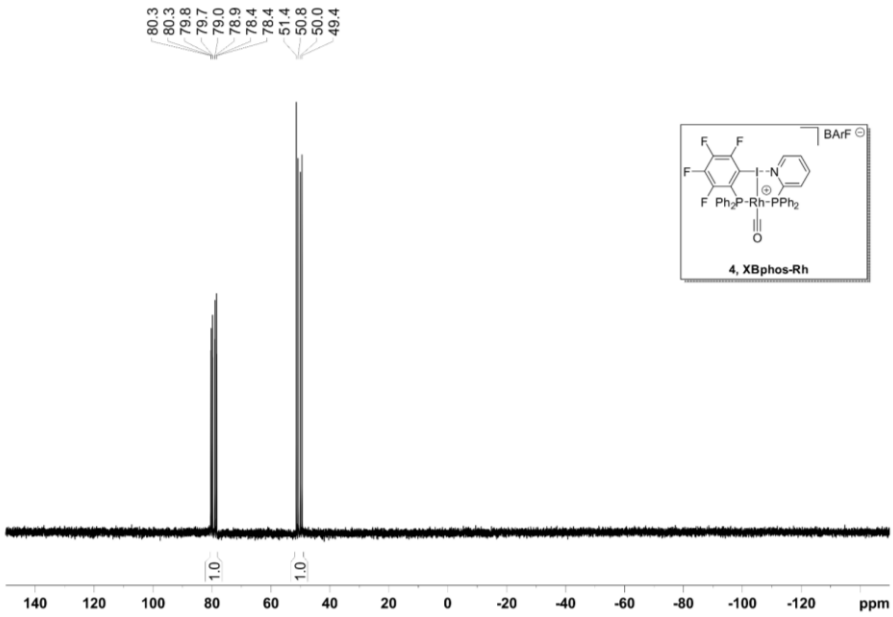

Figure 58. $^{31}P\{^{1}H\}$ NMR spectrum (202 MHz, CD_2Cl_2) for complex **4**.

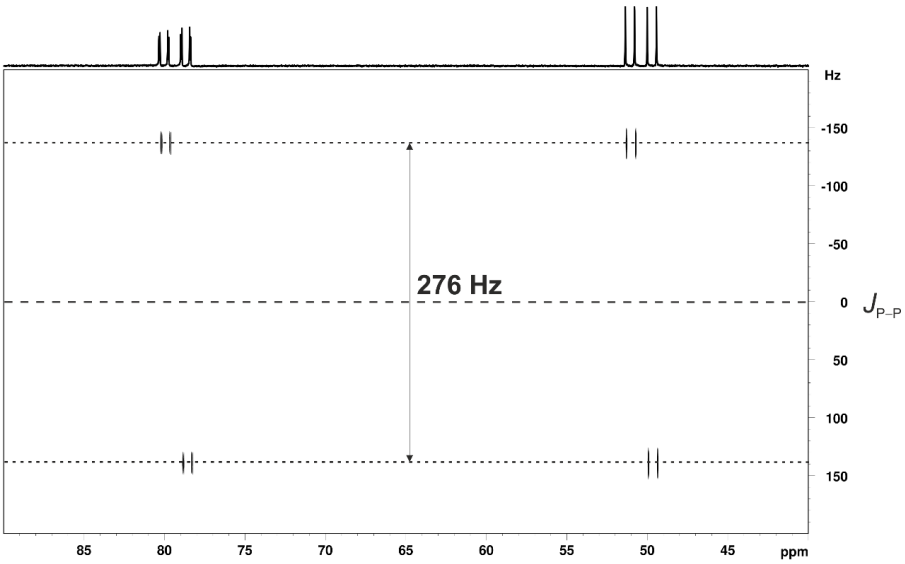

Figure 59. Two-dimensional heteronuclear $^{31}P\{^{1}H\}$ *J*-resolved NMR experiment (202 MHz, CD_2Cl_2) for complex **4**.

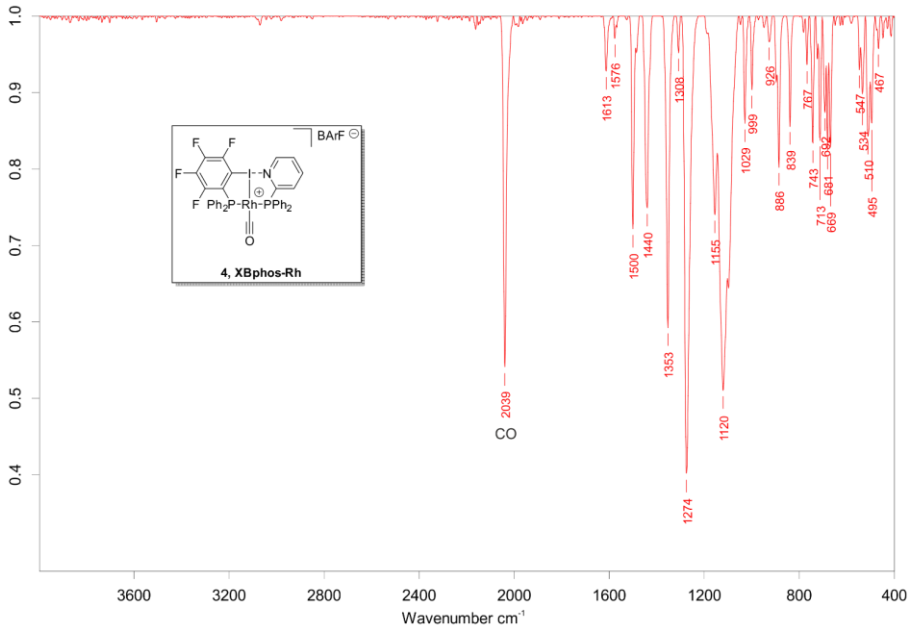

Figure 60. IR spectrum for complex **4**.

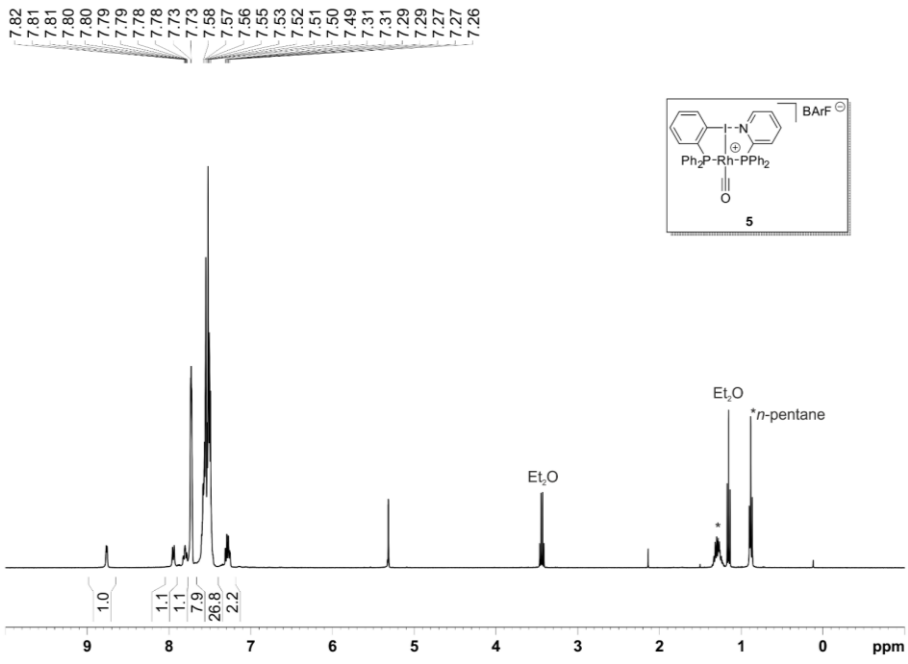

Figure 61. ^{1}H NMR spectrum (400 MHz, CD_2Cl_2) for complex **5**.

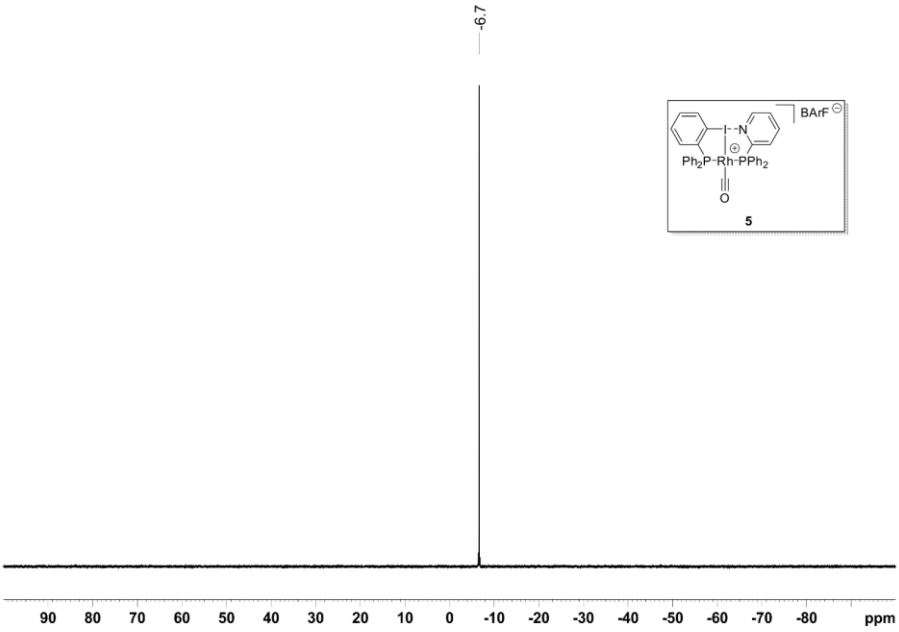

Figure 62. $^{11}B\{^1H\}$ NMR spectrum (128 MHz, CD_2Cl_2) for complex **5**.

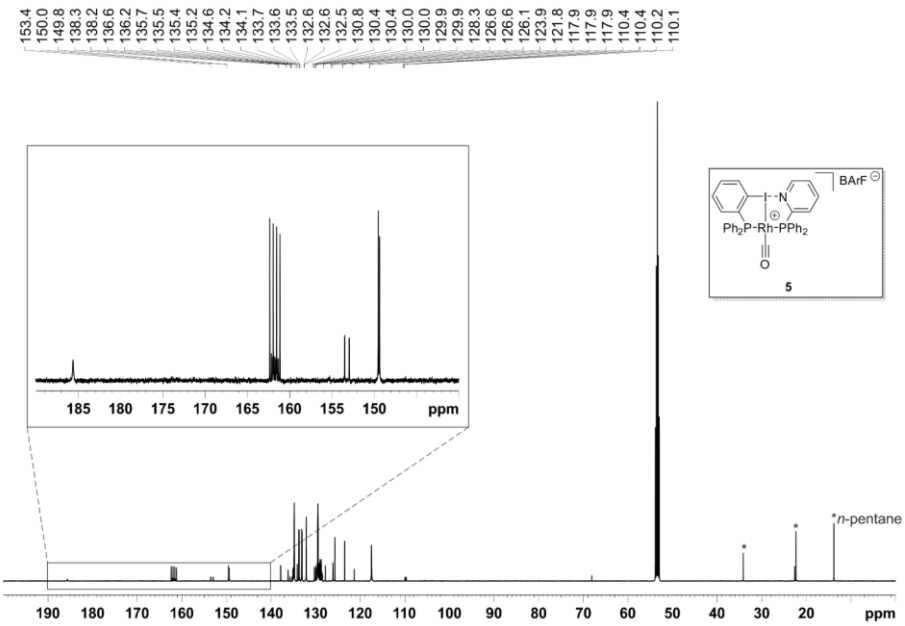

Figure 63. $^{13}C\{^1H\}$ NMR spectrum (126 MHz, CD_2Cl_2) for complex **5**.

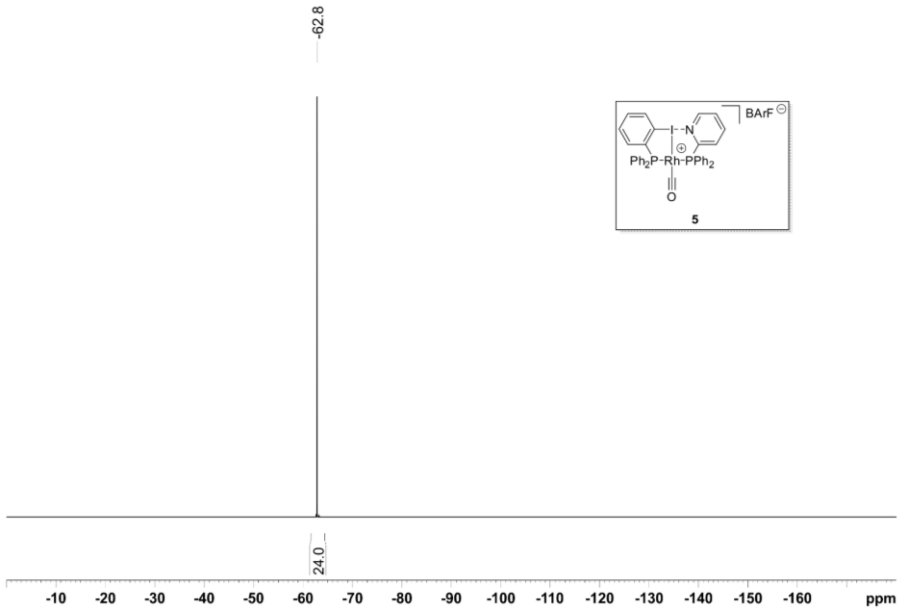

Figure 64. $^{19}F\{^{1}H\}$ NMR spectrum (471 MHz, CD_2Cl_2) for complex **5**.

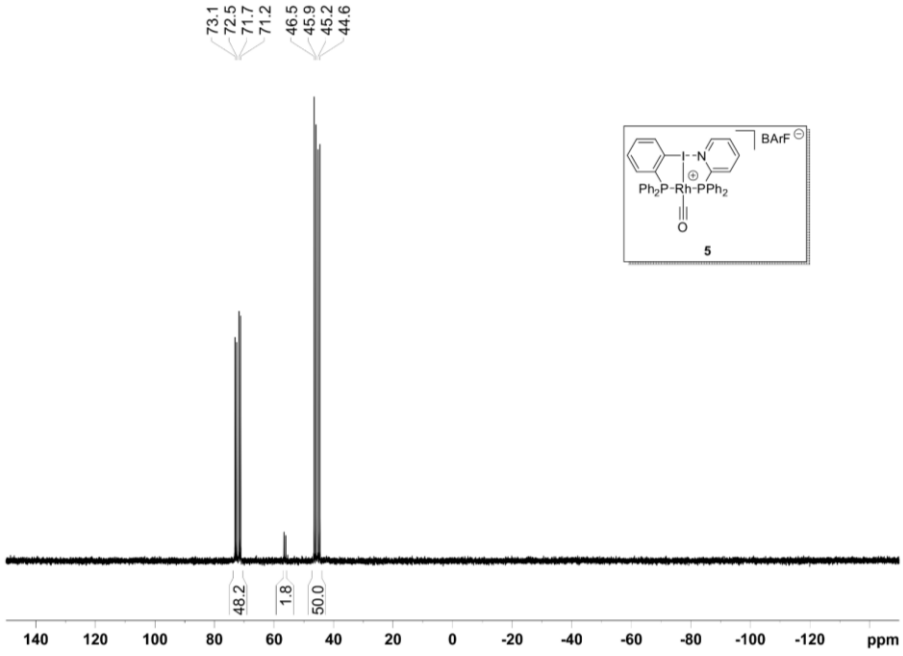

Figure 65. $^{31}P\{^{1}H\}$ IGD (inverse gated decoupled) NMR spectrum (202 MHz, CD_2Cl_2) for complex **5**.

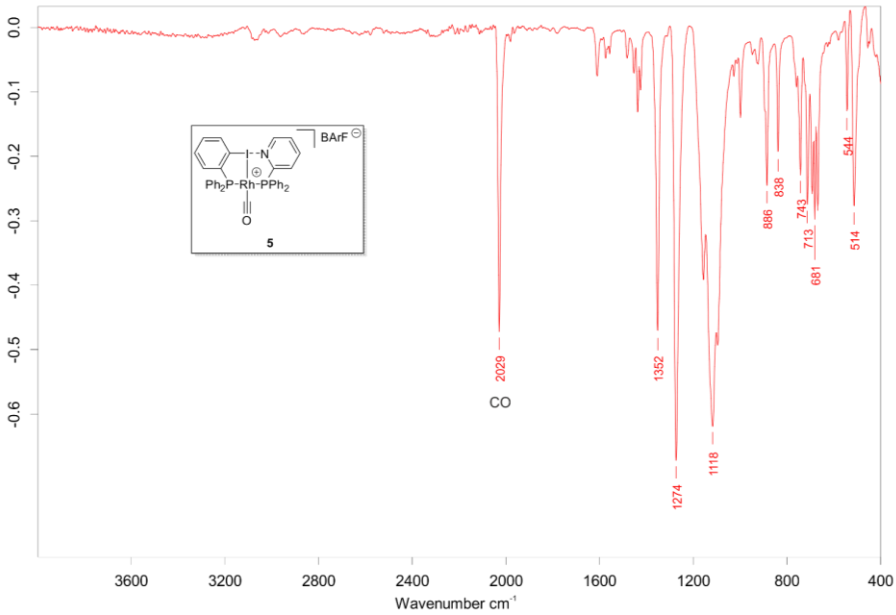

Figure 66. IR spectrum for complex **5**.

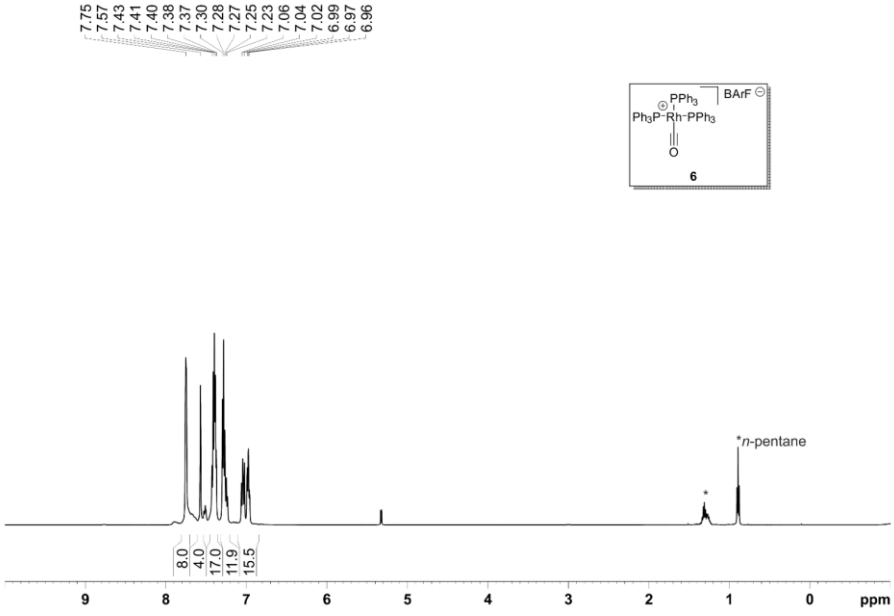

Figure 67. ^{1}H NMR spectrum (500 MHz, CD_2Cl_2) for complex **6**.

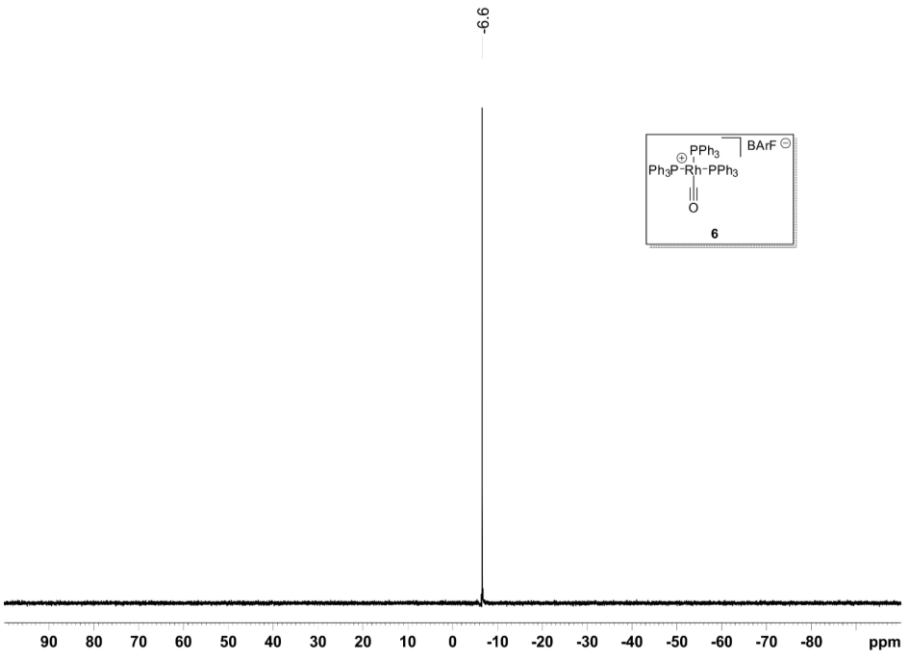

Figure 68. $^{11}B\{^1H\}$ NMR spectrum (128 MHz, CD_2Cl_2) for complex **6**.

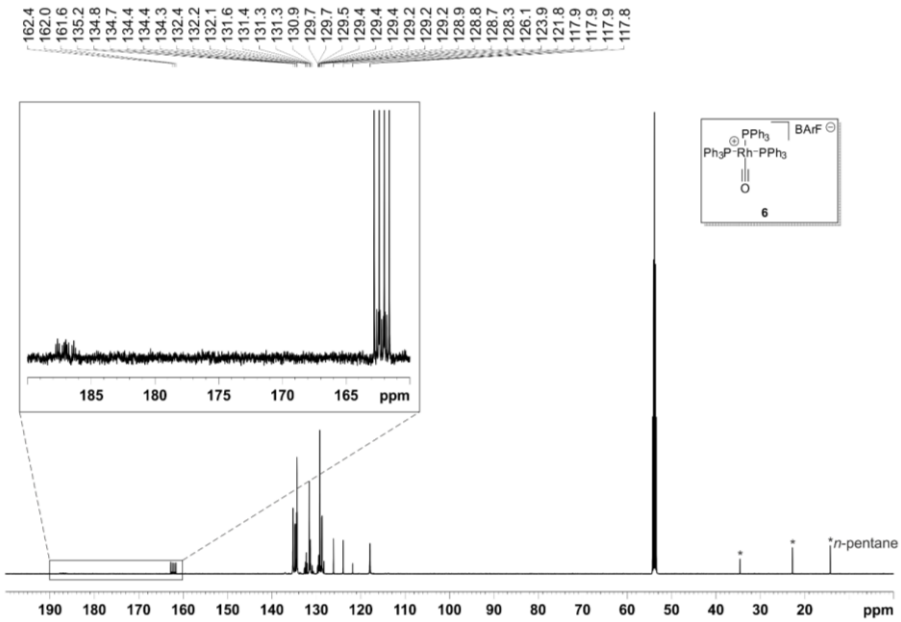

Figure 69. $^{13}C\{^1H\}$ spectrum NMR (126 MHz, CD_2Cl_2) for complex **6**.

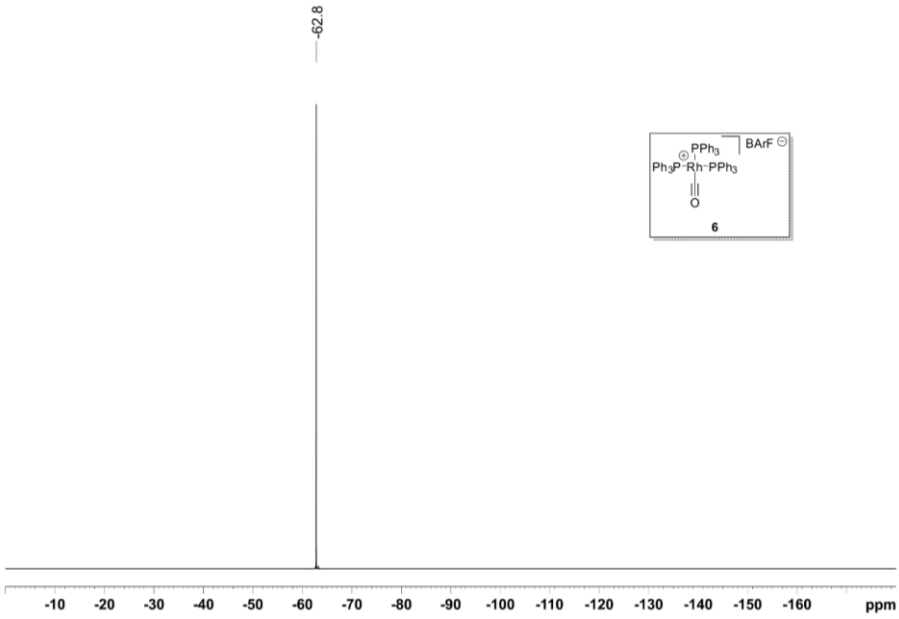

Figure 70. $^{19}F\{^{1}H\}$ NMR spectrum (471 MHz, CD_2Cl_2) for complex **6**.

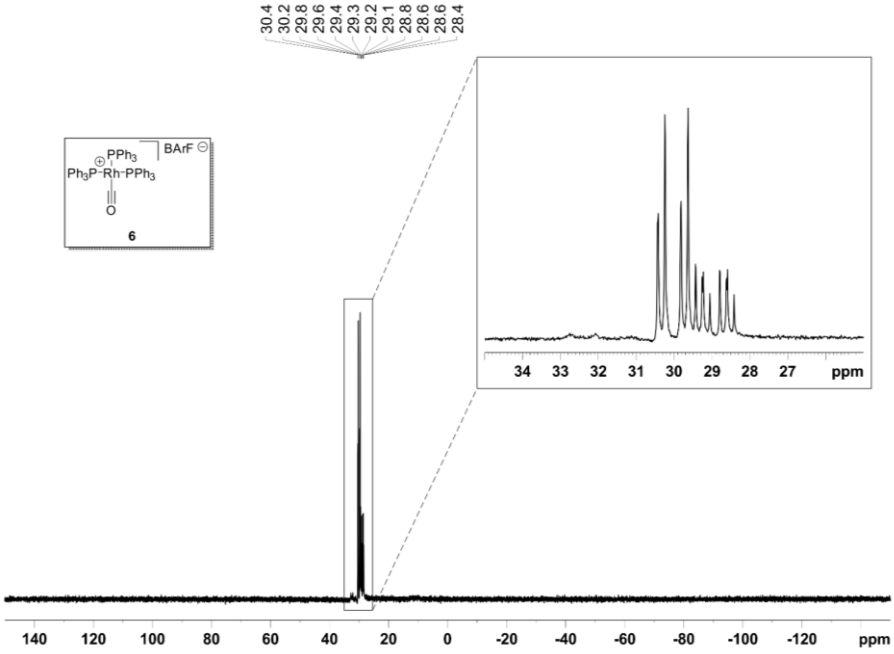

Figure 71. $^{31}P\{^{1}H\}$ NMR spectrum (202 MHz, CD_2Cl_2) for complex **6**.

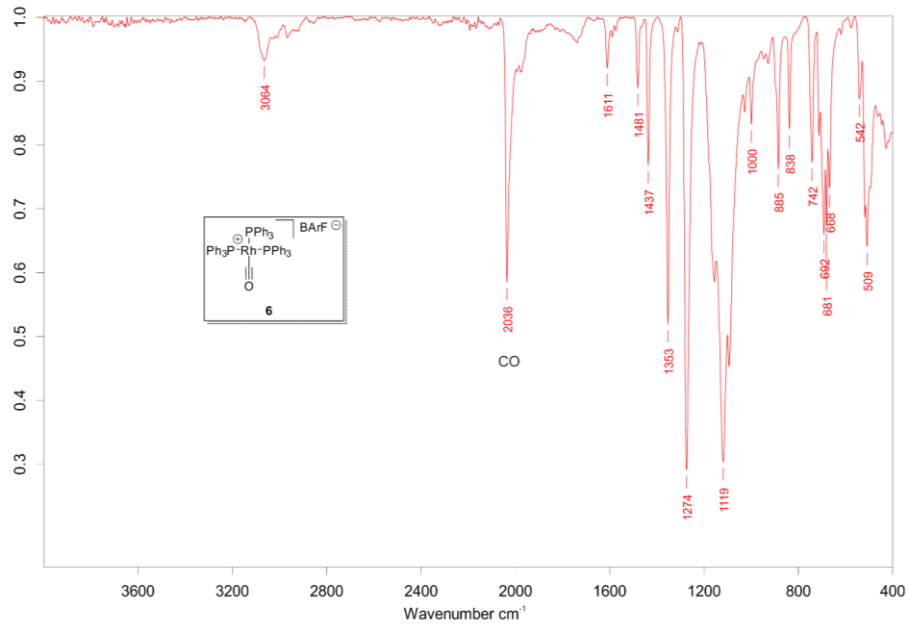

Figure 72. IR spectrum for complex **6**.

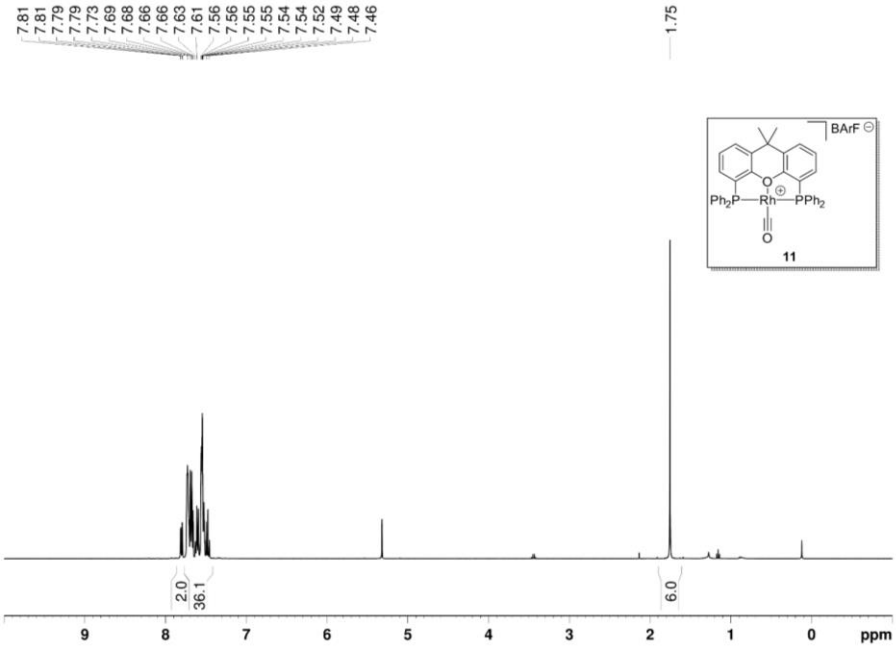

Figure 73. ^{1}H NMR spectrum (400 MHz, CD_2Cl_2) for complex **11**.

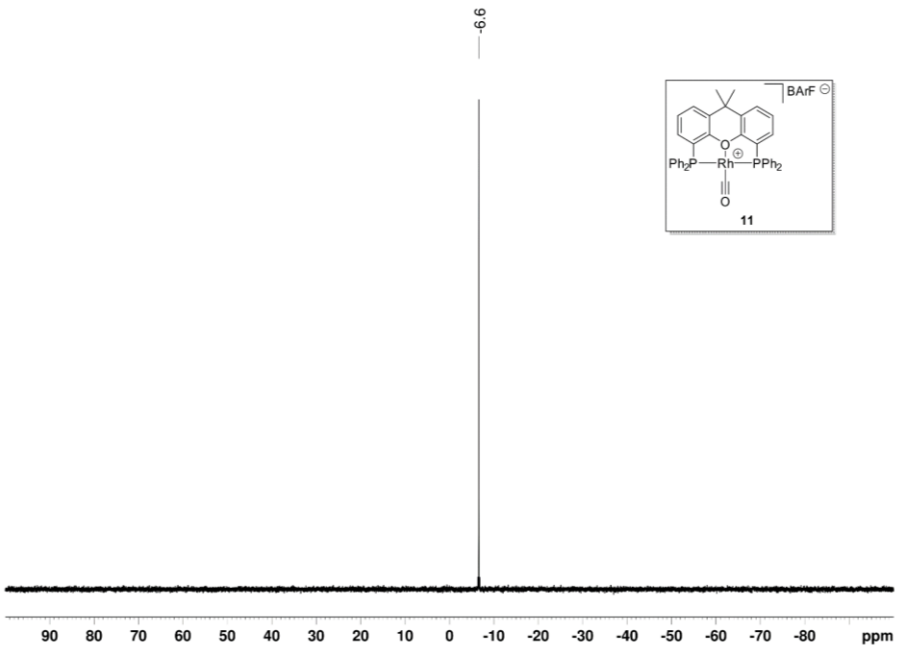

Figure 74. $^{11}B\{^1H\}$ NMR spectrum (128 MHz, CD_2Cl_2) for complex **11**.

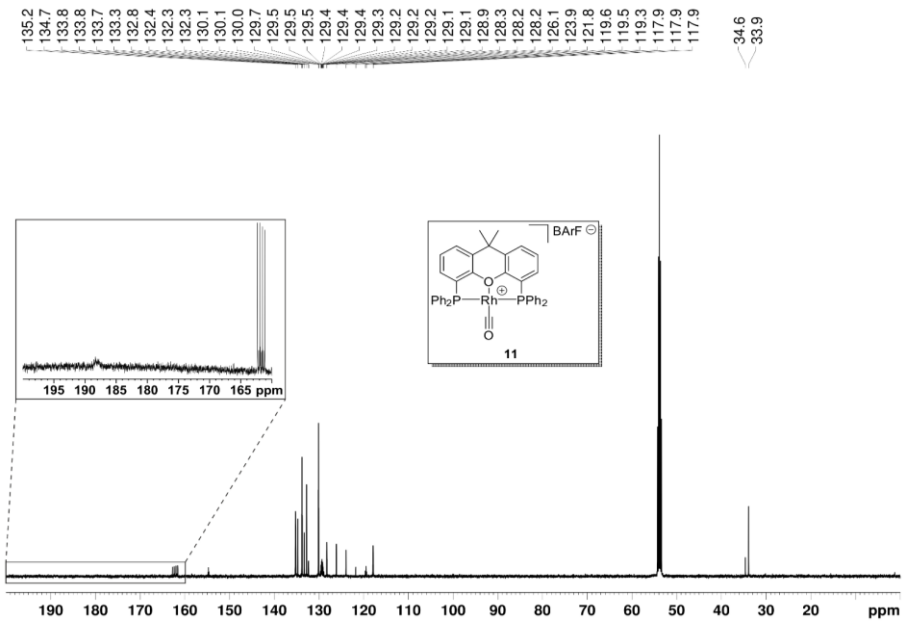

Figure 75. $^{13}C\{^1H\}$ NMR spectrum (126 MHz, CD_2Cl_2) for complex **11**.

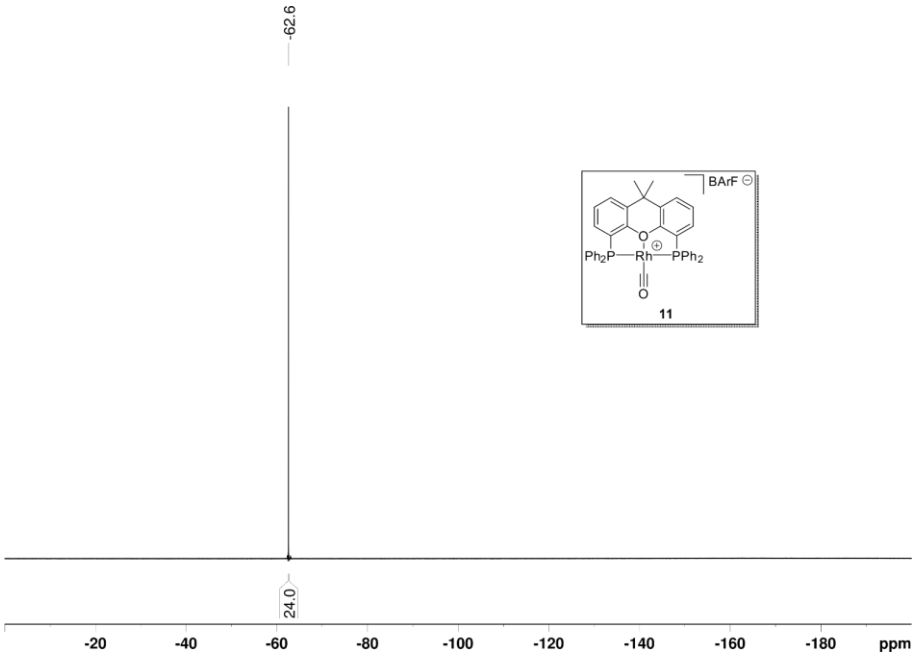

Figure 76. $^{19}F\{^{1}H\}$ NMR spectrum (376 MHz, CD_2Cl_2) for complex **11**.

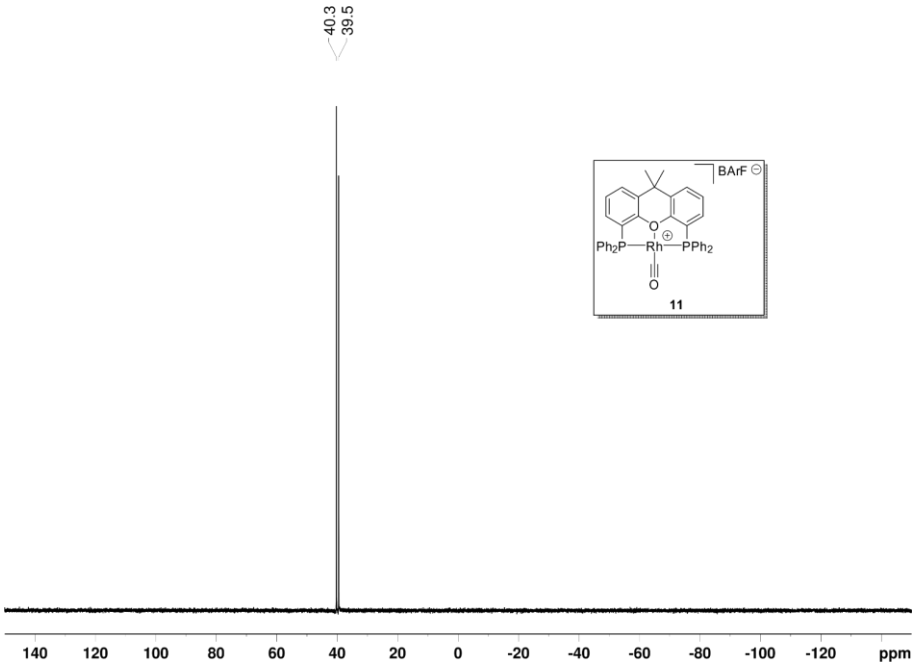

Figure 77. $^{31}P\{^{1}H\}$ NMR spectrum (162 MHz, CD_2Cl_2) for complex **11**.

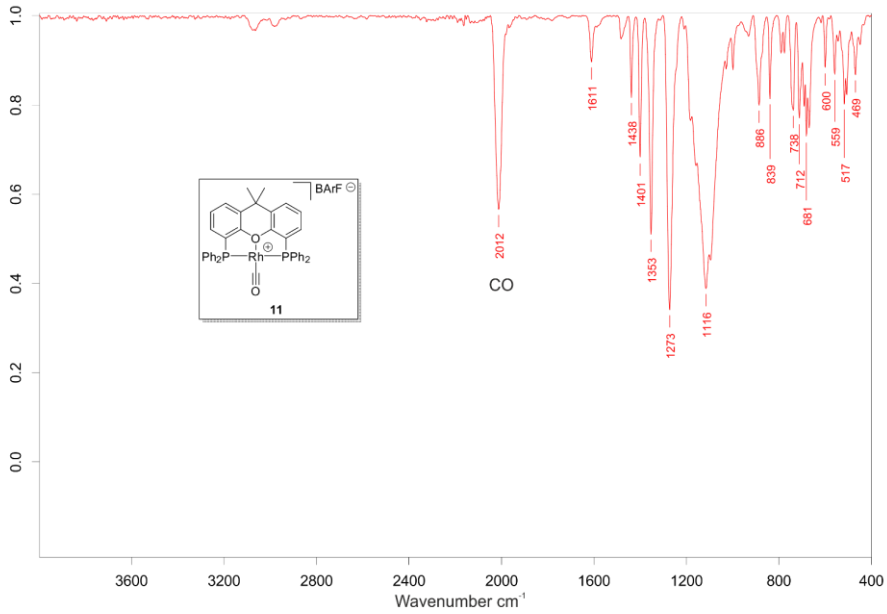

Figure 78. IR spectrum for complex **11**.

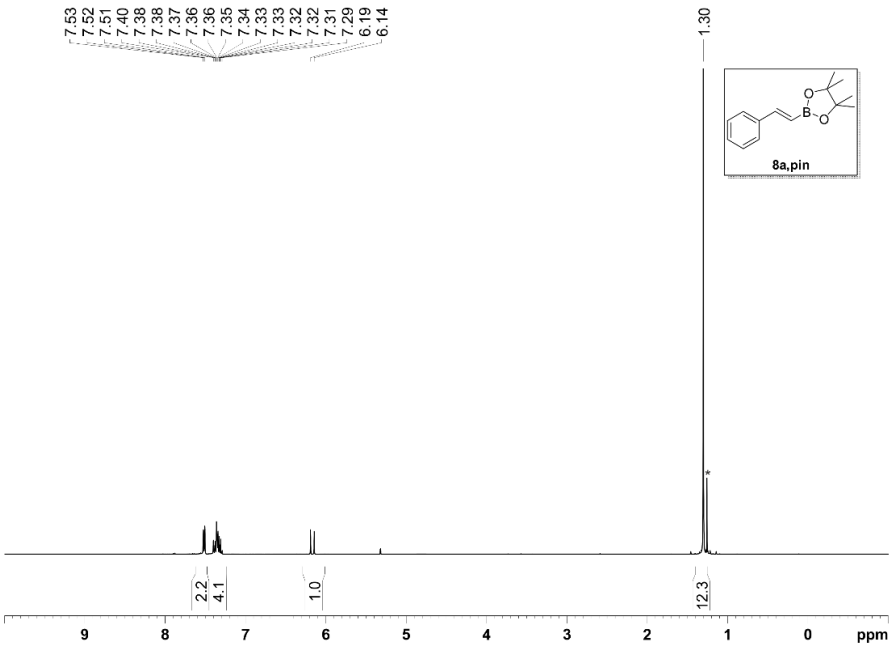

Figure 79. ^{1}H NMR spectrum (400 MHz, CD_2Cl_2) for product **8a,pin**.

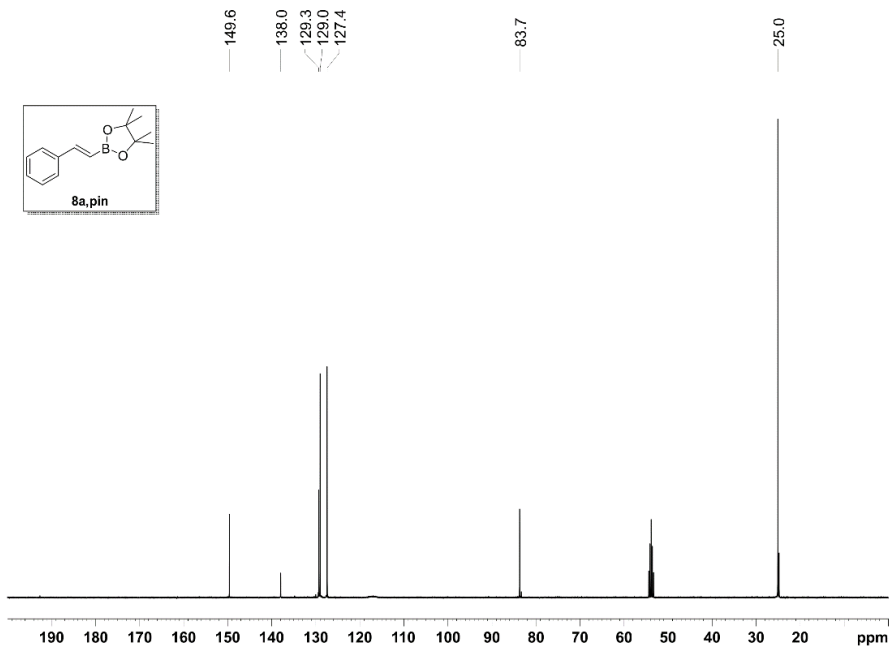

Figure 80. $^{13}C\{^{1}H\}$ NMR spectrum (100 MHz, CD_2Cl_2) for product **8a,pin**.

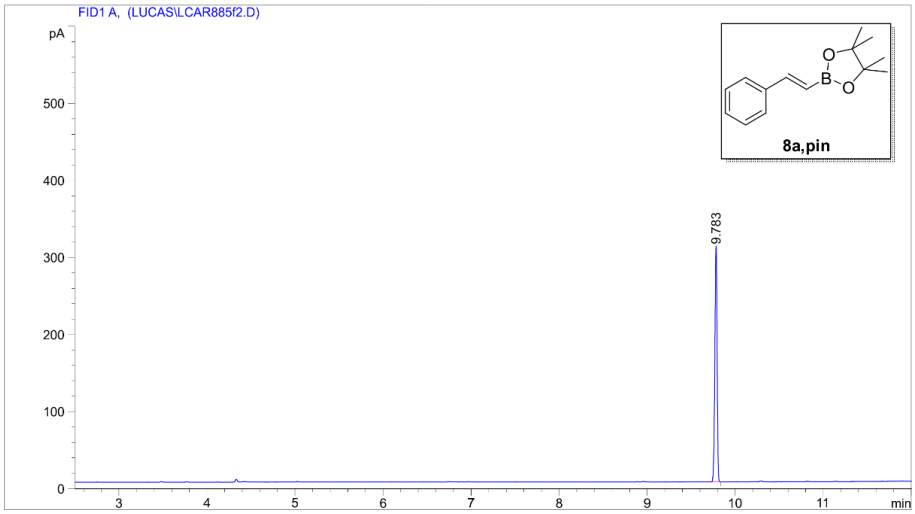

Figure 81. GC-FID chromatogram for product **8a,pin**.

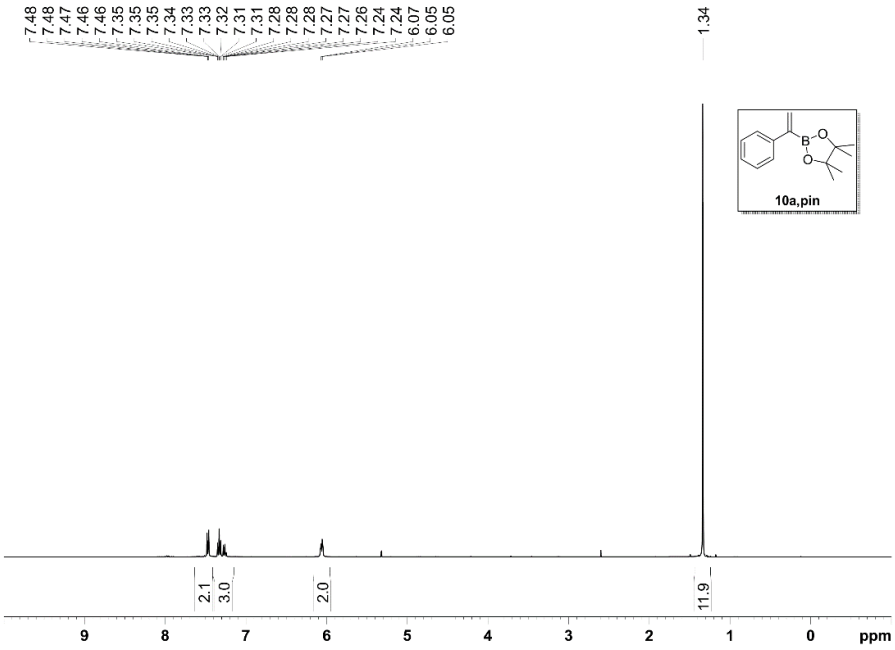

Figure 82. ^{1}H NMR spectrum (400 MHz, CD_2Cl_2) for product **10a,pin**.

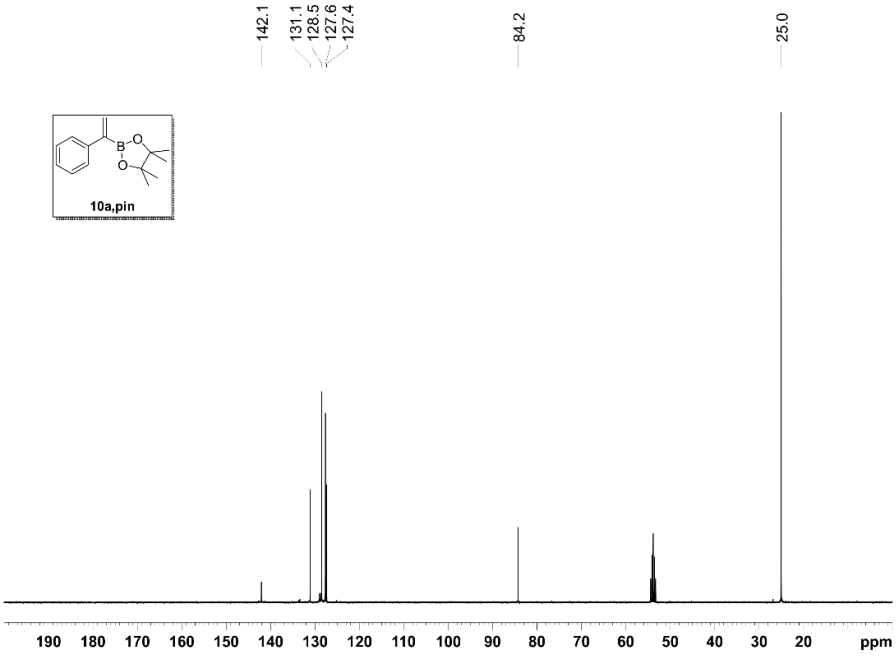

Figure 83. $^{13}C\{^{1}H\}$ NMR spectrum (100 MHz, CD_2Cl_2) for product **10a,pin**.

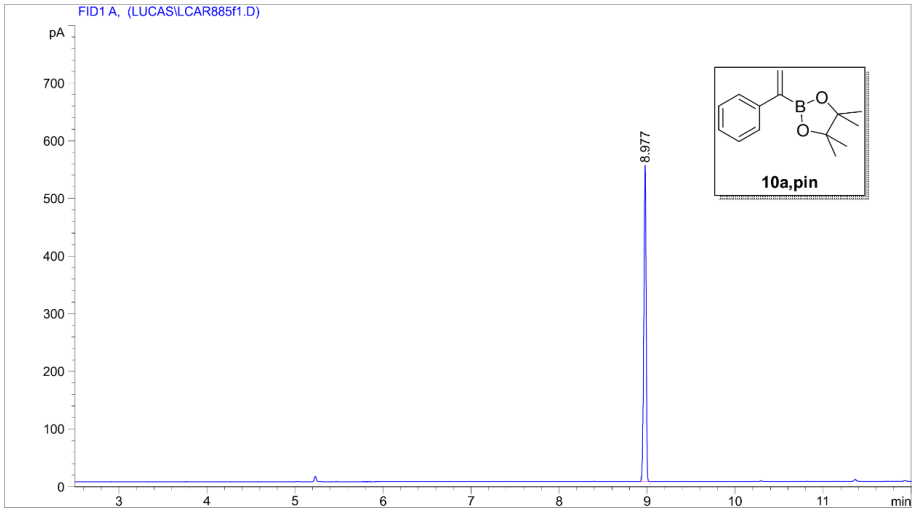

Figure 84. GC-FID chromatogram for product **10a,pin**.

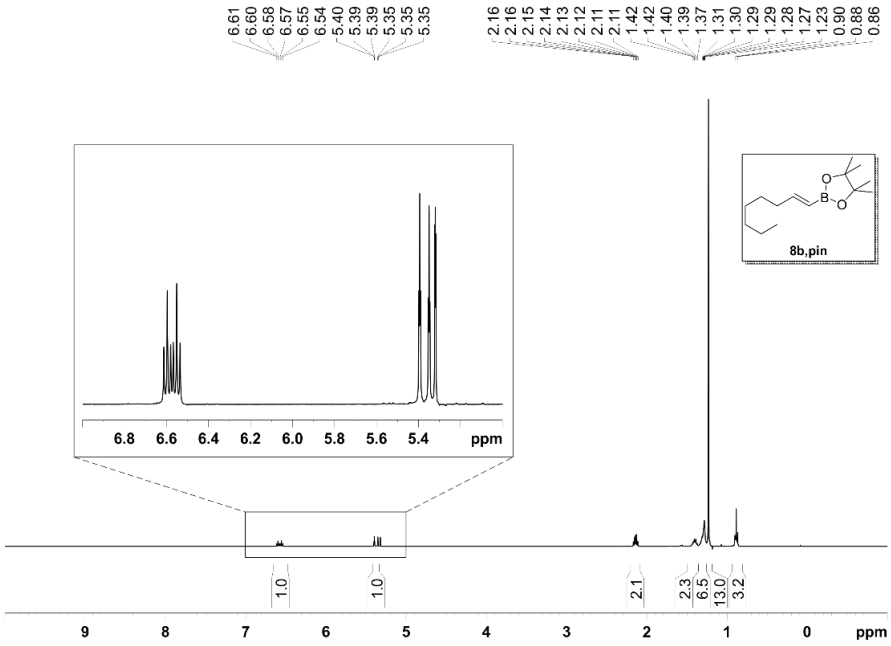

Figure 85. ^{1}H NMR spectrum (400 MHz, CD_2Cl_2) for product **8b,pin**.

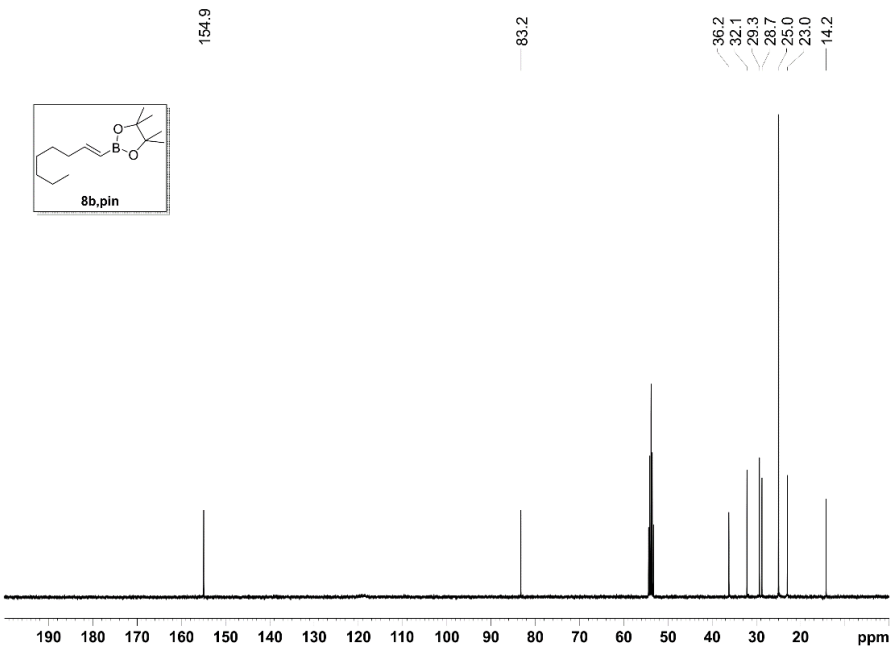

Figure 86. $^{13}C\{^{1}H\}$ NMR spectrum (100 MHz, CD_2Cl_2) for product **8b,pin**.

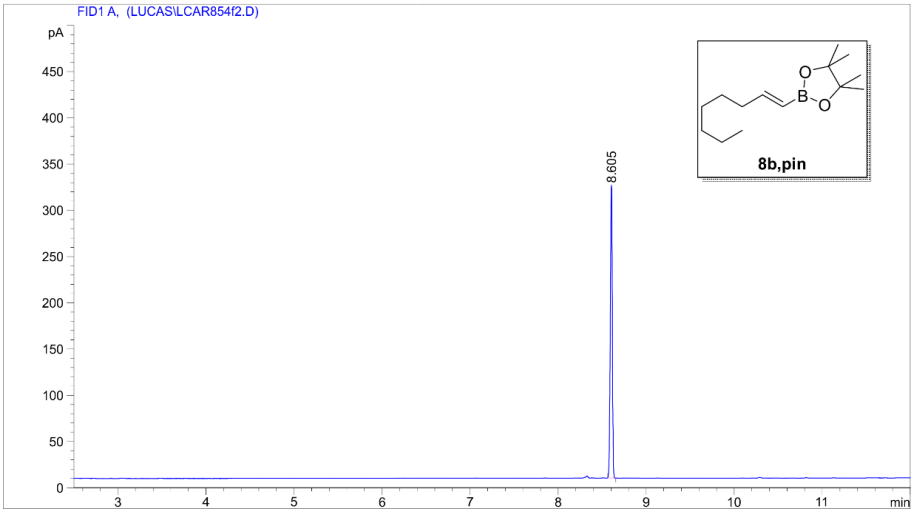

Figure 87. GC-FID chromatogram for product **8b,pin**.

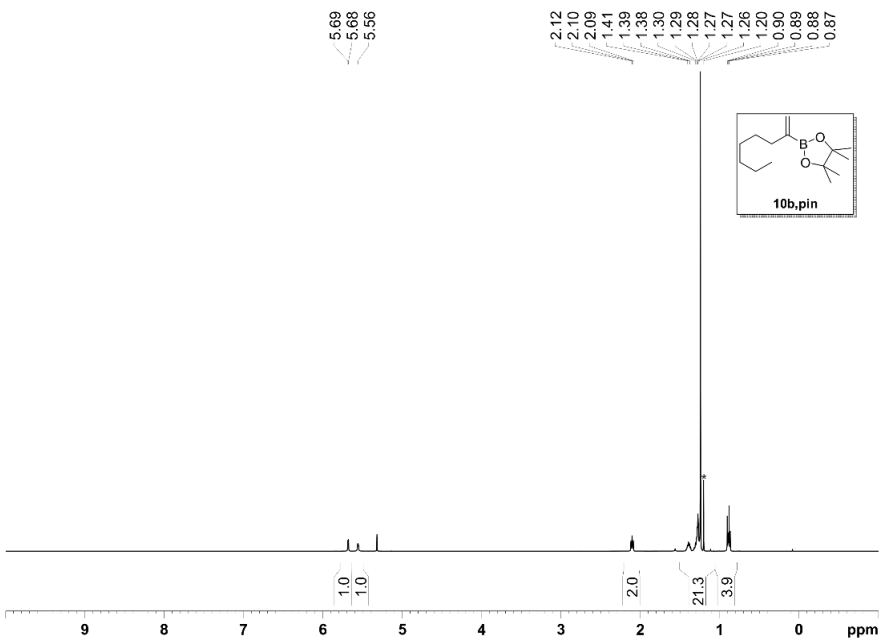

Figure 88. ^{1}H NMR spectrum (400 MHz, CD_2Cl_2) for product **10b,pin**.

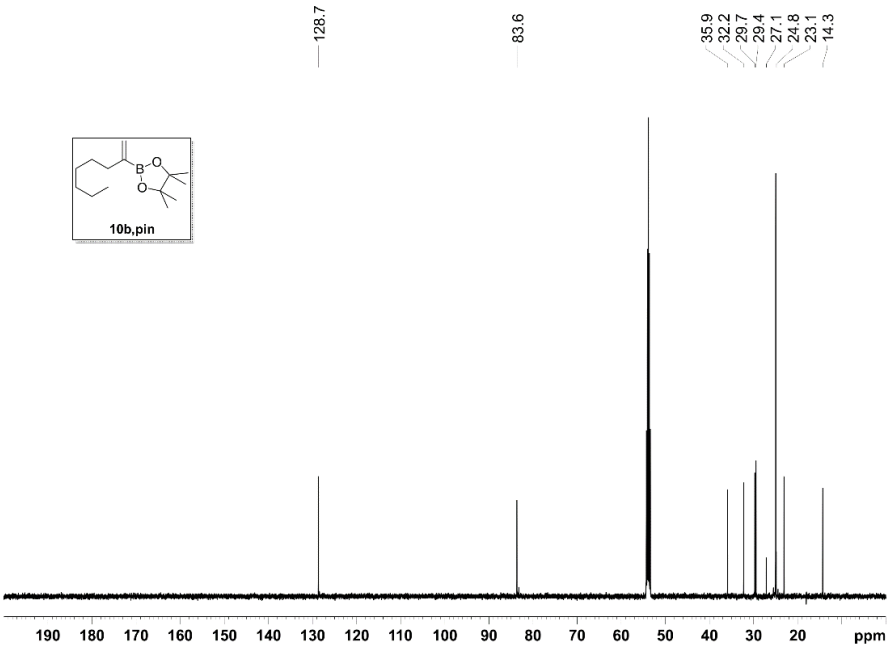

Figure 89. $^{13}C\{^{1}H\}$ NMR spectrum (100 MHz, CD_2Cl_2) for product **10b,pin**.

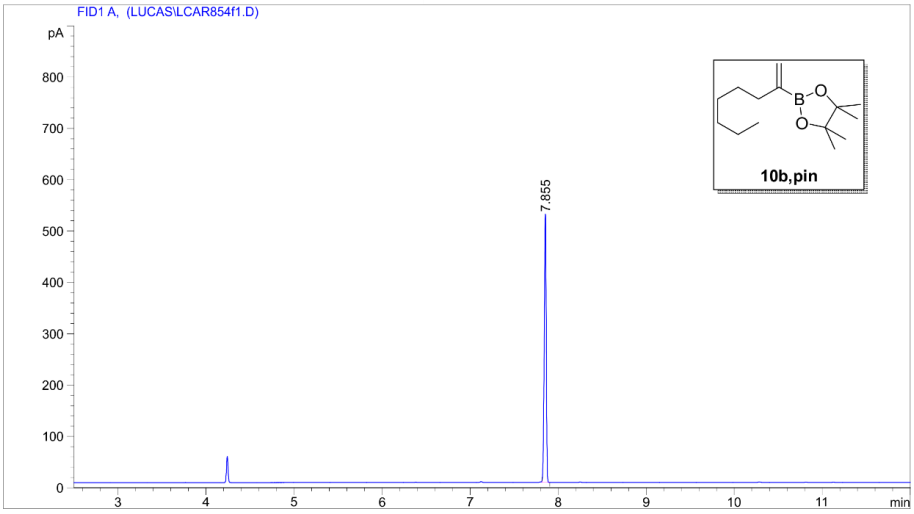

Figure 90. GC-FID chromatogram for product **10b,pin**.

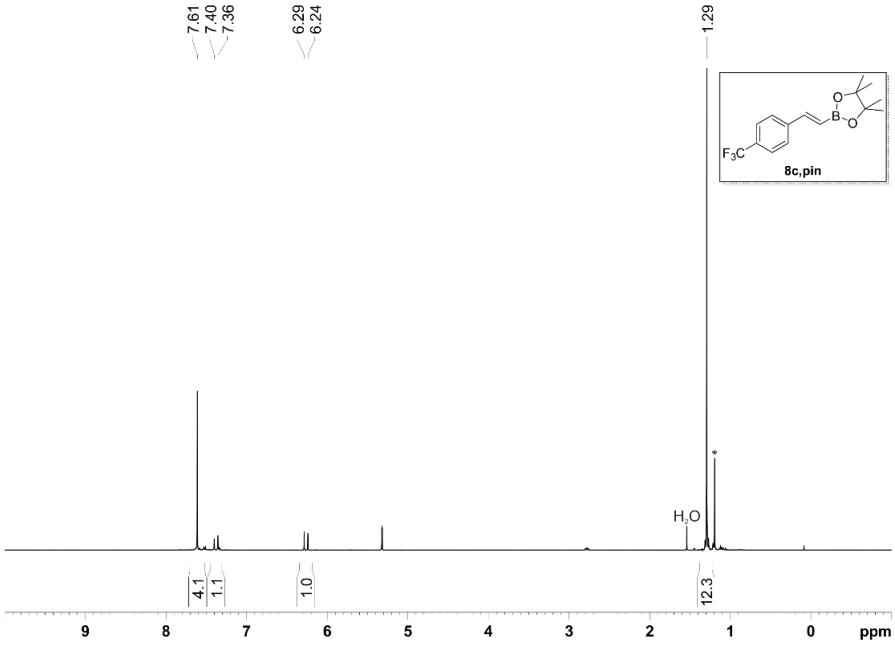

Figure 91. ^{1}H NMR spectrum (400 MHz, CD_2Cl_2) for product **8c,pin**.

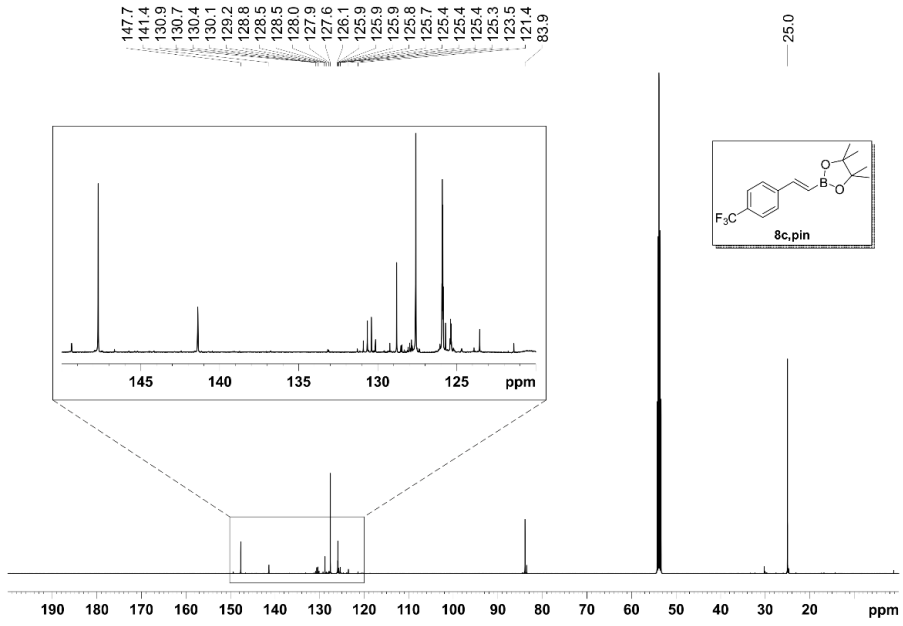

Figure 92. $^{13}C\{^{1}H\}$ NMR spectrum (126 MHz, CD_2Cl_2) for product **8c,pin**.

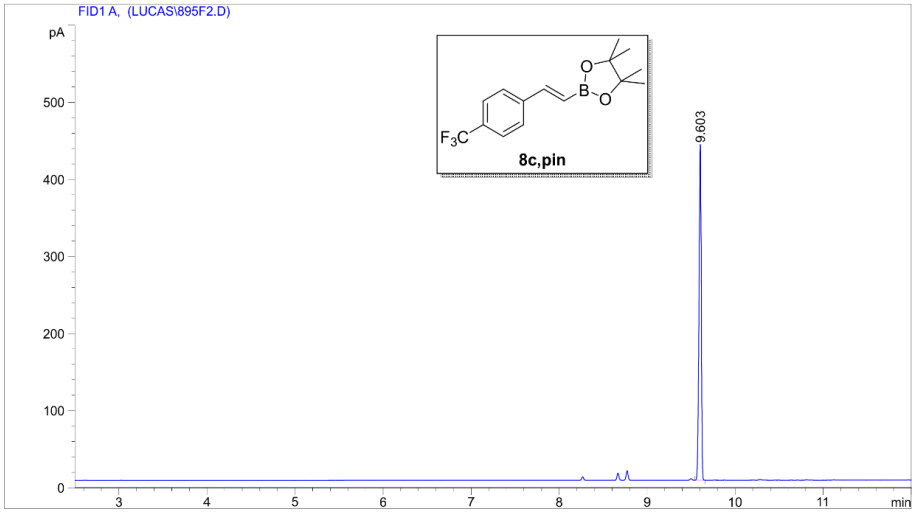

Figure 93. GC-FID chromatogram for product **8c,pin**.

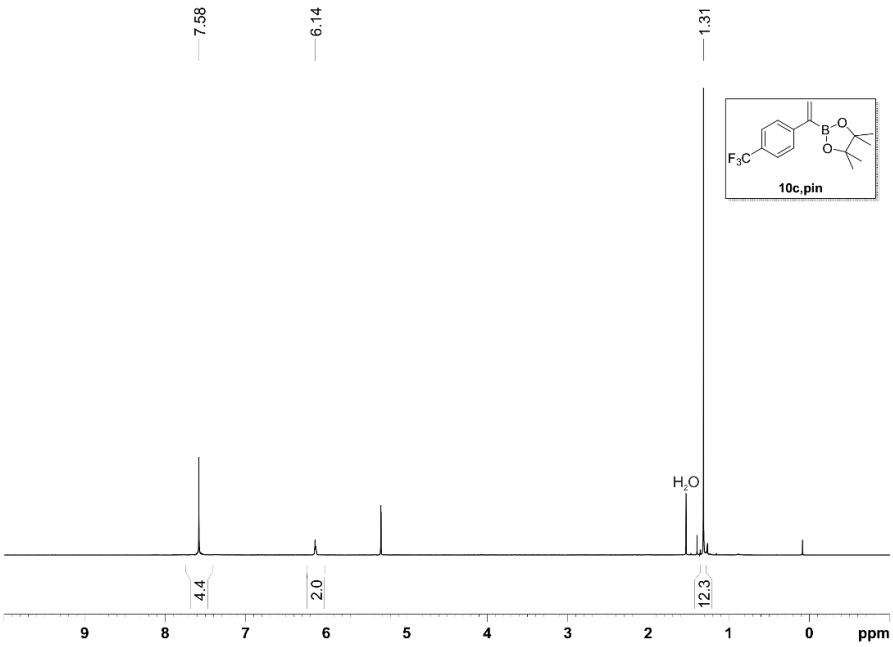

Figure 94. ^{1}H NMR spectrum (400 MHz, CD_2Cl_2) for product **10c,pin**.

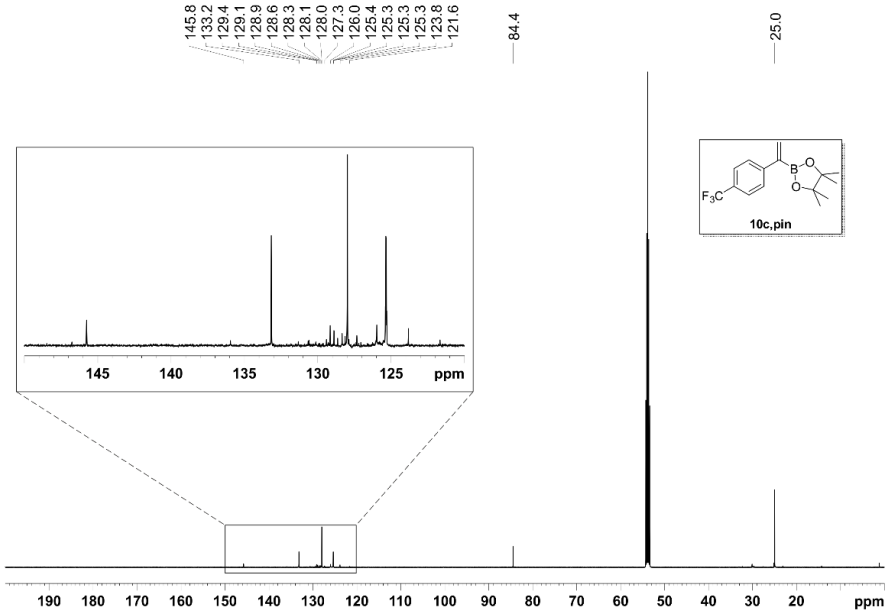

Figure 95. $^{13}C\{^{1}H\}$ NMR spectrum (126 MHz, CD_2Cl_2) for product **10c,pin**.

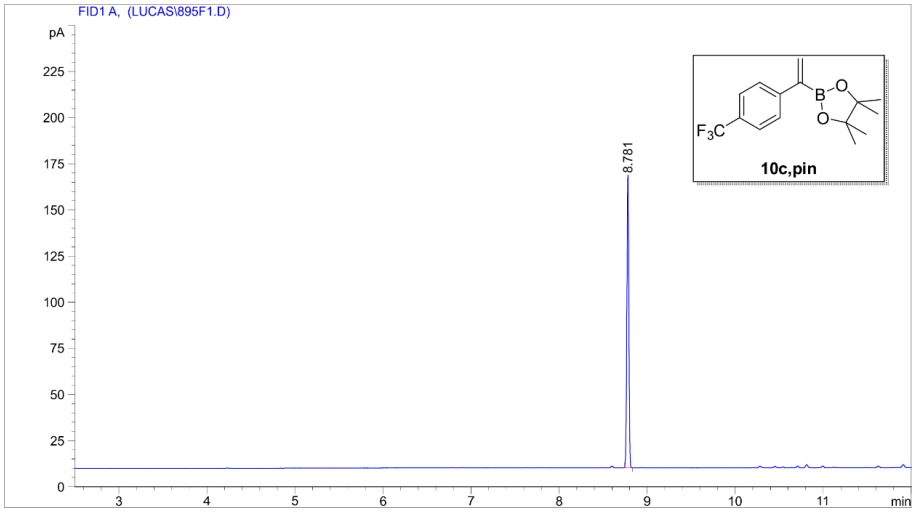

Figure 96. GC-FID chromatogram for product **10c,pin**.

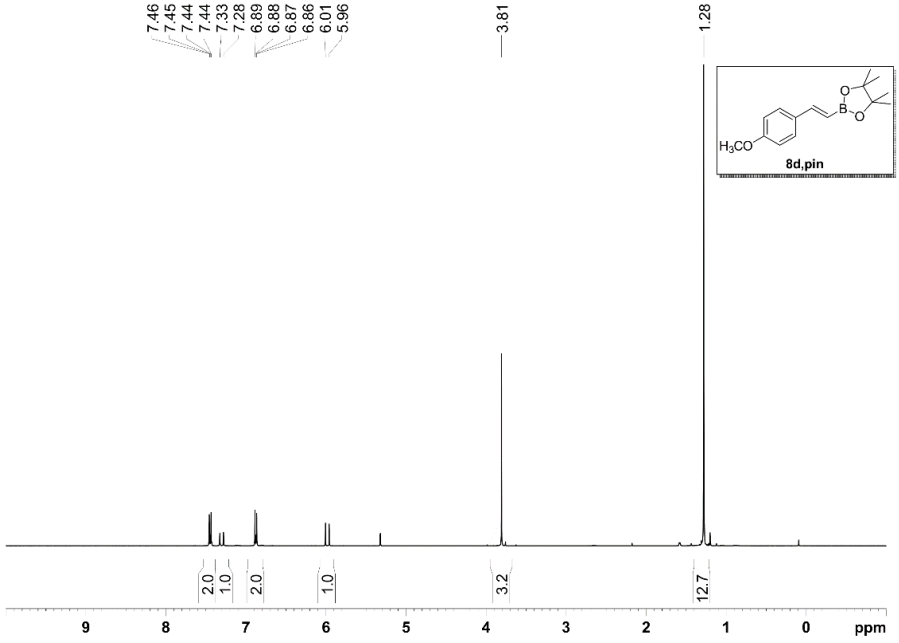

Figure 97. ^{1}H NMR spectrum (400 MHz, CD_2Cl_2) for product **8d,pin**.

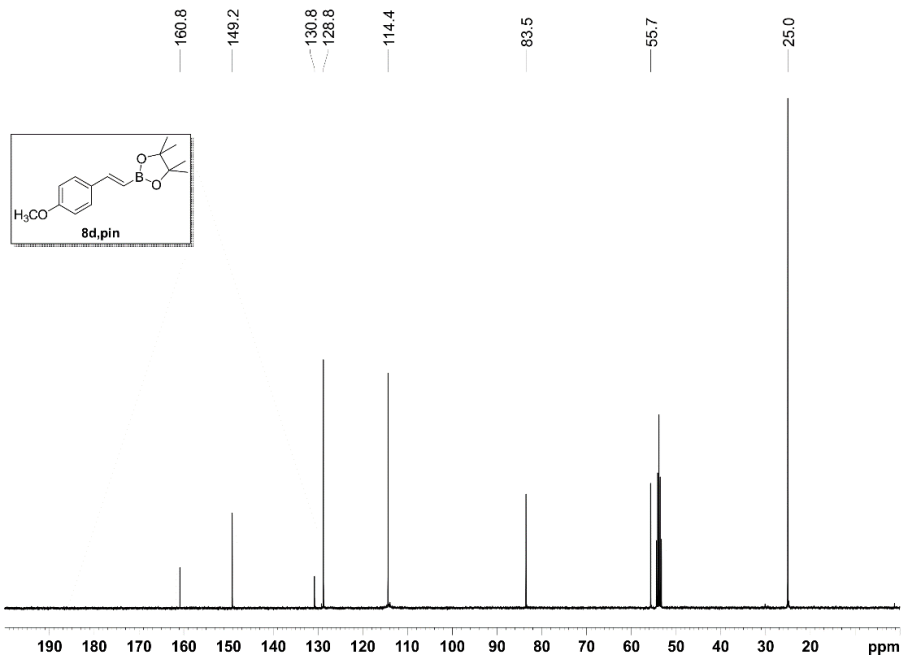

Figure 98. $^{13}C\{^{1}H\}$ NMR spectrum (100 MHz, CD_2Cl_2) for product **8d,pin**.

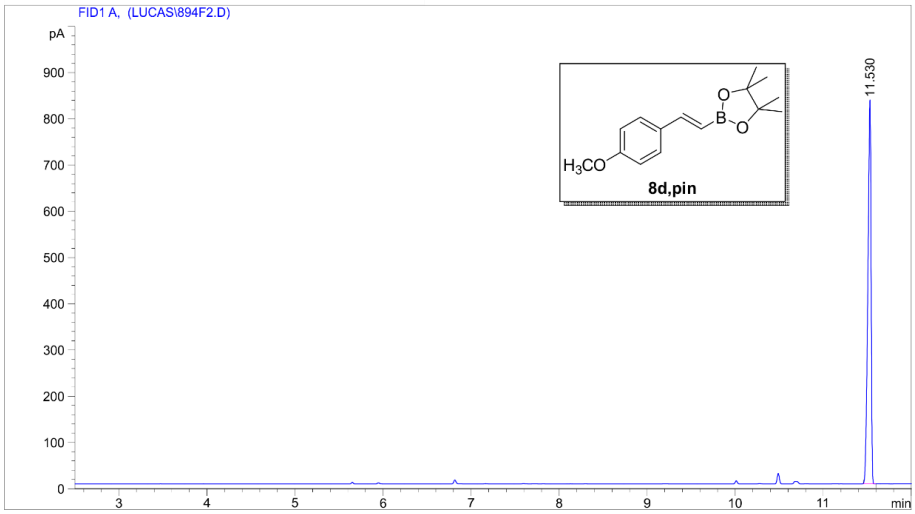

Figure 99. GC-FID chromatogram for product **8d,pin**.

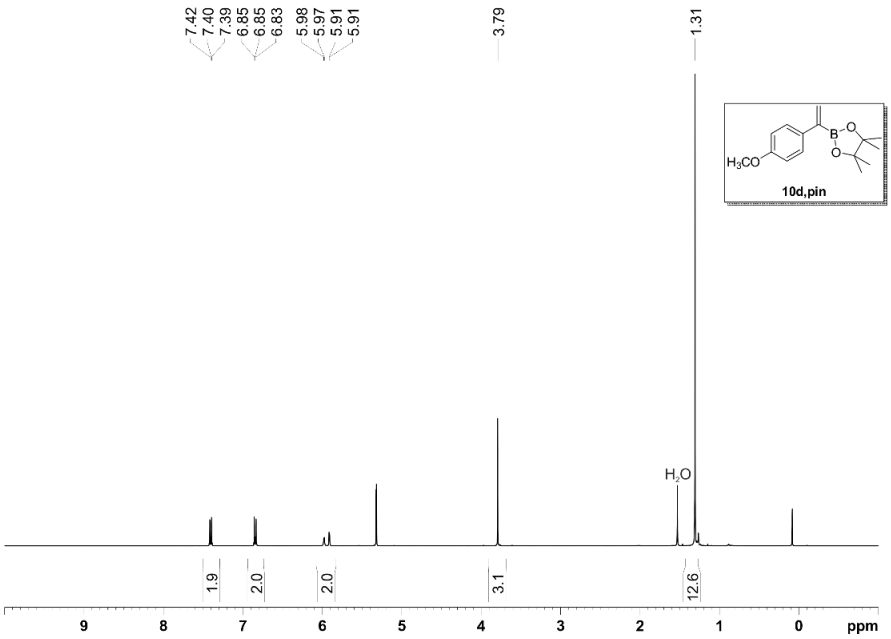

Figure 100. ^{1}H NMR spectrum (400 MHz, CD_2Cl_2) for product **10d,pin**.

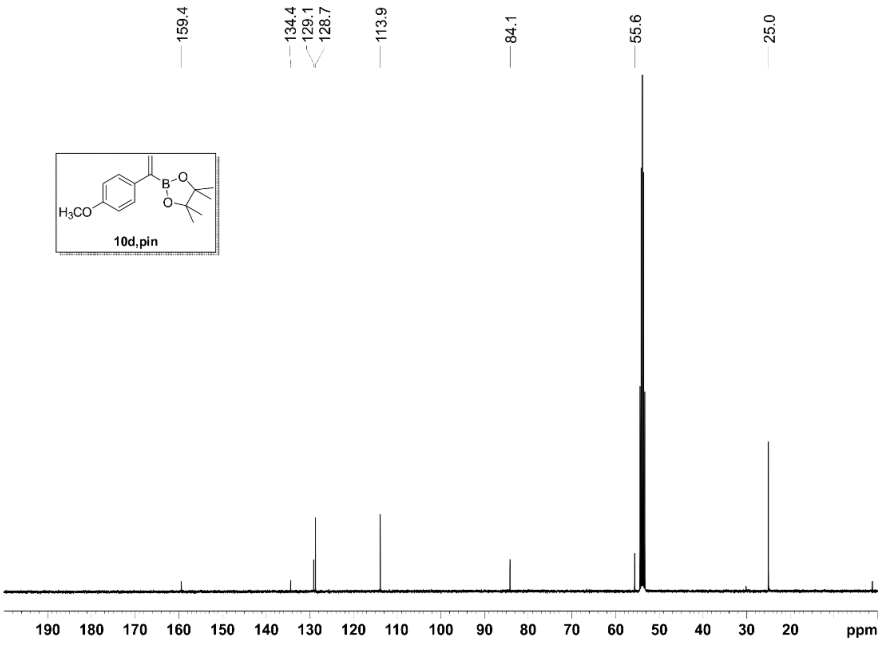

Figure 101. $^{13}C\{^{1}H\}$ NMR spectrum (100 MHz, CD_2Cl_2) for product **10d,pin**.

Figure 102. GC-FID chromatogram for product **10d,pin**.

CHAPTER II

Halogen Bonding Effects on the Outcome of Reactions at Rhodium

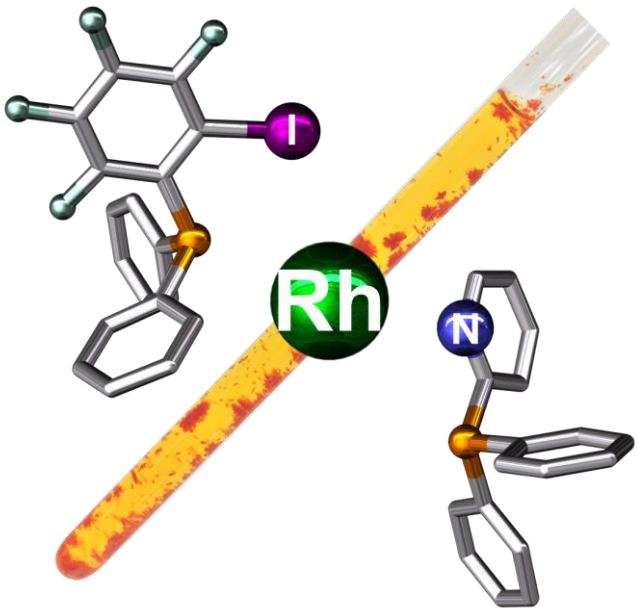

Halogen Bonding Effects on the Outcome of Reactions at Rhodium

Chem. Commun. **2019**, *55*, 2380-2383

Lucas Carreras,[a,b] Jordi Benet-Buchholz,[b] Antonio Franconetti,[c] Antonio Frontera,[c] Piet W. N. M. van Leeuwen,[d] and Anton Vidal-Ferran[b,e]*

a Universitat Rovira i Virgili, Departament de Química Analítica i Química Orgànica, C. Marcel·lí Domingo 1, 43007, Tarragona, Spain.
b Institut Català d'Investigació Química (ICIQ) & Barcelona Institute of Science and Technology (BIST), Av. Països Catalans 16, 43007, Tarragona, Spain.
c Universitat de les Illes Balears, Departament de Química, Crta. de Valldemossa km 7.5, 07122, Palma de Mallorca, Spain.
d Laboratoire de Physique et Chimie des Nano-Objets (LPCNO), Institut National des Sciences Appliquées (INSA), Av. De Rangueil, F-31077, Toulouse, France.
e Institució Catalana de Recerca i Estudis Avançats (ICREA), Pg. Lluís Companys 23, 08010, Barcelona, Spain.

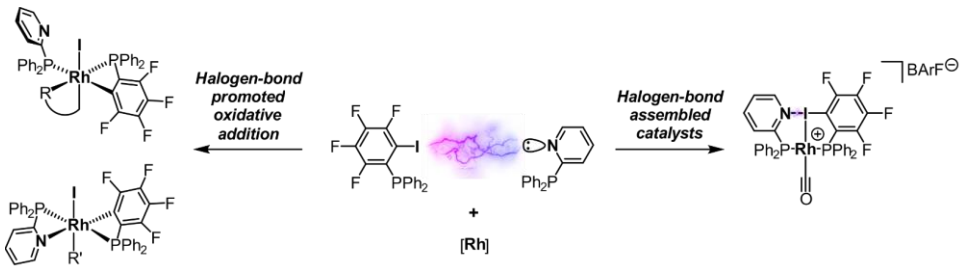

2.1. ABSTRACT

Key findings regarding the effects of ligand preorganization *via* halogen bonding on the outcome of reactions at rhodium are reported. An unprecedented halogen bonding-mediated oxidative addition of C_{Ar}–I bonds to rhodium with efficient formation of cyclometallated species deserves special mention.

2.2. INTRODUCTION

Halogen bond has been under the spotlight as a promising non-conventional supramolecular interaction, resembling hydrogen bonding

in many aspects but becoming a genuine non-covalent interaction due to its inherent features.[7] In contrast to the numerous reports of halogen bonding applied to crystal engineering[17] or functional materials,[18,19] its application to solution chemistry has progressed at a much slower pace and mainly involves molecular recognition events[20] and organocatalysis processes.[21] In sharp contrast, transition metal-based catalysis remained residual, and rational design of halogen bonding metal catalysts was inexistent. As discussed in the previous chapter, our group has pioneered the use of halogen bonding as the driving force to construct the backbone of rhodium chelates, successfully using the resulting Rh(I) complexes as efficient catalysts for the hydroboration of terminal alkynes. This breakthrough in the use of halogen bonding for easily constructing metal catalysts prompted us to further explore the use of this interaction for influencing the coordination sphere at the metal center. By expanding the structural diversity of our approach, we aimed to gain new insights into the reactivity of these complexes and induce transformations at the metal that would not take place in the absence of halogen bonding. Herein, we summarize our work on the formation of five- and six-coordinate rhodium complexes, in which halogen bonding drives ligand preorganization and determines the structure of the final products.

2.3. RESULTS AND DISCUSSION

The underlying strategy for the preparation of **XBphos-Rh** relied on the *in situ* formation of a putative $[Rh(CO)_2]X$ intermediate from $[Rh(Cl)(CO)_2]_2$ and a halide scavenger (*i.e.* NaBArF). Although this strategy proved to be useful for the preparation of four-coordinate rhodium complexes such as **XBphos-Rh**, herein we broaden our approach to include a wider array of rhodium precursors. We began by studying $[Rh(nbd)_2]BF_4$ as the rhodium precursor in the complexation reaction, since phosphorus-containing complexes derived from this cationic metal precursor have found wide application in pivotal organic transformations[98] such as (enantioselective)

(98) For selected examples, see: (a) Togni, A.; Breutel, C.; Schnyder, A.; Spindler, F.; Landert, H.; Tijani, A. *J. Am. Chem. Soc.* **1994**, *116*, 4062-4066. (b) Yamanoi, Y.; Imamoto, T. *J. Org. Chem.* **1999**, *64*, 2988-2989. (c) Imamoto, T.; Sugita, K.; Yoshida, K. *J. Am. Chem. Soc.* **2005**, *127*, 11934-11935.

hydrogenations.[99] When an equimolar mixture of ligands **1** and **2** were added to stoichiometric amounts of $[Rh(nbd)_2]BF_4$, heterocomplex $[Rh(nbd)(\mathbf{1})(\mathbf{2})]BF_4$ **3** was isolated in 90% yield (Scheme 32). X-ray analysis confirmed the structure of the rhodium complex derived from **1** and **2** (Figure 103) as a 5-coordinate square-pyramidal complex.

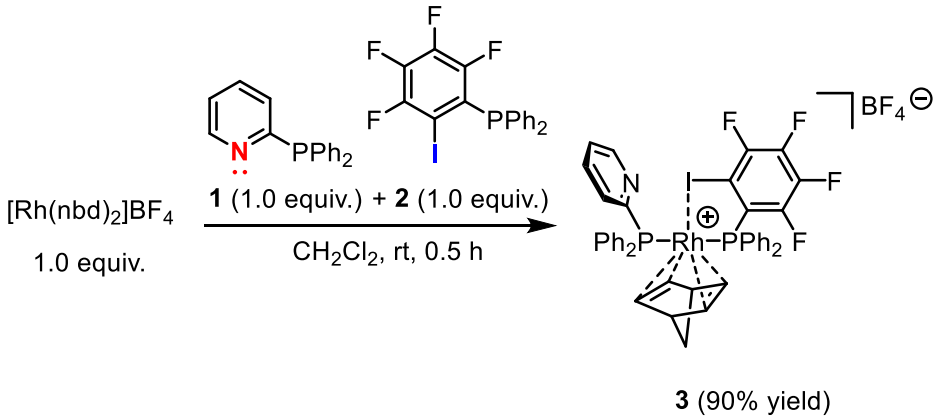

Scheme 32. Preparation of $[Rh(nbd)(\mathbf{1})(\mathbf{2})]BF_4$ complex **3**.

In addition to a coordinated norbornadiene unit, X-ray analysis also revealed phosphines **1** and **2** coordinated in a relative *cis*-arrangement as well as a I–Rh interaction in the apical position (2.7726(5) Å). This arrangement of the P-ligands containing the halogen bond donor and acceptor motifs in the slightly distorted square-pyramidal environment (P–Rh–P angle = 95.31(5)°) does not allow the required linear N···I–C alignment for effective halogen bonding (N···I–C angle = 59.1(2)°). However, preorganization of ligands **1** and **2** *via* halogen bonding interactions (*i.e. in situ* formation of supramolecular bisphosphine **1·2**) before coordination to the rhodium center may account for the high selectivity obtained in the formation of heterocomplex $[Rh(nbd)(\mathbf{1})(\mathbf{2})]BF_4$ **3** (90% yield), with the corresponding homocomplexes not being

(99) Brown, J. M. *Organometallics* **2014**, *33*, 5912-5923.

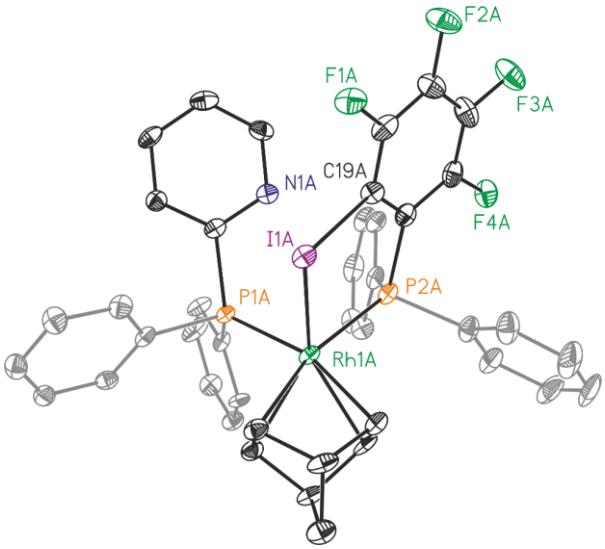

Figure 103. X-Ray structure of **3** with hydrogen atoms and the BF_4^- unit having been omitted for the sake of clarity. Color scheme: C: black, P: orange, Rh: green, F: green, N: blue, I: purple. Atomic displacement ellipsoids are drawn at a 50% probability. For crystallographic data in CIF or other electronic format see CCDC 1874508.

detected.[100] These observations are in agreement with the results of DOSY experiments of ligands **1**, **2** and a 1:1 mixture of **1** and **2**, in which the value of the diffusion coefficient of the ligand mixture is lower than the same values for free ligand **1** or **2**. A lower diffusion coefficient is associated to a larger molecular size, thus pointing to a favorable halogen-bond-mediated assembly of the two ligands in solution (see section 2.5.5 in the Experimental Section).

We then turned our attention to the use of $[Rh(acac)(CO)_2]$ as the rhodium precursor. The combination of this derivative and phosphorus ligands has been widely employed to generate active hydroformylation catalysts.[101] In this case, when an equimolar mixture of ligands **1** and **2** was added to stoichiometric amounts of $[Rh(acac)(CO)_2]$, $^{31}P\{^1H\}$ NMR analysis showed that complex [Rh(acac)(CO)(**1**)] **4** was formed, with iodo-substituted phosphine **2** remaining uncoordinated (Scheme 33).

(100) Homocomplexes $[Rh(nbd)(\mathbf{1})_2]BF_4$ or $[Rh(nbd)(\mathbf{2})_2]BF_4$ were not observed during the complexation reaction. See section 2.5.4 for details.
(101) van Leeuwen, P. W. N. M.; Claver, C., Eds. *Rhodium Catalyzed Hydroformylation*, Dordrecht, **2000**.

Therefore, we envisaged that a stepwise coordination protocol using first ligand **2** followed by phosphine **1** could lead to the target complex [Rh(acac)(**1**)(**2**)]. The reaction between [Rh(acac)$(CO)_2$] and ligand **2** efficiently led to complex [Rh(acac)(CO)(**2**)] **5**, which was successfully isolated. Unfortunately, the reaction of **5** with equimolar amounts of the ligand **1** reverted to complex **4** (Scheme 34) by ligand displacement. The halogen bonding interaction between ligands **1** and **2** does not appear to be strong enough to displace the acetylacetonato or carbonyl ligands. Furthermore, the lower donicity of the phosphorus electron pair in **2** (see section 2.5.6 for the determination of the Tolman electronic parameter[102] and the percent buried volume[103]) compared to **1** ensured that **2** remained uncoordinated.

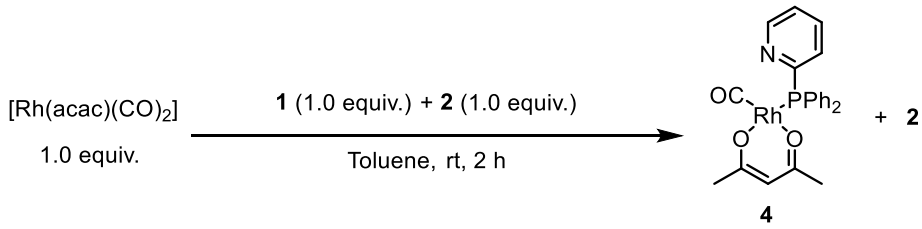

Scheme 33. Reaction of ligands **1** and **2** with [Rh(acac)$(CO)_2$].

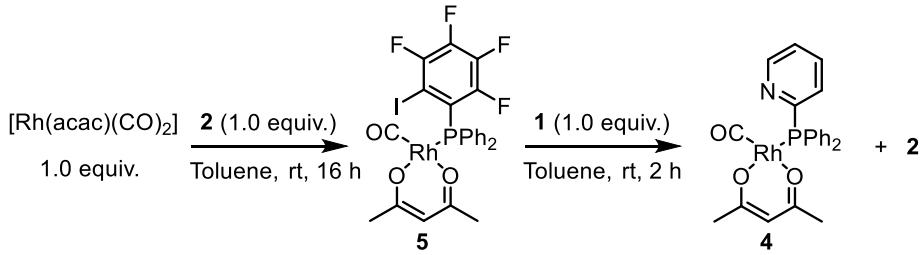

Scheme 34. Reaction of ligand **1** with complex **5**.

(102) Roodt, A.; Otto, S.; Steyl, G. *Coord. Chem. Rev.* **2003**, *245*, 121-137.
(103) Percent buried volume (%V_{Bur}) was used as steric descriptor, see: Clavier, H.; Nolan, S. P. *Chem. Commun.* **2010**, *46*, 841-861. SambVca 2.0 web application was used to calculate %V_{Bur}, see: Falivene, L.; Credendino, R.; Poater, A.; Petta, A.; Serra, L.; Oliva, R.; Scarano, V.; Cavallo, L. *Organometallics* **2016**, *35*, 2286-2293, and section 2.5.6 for details.

We then moved to the [Rh(acac)(C_2H_4)$_2$] precursor,[104] with the reasoning that the ethylene ligands would be more labile and thus more readily displaced by the supramolecular phosphine assembly compared to carbonyl ligands. Interestingly, the reaction of [Rh(acac)(C_2H_4)$_2$] with phosphines **1** and **2** led to complex **6** that incorporated both phosphines and an acetylacetonato ligand. A closer inspection of the NMR spectral data pointed to the formation of a Rh(III) complex in which a C–I oxidative addition process had taken place (Scheme 35). Single crystals of complex **6** suitable for X-ray analysis were obtained and the structure of the Rh(III) complex was confirmed (Figure 104). Indeed, it is reported in the literature that *ortho*-haloarylphosphines such as **2** undergo oxidative addition (OA) processes with rhodium (and other transition metals) at high temperatures or under UV/Vis irradiation.[105] According to these literature reports, the mild conditions employed in the complexation reaction of [Rh(acac)(C_2H_4)$_2$] with **1** and **2** should not favor the C_{Ar}–I oxidative addition process. However, as we observed OA even at 25 °C, we wondered whether ligand preorganization around the rhodium center due to halogen bonding between **1** and **2** could be facilitating the OA process.

(104) The reactivity observed for precursor [Rh(acac)(C_2H_4)$_2$] was identical to that observed for the related precursor [Rh(acac)(cod)].

(105) For a selected example see: (a) Besteiro, J. C.; Lahuerta, P.; Sanaú, M.; Solana, I.; Cotton, F. A.; Llusar, R.; Schwotzer, W. *Polyhedron* **1988**, *7*, 87-96, and references cited therein. For a review on *ortho*-metallated transition metal complexes derived from tertiary phosphines see: (b) Mohr, F.; Privér, S. H.; Bhargava, S. K.; Bennett, M. A. *Coord. Chem. Rev.* **2006**, *250*, 1851-1888.

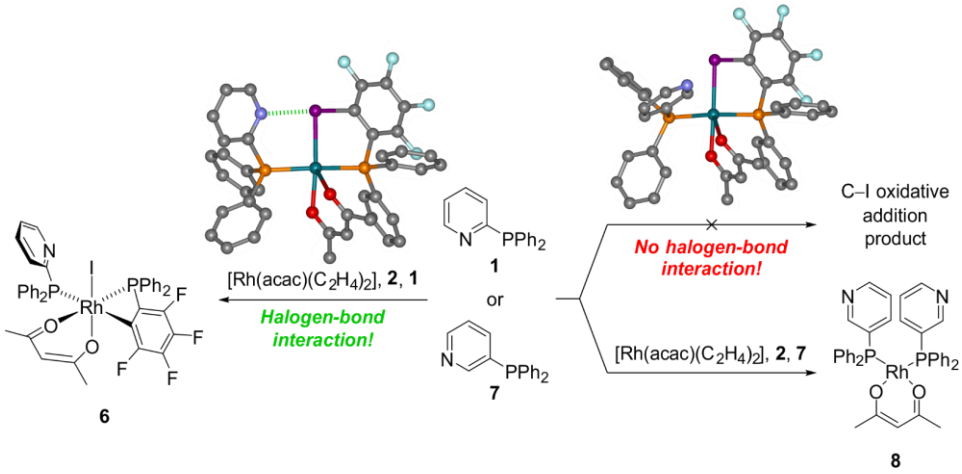

Scheme 35. Reactivity of 2-iodo-3,4,5,6-tetrafluorophenyldiphenylphosphine **2** and [Rh(acac)(C_2H_4)$_2$] with 2-pyridyldiphenylphosphine **1** and 3-pyridyldiphenylphosphine **7**.

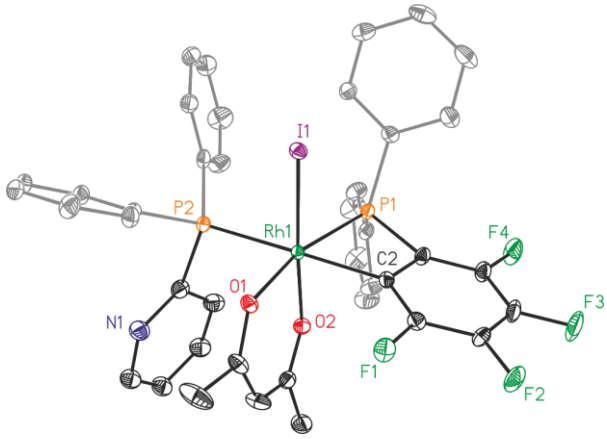

Figure 104. X-Ray structure of **6** with hydrogen atoms having been omitted for the sake of clarity. Color scheme: C: black, P: orange, Rh: green, F: green, N: blue, I: purple, O: red. Atomic displacement ellipsoids are drawn at a 50% probability. For crystallographic data in CIF or other electronic format see CCDC 1874511.

It has been demonstrated that, when ligands **1** and **2** are coordinated to a rhodium(I) center, a square planar (**XBphos-Rh**, see Chapter I) or square-pyramidal geometry (Figure 103) is adopted depending on the nature of the precursor. Moreover, the iodine atom is coordinated to the metal center in both cases. In the case of six-coordinate complex **6**, we reasoned that a transient N···I–C alignment *via* halogen bonding with simultaneous coordination of the I-atom to the rhodium center could be taking place,

ultimately favoring the oxidative addition of the C–I bond to the electron-rich rhodium center. To support this statement, we decided to study the interplay between [Rh(acac)(C_2H_4)$_2$], ligand **2** and 3-pyridyldiphenylphosphine **7**. In this case, alignment of the N···I–C atoms with simultaneous coordination of the phosphorus ligating groups is not possible, suggesting that oxidative addition in ligand **7** (in the presence of ligand **2**) should be disfavored with respect to the same process employing halogen bond complementary ligands **1** and **2**. Consistent with this line of reasoning, the complexation reaction using **2** and 3-pyridyldiphenylphosphine **7** as the halogen bond acceptor with [Rh(acac)(C_2H_4)$_2$] had a different reaction outcome. Unlike in the case of the reaction of **1** with **2**, where chemoselective formation of the oxidative addition Rh(III) complex **6** was observed, the reaction of **7** and **2** led to homocomplex **8** (Scheme 35) with no traces of the OA product being detected by NMR analysis. To further demonstrate the influence of halogen bonding in this transformation, we monitored the reaction of [Rh(acac)(C_2H_4)$_2$] with an equimolar mixture of ligands either **1** and **2** or of ligands **7** and **2** by ^{31}P NMR spectroscopy. It is interesting to note that, whilst no heterocomplex for **7** and **2** was observed by ^{31}P NMR analysis, this technique clearly demonstrated that rhodium species containing the halogen-bonded **1·2** assembly were formed (see section 2.5.7).

Theoretical calculations[106] were also carried out in order to understand the selective formation of complex **6** (see section 2.5.8 in the Experimental Section for details). The examination of the reaction path reveals the formation of an intermediate displaying a short and directional halogen bonding contact N···I–C (see Figure 105a). In fact, the molecular electronic potential (MEP) surface of ligand **2** reveals the existence of a strong σ-hole (*ca.* 30 kcal·mol^{-1}, see Figure 106) on the extension of the C–I bond. The MEP surfaces of phosphine **1** (Figure 106a) and **2** (Figure 106b) show that the MEP at the N atom of **1** is large and negative (–38 kcal·mol^{-1}) and at the extension of the C–I bond in **2** is large and positive, thus anticipating a strong halogen bonding interaction between both ligands.

(106) Work performed in collaboration with the research group of Prof. A. Frontera (*Universitat de les Illes Balears*).

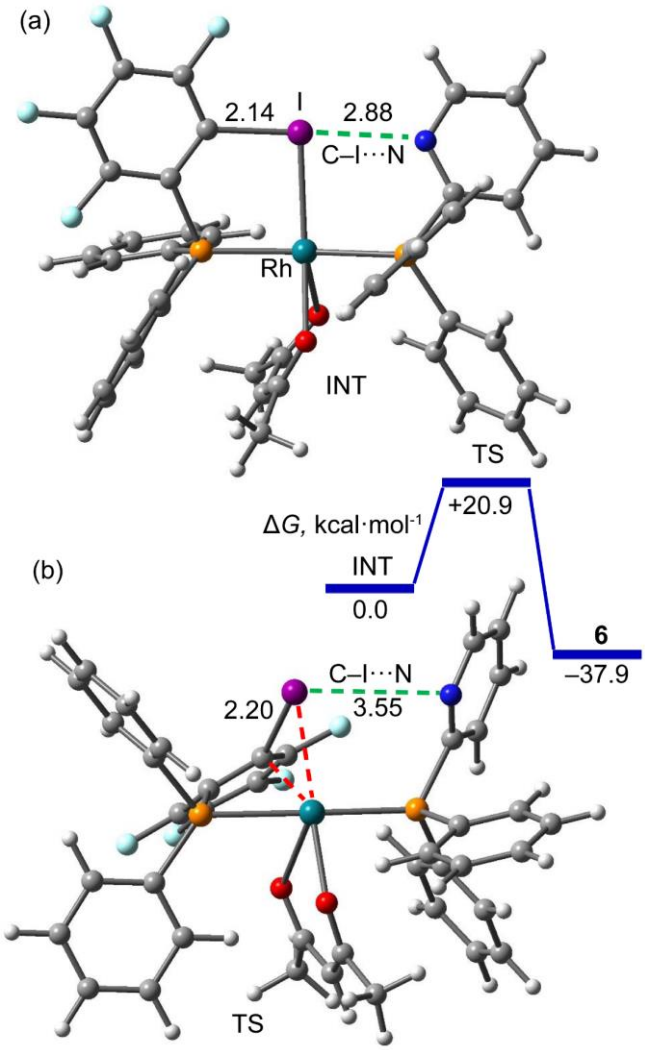

Figure 105. M06-2X/LANL2DZ optimized structures of the intermediate and transition state to yield **6**. Distances in Å. Halogen bonds are represented by green dashes.

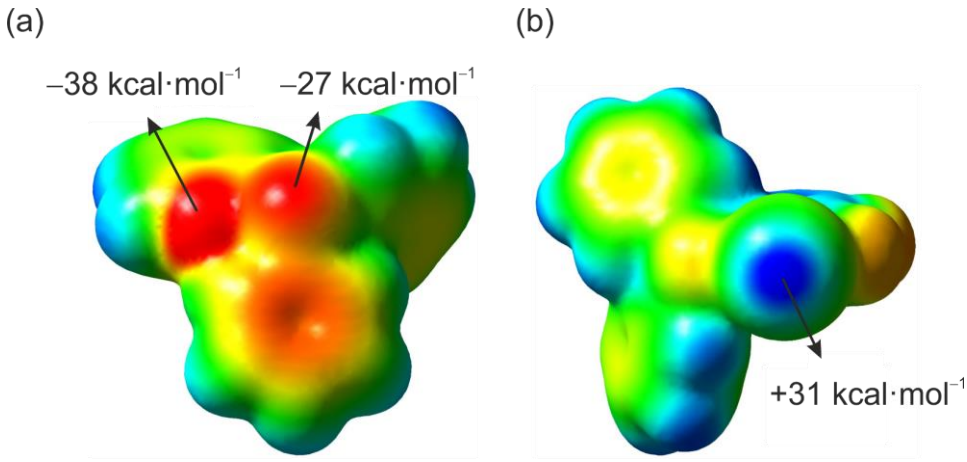

Figure 106. Molecular electrostatic potential (MEP) of ligands: (a) **1** and (b) **2**, computed with an isovalue = 0.001 a.u. at the M06-2X/LANL2DZ level. See section 2.5.8 for details.

Remarkably, this halogen bonding interaction enlarges the C–I distance from 2.11 Å in the ligand to 2.14 Å in the intermediate thus facilitating the subsequent oxidative addition. Interestingly, the calculation of the equivalent intermediate using phosphine **7** (no halogen bond is possible, see Figure 107) is 6.9 kcal·mol^{-1} less stable, thus explaining the absence of oxidative addition reaction (Scheme 35). The TS structure is characterized by a lengthening of the C_{Ar}–I bond (from 2.14 to 2.20 Å) as well as a shortening of the C–Rh distance (1.06 Å). The N···I–C halogen bond is less directional and longer in the TS, but the interaction still exists as evidenced by the non-covalent interaction plot (NCIplot, see Figure 108). The NCIplot is an intuitive visualization index that enables the identification of non-covalent interactions efficiently. The NCIplot is convenient to analyze host-guest interactions since it clearly shows which molecular regions interact. The color scheme is a red-yellow-green-blue scale with red (repulsive) and blue (attractive). Yellow and green surfaces correspond to weak repulsive and weak attractive interactions, respectively. As noted, the intermolecular C–I···N contact is characterized by a small and green isosurfaces located between both donor N-atom and the iodine. Overall, these results illustrate that the combined use of an electron-rich metal precursor such as [Rh(acac)(C_2H_4)$_2$] together with complementary ligands **1** and **2** efficiently leads to a new class of cyclometallated rhodium(III) complexes.

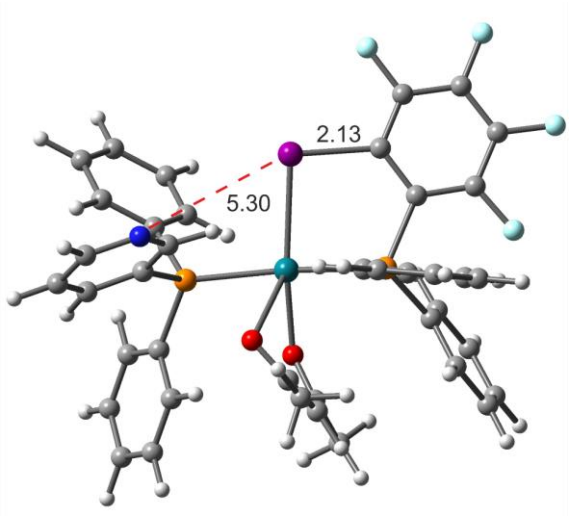

Figure 107. Optimized intermediate (N_{imag} = 0) derived from ligand **7** at M06-2X/LANL2DZ level.

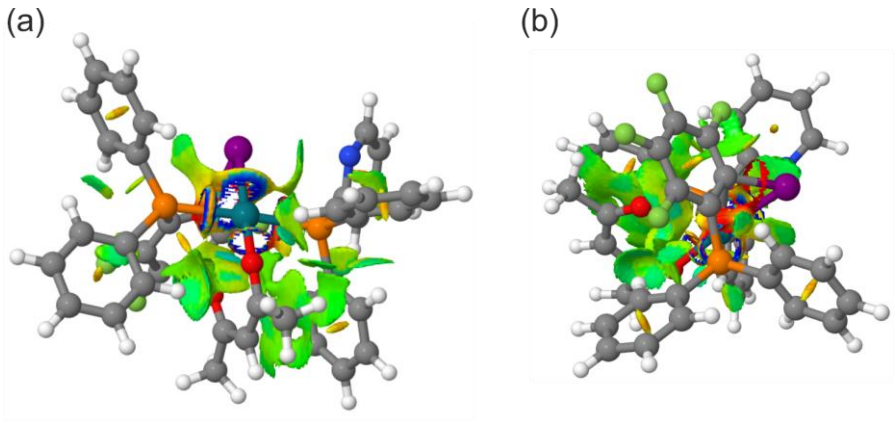

Figure 108. Non-covalent interaction plot of transition state (TS) from orientation (a) and (b). The gradient cut-off is s = 0.50 a.u., and the color scale is –0.04 < ρ < 0.04 a.u. See section 2.5.8 for details.

Analogous behavior was observed for the reaction between **1** and **2** and $[Rh(Cl)(CO)_2]_2$ in the absence of a halide scavenger, in contrast to the preparation of **XBphos-Rh** (see Chapter I). In this case, the CO ligands were preferentially displaced by phosphines **1** and **2**. The complementarity of the halogen-bonded complex **1·2** for simultaneous complexation of the two phosphine groups to the rhodium center and the absence of strong π back-donating carbonyl ligands facilitated the formation of complex **9**

arising from coordination of the P-atoms and a C_{Ar}–I oxidative addition process (Scheme 36).[107]

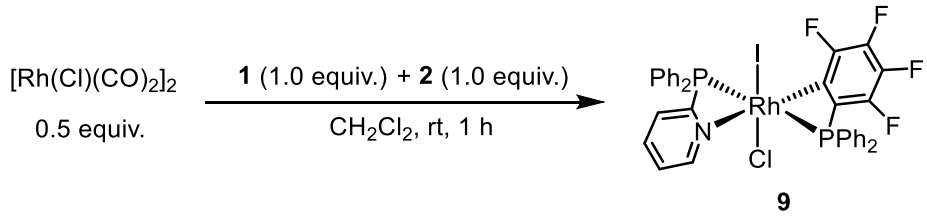

Scheme 36. Preparation of complex **9**.

The structure of the final complex was determined by standard spectroscopic techniques and confirmed by X-ray analysis (Figure 109). In this case, the pyridine group is coordinated to the rhodium center with the two halogen ligands placed axially and the two phosphino groups coordinated in a *trans*-arrangement.

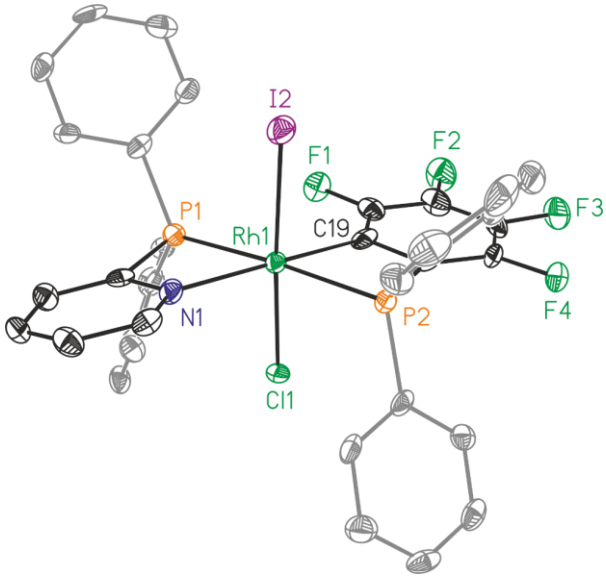

Figure 109. X-Ray structure of **9** with hydrogen atoms having been omitted for the sake of clarity. Color scheme: C: black, P: orange, Rh: green, F: green, Cl: green, N: blue, I: purple. Atomic displacement ellipsoids are drawn at a 50% probability. For crystallographic data in CIF or other electronic format see CCDC 1874513.

(107) The complexation of phosphines **7** and **2** using $[Rh(Cl)(CO)_2]_2$ as the Rh(I) source led to a mixture of hetero- and homocomplexes, but no oxidative addition products were observed.

Interestingly, cyclometallated Rh(III) complexes have been reported as therapeutic agents in medicinal chemistry, suggesting a potential application of these cyclometallated species as drug-like species.[108]

(108) (a) Geldmacher, Y.; Oleszak, M.; Sheldrick, W. S. *Inorg. Chim. Acta* **2012**, *393*, 84-102. (b) Leung, C.-H.; Lin, S.; Zhong, H.-J.; Ma, D.-L. *Chem. Sci.* **2015**, *6*, 871-884.

2.4. CONCLUSIONS

In conclusion, these results illustrate how the careful selection of the rhodium precursor and the geometry of the halogen bond donor and acceptor ligands determines the outcome of the Rh–P complexation chemistry, either to P–I–P pincer-like Rh(I) complexes with a permanent halogen bonding interaction (**XBphos-Rh**, Chapter I) or to the P–P Rh(III) complexes described in this section of the PhD thesis (Chapter II) that arise from an unprecedented halogen-bond-driven C_{Ar}–I oxidative addition process. It has been both experimentally and computationally demonstrated that the N···I halogen bond interaction and the electron density at the metal center are key factors that control the reactivity towards oxidative addition processes as observed in complexes **6** and **9**. Selectivity in the inner coordination sphere chemistry at rhodium has also been controlled by employing building blocks **1** and **2**. Ligand preorganization by *in situ* formation of supramolecular halogen-bonded complex **1·2** appears to translate to a selective formation of complex **3**. Further work is currently underway to study the application[108] and catalytic activity of these new complexes, to ultimately set the basis for the use of halogen bonding in transition metal chemistry and catalysis.

2.5. EXPERIMENTAL SECTION

2.5.1. General considerations

All syntheses were carried out using chemicals as purchased from commercial sources unless otherwise stated. Air- and moisture-sensitive manipulations or reactions were performed under inert atmosphere, either in a glove box or with standard Schlenk techniques. Glassware was dried under vacuum before use with a hot air gun. All solvents were dried and deoxygenated by using a solvent purification system (SPS). Silica gel 60 (230-400 mesh) was used for column chromatography. NMR spectra were recorded at room temperature in 400 MHz or 500 MHz spectrometers in $CDCl_3$ or CD_2Cl_2 unless otherwise cited. ^{1}H and $^{13}C\{^{1}H\}$ NMR chemical shifts are quoted in ppm relative to residual solvent peaks. $^{11}B\{^{1}H\}$ NMR chemical shifts are quoted in ppm relative to $BF_3{\cdot}Et_2O$ in $CDCl_3$. $^{19}F\{^{1}H\}$ NMR chemical shifts are quoted in ppm relative to $CFCl_3$ in $CDCl_3$. $^{31}P\{^{1}H\}$ NMR chemical shifts are quoted in ppm relative to 85% phosphoric acid in water. HRMS and MS spectra were recorded using ESI ionization method in positive mode. IR spectra were recorded using Attenuated Total Reflection (ATR) technique. Ligands **1** and **2** were prepared according to the methodologies described in Chapter I, section 1.5.3.

2.5.2. General structural comments on X-ray crystals

Crystals of **3**, **4**, **5**, **6**, **8** and **9** were grown by solvent diffusion, using CH_2Cl_2 and *n*-pentane at –20 °C under inert atmosphere. 2-iodo-3,4,5,6-tetrafluorophenyldiphenylphosphine **2** was obtained as a thick oil that after some time evolved to a colorless solid, with crystals suitable for single crystal X-ray diffraction. The crystals used for structure determination were selected using a Zeiss stereomicroscope using polarized light and prepared under inert conditions immersed in perfluoropolyether as protecting oil for manipulation.

Crystal structure determination for samples **2**, **3**, **4**, **5**, **6**, **8** and **9** were carried out using an Apex DUO Kappa 4-axis goniometer equipped with an APEX 2 4K CCD area detector, a Microfocus Source E025 IuS using MoK_α radiation, Quazar MX multilayer Optics as monochromator and an Oxford Cryosystems low temperature device Cryostream 700 plus (T = –173 °C). Full-sphere data collection was used with ω and φ scans. Programs used:

Bruker Device: Data collection APEX-2,[109] data reduction Bruker Saint[110] V/60A and absorption correction SADABS[111] or TWINABS.[112] Crystal structure solution was achieved using the computer program SHELXT.[79] Visualization was performed with the program SHELXle.[80] Missing atoms were subsequently located from difference Fourier synthesis and added to the atom list. Least-squares refinement on F2 using all measured intensities was carried out using the program SHELXL 2015.[81] All non-hydrogen atoms were refined including anisotropic displacement parameters.

Comments to complex **3**: The asymmetric unit contains two molecules of the metal complex, two tetrafluoroborate anions and two highly disordered dichloromethane molecules. The tetrafluoroborate anions are disordered in two orientations (ratios 62:38 and 56:44). The two dichloromethane molecules are disordered in respectively two and five positions with ratios of 59:41 and 33:24:22:14:7. The measured sample is formed by a minimum of two crystals with a ratio of 57:43. The collected data were processed with TWINABS taking in account overlapping reflections.

Comments to complex **5**: The asymmetric unit contains one molecule of the metal complex. The measured sample is formed by a minimum of two crystals with a ratio of 68:32. The collected data were processed with TWINABS taking in account overlapping reflections.

Comments to complex **6**: The asymmetric unit contains one molecule of the metal complex. The pyridine ring present in the structure is disordered in two inverted orientations (ratio 69:31).

Comments to complex **8**: The asymmetric unit contains one molecule of the metal complex. This compound was measured three times and special tests (checking general remaining electron densities) were performed to ensure the location and presence of the nitrogen atoms in the complex.

---

(109) Data collection with APEX II version v2013.4-1. Bruker, **2007**. Bruker AXS Inc., Madison, Wisconsin, USA.
(110) Data reduction with Bruker SAINT version V8.30c. Bruker, **2007**. Bruker AXS Inc., Madison, Wisconsin, USA.
(111) SADABS: V2012/1 Bruker, **2001**. Bruker AXS Inc., Madison, Wisconsin, USA. Blessing, R. H. *Acta Cryst.* **1995**, *A51*, 33-38.
(112) TWINABS Version 2012/1 Bruker AXS scaling for twinned crystals. Blessing, R. H. *Acta Cryst.* **1995**, *A51*, 33-38.

Comments to complex **9**: The asymmetric unit contains one molecule of the metal complex and two molecules of dichloromethane. One of the halogen atoms coordinated to the metal atom shows a shared occupancy of 83 % Chlorine and 17 % Iodine.

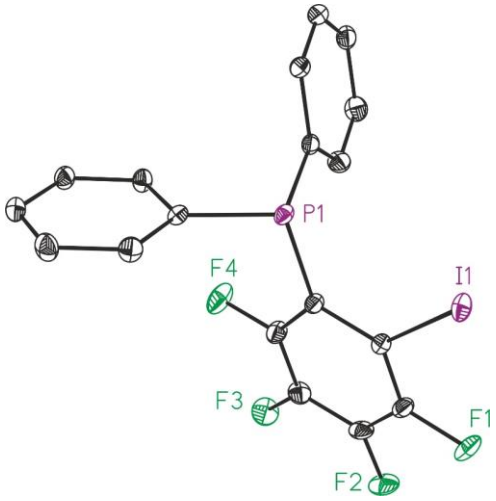

Figure 110. X-Ray structure of **2** with hydrogen atoms having been omitted for the sake of clarity. Color scheme: C: black, P: purple, F: green, I: purple. Atomic displacement ellipsoids are drawn at a 50% probability. For crystallographic data in CIF or other electronic format see CCDC 1874507.

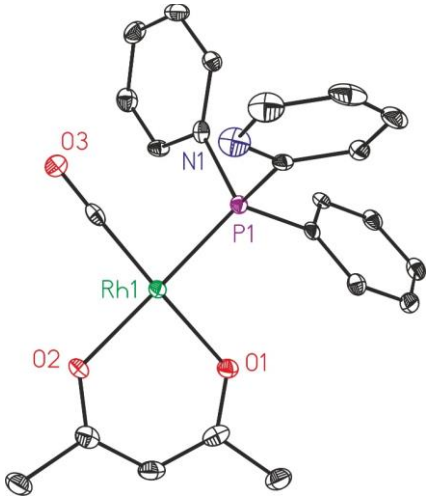

Figure 111. X-Ray structure of **4** with hydrogen atoms having been omitted for the sake of clarity. Color scheme: C: black, P: purple, Rh: green, N: blue, O: red. Atomic displacement ellipsoids are drawn at a 50% probability. For crystallographic data in CIF or other electronic format see CCDC 1874509.

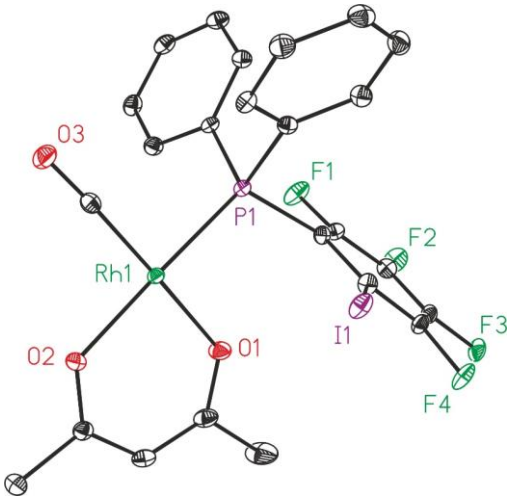

Figure 112. X-Ray structure of **5** with hydrogen atoms having been omitted for the sake of clarity. Color scheme: C: black, P: purple, Rh: green, F: green, O: red, I: purple. Atomic displacement ellipsoids are drawn at a 50% probability. For crystallographic data in CIF or other electronic format see CCDC 1874510.

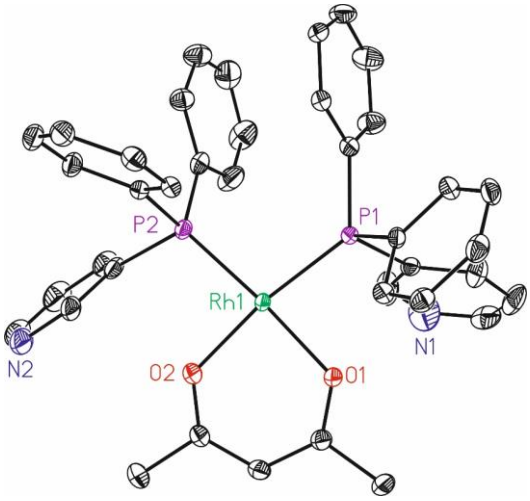

Figure 113. X-Ray structure of **8** with hydrogen atoms having been omitted for the sake of clarity. Color scheme: C: black, P: purple, Rh: green, N: blue, O: red. Atomic displacement ellipsoids are drawn at a 50% probability. For crystallographic data in CIF or other electronic format see CCDC 1874512.

2.5.3. Synthesis of ligand 7

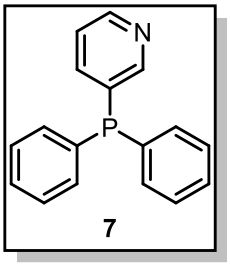

3-pyridyldiphenylphosphine (**7**): Ligand **7** was prepared according to a described procedure,[113] leading to 851.0 mg of white solid 3-diphenylphosphino pyridine (66% yield). ^{1}H NMR, ^{13}C{^{1}H} NMR and ^{31}P{^{1}H} NMR data were in agreement with those previously reported.[114] ^{1}H NMR (500 MHz, $CDCl_3$) δ: 8.49 (dt, J = 4.8, 1.5 Hz, 1 H), 8.49-8.44 (m, 1 H), 7.49-7.46 (m, 1 H), 7.31-7.20 (m, 10 H), 7.18-7.16 (m, 1 H) ppm. ^{13}C{^{1}H} NMR (100 MHz, $CDCl_3$) δ: 154.3 (d, J_{C-P} = 24.0 Hz), 149.7, 141.0 (d, J_{C-P} = 15.7 Hz), 135.8 (d, J_{C-P} = 10.3 Hz), 133.7 (d, J_{C-P} = 19.9 Hz), 133.6 (d, J_{C-P} = 16.0 Hz), 129.2, 128.8 (d, J_{C-P} = 7.0 Hz), 123.5 (d, J_{C-P} = 4.1 Hz) ppm. ^{31}P{^{1}H} NMR (202 MHz, $CDCl_3$) δ: −8.8 ppm. ESI-MS: $[M+H]^+$, 264.0.

2.5.4. Syntheses of complexes 3, 4, 5, 6, 8, 9, 10 and 11

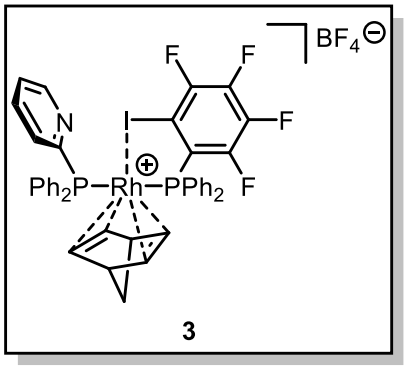

[Rh(nbd)(**1**)(**2**)]BF_4 (**3**): In a glove box filled with N_2, 66.8 mg (0.18 mmol) of [Rh(nbd)$_2$]BF_4 were weighed in a glass vial provided with a magnetic stirrer and dissolved in 1 mL of CH_2Cl_2. Then, a solution of 2-PyPPh$_2$, **1** (46.1 mg, 0.18 mmol) and 2-iodo-3,4,5,6-tetrafluorophenyldiphenylphosphine, **2** (80.5 mg, 0.18 mmol) in 1 mL of dichloromethane was prepared in a vial provided with a magnetic stirrer. The solution was stirred for 5 minutes at 25 °C. Afterwards, the ligands' solution was added dropwise to the rhodium solution. This mixture was stirred for 30 minutes at 25 °C. The resulting solution was evaporated, and then washed with *n*-pentane (3 x 2 mL) and dried under vacuum to afford

(113) Ponsico, S.; Gulyas, H.; Martínez-Belmonte, M.; Escudero-Adán, E. C.; Freixa, Z.; van Leeuwen, P. W. N. M. *Dalton Trans.* **2011**, *40*, 10686-10697.
(114) Sun, M.; Zhang, H.-Y.; Han, Q.; Yang, K.; Yang, S.-D. *Chem. - Eur. J.* **2011**, *17*, 9566-9570.

159.0 mg of **3** as an orange solid in 90% yield. ^{1}H NMR (500 MHz, CD_2Cl_2) δ: 7.94 (br s, 1 H), 7.52 (t, J = 7.3 Hz, 1 H), 7.48-7.18 (m, 14 H), 7.11-7.08 (m, 3 H), 7.02-6.88 (m, 4 H), 6.58 (dm, J = 7.9 Hz, 1 H), 3.80-3.60 (m, 6 H), 1.34 (s, 2 H) ppm. ^{13}C{^{1}H} NMR (126 MHz, CD_2Cl_2) δ:[115] 156.5 (d, J_{C-P} = 64.5 Hz, C_{Py}), 149.0 (d, J_{C-P} = 18.7 Hz, C_{Py}), 136.8 (d, J_{C-P} = 4.1 Hz, C_{Ph}), 134.7 (d, J_{C-P} = 11.6 Hz, C_{Ph}), 132.7 (d, J_{C-P} = 11.4 Hz, C_{Ph}), 131.6 (C_{Py}), 131.2 (C_{Ph}), 130.9 (C_{Ph}), 130.5 (d, J_{C-P} = 8.8 Hz, C_{Ph}), 129.5-129.0 (C_{Ph}, C_{Py}), 128.0 (d, J_{C-P} = 11.0 Hz, C_{Ph}), 125.2 (d, J_{C-P} = 1.4 Hz, C_{Py}), 64.0 (C_{nbd}), 57.6 (C_{nbd}), 57.3 (C_{nbd}), 47.2 (C_{nbd}) ppm. ^{11}B{^{1}H} NMR (CD_2Cl_2, 160 MHz) δ: –1.1 ppm. ^{19}F{^{1}H} NMR (471 MHz, CD_2Cl_2) δ: –108.6 - –108.7 (m, 1 F), –112.9 - –113.0 (m, 1 F), –145.6 - –145.7 (m, 1 F), –149.0 - –149.1 (m, 1 F), –152.6 (s, 4 F) ppm. ^{31}P{^{1}H} NMR (162 MHz, CD_2Cl_2) δ: 77.3 (ddd, J_{P-Rh} = 140.3 Hz, J_{P-F} = 30.1, 15.3 Hz), 30.8 (br d, J_{P-Rh} = 136.7 Hz) ppm. IR (neat): 3057, 2922, 1614, 1571, 1495, 1433, 1333, 1303, 1184, 1162, 1107, 1052, 1027, 996, 844, 777, 742, 719, 695, 514, 437, 415 cm^{-1}. HRMS ESI-MS (m/z): $[M-BF_4]^+$ calcd. for $C_{42}H_{32}F_4INP_2Rh^+$ 918.0040, found 918.0069.

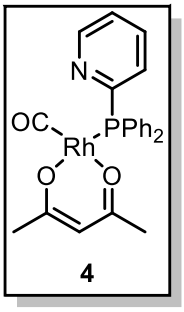

4

Acetylacetonato carbonyl 2-pyridyldiphenylphosphine rhodium(I), [Rh(acac)(CO)(**1**)] (**4**): In a glove box filled with N_2, 14.8 mg (0.06 mmol) of [Rh(acac)$(CO)_2$] were weighed in a vial provided with a magnetic stirrer and dissolved in 0.5 mL of toluene. The green crystals turned into a yellow solution. Then a solution of 0.5 mL of 2-pyridyldiphenylphosphine, **1** (15.8 mg, 0.06 mmol) in toluene was added dropwise to the rhodium precursor solution, observing some bubbling due to the release of CO and a change in the color of the solution from yellow to orange. Finally, 0.5 mL of toluene were added and the solution was stirred for 2 hours. Precipitation with *n*-pentane yielded 30 mg of a yellow powder (quantitative amounts of

(115) A heavily overlapped ^{13}C{^{1}H} NMR spectrum was observed due to the splitting of the carbon signals with other NMR active nuclei present in the molecule. Whenever possible the carbons where assigned with the help of other NMR experiments as follows: C_{nbd} (norbornadiene carbons), C_{Ph} (phenyl ring carbons), C_{Py} (pyridyl ring carbons), C_F (fluorine-containing ring carbons), C_{CO} (carbonyl carbon), C_{acac} (acetylacetonate carbons). This also applies for complexes **4**, **5**, **6**, **8**, **9**, **10** and **11**.

4). ^{1}H NMR, ^{13}C{^{1}H} NMR, ^{31}P{^{1}H} NMR and IR data were in agreement with those previously reported.[116] ^{1}H NMR (400 MHz, $CDCl_3$) δ: 8.68 (d, J = 4.7 Hz, 1 H), 7.95-7.92 (m, 1 H), 7.80-7.70 (m, 4 H), 7.59 (tq, J = 9.5, 1.8 Hz, 1 H), 7.40-7.25 (m, 6 H), 7.20-7.17 (m, 1 H), 5.34 (s, 1 H), 2.01 (s, 3 H), 1.44 (s, 3 H) ppm. ^{13}C{^{1}H} NMR (100 MHz, $CDCl_3$) δ:[115] 188.9 (dd, J_{C-Rh} = 75.4 Hz, J_{C-P} = 24.5 Hz, C_{CO}), 187.6 (C_{acac}), 185.5 (C_{acac}), 157.7 (d, J_{C-P} = 71.4 Hz, C_{Py}), 150.1 (d, J_{C-P} = 14.5 Hz, C_{Py}), 135.5 (d, J_{C-P} = 9.4 Hz, C_{Py}), 135.0 (d, J_{C-P} = 11.4 Hz, C_{Ph}), 132.3 (d, J_{C-P} = 51.6 Hz, C_{Ph}), 131.3 (d, J_{C-P} = 27.0 Hz, C_{Py}), 130.4 (d, J_{C-P} = 2.5 Hz, C_{Ph}), 128.0 (d, J_{C-P} = 10.6 Hz, C_{Ph}), 123.9 (d, J_{C-P} = 2.2 Hz, C_{Py}), 100.8 (d, J_{C-Rh} = 2.2 Hz, C_{acac}), 27.7 (d, J_{C-Rh} = 5.3 Hz, C_{acac}), 26.7 (C_{acac}) ppm. ^{31}P{^{1}H} NMR (202 MHz, $CDCl_3$) δ: 53.6 (d, J_{P-Rh} = 174.6 Hz) ppm. IR (neat): 1962 (CO), 1567, 1515, 1479, 1447, 1434, 1420, 1381, 1309, 1271, 1194, 1154, 1097, 1025, 999, 987, 930, 769, 743, 724, 709, 693, 590, 537, 526, 512, 496 cm^{-1}. ESI-MS: $[M+Na]^+$, 516.0.

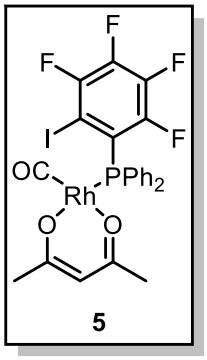

5

Acetylacetonato carbonyl 2-iodo-3,4,5,6-tetrafluorophenyldiphenylphosphine rhodium(I), [Rh(acac)(CO)(**2**)] (**5**): In a glove box filled with N_2, 46.1 mg (0.18 mmol) of [Rh(acac)$(CO)_2$] were weighed in a vial provided with a magnetic stirrer and dissolved in 1 mL of toluene. The green crystals turned into a yellow solution. Then a solution of 1 mL of 2-iodo-3,4,5,6-tetrafluorophenyldiphenylphosphine **2** (81.4 mg, 0.18 mmol) in toluene was added dropwise to the rhodium precursor solution. The color of the solution changed from yellow to orange, indicating that the ligand coordination was taking place. The solution was stirred overnight at room temperature. Precipitation with *n*-pentane yielded a yellow powder that after washing with *n*-pentane (3 x 2 mL) and drying under vacuum yielded the desired complex (75.8 mg, 62% yield). ^{1}H NMR (400 MHz, CD_2Cl_2) δ: 7.90-7.80 (m, 4 H), 7.55-7.40 (m, 6 H), 5.48 (s, 1 H), 2.09 (s, 3 H), 1.59 (s, 3 H) ppm. ^{13}C{^{1}H} NMR (126 MHz, CD_2Cl_2) δ:[115] 189.8 (dd, J_{C-Rh} = 75.4 Hz, J_{C-P} = 24.5 Hz, C_{CO}), 188.2 (C_{acac}), 185.4 (C_{acac}), 149.4 (ddm, J_{C-F} = 254.9 Hz, J = 11.5 Hz, C_F), 148.0 (dtm, J_{C-F} =

(116) Purcell, W.; Conradie, J.; Chiweshe, T. T.; Venter, J. A.; Visser, H. G.; Coetzee, M. P. *J. Mol. Struct.* **2013**, *1038*, 220-229.

242.0 Hz, J = 11.0 Hz, C_F), 140.8 (dm, J_{C-F} = 256.1 Hz, C_F), 140.4 (dm, J_{C-F} = 260.8 Hz, C_F), 134.6 (d, J = 12.8 Hz, C_{Ph}), 132.4 (dd, J = 53.0, 3.2 Hz, C_{Ph}), 131.3 (d, J = 2.5 Hz, C_{Ph}), 128.9 (d, J = 11.1 Hz, C_{Ph}), 120.0 (ddm, J = 40.7, 14.5 Hz, C_F), 100.8 (d, J_{C-Rh} = 2.0 Hz, C_{acac}), 87.9-87.6 (m, C_F), 27.7 (d, J_{C-Rh} = 6.5 Hz, C_{acac}), 27.0 (C_{acac}) ppm. $^{19}F\{^1H\}$ NMR (376 MHz, CD_2Cl_2) δ: −109.7 (dm, J = 24.0 Hz, 1 F), −121.9 - −122.0 (m, 1 F), −149.6 - −149.7 (m, 1 F), −153.5 (tm, J = 18.8 Hz, 1 F) ppm. $^{31}P\{^1H\}$ NMR (162 MHz, CD_2Cl_2) δ: 66.3 (dt, J_{P-Rh} = 183.9 Hz, J_{P-F} = 7.7 Hz) ppm. IR (neat): 1968 (CO), 1571, 1552, 1517, 1483, 1427, 1377, 1332, 1301, 1271, 1233, 1186, 1121, 1103, 1088, 1026, 999, 782, 774, 758, 746, 717, 693, 504 cm^{-1}. HRMS ESI-MS (m/z): $[M-CO+H]^+$ calcd. for $C_{23}H_{18}F_4IO_2PRh$ 662.9075, found 662.9085.

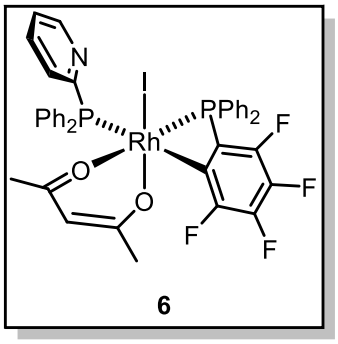

6

Iodo acetylacetonato 3,4,5,6-tetrafluorophenyldiphenylphosphine 2-pyridyldiphenylphosphine rhodium(III), [Rh(I)(acac)(2-$C_6F_4PPh_2$)(**1**)] (**6**): In a glove box filled with N_2, 65.8 mg (0.21 mmol) of [Rh(acac)(cod)][104] were weighed in a vial provided with a magnetic stirrer and dissolved in 1 mL of diethyl ether, forming a yellow solution. Then a solution of 1 mL of 2-iodo-3,4,5,6-tetrafluorophenyldiphenylphosphine, **2** (95.7 mg, 0.21 mmol) and 2-$PyPPh_2$, **1** (54.7 mg, 0.21 mmol) in Et_2O, previously stirred for five minutes, was added dropwise to the rhodium precursor solution. During the addition, a change in color from yellow to deep red was observed. After *ca.* 15 minutes an orange precipitate was formed. Following stirring for 1 hour, the mother liquors were decanted, and the solid was washed with Et_2O (3 x 2 mL) and *n*-pentane (3 x 2 mL) and dried under vacuum, affording complex **6** as an orange solid (118.0 mg) in 61% yield. ^1H NMR (500 MHz, CD_2Cl_2) δ: 8.40 (d, J = 4.8 Hz, 1 H), 7.85 (t, J = 8.3 Hz, 2 H), 7.56-7.14 (m, 21 H), 5.04 (s, 1 H), 1.90 (s, 3 H), 1.16 (s, 3 H) ppm. $^{13}C\{^1H\}$ NMR (126 MHz, CD_2Cl_2) δ:[115] 188.4 (d, J = 3.4 Hz, C_{acac}), 185.0 (s, C_{acac}), 159.0 (d, J = 58.2 Hz), 149.8 (d, J = 15.1 Hz), 136.5 (d, J = 9.4 Hz), 135.7 (d, J = 6.2 Hz), 135.4 (d, J = 9.8 Hz), 135.2 (d, J = 9.9 Hz), 134.6 (d, J = 11.0 Hz), 132.9 (d, J = 9.9 Hz), 132.0-130.0 (m), 129.0-127.0 (m), 126.8, 124.1, 123.7 (d, J = 1.4 Hz), 99.4, 99.1, 27.3, 26.4 ppm. $^{19}F\{^1H\}$ NMR (376 MHz, CD_2Cl_2) δ: −133.9 (t, J_{F-P}

= 20.7 Hz, 1 F), –134.7 - –134.8 (m, 1 F), –149.7 - –149.8 (m, 1 F), –162.6 (t, J_{F-P} = 19.3 Hz, 1 F) ppm. $^{31}P\{^1H\}$ NMR (202 MHz, CD_2Cl_2) δ: 15.6 (d, J_{P-Rh} = 81.9 Hz), –36.8 (d, J_{P-Rh} = 101.6 Hz) ppm. IR (neat): 3054, 1576, 1513, 1466, 1434, 1094, 1015, 740, 689, 512 cm^{-1}. HRMS ESI-MS (m/z): $[M+Na]^+$ calcd. for $C_{40}H_{31}F_4INO_2P_2RhNa^+$ 947.9758, found 947.9763.

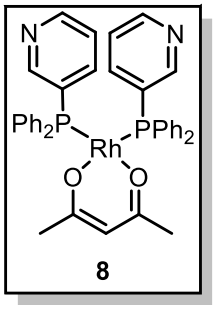

8

Acetylacetonato bis(3-pyridyldiphenylphosphine) rhodium(I), [Rh(acac)(**7**)$_2$] (**8**): In a glove box filled with N_2, 65.3 mg (0.21 mmol) of [Rh(acac)(cod)][104] were weighed in a vial provided with a magnetic stirrer and dissolved in 1 mL of diethyl ether, forming a yellow solution. Then a solution of 2-iodo-3,4,5,6-tetrafluorophenyldiphenylphosphine, **2** (94.9 mg, 0.21 mmol) and 3-PyPPh$_2$, **7** (54.3 mg, 0.21 mmol) in 1 mL of Et_2O, previously stirred for five minutes, was added dropwise to the rhodium precursor solution. During the addition, a change in color from yellow to deep orange was observed and approximately, after 15 minutes, a precipitate was formed. After stirring for 1 hour, the mother liquors were decanted, and the solid was washed with Et_2O (3 x 2 mL) and *n*-pentane (3 x 2 mL) and dried under vacuum, affording 48.1 mg of homocomplex **8** (32% yield) as a yellow solid. ^1H NMR (500 MHz, CD_2Cl_2) δ: 8.53 (d, J = 2.0 Hz, 2 H), 8.37 (d, J = 4.7 Hz, 2 H), 7.70-7.55 (m, 10 H), 7.27 (t, J = 7.4 Hz, 4 H), 7.14 (t, J = 7.4 Hz, 8 H), 7.01-6.98 (m, 2 H), 5.29 (s, 1 H), 1.43 (s, 6 H) ppm. $^{13}C\{^1H\}$ NMR (126 MHz, CD_2Cl_2) δ:[115] 185.0 (C_{acac}), 154.6 (t, J_{C-P} = 5.9 Hz, C_{Py}), 149.6 (C_{Py}), 141.5 (t, J_{C-P} = 4.6 Hz, C_{Py}), 135.1 (t, J_{C-P} = 5.9 Hz, C_{Ph}), 134.5 (t, J_{C-P} = 22.3 Hz, C_{Ph}), 132.2 (t, J_{C-P} = 19.3 Hz, C_{Py}), 129.7 (C_{Ph}), 127.8 (t, J_{C-P} = 4.9 Hz, C_{Ph}), 122.5 (t, J_{C-P} = 3.4 Hz, C_{Py}), 99.8 (d, J_{C-Rh} = 1.4 Hz, C_{acac}), 26.9 (d, J_{C-Rh} = 2.9 Hz, C_{acac}) ppm. $^{31}P\{^1H\}$ NMR (162 MHz, CD_2Cl_2) δ: 54.3 (d, J_{P-Rh} = 193.1 Hz) ppm. IR (neat): 3046, 1567, 1515, 1477, 1433, 1395, 1270, 1179, 1090, 1021, 931, 794, 753, 692, 620, 599, 551, 525, 436 cm^{-1}. HRMS ESI-MS (m/z): $[M]^{+\bullet}$ calcd. for $C_{39}H_{35}N_2O_2P_2Rh$ 728.1223, found 728.1241.

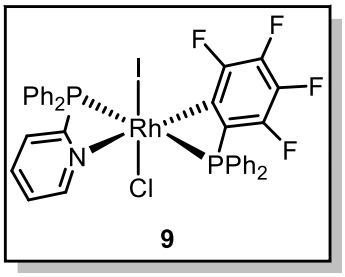

9

Iodo chloro 3,4,5,6-tetrafluorophenyldiphenylphosphine 2-pyridyldiphenylphosphine rhodium(III), [Rh(Cl)(I)(2-$C_6F_4PPh_2$)(**1**)] (**9**): In a glove box filled with N_2, 25.5 mg (0.06 mmol) of $[Rh(Cl)(CO)_2]_2$ dimer were weighed in a vial provided with a magnetic stirrer and dissolved in 1 mL of CH_2Cl_2. Then, a solution of 2-$PyPPh_2$, **1** (34.5 mg, 0.12 mmol) and 2-iodo-3,4,5,6-tetrafluorophenyldiphenylphosphine, **2** (61.6 mg, 0.12 mmol) in 2 mL of dichloromethane was prepared in a vial provided with a magnetic stirrer. The resulting solution was stirred for 5 minutes at 25 °C. Afterwards, the ligands' solution was added dropwise to the rhodium solution, observing some bubbling due to the release of CO. This mixture was stirred for 1 hour at 25 °C. The resulting red solution was evaporated and complex **9** was obtained after crystallization using CH_2Cl_2 and *n*-pentane, obtaining 20.3 mg (19% yield) of the complex **9** as red crystals. ^{1}H NMR (500 MHz, CD_2Cl_2) δ: 8.74 (d, J = 5.0 Hz, 1 H), 8.02 (tt, J = 7.9, 1.8 Hz, 1 H), 7.90-7.65 (m, 10 H), 7.55-7.35 (m, 12 H) ppm. ^{13}C{^{1}H} NMR (126 MHz, CD_2Cl_2) δ:[115] 167.9 (d, J_{C-P} = 56.2 Hz, C_{Py}), 152.6 (dm, J_{C-P} = 17.9 Hz, C_{Py}), 137.7 (d, J_{C-P} = 3.4 Hz, C_{Py}), 135.3 (d, J_{C-P} = 9.7 Hz, C_{Ph}), 134.8 (d, J_{C-P} = 9.5 Hz, C_{Ph}), 134.1 (d, J_{C-P} = 10.0 Hz, C_{Ph}), 131.5 (dd, J = 15.5, 2.5 Hz, C_{Ph}), 131.2 (dd, J = 13.3, 2.6 Hz, C_{Ph}), 130.7-130.5 (m, C_{Py}), 130.2-128.8 (m, C_{Py}), 128.7 (d, J_{C-P} = 4.0 Hz, C_{Ph}), 128.6 (t, J_{C-P} = 3.6 Hz, C_{Ph}), 128.5 (d, J_{C-P} = 4.5 Hz, C_{Ph}) ppm. ^{19}F{^{1}H} NMR (471 MHz, CD_2Cl_2) δ: −131.3 (tm, J = 19.4 Hz, 1 F), −132.8 - −133.0 (m, 1 F), −148.7 (t, J = 22.0 Hz, 1 F), −161.5 (t, J = 20.2 Hz, 1 F) ppm. ^{31}P{H} NMR (202 MHz, CD_2Cl_2) δ: −17.7 (ddd, J_{P-P} = 568.6 Hz, J_{P-Rh} = 85.8 Hz, J_{P-F} = 17.7 Hz), −31.2 (dd, J_{P-P} = 568.4 Hz, J_{P-Rh} = 74.6 Hz) ppm. IR (neat): 3055, 2085, 1980, 1615, 1584, 1467, 1447, 1434, 1329, 1294, 1185, 1092, 1015, 843, 789, 740, 707, 688, 617, 526, 506, 434 cm^{-1}. HRMS ESI-MS (m/z): $[M+Na]^+$ calcd. for $C_{35}H_{24}ClF_4INNaP_2Rh$ 883.9001, found 883.8986.

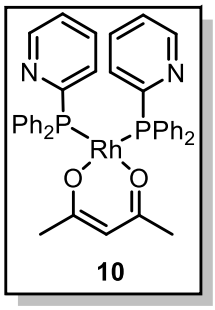

10

Acetylacetonato bis(2-pyridyldiphenylphosphine) rhodium(I), [Rh(acac)(**1**)$_2$] (**10**): In a glove box filled with N_2, 21.1 mg (0.07 mmol) of [Rh(acac)(cod)][104] were weighed in a vial provided with a magnetic stirrer and dissolved in 0.5 mL of diethyl ether, forming a yellow solution. Then a solution of 0.5 mL of 2-PyPPh$_2$, **2** (36.2 mg, 0.13 mmol) in Et_2O was added dropwise to the rhodium precursor solution. During the addition, a change in color from yellow to deep orange was observed. 0.5 mL of Et_2O were further added to quantitatively transfer the ligand, and after *ca.* 15 minutes, a precipitate was formed. After stirring for 1 hour, the mother liquors were decanted. The solid was washed with Et_2O (3 x 2 mL) and *n*-pentane (3 x 2 mL) and dried under vacuum, affording 47.4 mg (98% yield) of **10** as an orange solid. ^{1}H NMR, ^{13}C{^{1}H} NMR, ^{31}P{^{1}H} NMR and IR data were in agreement with those previously reported.[117] ^{1}H NMR (500 MHz, CD_2Cl_2) δ: 8.38 (d, J = 4.5 Hz, 2 H), 8.14 (d, J = 7.7 Hz, 2 H), 7.70-7.60 (m, 8 H), 7.41 (tm, J = 7.7 Hz, 2 H), 7.21 (t, J = 7.3 Hz, 4 H), 7.10 (t, J = 7.5 Hz, 8 H), 7.05-7.02 (m, 2 H), 5.27 (s, 1 H), 1.42 (s, 6 H) ppm. ^{13}C{^{1}H} NMR (100 MHz, CD_2Cl_2) δ:[115] 184.8 (C_{acac}), 160.6 (t, J_{C-P} = 30.9 Hz, C_{Py}), 149.0 (t, J_{C-P} = 6.3 Hz, C_{Py}), 135.8 (t, J_{C-P} = 22.4 Hz, C_{Py}), 135.3 (t, J_{C-P} = 5.6 Hz, C_{Ph}), 134.6 (t, J_{C-P} = 4.7 Hz, C_{Ph}), 132.2 (t, J_{C-P} = 14.0 Hz, C_{Py}), 129.0 (C_{Ph}), 127.2 (t, J_{C-P} = 4.9 Hz, C_{Ph}), 122.9 (C_{Py}), 99.6 (d, J_{C-Rh} = 1.6 Hz, C_{acac}), 26.9 (t, J_{C-Rh} = 2.8 Hz, C_{acac}) ppm. ^{31}P{^{1}H} NMR (202 MHz, CD_2Cl_2) δ: 59.2 (d, J_{P-Rh} = 192.8 Hz) ppm. IR (neat): 3046, 2985, 2911, 1567, 1513, 1478, 1445, 1433, 1418, 1393, 1308, 1268, 1194, 1181, 1152, 1127, 1091, 1045, 1026, 998, 986, 931, 791, 765, 740, 724, 693, 618, 597, 551, 526, 517, 510, 499, 461, 436, 417 cm^{-1}.

(117) Kartashova, K.; Mallet-Ladeira, S.; Axet, M. R. *J. Organomet. Chem.* **2015**, *799-800*, 226-231.

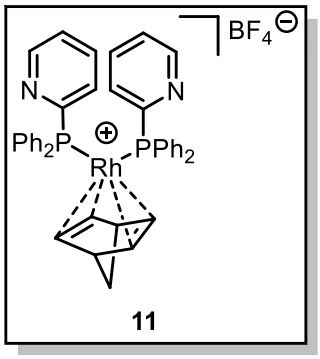

11

Norbornadiene bis(2-pyridyldiphenylphosphine) rhodium(I) tetrafluoroborate, [Rh(nbd)(**1**)$_2$]BF$_4$ (**11**):[118] In a glove box filled with N_2, 51.8 mg (0.14 mmol) of [Rh(nbd)$_2$]BF$_4$ were weighed in a glass vial provided with a magnetic stirrer and dissolved in 1 mL of CH_2Cl_2. Then, a solution of 2-PyPPh$_2$, **1** (75.2 mg, 0.28 mmol) in 1 mL of dichloromethane was prepared and then added dropwise to the rhodium solution. This mixture was stirred for 30 minutes at 25 °C. The resulting solution was evaporated and then washed with *n*-pentane (3 x 2 mL) and dried under vacuum to afford 98.0 mg of **11** as an orange solid in 88% yield. ^{1}H NMR (500 MHz, CD_2Cl_2) δ: 8.02 (d, J = 4.7 Hz, 2 H), 7.54-7.44 (m, 14 H), 7.42-7.34 (m, 8 H), 7.11 (t, J = 6.2 Hz, 2 H), 7.02 (d, J = 7.8 Hz, 2 H), 3.92 (d, J = 2.1 Hz, 4 H), 3.53 (s, 2 H), 1.30 (s, 2 H) ppm. ^{13}C{^{1}H} NMR (126 MHz, CD_2Cl_2) δ:[115] 161.4 (d, J_{C-P} = 57.4 Hz, C_{Py}), 150.8 (d, J_{C-P} = 19.3 Hz, C_{Py}), 136.9 (d, J_{C-P} = 1.8 Hz, C_{Ph}), 134.1 (d, J_{C-P} = 13.5 Hz, C_{Ph}), 132.4 (d, J_{C-P} = 10.0 Hz, C_{Ph}), 131.3 (d, J_{C-P} = 32.4 Hz, C_{Py}), 131.1 (C_{Ph}), 129.3 (d, J_{C-P} = 9.7 Hz, C_{Ph}), 128.2 (d, J_{C-P} = 11.6 Hz, C_{Ph}), 125.3 (C_{Py}), 63.9 (C_{nbd}), 59.5 (d, J_{C-P} = 4.1 Hz, C_{nbd}), 49.7 (C_{nbd}) ppm. ^{11}B{^{1}H} NMR (CD_2Cl_2, 128 MHz) δ: −1.1 ppm. ^{19}F{^{1}H} NMR (376 MHz, CD_2Cl_2) δ: −153.0 (s) ppm. ^{31}P{^{1}H} NMR (162 MHz, CD_2Cl_2) δ: 10.4 (d, J_{P-Rh} = 124.2 Hz) ppm. IR (neat): 3053, 2989, 2926, 2861, 1585, 1570, 1479, 1449, 1434, 1422, 1305, 1280, 1159, 1090, 1049, 997, 741, 693, 504 cm^{-1}. HRMS ESI-MS (m/z): [M−BF$_4$]$^+$ calcd. for $C_{41}H_{36}N_2P_2Rh^+$ 721.1403, found 721.1393.

(118) The synthesis of homocomplex [Rh(nbd)(**2**)$_2$]BF$_4$ was also attempted but a complex mixture of products was obtained according to the ^{31}P{^{1}H} NMR.

2.5.5. DOSY NMR experiments

Diffusion Ordered SpectroscopY (DOSY) NMR spectra were recorded at 25 °C in a 500 MHz spectrometer equipped with a cryoprobe. All DOSY experiments were obtained with a longitudinal eddy-current delay (LED) bipolar gradient pulse pair and two spoil gradients pulse sequence (ledbpgp2s) in the standard Bruker pulse sequence library.[119] All experiments were processed with standard Bruker 1D and 2D DOSY software. $CDCl_3$ was used as solvent and the concentration of the ligands was chosen to be 0.3 M. Bis(2-diphenylphosphinophenyl)ether (DPEphos) was included as control bidentate ligand. Reproducibility of DOSY experiments was proven by successfully repeating the experiments two times.

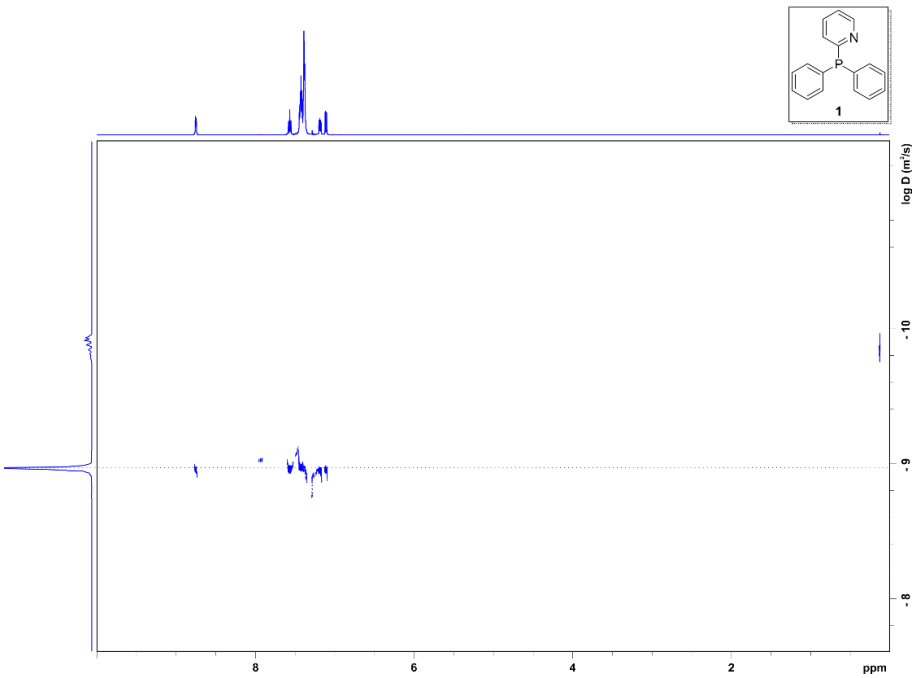

Figure 114. 2D DOSY for ligand **1**. Log D = −8.99±0.01 → D = 1.03±0.01·10^{-9} m^2·s^{-1}.

(119) Bruker User Library (accessed 23 October 2018). https://www.bruker.com/service/information-communication/nmr-pulse-program-lib/bruker-user-library.html

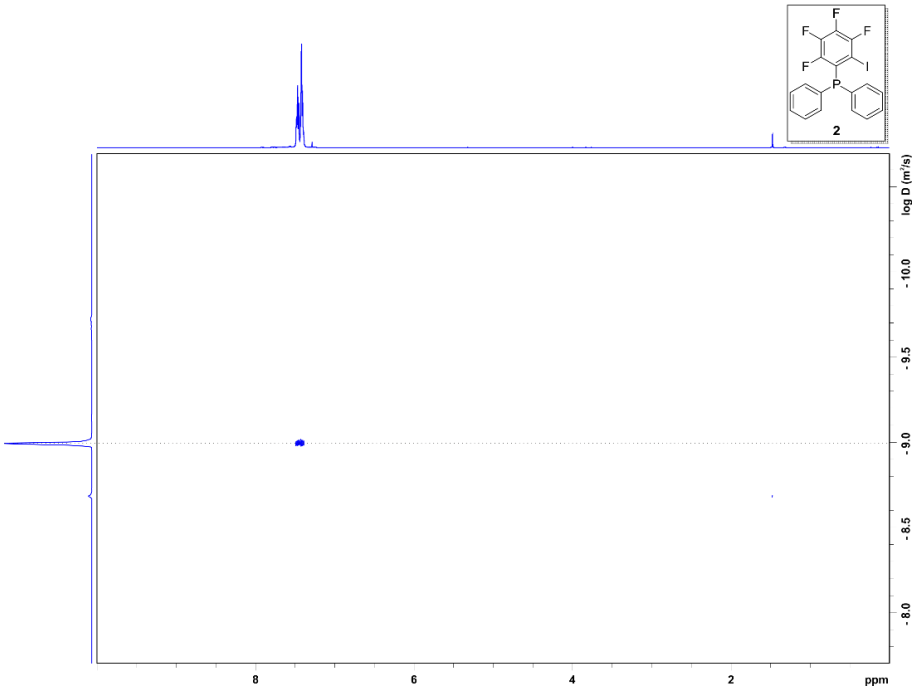

Figure 115. 2D DOSY for ligand **2**. Log D = –9.02±0.03 → D = 9.47±0.75·10^{-10} m^2·s^{-1}.

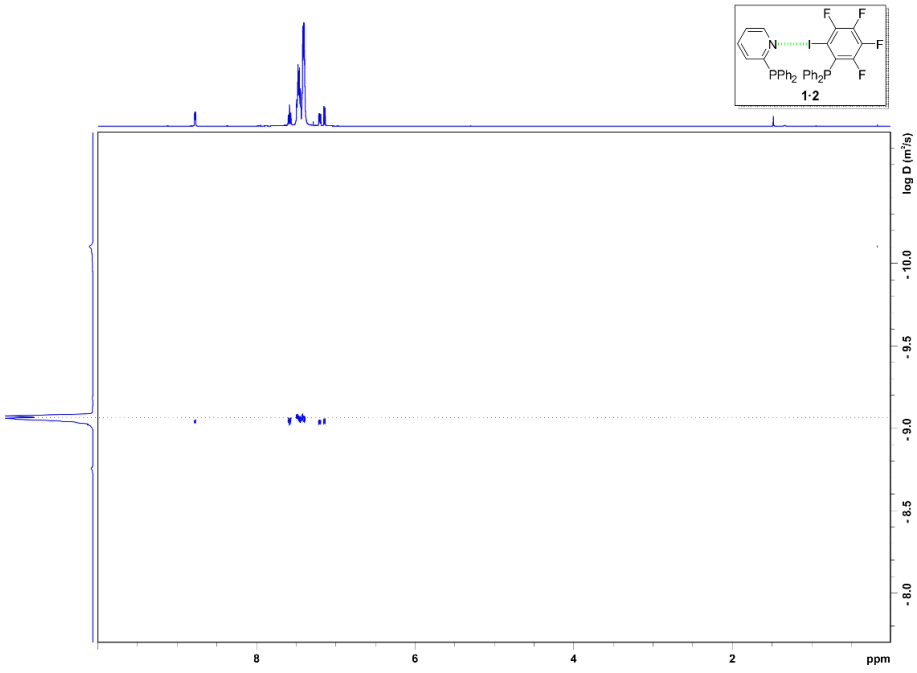

Figure 116. 2D DOSY for ligands **1·2**. Log D = –9.06±0.01 → D = 8.66±0.21·10^{-10} m^2·s^{-1}.

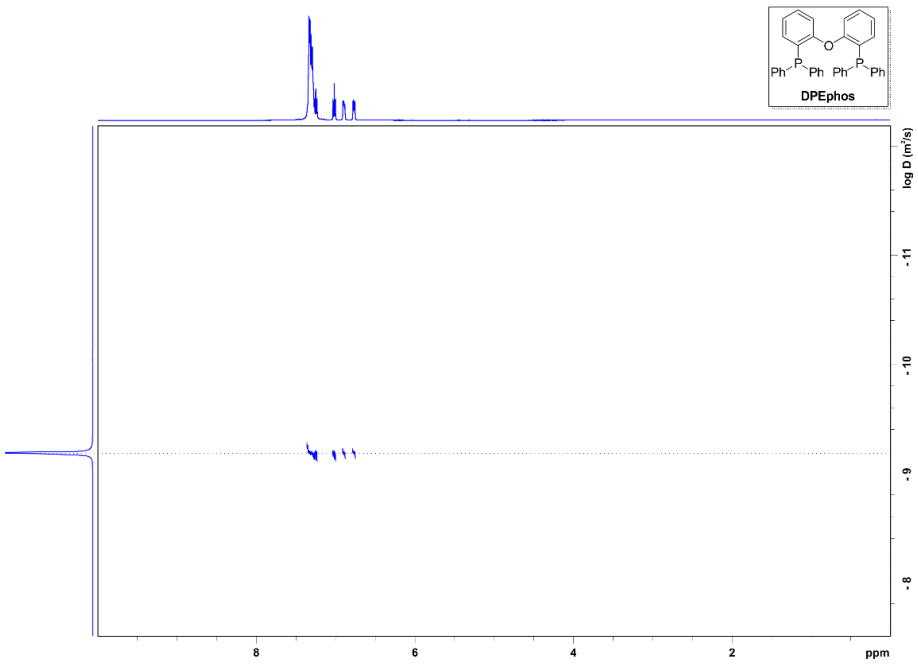

Figure 117. 2D DOSY for ligand DPEphos. Log D = –9.19 → D = 6.46·10^{-10} m^2·s^{-1}.

2.5.6. Tolman Electronic Parameter and Percent Buried Volume calculation

The Tolman electronic parameter was measured considering the CO stretching frequencies of carbonylrhodium(I) complexes **4** (1962 cm^{-1}) and **5** (1968 cm^{-1}).[102]

The percent buried volume (%V_{Bur}) was calculated using SambVca 2.0 web application.[120] Bond distances from the X-ray structures of **4** and **5** were used to determine %V_{Bur} of ligands **1** and **2** respectively.

(120) SambVca 2.0: https://www.molnac.unisa.it/OMtools/sambvca2.0/. For details see ref. 103.

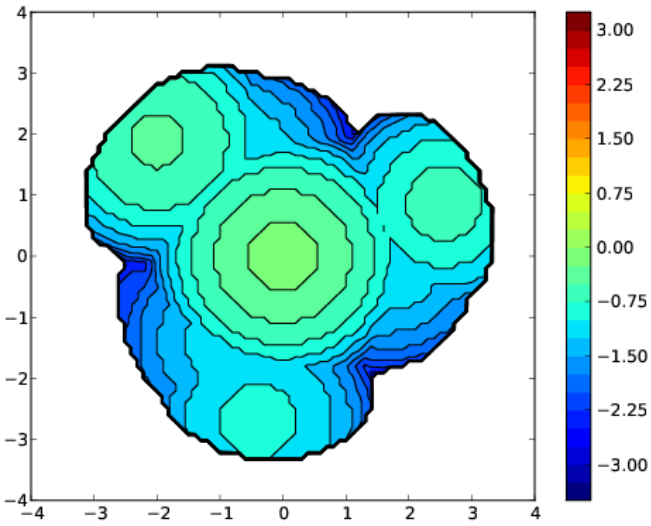

Figure 118. Generated steric map for ligand **1** ($\%V_{Bur}$ = 28.9).

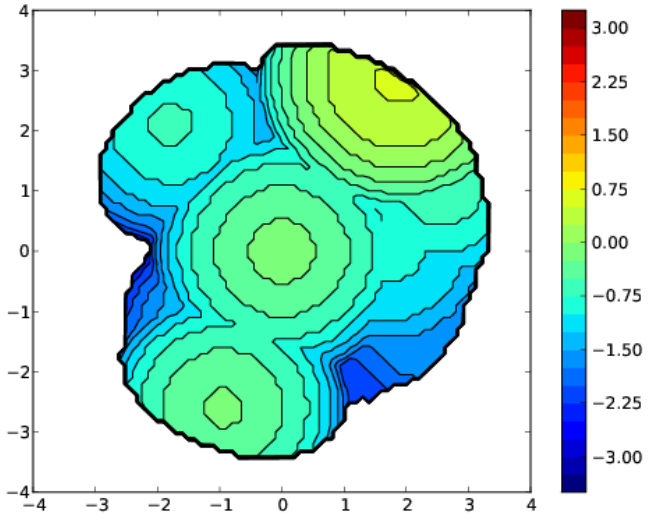

Figure 119. Generated steric map for ligand **2** ($\%V_{Bur}$ = 34.4).

2.5.7. ^{31}P NMR reaction monitoring

In a glove box filled with N_2, 20.0 mg (0.06 mmol) of [Rh(acac)(cod)] were weighed in a flask provided with a magnetic stirrer and dissolved in 0.5 mL of diethyl ether, forming a yellow solution. Then a solution of 0.5 mL of 2-iodo-3,4,5,6-tetrafluorophenyldiphenylphosphine **2** (29.1 mg, 0.06 mmol) and 2-PyPPh$_2$ **1** or 3-PyPPh$_2$ **7** (17.1 mg, 0.06 mmol) in Et_2O, previously stirred for five minutes, was added dropwise to the rhodium precursor solution. A change in color from yellow to orange was observed during the addition. This solution was immediately transferred to a screw-capped NMR tube provided with a septum and a $(CD_3)_2CO$ insert. $^{31}P\{^1H\}$ NMR were recorded at 25 °C in a 500 MHz spectrometer equipped with a cryoprobe every 10 minutes for 2 hours.

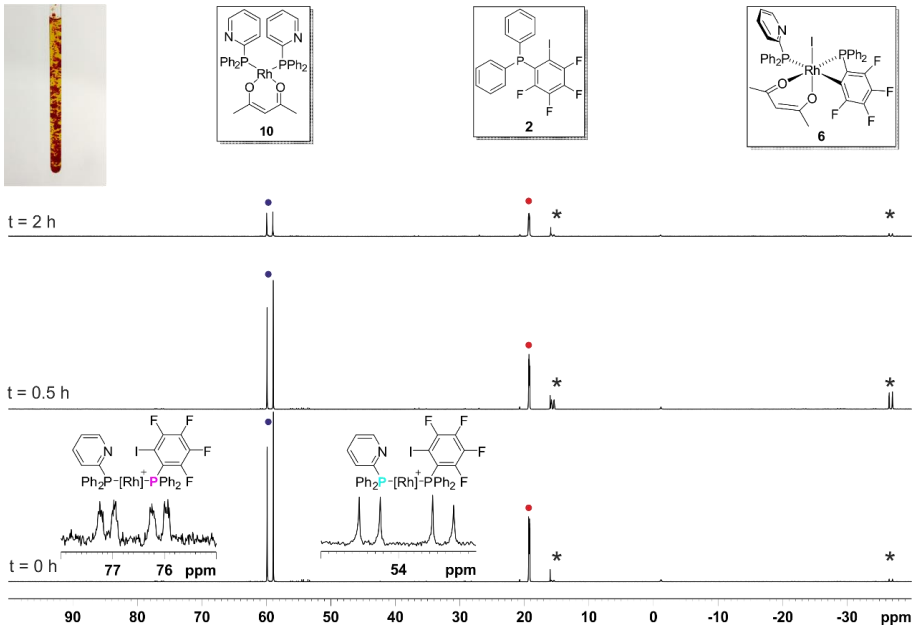

Figure 120. $^{31}P\{^1H\}$ NMR (202 MHz, CD_2Cl_2) stacked spectra for ligands **1**·**2**. Upon time, consumption of **10** (●) and **2** (●) was observed, whilst **6** (*) was generated. After 0.5 hours, **6** started to crystallize (see picture), leading to a decrease in the intensity of the signals. Heterocomplexes were observed in the mixture (δ: 76.6 (dd, J = 207.5, 58.7 Hz), 53.9 (dd, J = 191.1, 54.9 Hz) ppm).

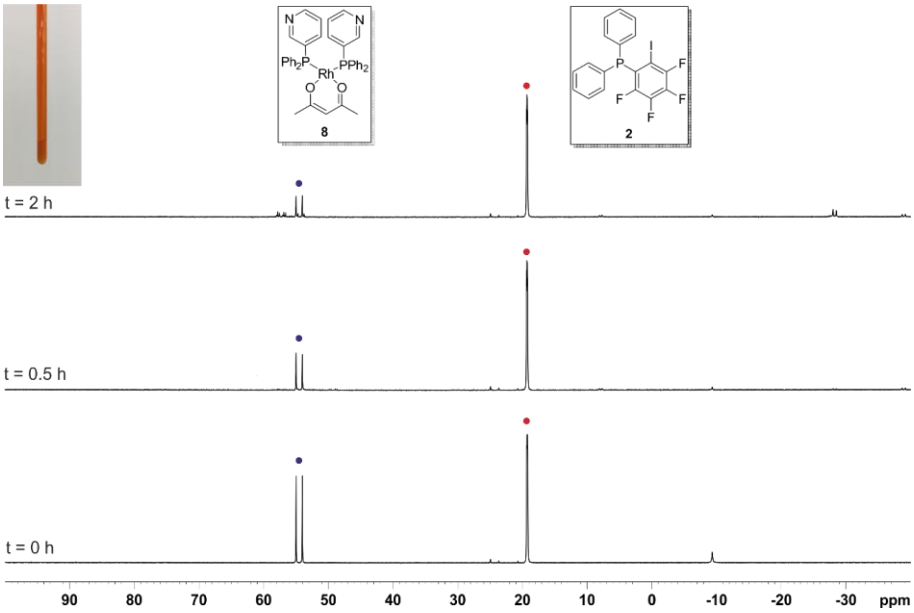

Figure 121. $^{31}P\{^{1}H\}$ NMR (202 MHz, CD_2Cl_2) stacked spectra for ligands **7·2**, observing the formation of of **8** (●). After 0.5 hours, **8** started to precipitate (see picture), leading to a decrease in the intensity of the signals, whilst the concentration of **2** (●) was maintained.

2.5.8. Computational methods

All geometry optimizations were carried out using the M06-2X hybrid functional[121] at LANL2DZ level of theory implemented in Gaussian 09 package.[65] Analysis of corresponding frequencies were performed to characterize structures of minima ($N_{imag} = 0$) or transition states ($N_{imag} = 1$). Product of oxidative addition (**6**) was optimized from X-ray structure as jumping-off place and the transition state connecting reagent/intermediate and products was calculated using the quadratic synchronous transit (QST3) approach[122] and verified by having only one imaginary frequency.

Molecular Electrostatic Potential (MEP) surfaces (isosurface, 0.001 a.u.) have been computed at the same level for optimizations. Solvent effects (diethyl ether) on the energies (kcal·mol^{-1}) were considered using the polarizable continuum model (PCM) with the integral equation formalism variant (IEFPCM).[123]

The NCIplot[124] isosurfaces have been used to confirm the halogen bonding interaction in the transition state. The favorable or unfavorable interaction is evaluated by the isosurface color from red for ρ^{+}cut (repulsive) to blue for ρ^{-}cut (attractive).

(121) Zhao, Y.; Truhlar, D. G. *Theor. Chem. Acc.* **2008**, *120*, 215-241.
(122) Foresman, J. B.; Frisch, Æ. *Exploring Chemistry with Electronic Structure Methods*, 3rd Ed. (Gaussian, Inc., Wallingford, CT, **2015**). ISBN: 978-1-935522-03-4.
(123) Tomasi, J.; Mennucci, B.; Cammi, R. *Chem. Rev.* **2005**, *105*, 2999-3093.
(124) Contreras-García, J.; Johnson, E. R.; Keinan, S.; Chaudret, R.; Piquemal, J.-P.; Beratan, D. N.; Yang, W. *J. Chem. Theory Comput.* **2011**, *7*, 625-632.

Cartesian coordinates:

Ligand **1**:

P	0.03715300	0.01758800	−1.28137400
C	0.68988100	1.54650000	−0.38961600
C	−0.12928100	2.42856000	0.33971500
C	2.54811400	2.92045200	−0.06080900
C	0.43691100	3.59383200	0.87701800
H	−1.18041400	2.20762800	0.48316400
C	1.80154100	3.84821200	0.67938500
H	3.60562700	3.07354100	−0.24706500
H	−0.17782600	4.28726700	1.44123700
H	2.27574600	4.73693200	1.07851500
N	2.00758700	1.80278100	−0.59109700
C	0.98875900	−1.37246900	−0.43202600
C	0.33414100	−2.59664400	−0.19119100
C	2.36150200	−1.26093100	−0.14557900
C	1.03515600	−3.68401600	0.34967900
H	−0.72362700	−2.70370400	−0.41679100
C	3.05809100	−2.35026300	0.40149500
H	2.87681200	−0.32880600	−0.35206000
C	2.40017300	−3.56331000	0.65223200
H	0.51669800	−4.61993700	0.53226700
H	4.11590700	−2.24988400	0.62366900
H	2.94294000	−4.40432300	1.07191600
C	−1.63564500	−0.15142800	−0.44388300
C	−1.78042900	−0.41850700	0.93214900
C	−2.78624400	0.02540000	−1.23064000
C	−3.05462700	−0.50480200	1.50844600
H	−0.89510700	−0.56419900	1.54686400
C	−4.06641700	−0.05748600	−0.65516500
H	−2.68076400	0.22443900	−2.29362000
C	−4.20091600	−0.32267300	0.71439900
H	−3.15517800	−0.71274800	2.56887000
H	−4.94767700	0.07988800	−1.27338600
H	−5.18780700	−0.39194500	1.16104200

Ligand **2**:

P	−0.92845700	0.65319700	−0.86233300
C	−1.73569700	1.62558200	0.53173200
C	−1.25482600	2.93766200	0.70408700
C	−2.74682700	1.14266900	1.38260300
C	−1.75954600	3.75273100	1.72821100
H	−0.48916400	3.32283500	0.03508800
C	−3.25926600	1.96333000	2.39768400
H	−3.12934700	0.13475100	1.25994800
C	−2.76408900	3.26518500	2.57678000
H	−1.37697700	4.75989000	1.85576300
H	−4.03712300	1.58330500	3.05171400
H	−3.16073600	3.89390800	3.36739300
C	−2.18343400	−0.67075200	−1.27835600
C	−1.78096900	−1.98437700	−1.57346200
C	−3.53120300	−0.30880800	−1.45289500
C	−2.71655800	−2.93065700	−2.01377200
H	−0.73972800	−2.27821200	−1.46335600
C	−4.46674200	−1.25601500	−1.89467900
H	−3.85650100	0.70780200	−1.24579500
C	−4.06305500	−2.57001900	−2.17414700
H	−2.39483100	−3.94363000	−2.23244400
H	−5.50476800	−0.96655200	−2.02162000
H	−4.78672000	−3.30243200	−2.51622900
C	0.34348600	−0.34006100	0.14443100
C	1.73099400	−0.16556400	−0.06640400
C	−0.04061400	−1.23115600	1.15263800
C	2.64829700	−0.87775100	0.71180200
C	0.87358500	−1.94279800	1.92533100
C	2.23261600	−1.76295800	1.70254900
I	2.53226100	1.15549000	−1.50802300
F	−1.37418700	−1.44481500	1.42740000
F	0.44627600	−2.80853900	2.89950000
F	3.15091400	−2.44815700	2.45414100
F	4.00321900	−0.72382600	0.52395100

Intermediate, **INT**:

I	0.17012900	−2.33449000	−0.71428300
Rh	−0.45604200	0.24522800	−0.12187100
P	1.87177800	0.69336500	−0.02114700
P	−2.79727100	−0.22335400	0.07886500
F	2.35148400	−4.56181600	−0.25583300
F	4.93793400	−4.53311500	0.64591700
F	6.15546800	−2.12952700	1.27587800
F	4.81012600	0.20792600	0.97795100
O	−0.74479100	2.31584400	−2.13504800
O	−0.94937500	2.04208200	0.85166300
C	2.81423600	−0.93588300	0.24055600
C	2.20579200	−2.16642600	−0.07806900
C	2.93294400	−3.34862100	0.05680400
C	4.24888100	−3.35542500	0.51037700
C	4.85815100	−2.14732000	0.82842100
C	4.14166600	−0.96228100	0.67729200
C	0.57346500	4.19887600	−2.85722600
H	0.23142100	5.23961600	−2.82800100
H	0.36664500	3.77003200	−3.84028000
H	1.65804500	4.19465800	−2.68672500
C	−0.12380700	3.37063400	−1.78371500
C	−0.02539200	3.87330900	−0.43895200
H	0.41605600	4.85922700	−0.32798800
C	−0.48120500	3.25800700	0.73054800
C	−0.42696200	4.02251400	2.03898500
H	−0.01869300	5.02847300	1.91558100
H	0.19251500	3.46289300	2.75140700
H	−1.43893700	4.08845900	2.45401900
C	−3.48891700	−1.53594800	−1.06859300
C	−4.79564900	−1.51405700	−1.57926300
C	−3.01978900	−3.52891000	−2.19838600
C	−5.20963900	−2.55171100	−2.42942700
H	−5.46222200	−0.69764100	−1.32390600
C	−4.31182500	−3.58166900	−2.74149600
H	−2.28378700	−4.29526600	−2.41756700
H	−6.21371500	−2.55262700	−2.83944600
H	−4.59364400	−4.40040000	−3.39250100
N	−2.61877400	−2.52669400	−1.38889300
C	2.75028700	1.32035500	−1.54064900
C	4.06447700	1.82581300	−1.52648600
C	2.05474600	1.19289400	−2.75652600
C	4.67526900	2.20512900	−2.72934600
H	4.61010900	1.91637800	−0.59239900
C	2.67850200	1.56267000	−3.95832900
H	1.02324600	0.84870600	−2.75573800
C	3.98556600	2.06948200	−3.94654700
H	5.68757700	2.59565100	−2.71763300
H	2.13671500	1.46732400	−4.89335400
H	4.46505900	2.36027000	−4.87591500
C	2.41527300	1.72852300	1.42328100
C	2.85421100	3.05188300	1.27006100
C	2.27902400	1.17849800	2.70927300
C	3.18833200	3.81129800	2.40178700
H	2.91849000	3.49682100	0.28143700
C	2.62007700	1.93653900	3.83731800
H	1.89560100	0.16741900	2.83143500
C	3.08104800	3.25448400	3.68459900
H	3.52801300	4.83448000	2.27938600
H	2.51989900	1.50504900	4.82782100
H	3.34519900	3.84264400	4.55751900
C	−4.01745700	1.16831000	−0.07098100
C	−5.22023200	1.17766800	0.65631600
C	−3.69753100	2.23053600	−0.93440900
C	−6.11924300	2.24344200	0.50527400
H	−5.44520700	0.37148300	1.35080500
C	−4.60401900	3.29272300	−1.08255300
H	−2.74133500	2.23174800	−1.45689600
C	−5.81251900	3.29952100	−0.36855000
H	−7.04517900	2.25409900	1.07118800
H	−4.35630100	4.11713400	−1.74311100
H	−6.50601000	4.12714800	−0.48132200
C	−3.15197000	−0.92402300	1.76895100
C	−3.94918200	−2.05451900	2.00028700
C	−2.55840200	−0.24255000	2.85046200
C	−4.16150200	−2.50466500	3.31423400
H	−4.40175600	−2.59084000	1.16985500

C	−2.78398600	−0.68860300	4.15930000
H	−1.92796900	0.62411000	2.65224400
C	−3.58389000	−1.82046100	4.39325600
H	−4.77389300	−3.38295200	3.49177300
H	−2.33144800	−0.16116300	4.99277200
H	−3.75034700	−2.16836300	5.40780300

Intermediate 2, **INT 2:**

I	0.46948000	2.40011300	0.56841400
Rh	−0.40608700	−0.06787300	−0.18094000
P	1.85562000	−0.74977700	−0.06302600
P	−2.75456300	0.40732900	−0.19127400
F	2.87053800	4.41428200	0.32702400
F	5.52766000	4.11771500	−0.28480400
F	6.55067400	1.60273400	−0.80680400
F	4.94945800	−0.58063700	−0.70436000
O	−1.51844900	−1.97158900	1.62847500
O	−0.87196900	−1.79710700	−1.25264300
C	3.00908800	0.75888100	−0.17967500
C	2.51104700	2.04617900	0.09308200
C	3.35802600	3.15336200	0.06021200
C	4.70993400	3.01979900	−0.24451900
C	5.22090900	1.75483300	−0.51049200
C	4.37347200	0.64938400	−0.46271200
C	−0.70685800	−3.95806600	2.72132100
H	−1.30249100	−4.87781400	2.68042100
H	−0.98476200	−3.38987300	3.61197600
H	0.35004000	−4.24321200	2.78056300
C	−0.96237800	−3.11102300	1.48210800
C	−0.58570600	−3.68999800	0.22221700
H	−0.27624500	−4.73054200	0.23832100
C	−0.64894700	−3.06339800	−1.02911600
C	−0.45124900	−3.88116500	−2.28919400
H	−0.16655500	−4.91385600	−2.07206100
H	0.31729600	−3.40755100	−2.91159900
H	−1.38903300	−3.87474400	−2.85751000
C	−3.55475500	0.43996900	1.48738600
C	−4.94178800	0.31204900	1.66214100
C	−5.47012700	0.34513000	2.95996000
H	−5.59201900	0.16869300	0.80232700
C	−4.58847800	0.50618300	4.03964800
H	−6.53459200	0.24383800	3.13576700
H	−4.95459300	0.54327400	5.06007600
C	2.41923500	−1.46576600	1.56178200
C	3.69802600	−2.02792500	1.74437900
C	1.52617300	−1.37423300	2.64341100
C	4.07651100	−2.49506300	3.00943200
H	4.39118100	−2.10476000	0.91195700
C	1.91546400	−1.83878600	3.91025800
H	0.52793700	−0.96875700	2.49076200
C	3.18788000	−2.39781100	4.09424000
H	5.06108900	−2.92934200	3.14914400
H	1.22130200	−1.76801700	4.74095900
H	3.48700300	−2.75785900	5.07336400
C	2.47632100	−1.87250100	−1.40345400
C	2.74538600	−3.22734600	−1.16144400
C	2.58080000	−1.35429900	−2.70505900
C	3.15490300	−4.05480400	−2.21829500
H	2.62162700	−3.64094100	−0.16492300
C	2.99415400	−2.18139300	−3.75695100
H	2.32904600	−0.31399300	−2.90098300
C	3.28782700	−3.53347300	−3.51344500
H	3.36314900	−5.10262100	−2.02889100
H	3.07932200	−1.77740000	−4.76014700
H	3.60713300	−4.17458200	−4.32853700
C	−3.86081200	−0.77150100	−1.11765400
C	−4.65689800	−0.36541200	−2.19859700
C	−3.86626100	−2.11650200	−0.70076200
C	−5.46331400	−1.30415100	−2.86473300
H	−4.65496700	0.67092700	−2.52526200
C	−4.67592000	−3.04600500	−1.36449500
H	−3.23634200	−2.41912100	0.13219600
C	−5.47472800	−2.64260700	−2.44899900
H	−6.07733600	−0.98806400	−3.70201200
H	−4.67763500	−4.08196700	−1.04073100
H	−6.09815600	−3.36641900	−2.96457500
C	−3.17392100	2.07201700	−0.93233600

C	−4.15379600	2.94043600	−0.42420700
C	−2.43677300	2.44993700	−2.07264800
C	−4.39689300	4.17358300	−1.05184400
H	−4.71867000	2.66943700	0.46299100
C	−2.68773900	3.67508000	−2.70511000
H	−1.66469800	1.78296500	−2.45210200
C	−3.66906000	4.54023400	−2.19371600
H	−5.14907300	4.84372600	−0.64854900
H	−2.11673600	3.95647900	−3.58379800
H	−3.85833200	5.49368900	−2.67615600
N	−3.24878800	0.60862600	3.88641400
C	−2.74897800	0.56277600	2.63220100
H	−1.66707900	0.58616500	2.54086900

Transition state, **TS** (frequency: −145.41 cm^{-1}):

I	−0.26791600	−2.64315100	0.69098000
Rh	0.09897000	−0.25092300	−0.66779100
P	−2.40553600	−0.28003800	−0.79467000
P	2.45181500	−0.16939700	−0.34746400
F	0.69588900	−0.84214600	3.21931800
F	−0.63358500	0.99746100	4.74397800
F	−3.08017800	1.99593300	3.92702900
F	−4.11179300	1.27210000	1.49770500
O	−0.65212700	2.10167200	0.76809100
O	0.41069800	1.46048900	−1.90110500
C	−2.24605200	−0.17999300	1.07254400
C	−1.03502200	−0.75278800	1.53870200
C	−0.51265700	−0.34534500	2.76152900
C	−1.18481900	0.58596800	3.55290000
C	−2.40937400	1.08911600	3.14068200
C	−2.92267300	0.70076500	1.90206000
C	−0.34661900	4.35417400	1.52947600
H	0.44916000	5.10208300	1.46842100
H	−0.37111600	3.91295200	2.53099500
H	−1.30912800	4.85336700	1.36013700
C	−0.17420600	3.25117500	0.49599800
C	0.48264600	3.59003200	−0.73235000
H	0.84188800	4.60818300	−0.83121600
C	0.74687500	2.72258700	−1.79664000
C	1.49233600	3.25656700	−3.00650500
H	1.67428000	4.33139300	−2.93860800
H	0.91630700	3.03583500	−3.91152100
H	2.45339600	2.73355700	−3.09288200
C	3.26035900	−1.44035700	0.76733500
C	3.78861200	−1.14513200	2.03098700
C	3.78859100	−3.69413800	0.98500100
C	4.33023800	−2.19419200	2.79197000
H	3.77974600	−0.13045300	2.41030700
C	4.33438200	−3.49086600	2.26372100
H	3.76970100	−4.67948300	0.53224500
H	4.73838900	−1.99751600	3.77734700
H	4.74404500	−4.32611600	2.81942300
N	3.25609800	−2.69442600	0.25532100
C	−3.47350200	1.13035900	−1.35057600
C	−4.85603500	0.98939900	−1.55256300
C	−2.84176500	2.36217800	−1.58954000
C	−5.61085500	2.09085500	−1.97806300
H	−5.34366300	0.03466200	−1.37708200
C	−3.60364200	3.46247500	−2.00778200
H	−1.76948500	2.45259600	−1.45276800
C	−4.98697800	3.32953500	−2.20008300
H	−6.67987600	1.98459300	−2.13091000
H	−3.11312900	4.41420000	−2.18444900
H	−5.57606700	4.18210500	−2.52348600
C	−3.42109100	−1.80517700	−1.09989200
C	−3.24251900	−2.48094700	−2.31891000
C	−4.34523800	−2.28824400	−0.15863200
C	−3.99084400	−3.63303300	−2.59928900
H	−2.51341100	−2.11590200	−3.03798100
C	−5.08932500	−3.44472800	−0.43790100
H	−4.47574900	−1.77030500	0.78857900
C	−4.91414100	−4.11611100	−1.65811500
H	−3.84900400	−4.15316500	−3.54066200
H	−5.79903500	−3.81943300	0.29235100
H	−5.48910100	−5.01112800	−1.87262800

C	3.00348200	1.45996900	0.36017100
C	3.93268600	2.28023000	−0.29853400
C	2.41912300	1.89434000	1.56468400
C	4.27699800	3.52797800	0.24430600
H	4.37943700	1.95888200	−1.23534500
C	2.77939400	3.13081100	2.11501300
H	1.65816900	1.28865400	2.05247000
C	3.70595400	3.95259400	1.45250100
H	4.98667600	4.16279100	−0.27631100
H	2.32475700	3.45737000	3.04505100
H	3.97482600	4.91660900	1.87282000
C	3.42346400	−0.36224000	−1.92030900
C	4.79227900	−0.68374600	−1.88695700
C	2.77265500	−0.17817500	−3.15133500
C	5.51115200	−0.81765000	−3.08186200
H	5.29229300	−0.83833700	−0.93385300
C	3.49760600	−0.31307700	−4.34709000
H	1.71803900	0.08588200	−3.16474500
C	4.86287700	−0.63178500	−4.31465700
H	6.56626900	−1.06969800	−3.05352400
H	2.99422400	−0.17174200	−5.29796000
H	5.41853100	−0.73908500	−5.24093500

Compound **6**:

I	−0.02591500	−0.55893700	−2.78274500
Rh	0.05901200	−0.83111600	−0.08200500
P	−1.60306500	0.91210500	0.24384300
P	2.20257000	0.39517100	−0.02610400
F	−1.51445700	−4.03209100	−0.41833400
F	−4.21330100	−4.41189400	−0.27832500
F	−5.93754600	−2.31021500	0.10734400
F	−4.95043900	0.26820800	0.37284600
O	1.05854200	−2.63462500	−0.26211200
O	0.06801200	−1.04137200	1.97885800
C	−2.70359700	−0.57701900	0.11892400
C	−1.80154500	−1.64386900	−0.09141100
C	−2.32040700	−2.92382500	−0.22079600
C	−3.70161400	−3.14056700	−0.15355700
C	−4.58140600	−2.07530500	0.04356300
C	−4.07251500	−0.78334100	0.18101500
C	1.68114400	−4.86017500	0.21403300
H	1.93626700	−5.51437900	1.04940300
H	2.55571800	−4.70821100	−0.42552500
H	0.90123600	−5.33295900	−0.39318300
C	1.15884500	−3.52175900	0.67356900
C	0.82400200	−3.33142300	2.03898300
H	0.97155900	−4.17571700	2.69958000
C	0.34059300	−2.14368600	2.61628300
C	0.13055400	−2.05325500	4.10928600
H	0.27775300	−3.01374600	4.60630700
H	−0.87908800	−1.68020300	4.30671500
H	0.83372600	−1.31644600	4.51628600
C	2.08658600	1.99171500	−0.97948600
C	2.85777600	2.25119600	−2.12077600
C	0.90856300	3.98010800	−1.22633300
C	2.61751900	3.43399300	−2.83602400
H	3.60654600	1.53973900	−2.44980700
C	1.62924600	4.31637700	−2.38205100
H	0.13171300	4.63206800	−0.84575300
H	3.18565200	3.65412000	−3.73316400
H	1.40762700	5.23676400	−2.90875100
N	1.12083500	2.83657700	−0.54130400
C	−2.30443700	2.19459200	−0.89770200
C	−2.29921500	3.54428000	−0.50982200
C	−2.85291000	1.81816100	−2.13488900
C	−2.83816900	4.51859000	−1.36222200
H	−1.88710300	3.83328000	0.45346700
C	−3.38566300	2.79646100	−2.98527800
H	−2.85496300	0.77596700	−2.44060100
C	−3.37793300	4.14688900	−2.60285200
H	−2.84185000	5.55983900	−1.05519100
H	−3.80558500	2.50194200	−3.94099500
H	−3.79587900	4.90020300	−3.26283900
C	−1.79019300	1.63342100	1.93965300
C	−0.65367100	1.79265000	2.74487400
C	−3.05676700	2.02837200	2.40802700
C	−0.78053800	2.35415500	4.02483700

H	0.31619400	1.46539400	2.38715700
C	−3.17903800	2.58278700	3.68980900
H	−3.93622700	1.91210100	1.77961100
C	−2.04128600	2.74706100	4.49802800
H	0.10322500	2.47546500	4.64337000
H	−4.15534700	2.88464800	4.05389100
H	−2.14049000	3.17735600	5.48973400
C	3.72686400	−0.42713100	−0.71278900
C	3.59656400	−1.51007700	−1.59964200
C	5.00641900	0.04670400	−0.36396800
C	4.74758300	−2.10787800	−2.14002000
H	2.61198800	−1.88830600	−1.85643300
C	6.15051600	−0.55367800	−0.90551300
H	5.10696600	0.87436600	0.33418600
C	6.02125300	−1.63225900	−1.79706400
H	4.64307500	−2.94136300	−2.82667000
H	7.13424800	−0.18564300	−0.63322400
H	6.90749700	−2.09792900	−2.21642100
C	2.77573100	0.90036900	1.67691600
C	3.06813400	−0.14109600	2.57875300
C	2.89945800	2.23438300	2.09464900
C	3.48677900	0.15064600	3.88312400
H	2.98091600	−1.17829200	2.25838400
C	3.31462600	2.52516500	3.40509200
H	2.65869400	3.04403300	1.41432800
C	3.60827900	1.48694400	4.30092000
H	3.71802900	−0.65900000	4.56807600
H	3.40846100	3.55934500	3.72041100
H	3.93144800	1.71409300	5.31180200

Product from "**INT 2**" (not observed experimentally):

I	−0.02145300	−0.40793800	−2.76947000
Rh	−0.00038000	−0.85578200	−0.09785800
P	−1.50994000	1.00165600	0.30525900
P	2.21054000	0.23791200	0.03408500
F	−1.87526000	−3.86633800	−0.72897800
F	−4.59472300	−4.00237100	−0.57354100
F	−6.11109900	−1.79053900	0.01124000
F	−4.87628500	0.66235400	0.45575600
O	0.85233800	−2.73448600	−0.36823000
O	−0.10803300	−1.24102000	1.94291300
C	−2.72964200	−0.37574900	0.10643800
C	−1.92889800	−1.50041700	−0.19081800
C	−2.56968700	−2.70906100	−0.42077400
C	−3.96476600	−2.79988100	−0.35096000
C	−4.74027400	−1.67747600	−0.05367800
C	−4.11134700	−0.45325900	0.17424800
C	1.11594500	−5.06611700	−0.09151900
H	1.23260800	−5.81832000	0.69043700
H	2.04134900	−4.97495000	−0.66705800
H	0.32371700	−5.38070800	−0.78030200
C	0.73065300	−3.71811400	0.46331300
C	0.27572100	−3.61772700	1.80437300
H	0.22858900	−4.53755200	2.37231000
C	−0.07400000	−2.43193900	2.47232300
C	−0.40498500	−2.45939600	3.94568200
H	−0.45406500	−3.47650700	4.33812400
H	−1.36016400	−1.95103000	4.10917800
H	0.36248400	−1.89539400	4.48923800
C	2.10601300	2.02622400	−0.46951400
C	2.41451100	2.42070200	−1.78356400
C	2.22576900	3.75866200	−2.15294400
H	2.78295200	1.69501500	−2.50251800
C	1.74007500	4.66365800	−1.19780800
H	2.44294400	4.09327500	−3.16006500
H	1.58640900	5.70898500	−1.44213900
C	−2.01675400	2.35466100	−0.85324100
C	−1.67638300	3.68504700	−0.55763900
C	−2.72116600	2.04612200	−2.02920500
C	−2.03700100	4.70739500	−1.44673300
H	−1.13797000	3.93504600	0.35167600
C	−3.08646000	3.07359600	−2.90795700
H	−2.96977500	1.01584600	−2.26703700
C	−2.74271600	4.40425600	−2.62043600
H	−1.76801200	5.73300200	−1.21557900
H	−3.63259400	2.83394500	−3.81379000

H	−3.02546800	5.19736100	−3.30506100
C	−1.65442400	1.73076700	2.00411200
C	−0.62662000	1.54129300	2.94240600
C	−2.79604300	2.48163900	2.34110300
C	−0.73530200	2.11898400	4.21656800
H	0.22971300	0.91882000	2.69818400
C	−2.90145700	3.04888300	3.61795700
H	−3.59200300	2.62396700	1.61493600
C	−1.86949500	2.87256800	4.55449000
H	0.06200200	1.97584700	4.93850700
H	−3.78218800	3.62576600	3.87903300
H	−1.95224500	3.31810300	5.54070100
C	3.61353700	−0.41349300	−1.00990300
C	3.43618800	−1.56972200	−1.78523700
C	4.85869200	0.24230900	−0.98905200
C	4.50994100	−2.06231200	−2.54692400
H	2.47585600	−2.07636500	−1.79604500
C	5.92382300	−0.25176700	−1.75102700
H	4.99680300	1.13318400	−0.37966300
C	5.74857300	−1.40699700	−2.53277900
H	4.37122200	−2.95245300	−3.15157300
H	6.88235300	0.25639600	−1.73470200
H	6.57350000	−1.79032500	−3.12501400
C	2.98780100	0.25961800	1.73498900
C	2.95214800	−0.95658000	2.44309800
C	3.63564300	1.36988400	2.30141900
C	3.54265900	−1.05720800	3.70942300
H	2.47693700	−1.82854800	1.99830500
C	4.21789200	1.27103400	3.57558900
H	3.69748900	2.31005300	1.76120800
C	4.16926200	0.06112400	4.28320200
H	3.51614500	−2.00238700	4.24231700
H	4.71297700	2.13464200	4.00736100
H	4.62288000	−0.01354800	5.26625900
N	1.43153100	4.29691800	0.06630900
C	1.60193900	3.00094800	0.41147500
H	1.32563200	2.75094000	1.43320500

2.5.9. Collection of spectra

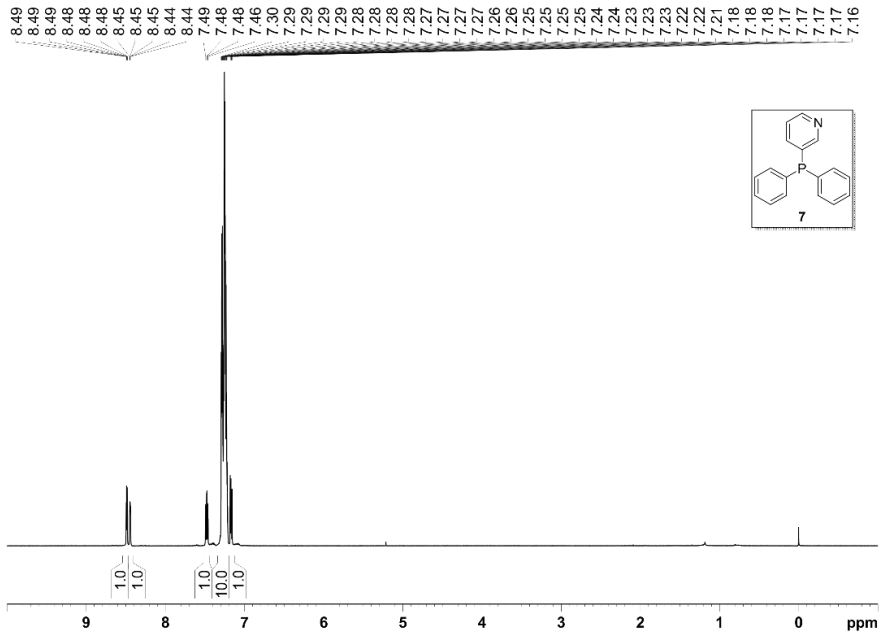

Figure 122. ^{1}H NMR spectrum (500 MHz, $CDCl_3$) for ligand **7**.

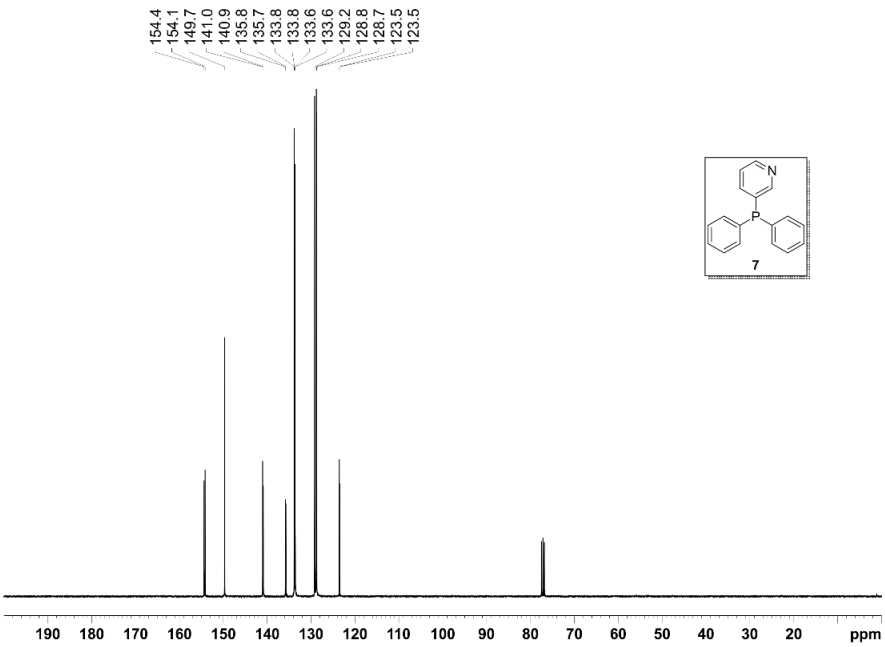

Figure 123. $^{13}C\{^{1}H\}$ NMR spectrum (100 MHz, $CDCl_3$) for ligand **7**.

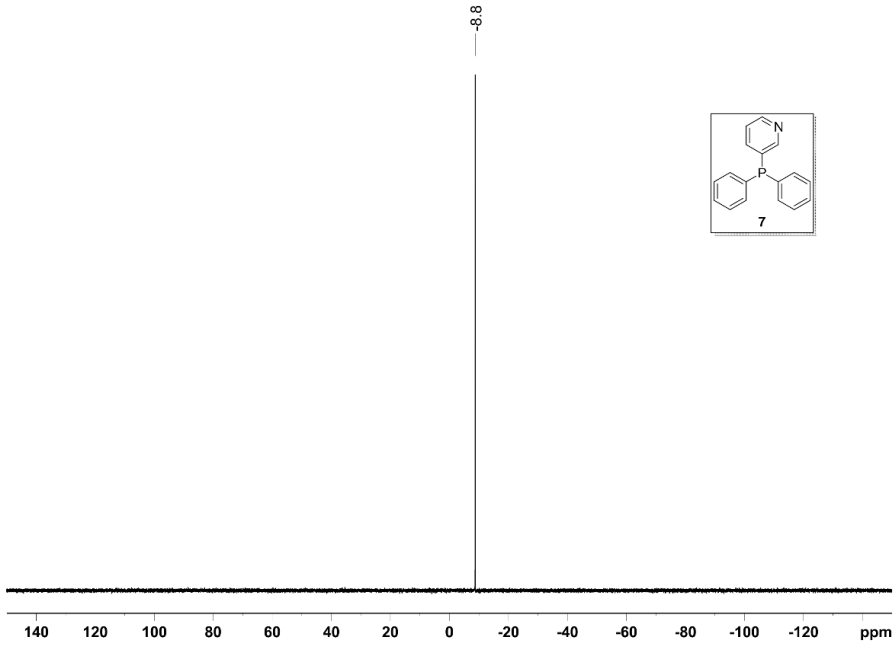

Figure 124. $^{31}P\{^{1}H\}$ NMR spectrum (202 MHz, $CDCl_3$) for ligand **7**.

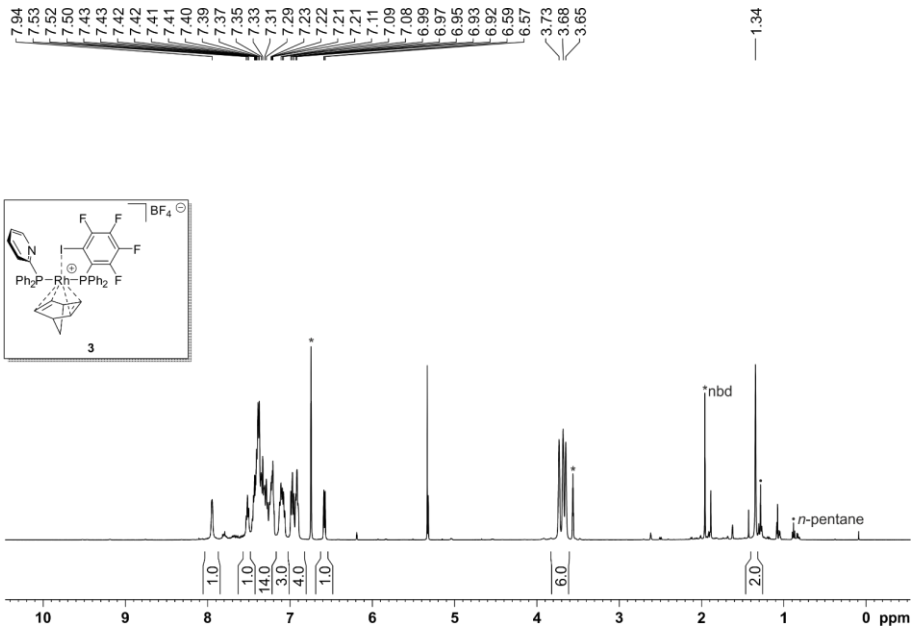

Figure 125. ^{1}H NMR spectrum (500 MHz, CD_2Cl_2) for complex **3**.

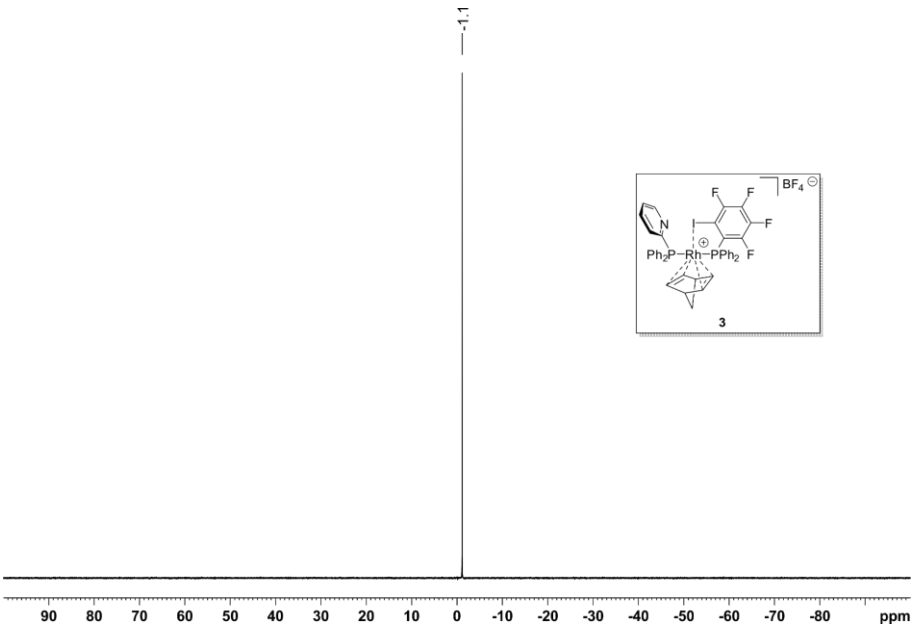

Figure 126. $^{11}B\{^{1}H\}$ NMR spectrum (160 MHz, CD_2Cl_2) for complex **3**.

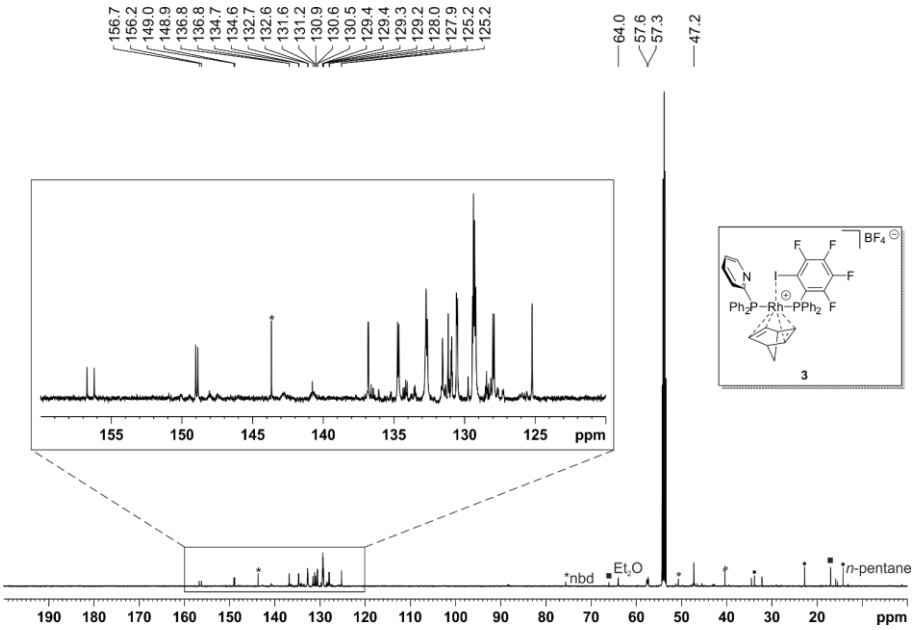

Figure 127. $^{13}C\{^{1}H\}$ NMR spectrum (126 MHz, CD_2Cl_2) for complex **3**.

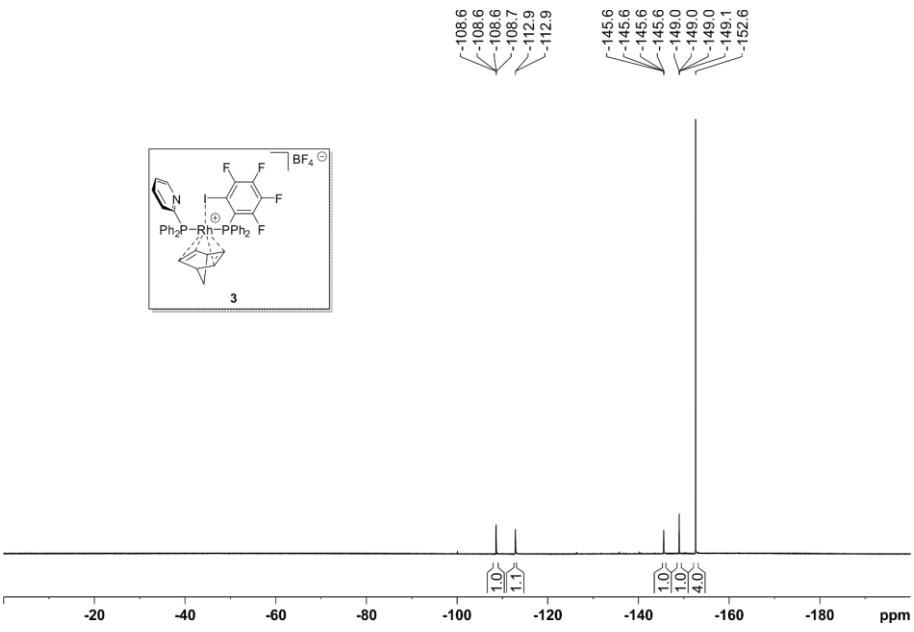

Figure 128. $^{19}F\{^{1}H\}$ NMR spectrum (471 MHz, CD_2Cl_2) for complex **3**.

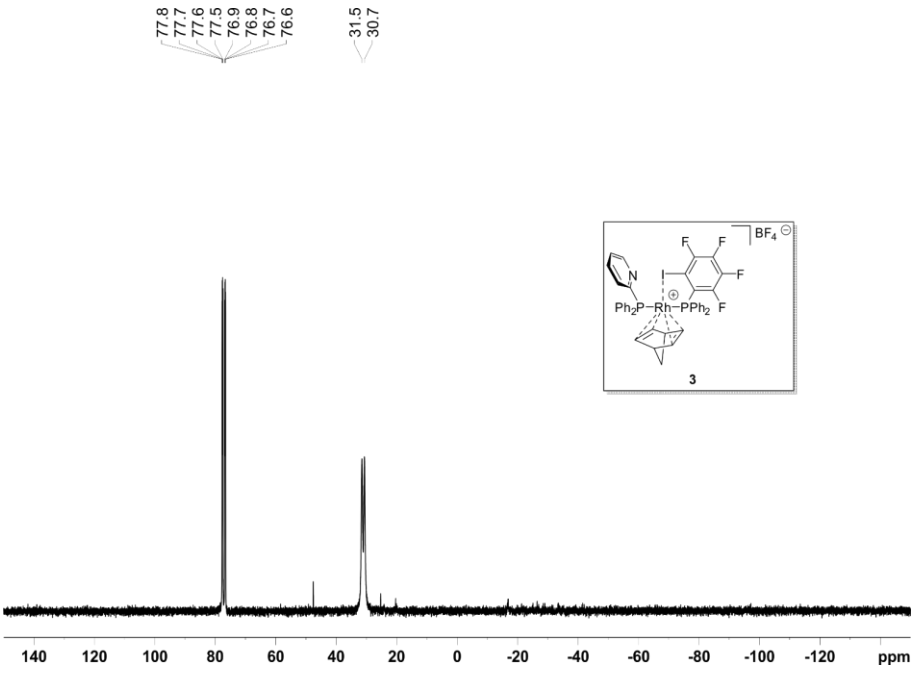

Figure 129. $^{31}P\{^{1}H\}$ NMR spectrum (162 MHz, CD_2Cl_2) for complex **3**.

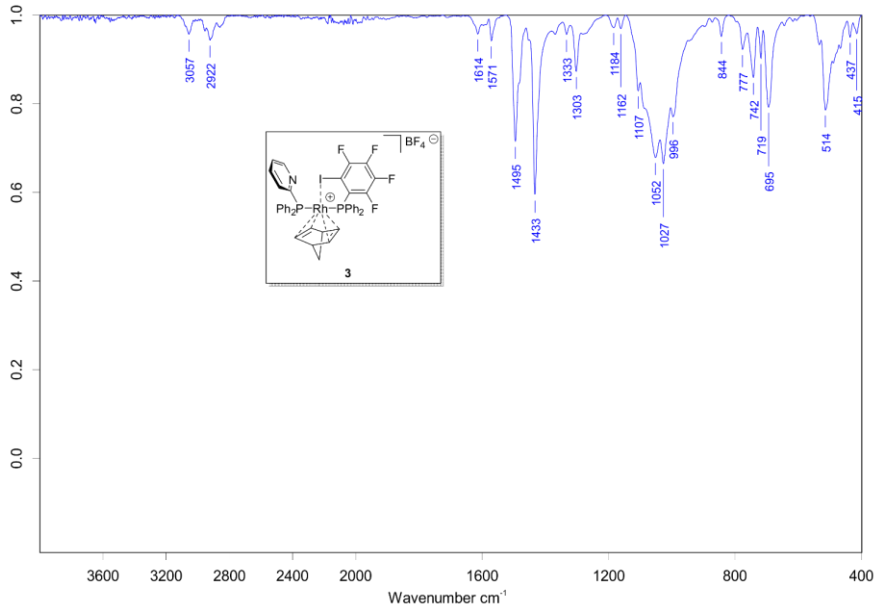

Figure 130. IR spectrum for complex **3**.

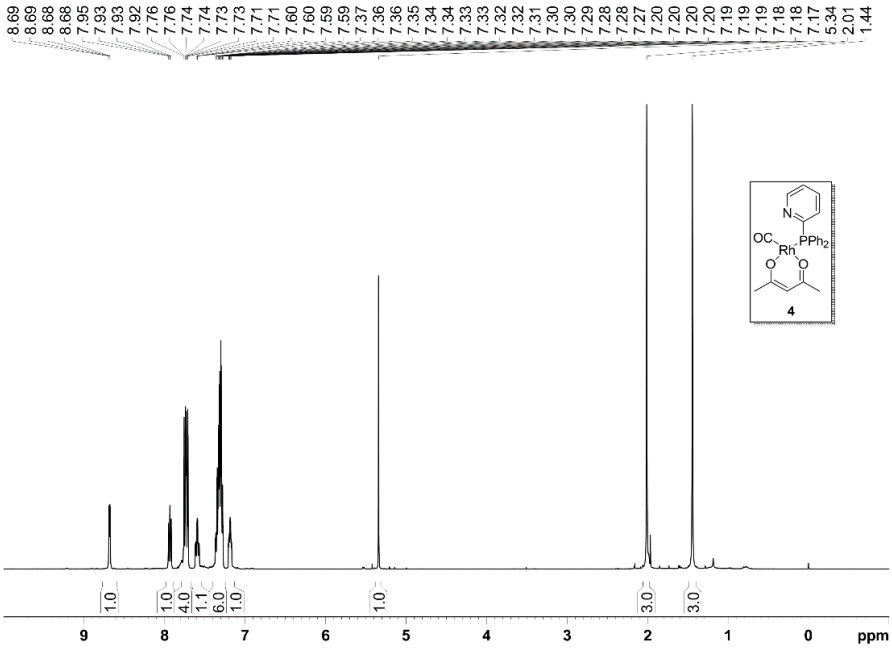

Figure 131. ^{1}H NMR spectrum (400 MHz, $CDCl_3$) for complex **4**.

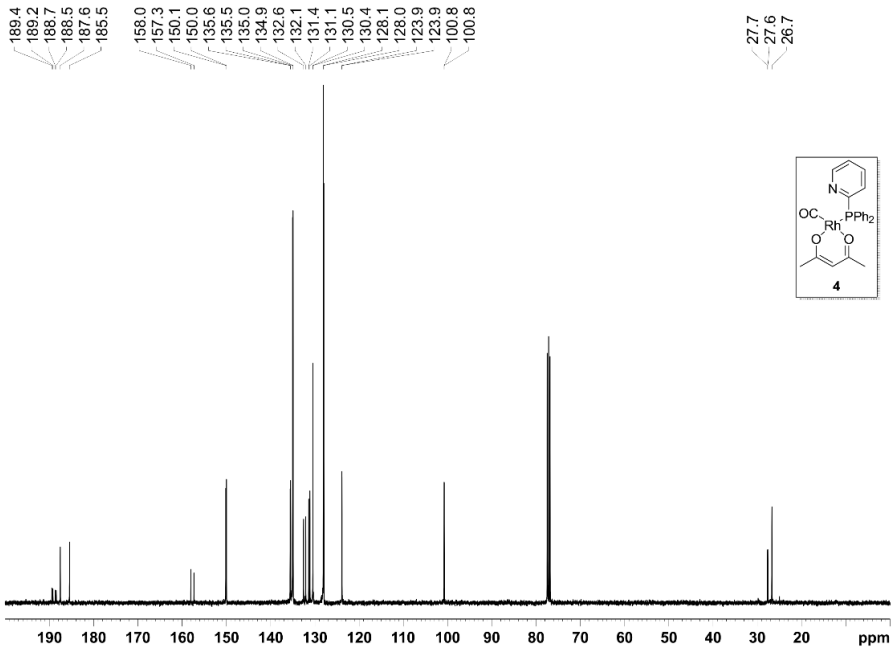

Figure 132. $^{13}C\{^{1}H\}$ NMR spectrum (100 MHz, $CDCl_3$) for complex **4**.

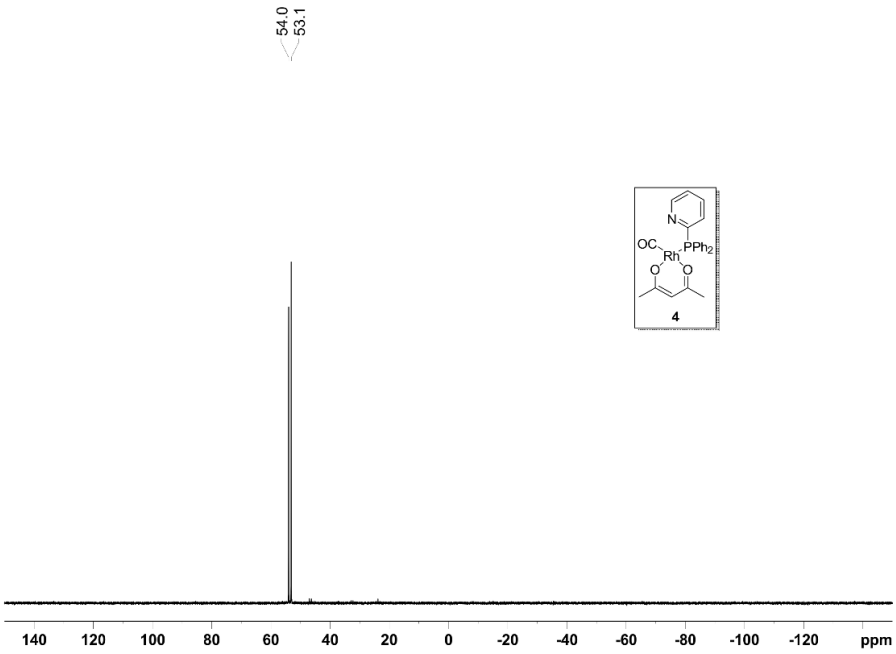

Figure 133. $^{31}P\{^{1}H\}$ NMR spectrum (202 MHz, $CDCl_3$) for complex **4**.

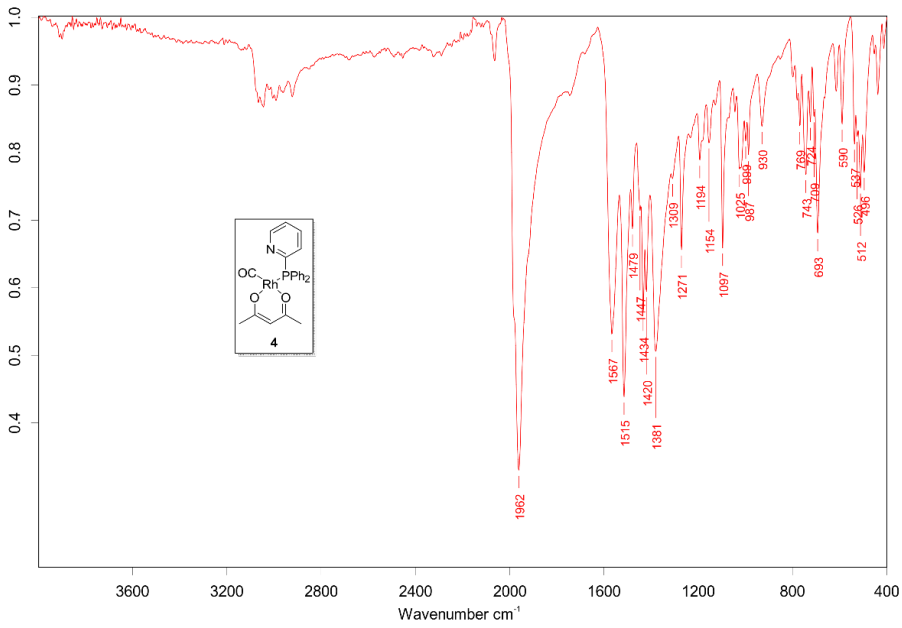

Figure 134. IR spectrum for complex **4**.

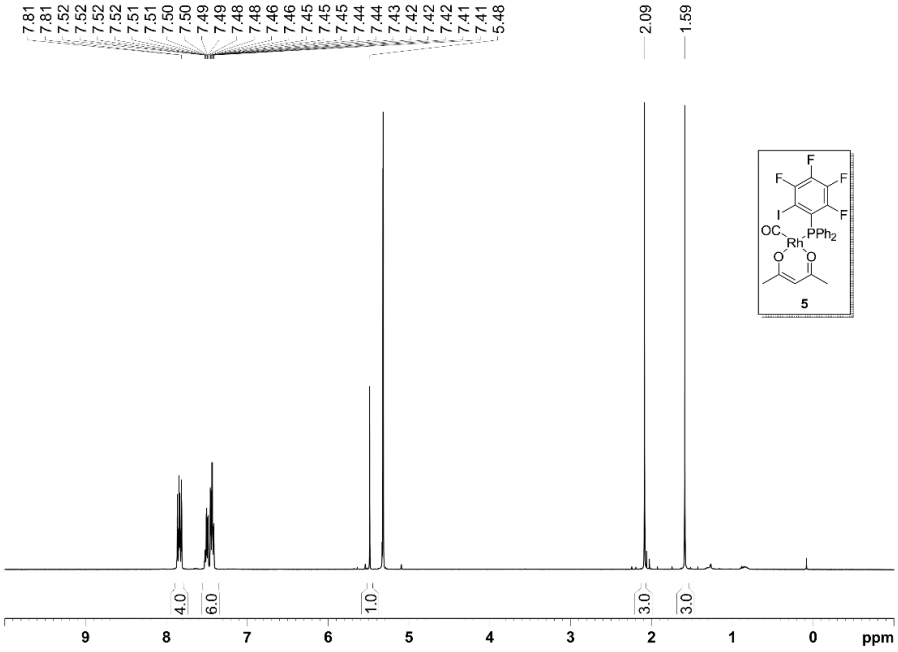

Figure 135. ^{1}H NMR spectrum (400 MHz, CD_2Cl_2) for complex **5**.

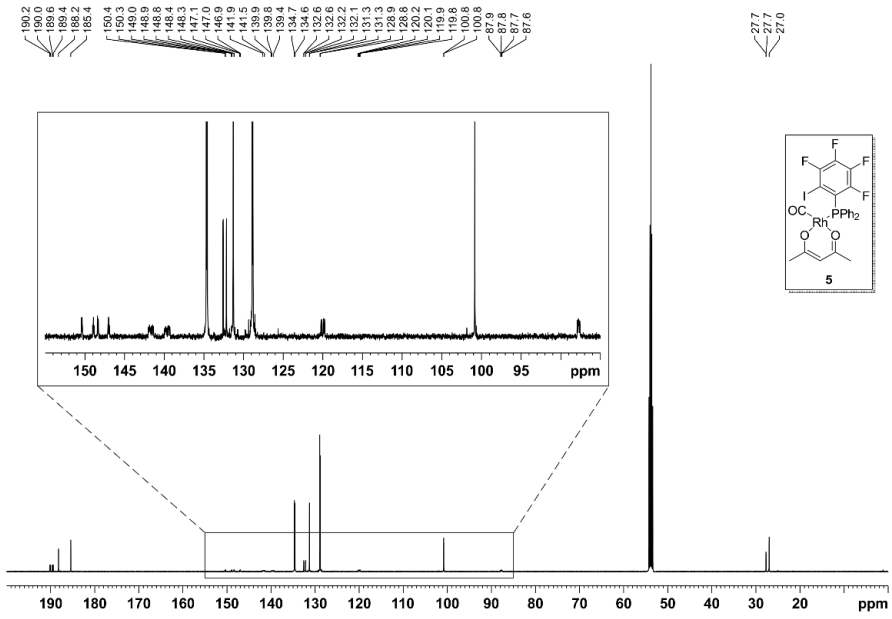

Figure 136. $^{13}C\{^{1}H\}$ NMR spectrum (126 MHz, CD_2Cl_2) for complex **5**.

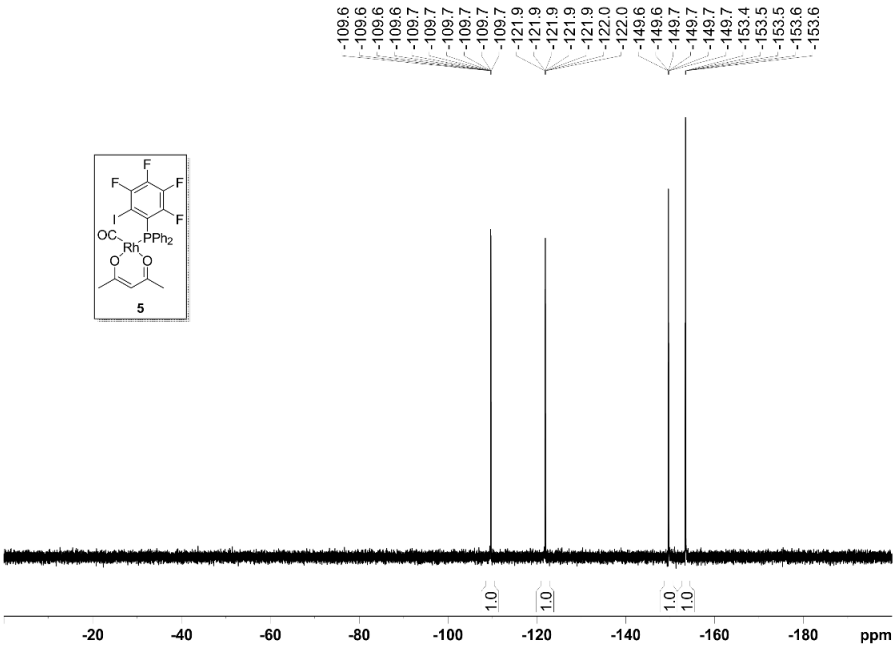

Figure 137. $^{19}F\{^{1}H\}$ NMR spectrum (376 MHz, CD_2Cl_2) for complex **5**.

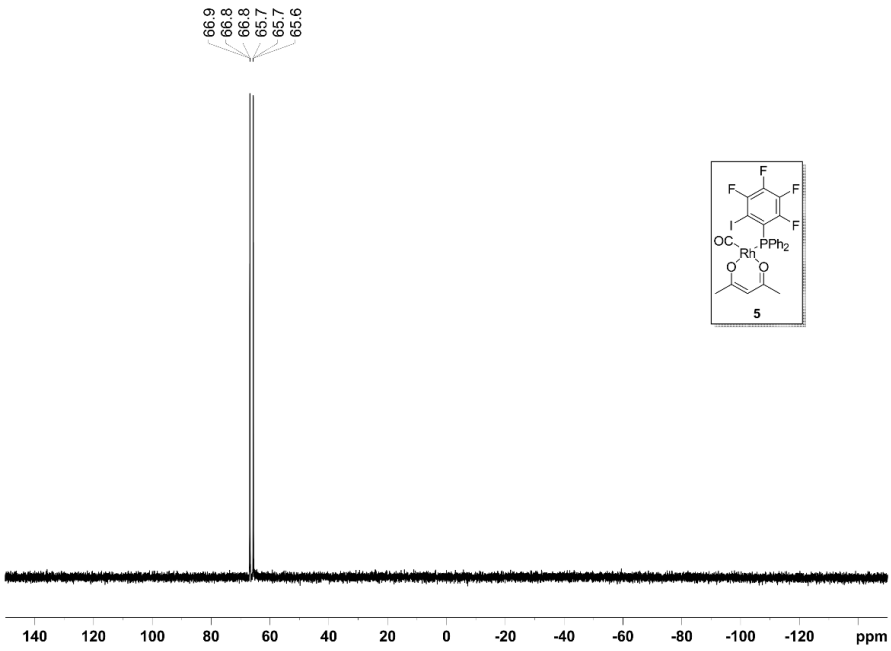

Figure 138. $^{31}P\{^{1}H\}$ NMR spectrum (162 MHz, CD_2Cl_2) for complex **5**.

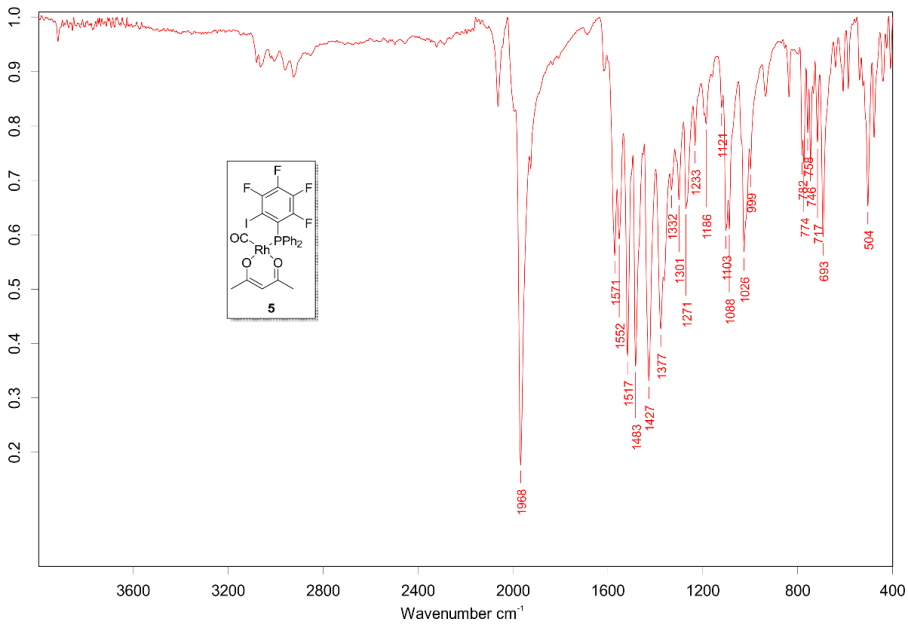

Figure 139. IR spectrum for complex **5**.

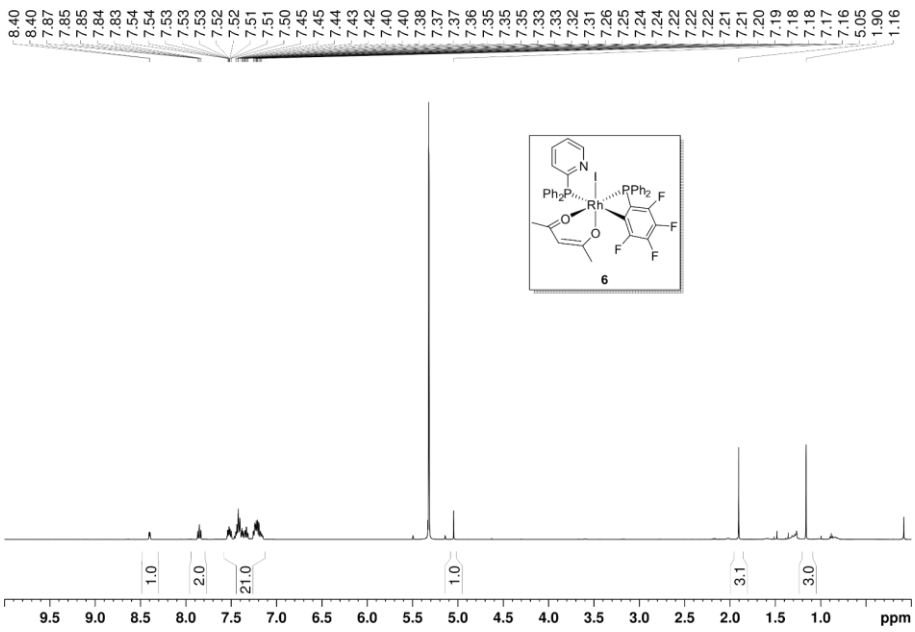

Figure 140. ^{1}H NMR spectrum (500 MHz, CD_2Cl_2) for complex **6**.

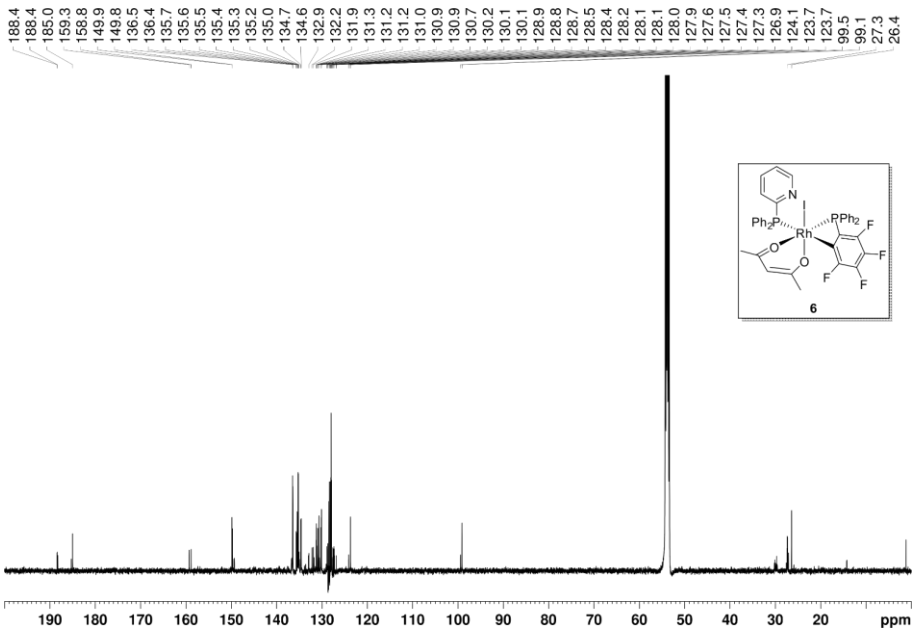

Figure 141. $^{13}C\{^{1}H\}$ NMR spectrum (126 MHz, CD_2Cl_2) for complex **6**.

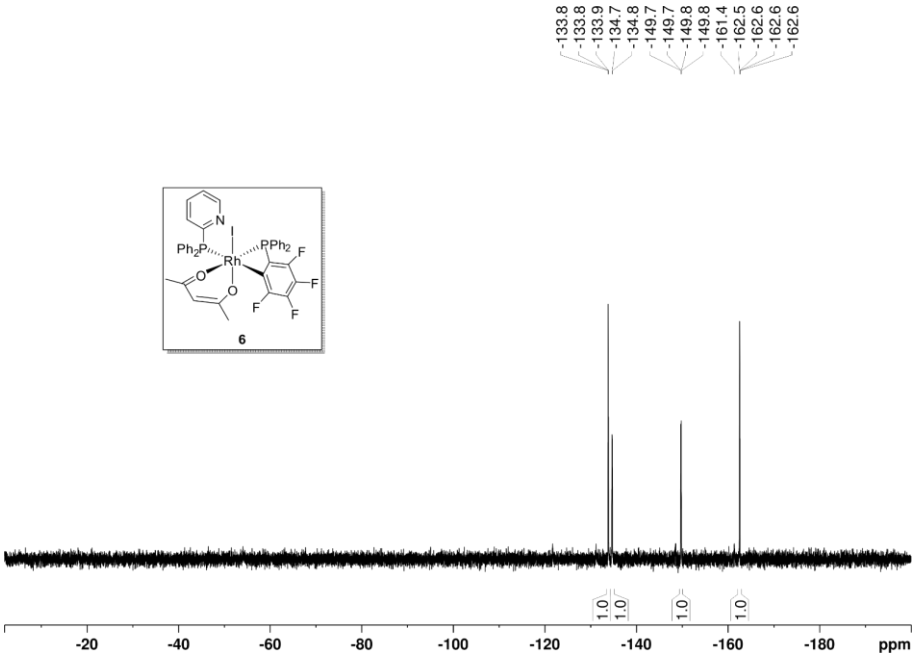

Figure 142. $^{19}F\{^{1}H\}$ NMR spectrum (376 MHz, CD_2Cl_2) for complex **6**.

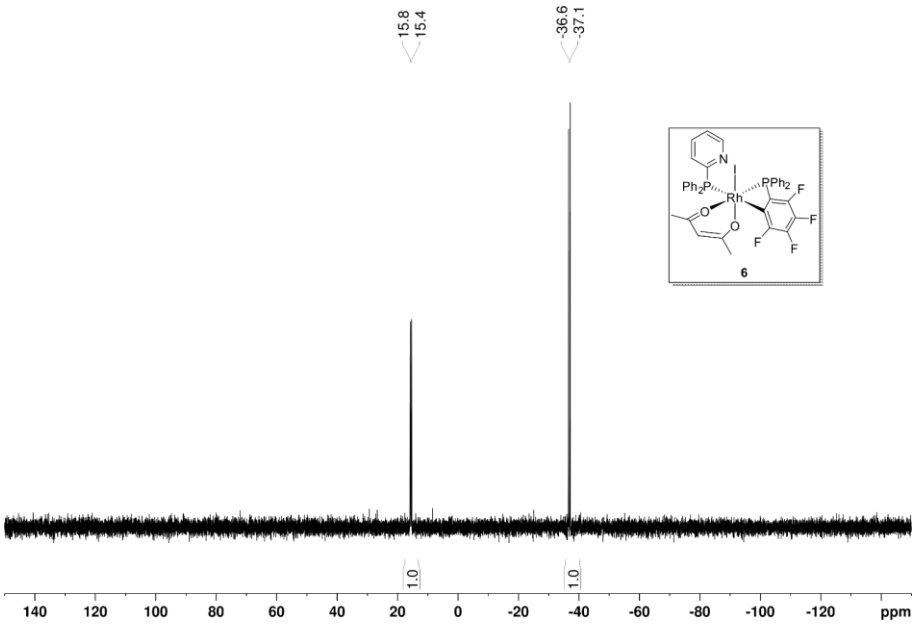

Figure 143. $^{31}P\{^{1}H\}$ NMR spectrum (202 MHz, CD_2Cl_2) for complex **6**.

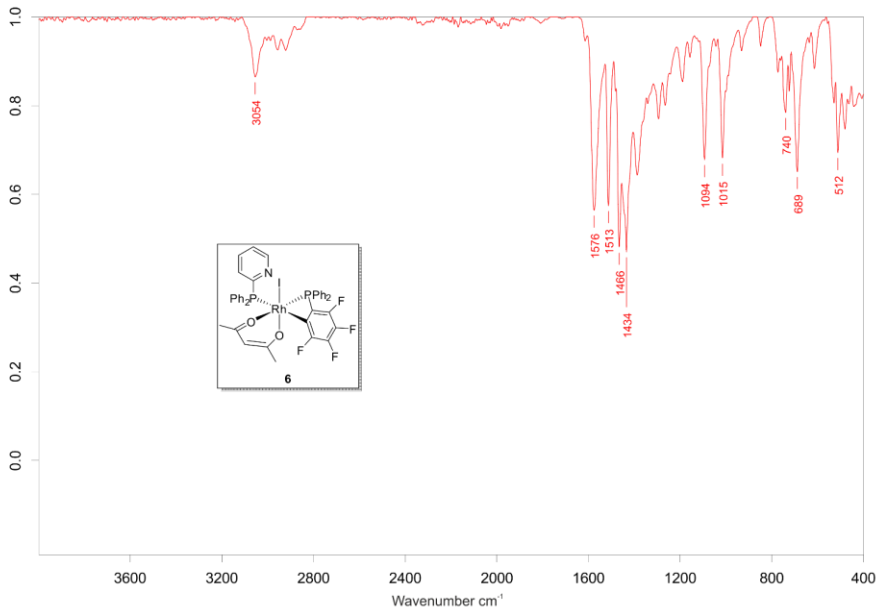

Figure 144. IR spectrum for complex **6**.

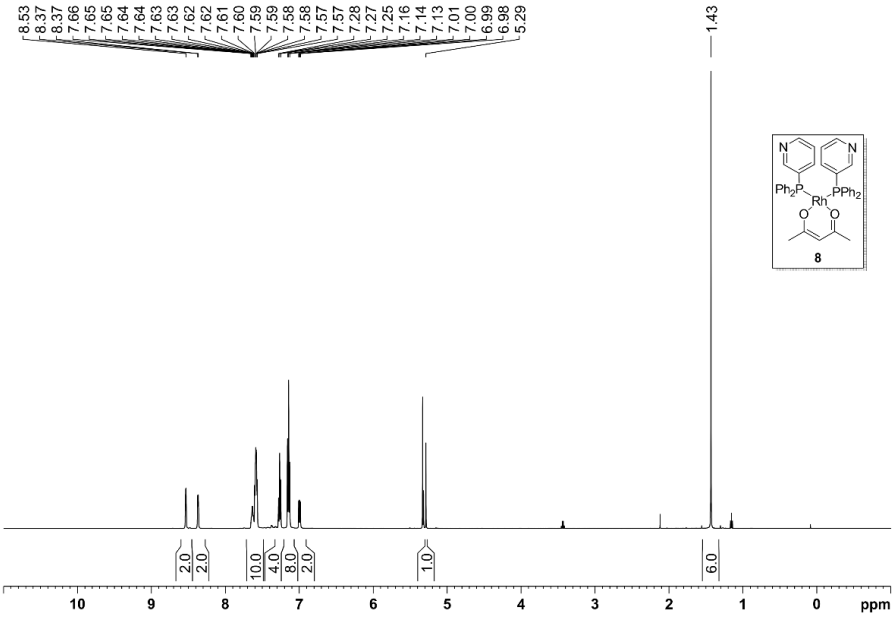

Figure 145. ^{1}H NMR spectrum (500 MHz, CD_2Cl_2) for complex **8**.

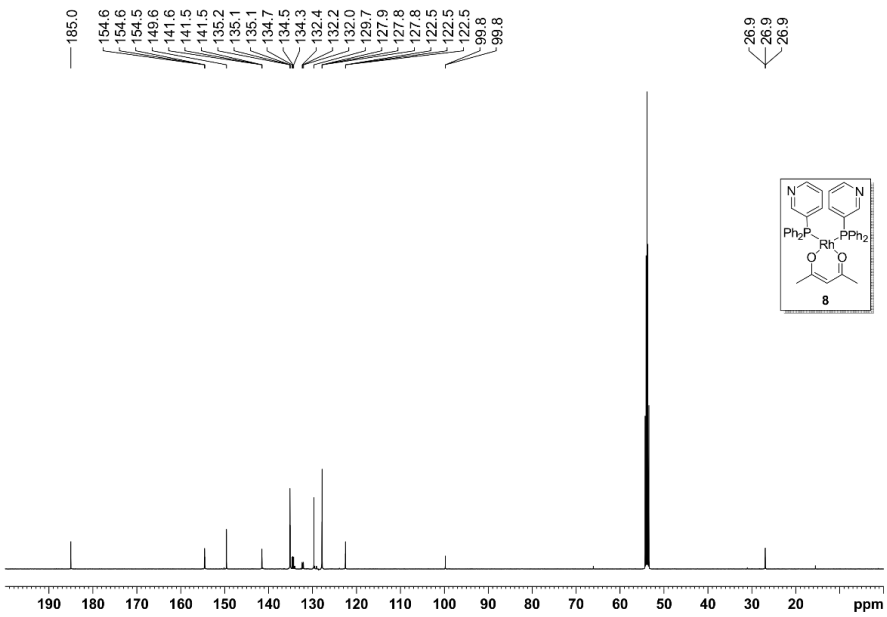

Figure 146. $^{13}C\{^{1}H\}$ NMR spectrum (126 MHz, CD_2Cl_2) for complex **8**.

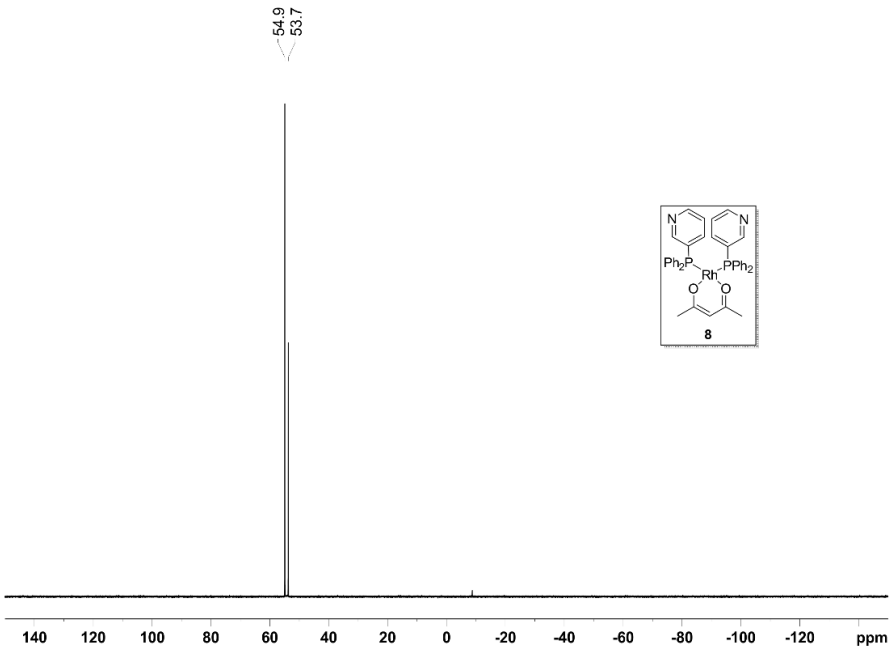

Figure 147. $^{31}P\{^{1}H\}$ NMR spectrum (162 MHz, CD_2Cl_2) for complex **8**.

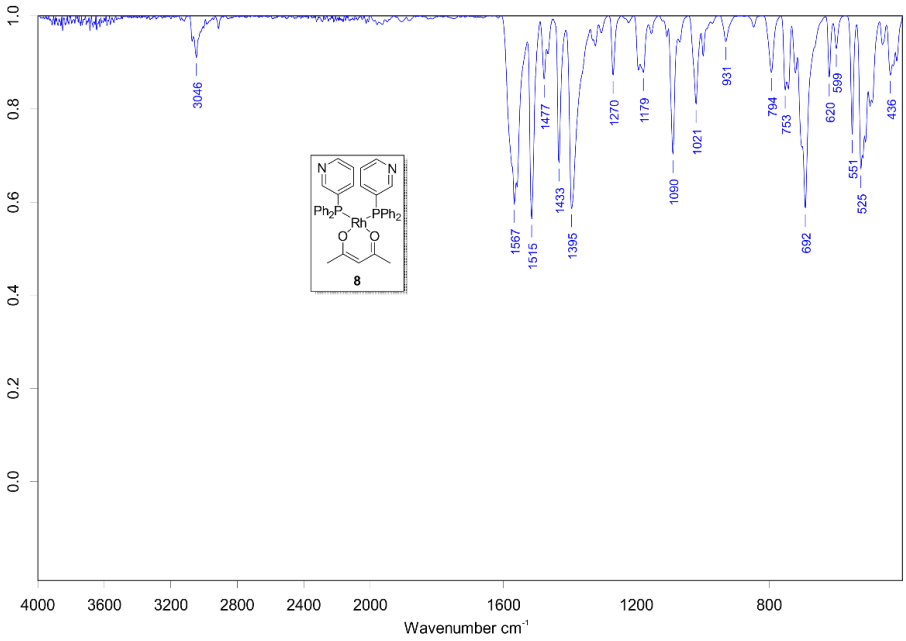

Figure 148. IR spectrum for complex **8**.

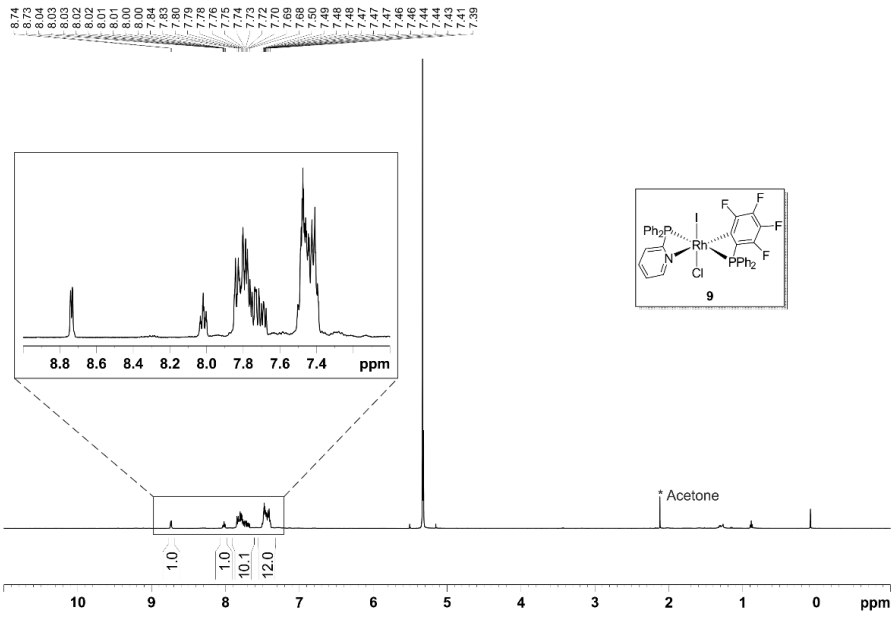

Figure 149. ^{1}H NMR spectrum (500 MHz, CD_2Cl_2) for complex **9**.

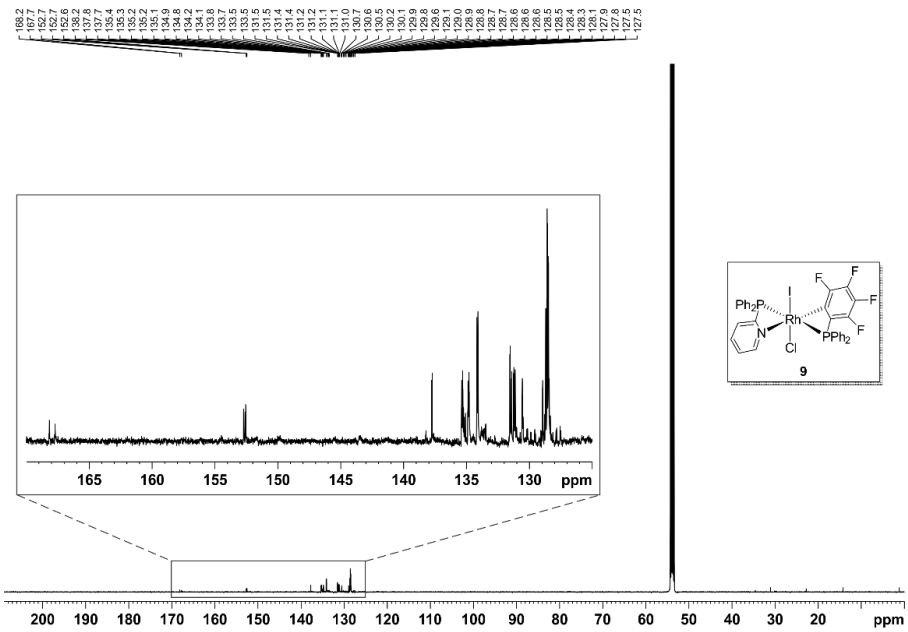

Figure 150. $^{13}C\{^{1}H\}$ NMR spectrum (126 MHz, CD_2Cl_2) for complex **9**.

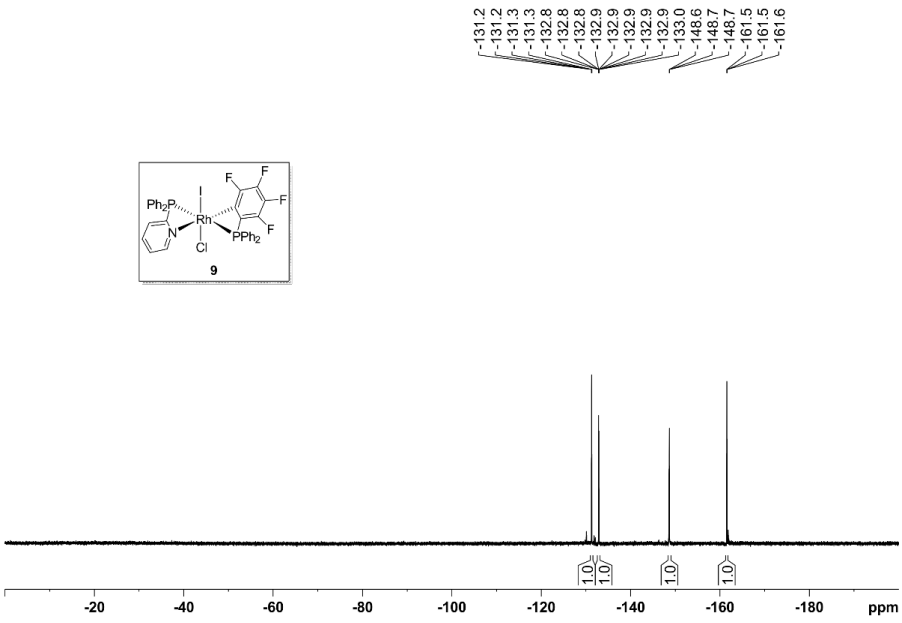

Figure 151. $^{19}F\{^{1}H\}$ NMR spectrum (471 MHz, CD_2Cl_2) for complex **9**.

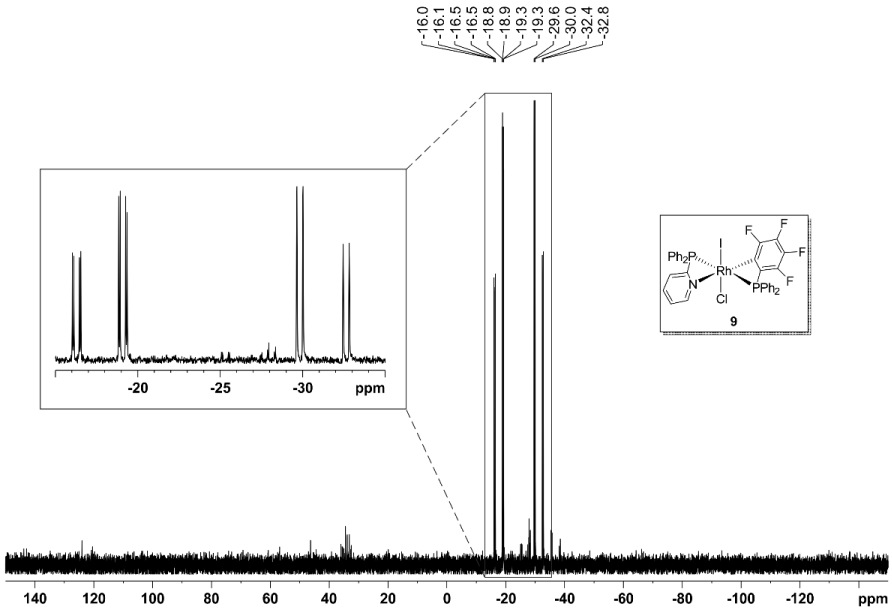

Figure 152. $^{31}P\{^{1}H\}$ NMR spectrum (202 MHz, CD_2Cl_2) for complex **9**.

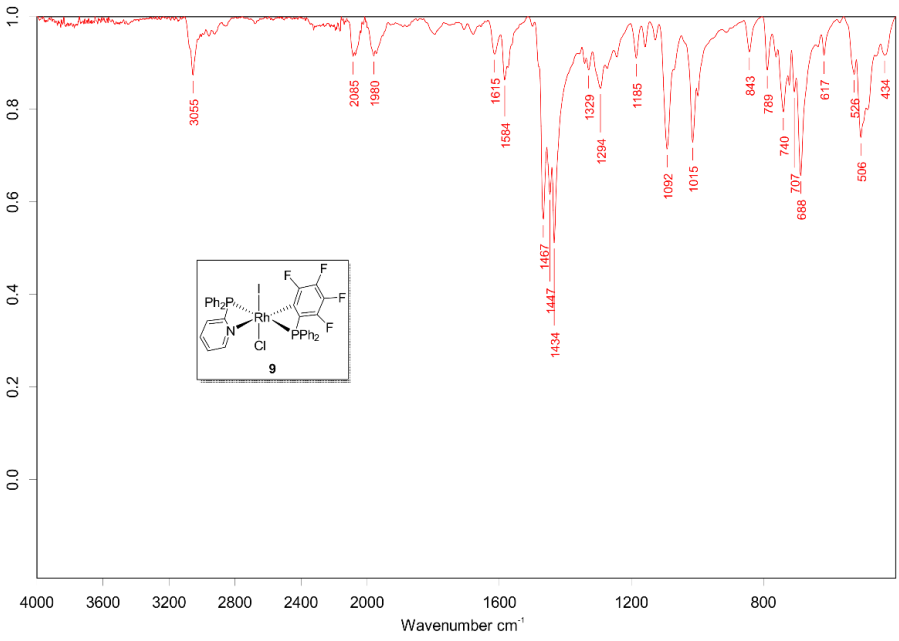

Figure 153. IR spectrum for complex **9**.

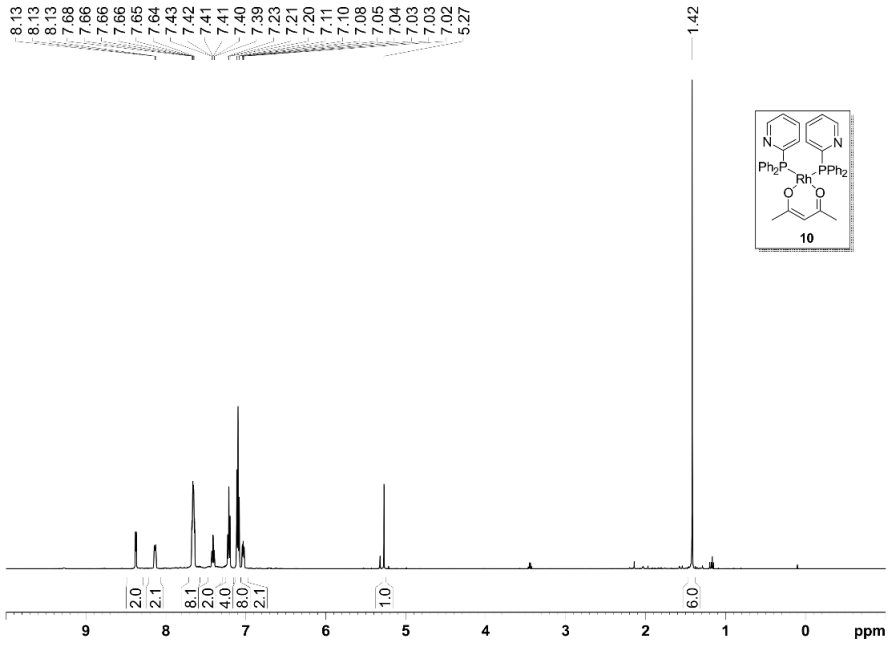

Figure 154. ^{1}H NMR spectrum (500 MHz, CD_2Cl_2) for complex **10**.

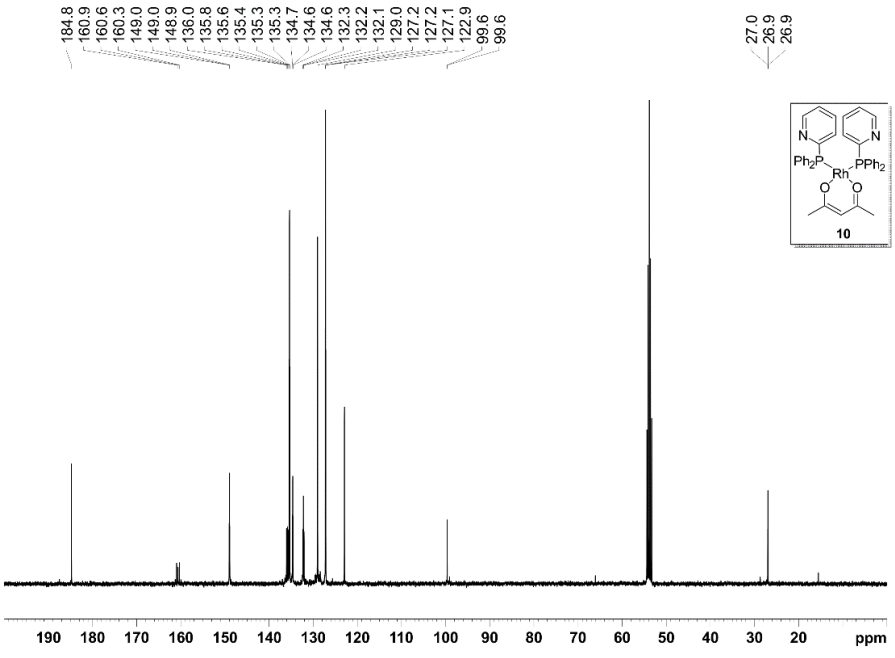

Figure 155. $^{13}C\{^{1}H\}$ NMR spectrum (100 MHz, CD_2Cl_2) for complex **10**.

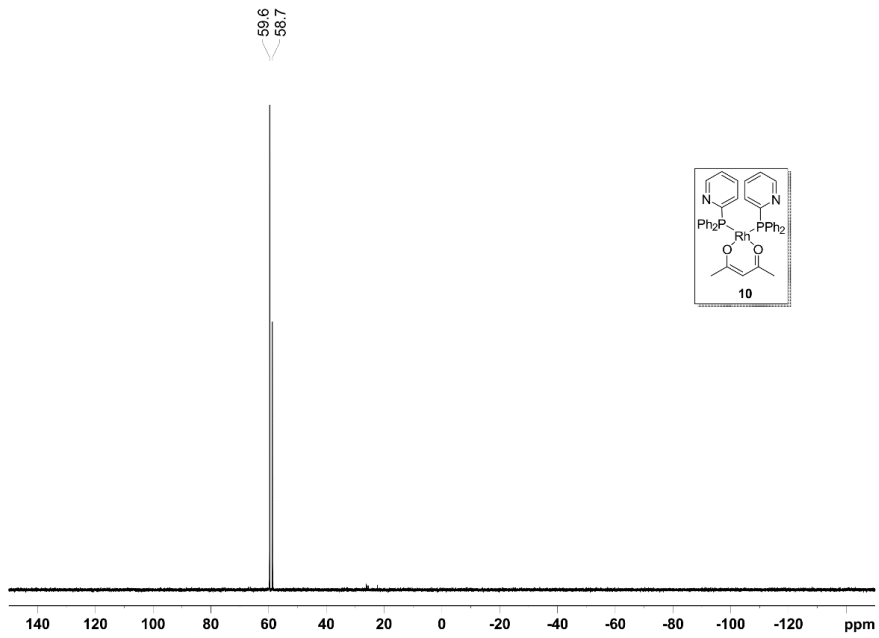

Figure 156. $^{31}P\{^{1}H\}$ NMR spectrum (202 MHz, CD_2Cl_2) for complex **10**.

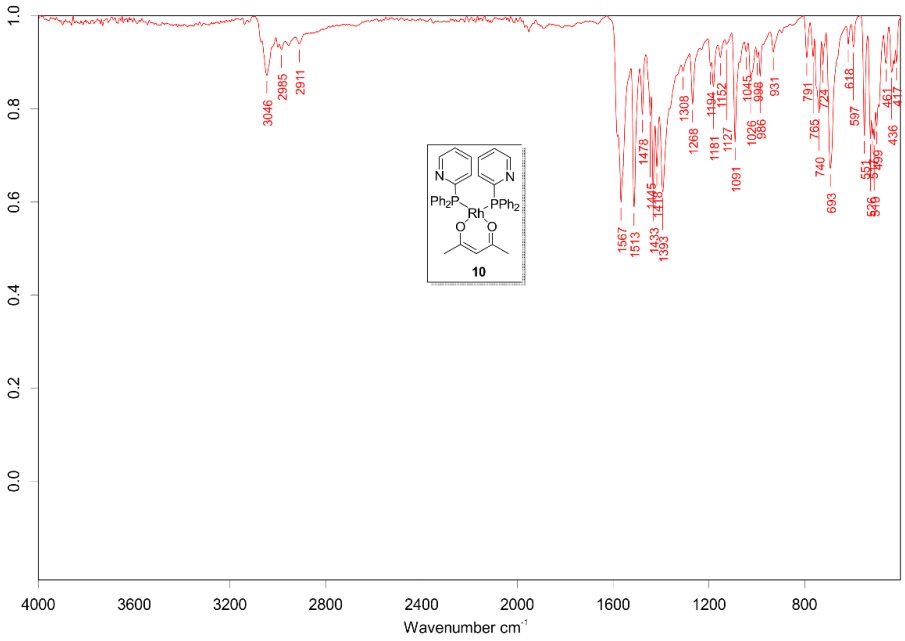

Figure 157. IR spectrum for complex **10**.

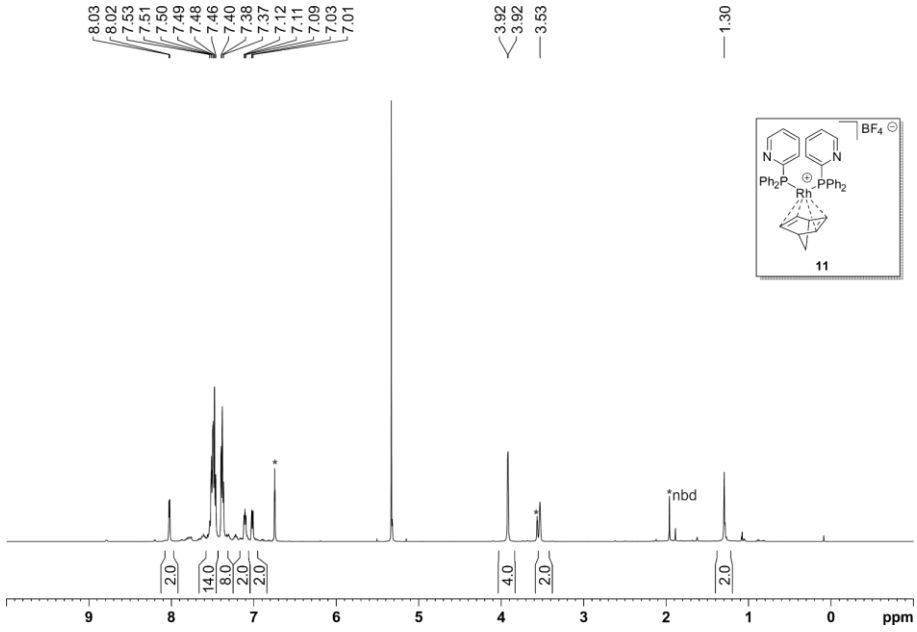

Figure 158. ^{1}H NMR spectrum (500 MHz, CD_2Cl_2) for complex **11**.

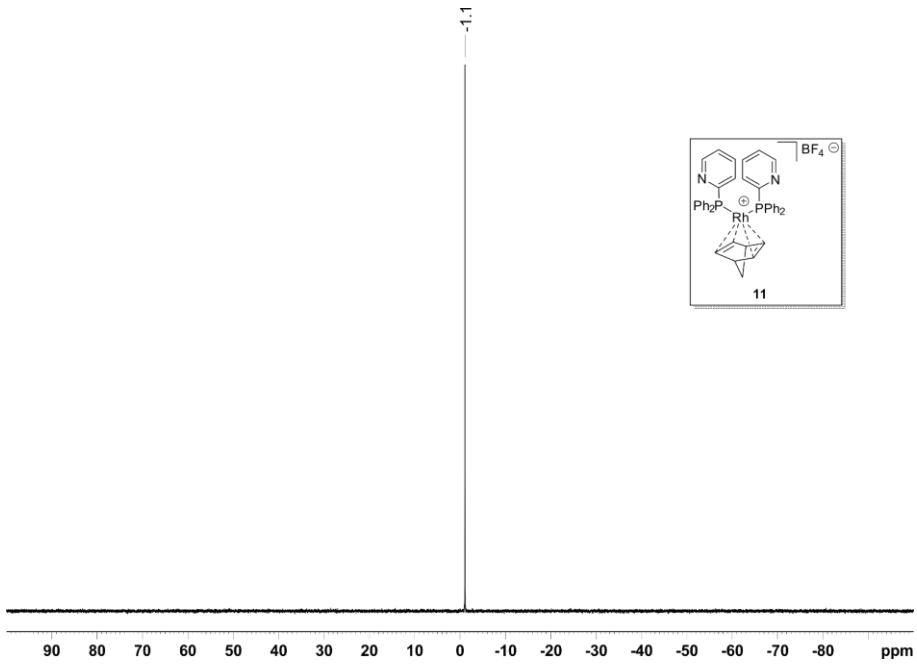

Figure 159. $^{11}B\{^{1}H\}$ NMR spectrum (128 MHz, CD_2Cl_2) for complex **11**.

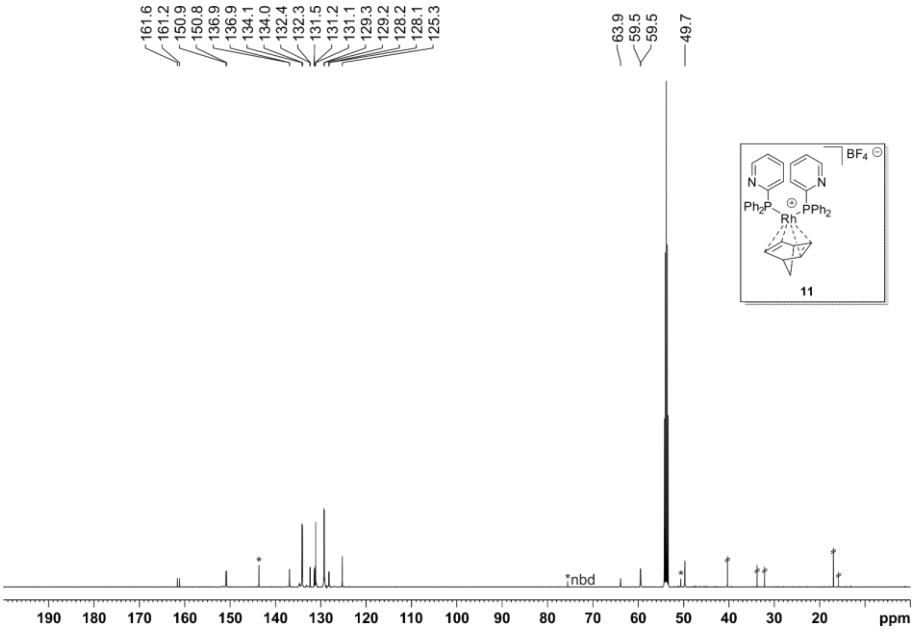

Figure 160. $^{13}C\{^{1}H\}$ NMR spectrum (126 MHz, CD_2Cl_2) for complex **11**.

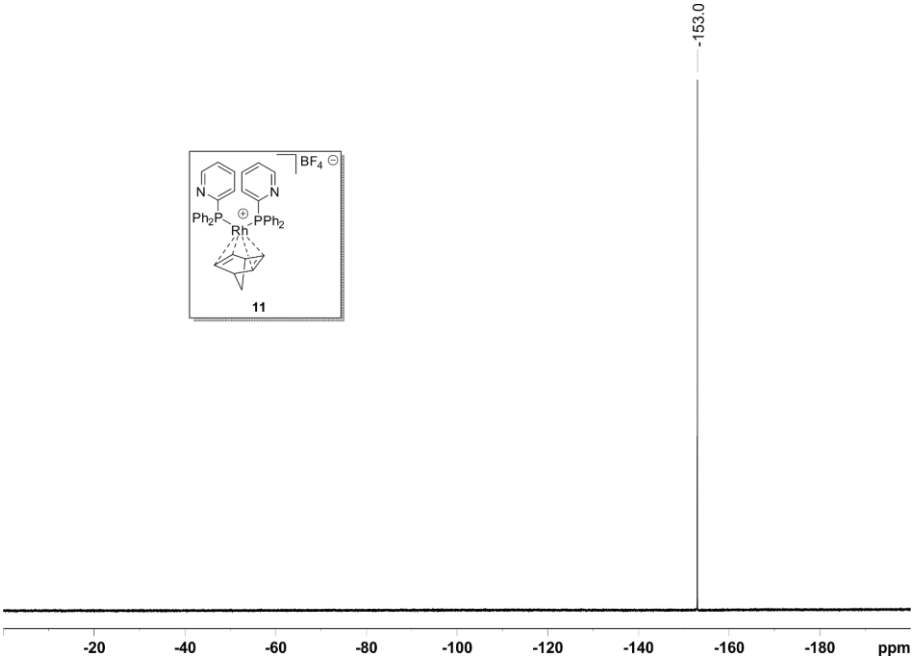

Figure 161. $^{19}F\{^{1}H\}$ NMR spectrum (376 MHz, CD_2Cl_2) for complex **11**.

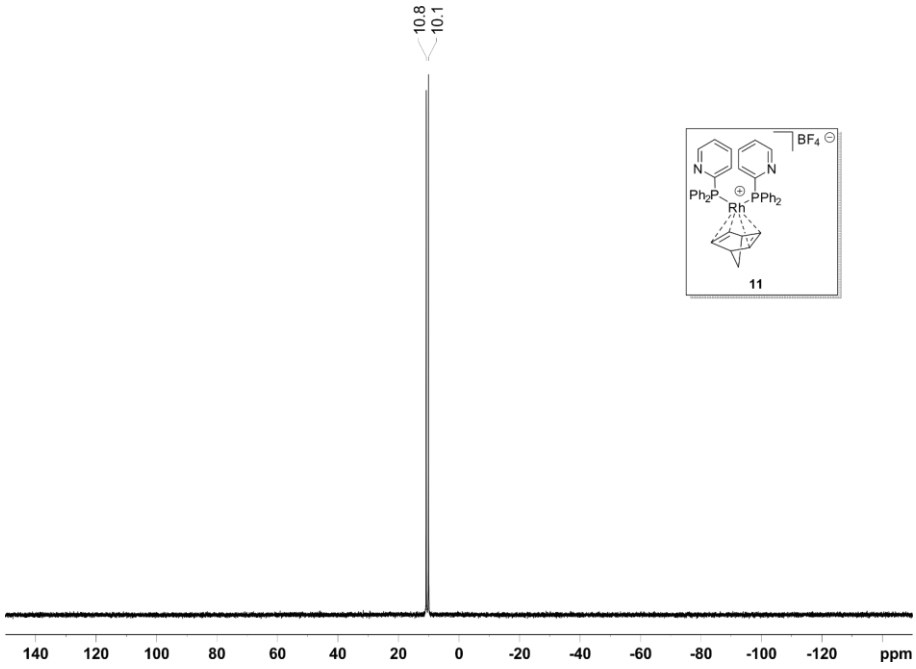

Figure 162. $^{31}P\{^{1}H\}$ NMR spectrum (162 MHz, CD_2Cl_2) for complex **11**.

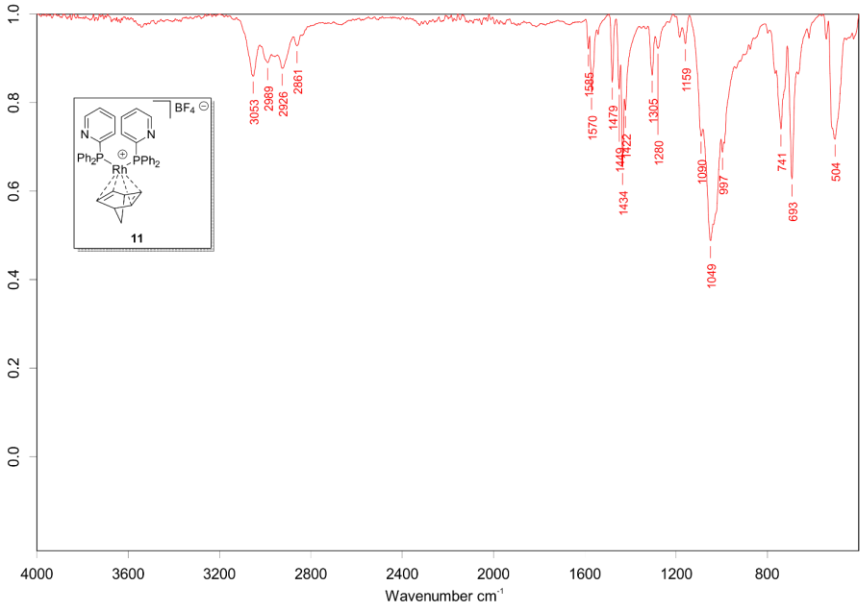

Figure 163. IR spectrum for complex **11**.

CHAPTER III

Supramolecular Regulation in Gold(I) Catalysts for the Selective Functionalization of Aromatic Alcohols

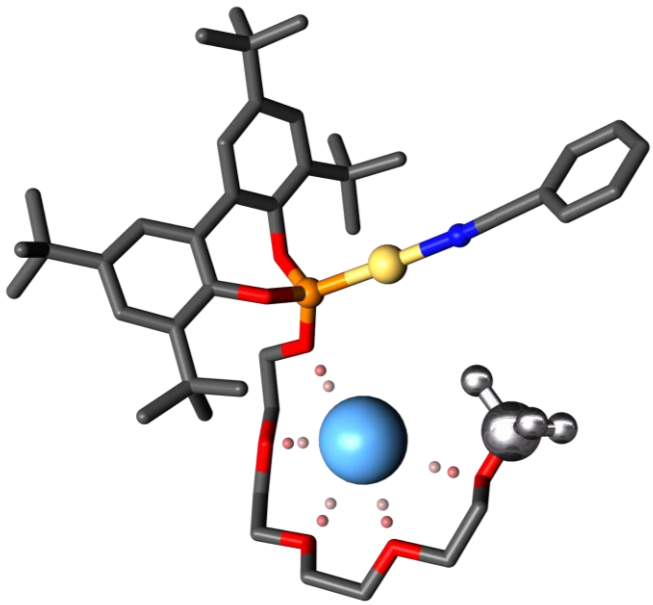

Supramolecular Regulation in Gold(I) Catalysts for the Selective Functionalization of Aromatic Alcohols

(*To be submitted*)

Lucas Carreras,[a,b] Antonio Franconetti,[c] Antonio Frontera,[c] Christopher A. Hunter,[d] and Anton Vidal-Ferran[b,e]*

a Universitat Rovira i Virgili, Departament de Química Analítica i Química Orgànica, C. Marcel·lí Domingo 1, 43007, Tarragona, Spain.
b Institut Català d'Investigació Química (ICIQ) & Barcelona Institute of Science and Technology (BIST), Av. Països Catalans 16, 43007, Tarragona, Spain.
c Universitat de les Illes Balears, Departament de Química, Crta. de Valldemossa km 7.5, 07122, Palma de Mallorca, Spain.
d Department of Chemistry, University of Cambridge, Lensfield Road, CB2 1EW, Cambridge, United Kingdom.
e Institució Catalana de Recerca i Estudis Avançats (ICREA), Pg. Lluís Companys 23, 08010, Barcelona, Spain.

Supramolecularly regulated gold(I) carbene C–H insertions

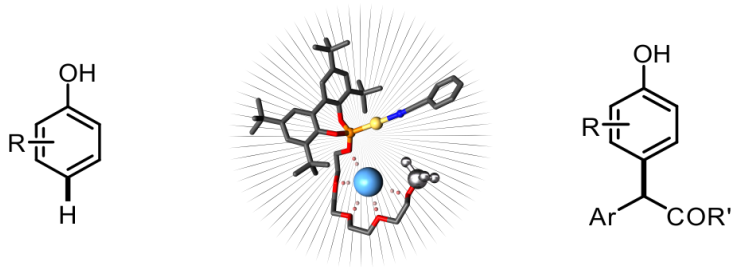

3.1. ABSTRACT

Phosphite-based Au(I) catalytic systems containing a polyether-based regulation site and steric effectors of different sizes were designed and synthesized. These catalysts have been successfully tested in the Au(I)-catalyzed C–H functionalization of phenols and related derivatives with gold-carbenes derived from diazo compounds. Regulation of the steric congestion around the catalytic Au(I) center *via* ion-dipole interactions by an external regulation agent led to an enhancement of both the activity (up

to 20%) and selectivity of the reaction (from 28:1 to >50:1 in terms of C–H *vs.* O–H functionalization products). This new approach in supramolecular gold(I) catalysis has been applied to the derivatization of an array of substituted phenols and related substrates and to the preparation of an advanced synthetic intermediate of anticancer agent Tamoxifen. The effect of the regulation agent on the selectivity and yield of the reaction has been studied and rationalized using DFT-D calculations.

3.2. INTRODUCTION

Homogenous gold(I) catalysis emerged in the last decades and has become a firmly established area of research.[125] The unique properties of Au(I)[126] as an activating agent for nucleophilic reagents has revolutionized homogeneous catalysis as it has allowed a number of unprecedented organic transformations to be developed.[127] Ligand design in gold chemistry both takes advantage of, and is at the same time at a disadvantage from, one of the most characteristic features of Au(I) complexes: their linear nature. Unlike other transition metal catalysts, gold(I) complexes normally place the activated substrate away from the ligand that aimed to tune the reactivity of the metal center. This can prevent the ligand from sterically influencing the outcome of the reaction. To overcome this limitation, typical ligand design has been based on large backbones with the aim of influencing both the metal center and the activated substrate.[128] This approach ultimately leads to a high synthetic cost and to limited libraries of ligands available for screening in catalysis.[13] The design of supramolecular ligands or catalytic systems has contributed in a number of ways to the engineering of sterically-based modes of activation for substrates coordinated linearly at the gold center: (i) use of reversible interactions to build the ligand backbone,[129] (ii)

(125) Echavarren, A. M.; Hashmi, A. S. K.; Toste, F. D. *Adv. Synth. Catal.* **2016**, *358*, 1347-1347.
(126) Gorin, D. J.; Toste, F. D. *Nature* **2007**, *446*, 395-403.
(127) For selected reviews, see: (a) Dorel, R.; Echavarren, A. M. *Chem. Rev.* **2015**, *115*, 9028-9072. (b) Li, Y.; Li, W.; Zhang, J. *Chem. - Eur. J.* **2017**, *23*, 467-512.
(128) Zi, W.; Toste, F. D. *Chem. Soc. Rev.* **2016**, *45*, 4567-4589.
(129) Gramage-Doria, R.; Bellini, R.; Rintjema, J.; Reek, J. N. H. *ChemCatChem* **2013**, *5*, 1084-1087.

utilization of multiple catalyst-substrate interactions,[130] (iii) encapsulation of the gold-based catalyst[48] and (iv) supramolecular regulation of activity of the catalytic system.[49-51]Regulation strategies in gold chemistry have, to this date, relied on influencing the activity/selectivity of stimuli-responsive gold rotaxanes by modifying their conformation[49] or by changing the aggregation state of the backbone of the catalyst.[50,51]

Our research group has designed supramolecularly regulated catalysts that contain linear polyethyleneoxy chains as regulation sites and stereogenic phosphite ligating groups for rhodium-[40,43,44] and palladium-[45] catalyzed reactions. The addition of an external regulation agent (RA) capable of interacting with the polyethyleneoxy chain through ion-dipole or hydrogen bonding interactions triggers the regulation mechanism. The choice of the regulation agent determines the rigidity and conformational flexibility of the whole system, which translates into a modulation of the activity and stereoselectivity of the catalyst. Moreover, this strategy offers the advantage of providing access to libraries of catalysts with reduced synthetic effort when compared to their preparation following standard synthetic protocols.[53] As the regulation effects on the activity, regio- and stereo-selectivity of previously studied transformations in the group were significant,[14] we envisioned a related regulation mechanism for gold catalysis. Unlike the bidentate ligands already studied by our group, the linear nature of gold(I) complexes prompted us to design ligands featuring a linear polyethyleneoxy regulation site and a phosphite ligating group. This P-group was placed at one end of the polyethyleneoxy chain and a steric effector was appended at the other end of the chain. We postulated that the choice of regulation agents (*i.e.* polyethyleneoxy binders) of different sizes would translate into the modulation of the outcome of the reaction by modification of the steric congestion around the gold center. Herein, we report the results on the synthesis of gold-complexes that can be structurally modified by an external regulation agent. We also describe the general application of these supramolecularly regulated gold catalysts for the selective C–H functionalization reaction of phenols and related substrates with carbenes derived from diazo compounds, affording synthetically useful 2-(hydroxyaryl)-2-aryl-1-oxo-ethyl derivatives (Scheme 37).

(130) Hamilton, G. L.; Kang, E. J.; Mba, M.; Toste, F. D. *Science* **2007**, *317*, 496-499.

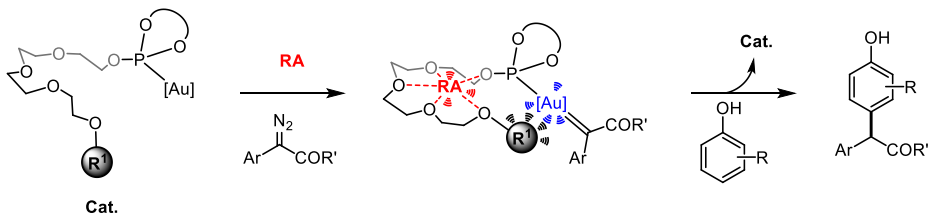

Scheme 37. Design principle of supramolecularly regulated Au(I)-phosphite catalysts incorporating a steric effector for the selective C–H functionalization reaction of phenols with gold-carbenes derived from diazo compounds.

3.3. RESULTS AND DISCUSSION

Our research activities began with the synthesis of the polyethyleneoxy-containing phosphite ligands **L1**-**L3** and the corresponding gold complexes **C1**-**C3** (Scheme 38). With regard to the regulation site, we chose a tetraethyleneglycol fragment due to its availability and affinity towards metal and ammonium salts through ion-dipole or hydrogen bonding interactions, respectively.[131] The choice of conformationally labile phosphite groups derived from commercially available 3,3',5,5'-tetra-*tert*-butyl-[1,1'-biphenyl]-2,2'-diol (Scheme 38) was based on the higher stability of phosphite groups derived from 3,3'-disubstituted [1,1'-biaryl]-2,2'-diols than those derived from their 3,3'-unsubstituted analogues,[132] and the better performance of sterically encumbered phosphite ligands in the chemistry to be studied.[133] In terms of the steric effectors to be linked to the polyethyleneoxy motif, we planned to use a set of substituents covering a range of sizes (*e.g.*, methyl, *tert*-butyl and 1-adamantyl), in order to identify the steric effector providing maximized regulation effects.

(131) (a) Cram, D. J. *Angew. Chem., Int. Ed. Engl.* **1988**, *27*, 1009-1020. (b) Pedersen, C. J. *Angew. Chem., Int. Ed. Engl.* **1988**, *27*, 1021-1027. (c) Jose, D. A.; Mon, I.; Fernández-Pérez, H.; Escudero-Adán, E. C.; Benet-Buchholz, J.; Vidal-Ferran, A. *Org. Lett.* **2011**, *131*, 3632-3635.

(132) Gual, A.; Godard, C.; de la Fuente, V.; Castillón, S. *Design and synthesis of phosphite ligands for homogeneous catalysis*, p. 81-131. In *Phosphorus(III) Ligands in Homogeneous Catalysis: Design and Synthesis*, Kamer, P. C. J.; van Leeuwen, P. W. N. M., Eds., John Wiley & Sons Ltd., **2012**.

(133) (a) Yu, Z.; Ma, B.; Chen, M.; Wu, H.-H.; Liu, L.; Zhang, J. *J. Am. Chem. Soc.* **2014**, *136*, 6904-6907. (b) Xi, Y.; Su, Y.; Yu, Z.; Dong, B.; McClain, E. J.; Lan, Y.; Shi, X. *Angew. Chem., Int. Ed.* **2014**, *53*, 9817-9821.

The required monosubstituted tetraethyleneglycol moieties for synthesizing ligands **L1**-**L3** were either commercially available (R^1 = Me) or synthesized following well-established synthetic protocols (R^1 = *tert*-butyl and 1-adamantyl).[134] Phosphite ligands **L1**-**L3** were subsequently prepared by *O*-phosphorylation[135] of the required chlorophosphite with monosubstituted tetraethyleneglycol moieties (40-80% yield). Subsequent reaction of ligands **L1**-**L3** with stoichiometric amounts of $(Me)_2SAuCl$ afforded the corresponding chlorogold(I) complexes quantitatively. The target cationic gold(I) complexes **C1**-**C3** were isolated in 70 to 90% yield from their precursors by using equimolar amounts of silver tetrafluoroborate as the halide scavenger (Scheme 38, see section 3.5.4 in the Experimental Section for details).

(134) (a) For the preparation of tetraethyleneglycol mono-*tert*-butyl ether, see: French, A. C.; Thompson, A. L.; Davis, B. G. *Angew. Chem., Int. Ed.* **2009**, *48*, 1248-1252. (b) For the preparation of tetraethyleneglycol mono-1-adamantyl ether, see: Agasti, S. S.; Liong, M.; Tassa, C.; Chung, H. J.; Shaw, S. Y.; Lee, H.; Weissleder, R. *Angew. Chem., Int. Ed.* **2012**, *51*, 450-454.

(135) Buisman, G. J. H.; Kamer, P. C. J.; van Leeuwen, P. W. N. M. *Tetrahedron: Asymmetry* **1993**, *4*, 1625-1634.

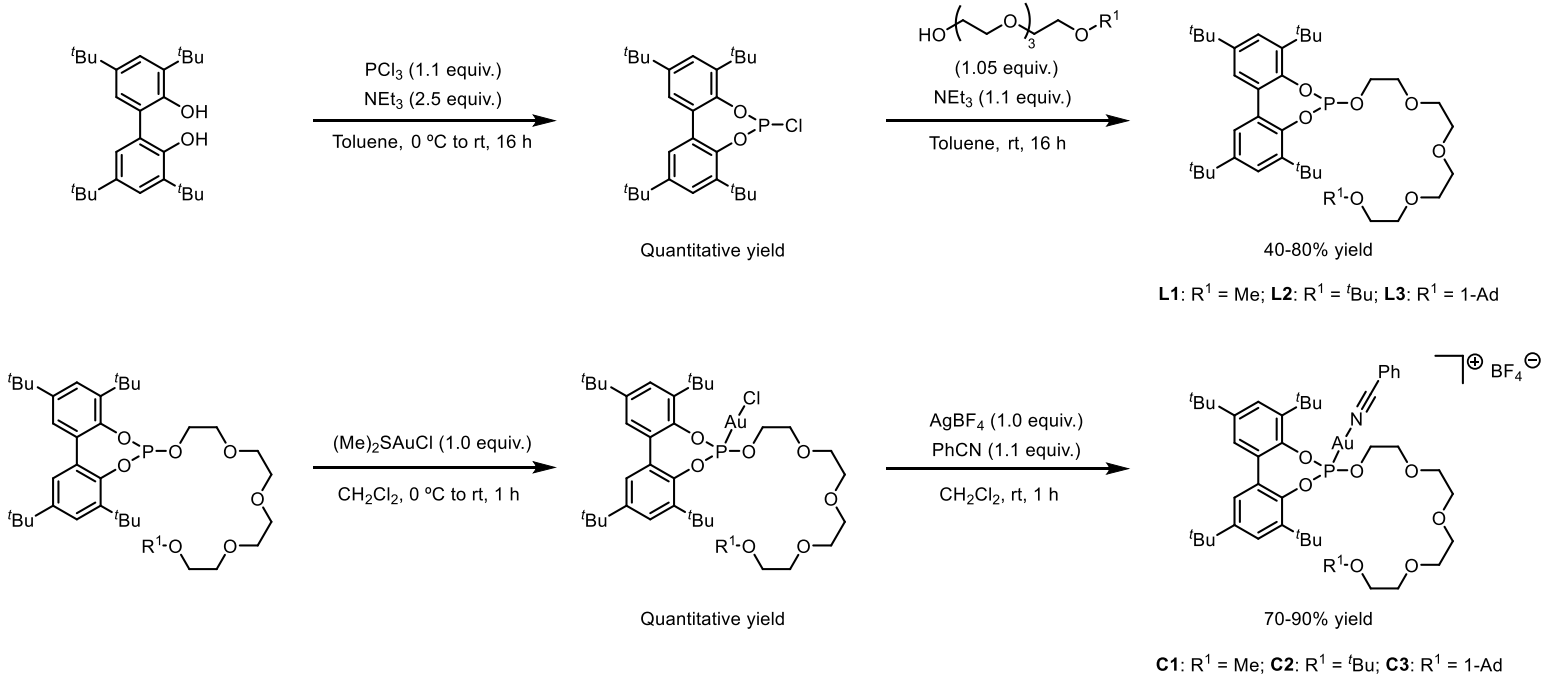

Scheme 38. Synthesis of Au(I)-phosphite catalysts **C1**-**C3** incorporating a steric effector in the regulation site.

The design principle of the regulation mechanism proposed herein is the binding of suitable regulation agents to the regulation site. Metal salts bind to polyethyleneoxy chains through ion-dipole interactions.[131] In terms of the metal salts to be employed in our studies, we envisaged that tetrafluoroborates could be suitable: the catalysts to be studied (**C1**-**C3**) contained this counterion and we deemed it necessary to include the same counterion both for the gold center and the regulation agent, given the significant counterion effects observed in gold(I) chemistry.[136] To begin the binding studies of phosphite ligands **L1**-**L3**, we considered measuring the binding constants between ligands **L1**-**L3** and two representative tetrafluoroborates (*i.e.*, those containing cationic species with a small and large ionic radius: Na^+ [0.98 Å] and Cs^+ [1.67 Å], respectively).[137] Unfortunately, the accurate measurement of the association constants between $NaBF_4$ or $CsBF_4$ and ligands **L1**-**L3** turned out to be very difficult due to the poor solubility of these salts (particularly $CsBF_4$) in dichloromethane.[138] For the sake of convenience, we turned our attention to alternative alkali metal salts such as NaBArF (BArF = $[B(3,5\text{-}(CF_3)_2C_6H_3)_4]^-$) or CsBArF. Interestingly, addition of increasing amounts of the BArF salts to a solution of the phosphite ligands led to changes in the ^{31}P NMR spectra (see section 3.5.6 for details).[139] In all cases, the binding isotherms pointed to very strong binding processes resulting in complete complexation of the guest after each addition. Association constants between ligands **L1**-**L3** and the BArF salts were determined by multivariate factor analysis of titration data with software developed in-house.[140] Binding constants were high in all cases and ranged from 10^3 to 10^7 M^{-1}. In

(136) Jia, M.; Bandini, M. *ACS Catal.* **2015**, *5*, 1638-1652.
(137) Cotton, F. A.; Wilkinson, G. *Advanced Inorganic Chemistry: A Comprehensive Text*, 3rd Ed., Wiley, New York, **1972**.
(138) Whilst $CsBF_4$ was poorly soluble in dichloromethane, its solubility increased in the presence of gold complex [Au(Cl)(**L1**)], phenol **1a** and diazo derivative **2a**, with all the components of the mixture having the same concentrations than those in catalytic experiments (^{133}Cs NMR (D_2O, 53 MHz): δ –28.9 ppm. ^{133}Cs shifts are quoted in ppm relative to $CsNO_3$ as external reference standard in D_2O using a coaxial insert for NMR tubes).
(139) Binding constants could not be determined by UV/Vis titrations because host and guest had heavily overlapping UV/Vis spectra.
(140) Software developed in-house by Prof. C. A. Hunter.

the case of NaBArF, as a complementary binder to the tetraethyleneoxy motif, binding affinity was very high for all ligands (>10^5 M^{-1}) and increased with the size of the substituent at the end of the tetraethyleneoxy chain (R^1) (see third column in Table 5). In the case of the bulkier CsBArF, binding constants decreased with the size of the steric effector (see fourth column in Table 5). These studies are evidence for highly favorable binding processes between phosphite ligands **L1**-**L3** and alkali metal salts of weakly coordinating anions and are in agreement with already published binding studies for related supramolecular ligands.[43a]

Table 5. Binding constant data for complexation between ligands **L1**-**L3** and Na and Cs alkali metal salts[a]

Entry	Ligand	K_a, NaBArF (M^{-1})	K_a, CsBArF (M^{-1})
1	**L1**	*ca.* $1{\cdot}10^5$	*ca.* $1{\cdot}10^5$
2	**L2**	*ca.* $1{\cdot}10^6$	*ca.* $5{\cdot}10^4$
3	**L3**	*ca.* $1{\cdot}10^7$	*ca.* $4{\cdot}10^3$

[a] Measured by NMR spectroscopy at 25 °C. See section 3.5.6 for details.

Transformations involving Au(I)-carbenes derived from diazo compounds have experienced significant growth,[141] since the discovery of this chemistry by Nolan, Pérez and co-workers in 2005.[142] In 2014, Zhang[133a] and Shi[133b] independently reported that Au(I)-phosphite complexes catalyzed the C–H functionalization of the *para*-C_{sp2}–H position of phenols with gold-carbenes. Although reactions were described to proceed in good to high yields on an electronically and

(141) (a) Liu, L.; Zhang, J. *Chem. Soc. Rev.* **2016**, *45*, 506-516. (b) Fructos, M. R.; Díaz-Requejo, M. M.; Pérez, P. J. *Chem. Commun.* **2016**, *52*, 7326-7335.
(142) Fructos, M. R.; Belderrain, T. R.; de Frémont, P.; Scott, N. M.; Nolan, S. P.; Díaz-Requejo, M. M.; Pérez, P. J. *Angew. Chem., Int. Ed.* **2005**, *44*, 5284-5288.

structurally diverse array of phenols, naphthols,[143] non-phenolic aromatic alcohols and diazoketones were understudied. We considered that this chemistry was a suitable benchmark to demonstrate our proposed regulation mechanism and, given also the interest in further developing strategies for the site-selective C_{sp2}–H bond functionalization, subsequent investigations within the present PhD thesis involved the evaluation of the catalytic activity of gold complexes **C1**-**C3** in the functionalization of phenols and related substrates with diazo compounds.

At the outset of our studies, we were not also interested in determining the suitability of our initial catalyst design, but in evaluating our design principle, namely, whether the addition of a regulation agent would affect the catalytic activity of gold-complexes **C1**-**C3** through distal regulation. Reactions were performed using gold complexes **C1**-**C3** in catalytic amounts (5 mol%) and an excess of the tetrafluoroborate regulation agent (10 mol%) to ensure quantitative formation of the supramolecular complex. Initial catalytic studies were performed on 2-diazo-2-phenylacetate (**2a**) and phenol (**1a**) as model substrates, with the former being used as the limiting reagent. The experimental conditions employed in this study, together with the results obtained, are summarized in Table 6.

(143) The C–H functionalization of 1- and 2-naphthol derivatives with alkyl 2-diazo-2-phenylacetates using gold(I)-catalysts was published during the preparation of the present thesis: Yu, Z.; Li, Y.; Zhang, P.; Liu, L.; Zhang, J. *Chem. Sci.* **2019**, DOI: 10.1039/C9SC01657K.

Table 6. Au(I)-catalyzed C_{sp2}–H functionalization of phenol **1a** with diazoderivative **2a**[a]

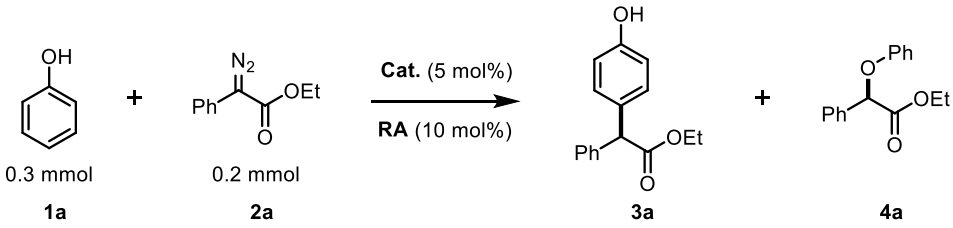

0.3 mmol **1a** + 0.2 mmol **2a** → **3a** + **4a**

Entry	Catalyst	RA	Yield (%)	3a : 4a Ratio
1	[Au(Cl)(**L1**)]	none	<1	-
2	[Au(CH_3CN)(**L1**)]BF_4	none	76	>50 : 1
3	[Au(2,4,6-$(MeO)_3$ (C_6H_2)CN)(**L1**)]BF_4	none	66	11:1
4	**C1**	none	83	28 : 1
5	**C1**	NH_4BF_4	73	24 : 1
6	**C1**	$LiBF_4$	84	35 : 1
7	**C1**	$NaBF_4$	87	30 : 1
8	**C1**	KBF_4	86	37 : 1
9	**C1**	$RbBF_4$	86	31 : 1
10	**C1**	$CsBF_4$	88 (80)	>50 : 1
11	**C2**	none	83	42 : 1
12	**C2**	$LiBF_4$	74	15 : 1
13	**C2**	$CsBF_4$	75	38 : 1
14	**C3**	none	66	13 : 1
15	**C3**	$LiBF_4$	71	18 : 1
16	**C3**	$CsBF_4$	67	13 : 1

[a] Reactions were performed in CH_2Cl_2 (0.1 M) under N_2 and reacted for 1 h at 25 °C. Yield was determined by ^1H NMR using 1,3,5-trimethoxybenzene as an internal standard. Isolated yield in parentheses.

Initial experiments demonstrated that gold complexes **C1**-**C3** catalyzed the *para*-C_{sp2}–H functionalization reaction of phenol **1a** with carbenes derived from diazoester **2a** in the absence of regulation agent (entries 4, 11 and 14, Table 6). Gold catalysts **C1**-**C3** were very active in the transformation, as the diazoester **2a** was fully consumed after 1 h at room

temperature with yields ranging from 66% (for **C3**) to 83% (for **C1** and **C2**). In order decouple activation effects in the gold chemistry that were not related to the envisioned regulation mechanism, a number of control experiments were performed. For instance, $(Me_2S)AuCl$ and $CsBF_4$ (as a representative example of a regulation agent) were studied as potential catalysts, and both displayed negligible activity. The effects of $AgBF_4$ in the reaction between **1a** and **2a** were also studied, with the *para*-C_{sp2}–H functionalization product being obtained in 7% yield (see section 3.5.8.1 for details). Plausible changes to the outcome of the reaction due to changes in the inner coordination sphere of the gold(I) center were also investigated, with [Au(Cl)(**L1**)], $[Au(CH_3CN)(\mathbf{L1})]BF_4$, $[Au(2,4,6\text{-}(MeO)_3(C_6H_2)CN)(\mathbf{L1})]BF_4$ and $[Au(PhCN)(\mathbf{L1})]BF_4$ (referred to as **C1**) catalysts being tested in this chemistry (entries 1-4, Table 6). Whilst the chlorogold complex [Au(Cl)(**L1**)] was, as expected, inactive in this transformation, the three cationic complexes catalyzed the transformation in good yields (entries 2-4, Table 6), with **C1** being the catalyst leading to the *para*-C_{sp2}–H functionalization product in a higher yield (83%, entry 4, Table 6). It is interesting to note that the reaction took place in a selective way with minor amounts of the O–H insertion product being detected. *Ortho*-C_{sp2}–H or *meta*-C_{sp2}–H functionalization products were not detected in the reaction mixtures by NMR or GC analyses either. Further reactivity studies used the cationic gold complex derived from benzonitrile (**C1**) as catalyst, as this complex provided the highest yield.

We next evaluated whether the use of different external regulation agents translated into a maximized output of the reaction in terms of yield and selectivity. The effects produced by alkali metal and ammonium tetrafluoroborate salts on the catalytic activity have been summarized in Table 6. Of all the RAs tested, the catalyst incorporating $CsBF_4$ (*i.e.*, $[Au(PhCN)(\mathbf{L1}{\cdot}CsBF_4)]BF_4$) provided the highest yield and selectivity, with positive regulation effects in the yield (+5%) and selectivity (from 28:1 to >50:1 in terms of *para*-C_{sp2}–H *vs.* O–H functionalization products). Although the use of regulation agents with a counterion different to that in **C1** was *a priori* considered inappropriate due to the potential importance of "counterion effects"[136] in gold chemistry, we also decided to study the effects of NaBArF as regulation agent. A very poor reactivity was observed for NaBArF (see section 3.5.8.1), so regulation agents derived from counterions other than tetrafluoroborate were not further considered.

Regarding the influence of the steric effector in the outcome of the reaction, the general trend observed was that bulky steric effectors such as *tert*-butyl (**C2**) or 1-adamantyl (**C3**) were less favorable for catalytic activity than **C1**. For **C2**, the addition of a regulation agent (for instance $LiBF_4$ or $CsBF_4$) was detrimental to its activity, regardless of the ionic radius of the cationic component of the regulation agent (entries 11-13, Table 6). However, it should be noted that $CsBF_4$ maintained the selectivity of the reaction with respect to **C1** (compare entries 10 and 13, Table 6). 1-Adamantyl-substituted catalyst (**C3**) displayed the poorest catalytic activity of the whole series in terms of the yield in the transformation under study (entries 14-16, Table 6), although addition of $LiBF_4$ led to positive regulation effects in the yield (+5%) and selectivity (from 13:1 to 18:1 in terms of C–H *vs.* O–H functionalization products, entry 15, Table 6). To conclude with this study on the reactivity of **1a** and **2a**, methyl-substituted catalyst **C1** displayed the highest overall performance (entry 10, Table 6) by combining complex **C1** with the regulation agent containing the largest alkali metal cation ($CsBF_4$).

After determining the optimal catalyst (**C1**), and having demonstrated that the yield of the reaction can be improved by the choice of the regulation agent ($CsBF_4$ for substrates **1a** and **2a**), we decided to explore the substrate scope of the reaction with a set of phenols incorporating substituents with different electronic properties at different positions of the aromatic ring. Typically challenging substrates, such as electron-poor phenols, or understudied analogues of phenol, such as naphthol derivatives[143] and tropolone, were included in the study. For each substrate, the whole set of alkali metal tetrafluoroborate salts was tested, with the yield and selectivity (ratio of C–H *vs.* O–H functionalization products) for the optimal regulation agent being indicated in Scheme 39 (see section 3.5.8 for the complete set of results). The yield for fluoro-substituted phenols **1b** and **1c** was lower than for phenol due to the reduced reactivity of electron poor phenols.[133a] Nevertheless, 2-fluorophenol **1b** experienced a noticeable increase in the yield (+20%) when $RbBF_4$ was employed. Alternatively, the use of $CsBF_4$ as the regulation agent for the *para*-C_{sp2}–H functionalization of 3-fluorophenol **1c** led to a moderate increase of the yield towards **3c** (+3%). When moving to electron-rich aromatic systems such as methoxy-substituted phenol **1d**, the yield of the reaction product was higher. It is important to note in this

case that two possible C–H insertion products could be obtained, namely the corresponding C–H insertion products *para*-OH **3d** and *para*-OMe **3d'**. Products **3d** and **3d'** were obtained in a similar ratio (*ca.* 1:1), as a separable mixture of compounds by column chromatography on SiO_2 (see section 3.5.9). Though the reaction yield could be improved upon using $CsBF_4$, none of the alkali metal tetrafluoroborates had an effect on biasing the regioselectivity of the reaction, with a *ca.* 1:1 ratio for the two possible products being detected in all cases (see section 3.5.8.5).[144] After studying electronic and the substitution effects in phenols, we moved to naphthol derivatives. The functionalization of naphthols employing this approach was understudied,[143] therefore, we deemed these substrates to be highly interesting in terms of developing an attractive synthetic entry point for functionalized naphthol derivatives. Catalyst **C1** displayed a high activity on 1-naphthol **1e** and diazoderivative **2a** with the functionalized product being formed in 89% yield without using a RA. Subsequent studies demonstrated that the activity of catalyst **C1** for this substrate could be maximized, leading to almost quantitative yield for **3e** when employing $CsBF_4$ as the regulation agent. It was not trivial to unequivocally establish the structure of the C_{sp2}–H insertion product with standard spectroscopic techniques. Fortunately, single crystals of the reaction product were grown and the structure was established to be the (4-hydroxynaphthalen-1-yl)-2-phenylacetate derivative **3e** by X-ray diffraction analysis.

(144) It should be noted that 2-methoxyphenol was also screened with our catalytic system (see section 3.5.8.10). Unfortunately, the two positional isomers from the *para*-OH and *para*-OMe C–H functionalization could not be separated using preparative techniques (see section 3.5.11). Nitrophenols were also tested, but their lack of reactivity rendered diazo coupling products **5** and **6**.

Scheme 39. Substrate scope of Au(I)-catalyzed aromatic alcohols functionalization[a]

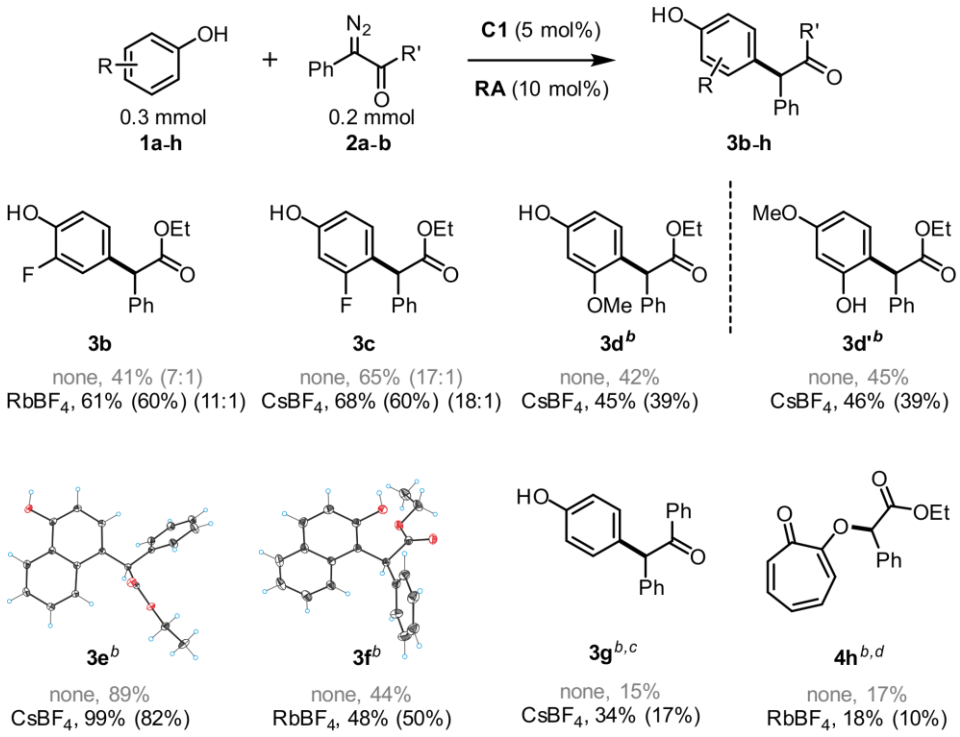

[a] Reactions were performed in CH_2Cl_2 (0.1 M) under N_2 and reacted for 1 h at 25 °C. Yield determined by ^1H NMR using 1,3,5-trimethoxybenzene as an internal standard. Values in parentheses indicate the ratio of the *para*-C–H insertion product to the O–H insertion product. Isolated yield in parentheses. The table displays the results when using the best performing regulation agent (in black) and no RA (in grey). [b] O–H insertion product not detected. [c] Reaction between **1a** and 2-diazo-1,2-diphenylethan-1-one **2b**. [d] Reaction between tropolone **1h** and **2a**.

The study of the reactivity of 2-naphthol **1f** was also interesting since the insertion of the corresponding metal carbene at the *para*-C_{sp2}–H position is not possible for this substrate and the two *ortho* positions are inequivalent. With our supramolecular catalyst **C1**, an insertion product was obtained in moderate yield in the absence of regulation agent, and the reaction outcome was improved upon using $RbBF_4$ as regulation agent (+4%). Again, X-Ray studies were required to establish the structure of the reaction product, which was determined to be the (2-hydroxynaphthalen-1-yl)-2-phenylacetate isomer **3f**. Supramolecular catalysts

[Au(PhCN)(**L1**·RA)]BF_4 did not tolerate changes in the nature of the diazo derivative employed. Studies of the reactivity of phenol with unsubstituted ethyl 2-diazoacetate, *tert*-butyl 2-diazoacetate, methyl ethyl 2-diazoacetate, diazoacetophenone or diazophosphonates gave no reaction or very poor conversions. These results showed that the substructure Ar(C=N_2)CO in the diazo compound was key to reactivity. 2-Diazo-1,2-diphenylethan-1-one **2b** was a potential candidate for our studies since it would incorporate a phenyl group into the required substructure. Moreover, the *para*-C–H insertion product of this substrate leads to an advanced synthetic intermediate of Tamoxifen,[145] which is the world's largest selling drug for the hormonal treatment of breast cancer. The reaction of **1a**, **2b** and **C1** gave poor results (15% yield of **3g**). However, the output of the reaction could be maximized by using $CsBF_4$ as the regulation agent under standard reaction conditions (+19% enhancement in the yield). The yield could be further enhanced by performing the reaction in chlorobenzene at 60 °C (39% overall yield, +24% enhancement in the yield). Tropolone **1h**, a seven-membered aromatic alcohol, had never been studied as substrate in this chemistry and was included in our studies. Many natural products with interesting biological properties contain the tropolone fragment.[146] Surprisingly, the C–H insertion products were not detected in any of the reaction mixtures involving [Au(PhCN)(**L1**·RA)]BF_4 as catalysts. Instead, the O–H functionalization product **4h** was obtained. The regulation effects were limited in this case, with almost the same results with and without regulation agent ($RbBF_4$). The ketone functional group of tropolone could account for this change in reactivity as it may establish weak interactions during the catalytic process with the gold center.

To shed light on the mechanism of the reaction and to rationalize the regulation effects in the activity and selectivity of the reaction between phenol **1a** and diazoester **2a** (see Table 6, entries 4, 6, 10), we performed a theoretical investigation into the reactivity of the Au(PhCN)(**L1**·RA)]BF_4 catalytic systems.[147] Optimization of the structures was performed at the

(145) Danoun, G.; Tlili, A.; Monnier, F.; Taillefer, M. *Angew. Chem., Int. Ed.* **2012**, *51*, 12815-12819.
(146) Ronald, B. *Nat. Prod. Rep.* **2008**, *25*, 118-138.
(147) These studies were performed in collaboration with the group of Prof. A. Frontera (*Universitat de les Illes Balears*).

BD86[148]-D3/def2-SVP[68a] level of theory, whilst energies of all structures included in this computational study were computed at the BP86-D3/def2-TZVPD level of theory considering the solvent effects of dichloromethane (the conductor-like screening model COSMO[149], which is a variant of the dielectric continuum solvation model[150], was used). The TURBOMOLE software[151] was used in all cases with the latest available correction for dispersion (D3[67]). The computational method is a good compromise between the size of the system (up to 106 atoms including the alkali metal center, gold catalyst and reagents) and the accuracy of the results.[152] Transition state structures were characterized by means of frequency analysis calculations.

Our studies started with the calculation of the gold carbenes **C1-2a** derived from the highest performing catalyst (Figure 164), which is the mechanistic step in which the O–H *vs* *para*-C_{sp2}–H insertion is determined.[153] The smallest and biggest possible regulation agents in our catalytic system (*i.e.*, lithium and cesium derivatives, respectively) were chosen as representative examples and included in the theoretical investigations.

(148) (a) Perdew, J. P. *Phys. Rev. B* **1986**, *33*, 8822-8824; (b) Becke, A. D. *Phys. Rev. A* **1988**, *38*, 3098-3100.
(149) Klamt, A.; Schueuermann, G. *J. Chem. Soc., Perkin Trans. 2* **1993**, 799-805.
(150) Klamt, A. *WIREs Comput. Mol. Sci.* **2011**, *1*, 699-709.
(151) Ahlrichs, R.; Baer, M.; Haeser, M.; Horn, H.; Koelmel, C. *Chem. Phys. Lett.* **1989**, *162*, 165-169.
(152) Balakrishna, B.; Bauzá, A.; Frontera, A.; Vidal-Ferran, A. *Chem. - Eur. J.* **2016**, *22*, 10607-10613.
(153) For other computational studies on the insertion of gold (I) carbenes to phenols, see: (a) Liu, Y.; Yu, Z.; Zhang, J. Z.; Liu, L.; Xia, F.; Zhang, J. *Chem. Sci.* **2016**, *7*, 1988-1995. (b) Liu, Y.; Yu, Z.; Luo, Z.; Zhang, J. Z.; Liu, L.; Xia, F. *J. Phys. Chem. A* **2016**, *120*, 1925-1932. (c) Liu, Y.; Luo, Z.; Zhang, J. Z.; Xia, F. *J. Phys. Chem. A* **2016**, *120*, 6485-6492. (d) Luo, Z.; Gao, Y.; Zhu, T.; Zhang, J. Z.; Xia, F. *J. Phys. Chem. A* **2017**, *121*, 6523-6529.

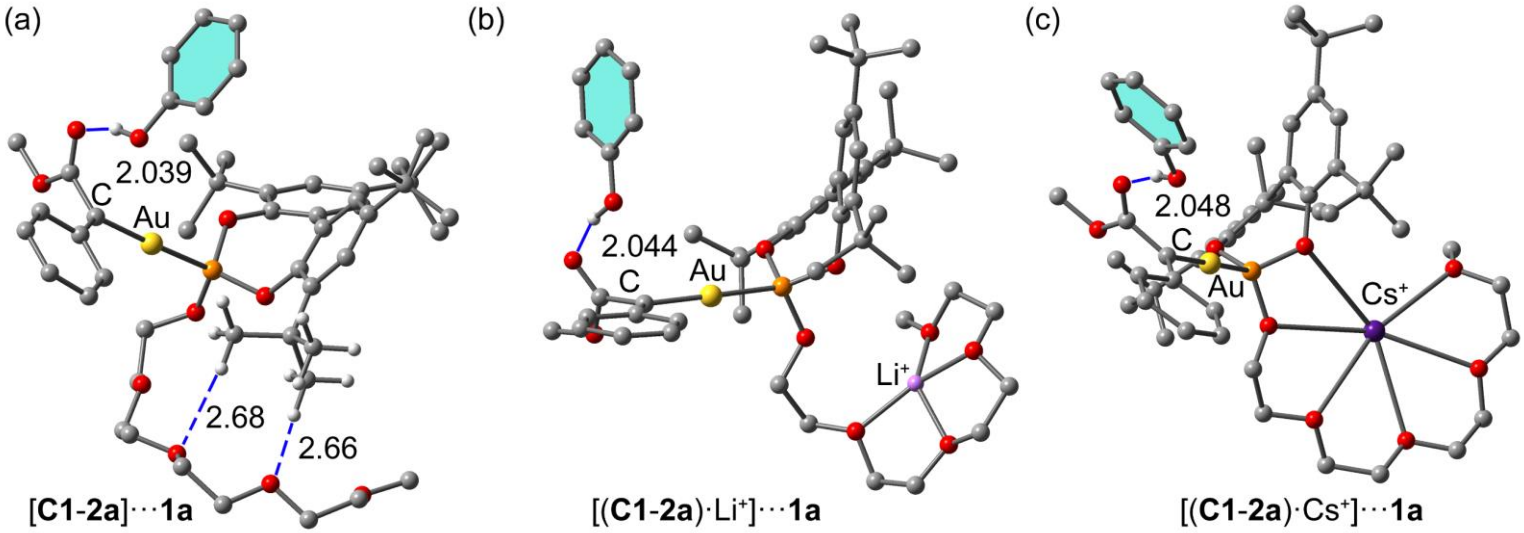

Figure 164. Optimized geometry of **C1**-**2a** complexes interacting with **1a** in the absence of RA (a), and in the presence of Li^+ (b) and Cs^+ (c). Distances in Å.

The optimized geometries for the three representative cases studied in this work (**C1-2a**, (**C1-2a**)·Li^+ and (**C1-2a**)·Cs^+) are represented in Figure 164. There are significant differences in their structures depending on the size of the alkali metal cation bound to the tetraethyleneoxy moiety. That is, in the absence of RA, one *tert*-butyl group of the biphenyl moiety interacts with the tetraethyleneoxy group, determining the final geometry. In case of lithium, four O-atoms of the regulation site bind the alkali metal center and for cesium two additional O-atoms of the phosphite group also bind the alkali metal center, thus affecting the electronic nature of the P–Au–C bonds. Binding of the regulation agent to the tetraethyleneoxy moiety brings the methyl substituents of the phosphite group closer to the gold center (the distance between the closest C-methyl group of the *tert*-butyl substituent is 0.06 Å shorter in (**C1-2a**)·Cs^+ than in the naked **C1-2a** adduct), thus affecting the steric environment around the gold center. In a parallel way, an increase in the size of the tetraethyleneoxy binder translates into an elongation of the C–Au bond (the C–Au bond distance is 0.04 Å longer (**C1-2a**)·Cs^+ than in (**C1-2a**)·Li^+ and 0.09 Å longer than in the naked **C1-2a** adduct).

The C–H/O–H insertion ability of the carbene into the corresponding phenol bonds increases as the C–Au bond enlarges because the donor-acceptor orbital interaction between the occupied *d* atomic orbitals of gold with the empty *p* orbital of carbon is less effective, thus increasing the electrophilicity of the carbene carbon. We have studied the O–H *vs para*-C_{sp2}–H insertion by computing the energetic barriers for the three cases considered. The energetic results are given in Table 7 and the energy profiles in the absence of regulation agent, for lithium and for cesium are given in Figure 165, Figure 166 and Figure 167, respectively.

Table 7. Energy barriers[a] (forward and backward, $\Delta G^{\#}_{f}$ and $\Delta G^{\#}_{b}$, respectively) in kcal·mol^{-1} and reaction energies (ΔG) for the O–H and *para*-C_{sp2}–H insertion reactions of phenol for catalyst **C1** and substrate **2a**

Entry	Adduct	O–H insertion			*para*-C_{sp2}–H insertion		
		$\Delta G^{\#}_{f}$	$\Delta G^{\#}_{b}$	ΔG	$\Delta G^{\#}_{f}$	$\Delta G^{\#}_{b}$	ΔG
1	**C1-2a**	3.1	7.3	–4.2	6.1	24.8	–18.7
2	**(C1-2a)·Li^+**	2.7	6.8	–4.1	6.4	24.4	–18.0
3	**(C1-2a)·Cs^+**	1.9	6.8	–4.9	4.3	25.5	–19.3

[a] BP86(COSMO=CH_2Cl_2)/def2-TZVP//BP86/def2-SVP level of theory.

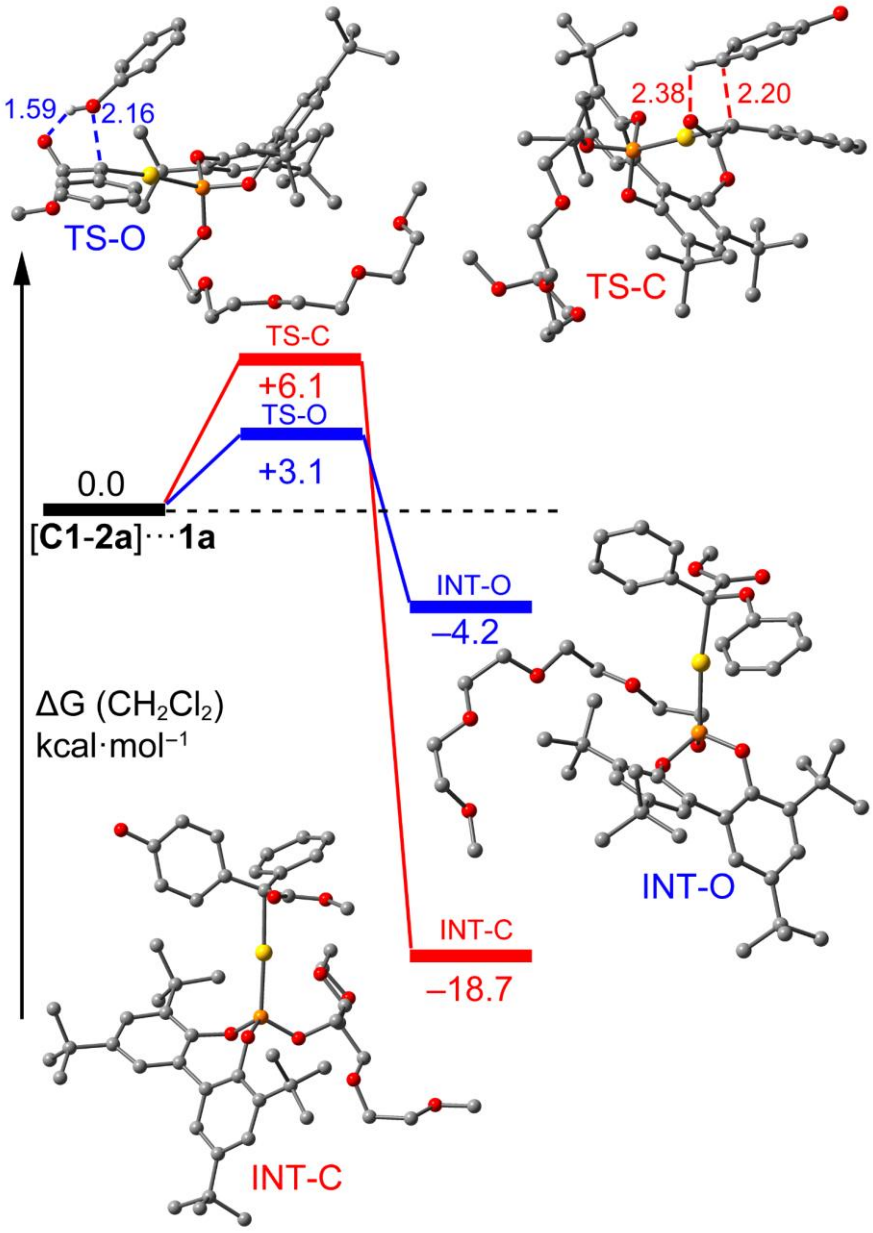

Figure 165. Energetic profile obtained for the O–H (in blue) and *para*-C_{sp2}–H (in red) insertion reactions of catalyst **C1** and substrate **2a** into phenol **1a** in the absence of RA. Distances in Å.

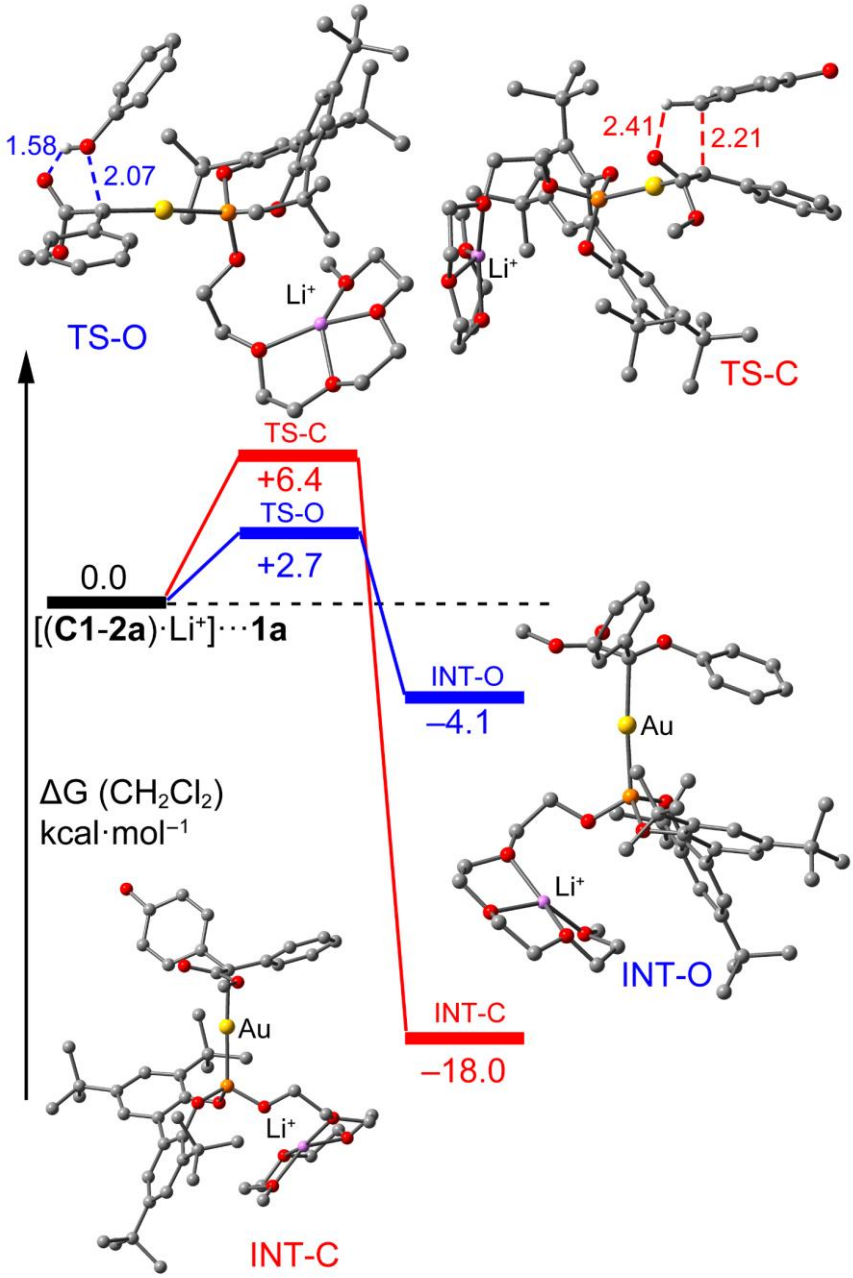

Figure 166. Energetic profile obtained for the O–H (in blue) and *para*-C_{sp2}–H (in red) insertion reactions of catalyst **C1** and substrate **2a** into phenol **1a** for Li^+. Distances in Å.

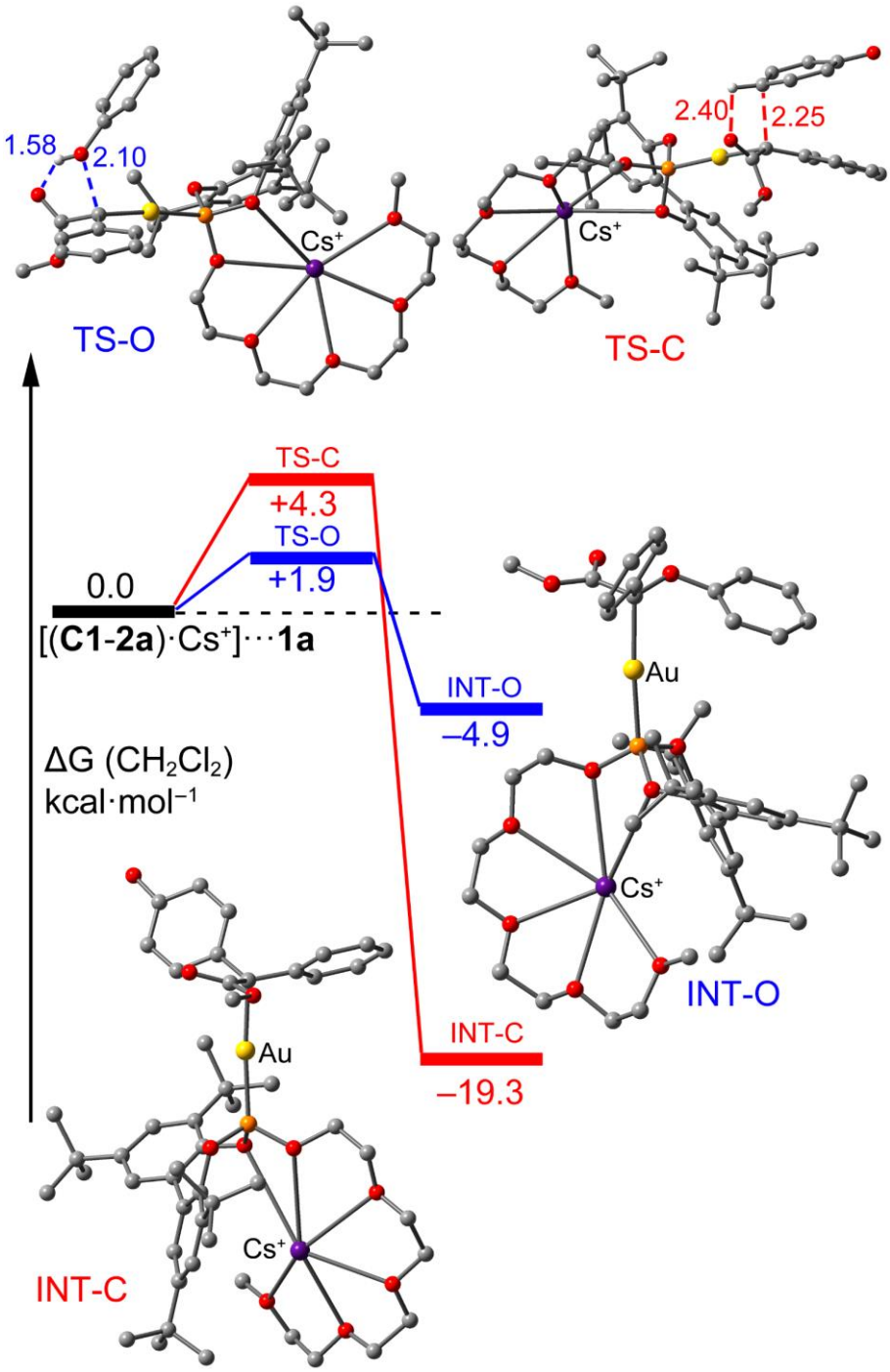

Figure 167. Energetic profile obtained for the O–H (in blue) and *para*-C_{sp2}–H (in red) insertion reactions of catalyst **C1** and substrate **2a** into phenol **1a** for Cs^+. Distances in Å.

It has been previously demonstrated that the generation of Au-carbene species is highly exergonic.[142,153,154] Therefore, gold carbenes and phenol are considered the reactants for the insertion reactions. The free energies given in Table 7, Figure 165, Figure 166 and Figure 167 are relative to these precursors [**C1**-**2a**]···**1a**, which are shown in Figure 164. Previous work has demonstrated that the insertion is the rate determining step and that the insertion into the O–H bond is the kinetic product whilst that into the *para*-C_{sp2}–H is thermodynamically favored.[153a] The experimental results in Table 6 reveal that the major product arises from insertion into the *para*-C_{sp2}–H bond and consequently the reaction should be thermodynamically controlled. The results gathered in Table 7 show that the barrier for insertion into O–H bonds are very low, ranging from 1.9 to 3.1 kcal·mol^{-1} and those for insertion into the *para*-C_{sp2}–H bonds are significantly higher, in agreement with previous calculations.[153a] However, the resulting products of insertion into the O–H bond (see Figure 167 for cesium) are not thermodynamically very stable (ΔG values in Table 7), with backward barriers ($\Delta G^{\#}_{b}$) that are low, thus allowing the reverse reaction to occur. In sharp contrast, the insertion into the *para*-C_{sp2}–H bond yields thermodynamically very stable intermediates and, concomitantly, large backward energy barriers ($\Delta G^{\#}_{b}$ >24 kcal·mol^{-1}) that prevent the reverse reaction from occurring. Therefore, the DFT calculations confirm that these reactions take place under thermodynamic control thus explaining the predominant formation of **3a**. Insertion into O–H bonds presents low barriers due to the existence of a strong O–H···O hydrogen bonding interactions in the transition state (see Figure 167, TS-O, 1.58 Å). For the insertion at the *para*-C_{sp2}–H bond, a weaker (C–H instead of O–H) and poorly directional C–H···O hydrogen bond is also established (Figure 167, TS-C, 2.40 Å). Interestingly, insertion into either O–H or *para*-C_{sp2}–H bonds and the hydrogen transfer to the ester group take place in the same step. This has been confirmed by intrinsic reaction coordinate (IRC) calculations. This is likely provoked by the presence of the regulation site since previous work[153] that used a simpler catalyst with $(PhO)_3P$ as the ligand reported two intermediates for this reaction, one derived from the

(154) (a) Rivilla, I.; Gómez-Emeterio, B. P.; Fructos, M. R.; Díaz-Requejo, M. M.; Pérez, P. J. *Organometallics* **2011**, *30*, 2855-2860. (b) Barluenga, J.; Lonzi, G.; Tomás, M.; López, L. A. *Chem. - Eur. J.* **2013**, *19*, 1573-1576. (c) López, E.; Lonzi, G.; López, L. A. *Organometallics* **2014**, *33*, 5924-5927.

insertion and another one from the proton transfer. The energetic results summarized in Table 7 are in good agreement with the experimental results. That is, in the absence of RA the proportion of **3a** is the smallest of the series because the barrier of the backward O–H insertion reaction is the largest ($\Delta G^{\#}_{b}$ = 7.3 kcal·mol^{-1}, Table 7). For lithium and cesium, the backward reaction presents the same energy barrier ($\Delta G^{\#}_{b}$ = 6.8 kcal·mol^{-1}); however, for cesium the barrier for the forward reaction of the insertion into the *para*-C_{sp2}–H bond is lower than that for lithium, thus explaining the larger **3a**:**4a** ratio (>50:1) and activity in the former.

3.4. CONCLUSIONS

An array of supramolecularly regulated phosphite-based Au(I) catalytic systems containing a polyether-based regulation site and steric effectors of different sizes has been described. The polyether-containing phosphite ligands had a high affinity for alkali metal salts according to binding studies carried out with NMR techniques. These Au(I) complexes have been successfully used as catalysts in the C–H selective functionalization of phenols and related derivatives with gold-carbenes derived from diazo compounds. The regulation of the steric congestion around the catalytic Au(I) center by the choice of a suitable external regulation agent provided an enhancement in the activity (up to 20%) and selectivity of the reaction (from 28:1 to >50:1 in terms of *para*-C_{sp2}C–H *vs.* O–H functionalization products). The catalytic performance and selectivity of the supramolecularly regulated catalysts has been rationalized using DFT calculations. These studies demonstrated that regulation agents of large size (*i.e.*, $CsBF_4$ and $RbBF_4$) favor the insertion of the carbene into the *para*-C_{sp2}–H bond. This new approach in supramolecular gold(I) catalysis has been applied to the derivatization of an array of substituted phenols, naphthols, seven-membered aromatic alcohols and to the preparation of an advanced synthetic intermediate of anticancer agent Tamoxifen.

3.5. EXPERIMENTAL SECTION

3.5.1. General considerations

All syntheses were carried out using chemicals as purchased from commercial sources unless otherwise stated. Tetrafluoroborate salts (NH_4BF_4, $LiBF_4$, $NaBF_4$, KBF_4 and $RbBF_4$) were purchased from commercial sources. $CsBF_4$ was prepared reacting Cs_2CO_3 with HBF_4.[155] All regulation agents were azeotropically dried with toluene prior to their use. Air- and moisture-sensitive manipulations or reactions were performed under inert atmosphere (N_2 or argon), either in a glove box or with standard Schlenk techniques. Glassware was dried under vacuum before use with a hot air gun. All solvents were dried and deoxygenated by using a solvent purification system (SPS). Silica gel 60 (230-400 mesh) was used for column chromatography. NMR spectra were recorded at room temperature in 400 MHz or 500 MHz spectrometers in $CDCl_3$ or CD_2Cl_2 unless otherwise cited. ^1H and ^{13}C NMR chemical shifts are quoted in ppm relative to residual solvent peaks. $^{11}B\{^1H\}$ NMR chemical shifts are quoted in ppm relative to $BF_3{\cdot}Et_2O$ in $CDCl_3$. $^{19}F\{^1H\}$ NMR chemical shifts are quoted in ppm relative to $CFCl_3$ in $CDCl_3$. $^{31}P\{^1H\}$ NMR chemical shifts are quoted in ppm relative to 85% phosphoric acid in water. HRMS and MS spectra were recorded using ESI ionization method. IR spectra were recorded using Attenuated Total Reflection (ATR) technique.

(155) A round-bottomed flask provided with a stirrer was loaded with Cs_2CO_3 (3.27 g, 9.9 mmol) and 50 mL of MilliQ water. An aqueous HBF_4 solution (50 wt%, 19.9 mmol) was added dropwise to the cesium carbonate-containing solution, observing some bubbling due to the release of CO_2. This solution was stirred for 24 hours at room temperature. Then, water was evaporated, and the solid residue was further dried in a vacuum oven at 120 °C for 24 hours, quantitatively yielding $CsBF_4$ as a white solid. The cesium content was determined by ICP-MS (calcd. for $CsBF_4$ 60.5%, found 60.0$\pm$0.5 %).

3.5.2. General structural comments on X-ray crystals

Crystals of **3e** and **3f** were grown by solvent diffusion, using CH_2Cl_2 and *n*-pentane at room temperature. The crystals used for structure determination were selected using a Zeiss stereomicroscope using polarized light and prepared under inert conditions immersed in perfluoropolyether as protecting oil for manipulation.

Crystal structure determination for samples **3e** and **3f** were carried out using an Apex DUO Kappa 4-axis goniometer equipped with an APEX 2 4K CCD area detector, a Microfocus Source E025 IuS using MoKα radiation, Quazar MX multilayer Optics as monochromator and an Oxford Cryosystems low temperature device Cryostream 700 plus (T = −173 °C). Full-sphere data collection was used with ω and φ scans. Programs used: Data collection APEX-2,[109] data reduction Bruker Saint[110] V/.60A and absorption correction SADABS.[111] Structure Solution and Refinement: Crystal structure solution was achieved using the computer program SHELXT.[79] Visualization was performed with the program SHELXle.[80] Missing atoms were subsequently located from difference Fourier synthesis and added to the atom list. Least-squares refinement on F2 using all measured intensities was carried out using the program SHELXL 2015.[81] All non-hydrogen atoms were refined including anisotropic displacement parameters.

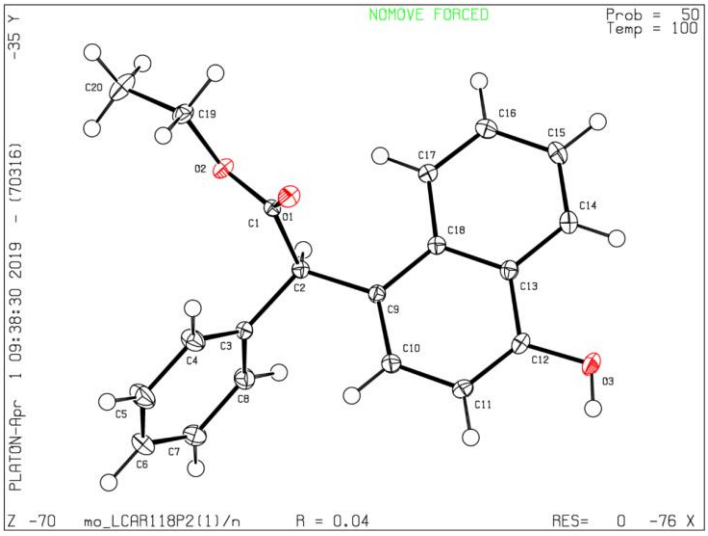

Figure 168. CheckCIF-generated[156] ORTEP drawing (thermal ellipsoids drawn at a 50 % probability level) showing the structure of **3e**. Color scheme: C: black, O: red. (To be deposited at the Cambridge Crystallographic Data Center, CCDC).

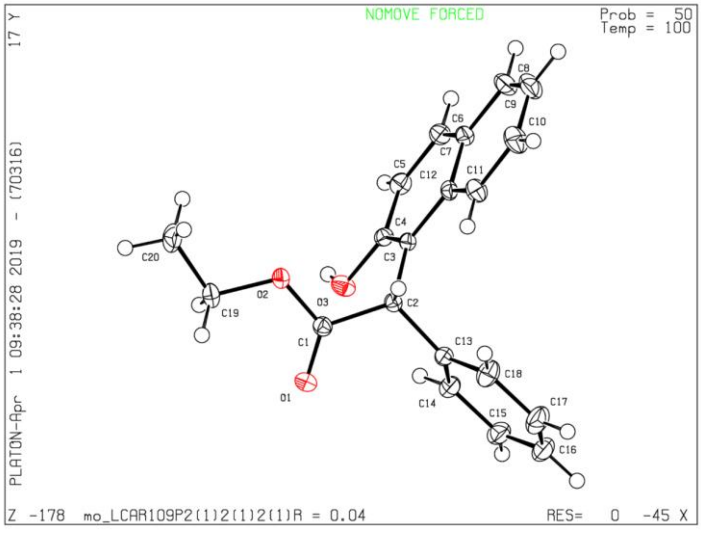

Figure 169. CheckCIF-generated[156] ORTEP drawing (thermal ellipsoids drawn at a 50 % probability level) showing the structure of **3f**. Color scheme: C: black, O: red. (To be deposited at the Cambridge Crystallographic Data Center, CCDC).

(156) CheckCIF reports on the consistency and integrity of crystal structure determinations reported in CIF format. https://checkcif.iucr.org/

Table 8. Crystal data and structural parameters for **3e** and **3f**

Compound	3e	3f
Formula	$C_{20}H_{18}O_3$	$C_{20}H_{18}O_3$
Solvent	CH_2Cl_2	CH_2Cl_2
Formula weight	306.34	306.34
Crystal size (mm^3)	0.10 x 0.10 x 0.10	0.25 x 0.10 x 0.06
Temperature (K)	100(2)	100(2)
Crystal system	Monoclinic	Orthorhombic
Space group	*P2*(1)/n	*P2*(1)2(1)2(1)
a (Å)	11.9062(6)	8.8530(4)
b (Å)	7.6280(4)	9.9104(4)
c (Å)	17.1199(10)	18.1445(7)
α (°)	90	90
β (°)	92.8492(18)	90
γ (°)	90	90
Volume ($Å^3$)	1552.92(14)	1591.94(11)
Z	4	4
ρ ($g{\cdot}cm^{-3}$)	1.310	1.278
μ (mm^{-1})	0.087	0.085
θ_{max} (°)	31.688	31.547
Reflect. collected	11833	9947
Unique reflect.	5044 [R(int) = 0.0203]	5308 [R(int) = 0.0285]
Absorpt. correction	Multi-Scan	Multi-Scan
Parameters/restrains	210/0	210/0
R1/wR2 [I>2σ(I)]	0.0432/0.1133	0.0416/0.1100
R1/wR2 (all data)	0.0555/0.1219	0.0469/0.1147
Goodnes-of-fit (F^2)	1.040	1.057
Peak/hole ($e/Å^3$)	0.486/−0.208	0.500/−0.184

Table 9. Bond lengths (Å) for **3e** and **3f**

	Compound 3e		Compound 3f	
Entry	**Atoms**	**Length (Å)**	**Atoms**	**Length (Å)**
1	O1 C1	1.2152(13)	C1 O1	1.2111(19)
2	O2 C1	1.3346(11)	C1 O2	1.3308(19)
3	O2 C19	1.4625(13)	C1 C2	1.523(2)
4	O3 C12	1.3609(11)	C2 C13	1.522(2)
5	C18 C17	1.4185(14)	C2 C3	1.527(2)
6	C18 C13	1.4288(13)	O2 C19	1.462(2)
7	C18 C9	1.4341(13)	C3 C4	1.381(2)
8	C12 C11	1.3705(14)	C3 C12	1.4306(19)
9	C12 C13	1.4245(14)	O3 C4	1.3656(18)
10	C13 C14	1.4183(13)	C4 C5	1.416(2)
11	C1 C2	1.5189(14)	C5 C6	1.369(2)
12	C9 C10	1.3756(14)	C6 C7	1.415(2)
13	C9 C2	1.5211(13)	C7 C8	1.419(2)
14	C17 C16	1.3750(13)	C7 C12	1.431(2)
15	C19 C20	1.5068(15)	C8 C9	1.366(3)
16	C11 C10	1.4124(14)	C9 C10	1.407(3)
17	C14 C15	1.3685(15)	C10 C11	1.375(2)
18	C2 C3	1.5265(13)	C11 C12	1.422(2)
19	C16 C15	1.4111(15)	C13 C14	1.393(2)
20	C6 C5	1.3817(18)	C13 C18	1.398(2)
21	C6 C7	1.3891(16)	C14 C15	1.391(2)
22	C3 C4	1.3913(14)	C15 C16	1.388(3)
23	C3 C8	1.3938(16)	C16 C17	1.382(3)
24	C7 C8	1.3910(15)	C17 C18	1.401(3)
25	C4 C5	1.3937(15)	C19 C20	1.498(3)

Table 10. Bond angles (°) for **3e** and **3f**

	Compound 3e		Compound 3f	
Entry	**Atoms**	**Angle (°)**	**Atoms**	**Angle (°)**
1	C1 O2 C19	117.26(8)	O1 C1 O2	123.83(15)
2	C17 C18 C13	117.59(8)	O1 C1 C2	125.76(15)
3	C17 C18 C9	122.95(9)	O2 C1 C2	110.24(13)
4	C13 C18 C9	119.42(9)	C13 C2 C1	113.30(12)
5	O3 C12 C11	123.69(9)	C13 C2 C3	111.39(12)
6	O3 C12 C13	115.83(9)	C1 C2 C3	112.48(12)
7	C11 C12 C13	120.47(9)	C1 O1 C19	115.43(13)
8	C14 C13 C12	121.08(9)	C4 C3 C12	118.77(13)
9	C14 C13 C18	119.68(9)	C4 C3 C2	120.61(12)
10	C12 C13 C18	119.22(9)	C12 C3 C2	120.52(13)
11	O1 C1 O2	123.15(9)	O3 C4 C3	117.83(13)
12	O1 C1 C2	126.08(9)	O3 C4 C5	120.15(14)
13	O2 C1 C2	110.73(8)	C3 C4 C5	122.02(14)
14	C10 C9 C18	118.75(9)	C6 C5 C4	119.67(15)
15	C10 C9 C2	121.73(8)	C5 C6 C7	120.82(15)
16	C18 C9 C2	119.31(8)	C6 C7 C8	120.76(15)
17	C16 C17 C18	121.61(9)	C6 C7 C12	119.41(14)
18	O2 C19 C20	107.17(9)	C8 C7 C12	119.82(15)
19	C12 C11 C10	119.94(9)	C9 C8 C7	121.04(17)
20	C15 C14 C13	120.81(9)	C8 C9 C10	119.61(16)
21	C1 C2 C9	113.52(8)	C11 C10 C9	121.00(17)
22	C1 C2 C3	108.82(8)	C10 C11 C12	121.14(16)
23	C9 C2 C3	114.49(8)	C11 C12 C3	123.34(14)
24	C17 C16 C15	120.17(10)	C11 C12 C7	117.38(14)
25	C9 C10 C11	122.17(9)	C3 C12 C7	119.27(13)
26	C5 C6 C7	119.31(10)	C14 C13 C18	118.89(15)
27	C14 C15 C16	120.09(9)	C14 C13 C2	120.94(14)
28	C4 C3 C8	118.78(9)	C18 C13 C2	120.09(15)
29	C4 C3 C2	122.74(10)	C15 C14 C13	120.62(16)
30	C8 C3 C2	118.48(9)	C16 C15 C14	120.38(18)
31	C6 C7 C8	120.28(11)	C17 C16 C15	119.58(17)

32	C7 C8 C3	120.61(10)	C16 C17 C18	120.44(18)
33	C3 C4 C5	120.35(11)	C13 C18 C17	120.08(17)
34	C6 C5 C4	120.65(11)	O2 C19 C20	107.74(14)

Table 11. Torsion angles (°) for **3e** and **3f**

	Compound 3e		Compound 3f	
Entry	**Atoms**	**T. angle (°)**	**Atoms**	**T. angle (°)**
1	O3 C12 C13 C14	−1.53(15)	O1 C1 C2 C13	0.5(2)
2	C11 C12 C13 C14	179.44(11)	O2 C1 C2 C13	175.79(13)
3	O3 C12 C13 C18	176.78(9)	O1 C1 C2 C3	127.95(16)
4	C11 C12 C13 C18	−2.25(16)	O2 C1 C2 C3	−56.75(16)
5	C17 C18 C13 C14	2.27(15)	O1 C1 O2 C19	−3.9(2)
6	C9 C18 C13 C14	179.96(10)	C2 C1 O2 C19	−179.28(14)
7	C17 C18 C13 C12	−176.06(10)	C13 C2 C3 C4	86.92(17)
8	C9 C18 C13 C12	1.63(15)	C1 C2 C3 C4	−41.54(18)
9	C19 O2 C1 O1	−6.75(14)	C13 C2 C3 C12	−89.48(16)
10	C19 O2 C1 C2	171.24(8)	C1 C2 C3 C12	142.06(14)
11	C17 C18 C9 C10	177.56(10)	C12 C3 C4 O3	−178.71(13)
12	C13 C18 C9 C10	0.00(15)	C2 C3 C4 O3	4.8(2)
13	C17 C18 C9 C2	2.82(15)	C12 C3 C4 C5	1.6(2)
14	C13 C18 C9 C2	−174.74(9)	C2 C3 C4 C5	−174.84(14)
15	C13 C18 C17 C16	−0.65(16)	O3 C4 C5 C6	178.35(15)
16	C9 C18 C17 C16	−178.26(10)	C3 C4 C5 C6	−2.0(2)
17	C1 O2 C19 C20	−169.17(9)	C4 C5 C6 C7	0.5(2)
18	O3 C12 C11 C10	−177.73(10)	C5 C6 C7 C8	179.91(16)
19	C13 C12 C11 C10	1.22(17)	C5 C6 C7 C12	1.3(2)
20	C12 C13 C14 C15	176.41(11)	C6 C7 C8 C9	−178.44(17)
21	C18 C13 C14 C15	−1.89(17)	C12 C7 C8 C9	0.2(3)
22	O1 C1 C2 C9	−29.20(13)	C7 C8 C9 C10	−0.1(3)
23	O2 C1 C2 C9	152.88(8)	C8 C9 C10 C11	0.3(3)
24	O1 C1 C2 C3	99.55(11)	C9 C10 C11 C12	−0.5(3)
25	O2 C1 C2 C3	−78.37(9)	C10 C11 C12 C3	−179.58(16)
26	C10 C9 C2 C1	118.17(11)	C10 C11 C12 C7	0.5(2)
27	C18 C9 C2 C1	−67.25(12)	C4 C3 C12 C11	−179.71(15)
28	C10 C9 C2 C3	−7.62(14)	C2 C3 C12 C11	−3.2(2)
29	C18 C9 C2 C3	166.96(9)	C4 C3 C12 C7	0.2(2)
30	C18 C17 C16 C15	−1.40(18)	C2 C3 C12 C7	176.65(13)
31	C18 C9 C10 C11	−1.08(16)	C6 C7 C12 C11	178.29(15)

32	C2 C9 C10 C11	173.53(10)	C8 C7 C12 C11	−0.4(2)
33	C12 C11 C10 C9	0.48(17)	C6 C7 C12 C3	−1.6(2)
34	C13 C14 C15 C16	−0.18(18)	C8 C7 C12 C3	179.74(15)
35	C17 C16 C15 C14	1.83(19)	C1 C2 C13 C14	63.34(19)
36	C1 C2 C3 C4	−23.84(12)	C3 C2 C13 C14	−64.69(18)
37	C9 C2 C3 C4	104.37(11)	C1 C2 C13 C18	−120.18(17)
38	C1 C2 C3 C8	156.33(9)	C3 C2 C13 C18	111.80(17)
39	C9 C2 C3 C8	−75.46(12)	C18 C13 C14 C15	−0.4(2)
40	C5 C6 C7 C8	−0.75(18)	C2 C13 C14 C15	176.13(15)
41	C6 C7 C8 C3	1.18(17)	C13 C14 C15 C16	−0.4(3)
42	C4 C3 C8 C7	−0.34(16)	C14 C15 C16 C17	1.0(3)
43	C2 C3 C8 C7	179.50(9)	C15 C16 C17 C18	−0.7(3)
44	C8 C3 C4 C5	−0.91(16)	C14 C13 C18 C17	0.7(3)
45	C2 C3 C4 C5	179.25(10)	C2 C13 C18 C17	−175.90(17)
46	C7 C6 C5 C4	−0.50(19)	C16 C17 C18 C13	−0.1(3)
47	C3 C4 C5 C6	1.35(19)	C1 O2 C19 C20	174.30(16)

3.5.3. Syntheses of ligands L1-L3

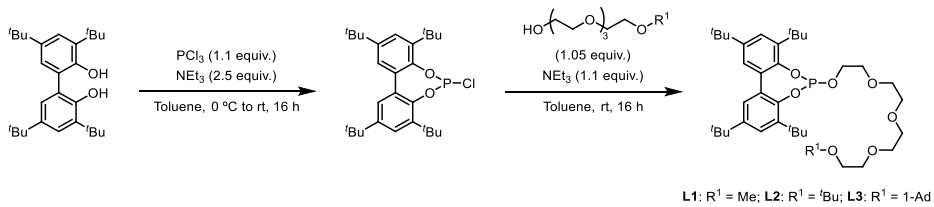

L1: R^1 = Me; **L2**: R^1 = ^{t}Bu; **L3**: R^1 = 1-Ad

Scheme 40. General synthesis for ligands **L1**-**L3**.

3,3',5,5'-tetra-*tert*-butylbiphenyl-2,2'-diyl chlorophosphite: The preparation of 3,3',5,5'-tetra-*tert*-butylbiphenyl-2,2'-diyl chlorophosphite was performed by slightly varying a reported procedure.[135] Under inert atmosphere, a flame-dried Schlenk flask provided with a stirrer was loaded with PCl_3 (500 µL, 5.73 mmol), dry toluene (30 mL) and triethylamine (1.74 mL, 12.4 mmol). The resulting solution was cooled to 0 °C. In parallel, a flame-dried Schlenk flask provided with a stirrer was loaded under Ar with 3,3',5,5'-tetra-*tert*-butyl-2,2'-dihydroxybiphenyl (2 g, 4.77 mmol) and was azeotropically dried with toluene (3 x 10 mL), after which anhydrous toluene was added (30 mL). The diol solution was then slowly added dropwise to the PCl_3 and NEt_3 solution. Subsequently, the mixture was allowed to reach room temperature. After stirring for 16 hours, the mixture was filtered under inert atmosphere through Celite® 521, and the precipitate was further washed with toluene (20 mL). Volatiles were removed from the combined filtrates under reduced pressure to afford a yellowish solid (quantitative yield). This compound was used in the following syntheses with no further purification. Spectroscopic data for this compound were in agreement with those already reported in the literature.[135] ^{1}H NMR (400 MHz, $CDCl_3$) δ: 7.46 (d, J = 2.4 Hz, 2 H), 7.17 (d, J = 2.4 Hz, 2 H), 1.48 (s, 18 H), 1.35 (s, 18 H) ppm. $^{31}P\{^1H\}$ NMR (162 MHz, $CDCl_3$) δ: 174.6 ppm.

General procedure for ligands syntheses: A solution of 3,3',5,5'-tetra-*tert*-butylbiphenyl-2,2'-diyl chlorophosphite, *vide supra*, (4.77 mmol) in 30 mL of anhydrous toluene was prepared under Ar in a flame-dried Schlenk flask provided with a stirrer. Then, NEt_3 (5.72 mmol) was added dropwise. In parallel, a flame-dried Schlenk flask provided with a stirrer was loaded under Ar with the corresponding mono-functionalized tetraethyleneglycol derivative (TEG) (5.25 mmol) and was azeotropically dried with toluene (3 x

10 mL), after which 30 mL of anhydrous toluene were added. The monofunctionalized-TEG solution was slowly added dropwise to the chlorophosphite solution at room temperature. Then, the mixture was stirred for 16 h and filtered afterwards under N_2 atmosphere through Celite® 521. Volatiles were evaporated to dryness to give the crude product as a yellowish oil. The ligand was purified by flash chromatography, using SiO_2 as the stationary phase and a mixture of cyclohexane and ethyl acetate as the eluents.

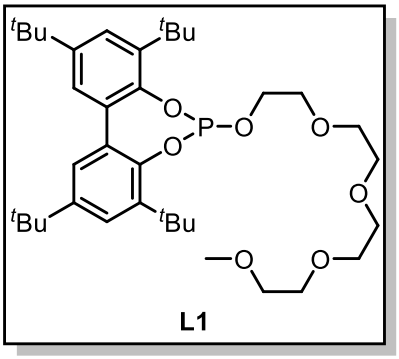

L1

Ligand **L1**: Ligand **L1** was prepared according to the described general procedure, using commercially available tetraethyleneglycol mono-methyl ether and purified by flash chromatography (SiO_2, cyclohexane:AcOEt, 1:0→5:1), yielding 2.3 g of a colorless thick oil (76% yield). ^{1}H NMR (400 MHz, $CDCl_3$) δ: 7.41 (d, J = 2.4 Hz, 2 H), 7.15 (d, J = 2.4 Hz, 2 H), 3.93-3.88 (m, 2 H), 3.70-3.50 (m, 14 H), 3.36 (s, 3 H), 1.48 (s, 18 H), 1.34 (s, 18 H) ppm. ^{13}C{^{1}H} NMR (100 MHz, $CDCl_3$) δ: 146.5, 140.0, 132.7, 126.7, 124.4, 72.1, 70.9, 70.8, 70.7, 63.7, 59.2, 35.5, 34.8, 31.7, 31.2 ppm. ^{31}P{^{1}H} NMR (162 MHz, $CDCl_3$) δ: 138.8 ppm. IR (neat): 2956, 2905, 2870, 1437, 1395, 1362, 1281, 1229, 1200, 1108, 1090, 1031, 941, 868, 850, 802, 777, 764, 735, 697, 615 cm^{-1}. HRMS ESI-MS (m/z): $[M+H]^+$ calcd. for $C_{37}H_{60}O_7P^+$ 647.4085, found 647.4084.

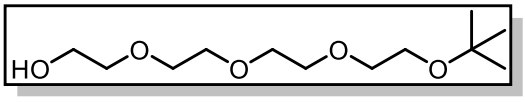

Tetraethyleneglycol mono-*tert*-butyl ether: The preparation of mono-*tert*-butyl ether was performed by adapting a reported procedure.[134a] Tetraethyleneglycol (400 mL, 2.32 mol), Amberlyst® 15 macroreticular cation exchange resin (17.5 g, H^+ form) and CH_2Cl_2 (1 L) were placed in a 2 L two-necked round bottomed flask equipped with a dry ice/acetone condenser. The flask was kept under Ar and under mild stirring. 500 mL of isobutene (8% in CH_2Cl_2, 0.86 mmol) were then slowly added *via* cannula. After 6 hours, the reaction mixture was poured into 200 mL of saturated aqueous $NaHCO_3$ and the mixture extracted with water (2 x 500 mL). The

organic layer was dried over anhydrous $MgSO_4$ and evaporated to give a colorless oil (62.3 g, 29% yield) consisting only of the mono-substituted product. No further purification was performed. Spectroscopic data for this compound were in agreement with those already reported in the literature.[134a] ^{1}H NMR (400 MHz, $CDCl_3$) δ: 3.71-3.69 (m, 2 H), 3.66-3.64 (m, 8 H), 3.59-3.57 (m, 4 H), 3.51-3.49 (m, 2 H), 2.27 (br s, 1 H), 1.17 (s, 9 H) ppm. ^{13}C{^{1}H} NMR (100 MHz, $CDCl_3$) δ: 73.1, 72.6, 71.3, 70.7, 70.4, 61.8, 61.2, 27.5 ppm.

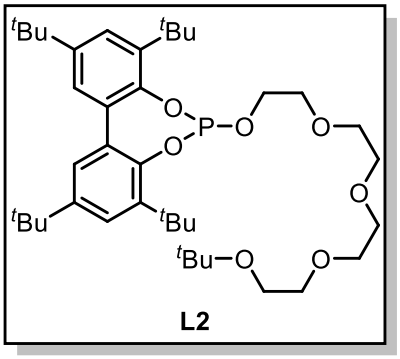

L2

Ligand **L2**: Ligand **L2** was prepared according to the described general procedure, using tetraethyleneglycol mono-*tert*-butyl ether (*vide supra*) and purified by flash chromatography (SiO_2, cyclohexane:AcOEt, 1:0→5:1), yielding 2.9 g of a colorless thick oil (84% yield). ^{1}H NMR (400 MHz, $CDCl_3$) δ: 7.41 (d, J = 2.5 Hz, 2 H), 7.16 (d, J = 2.4 Hz, 2 H), 3.93-3.88 (m, 2 H), 3.70-3.53 (m, 12 H), 3.52-3.49 (m, 2 H), 1.48 (s, 18 H), 1.34 (s, 18 H), 1.18 (s, 9 H) ppm. ^{13}C{^{1}H} NMR (100 MHz, $CDCl_3$) δ: 146.5, 146.3 (d, J_{C-P} = 5.8 Hz), 139.9 (d, J_{C-P} = 1.0 Hz), 132.7 (d, J_{C-P} = 3.6 Hz), 126.6, 124.3, 73.1, 71.3, 70.9, 70.8, 70.7, 63.7 (d, J_{C-P} = 2.1 Hz), 61.3, 35.5, 34.7, 31.6, 31.1 (d, J_{C-P} = 2.6 Hz), 27.6 ppm. ^{31}P{^{1}H} NMR (162 MHz, $CDCl_3$) δ: 138.8 ppm. IR (neat): 2959, 2906, 2869, 1437, 1394, 1362, 1281, 1229, 1198, 1124, 1090, 1036, 941, 869, 851, 777, 764, 736, 697, 615 cm^{-1}. HRMS ESI-MS (m/z): $[M+Na]^+$ calcd. for $C_{40}H_{65}O_7PNa^+$ 711.4360, found 711.4363.

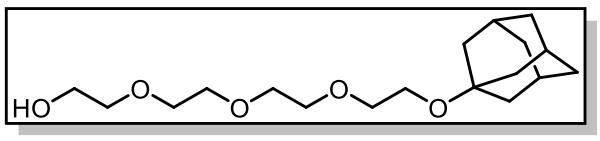

Tetraethyleneglycol mono-1-adamantyl ether: The preparation of tetraethyleneglycol mono-1-adamantyl ether was performed as reported in the literature.[134b] Tetraethyleneglycol (41.5 mL, 0.239 mol) was transferred to a round-bottom flask. The flask was heated to 60 °C and triethylamine (5 mL, 0.036 mol) was added. After stirring the solution for 5 minutes at 60 °C, 1-bromoadamantane (2.5 g, 0.012 mol) was added. A condenser was then attached to the set-up and the reaction mixture was heated to 180 °C and

stirred for 18 hours. After cooling at room temperature, 50 mL of dichloromethane were added to the reaction mixture. The organic layer was washed with 2 M HCl (4 x 50 mL) and a saturated NaCl solution (2 x 50 mL). The organic layer was subsequently dried over $MgSO_4$, and evaporated to dryness to afford a brown oil (3.69 g, 97% yield). This product was used without further purification. Spectroscopic data for this compound were in agreement with those already reported in the literature.[134b] ^{1}H NMR (400 MHz, $CDCl_3$) δ: 3.80-3.50 (m, 16 H), 2.56 (br s, 1 H), 2.13 (br s, 3 H), 1.80-1.50 (m, 12 H) ppm. ^{13}C{1H} NMR (100 MHz, CDCl3) δ: 72.7, 72.4, 71.4, 70.7, 70.6, 70.4, 61.8, 59.3, 41.5, 36.5, 30.6 ppm.

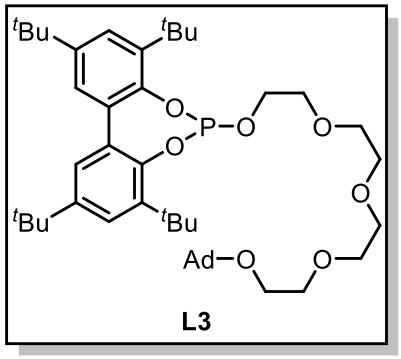

L3

Ligand **L3**: Ligand **L3** was prepared according to the described general procedure, using tetraethyleneglycol mono-1-adamantyl ether (*vide supra*) and purified by flash chromatography (SiO_2, cyclohexane:AcOEt, 1:0→5:1), yielding 1.3 g of a colorless thick oil that solidified upon standing (72% yield). ^{1}H NMR (400 MHz, $CDCl_3$) δ: 7.47-7.45 (m, 2 H), 7.21-7.19 (m, 2 H), 3.96-3.94 (m, 2 H), 3.75-3.55 (m, 14 H), 2.16 (br s, 3 H), 1.80-1.55 (m, 12 H) 1.53 (s, 18 H), 1.38 (s, 18 H) ppm. ^{13}C{^{1}H} NMR (100 MHz, $CDCl_3$) δ: 146.4, 146.2 (d, J_{C-P} = 5.8 Hz), 139.9, 132.7 (d, J_{C-P} = 3.4 Hz), 126.5, 124.2, 72.1, 71.3, 70.9, 70.8, 70.7, 70.6, 63.6, 59.3, 41.6, 36.5, 35.4, 34.7, 31.6, 31.1 (d, J_{C-P} = 2.2 Hz), 30.5 ppm. ^{31}P{^{1}H} NMR (162 MHz, $CDCl_3$) δ: 138.9 ppm. IR (neat): 2954, 2905, 1438, 1395, 1362, 1282, 1229, 1201, 1115, 1090, 1036, 941, 913, 869, 851, 777, 764, 733, 697, 615 cm^{-1}. HRMS ESI-MS (m/z): $[M+Na]^+$ calcd. for $C_{46}H_{71}O_7PNa^+$ 789.4830, found 789.4862.

3.5.4. Syntheses of complexes C1-C3, $[Au(CH_3CN)(L1)]BF_4$ and $[Au(2,4,6\text{-}(MeO)_3(C_6H_2)CN)(L1)]BF_4$

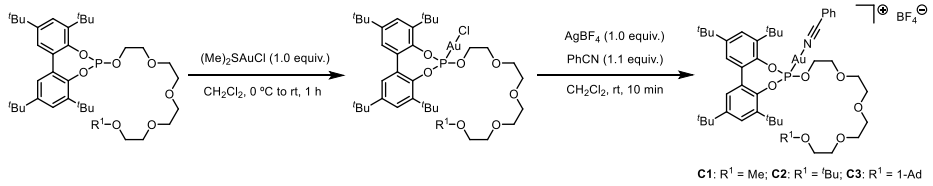

Scheme 41. General synthesis for complexes **C1-C3**.

General procedure for the synthesis of the complexes: The Au(I) complexes were prepared in two steps adapting reported procedures: The corresponding gold(I) chloride[157] was generated in the first and the cationic gold(I) complex[158] in the second. In a typical experiment, a solution of the desired ligand (0.3 mmol) in CH_2Cl_2 (3 mL) was added dropwise to a solution of $(Me)_2SAuCl$ (0.3 mmol) in CH_2Cl_2 (3 mL) at 0 °C. The resulting solution was allowed to reach room temperature and stirred for another 30 min. The volatiles were removed under vacuum to quantitatively yield the corresponding Au(I) chloride phosphite complex as a white solid. Subsequently, a solution of the desired gold(I) chlorophosphite (0.3 mmol) and benzonitrile (0.33 mmol) in CH_2Cl_2 (6 mL) was added to a solution of $AgBF_4$ (0.3 mmol) in CH_2Cl_2 (3 mL), observing the immediate formation of a white precipitate (AgCl). After stirring for 5 min, the mixture was filtered using a 0.22 μm pore size PTFE syringe filter. The filtrate was concentrated under vacuum. The cationic tetrafluoroborate complex was obtained as a white, foamy solid.

(157) Delpont, N.; Escofet, I.; Pérez-Galan, P.; Spiegl, D.; Raducan, M.; Bour, C.; Sinisi, R.; Echavarren, A. M. *Catal. Sci. Technol.* **2013**, *3*, 3007-3012.
(158) Amijs, C. H. M.; López-Carrillo, V.; Raducan, M.; Pérez-Galan, P.; Ferrer, C.; Echavarren, A. M. *J. Org. Chem.* **2008**, *73*, 7721-7730.

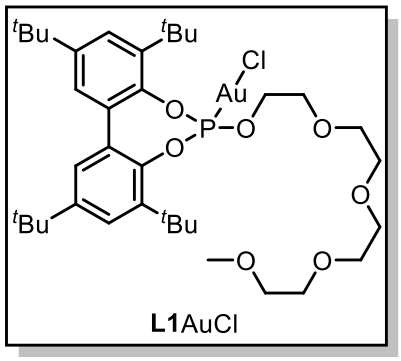

L1AuCl

Ligand **L1** gold(I) chloride: **L1**AuCl was prepared according to the described general procedure, quantitatively yielding the gold(I) chloride as a white solid. ^{1}H NMR (500 MHz, CD_2Cl_2) δ: 7.54 (d, J = 2.0 Hz, 2 H), 7.22 (d, J = 2.5 Hz, 2 H), 4.37-4.33 (m, 2 H), 3.71-3.69 (m, 2 H), 3.65-3.54 (m, 10 H), 3.50-3.48 (m, 2 H), 3.32 (s, 3 H), 1.53 (s, 18 H), 1.37 (s, 18 H) ppm. ^{13}C{^{1}H} NMR (100 MHz, CD_2Cl_2) δ: 149.1, 144.2 (d, J_{C-P} = 10.5 Hz), 140.4 (d, J_{C-P} = 3.9 Hz), 131.3 (d, J_{C-P} = 2.0 Hz), 127.5, 126.1, 72.3, 71.2, 71.0, 70.9, 70.7, 70.0 (d, J_{C-P} = 6.4 Hz), 69.3, 59.0, 36.0, 35.0, 31.9, 31.5 ppm. ^{31}P{^{1}H} NMR (162 MHz, CD_2Cl_2) δ: 122.9 ppm. IR (neat): 2957, 2870, 1589, 1436, 1396, 1363, 1282, 1221, 1202, 1119, 1084, 1032, 950, 915, 895, 799, 715, 645, 627, 537 cm^{-1}. HRMS ESI-MS (m/z): [M+Na]$^{+}$ calcd. for $C_{37}H_{59}O_7PAuClNa^{+}$ 901.3245, found 901.3205.

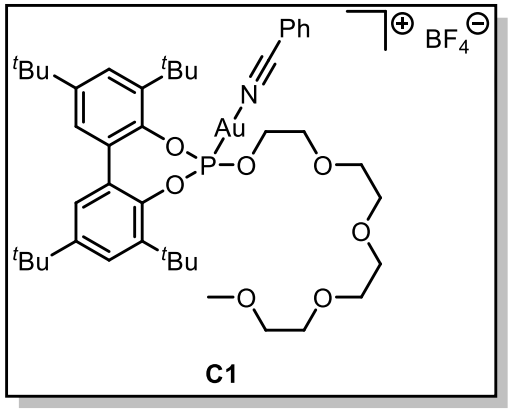

C1

Complex **C1**: **C1** was prepared according to the described general procedure, obtaining 283 mg (92% yield) of the cationic complex as a white solid. ^{1}H NMR (400 MHz, CD_2Cl_2) δ: 7.85-7.83 (m, 2 H), 7.79 (tm, J = 7.7 Hz, 1 H), 7.60 (tm, J = 7.9 Hz, 2 H), 7.57 (d, J = 1.9 Hz, 2 H), 7.24 (d, J = 2.4 Hz, 2 H), 4.51 (br d, J = 13.2 Hz, 2 H), 3.78 (br s, 2 H), 3.75-3.60 (m, 10 H), 3.56-3.54 (m, 2 H), 3.32 (s, 3 H), 1.54 (s, 18 H), 1.37 (s, 18 H) ppm. ^{11}B{^{1}H} NMR (128 MHz, CD_2Cl_2) δ: –1.2 ppm. ^{13}C{^{1}H} NMR (100 MHz, CD_2Cl_2) δ: 149.6, 143.9 (d, J_{C-P} = 10.4 Hz), 140.4 (d, J_{C-P} = 4.1 Hz), 135.9, 133.9, 131.0 (d, J_{C-P} = 2.3 Hz), 130.1, 127.7, 126.3, 120.6, 108.4, 72.1, 70.9, 70.7, 70.3, 70.0 (d, J_{C-P} = 4.7 Hz), 59.1, 36.0, 35.1, 31.8, 31.4 ppm. ^{19}F{^{1}H} NMR (376 MHz, CD_2Cl_2) δ: –152.5 ppm. ^{31}P{^{1}H} NMR (162 MHz, CD_2Cl_2) δ: 112.6 (br s) ppm. IR (neat): 2958, 2283, 1594, 1448, 1397, 1363, 1282, 1221, 1029, 931, 800, 760, 715, 686, 644, 627, 550

cm^{-1}. HRMS ESI-MS (m/z): [M–PhCN–BF_4]$^+$ calcd. for $C_{37}H_{59}O_7PAu^+$ 843.3659, found 843.3634.

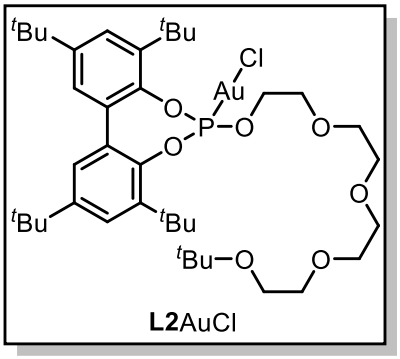

L2AuCl

Ligand **L2** gold(I) chloride: **L2**AuCl was prepared according to the described general procedure, quantitatively yielding the gold(I) chloride as a white solid. ^{1}H NMR (400 MHz, CD_2Cl_2) δ: 7.57 (d, J = 2.0 Hz, 2 H), 7.24 (d, J = 2.4 Hz, 2 H), 4.40-4.35 (m, 2 H), 3.74-3.72 (m, 2 H), 3.67-3.57 (m, 8 H), 3.55-3.47 (m, 4 H), 1.56 (s, 18 H), 1.39 (s, 18 H), 1.19 (s, 9 H) ppm. ^{13}C{^{1}H} NMR (100 MHz, CD_2Cl_2) δ: 149.2 (d, J_{C-P} = 1.2 Hz), 144.3 (d, J_{C-P} = 10.6 Hz), 140.5 (d, J_{C-P} = 3.8 Hz), 131.4 (d, J_{C-P} = 2.5 Hz), 127.5 (d, J_{C-P} = 0.8 Hz), 126.2, 73.1, 71.7, 71.3, 71.1, 70.9, 70.1 (d, J_{C-P} = 6.4 Hz), 69.3, 61.5, 36.1, 35.1, 32.0, 31.6, 27.7 ppm. ^{31}P{^{1}H} NMR (162 MHz, CD_2Cl_2) δ: 123.0 ppm. IR (neat): 2961, 2869, 1589, 1437, 1396, 1362, 1221, 199, 1120, 1084, 1034, 950, 915, 895, 799, 715, 645, 627, 537 cm^{-1}. HRMS ESI-MS (m/z): [M+Na]$^+$ calcd. for $C_{40}H_{65}O_7PAuClNa^+$ 943.3714, found 943.3754.

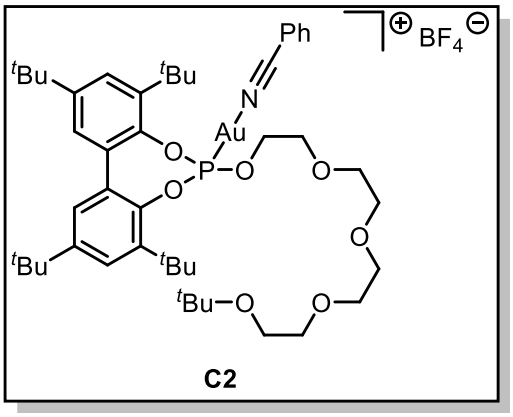

C2

Complex **C2**: **C2** was prepared according to the described general procedure, obtaining 162 mg (78% yield) of the cationic complex as a white solid. ^{1}H NMR (400 MHz, CD_2Cl_2) δ: 7.85-7.65 (m, 3 H), 7.60-7.50 (m, 4 H), 7.23 (d, J = 2.4 Hz, 2 H), 4.52 (br d, J = 14.7 Hz, 2 H), 3.90-3.62 (m, 12 H), 3.59-3.57 (m, 2 H), 1.53 (s, 18 H), 1.36 (s, 18 H), 1.22 (s, 9 H) ppm. ^{11}B{^{1}H} NMR (128 MHz, CD_2Cl_2) δ: –1.1 ppm. ^{13}C{^{1}H} NMR (100 MHz, CD_2Cl_2) δ: 149.7, 143.9 (d, J_{C-P} = 10.6 Hz), 140.5 (d, J_{C-P} = 4.0 Hz), 135.0, 133.4, 131.1 (d, J_{C-P} = 2.3 Hz), 130.0, 127.8, 126.4, 120.2, 110.1, 75.0, 71.7, 70.9, 70.8, 70.7, 70.4, 70.3, 61.6, 36.1, 35.2,

31.9, 31.5, 27.8 ppm. $^{19}F\{^1H\}$ NMR (376 MHz, CD_2Cl_2) δ: –152.6 ppm. $^{31}P\{^1H\}$ NMR (162 MHz, CD_2Cl_2) δ: 113.8 (br s) ppm. IR (neat): 2961, 2284, 1594, 1448, 1396, 1364, 1282, 1221, 1202, 1032, 932, 800, 760, 687, 644, 627, 550 cm^{-1}. HRMS ESI-MS (m/z): $[M–PhCN–BF_4]^+$ calcd. for $C_{40}H_{65}O_7PAu^+$ 885.4128, found 885.4102.

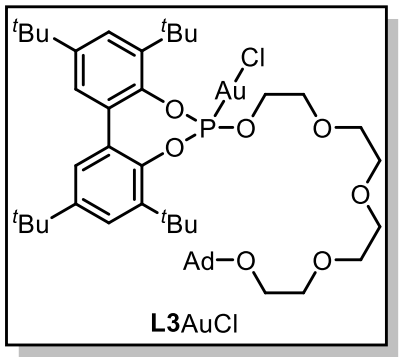

L3AuCl

Ligand **L3** gold(I) chloride: **L3**AuCl was prepared according to the described general procedure, quantitatively yielding the gold(I) chloride as a white solid. ^1H NMR (400 MHz, CD_2Cl_2) δ: 7.56 (d, J = 2.0 Hz, 2 H), 7.23 (d, J = 2.4 Hz, 2 H), 4.38-4.33 (m, 2 H), 3.73-3.71 (m, 2 H), 3.68-3.50 (m, 12 H), 2.13 (br s, 3 H), 1.80-1.57 (m, 12 H) 1.55 (s, 18 H), 1.38 (s, 18 H) ppm. $^{13}C\{^1H\}$ NMR (100 MHz, CD_2Cl_2) δ: 149.2, 144.3 (d, $J_{C–P}$ = 10.5 Hz), 140.5 (d, $J_{C–P}$ = 4.0 Hz), 131.4 (d, $J_{C–P}$ = 2.1 Hz), 127.6, 126.2, 72.3, 71.8, 71.3, 71.1, 71.0, 70.1 (d, $J_{C–P}$ = 6.5 Hz), 69.4, 59.7, 42.0, 36.9, 36.1, 35.1, 32.0, 31.6, 31.1 ppm. $^{31}P\{^1H\}$ NMR (162 MHz, CD_2Cl_2) δ: 122.9 ppm. IR (neat): 2905, 1437, 1396, 1363, 1221, 1116, 1085, 1035, 950, 915, 895, 798, 645, 627 cm^{-1}. HRMS ESI-MS (m/z): $[M+Na]^+$ calcd. for $C_{46}H_{71}O_7PAuClNa^+$ 1021.4184, found 1021.4180.

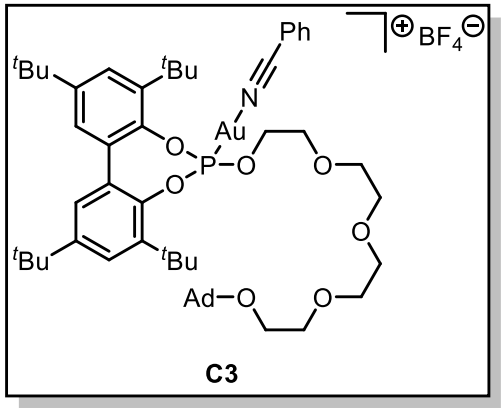

C3

Complex **C3**: **C3** was prepared according to the described general procedure, obtaining 114 mg (93% yield) of the cationic complex as a white solid. ^1H NMR (400 MHz, CD_2Cl_2) δ: 7.90-7.69 (m, 3 H), 7.65-7.50 (m, 4 H), 7.24 (d, J = 2.2 Hz, 2 H), 4.52 (br d, J = 14.2 Hz, 2 H), 3.90-3.50 (m, 14 H), 2.14 (br s, 3 H), 1.90-1.57 (m, 12 H) 1.54 (s, 18 H), 1.37 (s, 18 H) ppm. $^{11}B\{^1H\}$ NMR (128 MHz, CD_2Cl_2) δ: –1.1 ppm. $^{13}C\{^1H\}$ NMR (100 MHz, CD_2Cl_2) δ: 149.8, 143.9 (d, $J_{C–P}$ = 10.4 Hz), 140.5 (d, $J_{C–P}$ =

3.9 Hz), 135.0, 133.4, 131.1 (d, J_{C-P} = 2.0 Hz), 130.0, 127.8, 126.4, 120.2, 110.2, 74.1, 71.9, 71.0, 70.9, 70.4, 70.3, 59.8, 42.2, 36.6, 36.1, 35.2, 32.0, 31.5, 31.2 ppm. $^{19}F\{^1H\}$ NMR (376 MHz, CD_2Cl_2) δ: –152.5 ppm. $^{31}P\{^1H\}$ NMR (162 MHz, CD_2Cl_2) δ: 114.3 (br s) ppm. IR (neat): 2097, 2284, 1594, 1449, 1397, 1363, 1282, 1221, 1032, 932, 800, 760, 687, 644, 627, 550 cm^{-1}. HRMS ESI-MS (m/z): $[M–PhCN–BF_4]^+$ calcd. for $C_{46}H_{71}O_7PAu^+$ 963.4598, found 963.4594.

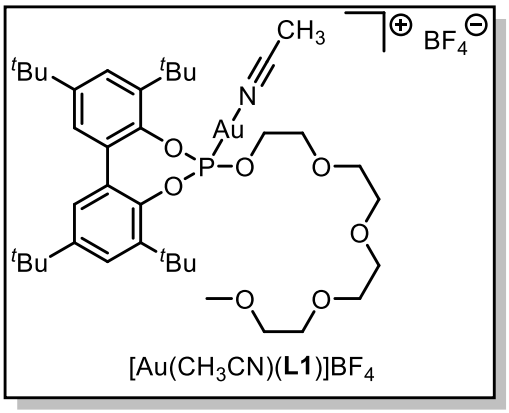

Complex $[Au(CH_3CN)(\mathbf{L1})]BF_4$: The complex was prepared according to the described general procedure, using **L1**AuCl and acetonitrile instead of benzonitrile. 158 mg (82% yield) of the cationic complex were obtained as a white solid. ^1H NMR (400 MHz, CD_2Cl_2) δ: 7.56 (d, J = 2.1 Hz, 2 H), 7.23 (d, J = 2.4 Hz, 2 H), 4.45 (br d, J = 13.9 Hz, 2 H), 3.80-3.50 (m, 14 H), 3.29 (s, 3 H), 2.47 (s, 3 H), 1.52 (s, 18 H), 1.36 (s, 18 H) ppm. $^{11}B\{^1H\}$ NMR (128 MHz, CD_2Cl_2) δ: –1.2 ppm. $^{13}C\{^1H\}$ DEPTQ135 NMR (100 MHz, CD_2Cl_2) δ: 149.7, 143.9 (d, J_{C-P} = 12.1 Hz), 140.5 (d, J_{C-P} = 4.2 Hz), 131.1, 127.7, 126.3, 120.6, 108.4, 72.1, 71.2, 70.8, 70.7, 70.4, 70.1, 59.3, 36.0, 35.1, 31.9, 31.5 ppm. $^{19}F\{^1H\}$ NMR (376 MHz, CD_2Cl_2) δ: –153.0 ppm. $^{31}P\{^1H\}$ NMR (162 MHz, CD_2Cl_2) δ: 111.2 (br s) ppm. IR (neat): 2958, 2871, 1589, 1438, 1397, 1363, 1282, 1246, 1221, 1203, 1167, 1081, 1029, 931, 916, 897, 880, 853, 800, 760, 715, 685, 645, 628, 537 cm^{-1}. ESI-MS (m/z): $[M–CH_3CN–BF_4]^+$, 843.4.

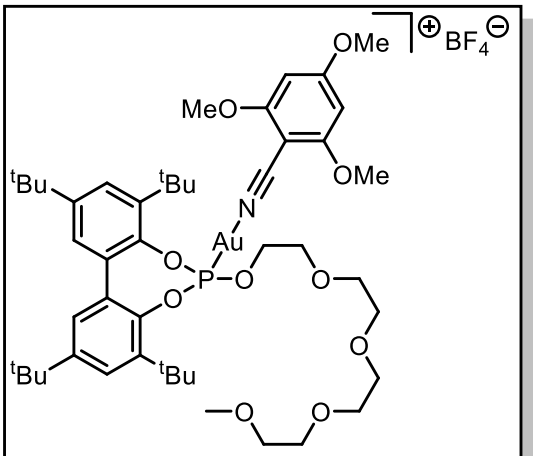

[Au(2,4,6-(MeO)$_3$(C$_6$H$_2$)CN)(**L1**)]BF$_4$

Complex [Au(2,4,6-(MeO)$_3$(C$_6$H$_2$)CN)(**L1**)]BF$_4$: The complex was prepared according to the described general procedure, but adding stoichiometric amounts of 2,4,6-trimethoxybenzonitrile. The cationic complex was obtained as a white solid (250 mg, 87% yield). ^{1}H NMR (400 MHz, CD_2Cl_2) δ: 7.58 (d, J = 1.8 Hz, 2 H), 7.24 (d, J = 2.4 Hz, 2 H), 6.2 (s, 2 H), 4.37-4.32 (m, 2 H), 3.92 (s, 9 H), 3.75-3.45 (m, 14 H), 3.31 (s, 3 H), 1.55 (s, 18 H), 1.37 (s, 18 H) ppm. ^{11}B{^{1}H} NMR (128 MHz, CD_2Cl_2) δ: –1.2 ppm. ^{13}C{^{1}H} NMR (100 MHz, CD_2Cl_2) δ: 169.4, 166.3, 150.0, 143.9 (d, J_{C-P} = 10.4 Hz), 140.4 (d, J_{C-P} = 4.0 Hz), 131.0 (d, J_{C-P} = 2.1 Hz), 127.9, 126.5, 120.1, 91.6, 72.3, 71.2, 71.0, 70.9, 70.8, 70.7, 70.6, 69.9, 69.8, 59.0, 57.1, 56.9, 36.1, 35.2, 31.9, 31.5 ppm. ^{19}F{^{1}H} NMR (376 MHz, CD_2Cl_2) δ: –153.5 ppm. ^{31}P{^{1}H} NMR (162 MHz, CD_2Cl_2) δ: 110.1 (br s) ppm. IR (neat): 2956, 2871, 2249, 1604, 1577, 1461, 1437, 1422, 1397, 1354, 1237, 1210, 1162, 1133, 1081, 1025, 933, 916, 897, 880, 800, 778, 644, 626, 521 cm^{-1}. HRMS ESI-MS (m/z): [M–(2,4,6-(MeO)$_3$(C$_6$H$_2$)CN)–BF$_4$]$^+$ calcd. for $C_{37}H_{59}O_7PAu^+$ 843.3658, found 843.3648.

3.5.5. Syntheses of diazo compounds 2a and 2b

Tosyl azide:[159] The preparation of tosyl azide (TsN_3) was performed adapting a reported procedure.[160] A solution of sodium azide (4.08 g, 62.8 mmol) in water (20 mL) was added dropwise over 1 h to a solution of *p*-toluenesulfonyl chloride (7.7 g, 40.4 mmol) in acetone (30 mL) at 0 °C. The reaction was warmed at room temperature and stirred for 11 h. The acetone was then removed under vacuum and the reaction mixture was extracted with AcOEt (3 x 25 mL). The combined organic layers were washed with water (25 mL), a saturated Na_2CO_3 solution (25 mL), dried over $MgSO_4$ and concentrated under vacuum. The crude product was used with no further purification.

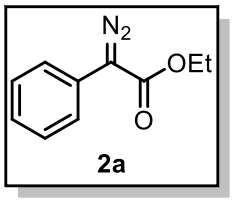

2a

Phenyl ethyl diazoacetate (PhEDA), **2a**: The preparation of PhEDA was carried as reported in the literature.[161] A solution of 1,8-diazabicyclo-[5.4.0]-undec-7-ene (DBU) (7.56 mL, 50.6 mmol) in anhydrous CH_3CN (20 mL) was added dropwise at room temperature to a solution of ethyl phenyl acetate (5.42 mL, 33.7 mmol) and *p*-toluenesulfonyl azide (*vide supra*, TsN_3, 7.97 g, 40.4 mmol) in anhydrous CH_3CN (30 mL). The reaction mixture was stirred at room temperature for 15 hours. After adding water (20 mL), the resulting mixture was extracted with diethyl ether (3 × 40 mL). The combined organic layers were washed with brine (20 mL) and dried over anhydrous $MgSO_4$. After the removal of the solvent under vacuum, the residue was purified by silica gel column chromatography with cyclohexane/ethyl acetate (30:1) as the eluent to give **2a** as a red oil (3.21 g, 50% yield). ^1H and $^{13}C\{^1H\}$ NMR data were in agreement with those

(159) Azide and, especially, diazo compounds are potentially explosive and presumed to be toxic (see: Ford, A.; Miel, H.; Ring, A.; Slattery, C. N.; Maguire, A. R.; McKervey, M. A. *Chem. Rev.* **2015**, *115*, 9981-10080). For this reason, these compounds should not be heated and contact with metallic accessories should be avoided. One should take all reported steps to handle these compounds safely.

(160) Wang, N.; Li, R.; Li, L.; Xu, S.; Song, H.; Wang, B. *J. Org. Chem.* **2014**, *79*, 5379-5385.

(161) Hu, M.; He, Z.; Gao, B.; Li, L.; Ni, C.; Hu, J. *J. Am. Chem. Soc.* **2013**, *135*, 17302-17305.

previously reported.[161] ^{1}H NMR (400 MHz, $CDCl_3$) δ: 7.49 (dm, J = 8.6 Hz, 2 H), 7.39 (tm, J = 7.8 Hz, 2 H), 7.19 (tm, J = 7.4 Hz, 1 H), 4.34 (q, J = 7.1 Hz, 2 H), 1.35 (t, J = 7.1 Hz, 3 H) ppm. ^{13}C{^{1}H} NMR (100 MHz, $CDCl_3$) δ: 165.3, 129.0, 125.8, 125.7, 124.1, 61.1, 14.6 ppm.

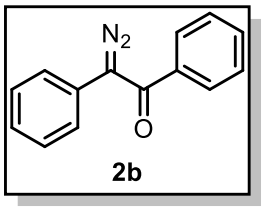

2b

2-Diazo-1,2-diphenylethan-1-one, **2b**: The preparation of substrate **2b** was performed by a Swern-type oxidation as reported in the literature.[162] Dry DMSO (0.634 mL, 8.92 mmol) and THF (30 mL) were placed into a flame-dried Schlenk flask under Ar and stirred at –55 °C. Oxalyl chloride (0.64 mL, 6.69 mmol) was added dropwise to this solution, observing bubbling due to the release of CO_2. The reaction was maintained at –55 °C until gas evolution ceased (*ca.* 20 min), at which point the reaction was cooled to –78 °C. A solution of benzil monohydrazone ((*E*)-2-hydrazineylidene-1,2-diphenylethan-1-one, 1 g, 4.46 mmol) and NEt_3 (1.88 mL, 13.4 mmol) in THF (15 mL) was added dropwise to the previous solution to obtain a bright yellow solution containing a white precipitate. The reaction mixture was maintained at –78 °C for 1 h and was then vacuum filtered under N_2 through a medium porosity sintered glass funnel. The filtrate was diluted with diethyl ether (200 mL), washed with water (400 mL), sat. aq. $NaHCO_3$ (2 x 200 mL), brine (200 mL), dried over Na_2SO_4 and concentrated under vacuum to provide **2b** (0.35 g, 36% yield) as a fair orange solid. ^{1}H and ^{13}C{^{1}H} NMR data were in agreement with those previously reported.[163] ^{1}H NMR (500 MHz, $CDCl_3$) δ: 7.57-7.50 (m, 2H), 7.46-7.36 (m, 3H), 7.36-7.28 (m, 4H), 7.21-7.14 (m, 1H) ppm. ^{13}C{^{1}H} NMR (126 MHz, $CDCl_3$) δ: 188.5, 138.1, 131.8, 129.2, 128.6, 127.9, 127.1, 126.2, 126.1 ppm.

(162) Javed, M. I.; Brewer, M. *Org. Lett.* **2007**, *9*, 1789-1792.
(163) Keipour, H.; Jalba, A.; Delage-Laurin, L.; Ollevier, T. *J. Org. Chem.* **2017**, *82*, 3000-3010.

3.5.6. Binding studies for ligands L1-L3

$^{31}P\{^{1}H\}$ NMR titrations were carried out using a Bruker Avance III HD 500 MHz Smart Probe spectrometer. In a typical experiment, a screw-capped NMR tube (diam. 5 mm, length 7 in, provided with a cap with a septum) was filled with 400 μL of a 0.002 M solution of the respective host (ligands **L1**-**L3**) in a mixture of CH_2Cl_2:THF (from 97:3 to 95:5). In order to provide a deuterium lock signal, a sealed $(CD_3)_2CO$ insert containing PPh_3 (40 mM) as the ^{31}P NMR reference was placed inside the NMR tube. The host solution was used to prepare the solution of guest, so that the concentration of the host remained constant throughout the titration. Aliquots of the solution containing the guest (NaBArF or CsBArF) were successively added to the host-containing solution. The choice of concentration of the guest solution was based on the stability of the complex ([Guest] ≥ $10/K_a$). A spectrum was recorded after each addition. Changes in the ^{31}P NMR chemical shift of the host-guest mixtures with respect to that in the host were used determine the association constants between ligands **L1**-**L3** and the BArF salts by fitting the titration data to a 1:1 binding isotherm with software developed in-house.[140] NaBArF was purchased from commercial sources. CsBArF was prepared according to a well-established synthetic protocol.[42]

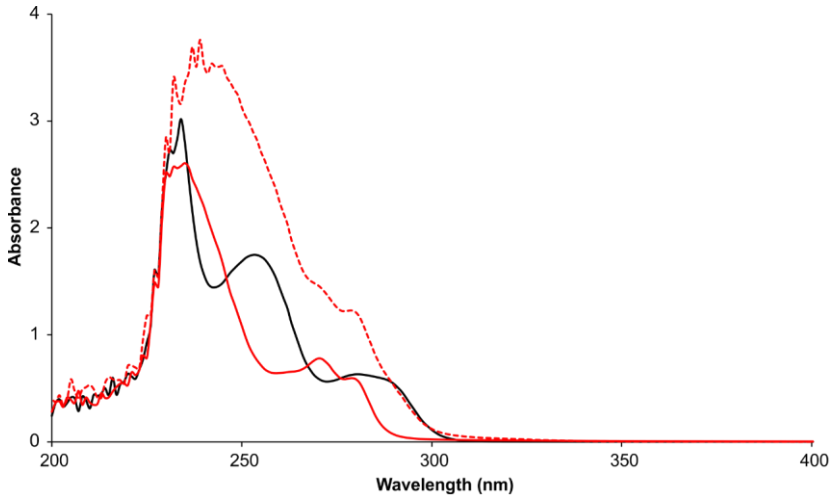

Figure 170. Stacked UV/Vis spectra in CH_2Cl_2:THF (97:3) of host **L1** (0.0001 M, black line) and guest NaBArF (0.0001 M, red line). The dashed red line corresponds to a 1:1 mixture of **L1**:NaBArF (0.0001 M).

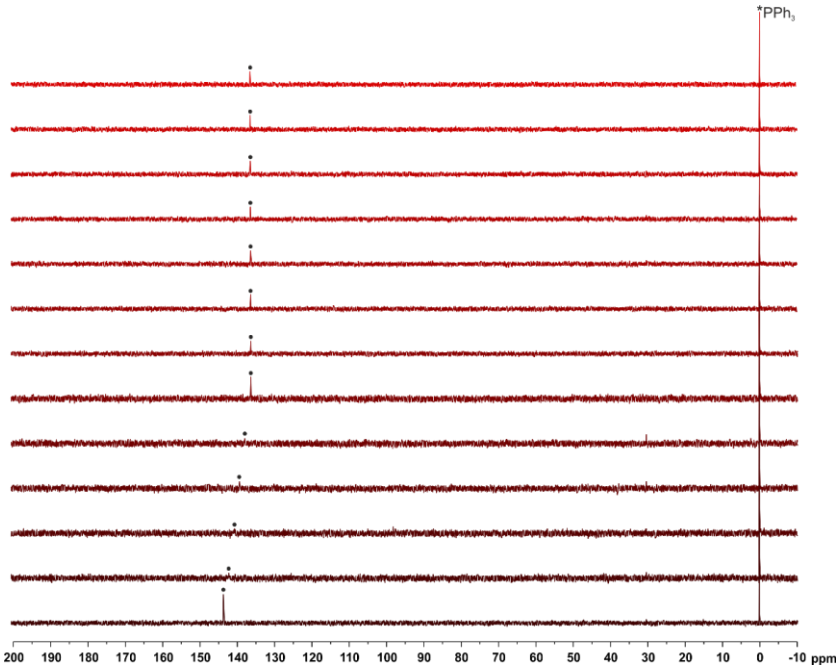

Figure 171. Stacked plot of the $^{31}P\{^{1}H\}$ NMR spectra (500 MHz, CH_2Cl_2:THF (97:3), $(CD_3)_2CO$ capillary insert) of the titration between **L1** and NaBArF.

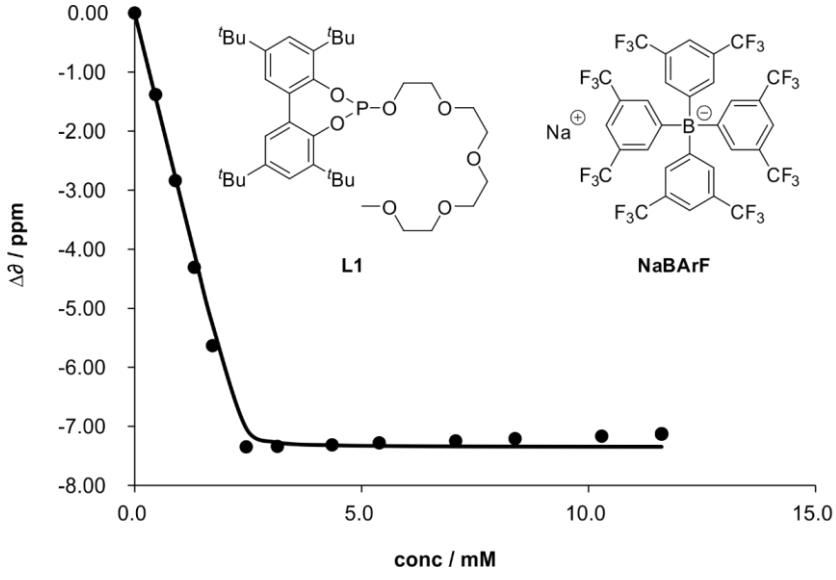

Figure 172. Plot of the changes in the $^{31}P\{^{1}H\}$ NMR chemical shifts against the concentration of NaBArF for **L1** (2 mM) in CH_2Cl_2:THF (97:3) at 25 °C. The line connecting the data points is the best fit for a 1:1 binding isotherm (K_a (1:1) = $1.08 \cdot 10^5\ M^{-1}$).

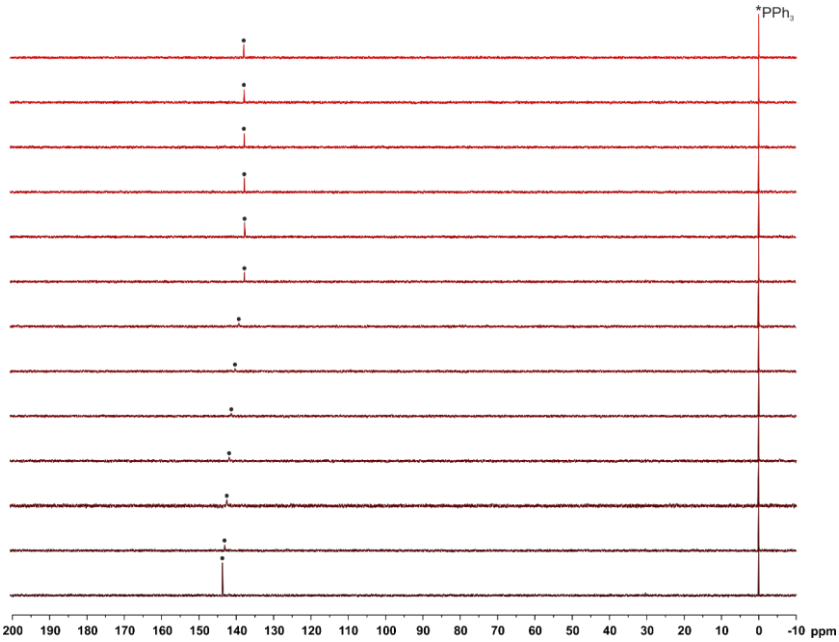

Figure 173. Stacked plot of the $^{31}P\{^{1}H\}$ NMR spectra (500 MHz, CH_2Cl_2:THF (97:3), $(CD_3)_2CO$ capillary insert) of the titration between **L2** and NaBArF.

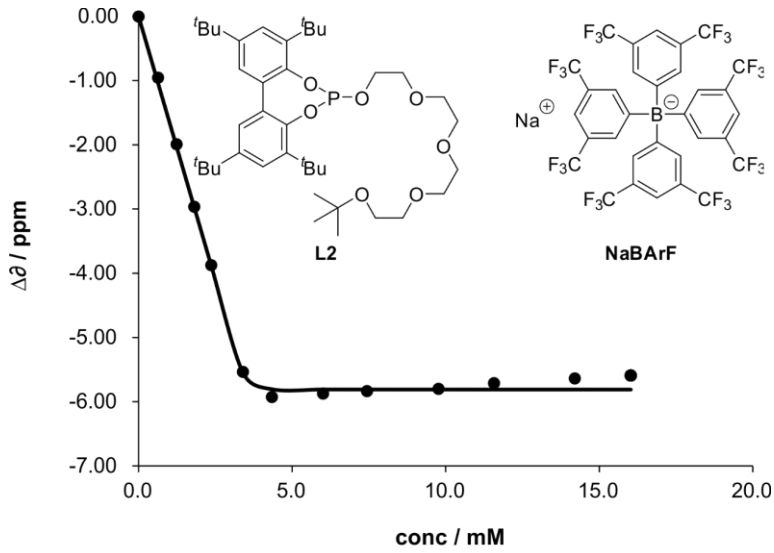

Figure 174. Plot of the changes in the $^{31}P\{^{1}H\}$ NMR chemical shifts against the concentration of NaBArF for **L2** (4 mM) in CH_2Cl_2:THF (97:3) at 25 °C. The line connecting the data points is the best fit for a 1:1 binding isotherm (K_a (1:1) = $1.27 \cdot 10^6$ M^{-1}).

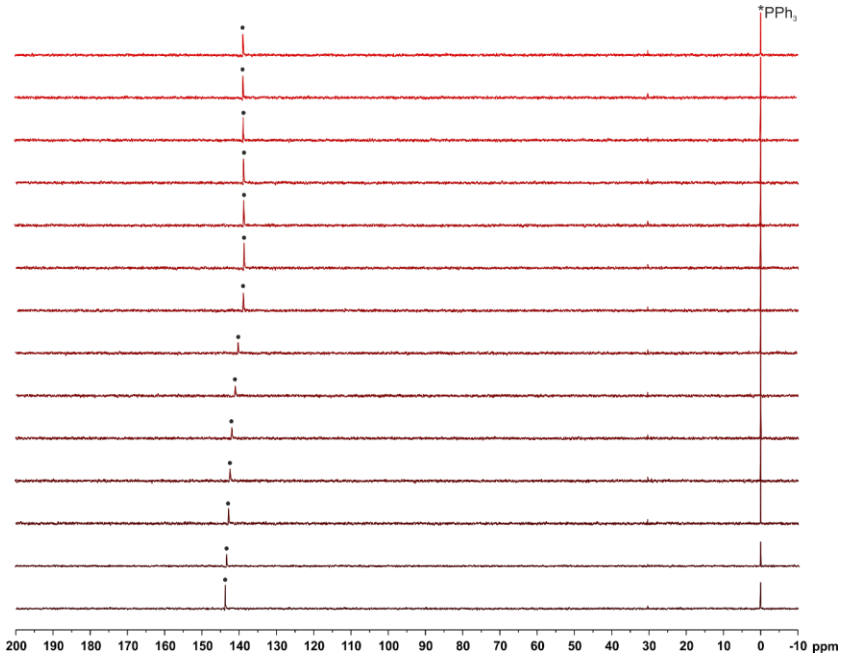

Figure 175. Stacked plot of the $^{31}P\{^{1}H\}$ NMR spectra (500 MHz, CH_2Cl_2:THF (97:3), $(CD_3)_2CO$ capillary insert) of the titration between **L3** and NaBArF.

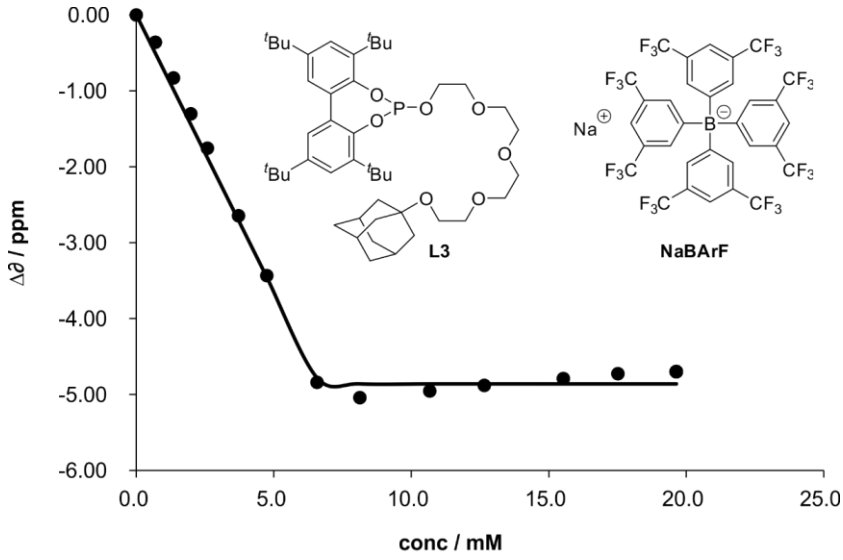

Figure 176. Plot of the changes in the $^{31}P\{^{1}H\}$ NMR chemical shifts against the concentration of NaBArF for **L3** (7 mM) in CH_2Cl_2:THF (97:3) at 25 °C. The line connecting the data points is the best fit for a 1:1 binding isotherm (K_a (1:1) = $9.84 \cdot 10^6\ M^{-1}$).

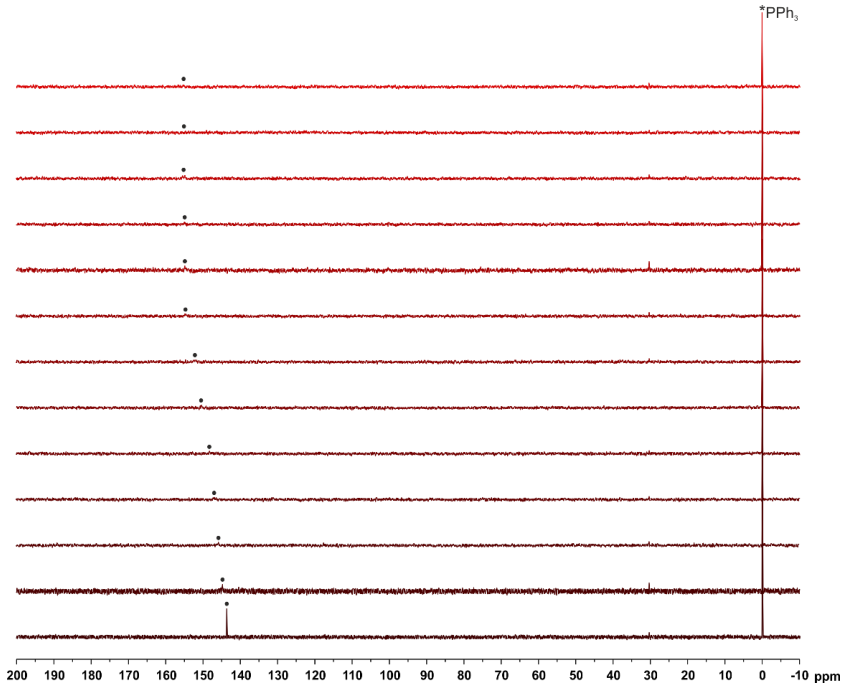

Figure 177. Stacked plot of the $^{31}P\{^{1}H\}$ NMR spectra (500 MHz, CH_2Cl_2:THF (95:5), $(CD_3)_2CO$ capillary insert) of the titration between **L1** and CsBArF.

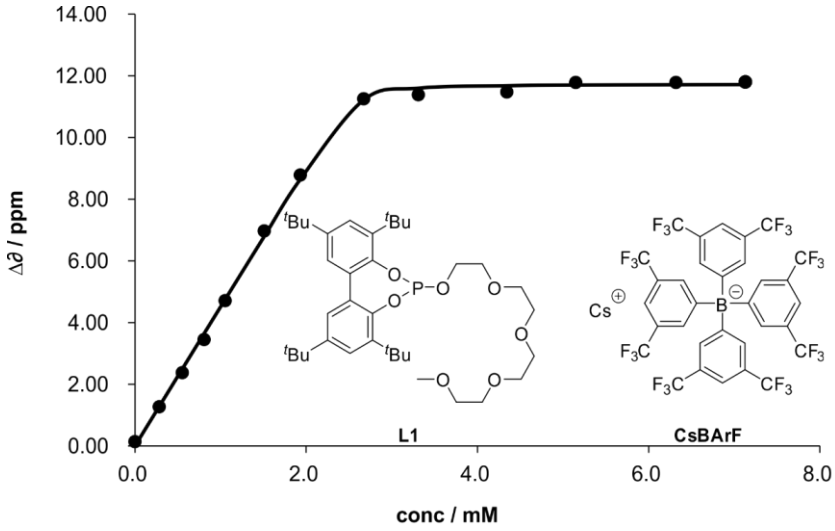

Figure 178. Plot of the changes in the $^{31}P\{^{1}H\}$ NMR chemical shifts against the concentration of CsBArF for **L1** (3 mM) in CH_2Cl_2:THF (95:5) at 25 °C. The line connecting the data points is the best fit for a 1:1 binding isotherm (K_a (1:1) = $1.08 \cdot 10^5$ M^{-1}).

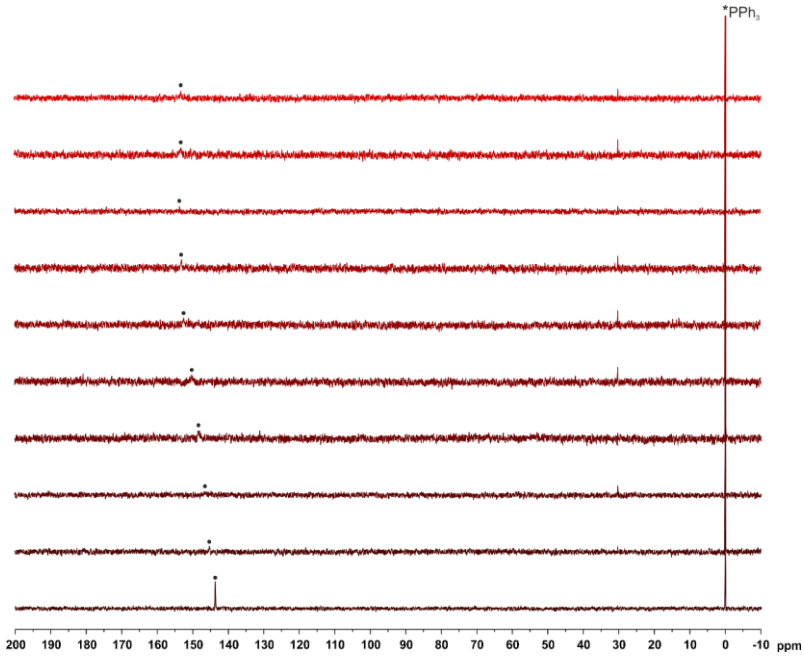

Figure 179. Stacked plot of the $^{31}P\{^{1}H\}$ NMR spectra (500 MHz, CH_2Cl_2:THF (95:5), $(CD_3)_2CO$ capillary insert) of the titration between **L2** and CsBArF.

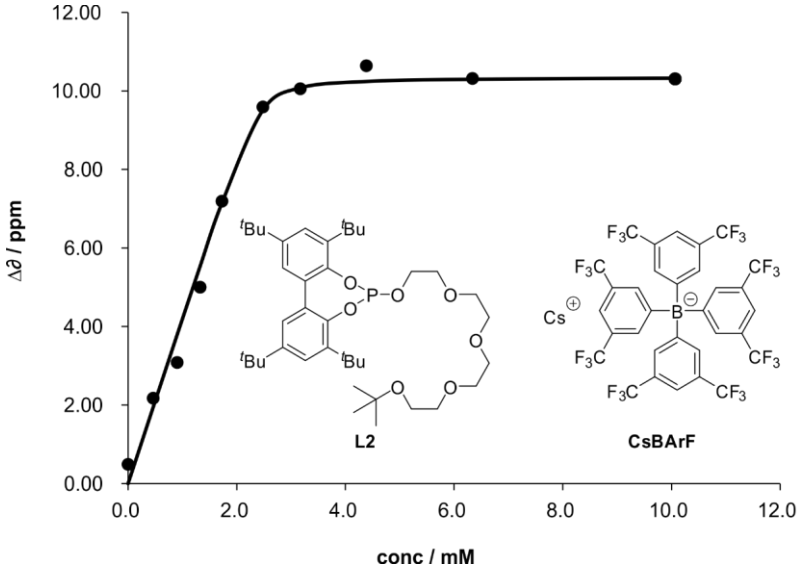

Figure 180. Plot of the changes in the $^{31}P\{^{1}H\}$ NMR chemical shifts against the concentration of CsBArF for **L2** (2 mM) in CH_2Cl_2:THF (95:5) at 25 °C. The line connecting the data points is the best fit for a 1:1 binding isotherm (K_a (1:1) = $4.57 \cdot 10^4$ M^{-1}).

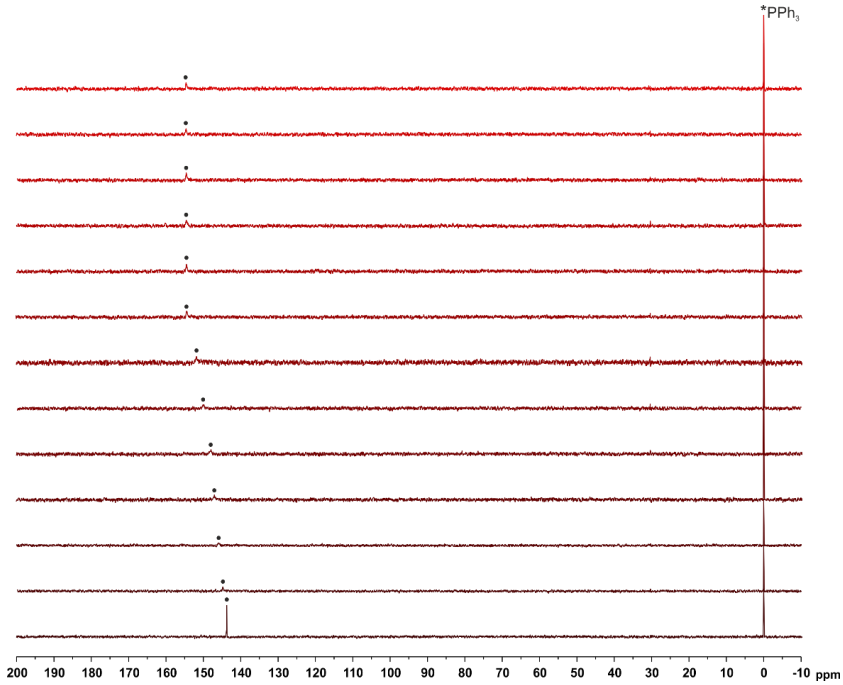

Figure 181. Stacked plot of the $^{31}P\{^{1}H\}$ NMR spectra (500 MHz, CH_2Cl_2:THF (95:5), $(CD_3)_2CO$ capillary insert) of the titration between **L3** and CsBArF.

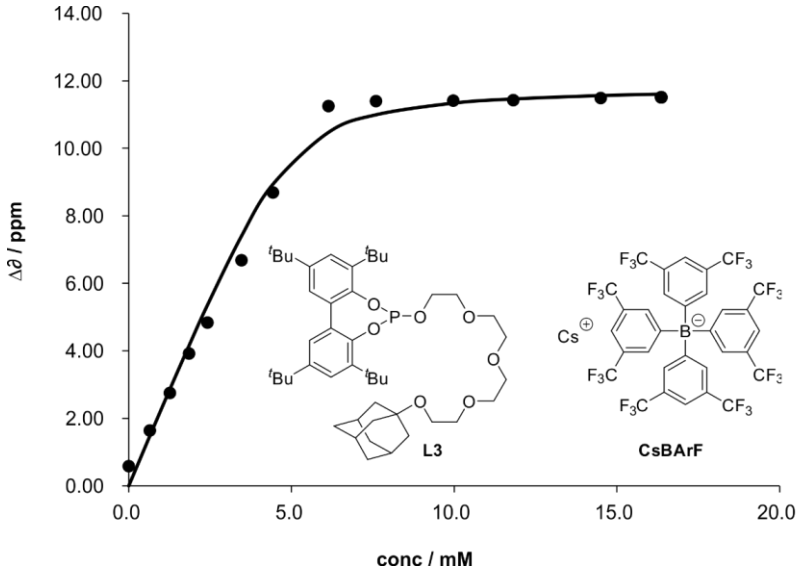

Figure 182. Plot of the changes in the $^{31}P\{^{1}H\}$ NMR chemical shifts against the concentration of CsBArF for **L3** (5 mM) in CH_2Cl_2:THF (95:5) at 25 °C. The line connecting the data points is the best fit for a 1:1 binding isotherm (K_a (1:1) = $4.29 \cdot 10^3$ M^{-1}).

3.5.7. General procedure for the selective gold(I)-catalyzed functionalization of aromatic alcohols

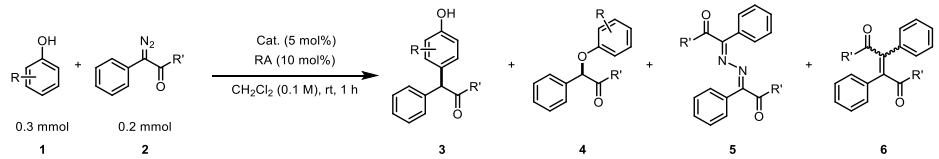

Scheme 42. General procedure for gold(I)-catalyzed functionalization reactions of aromatic alcohols **1** with diazo derivatives **2**.

A solution of the catalyst (5 mol%) and the regulation agent (RA, 10 mol%) in 0.5 mL of CH_2Cl_2 were transferred in the glove box (N_2 atmosphere) to a dried screw-capped vial (10 mL) provided with a septum and a stirrer. The solution was stirred for 5 minutes. A solution of the phenol (**1**, 0.3 mmol) in 0.5 mL of CH_2Cl_2 was subsequently added and the final solution was stirred for 5 minutes. After that time, a solution of the diazo derivative (**2**, 0.2 mmol) in 1 mL of CH_2Cl_2 was added dropwise, observing bubbling due to the release of N_2 (the final concentration of the reaction mixture was 0.1 M). Once the addition was complete, the solution was stirred for 1 hour to ensure the complete consumption of the diazo compound (checked by TLC analysis, AcOEt:Cy 1:6). This solution was filtered through a nylon filter (0.45 μm), evaporated to dryness under vacuum and then analyzed by NMR. The yield towards functionalized aromatic alcohols was calculated using ^{1}H qNMR, employing 1,3,5-trimethoxybenzene (TMB) as internal standard. The different isomers (**3**, C–H functionalization product) and (**4**, O–H functionalization product) were quantified by analyzing the corresponding characteristic methylene proton signals located at chemical shifts ranging from 6.0 to 4.5 ppm for the whole set of functionalized aromatic alcohols.

3.5.8. Complete set of results for the selective gold(I)-catalyzed functionalization of aromatic alcohols

3.5.8.1 Control experiments

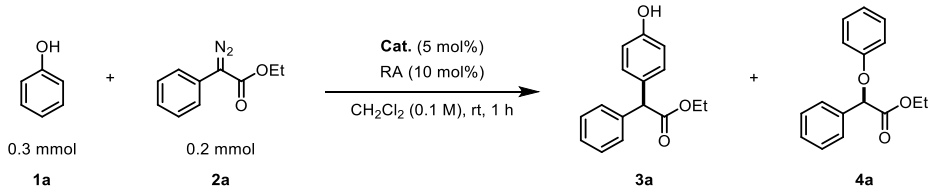

Scheme 43. Control experiments for the gold(I)-catalyzed selective functionalization of **1a** with **2a**.

Table 12. Control experiments for the gold(I)-catalyzed selective functionalization of **1a** with **2a**[a]

Entry	Cat.	RA	Yield (%) 3a	Yield (%) 4a	3:4 Ratio
1	$AgBF_4$	none	6.7	55.6	1:8
2	$(Me_2S)AuCl$	none	<1	<1	-
3	none	$CsBF_4$	n.d.	n.d.	-
4[b]	**C1**	NaBArF	1.4	7.0	1:5
5	**L1**AuCl	none	<1	<1	-
6[c]	[Au(*A*)(**L1**)]BF_4	none	76.0	1.0	>50 : 1
7[d]	[Au(*B*)(**L1**)]BF_4	none	66.0	5.7	11:1

[a] Reactions were performed under inert atmosphere for 1 h at 25 °C. Yields determined by ^1H NMR using 1,3,5-trimethoxybenzene as internal standard. [b] 15 mol% of NaBArF. [c] *A* = CH_3CN. [d] *B* = 2,4,6-$(CH_3O)_3(C_6H_2)CN$.

3.5.8.2 Gold(I)-catalyzed selective functionalization of 1a with 2a using complex C1

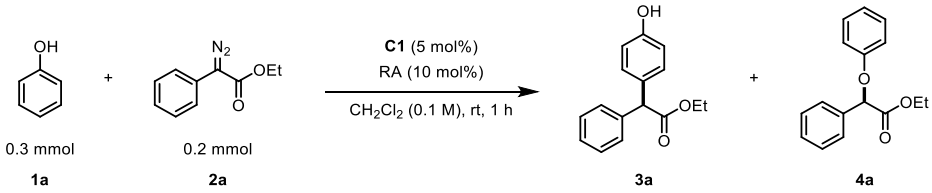

0.3 mmol **1a** + 0.2 mmol **2a** → **3a** + **4a**

Scheme 44. Gold(I)-catalyzed selective functionalization of **1a** with **2a** using complex **C1**.

Table 13. Gold(I)-catalyzed selective functionalization of **1a** with **2a** using complex **C1**[a]

Entry	RA	Yield (%) 3a	Yield (%) 4a	3:4 Ratio	Regulation effects 3/4
1	none	83.0	2.9	28:1	-
2	$LiBF_4$	83.5	2.4	35:1	+0.5/–0.5
3	$NaBF_4$	87.3	3.0	30:1	+4.3/+0.1
4	KBF_4	86.1	2.4	37:1	+3.1/–0.5
5	$RbBF_4$	85.5	2.8	31:1	+2.5/–0.1
6	$CsBF_4$	87.7 (80.0)	1.5	>50:1	+4.7/–1.4
7	NH_4BF_4	72.6	3.1	24:1	–10.4/+0.2

[a] Reactions were performed under inert atmosphere for 1 h at 25 °C. Yields determined by ^1H NMR using 1,3,5-trimethoxybenzene as internal standard. Isolated yields in parentheses.

3.5.8.3 Gold(I)-catalyzed selective functionalization of 1b with 2a using complex C1

Scheme 45. Gold(I)-catalyzed selective functionalization of **1b** with **2a** using complex **C1**.

Table 14. Gold(I)-catalyzed selective functionalization of **1b** with **2a** using complex **C1**[a]

Entry	RA	Yield (%) 3b	Yield (%) 4b	3:4 Ratio	Regulation effects 3/4
1	none	41.0	6.2	7:1	-
2	$LiBF_4$	46.3	6.7	7:1	+5.3/+0.5
3	$NaBF_4$	46.7	5.3	9:1	+5.7/–0.9
4	KBF_4	50.6	4.2	12:1	+9.6/–2.0
5	$RbBF_4$	60.6 (59.6)	5.6	11:1	+19.6/–0.6
6	$CsBF_4$	40.6	7.8	5:1	–0.4/+1.6

[a] Reactions were performed under inert atmosphere for 1 h at 25 °C. Yields determined by ^1H NMR using 1,3,5-trimethoxybenzene as internal standard. Isolated yields in parentheses.

3.5.8.4 Gold(I)-catalyzed selective functionalization of 1c with 2a using complex C1

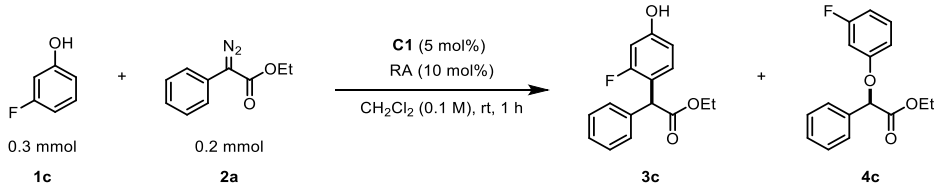

Scheme 46. Gold(I)-catalyzed selective functionalization of **1c** with **2a** using complex **C1**.

Table 15. Gold(I)-catalyzed selective functionalization of **1c** with **2a** using complex **C1**[a]

Entry	RA	Yield (%) 3c	Yield (%) 4c	3:4 Ratio	Regulation effects 3/4
1	none	65.0	3.9	17:1	-
2	$LiBF_4$	63.0	3.4	18:1	−2.0/−0.5
3	$NaBF_4$	63.4	5.3	12:1	−1.6/+1.4
4	KBF_4	61.6	5.4	11:1	−3.4/+1.5
5	$RbBF_4$	66.1	6.5	10:1	+1.1/+2.6
6	$CsBF_4$	68.3 (60.2)	3.9	18:1	+3.3/0

[a] Reactions were performed under inert atmosphere for 1 h at 25 °C. Yields determined by ^1H NMR using 1,3,5-trimethoxybenzene as internal standard. Isolated yields in parentheses.

3.5.8.5 Gold(I)-catalyzed selective functionalization of 1d with 2a using complex C1

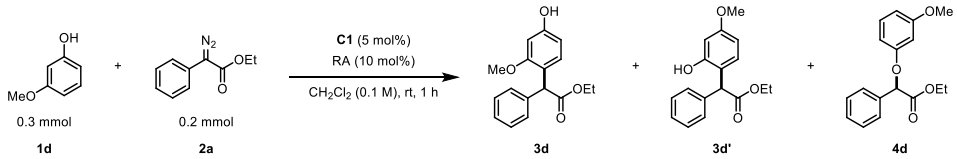

Scheme 47. Gold(I)-catalyzed selective functionalization of **1d** with **2a** using complex **C1**.

Table 16. Gold(I)-catalyzed selective functionalization of **1d** with **2a** using complex **C1**[a]

Entry	RA	Yield (%) 3d	Yield (%) 3d'	Yield (%) 4d[b]	3:4 Ratio	Regulation effects 3/4
1	none	42.1	44.6	n.d.	-	-
2	$LiBF_4$	40.6	43.0	n.d.	-	–3.1/-
3	$NaBF_4$	38.0	43.4	n.d.	-	–5.3/-
4	KBF_4	43.7	44.8	n.d.	-	+1.8/-
5	$RbBF_4$	39.0	39.7	n.d.	-	–8.0/-
6	$CsBF_4$	44.7 (38.8)	45.9 (38.8)	n.d.	-	+3.9/-

[a] Reactions were performed under inert atmosphere for 1 h at 25 °C. Yields determined by ^1H NMR using 1,3,5-trimethoxybenzene as internal standard. Isolated yields in parentheses. [b] O–H insertion product could not be isolated.

3.5.8.6 Gold(I)-catalyzed selective functionalization of 1e with 2a using complex C1

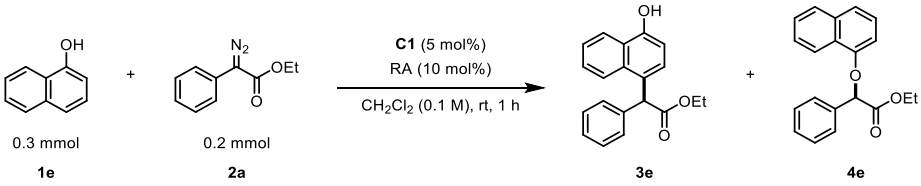

Scheme 48. Gold(I)-catalyzed selective functionalization of **1e** with **2a** using complex **C1**.

Table 17. Gold(I)-catalyzed selective functionalization of **1e** with **2a** using complex **C1**[a]

Entry	RA	Yield (%) 3e	Yield (%) 4e[b]	3:4 Ratio	Regulation effects 3/4
1	none	88.9	n.d.	-	-
2	$LiBF_4$	94.3	n.d.	-	+5.4/-
3	$NaBF_4$	92.7	n.d.	-	+3.8/-
4	KBF_4	81.9	n.d.	-	−7.0/-
5	$RbBF_4$	98.5	n.d.	-	+9.6/-
6	$CsBF_4$	98.7 (81.6)	n.d.	-	+9.8/-

[a] Reactions were performed under inert atmosphere for 1 h at 25 °C. Yields determined by ^1H NMR using 1,3,5-trimethoxybenzene as internal standard. Isolated yields in parentheses. [b] O–H insertion product could not be isolated.

3.5.8.7 Gold(I)-catalyzed selective functionalization of 1f with 2a using complex C1

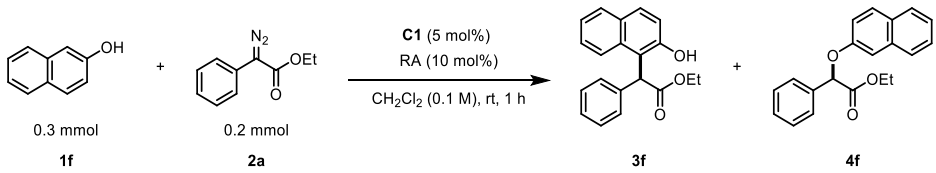

Scheme 49. Gold(I)-catalyzed selective functionalization of **1f** with **2a** using complex **C1**.

Table 18. Gold(I)-catalyzed selective functionalization of **1f** with **2a** using complex **C1**[a]

Entry	RA	Yield (%) 3f	Yield (%) 4f[b]	3:4 Ratio	Regulation effects 3/4
1	none	44.1	n.d.	-	-
2	$LiBF_4$	19.3	n.d.	-	–24.8/-
3	$NaBF_4$	36.8	n.d.	-	–7.3/-
4	KBF_4	46.1	n.d.	-	+2.0/-
5	$RbBF_4$	47.9 (50.1)	n.d.	-	+3.8/-
6	$CsBF_4$	43.9	n.d.	-	–0.2/-

[a] Reactions were performed under inert atmosphere for 1 h at 25 °C. Yields determined by ^1H NMR using 1,3,5-trimethoxybenzene as internal standard. Isolated yields in parentheses. [b] O–H insertion product could not be isolated.

3.5.8.8 Gold(I)-catalyzed selective functionalization of 1a with 2b using complex C1

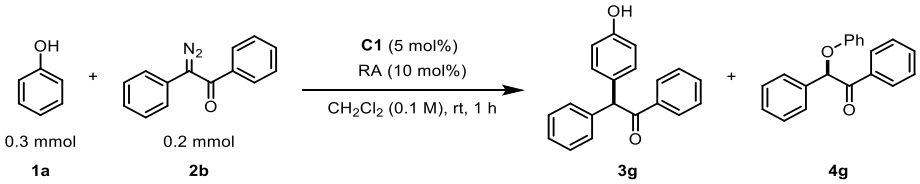

Scheme 50. Gold(I)-catalyzed selective functionalization of **1a** with **2b** using complex **C1**.

Table 19. Gold(I)-catalyzed selective functionalization of **1a** with **2b** using complex **C1**[a]

Entry	RA	Yield (%) 3g	Yield (%) 4g[b]	3:4 Ratio	Regulation effects 3/4
1	none	14.9	n.d.	-	-
2	$LiBF_4$	14.4	n.d.	-	–0.5/-
3	$NaBF_4$	14.2	n.d.	-	–0.7/-
4	KBF_4	15.9	n.d.	-	+1.0/-
5	$RbBF_4$	28.4	n.d.	-	+13.5/-
6	$CsBF_4$	34.4 (17.4)	n.d.	-	+19.5/-
7[c]	$CsBF_4$	39.0	n.d.	-	+24.1/-

[a] Reactions were performed under inert atmosphere for 1 h at 25 °C. Yields determined by ^1H NMR using 1,3,5-trimethoxybenzene as internal standard. Isolated yields in parentheses. [b] O–H insertion product could not be isolated. [c] Reaction performed at 60 °C using chlorobenzene as solvent.

3.5.8.9 Gold(I)-catalyzed selective functionalization of 1h with 2a using complex C1

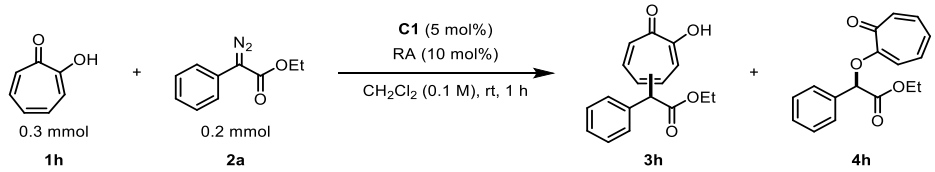

Scheme 51. Gold(I)-catalyzed selective functionalization of **1h** with **2a** using complex **C1**.

Table 20. Gold(I)-catalyzed selective functionalization of **1h** with **2a** using complex **C1**[a]

Entry	RA	Yield (%) 3h[b]	Yield (%) 4h	3:4 Ratio	Regulation effects 3/4
1	none	n.d.	16.7	-	-
2	$LiBF_4$	n.d.	11.7	-	-/–5.0
3	$NaBF_4$	n.d.	16.3	-	-/–0.4
4	KBF_4	n.d.	15.5	-	-/–1.2
5	$RbBF_4$	n.d.	17.7 (10.6)	-	-/+1.0
6	$CsBF_4$	n.d.	16.6	-	-/–0.1

[a] Reactions were performed under inert atmosphere for 1 h at 25 °C. Yields determined by ^1H NMR using 1,3,5-trimethoxybenzene as internal standard. Isolated yields in parentheses. [b] C–H insertion product could not be isolated.

3.5.8.10 Gold(I)-catalyzed selective functionalization of 1i with 2a using complex C1

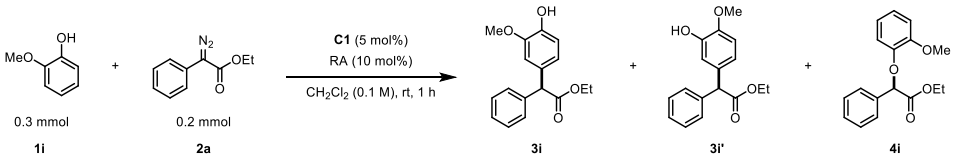

Scheme 52. Gold(I)-catalyzed selective functionalization of **1i** with **2a** using complex **C1**.

Table 21. Gold(I)-catalyzed selective functionalization of **1i** with **2a** using complex **C1**[a]

Entry	RA	Yield (%) 3i	Yield (%) 3i'	Yield (%) 4i	3:4 Ratio	Regulation effects 3/4
1	none	26.4	60.6	0.5	>50:1	-
2	$LiBF_4$	26.7 (18.5)	65.5(50.0)	1.4	>50:1	+5.2/+0.9
3	$CsBF_4$	25.3	61.7	1.5	>50:1	0/+1.0

[a] Reactions were performed under inert atmosphere for 1 h at 25 °C. Yields determined by ^1H NMR using 1,3,5-trimethoxybenzene as internal standard. Isolated yields in parentheses. Products **3i** and **3i'** were isolated as a mixture.

3.5.9. Characterization of functionalized products 3, 4, 5 and 6

Functionalized aromatic alcohols were isolated from the crude reaction mixtures by column chromatography using SiO_2 and ethyl acetate (AcOEt) and cyclohexane (Cy) mixtures as the eluents. O–H functionalization isomers **4** were formed in low amounts, which made isolation not possible. Thus, O–H functionalized isomers **4a**-**4c** and **4i** were prepared using $AgBF_4$ as catalyst. Aside of the functionalized aromatic alcohols, the corresponding dimerization products **5** and **6** from diazo derivative **2a** (Scheme 42) were obtained as minor components of the reaction mixture and their characterization data has been included in this section.

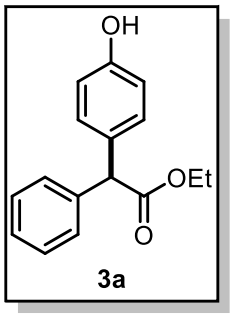

3a

Ethyl 2-(4-hydroxyphenyl)-2-phenylacetate, **3a**: Product **3a** was prepared following the general procedure employing complex **C1** and $CsBF_4$ as the regulation agent. The reaction crude mixture was purified by column chromatography using SiO_2 and Cy and AcOEt as the eluents (30:1→10:1, Cy:AcOEt), to afford **3a** as a colorless solid (41.0 mg, 80% yield). ^1H and $^{13}C\{1H\}$ NMR data were in agreement with those previously reported.[133a] ^1H NMR (400 MHz, $CDCl_3$) δ: 7.28-7.15 (m, 5 H), 7.11 (dm, J = 8.5 Hz, 2 H), 6.70 (dm, J = 8.6 Hz, 2 H), 4.88 (s, 1 H), 4.64 (br s, 1 H), 4.13 (q, J = 7.1 Hz, 2 H), 1.18 (t, J = 7.1 Hz, 3 H) ppm. $^{13}C\{^1H\}$ NMR (100 MHz, $CDCl_3$) δ: 173.3, 155.0, 139.1, 130.9, 130.0, 128.7, 128.6, 127.3, 115.6, 61.4, 56.5, 14.2 ppm.

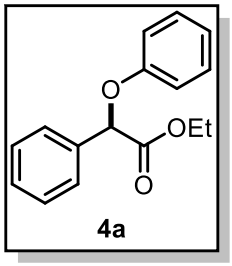

4a

Ethyl 2-phenoxy-2-phenylacetate, **4a**: Product **4a** was prepared following the general procedure employing $AgBF_4$ as the catalyst. The reaction crude mixture was purified by column chromatography using SiO_2 and Cy and AcOEt as the eluents (30:1, Cy:AcOEt), to afford **4a** as a yellow oil (22.0 mg, 43% yield). ^1H and $^{13}C\{^1H\}$ NMR data were in agreement with those previously reported.[164] ^1H NMR (400 MHz, $CDCl_3$) δ: 7.52 (dm, J = 7.9 Hz, 2 H), 7.36-7.26 (m, 3 H), 7.24-7.16 (m, 2 H), 6.94-6.86 (m, 3 H), 5.55 (s, 1 H),

(164) Tseberlidis, G.; Caselli, A.; Vicente, R. *J. Organomet. Chem.* **2017**, *835*, 1-5.

4.20-4.06 (m, 2 H), 1.13 (t, J = 7.1 Hz, 3 H) ppm. $^{13}C\{^1H\}$ NMR (100 MHz, $CDCl_3$) δ: 170.1, 157.5, 135.7, 129.7, 129.0, 128.9, 127.2, 121.9, 115.6, 78.8, 61.7, 14.1 ppm.

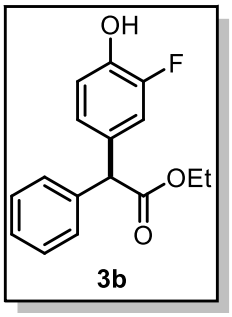

3b

Ethyl 2-(3-fluoro-4-hydroxyphenyl)-2-phenylacetate, **3b**: Product **3b** was prepared following the general procedure employing complex **C1** and $RbBF_4$ as the regulation agent. The reaction crude mixture was purified by column chromatography using SiO_2 and Cy and AcOEt as the eluents (30:1→10:1, Cy:AcOEt), to afford **3b** as a pale yellowish oil (32.7 mg, 60% yield). ^1H and $^{13}C\{^1H\}$ NMR data were in agreement with those previously reported.[133a] ^1H NMR (400 MHz, $CDCl_3$) δ: 7.37-7.27 (m, 5 H), 7.07 (dd, J = 11.6, 2.0 Hz, 1 H), 7.00-6.90 (m, 2 H), 5.02 (br s, 1 H), 4.92 (s, 1 H), 4.21 (q, J = 7.1 Hz, 2 H), 1.26 (t, J = 7.1 Hz, 3 H) ppm. $^{13}C\{^1H\}$ NMR (100 MHz, $CDCl_3$) δ: 172.6, 151.0 (d, J_{C-F} = 237.9 Hz), 142.9 (d, J_{C-F} = 14.5 Hz), 138.5, 131.7 (d, J_{C-F} = 6.0 Hz), 128.8, 128.5, 127.5, 125.1 (d, J_{C-F} = 3.5 Hz), 117.3 (d, J_{C-F} = 2.1 Hz), 116.0 (d, J_{C-F} = 19.4 Hz), 61.5, 56.2, 14.2 ppm. $^{19}F\{^1H\}$ NMR (376 MHz, $CDCl_3$) δ: –140.5 ppm.

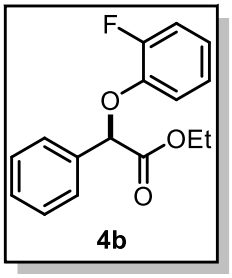

4b

Ethyl 2-(2-fluorophenoxy)-2-phenylacetate, **4b**: Product **4b** was prepared following the general procedure employing $AgBF_4$ as the catalyst. The reaction crude mixture was purified by column chromatography using SiO_2 and Cy and AcOEt as the eluents (30:1, Cy:AcOEt), to afford **4b** as a pale yellow oil (13.9 mg, 25% yield). ^1H NMR (400 MHz, $CDCl_3$) δ: 7.62-7.56 (m, 2 H), 7.44-7.34 (m, 3 H), 7.14-7.04 (m, 1 H), 7.03-6.90 (m, 3 H), 5.64 (s, 1 H), 4.25-4.16 (m, 2 H), 1.20 (t, J = 7.1 Hz, 3 H) ppm. $^{13}C\{^1H\}$ NMR (100 MHz, $CDCl_3$) δ: 169.7, 153.5 (d, J_{C-F} = 246.8 Hz), 145.3 (d, J_{C-F} = 10.8 Hz), 135.3, 129.2, 128.9, 127.3, 124.4 (d, J_{C-F} = 4.1 Hz), 123.0 (d, J_{C-F} = 7.2 Hz), 117.9 (d, J_{C-F} = 1.3 Hz), 116.8 (d, J_{C-F} = 18.4 Hz), 80.3, 61.8, 14.1 ppm. $^{19}F\{^1H\}$ NMR (376 MHz, $CDCl_3$) δ: –131.8 ppm. IR (neat): 3069, 2989, 2925, 2853, 1734, 1613, 1592, 1506, 1477, 1455, 1367, 1322, 1306, 1278, 1258, 1212, 1178, 1110, 1083, 1055, 1019, 947, 929, 915, 886, 843, 798, 779, 752,

725, 688, 615, 491 cm^{-1}. HRMS ESI-MS (m/z): $[M+Na]^+$ calcd. for $C_{16}H_{15}FO_3Na^+$ 297.0897, found 297.0887.

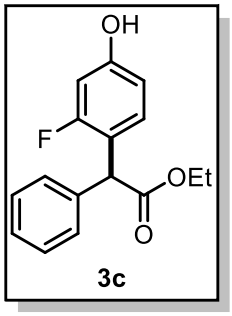

3c

Ethyl 2-(2-fluoro-4-hydroxyphenyl)-2-phenylacetate, **3c**: Product **3c** was prepared following the general procedure employing complex **C1** and $CsBF_4$ as the regulation agent. The reaction crude mixture was purified by column chromatography using SiO_2 and Cy and AcOEt as the eluents (30:1→10:1, Cy:AcOEt), to afford **3c** as a colorless oil that solidified upon standing (33 mg, 60% yield). ^1H NMR (400 MHz, $CDCl_3$) δ: 7.39-7.27 (m, 5 H), 6.94 (t, J = 8.6 Hz, 1 H), 6.49 (dd, J = 11.3, 2.5 Hz, 1 H), 6.44 (dd, J = 8.5, 2.5 Hz, 1 H), 6.01 (br s, 1 H), 5.19 (s, 1 H), 4.29-4.17 (m, 2 H), 1.26 (t, J = 7.1 Hz, 3 H) ppm. $^{13}C\{^1H\}$ NMR (76 MHz, $CDCl_3$) δ: 173.6, 160.9 (d, J_{C-F} = 245.9 Hz), 156.7 (d, J_{C-F} = 11.6 Hz), 137.1, 130.4 (d, J_{C-F} = 5.3 Hz), 128.9, 128.8, 127.6, 117.7 (d, J_{C-F} = 15.1 Hz), 111.5 (d, J_{C-F} = 2.9 Hz), 103.3 (d, J_{C-F} = 25.2 Hz), 61.9, 49.8 (d, J_{C-F} = 2.6 Hz), 14.1 ppm. $^{19}F\{^1H\}$ NMR (376 MHz, $CDCl_3$) δ: –115.1 ppm. IR (neat): 3400 (OH), 3321 (OH), 3061, 3029, 2983, 2903, 1713, 1624, 1596, 1507, 1493, 1454, 1371, 1340, 1300, 1272, 1238, 1191, 1151, 1109, 1089, 1021, 964, 846, 822, 791, 737, 699, 628, 599, 563, 547, 527 cm^{-1}. HRMS ESI-MS (m/z): $[M+Na]^+$ calcd. for $C_{16}H_{15}FO_3Na^+$ 297.0897, found 297.0894.

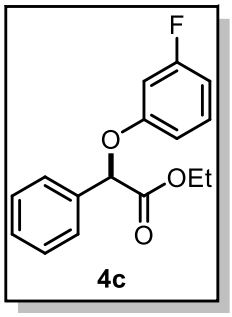

4c

Ethyl 2-(3-fluorophenoxy)-2-phenylacetate, **4c**: Product **4c** was prepared following the general procedure employing $AgBF_4$ as the catalyst. The reaction crude mixture was purified by column chromatography using SiO_2 and Cy and AcOEt as the eluents (30:1, Cy:AcOEt), to afford **4c** as a pale yellow oil (21.2 mg, 39% yield). ^1H NMR (400 MHz, $CDCl_3$) δ: 7.60-7.54 (m, 2 H), 7.44-7.34 (m, 3 H), 7.25-7.17 (m, 1 H), 6.77-6.65 (m, 3 H), 5.59 (s, 1 H), 4.26-4.15 (m, 2 H), 1.21 (t, J = 7.1 Hz, 3 H) ppm. $^{13}C\{^1H\}$ NMR (126 MHz, $CDCl_3$) δ: 169.6, 163.6 (d, J_{C-F} = 246.0 Hz), 158.7 (d, J_{C-F} = 10.7 Hz), 135.2, 130.5 (d, J_{C-F} = 10.0 Hz), 129.2, 129.0, 127.2, 111.2 (d, J_{C-F} = 2.8 Hz), 108.8 (d, J_{C-F} = 21.3 Hz), 103.6 (d, J_{C-F} = 25.0 Hz),

79.0, 61.9, 14.1 ppm. $^{19}F\{^{1}H\}$ NMR (376 MHz, $CDCl_3$) δ: −111.3 ppm. IR (neat): 2982, 1751, 1610, 1594, 1488, 1448, 1370, 1261, 1205, 1182, 1165, 1134, 1083, 1055, 1024, 964, 850, 831, 762, 726, 695, 678 cm^{-1}. HRMS ESI-MS (m/z): $[M+Na]^+$ calcd. for $C_{16}H_{15}FO_3Na^+$ 297.0897, found 297.0890.

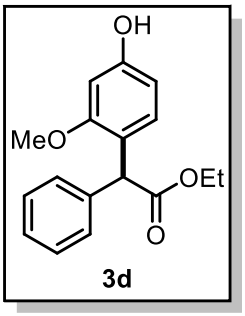

3d

Ethyl 2-(4-hydroxy-2-methoxyphenyl)-2-phenylacetate, **3d**: Product **3d** was prepared following the general procedure employing complex **C1** and $CsBF_4$ as the regulation agent. The reaction crude mixture was purified by column chromatography using SiO_2 and Cy and AcOEt as the eluents (30:1→10:1, Cy:AcOEt), to afford **3d** as a colorless oil (22.2 mg, 39% yield). Assignments were done by comparison with reported data for methyl 2-(4-hydroxy-2-methoxyphenyl)-2-phenylacetate.[133a] ^{1}H NMR (500 MHz, $CDCl_3$) δ: 7.30-7.15 (m, 5 H), 6.65 (d, J = 8.4 Hz, 1 H), 6.25 (d, J = 2.4 Hz, 1 H), 6.14 (dd, J = 8.3, 2.4 Hz, 1 H), 5.68 (br s, 1 H), 5.10 (s, 1 H), 4.17-4.05 (m, 2 H), 3.65 (s, 3 H), 1.16 (t, J = 7.1 Hz, 3 H). $^{13}C\{^{1}H\}$ NMR (100 MHz, $CDCl_3$) δ: 174.3, 157.8, 156.5, 137.9, 129.8, 129.1, 128.7, 127.2, 119.7, 107.0, 99.1, 61.3, 55.4, 50.8, 14.2 ppm. IR (neat): 3392 (OH), 2980, 2251, 1709, 1615, 1597, 1508, 1467, 1432, 1369, 1296, 1195, 1157, 1111, 1032, 957, 907, 834, 727, 698, 647, 539 cm^{-1}. HRMS ESI-MS (m/z): $[M-H]^-$ calcd. for $C_{17}H_{17}O_4^-$ 285.1132, found 285.1131.

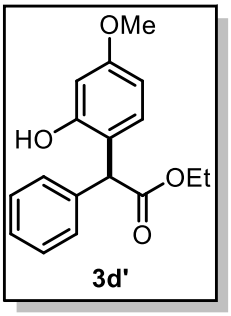

3d'

Ethyl 2-(2-hydroxy-4-methoxyphenyl)-2-phenylacetate, **3d'**: Product **3d'** was prepared following the general procedure employing complex **C1** and $CsBF_4$ as the regulation agent. The reaction crude mixture was purified by column chromatography using SiO_2 and Cy and AcOEt as the eluents (30:1→10:1, Cy:AcOEt), to afford **3d'** as a colorless oil (22.2 mg, 39% yield). Assignments were done by comparison with reported data for methyl 2-(2-hydroxy-4-methoxyphenyl)-2-phenylacetate.[133a] ^{1}H NMR (500 MHz, $CDCl_3$) δ: 7.77 (s, 1 H), 7.25-7.10 (m, 5 H), 6.92 (d, J = 8.4 Hz, 1 H), 6.42-6.34 (m, 2 H), 4.96 (s, 1 H), 4.25-4.14 (m, 2 H), 3.67 (s, 3 H), 1.23 (t, J = 7.1 Hz, 3 H). $^{13}C\{^{1}H\}$ NMR (100 MHz, $CDCl_3$) δ: 175.7, 160.7, 156.1, 137.4, 131.8, 128.7, 127.9, 127.4,

116.4, 106.6, 103.5, 62.2, 55.4, 54.3, 14.2 ppm. IR (neat): 3391 (OH), 2981, 2838, 1705, 1617, 1519, 1445, 1370, 1292, 1199, 1161, 1105, 1025, 960, 908, 831, 728, 698, 636 cm^{-1}. HRMS ESI-MS (m/z): $[M–H]^-$ calcd. for $C_{17}H_{17}O_4^-$ 285.1132, found 285.1133.

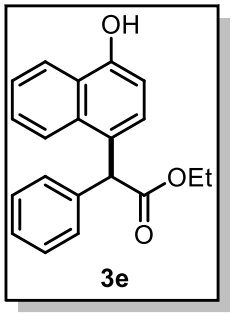

3e

Ethyl 2-(4-hydroxynaphthalen-1-yl)-2-phenylacetate, **3e**: Product **3e** was prepared following the general procedure employing complex **C1** and $CsBF_4$ as the regulation agent. The reaction crude mixture was purified by column chromatography using SiO_2 and Cy and AcOEt as the eluents (30:1→10:1, Cy:AcOEt), to afford **3e** as a pale yellow oil that solidified upon standing (50 mg, 82% yield). ^1H NMR (400 MHz, $CDCl_3$) δ: 8.23 (dd, J = 6.9, 2.0 Hz, 1 H), 7.95 (dd, J = 7.1, 1.8 Hz, 1 H), 7.53-7.46 (m, 2 H), 7.36-7.27 (m, 5 H), 7.13 (d, J = 7.8 Hz, 1 H), 6.69 (d, J = 7.9 Hz, 1 H), 5.68 (s, 1 H), 5.39 (br s, 1 H), 4.28-4.19 (m, 2 H), 1.25 (t, J = 7.1 Hz, 3 H) ppm. $^{13}C\{^1H\}$ NMR (100 MHz, $CDCl_3$) δ: 173.6, 151.4, 138.3, 132.8, 129.1, 128.8, 127.4, 127.1, 127.0, 126.6, 125.1, 123.2, 122.7, 108.1, 61.6, 53.4, 14.3 ppm. IR (neat): 3401 (OH), 3064, 3029, 2981, 2936, 1708, 1626, 1599, 1587, 1518, 1496, 1475, 1453, 1378, 1351, 1309, 1278, 1258, 1178, 1148, 1094, 1061, 1023, 907, 813, 759, 730, 710, 697, 648 cm^{-1}. HRMS ESI-MS (m/z): $[M–H]^-$ calcd. for $C_{20}H_{17}O_3^-$ 305.1183, found 305.1177.

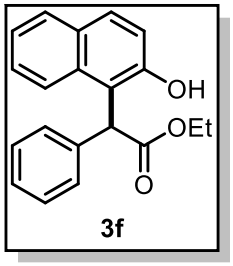

3f

Ethyl 2-(2-hydroxynaphthalen-1-yl)-2-phenylacetate, **3f**: Product **3f** was prepared following the general procedure employing complex **C1** and $RbBF_4$ as the regulation agent. The reaction crude mixture was purified by column chromatography using SiO_2 and Cy and AcOEt as the eluents (30:1→10:1, Cy:AcOEt), to afford **3f** as a colorless solid (30.7 mg, 50% yield). ^1H NMR (400 MHz, $CDCl_3$) δ: 8.39 (s, 1 H), 7.95 (d, J = 8.7 Hz, 1 H), 7.74 (d, J = 7.5 Hz, 1 H), 7.70 (d, J = 8.8 Hz, 1 H), 7.43 (t, J = 8.4 Hz, 1 H), 7.28 (t, J = 7.8 Hz, 1 H), 7.25-7.05 (m, 6 H), 5.93 (s, 1 H), 4.34-4.13 (m, 2 H), 1.24 (t, J = 7.1 Hz, 3 H) ppm. $^{13}C\{^1H\}$ NMR (100 MHz, $CDCl_3$) δ: 176.4, 154.4, 136.7, 133.5, 130.5, 129.6, 129.1, 128.8, 127.6, 127.5, 127.3, 123.4, 121.8, 120.8, 114.6, 62.7, 48.7, 14.2 ppm. IR (neat): 3378 (OH), 3066, 3025, 2978, 2951, 2923, 1709, 1627, 1606, 1581, 1511, 1497, 1474, 1453, 1438, 1390, 1367, 1356,

1342, 1305, 1275, 1256, 1207, 1176, 1111, 1066, 1024, 986, 938, 813, 771, 748, 729, 715, 698, 625, 597 cm 1. HRMS ESI-MS (m/z): $[M–H]^-$ calcd. for $C_{20}H_{17}O_3^-$ 305.1183, found 305.1181.

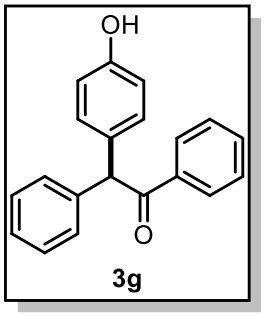

2-(4-hydroxyphenyl)-1,2-diphenylethan-1-one, **3g**: Product **3g** was prepared following the general procedure employing complex **C1** and $CsBF_4$ as the regulation agent. The reaction crude mixture was purified by column chromatography using SiO_2 and Cy and AcOEt as the eluents (10:1→5:1, Cy:AcOEt), to afford **3g** as a yellow oil (10 mg, 17% yield). ^1H and $^{13}C\{^1H\}$ NMR data were in agreement with those previously reported.[145] ^1H NMR (400 MHz, $CDCl_3$) δ: 8.00 (dm, J = 8.6 Hz, 2 H), 7.51 (tm, J = 7.4 Hz, 1 H), 7.41 (tm, J = 7.6 Hz, 2 H), 7.35-7.20 (m, 5 H), 7.13 (dm, J = 8.6 Hz, 2 H), 6.76 (dm, J = 8.6 Hz, 2 H), 5.98 (s, 1 H), 5.03 (br s, 1 H) ppm. $^{13}C\{^1H\}$ NMR (100 MHz, $CDCl_3$) δ: 198.8, 154.8, 139.5, 136.9, 133.2, 131.3, 130.5, 129.1, 129.1, 128.8, 128.7, 127.2, 115.8, 58.7 ppm.

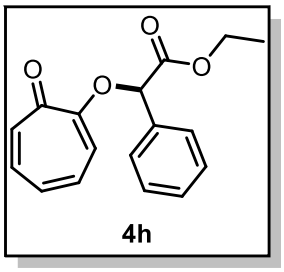

Ethyl 2-((7-oxocyclohepta-1,3,5-trien-1-yl)oxy)-2-phenylacetate, **4h**: Product **4h** was prepared following the general procedure employing complex **C1** and $RbBF_4$ as the regulation agent. The reaction crude mixture was purified by column chromatography using SiO_2 and Cy and AcOEt as the eluents (10:1→2:1, Cy:AcOEt), to afford **4h** as a red oil (6.0 mg, 10% yield). ^1H NMR (400 MHz, $CDCl_3$) δ: 7.58 (dd, J = 7.8, 1.6 Hz, 2 H), 7.42-7.31 (m, 3 H), 7.22-7.16 (m, 2 H), 7.04-6.84 (m, 3 H), 6.04 (s, 1 H), 4.24-4.14 (m, 2 H), 1.19 (t, J = 7.1 Hz, 3 H) ppm. $^{13}C\{^1H\}$ NMR (100 MHz, $CDCl_3$) δ: 181.0, 169.3, 16.4, 138.8, 136.3, 135.1, 132.5, 130.2, 129.1, 128.7, 127.5, 121.2, 79.1, 61.6, 14.0 ppm. IR (neat): 2979, 2925, 1745, 1627, 1575, 1496, 1469, 1391, 1369, 1260, 1228, 1171, 1086, 1028, 960, 912, 871, 773, 727, 695, 503 cm^{-1}. HRMS ESI-MS (m/z): $[M+Na]^+$ calcd. for $C_{17}H_{16}O_4Na^+$ 307.0941, found 307.0945.

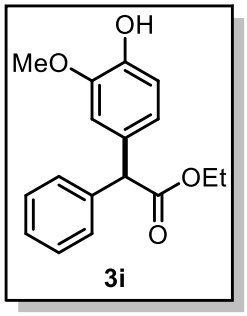

3i

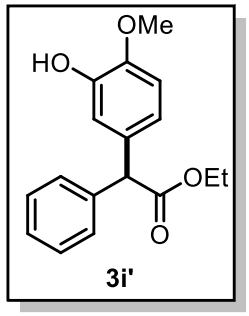

3i'

Ethyl 2-(4-hydroxy-3-methoxyphenyl)-2-phenylacetate, **3i** and ethyl 2-(3-hydroxy-4-methoxyphenyl)-2-phenylacetate, **3i'**: Products **3i**/**3i'** were prepared following the general procedure employing complex **C1** and $LiBF_4$ as the regulation agent. The reaction crude mixture was purified by column chromatography using SiO_2 and Cy and AcOEt as the eluents (30:1→10:1, Cy:AcOEt), to afford a colorless oil as mixture of positional isomers **3i**/**3i'** (ratio 1.0:2.5) that could not be separated with standard preparative techniques. Assignments were done by analyzing the aromatic region in ^{1}H NMR combined with GOESY (Gradient-enhanced nuclear Overhauser Effect SpectroscopY) analysis (see section 3.5.11). Isomers **3i**+**3i'** (39.2 mg, 69% yield). ^{1}H NMR (400 MHz, acetone-d6) δ: 7.55 (s, 1 H, **3i**), 7.53 (s, 1 H, **3i'**), 7.38-7.20 (m, 8 H, **3i**+**3i'**), 6.98 (d, *J* = 1.9 Hz, 1 H, **3i'**), 6.88 (d, *J* = 8.3 Hz, 1 H, **3i**), 6.86 (d, *J* = 2.2 Hz, 1 H, **3i**), 6.82 (dd, *J* = 8.2, 1.9 Hz, 1 H, **3i'**), 6.80-6.76 (m, 1 H, **3i**+**3i'**), 5.00 (s, 1 H, **3i'**), 4.97 (s, 1 H, **3i**), 4.20-4.13 (m, 2 H, **3i**+**3i'**), 3.81 (s, 3 H, **3i**), 3.79 (s, 3 H, **3i'**), 1.21 (t, *J* = 7.1 Hz, 3 H, **3i**+**3i'**). ^{13}C{^{1}H} NMR (126 MHz, acetone-d6) δ: 172.0, 147.3, 146.6, 146.4, 145.7, 139.8, 139.6, 132.0, 130.3, ,128.3, 128.2, 126.7, 121.1, 119.4, 115.3, 114.7, 112.1, 111.3, 60.4, 56.1, 55.9, 55.2, 13.4 ppm. IR (neat): 3438 (OH), 2962, 2934, 2849, 1728, 1602, 1511, 1452, 1368, 1270, 1144, 1025, 869, 800, 762, 725, 698, 645, 553 cm^{-1}. HRMS ESI-MS (m/z): $[M+Na]^+$ calcd. for $C_{17}H_{18}O_4Na^+$ 309.1097, found 309.1091.

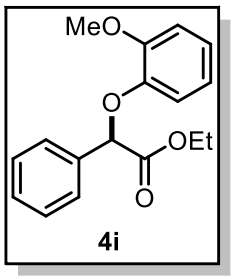

4i

Ethyl 2-(2-methoxyphenoxy)-2-phenylacetate, **4i**: Product **4i** was prepared following the general procedure employing $AgBF_4$ as the catalyst. The reaction crude mixture was purified by column chromatography using SiO_2 and Cy and AcOEt as the eluents (30:1, Cy:AcOEt), to afford **4i** as a yellow oil (14.6 mg, 26% yield). ^{1}H NMR (400 MHz, $CDCl_3$) δ: 7.65-7.55 (m, 2 H), 7.42-7.31 (m, 3 H), 7.01-6.78 (m, 4 H), 5.63 (s, 1 H), 4.24-4.17 (m, 2 H), 3.87 (s, 3 H), 1.21 (t, J = 7.1 Hz, 3 H) ppm. ^{13}C{^{1}H} NMR (100 MHz, $CDCl_3$) δ: 170.3, 150.7, 147.0, 136.0, 129.9, 128.9, 128.8, 128.2, 127.3,

123.3, 120.9, 117.8, 112.8, 80.4, 61.6, 56.2, 14.2 ppm. IR (neat): 3065, 2981, 2837, 1750, 1731, 1593, 1498, 1455, 1369, 1328, 1252, 1205, 1174, 1126, 1112, 1049, 1026, 916, 836, 741, 695, 521 cm^{-1}. HRMS ESI-MS (m/z): $[M+Na]^+$ calcd. for $C_{17}H_{18}O_4Na^+$ 309.1097, found 309.1092.

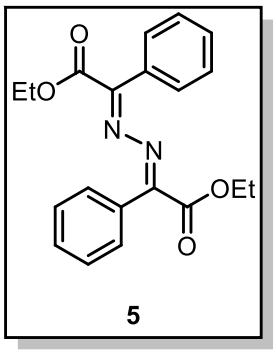

5

Ethyl benzoylformate azine, **5**: Product **5** was prepared by allowing to react PhEDA **2a** (45.4 μL, 0.26 mmol) with $AgBF_4$ (5.1 mg, 10 mol%) in 2 mL of CH_2Cl_2 for 1 hour. After evaporation, the reaction crude mixture was purified by column chromatography using SiO_2 and Cy and AcOEt as the eluents (30:1, Cy:AcOEt), to afford **5** as a yellow solid (9.1 mg, 10% yield). ^1H and $^{13}C\{^1H\}$ NMR data were in agreement with those previously reported.[165] ^1H NMR (400 MHz, $CDCl_3$) δ: 7.85-7.75 (m, 4 H), 7.55-7.35 (m, 6 H), 4.50 (q, J = 7.1 Hz, 4 H), 1.42 (t, J = 7.1 Hz, 6 H) ppm. $^{13}C\{^1H\}$ NMR (100 MHz, $CDCl_3$) δ: 165.3, 162.2, 132.0, 131.3, 128.8, 128.0, 61.7, 14.5 ppm.

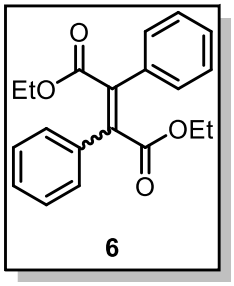

6

Diethyl 2,3-diphenylbutenoate, **6**: Product **6** was prepared by allowing to react PhEDA **2a** (45.4 μL, 0.26 mmol) with $AgBF_4$ (5.1 mg, 10 mol%) in 2 mL of CH_2Cl_2 for 1 hour. After evaporation, the reaction crude mixture was purified by column chromatography using SiO_2 and Cy and AcOEt as the eluents (30:1, Cy:AcOEt), to afford **6** as a pale yellow oil (18.3 mg, 22% yield). ^1H and $^{13}C\{^1H\}$ NMR data were in agreement with those previously reported.[166] ^1H NMR (400 MHz, $CDCl_3$) δ: 7.50-7.30 (m, 10 H), 4.00 (q, J = 7.1 Hz, 4 H), 0.94 (t, J = 7.1 Hz, 6 H) ppm. $^{13}C\{^1H\}$ NMR (100 MHz, $CDCl_3$) δ: 168.2, 137.8, 135.7, 128.8, 128.5, 128.3, 61.4, 13.7 ppm.

(165) Glaser, R.; Chen, G. S.; Barnes, C. L. *J. Org. Chem.* **1993**, *58*, 7446-7455.
(166) The *E* or *Z* configuration could not be univocally assigned according to previous reports. See: (a) Zhou, C.; Larock, R. C. *J. Org. Chem.* **2005**, *70*, 3765-3777. (b) Zhou, L.; Zhang, W.; Jiang, H. *Sci. China, Ser. B: Chem.* **2008**, *51*, 241-247.

3.5.10. Computational methods

The energies of all compounds included in this study were computed at the BP86[148]-D3/def2-TZVPD[68a]//BP86-D3/def2-SVP level of theory. The calculations have been performed by using the program TURBOMOLE (version 7.0).[151] For the calculations, we have used the DFT-D functional with the latest available correction for dispersion (D3).[67] TS structures were characterized by means of frequency analysis calculations. In order to reproduce solvent effects, we have used the conductor-like screening model COSMO,[149] which is a variant of the dielectric continuum solvation models.[150] CH_2Cl_2 has been used as solvent.

Cartesian coordinates:

[C1-2a]···1a:

Au	−1.2214603	−1.1604627	−0.9590938	C	0.8016636	−1.2491001	2.1466476
P	0.9649100	−0.4430327	−1.4596770	H	0.9364455	−2.1458754	2.7830536
O	2.0452627	0.0984267	−0.3597347	H	0.9545294	−1.5927676	1.1066096
O	0.7454777	0.8085173	−2.4932716	H	−0.2399958	−0.8814823	2.2621564
O	1.9484671	−1.5375505	−2.1471928	C	0.7925984	4.8677860	2.6343055
O	1.4453917	−3.9492906	−0.4544699	C	0.6908839	6.1286269	1.7521394
O	2.0227213	−4.5835728	2.5623046	H	1.6538244	6.3713657	1.2581493
O	3.3524657	−3.3299558	4.9061506	H	0.4145694	7.0022703	2.3759831
O	5.8090968	−1.7329232	4.4853204	H	−0.0850006	6.0239637	0.9662485
C	1.7422974	1.2594213	0.3850692	C	1.8822657	5.1094740	3.7102926
C	1.5822277	1.1578788	1.7907036	H	1.6373075	6.0084996	4.3124955
C	1.2791290	2.3610557	2.4579429	H	2.8755466	5.2700818	3.2441466
H	1.1336356	2.3222103	3.5449490	H	1.9732689	4.2549319	4.4108026
C	1.1582957	3.6126038	1.8131134	C	−0.5761500	4.6448723	3.3260057
C	1.4100792	3.6549295	0.4336474	H	−0.8533545	5.5354287	3.9273471
H	1.3609414	4.6053276	−0.1129948	H	−0.5572315	3.7738660	4.0117772
C	1.7275611	2.4904485	−0.3050567	H	−1.3782059	4.4704482	2.5804724
C	2.1499900	2.6355251	−1.7310877	C	4.4715997	5.0731025	−3.6469368
C	3.0503977	3.6747795	−2.0476980	C	3.9037430	6.4195029	−3.1299755
H	3.4523443	4.2691534	−1.2144088	H	4.6251614	7.2405475	−3.3204272
C	3.4528367	3.9472232	−3.3663411	H	3.7074373	6.3964957	−2.0392888
C	2.8821618	3.1622333	−4.3864857	H	2.9527878	6.6761608	−3.6401915
H	3.1549968	3.3800712	−5.4238024	C	5.7960566	4.7521559	−2.9083800
C	1.9740658	2.1052233	−4.1538936	H	6.5435246	5.5515132	−3.0920126
C	1.6683056	1.8350342	−2.7964356	H	6.2281761	3.7934325	−3.2608090
C	1.8177381	−0.1595839	2.5693916	H	5.6528232	4.6745294	−1.8118514
C	3.2642408	−0.6598987	2.3146471	C	4.7772648	5.2203666	−5.1517446
H	3.4644053	−1.5748884	2.9066779	H	5.5145035	6.0336821	−5.3065190
H	3.9982244	0.1112031	2.6236131	H	3.8726383	5.4818042	−5.7380227
H	3.4400511	−0.8911892	1.2479132	H	5.2137635	4.2953463	−5.5805846
C	1.6578558	0.0397258	4.0931429	C	1.3337808	1.3459478	−5.3456257
H	1.8816616	−0.9199585	4.5998230	C	−0.2110722	1.4760070	−5.2811667
H	0.6295566	0.3455631	4.3761859	H	−0.6698499	0.9555483	−6.1477899
H	2.3642197	0.7961732	4.4909813	H	−0.5171937	2.5409869	−5.3276506

H	−0.6298866	1.0401393	−4.3553796
C	1.7502639	−0.1449312	−5.3277622
H	1.3062500	−0.6741481	−6.1963979
H	1.4166510	−0.6539984	−4.4076073
H	2.8524579	−0.2504435	−5.3918580
C	1.7832503	1.9283352	−6.7050233
H	1.2852314	1.3686508	−7.5222672
H	2.8763248	1.8354736	−6.8645650
H	1.5031763	2.9948439	−6.8194199
C	1.5014819	−2.8397828	−2.5940486
H	1.8675157	−2.9554247	−3.6335769
H	0.3894430	−2.8853224	−2.6016311
C	2.0586682	−3.9519720	−1.7287348
H	1.8560981	−4.9123490	−2.2674159
H	3.1679645	−3.8516947	−1.6463757
C	1.6802028	−5.1683568	0.2458063
H	2.7728102	−5.3789451	0.3273176
H	1.2172310	−6.0143896	−0.3199299
C	1.0975791	−5.1383271	1.6492912
H	0.1307027	−4.5748110	1.6349027
H	0.8536598	−6.1897031	1.9457135
C	1.6373484	−4.7362004	3.9187337
H	1.1725429	−5.7413242	4.0770059
H	0.8756048	−3.9707040	4.2100281
C	2.8403616	−4.6450524	4.8397963
H	2.5215409	−4.9967064	5.8547386
H	3.6234661	−5.3567490	4.4790880
C	4.4736136	−3.2481189	5.7750072
H	5.2364837	−4.0159100	5.4996199
H	4.1628073	−3.4515492	6.8307921
C	5.1240941	−1.8800702	5.7100570
H	4.3509904	−1.0817355	5.8444320
H	5.8305238	−1.7945360	6.5752542
C	6.5384086	−0.5282355	4.4039237
H	7.0483577	−0.5099768	3.4216180
H	7.3113312	−0.4512937	5.2079443
H	5.8801774	0.3717366	4.4800250
C	−5.6541557	−3.4306789	1.5480768
C	−5.1249039	−2.7750010	0.4393328
C	−3.7299430	−2.4207650	0.3920391
C	−2.9103182	−2.7560163	1.5241038
C	−3.4493206	−3.4142559	2.6250844
C	−4.8205287	−3.7533728	2.6401887
H	−6.7216241	−3.6942677	1.5754937
H	−5.7816093	−2.5144555	−0.4031147
H	−1.8455571	−2.4794874	1.4971001
H	−2.8111392	−3.6664074	3.4844184
H	−5.2447924	−4.2718028	3.5138987
C	−3.1549193	−1.7662137	−0.7312027
C	−4.0231606	−1.4414289	−1.9009696
O	−4.8633214	−0.5365487	−1.8733456
O	−3.7651109	−2.1825489	−2.9762375
C	−4.5330797	−1.8930011	−4.1724558
H	−4.2086322	−2.6381478	−4.9177213
H	−5.6169624	−1.9879675	−3.9698182
H	−4.3154623	−0.8662630	−4.5236269
C	−5.2164682	3.7061756	2.3194065
C	−5.6093408	4.5436808	1.2557613
C	−5.7139741	4.0145114	−0.0453666
C	−5.4300743	2.6658608	−0.2895999
C	−5.0383790	1.8249954	0.7830710
C	−4.9308080	2.3563638	2.0923776
H	−5.1374574	4.1136027	3.3387265
H	−6.0227829	4.6625533	−0.8796063
H	−5.5109911	2.2473780	−1.3046564
H	−4.6278804	1.6855211	2.9092624
O	−4.7645089	0.5122075	0.6095487
H	−4.9056368	0.2449887	−0.3433840
H	−5.8363720	5.6038791	1.4412326

[(**C1**-**2a**)·Li^+]···**1a**:

Au	−1.8090043	−1.1548254	−0.4553659	H	−0.5534646	−1.3283173	2.1617805
P	0.4884510	−0.6617907	−0.3903831	H	−1.7858198	−0.2714444	2.9292394
O	1.3184012	−0.1758622	0.9420453	C	0.4497259	5.1165335	3.1097483
O	0.6800748	0.5269674	−1.4899500	C	0.8638232	6.2408901	2.1383954
O	1.5268058	−1.8934978	−0.7471145	H	1.9493122	6.2186897	1.9109798
O	2.9312681	−4.3495740	−0.3399772	H	0.6485294	7.2273117	2.5947724
O	4.5802308	−4.8062426	1.6773535	H	0.3048175	6.1927781	1.1817642
O	4.7361775	−2.3460797	2.5743888	C	1.2597094	5.2774020	4.4220717
O	5.0319481	−1.4777053	0.0875112	H	1.0814267	6.2798960	4.8622718
Li	4.0926369	−3.0654730	0.7820045	H	2.3485034	5.1774624	4.2369342
C	1.0883771	1.1167196	1.4888320	H	0.9731077	4.5266167	5.1854106
C	0.5553613	1.2424346	2.7991799	C	−1.0635592	5.2634316	3.4125706
C	0.3806686	2.5615666	3.2634779	H	−1.2720212	6.2662303	3.8377673
H	−0.0397812	2.7012556	4.2666887	H	−1.4173783	4.5127127	4.1477332
C	0.7142163	3.7153797	2.5199300	H	−1.6701345	5.1506096	2.4914591
C	1.3007070	3.5184491	1.2612512	C	5.3243192	3.9130834	−2.1227326
H	1.5977668	4.3786387	0.6480432	C	4.9187000	5.3810037	−1.8297950
C	1.5182554	2.2259488	0.7274494	H	5.7976787	6.0494104	−1.9306389
C	2.2601299	2.1185200	−0.5670075	H	4.5227869	5.5080795	−0.8019404
C	3.4006592	2.9307368	−0.7508918	H	4.1420950	5.7310378	−2.5394329
H	3.7471500	3.5229984	0.1083922	C	6.4036194	3.4647147	−1.1047933
C	4.0809571	3.0080972	−1.9797710	H	7.3007160	4.1120141	−1.1828394
C	3.5502990	2.2665546	−3.0540111	H	6.7263434	2.4202186	−1.2976172
H	4.0334435	2.3521216	−4.0324780	H	6.0422630	3.5265479	−0.0582765
C	2.4143163	1.4299906	−2.9527788	C	5.9328443	3.8481120	−3.5385580
C	1.8307923	1.3340150	−1.6650707	H	6.8272232	4.4997529	−3.5912441
C	0.2464694	0.0341748	3.7213309	H	5.2254802	4.2041838	−4.3146040
C	1.5392548	−0.7938795	3.9396633	H	6.2574708	2.8222470	−3.8084887
H	1.3309538	−1.6503598	4.6142215	C	1.8135740	0.7663846	−4.2209908
H	2.3220070	−0.1737224	4.4220616	C	0.3753129	1.3078200	−4.4393386
H	1.9497432	−1.1938522	2.9937709	H	−0.0584850	0.8661970	−5.3601831
C	−0.2497393	0.4872161	5.1133708	H	0.3863992	2.4086334	−4.5689493
H	−0.4378466	−0.4051702	5.7433523	H	−0.2954696	1.0689354	−3.5927302
H	−1.1994024	1.0557906	5.0583375	C	1.7858376	−0.7759514	−4.0943798
H	0.4982178	1.1089349	5.6439163	H	1.3918852	−1.2245711	−5.0292036
C	−0.8637226	−0.8587724	3.1156731	H	1.1399612	−1.1073762	−3.2626749
H	−1.1172463	−1.6787290	3.8191549	H	2.8060829	−1.1817613	−3.9316024

C	2.6327441	1.1028618	−5.4874107
H	2.1591446	0.6213274	−6.3659488
H	3.6746188	0.7284741	−5.4300751
H	2.6643515	2.1910787	−5.6913321
C	1.0476226	−3.1542227	−1.2736239
H	0.4888254	−2.9991051	−2.2212730
H	0.3719730	−3.6364341	−0.5355657
C	2.2353745	−4.0527977	−1.5572164
H	1.8460994	−4.9902053	−2.0118914
H	2.9210985	−3.5767020	−2.2939449
C	3.5547946	−5.6484499	−0.2787741
H	4.4893865	−5.6565931	−0.8844474
H	2.8730416	−6.4290900	−0.6817230
C	3.8460381	−5.9281806	1.1849432
H	2.8919951	−6.0354150	1.7513081
H	4.4252684	−6.8727828	1.2915706
C	4.6200366	−4.6630682	3.1033563
H	5.1586589	−5.5109557	3.5818510
H	3.5806305	−4.6397237	3.5070746
C	5.3476598	−3.3601174	3.3844202
H	5.2863165	−3.1087919	4.4664984
H	6.4230771	−3.4547274	3.1096029
C	5.5280225	−1.1627221	2.3964672
H	6.5991895	−1.4502334	2.2962051
H	5.4295917	−0.4774208	3.2674528
C	5.0543765	−0.4807829	1.1248707
H	4.0396118	−0.0375686	1.2409631
H	5.7597069	0.3377555	0.8636984
C	5.1290488	−0.9429639	−1.2376342
H	5.1095990	−1.7982496	−1.9385372
H	6.0892686	−0.3993501	−1.3675095
H	4.2863962	−0.2558897	−1.4644512
C	−6.9835474	−2.7877136	0.8457529
C	−6.1065311	−2.2675829	−0.1022591
C	−4.7147648	−2.0620938	0.2155683
C	−4.2721634	−2.4028220	1.5421385
C	−5.1554459	−2.9270640	2.4786987
C	−6.5132868	−3.1209426	2.1342705
H	−8.0432277	−2.9378263	0.5924577
H	−6.4826840	−2.0018597	−1.1004323
H	−3.2142099	−2.2386558	1.7964004
H	−4.8044466	−3.1880413	3.4877481
H	−7.2115111	−3.5333554	2.8788709
C	−3.7946424	−1.5520778	−0.7368297
C	−4.2819148	−1.2396359	−2.1160642
O	−5.0177589	−0.2800895	−2.3640200
O	−3.8109262	−2.0719293	−3.0415433
C	−4.2367833	−1.8388405	−4.4117583
H	−3.7785134	−2.6483046	−5.0036590
H	−5.3402811	−1.8792546	−4.4839527
H	−3.8836944	−0.8484045	−4.7559161
C	−5.8296251	4.2902952	1.3959823
C	−5.8793117	5.0802461	0.2282200
C	−5.7511958	4.4701630	−1.0363870
C	−5.5721223	3.0870505	−1.1417945
C	−5.5248196	2.2943226	0.0350018
C	−5.6531972	2.9069961	1.3081605
H	−5.9397289	4.7634600	2.3833644
H	−5.7976702	5.0826157	−1.9492957
H	−5.4781735	2.6039409	−2.1266857
H	−5.6252549	2.2710656	2.2048322
O	−5.3676518	0.9529904	−0.0051048
H	−5.3412496	0.6239627	−0.9510623
H	−6.0257003	6.1677014	0.3033513

[(**C1**-**2a**)·Cs^+]···**1a**:

Au	−2.0230624	−0.5795618	−0.5344900	H	−1.9376828	0.9095735	2.6513855
P	0.3190984	−0.4327390	−0.5342253	C	1.1657996	5.7630269	2.0241080
O	1.2105691	0.1246741	0.7392675	C	1.8059476	6.6370804	0.9262921
O	0.6893491	0.5485367	−1.7826219	H	2.8802442	6.4027237	0.7794827
O	1.1848204	−1.8260114	−0.6807519	H	1.7422934	7.7051933	1.2139525
O	2.4611489	−4.3971417	−0.3150778	H	1.2877237	6.5300368	−0.0485606
O	4.9625280	−4.9295471	1.1173702	C	1.9280503	6.0065033	3.3519028
O	6.2065941	−3.1046383	2.9836220	H	1.8995605	7.0828139	3.6172197
O	6.0814205	−0.1959242	2.6591476	H	2.9920889	5.7062483	3.2651256
C	1.1835426	1.5070599	1.0753891	H	1.4841945	5.4473639	4.2001362
C	0.6571483	1.9208349	2.3278523	C	−0.3154655	6.1903802	2.1903027
C	0.6913015	3.3082342	2.5729963	H	−0.3761008	7.2678077	2.4459366
H	0.2828553	3.6723458	3.5233243	H	−0.8236873	5.6287025	2.9997626
C	1.2187267	4.2613035	1.6734303	H	−0.8872415	6.0304842	1.2536587
C	1.7861432	3.7769675	0.4853711	C	5.8363230	2.9728035	−2.8074289
H	2.2275011	4.4714440	−0.2407872	C	5.6617407	4.5138522	−2.8001047
C	1.7975667	2.3985713	0.1677034	H	6.6346515	5.0126440	−2.9869237
C	2.5207491	1.9669993	−1.0688123	H	5.2794297	4.8851904	−1.8280148
C	3.7818412	2.5404619	−1.3425234	H	4.9553157	4.8395753	−3.5898985
H	4.2202981	3.1962409	−0.5755546	C	6.8243983	2.5620655	−1.6867832
C	4.4647376	2.3117215	−2.5510886	H	7.8143190	3.0336240	−1.8534690
C	3.8174229	1.5119474	−3.5133176	H	6.9739032	1.4622203	−1.6686156
H	4.3106194	1.3639155	−4.4791925	H	6.4723385	2.8841247	−0.6854611
C	2.5548588	0.9061162	−3.3199297	C	6.4406249	2.5557527	−4.1638323
C	1.9641884	1.1084856	−2.0483289	H	7.4296013	3.0373966	−4.2976074
C	0.1317607	0.9420934	3.4120467	H	5.8090865	2.8725389	−5.0182034
C	1.2414828	−0.0787048	3.7796329	H	6.5958546	1.4595294	−4.2329940
H	0.8905022	−0.7473797	4.5922502	C	1.8497044	0.1754295	−4.4935037
H	2.1522500	0.4415375	4.1402215	C	0.5232199	0.9114104	−4.8219753
H	1.5139076	−0.7116449	2.9136725	H	0.0223526	0.4188074	−5.6805425
C	−0.2543875	1.6831247	4.7126539	H	0.7180361	1.9653943	−5.1057270
H	−0.5987764	0.9457769	5.4645506	H	−0.1790017	0.9095446	−3.9671997
H	−1.0835080	2.4015041	4.5570569	C	1.5621892	−1.3053358	−4.1490075
H	0.6023504	2.2288312	5.1549190	H	1.0937112	−1.8114691	−5.0175420
C	−1.1330049	0.1967052	2.9217594	H	0.8731799	−1.4033557	−3.2918796
H	−1.5227664	−0.4637435	3.7235016	H	2.5016782	−1.8458954	−3.9103216
H	−0.9296981	−0.4420765	2.0398299	C	2.7130563	0.1825138	−5.7754561

H	2.1626048	−0.3337741	−6.5867200
H	3.6760145	−0.3507957	−5.6422816
H	2.9295447	1.2090470	−6.1311585
C	0.5477556	−3.0978121	−0.9858543
H	−0.1840188	−2.9765305	−1.8117558
H	0.0158157	−3.4621347	−0.0819442
C	1.6034640	−4.0986041	−1.4065668
H	1.0708785	−5.0187002	−1.7500460
H	2.1771937	−3.7051175	−2.2793241
C	3.3427683	−5.4891636	−0.5928029
H	4.0859290	−5.2047992	−1.3757248
H	2.7638979	−6.3587725	−0.9842953
C	4.0533456	−5.9306058	0.6692424
H	3.3022961	−6.1629287	1.4618457
H	4.6010363	−6.8768104	0.4430246
C	5.6951157	−5.3543827	2.2687484
H	6.1819036	−6.3392922	2.0736635
H	5.0063014	−5.4882314	3.1371070
C	6.7803432	−4.3565104	2.6165201
H	7.3697384	−4.7798500	3.4638342
H	7.4807732	−4.2291358	1.7557589
C	7.1502052	−2.2152470	3.5812859
H	8.0361513	−2.0813227	2.9143922
H	7.5275709	−2.6366292	4.5437822
C	6.4724530	−0.8794385	3.8513923
H	5.5469977	−1.0524081	4.4408787
H	7.1455246	−0.2421771	4.4685756
C	7.0997297	0.6352635	2.1080447
H	6.6787840	1.1264569	1.2105437
H	8.0036263	0.0597178	1.8030208
H	7.4112923	1.4234768	2.8299374
C	−7.1691486	−2.6114622	0.1083529
C	−6.3498948	−1.6262111	−0.4414299
C	−4.9323567	−1.5996546	−0.1561172
C	−4.4138168	−2.6075838	0.7371920
C	−5.2433974	−3.5721277	1.2896477
C	−6.6246242	−3.5805514	0.9720802
H	−8.2419765	−2.6303794	−0.1325633
H	−6.7804627	−0.8874074	−1.1302216
H	−3.3389568	−2.5848253	0.9740683
H	−4.8354828	−4.3312696	1.9731029
H	−7.2775163	−4.3540044	1.4052414
C	−4.0601323	−0.6448885	−0.7323645
C	−4.6341588	0.4699891	−1.5424258
O	−5.4760770	1.2578939	−1.0971478
O	−4.1061946	0.5706004	−2.7607594
C	−4.5970943	1.6432896	−3.6064245
H	−4.0758652	1.5204033	−4.5700117
H	−5.6923301	1.5577088	−3.7408359
H	−4.3586349	2.6237236	−3.1518472
C	−9.6654672	1.7062131	3.0420624
C	−10.1297903	2.7505056	2.2143946
C	−9.4074458	3.1014587	1.0552801
C	−8.2339805	2.4207426	0.7177784
C	−7.7686217	1.3705581	1.5536105
C	−8.4950790	1.0157869	2.7205993
H	−10.2272464	1.4339618	3.9482195
H	−9.7663999	3.9180252	0.4108834
H	−7.6612939	2.6915382	−0.1824896
H	−8.1132583	0.2007068	3.3524841
O	−6.6402662	0.6811717	1.2837612
H	−6.2162966	1.0101578	0.4387435
H	−11.0514802	3.2915999	2.4739904
Cs	4.0599410	−1.9233141	1.0324041

TS-O (no RA):

Au	−2.1733641	0.5517244	−0.1238980	H	−0.5541370	−1.6573981	2.7461868
P	0.0547641	0.6480111	−0.8512496	C	4.7469273	−0.0774667	4.1354466
O	1.1798207	−0.4365925	−0.3854866	C	5.6354954	1.1825605	4.1144943
O	0.6535761	2.1089407	−0.4077117	H	6.2977749	1.2107044	3.2252166
O	0.2540721	0.4829621	−2.4517310	H	6.2883722	1.1978050	5.0104924
O	−1.1079837	−2.0309154	−3.1429418	H	5.0358723	2.1154306	4.1276079
O	−0.1312345	−4.9093032	−2.7074068	C	5.6683770	−1.3232674	4.1507179
O	2.1908310	−6.2470567	−1.3176405	H	6.3447628	−1.2932152	5.0300135
O	4.5746740	−4.7915685	−0.3738878	H	6.2973942	−1.3660156	3.2381816
C	2.0179837	−0.3288688	0.7390243	H	5.0911907	−2.2679261	4.2085188
C	2.0090083	−1.3732781	1.7002344	C	3.8943799	−0.0509719	5.4294222
C	2.9205626	−1.2357164	2.7655597	H	4.5497377	−0.0033224	6.3235201
H	2.9380812	−2.0222666	3.5303347	H	3.2604471	−0.9551055	5.5292682
C	3.8101650	−0.1491003	2.9104682	H	3.2269562	0.8349642	5.4488667
C	3.7973692	0.8282820	1.9056343	C	5.9936906	3.5797580	−2.0458295
H	4.4700701	1.6939553	1.9628012	C	6.8814716	3.8947286	−0.8153302
C	2.9216600	0.7548044	0.7969341	H	7.9154038	4.1366073	−1.1373556
C	3.0533703	1.7998289	−0.2633106	H	6.9462621	3.0363346	−0.1165170
C	4.3450487	2.1744749	−0.6883516	H	6.4888883	4.7640171	−0.2490275
H	5.1960848	1.5892935	−0.3105228	C	6.5726100	2.3573691	−2.8030556
C	4.5620815	3.2447145	−1.5742426	H	7.6053139	2.5710157	−3.1481641
C	3.4337932	3.9831367	−1.9808672	H	5.9589828	2.1109047	−3.6936203
H	3.5884577	4.8528284	−2.6271263	H	6.6141512	1.4537233	−2.1625988
C	2.1087933	3.6680587	−1.6031863	C	6.0256876	4.7974860	−2.9917141
C	1.9557916	2.5199874	−0.7898923	H	7.0684297	4.9963249	−3.3108051
C	1.0811421	−2.6099454	1.6004822	H	5.6517311	5.7187252	−2.5001433
C	1.2674865	−3.3440989	0.2475972	H	5.4282175	4.6277018	−3.9106749
H	0.6449883	−4.2605224	0.2372533	C	0.9326616	4.6009429	−1.9968583
H	2.3153197	−3.6712449	0.0960275	C	0.2572159	5.1372570	−0.7064429
H	0.9696186	−2.7322202	−0.6216295	H	−0.5771478	5.8201144	−0.9696239
C	1.3796722	−3.6333550	2.7199188	H	0.9817657	5.7111491	−0.0939275
H	0.7081281	−4.5072578	2.6020188	H	−0.1491472	4.3194179	−0.0816075
H	1.2079536	−3.2219509	3.7356470	C	−0.1125407	3.8665612	−2.8719482
H	2.4198834	−4.0119428	2.6650018	H	−0.8861659	4.5847228	−3.2137978
C	−0.3928966	−2.1661544	1.7735934	H	−0.6272668	3.0628708	−2.3151025
H	−1.0603549	−3.0527906	1.7346320	H	0.3615852	3.4249013	−3.7721423
H	−0.7139472	−1.4718826	0.9709516	C	1.4214929	5.8230167	−2.8071240

H	0.5572257	6.4777040	−3.0382237
H	1.8811814	5.5316237	−3.7730144
H	2.1531601	6.4346638	−2.2429308
C	−0.8357704	0.3479768	−3.3926453
H	−0.7068986	1.1479979	−4.1484502
H	−1.8097784	0.4994746	−2.8747488
C	−0.8132927	−1.0065829	−4.0697163
H	−1.5758154	−0.9649615	−4.8888008
H	0.1790318	−1.1749740	−4.5546301
C	−1.4814190	−3.2426107	−3.7929207
H	−0.7884904	−3.4663523	−4.6377834
H	−2.5105118	−3.1390283	−4.2186420
C	−1.4510747	−4.4305612	−2.8471278
H	−1.9001849	−4.1449416	−1.8625433
H	−2.1079548	−5.2248205	−3.2846132
C	−0.0611837	−6.2269264	−2.1890021
H	−0.7519122	−6.8984119	−2.7588655
H	−0.3751061	−6.2644775	−1.1165976
C	1.3484602	−6.7738746	−2.3202703
H	1.3028028	−7.8912307	−2.2484345
H	1.7298025	−6.5285157	−3.3425591
C	3.5333891	−6.6686614	−1.4671229
H	3.9677696	−6.2837373	−2.4228409
H	3.5933289	−7.7864461	−1.5041590
C	4.3837198	−6.1908904	−0.3057800
H	3.8996472	−6.4864796	0.6590233
H	5.3665968	−6.7239014	−0.3560386
C	5.4705646	−4.3152818	0.6060793
H	5.5632735	−3.2203662	0.4735007
H	6.4838504	−4.7754216	0.5033879
H	5.1115205	−4.5191926	1.6448112
C	−7.1730468	−1.7437746	0.6794077
C	−6.4191024	−0.5815695	0.5115547
C	−4.9914741	−0.6353229	0.4885890
C	−4.3583879	−1.9029646	0.6534433
C	−5.1183152	−3.0636583	0.8179010
C	−6.5246499	−2.9866107	0.8307997
H	−8.2716214	−1.6903587	0.6958349
H	−6.9318260	0.3866125	0.4060439
H	−3.2588162	−1.9505855	0.6429546
H	−4.6187302	−4.0362211	0.9386058
H	−7.1223627	−3.9016307	0.9617547
C	−4.1950422	0.5596396	0.3225291
C	−4.8694129	1.8061315	−0.1918756
O	−5.0885280	2.8187272	0.4833944
O	−5.1531193	1.7111306	−1.4895705
C	−5.7157383	2.8894833	−2.1233336
H	−5.9104064	2.5958448	−3.1682503
H	−6.6531303	3.1879908	−1.6170550
H	−4.9943647	3.7277598	−2.0784817
C	−1.7160765	0.6888703	4.8246317
C	−0.9636559	1.8755311	4.7463064
C	−1.3376832	2.8862440	3.8415405
C	−2.4538577	2.7159051	3.0097985
C	−3.2051908	1.5256759	3.1040354
C	−2.8389780	0.5065345	4.0053490
H	−1.4322544	−0.0977683	5.5395984
H	−0.7550783	3.8175382	3.7820037
H	−2.7536804	3.5019611	2.3000447
H	−3.4539153	−0.4027762	4.0628487
O	−4.3275119	1.3216106	2.3362345
H	−4.6362879	2.1756389	1.8705279
H	−0.0869292	2.0153150	5.3952416

TS-O (Li^+):

Au	−2.2354032	−0.1665230	−0.3638127	H	−1.0352327	−0.6282646	2.2184672
P	0.0948361	−0.4519489	−0.3774095	H	−1.6732190	0.8391785	3.0327742
O	1.0878783	−0.3402196	0.9267702	C	2.6689529	4.7509514	3.1710027
O	0.6622397	0.6301667	−1.4560650	C	3.4790676	5.6197651	2.1875002
O	0.6130948	−1.9596178	−0.8001442	H	4.4337824	5.1386192	1.8928797
O	1.0003079	−4.7597612	−0.3289589	H	3.7360012	6.5864400	2.6642824
O	2.3962916	−5.7951697	1.6691843	H	2.9070339	5.8500726	1.2655798
O	3.5865896	−3.6042274	2.4765529	C	3.5338949	4.5002017	4.4330971
O	4.0449677	−2.9326120	−0.0486375	H	3.8293815	5.4651158	4.8931287
Li	2.6051307	−4.0204893	0.7396460	H	4.4614379	3.9468878	4.1808353
C	1.4445874	0.9181703	1.4814244	H	2.9908166	3.9190398	5.2053660
C	1.0794078	1.2209763	2.8203593	C	1.3870232	5.5259748	3.5684222
C	1.5092680	2.4723776	3.3048472	H	1.6540420	6.5058009	4.0139412
H	1.2383894	2.7475483	4.3310803	H	0.7812737	4.9760759	4.3162845
C	2.2698493	3.3946223	2.5527951	H	0.7447773	5.7176145	2.6846483
C	2.6452762	3.0091342	1.2577791	C	6.2255629	1.8752265	−2.4210975
H	3.2459102	3.6820847	0.6328506	C	6.4526712	3.3778485	−2.1101059
C	2.2627460	1.7654523	0.7007948	H	7.5151729	3.6476523	−2.2775786
C	2.8119164	1.4068314	−0.6438887	H	6.2076898	3.6284735	−1.0582915
C	4.1695277	1.6920303	−0.9093770	H	5.8315184	4.0207732	−2.7660563
H	4.7861547	2.0615348	−0.0767621	C	7.1074038	1.0164636	−1.4793447
C	4.7375476	1.5340104	−2.1862231	H	8.1787144	1.2652741	−1.6218563
C	3.8818969	1.1082862	−3.2215172	H	6.9846126	−0.0662600	−1.6920082
H	4.2939821	1.0260084	−4.2322331	H	6.8693341	1.1889732	−0.4099177
C	2.5134991	0.8008832	−3.0397274	C	6.6631266	1.6067624	−3.8756293
C	2.0289198	0.9063236	−1.7123505	H	7.7377147	1.8498010	−3.9950159
C	0.3215285	0.2357537	3.7485925	H	6.1067213	2.2325924	−4.6017584
C	1.1485588	−1.0662834	3.9077041	H	6.5332033	0.5429814	−4.1616489
H	0.6166515	−1.7740212	4.5772035	C	1.6118665	0.4872489	−4.2635575
H	2.1344597	−0.8493616	4.3667902	C	0.5240936	1.5885630	−4.3793143
H	1.3250972	−1.5727417	2.9405157	H	−0.1180362	1.3956075	−5.2628511
C	0.1121576	0.8244362	5.1624416	H	0.9886542	2.5860190	−4.5132348
H	−0.4158865	0.0817406	5.7934521	H	−0.1237475	1.6295866	−3.4833148
H	−0.5069512	1.7435389	5.1497237	C	0.9430475	−0.9029137	−4.1389016
H	1.0708302	1.0575377	5.6668462	H	0.3613336	−1.1246912	−5.0568905
C	−1.0833559	−0.0880831	3.1836942	H	0.2468656	−0.9473984	−3.2825412
H	−1.6393900	−0.7333761	3.8949392	H	1.7014827	−1.7037251	−4.0182884

C	2.4161666	0.4861892	−5.5833504
H	1.7301761	0.2746273	−6.4270405
H	3.2061796	−0.2923249	−5.5991814
H	2.8892378	1.4665649	−5.7891810
C	−0.2964806	−2.9638235	−1.3072984
H	−0.7504339	−2.6324393	−2.2654741
H	−1.1075397	−3.1449812	−0.5707495
C	0.4734548	−4.2455798	−1.5590691
H	−0.2336056	−4.9783290	−2.0070330
H	1.2925700	−4.0736336	−2.2928054
C	1.0438664	−6.1972962	−0.2259838
H	1.8732958	−6.6041064	−0.8485166
H	0.0900673	−6.6439228	−0.5827680
C	1.2477008	−6.5287331	1.2413008
H	0.3554020	−6.2178582	1.8329192
H	1.3914567	−7.6245397	1.3748018
C	2.5609622	−5.6609330	3.0871562
H	2.7270966	−6.6487457	3.5713718
H	1.6444838	−5.2058666	3.5300388
C	3.7723963	−4.7689379	3.2934828
H	3.8773263	−4.5002538	4.3679898
H	4.6983747	−5.3010286	2.9758421
C	4.7843658	−2.8586868	2.2151726
H	5.6291141	−3.5662940	2.0537655
H	5.0419335	−2.1957995	3.0709868
C	4.5487187	−2.0387255	0.9595304
H	3.8188924	−1.2155680	1.1303154
H	5.5094652	−1.5845840	0.6325121
C	4.2418228	−2.4671281	−1.3886565
H	3.8253920	−3.2346360	−2.0673811
H	5.3254520	−2.3525818	−1.6050098
H	3.7283769	−1.4977828	−1.5642449
C	−7.5183673	−1.0802132	1.1200543
C	−6.6196028	−0.6636532	0.1367409
C	−5.2332455	−0.4978752	0.4385932
C	−4.7953121	−0.7568953	1.7702282
C	−5.6976077	−1.1776141	2.7502065
C	−7.0594931	−1.3395624	2.4276861
H	−8.5840904	−1.2018445	0.8764547
H	−6.9908878	−0.4478875	−0.8765939
H	−3.7305307	−0.6205096	2.0134688
H	−5.3481330	−1.3787178	3.7735114
H	−7.7709669	−1.6671217	3.2010643
C	−4.2979767	−0.0416703	−0.5706018
C	−4.7188958	−0.1578516	−2.0198455
O	−4.9983431	0.8046653	−2.7428598
O	−4.7155261	−1.4191891	−2.4386752
C	−5.0813451	−1.6461750	−3.8285314
H	−5.0556481	−2.7400826	−3.9636356
H	−6.0955722	−1.2508753	−4.0258242
H	−4.3583098	−1.1453590	−4.4999593
C	−2.9268347	4.5036671	1.3484481
C	−2.1258380	5.0833125	0.3470951
C	−2.1871869	4.5994597	−0.9725265
C	−3.0419628	3.5361953	−1.2982824
C	−3.8510451	2.9773638	−0.2884279
C	−3.7942850	3.4471081	1.0377436
H	−2.8919562	4.8932340	2.3767423
H	−1.5717964	5.0605761	−1.7593311
H	−3.1066995	3.1595949	−2.3304527
H	−4.4562667	3.0026824	1.7947011
O	−4.7599237	1.9776418	−0.5724606
H	−4.9151874	1.8690190	−1.5795323
H	−1.4617555	5.9250571	0.5924637

TS-O (Cs^+):

Au	−2.9246053	−0.5661496	−0.0645346	H	−2.4639135	2.4068857	2.3027563
P	−0.6024025	−0.3383293	−0.2606948	C	1.7130287	6.0651319	0.6287274
O	0.3523724	0.4492148	0.8328167	C	2.4921369	6.4520124	−0.6448991
O	−0.2722656	0.3723772	−1.6943206	H	3.4648595	5.9235633	−0.7159977
O	0.2469637	−1.7407884	−0.2113574	H	2.7122385	7.5378362	−0.6343802
O	1.7175913	−4.0654028	0.6758369	H	1.9133826	6.2454480	−1.5683509
O	4.5494305	−4.1237415	1.4622191	C	2.5775684	6.4276242	1.8634896
O	6.1731906	−1.8247101	2.1917346	H	2.8229393	7.5089781	1.8548217
O	5.4622124	0.9196615	1.7142500	H	3.5328148	5.8643422	1.8638798
C	0.6381313	1.8373087	0.7809739	H	2.0557932	6.2160270	2.8182347
C	0.2818209	2.6692832	1.8750340	C	0.3945478	6.8807688	0.6637270
C	0.6668285	4.0210411	1.7642946	H	0.6164420	7.9667669	0.6393523
H	0.3990115	4.6989330	2.5838847	H	−0.1942175	6.6832315	1.5818679
C	1.3738132	4.5597411	0.6658637	H	−0.2450031	6.6438450	−0.2104461
C	1.7406169	3.6722691	−0.3576085	C	5.2228497	1.0081611	−3.3646284
H	2.2952628	4.0340621	−1.2328848	C	5.5933258	2.5071873	−3.4995224
C	1.3950563	2.3007216	−0.3187625	H	6.6555567	2.6121384	−3.7995355
C	1.8945859	1.4204062	−1.4205426	H	5.4661492	3.0624814	−2.5488045
C	3.2352285	1.5514310	−1.8455413	H	4.9729460	3.0050056	−4.2716508
H	3.8913364	2.2226682	−1.2720972	C	6.0895762	0.3605535	−2.2519601
C	3.7355665	0.8704167	−2.9719945	H	7.1678368	0.4740999	−2.4874392
C	2.8211633	0.0939702	−3.7122905	H	5.8815477	−0.7280900	−2.1716286
H	3.1749016	−0.3917034	−4.6274334	H	5.9128480	0.8240925	−1.2591822
C	1.4637194	−0.0841845	−3.3552372	C	5.5408476	0.3081569	−4.7016664
C	1.0586965	0.5422955	−2.1518087	H	6.6136986	0.4376924	−4.9459146
C	−0.4400016	2.1536981	3.1475772	H	4.9596739	0.7360952	−5.5433699
C	0.4022434	1.0369307	3.8200014	H	5.3453305	−0.7829360	−4.6631525
H	−0.0957045	0.6921657	4.7493759	C	0.4848971	−0.8171516	−4.3115273
H	1.4049508	1.4176882	4.1023118	C	−0.6161472	0.1845392	−4.7535571
H	0.5328457	0.1587403	3.1599945	H	−1.3110430	−0.3074711	−5.4649260
C	−0.6288864	3.2763373	4.1935008	H	−0.1697809	1.0572924	−5.2708815
H	−1.1325299	2.8600239	5.0882739	H	−1.2089706	0.5571622	−3.8971347
H	−1.2628231	4.1030237	3.8154410	C	−0.1658392	−2.0537420	−3.6437249
H	0.3363459	3.7031710	4.5314810	H	−0.8043312	−2.5821101	−4.3808026
C	−1.8502968	1.6228413	2.7911633	H	−0.8087270	−1.7789617	−2.7874603
H	−2.3790196	1.3005494	3.7120205	H	0.6050315	−2.7720220	−3.2962193
H	−1.8123634	0.7489095	2.1101718	C	1.2017624	−1.3155952	−5.5867835

H	0.4629119	−1.8059466	−6.2509917
H	1.9901533	−2.0630711	−5.3657305
H	1.6579495	−0.4873013	−6.1639548
C	−0.3653358	−3.0391694	0.0226115
H	−1.2399272	−3.1779208	−0.6464415
H	−0.7046085	−3.0960272	1.0778384
C	0.6506178	−4.1267928	−0.2571881
H	0.1149618	−5.1041141	−0.1785990
H	1.0246229	−4.0414509	−1.3060590
C	2.5691957	−5.2124089	0.6012565
H	3.0642697	−5.2675725	−0.3977216
H	1.9667524	−6.1427789	0.7285168
C	3.6170200	−5.1760094	1.6942570
H	3.1264730	−5.0588820	2.6906521
H	4.1401968	−6.1617590	1.6961860
C	5.6636426	−4.1761000	2.3561885
H	6.1477121	−5.1800671	2.3077972
H	5.3282021	−4.0156708	3.4087916
C	6.6951367	−3.1335228	1.9780589
H	7.6009509	−3.2973507	2.6087428
H	7.0034670	−3.2691858	0.9128185
C	7.1430343	−0.7991994	1.9829187
H	7.4203238	−0.7358491	0.9031022
H	8.0760175	−1.0247056	2.5520097
C	6.6097232	0.5330121	2.4676402
H	6.3561007	0.4694953	3.5531457
H	7.4210664	1.2916903	2.3580717
C	5.0185987	2.2311755	2.0442037
H	4.1150239	2.4475119	1.4415213
H	5.7956440	2.9948304	1.8113157
H	4.7579661	2.3177838	3.1242418
C	−7.6525154	−2.3280241	2.2583130
C	−6.9719196	−1.9615449	1.0966428
C	−5.6626505	−1.3920161	1.1670696
C	−5.0783903	−1.1959922	2.4541193
C	−5.7614446	−1.5692482	3.6134750
C	−7.0483362	−2.1355741	3.5177621
H	−8.6601239	−2.7640839	2.1925687
H	−7.4573316	−2.1032007	0.1190580
H	−4.0755339	−0.7461450	2.5168251
H	−5.2989820	−1.4201947	4.6002630
H	−7.5873695	−2.4274026	4.4320313
C	−4.9540828	−0.9971728	−0.0302990
C	−5.4286076	−1.5542637	−1.3546473
O	−5.9774981	−0.8845359	−2.2356137
O	−5.1402982	−2.8459288	−1.4779040
C	−5.5090805	−3.4824621	−2.7334672
H	−5.2133494	−4.5389017	−2.6239022
H	−6.5993328	−3.3949829	−2.8989003
H	−4.9725880	−3.0045056	−3.5749782
C	−4.6839444	4.0920449	0.6527848
C	−4.0752417	4.5602435	−0.5266124
C	−4.0711027	3.7581522	−1.6828808
C	−4.6662174	2.4881535	−1.6669482
C	−5.2834270	2.0367239	−0.4820781
C	−5.2903771	2.8280677	0.6832181
H	−4.7073921	4.7267819	1.5511369
H	−3.6104792	4.1291392	−2.6107114
H	−4.6812224	1.8613052	−2.5717597
H	−5.8008146	2.4542801	1.5822023
O	−5.9319626	0.8218836	−0.4296495
H	−6.0986448	0.4290587	−1.3600861
H	−3.6163005	5.5594872	−0.5498429
Cs	3.4457369	−1.2843262	0.7846025

TS-C (no RA):

Au	−1.9261899	−0.3609763	−0.5796413	H	−0.4790729	−1.8726283	1.3856230
P	0.3705417	−0.4587520	−0.9734754	C	1.7414353	4.1031768	3.7372000
O	1.4277768	−0.5087700	0.2714507	C	2.4425152	5.3054703	3.0719755
O	0.7938272	0.8871200	−1.8132347	H	3.4892989	5.0720293	2.7898523
O	0.9083767	−1.7410788	−1.8049634	H	2.4760757	6.1584974	3.7791633
O	0.5566132	−4.3388224	−0.5179577	H	1.9086213	5.6511323	2.1631557
O	2.4833431	−4.7706006	1.6447740	C	2.5366964	3.7183262	5.0104815
O	3.9050770	−2.6039690	2.9767478	H	2.6032825	4.5839175	5.7020108
O	6.2849829	−2.8882199	1.0814204	H	3.5700748	3.4048954	4.7576768
C	1.4527568	0.6038540	1.1398526	H	2.0583706	2.8861552	5.5648706
C	0.9333188	0.5157859	2.4544657	C	0.3068258	4.5340072	4.1351599
C	1.0628045	1.6866413	3.2361233	H	0.3411309	5.4077782	4.8183463
H	0.6667690	1.6532821	4.2611494	H	−0.2408441	3.7239011	4.6574609
C	1.6649141	2.8814186	2.7951008	H	−0.2844280	4.8235562	3.2420895
C	2.1825270	2.8935599	1.4886829	C	6.0863446	3.1940961	−2.1534167
H	2.6605422	3.7957216	1.0858349	C	6.7013020	3.5162044	−0.7763842
C	2.0943831	1.7656985	0.6442224	H	7.7195547	3.9345837	−0.9076597
C	2.7377374	1.8266816	−0.7028320	H	6.7963792	2.6114226	−0.1420184
C	4.0302123	2.3953341	−0.7982179	H	6.1062387	4.2687642	−0.2199876
H	4.5312682	2.6691082	0.1393011	C	7.0061124	2.1747032	−2.8726400
C	4.6673816	2.5979350	−2.0300398	H	8.0308317	2.5867829	−2.9785393
C	3.9463741	2.2467777	−3.1920287	H	6.6398239	1.9285234	−3.8896340
H	4.4168708	2.4335764	−4.1649850	H	7.0754284	1.2271734	−2.3007232
C	2.6586585	1.6745067	−3.1826726	C	6.0224951	4.5055548	−2.9781377
C	2.0972702	1.4299176	−1.9000089	H	7.0355519	4.9466624	−3.0781379
C	0.2639335	−0.7143803	3.1297924	H	5.3702031	5.2559182	−2.4865042
C	1.0764646	−1.0846605	4.4001827	H	5.6318550	4.3372030	−4.0018881
H	0.5611666	−1.9045063	4.9427460	C	1.9096135	1.4043615	−4.5145326
H	1.1792653	−0.2368696	5.1062989	C	0.5706524	2.1892606	−4.5292977
H	2.0884954	−1.4443943	4.1250806	H	0.0445748	2.0202217	−5.4917884
C	−1.1814817	−0.3200638	3.5314227	H	0.7537963	3.2786380	−4.4314533
H	−1.6831612	−1.1731613	4.0326359	H	−0.1012801	1.8789954	−3.7078657
H	−1.7849695	−0.0519616	2.6382922	C	1.6473674	−0.1101753	−4.6990519
H	−1.2105205	0.5407950	4.2286164	H	1.1275182	−0.2900977	−5.6629635
C	0.1807034	−1.9938493	2.2696150	H	1.0247656	−0.5248862	−3.8881450
H	−0.2759710	−2.7930539	2.8903043	H	2.5999693	−0.6770587	−4.7152986
H	1.1664890	−2.3539319	1.9230187	C	2.7266587	1.8774716	−5.7382578

H	2.1428690	1.6851438	−6.6607533
H	3.6867009	1.3330300	−5.8402986
H	2.9429380	2.9643262	−5.7064819
C	0.0495551	−2.8089491	−2.2845572
H	−0.0098246	−2.7192298	−3.3885693
H	−0.9718524	−2.6980418	−1.8577918
C	0.6296993	−4.1565825	−1.9099728
H	0.0441530	−4.9335096	−2.4671923
H	1.6847131	−4.2236108	−2.2747192
C	1.0769397	−5.5929113	−0.0954350
H	2.0330710	−5.8172884	−0.6261712
H	0.3583605	−6.4160318	−0.3333318
C	1.3550497	−5.5780494	1.3957667
H	0.4537590	−5.2094742	1.9473559
H	1.5322156	−6.6329205	1.7280238
C	2.9276129	−4.8001463	2.9901279
H	3.1415151	−5.8507290	3.3120902
H	2.1459675	−4.3966137	3.6803110
C	4.2032511	−3.9903764	3.1145333
H	4.6636283	−4.1938174	4.1137964
H	4.9222989	−4.3160786	2.3330616
C	5.0380965	−1.7631639	2.8192719
H	5.8603737	−2.0585641	3.5148064
H	4.7058083	−0.7430165	3.1050170
C	5.5809063	−1.7003315	1.3950270
H	4.7290475	−1.5406232	0.6883189
H	6.2558900	−0.8087597	1.3068984
C	6.7589292	−2.9186313	−0.2471733
H	7.2918023	−3.8779537	−0.3934984
H	7.4708375	−2.0825742	−0.4553759
H	5.9284626	−2.8525497	−0.9917677
C	−6.4704803	1.4561807	2.0002015
C	−5.9143810	0.4825904	1.1641853
C	−4.6304242	0.6692968	0.5711039
C	−3.9617221	1.9040362	0.8165830
C	−4.5218140	2.8793944	1.6479281
C	−5.7765099	2.6559280	2.2457000
H	−7.4518254	1.2822940	2.4663321
H	−6.4625919	−0.4535647	0.9871878
H	−2.9710881	2.0653199	0.3625653
H	−3.9750205	3.8141221	1.8426276
H	−6.2153718	3.4189679	2.9066989
C	−3.9913117	−0.3639913	−0.2388732
C	−4.4101617	−1.8136610	−0.0942252
O	−4.5936272	−2.6183881	−0.9941240
O	−4.4356086	−2.1412705	1.2203747
C	−4.5989701	−3.5457603	1.5154798
H	−4.6241701	−3.6170966	2.6163314
H	−5.5385957	−3.9305077	1.0742447
H	−3.7484938	−4.1272540	1.1086247
C	−6.1081377	−0.2262003	−2.1004550
C	−4.7015435	−0.0515651	−2.2991569
C	−4.2085675	1.2679888	−2.5567992
C	−5.0344851	2.3696519	−2.4125457
C	−6.4081347	2.1782641	−2.0781227
C	−6.9464522	0.8672470	−1.9546579
H	−6.5031633	−1.2492703	−2.0209461
H	−3.1499048	1.4073476	−2.8243693
H	−4.6493349	3.3899337	−2.5701287
H	−8.0231890	0.7593133	−1.7612428
O	−7.2517393	3.2008367	−1.8998272
H	−6.7888080	4.0544225	−2.0240934
H	−4.1167347	−0.9284623	−2.6082318

TS-C (Li^+):

Au	−1.8775878	−0.3350533	−0.2917048	H	1.2932800	−1.9794825	2.6715801
P	0.4367566	−0.3446396	−0.5561857	H	−0.3223579	−1.6329600	1.9570185
O	1.4563773	−0.3314966	0.7305615	C	1.8871159	4.5620742	3.7860261
O	0.8553401	0.9708583	−1.4225972	C	2.6400101	5.6749568	3.0285783
O	1.1117081	−1.6721808	−1.2622060	H	3.6836386	5.3847577	2.7902739
O	1.5690399	−4.4467525	−0.9570845	H	2.6901378	6.5865306	3.6562510
O	2.8039663	−5.5097404	1.1236330	H	2.1325876	5.9561174	2.0830904
O	3.7546502	−3.3267632	2.2181094	C	2.6462741	4.2663187	5.1048141
O	4.4424332	−2.4260057	−0.1856678	H	2.7314874	5.1898427	5.7128075
Li	2.9750819	−3.6463544	0.3461447	H	3.6725958	3.8962502	4.9047182
C	1.5165173	0.8583701	1.5053211	H	2.1274645	3.5091982	5.7266671
C	0.9854026	0.8998886	2.8169025	C	0.4593977	5.0702471	4.1127148
C	1.1390343	2.1323256	3.4918192	H	0.5117835	6.0000553	4.7148951
H	0.7249460	2.2072330	4.5070874	H	−0.1243301	4.3305294	4.6970851
C	1.7858137	3.2640386	2.9567451	H	−0.1065437	5.2973031	3.1860830
C	2.3236065	3.1418919	1.6638460	C	6.2727717	2.9233863	−1.9813811
H	2.8373869	3.9906725	1.1939637	C	6.9098295	3.3285915	−0.6366276
C	2.2051245	1.9493476	0.9185024	H	7.9432629	3.6909801	−0.8051973
C	2.8600178	1.8722522	−0.4235486	H	6.9739030	2.4755855	0.0704454
C	4.1800431	2.3548201	−0.5605451	H	6.3534236	4.1497617	−0.1411300
H	4.6937663	2.6978705	0.3473595	C	7.1487409	1.8187577	−2.6251074
C	4.8308852	2.3994035	−1.8059817	H	8.1857010	2.1847513	−2.7680538
C	4.0945036	1.9664450	−2.9265141	H	6.7696422	1.5079051	−3.6193226
H	4.5786620	2.0175913	−3.9120382	H	7.1956840	0.9170452	−1.9799888
C	2.7649170	1.4863897	−2.8794659	C	6.2489097	4.1676788	−2.9071466
C	2.1910700	1.4141266	−1.5867091	H	7.2759737	4.5624429	−3.0447478
C	0.2625368	−0.2423175	3.5863930	H	5.6276049	4.9777368	−2.4744835
C	0.9520508	−0.4364041	4.9641248	H	5.8472919	3.9330075	−3.9134698
H	0.4402612	−1.2394535	5.5324498	C	2.0986848	1.1232170	−4.2387661
H	0.9227658	0.4747732	5.5907001	C	0.5923491	0.7839539	−4.1760564
H	2.0154511	−0.7273366	4.8426789	H	0.2238103	0.6193397	−5.2088877
C	−1.2154990	0.1737225	3.8037479	H	−0.0036766	1.6024114	−3.7290981
H	−1.7569899	−0.6072694	4.3761434	H	0.3926821	−0.1410875	−3.6029605
H	−1.7377710	0.3066102	2.8329297	C	2.8380049	−0.0999249	−4.8406754
H	−1.3025600	1.1230938	4.3674495	H	2.4083194	−0.3652981	−5.8285223
C	0.2680775	−1.6250982	2.8947447	H	2.7441597	−0.9853318	−4.1774548
H	−0.2056453	−2.3578373	3.5799682	H	3.9184174	0.0958578	−4.9900743

C	2.2354498	2.3337699	−5.2023605
H	1.7658647	2.0940606	−6.1781186
H	3.2888135	2.6045347	−5.4065183
H	1.7298868	3.2306023	−4.7910985
C	0.3124403	−2.6501385	−1.9693863
H	−0.0116440	−2.2441022	−2.9515490
H	−0.5898443	−2.9087126	−1.3747436
C	1.1582690	−3.8851989	−2.2095336
H	0.5369919	−4.6152401	−2.7741363
H	2.0459129	−3.6412875	−2.8362968
C	1.7211389	−5.8793388	−0.9422434
H	2.6488772	−6.1752357	−1.4836282
H	0.8564807	−6.3702766	−1.4400645
C	1.7805627	−6.2987538	0.5150485
H	0.8021406	−6.1021838	1.0118004
H	2.0028403	−7.3865317	0.5972258
C	2.7989120	−5.4793142	2.5561494
H	2.9758494	−6.4911391	2.9842271
H	1.8103307	−5.1151134	2.9215523
C	3.9188214	−4.5398340	2.9665551
H	3.8850387	−4.3501238	4.0622617
H	4.9065554	−4.9936706	2.7221931
C	4.9317386	−2.5085875	2.1450760
H	5.8240509	−3.1635220	2.0223794
H	5.0637560	−1.9081762	3.0725989
C	4.7867264	−1.5989536	0.9392887
H	3.9997137	−0.8273807	1.0916490
H	5.7531916	−1.0787569	0.7583405
C	4.7283725	−1.8210948	−1.4517647
H	4.4361141	−2.5436625	−2.2362013
H	5.8162449	−1.6156910	−1.5474292
H	4.1630183	−0.8746117	−1.5886550
C	−6.6646854	1.5574039	1.7558071
C	−6.0204616	0.5231948	1.0681218
C	−4.6850754	0.6804493	0.5865962
C	−4.0591937	1.9482046	0.7808128
C	−4.7054283	2.9805888	1.4656075
C	−6.0102561	2.7860258	1.9599785
H	−7.6853873	1.4072296	2.1378819
H	−6.5398013	−0.4341848	0.9272151
H	−3.0340569	2.0939498	0.4031791
H	−4.1921111	3.9406887	1.6249086
H	−6.5188740	3.5956401	2.5054536
C	−3.9580670	−0.4001390	−0.0703119
C	−4.3205230	−1.8534652	0.1746786
O	−4.2383934	−2.7599310	−0.6411026
O	−4.6373524	−2.0462600	1.4759818
C	−4.8496329	−3.4181069	1.8787787
H	−5.0823784	−3.3792789	2.9565253
H	−5.6902624	−3.8636084	1.3126045
H	−3.9394750	−4.0220604	1.6960180
C	−5.9474948	−0.6210704	−2.0741062
C	−4.5513886	−0.3219266	−2.1967485
C	−4.1696072	1.0171172	−2.5356815
C	−5.1023088	2.0388895	−2.5356014
C	−6.4733453	1.7372743	−2.2712591
C	−6.8926408	0.3898547	−2.0737645
H	−6.2529214	−1.6690988	−1.9419097
H	−3.1136096	1.2408089	−2.7515227
H	−4.8067907	3.0766603	−2.7582381
H	−7.9662551	0.1904451	−1.9462590
O	−7.4204818	2.6745834	−2.2309209
H	−7.0469487	3.5632528	−2.4051585
H	−3.8677954	−1.1570032	−2.4015098

TS-C (Cs^+):

Au	18.6205325	10.1089021	5.9054331	H	20.1548427	10.1432540	8.3576632
P	20.7050834	11.0992846	5.6105841	C	19.0123491	16.8209078	8.6321511
O	21.4312851	11.8740150	6.8758265	C	19.2561493	17.9824119	7.6470754
O	20.6240315	12.2303103	4.4325910	H	20.3341987	18.2194070	7.5404574
O	21.9850079	10.1657392	5.1994915	H	18.7558524	18.8987767	8.0179414
O	24.4722855	8.6930891	5.3280435	H	18.8450780	17.7703018	6.6387838
O	27.1515721	9.8484730	5.5580176	C	19.5782576	17.2250083	10.0176376
O	27.6202292	12.2256661	7.1406432	H	19.1022935	18.1636565	10.3668140
O	25.6001980	14.1007297	7.9881930	H	20.6727510	17.3976002	9.9696906
C	20.8111603	13.0566914	7.3565493	H	19.3883911	16.4535109	10.7906420
C	20.1467098	13.0934496	8.6048446	C	17.4835930	16.5862875	8.7446646
C	19.5935513	14.3482950	8.9516890	H	16.9777079	17.5127012	9.0852354
H	19.0568029	14.4151965	9.9088447	H	17.2369804	15.7870307	9.4721257
C	19.6861806	15.5131070	8.1634578	H	17.0498460	16.3024689	7.7638219
C	20.4082606	15.4181764	6.9598296	C	24.5875600	16.3800509	3.6922745
H	20.5248944	16.2945800	6.3090902	C	24.8301070	17.2154833	4.9662732
C	20.9801423	14.1999028	6.5386485	H	25.6244942	17.9641460	4.7772756
C	21.7979053	14.1741402	5.2863139	H	25.1608362	16.5852259	5.8178012
C	22.7734320	15.1829499	5.0990074	H	23.9258823	17.7768757	5.2776938
H	22.9369223	15.8915605	5.9216052	C	25.9259775	15.7131631	3.2854675
C	23.5142694	15.2924798	3.9113603	H	26.7021188	16.4849808	3.1087839
C	23.2036570	14.3836005	2.8737264	H	25.8366579	15.1193732	2.3538270
H	23.7290393	14.4945114	1.9172093	H	26.2994941	15.0422227	4.0880939
C	22.2390444	13.3580875	2.9755204	C	24.1189450	17.3280374	2.5575496
C	21.5972334	13.2419435	4.2395921	H	24.8728029	18.1228520	2.3864544
C	20.0034773	11.9437422	9.6416661	H	23.1591022	17.8189453	2.8167914
C	20.6846859	12.3966719	10.9619686	H	23.9774736	16.7915563	1.5980398
H	20.5803208	11.6072493	11.7340058	C	21.8550720	12.5135865	1.7301551
H	20.2385198	13.3227753	11.3725468	C	20.3453393	12.7158648	1.4303308
H	21.7678463	12.5816264	10.8100574	H	20.0637675	12.1469411	0.5205522
C	18.4970071	11.6819124	9.9001355	H	20.1203716	13.7847057	1.2402916
H	18.3733030	10.8812285	10.6577346	H	19.7049646	12.3709380	2.2634824
H	17.9843600	11.3528977	8.9722379	C	22.1561729	11.0102424	1.9445475
H	17.9700522	12.5789000	10.2796794	H	21.9017918	10.4432776	1.0258164
C	20.6459194	10.5960391	9.2439763	H	21.5789876	10.5782246	2.7801252
H	20.5157846	9.8834290	10.0832995	H	23.2354337	10.8460665	2.1469463
H	21.7305066	10.6837916	9.0421605	C	22.6384631	12.9600755	0.4749573

H	22.3137467	12.3498431	−0.3907110
H	23.7325829	12.8141294	0.5821982
H	22.4509388	14.0207245	0.2150837
C	22.0756758	8.7474128	5.5141602
H	21.1498468	8.2269365	5.1889742
H	22.1944149	8.6213049	6.6108326
C	23.2694040	8.1642091	4.7883715
H	23.2345531	7.0544511	4.9145250
H	23.1872192	8.3771210	3.6957526
C	25.6382066	8.1622876	4.6911744
H	25.7443756	8.5799557	3.6614923
H	25.5499373	7.0550000	4.5935077
C	26.8789598	8.4507347	5.5110644
H	26.7522945	8.0435570	6.5430520
H	27.7317538	7.9043047	5.0417654
C	28.3745000	10.1263562	6.2417970
H	29.2326224	9.6551115	5.7060051
H	28.3453212	9.6982561	7.2719803
C	28.6185568	11.6192627	6.3240281
H	29.6319661	11.7783970	6.7626790
H	28.6279218	12.0720060	5.3019397
C	27.9052654	13.5794107	7.4840151
H	27.8672524	14.2349836	6.5794012
H	28.9330667	13.6638081	7.9093400
C	26.9199236	14.0661885	8.5265434
H	26.9580662	13.3988529	9.4208753
H	27.2315112	15.0859947	8.8551954
C	24.6529318	14.6208796	8.9144135
H	23.6598056	14.6074872	8.4248116
H	24.8953035	15.6697525	9.2009382
H	24.6065003	14.0077426	9.8440683
C	13.4674042	10.0355370	7.8918263
C	14.5172148	9.2858948	7.3516373
C	15.6368634	9.9254042	6.7355748
C	15.6099454	11.3496345	6.6352374
C	14.5568196	12.0961747	7.1703899
C	13.4844495	11.4404969	7.8062589
H	12.6271711	9.5247139	8.3849878
H	14.4958697	8.1910087	7.4356047
H	16.4573014	11.8593255	6.1487418
H	14.5702476	13.1941102	7.1023585
H	12.6575690	12.0265409	8.2358279
C	16.7816524	9.1776246	6.2370104
C	17.0740107	7.7714367	6.7301168
O	17.4886439	6.8429263	6.0551388
O	16.9264236	7.7151138	8.0745220
C	17.3320126	6.4767088	8.7033915
H	17.1599116	6.6216143	9.7834490
H	16.7280055	5.6317167	8.3205001
H	18.4007262	6.2696181	8.5003649
C	15.0906163	7.8209366	4.3933464
C	16.2471439	8.6186029	4.1213023
C	16.0622369	9.9172442	3.5493690
C	14.7974004	10.4712754	3.4504228
C	13.6624890	9.7053102	3.8557865
C	13.8188793	8.3605606	4.2986501
H	15.2312421	6.7796907	4.7175224
H	16.9395032	10.4967011	3.2233921
H	14.6524757	11.4842473	3.0419676
H	12.9157076	7.7797802	4.5341436
O	12.4182175	10.1852031	3.8112569
H	12.4058421	11.1011073	3.4645571
H	17.2150697	8.1069456	4.0321368
Cs	24.8060580	11.8962620	5.8859450

INT-O (no RA):

Au	19.6961637	10.0256595	5.1959801	H	20.2526062	11.0501030	8.4574584
P	21.4362749	11.4649752	4.6311951	C	19.4910878	16.8808829	8.1886908
O	22.2009537	12.4401797	5.6944934	C	19.0445434	17.9639288	7.1854573
O	20.7479658	12.4733499	3.5420950	H	19.9058409	18.4254125	6.6619690
O	22.7839192	10.8208645	3.9944398	H	18.5124304	18.7759757	7.7205923
O	23.1717757	8.5199077	5.8657060	H	18.3490139	17.5624206	6.4201763
O	23.7458694	8.3769087	8.9684968	C	20.4371932	17.5370634	9.2269151
O	24.3809912	10.1466594	11.2586281	H	19.9251209	18.3795200	9.7359851
O	26.1332646	12.4770415	10.7861941	H	21.3502829	17.9366187	8.7404483
C	21.5258125	13.5148018	6.3116460	H	20.7573832	16.8202055	10.0091497
C	21.3713514	13.5123240	7.7220258	C	18.2326130	16.3365945	8.9107543
C	20.7036842	14.6280565	8.2644946	H	17.6965452	17.1598349	9.4263983
H	20.5549506	14.6575281	9.3512140	H	18.4866913	15.5743639	9.6739432
C	20.2272778	15.7136619	7.4955351	H	17.5285961	15.8729705	8.1893535
C	20.4798750	15.6872008	6.1156452	C	22.9335478	17.5299082	1.8002164
H	20.1567336	16.5170676	5.4738643	C	21.9804153	18.6829439	2.2065187
C	21.1475097	14.6037649	5.4967526	H	22.4057678	19.6607498	1.9002952
C	21.5093013	14.7186758	4.0511677	H	21.8167080	18.7211512	3.3023125
C	22.0390542	15.9439017	3.5942132	H	20.9900108	18.5743377	1.7192917
H	22.2452117	16.7205217	4.3450306	C	24.3013811	17.7163579	2.5052974
C	22.3203616	16.1822558	2.2379890	H	24.7590926	18.6834346	2.2103241
C	22.0049735	15.1567243	1.3262138	H	25.0075746	16.9068841	2.2296246
H	22.1778774	15.3378588	0.2606969	H	24.2027602	17.7173597	3.6092734
C	21.4723726	13.9033102	1.7027498	C	23.1584913	17.6001285	0.2759256
C	21.2905477	13.7002138	3.0925088	H	23.6040561	18.5790691	0.0080721
C	21.9774999	12.4163200	8.6323517	H	22.2100407	17.5062592	−0.2907685
C	23.5147980	12.3645667	8.4240989	H	23.8552659	16.8134942	−0.0785447
H	23.9727974	11.6359488	9.1221248	C	21.0486196	12.8735995	0.6218126
H	23.9653463	13.3572708	8.6266208	C	19.5275054	12.5935568	0.7485701
H	23.7820277	12.0718357	7.3923448	H	19.2090747	11.8728817	−0.0333732
C	21.7208211	12.7082233	10.1275712	H	18.9437779	13.5252573	0.6056961
H	22.2015331	11.9120940	10.7294347	H	19.2609452	12.1728049	1.7359938
H	20.6401194	12.7208340	10.3778005	C	21.8454453	11.5533695	0.7614485
H	22.1624714	13.6740698	10.4462139	H	21.5723342	10.8590118	−0.0599007
C	21.3550862	11.0320009	8.3319043	H	21.6329475	11.0442627	1.7173718
H	21.7747127	10.2802342	9.0287899	H	22.9373656	11.7382399	0.7042192
H	21.5957765	10.6721006	7.3144279	C	21.3017336	13.4064651	−0.8066163

H	20.9648451	12.6486617	−1.5420258
H	22.3759919	13.5985172	−1.0019556
H	20.7382081	14.3380212	−1.0137738
C	22.9298664	9.4268019	3.6483711
H	23.3786889	9.4049288	2.6355541
H	21.9330431	8.9336835	3.6074125
C	23.8283012	8.6948383	4.6259106
H	24.0794582	7.7059673	4.1631816
H	24.7900950	9.2497066	4.7472326
C	23.8478459	7.5781745	6.6956852
H	24.9126014	7.8721048	6.8506374
H	23.8472877	6.5787117	6.1937573
C	23.1884497	7.4501391	8.0604171
H	22.0824391	7.5803116	7.9468074
H	23.3526094	6.4072508	8.4320925
C	23.3388414	8.1702872	10.3121627
H	23.2479428	7.0765558	10.5241487
H	22.3368066	8.6282940	10.5037818
C	24.3618288	8.7344046	11.2811198
H	24.1082500	8.3579875	12.3054464
H	25.3679890	8.3216271	11.0209106
C	25.3502706	10.6728438	12.1540464
H	26.3483168	10.2079262	11.9644684
H	25.0699414	10.4393273	13.2118891
C	25.4828844	12.1753441	12.0011692
H	24.4734951	12.6561377	12.0541041
H	26.0698228	12.5584895	12.8749364
C	26.3889947	13.8545488	10.6261719
H	26.9099161	13.9897019	9.6586837
H	27.0405033	14.2574585	11.4402117
H	25.4505347	14.4610111	10.6127402
C	15.9481983	8.0994204	8.7615594
C	16.2538598	8.4006639	7.4253268
C	17.5988846	8.5302690	7.0155520
C	18.6267406	8.3548421	7.9646291
C	18.3155699	8.0402711	9.2969804
C	16.9762339	7.9141747	9.7007021
H	14.8955255	8.0058344	9.0684052
H	15.4452578	8.5393731	6.6935566
H	19.6786480	8.4751101	7.6616179
H	19.1278415	7.9073092	10.0273711
H	16.7332890	7.6791941	10.7478833
C	17.9044528	8.8001938	5.5532773
C	18.3265435	7.6426998	4.7643655
O	17.9051040	7.5163411	3.5307573
O	19.0820893	6.7110486	5.2688658
C	19.4895196	5.5944347	4.4322454
H	20.0624059	4.9303462	5.0996582
H	18.5992147	5.0747905	4.0319006
H	20.1238598	5.9566216	3.6010526
C	16.3959539	12.8677483	5.8885647
C	15.5001493	13.3157385	4.9066595
C	15.0564517	12.4238009	3.9141119
C	15.5123063	11.0979650	3.8966521
C	16.4168084	10.6665689	4.8829042
C	16.8577961	11.5381464	5.8924955
H	16.7433301	13.5530437	6.6758578
H	14.3496481	12.7607012	3.1410157
H	15.1709922	10.3910374	3.1257336
H	17.5260366	11.1913682	6.6924343
O	16.8054612	9.3280553	4.7936185
H	15.1421039	14.3554563	4.9159953
H	17.2443805	8.2709523	3.4388743

INT-O (Li^+):

Au	19.1027494	9.8960989	5.4957534	H	20.1040916	10.4501754	8.1379554
P	21.0521311	11.1753986	5.5660856	H	18.5465745	11.0864987	8.7623179
O	21.5543788	12.0453429	6.8657710	C	18.9345270	16.9451345	8.4659722
O	20.8516062	12.2585668	4.3660100	C	19.0332743	18.0586170	7.4037426
O	22.4992651	10.4079205	5.3652152	H	20.0832526	18.3555808	7.2060089
O	24.6034759	8.7015670	6.3110090	H	18.5009679	18.9632399	7.7587952
O	26.1002199	9.1215417	8.4607336	H	18.5692525	17.7605658	6.4412571
O	25.4188469	11.6038922	8.9307666	C	19.5835967	17.4577993	9.7780118
O	25.5541361	12.1417299	6.3381811	H	19.0830805	18.3880353	10.1153093
Li	25.1650183	10.4506062	7.2733700	H	20.6592932	17.6849954	9.6319370
C	20.8829640	13.2327825	7.2605695	H	19.5002745	16.7212796	10.6025273
C	20.2659117	13.2931855	8.5384520	C	17.4359009	16.6375691	8.7160420
C	19.6564508	14.5210596	8.8651424	H	16.9057609	17.5543245	9.0456008
H	19.1607957	14.6049576	9.8395576	H	17.2907102	15.8717687	9.5044228
C	19.6500299	15.6526821	8.0191342	H	16.9426042	16.2749929	7.7908564
C	20.3292600	15.5434558	6.7968291	C	24.1226537	16.9280759	3.4121633
H	20.3653762	16.3965084	6.1073605	C	23.2252304	18.1887745	3.5137511
C	20.9733624	14.3480630	6.3972823	H	23.8278357	19.1038944	3.3433584
C	21.7683380	14.3701118	5.1296425	H	22.7517083	18.2839489	4.5114972
C	22.5812048	15.4953795	4.8683924	H	22.4167778	18.1677659	2.7549503
H	22.6719288	16.2544844	5.6594942	C	25.2302687	16.9960617	4.4939856
C	23.2532537	15.6730905	3.6453652	H	25.8559608	17.8995783	4.3483958
C	23.0552597	14.6906164	2.6550459	H	25.8997294	16.1124497	4.4362036
H	23.5306467	14.8332275	1.6794731	H	24.8117764	17.0469747	5.5197440
C	22.2596084	13.5358228	2.8360307	C	24.7980377	16.9200158	2.0252134
C	21.6769020	13.3832063	4.1182601	H	25.4220760	17.8279110	1.9072507
C	20.3110209	12.1354695	9.5702623	H	24.0579732	16.9262643	1.1994394
C	21.7883722	11.8118248	9.9145226	H	25.4642483	16.0437209	1.8881076
H	21.8320880	10.9927286	10.6628130	C	21.9777840	12.5829947	1.6431818
H	22.2899197	12.6958282	10.3574580	C	20.4560217	12.5967336	1.3367115
H	22.3674725	11.4982967	9.0259294	H	20.2398893	11.9404724	0.4686040
C	19.6043405	12.5172250	10.8908296	H	20.1174514	13.6194727	1.0757914
H	19.6752286	11.6696205	11.6015086	H	19.8519756	12.2447262	2.1944052
H	18.5269750	12.7333153	10.7461640	C	22.4432114	11.1375809	1.9451313
H	20.0730025	13.3937835	11.3800146	H	22.2886815	10.4981557	1.0522744
C	19.6006370	10.8708249	9.0298732	H	21.8756595	10.6897190	2.7802651
H	19.5902198	10.0782740	9.8063632	H	23.5239811	11.1092572	2.1957669

C	22.7145881	13.0357579	0.3622723
H	22.4726358	12.3369712	−0.4627465
H	23.8169313	13.0321841	0.4825114
H	22.4031824	14.0464577	0.0337149
C	22.5814078	9.0106387	5.0098690
H	22.1599034	8.8416557	3.9955613
H	22.0125335	8.3997964	5.7427431
C	24.0382658	8.5883086	4.9984933
H	24.0780576	7.5304863	4.6564874
H	24.6166518	9.2003691	4.2708425
C	25.5886964	7.7022203	6.6439237
H	26.5407535	7.9031565	6.1011393
H	25.2317724	6.6895603	6.3543136
C	25.7938506	7.7626051	8.1467072
H	24.8635647	7.4492637	8.6756454
H	26.6170535	7.0777990	8.4515002
C	25.9917755	9.4856033	9.8435010
H	26.7322887	8.9365773	10.4661968
H	24.9706167	9.2388792	10.2171739
C	26.2569407	10.9792587	9.9131747
H	26.0422977	11.3627416	10.9352751
H	27.3251316	11.1913883	9.6783928
C	25.8051777	12.9377529	8.5704765
H	26.9162601	12.9970449	8.5177608
H	25.4509385	13.6776848	9.3224831
C	25.2047560	13.2335936	7.2077122
H	24.0970983	13.3377845	7.2535917
H	25.6237964	14.1882981	6.8221741
C	25.5237889	12.4769997	4.9460470
H	25.8206382	11.5720063	4.3835222
H	26.2534342	13.2852826	4.7251743
H	24.5106827	12.8001587	4.6250275
C	14.5378506	8.0165056	7.8809930
C	15.1538645	8.4366466	6.6913422
C	16.5615462	8.4415211	6.5847330
C	17.3371999	8.0159281	7.6828332
C	16.7155529	7.5816537	8.8645728
C	15.3145413	7.5838045	8.9685360
H	13.4399277	8.0226329	7.9535299
H	14.5390241	8.7656246	5.8411581
H	18.4365854	8.0258405	7.6141542
H	17.3310132	7.2486554	9.7138105
H	14.8284426	7.2531137	9.8985024
C	17.2047111	8.8412877	5.2617950
C	17.5928719	7.6969792	4.4136126
O	17.3396516	7.7384698	3.1368586
O	18.1510240	6.6400378	4.9159474
C	18.4511490	5.5058853	4.0471755
H	18.8576370	4.7324972	4.7186026
H	17.5234745	5.1532395	3.5597552
H	19.1946597	5.8024028	3.2839893
C	16.0947065	13.0244160	5.7974608
C	15.6139036	13.7097825	4.6719831
C	15.3877454	13.0079343	3.4746356
C	15.6506074	11.6324764	3.3977388
C	16.1371120	10.9619910	4.5327148
C	16.3542621	11.6415623	5.7431020
H	16.2569107	13.5611121	6.7440029
H	15.0024051	13.5332691	2.5880359
H	15.4727118	11.0745371	2.4662635
H	16.6702316	11.1024499	6.6466016
O	16.3450050	9.5872995	4.3820874
H	15.4024363	14.7874534	4.7279696
H	16.8036159	8.5925352	3.0439462

INT-O (Cs^+):

Au	18.5469537	9.7553183	5.5854888	H	17.7786801	11.3588712	8.7830329
P	20.5807442	10.8841792	5.7297410	C	19.0563327	17.0159717	8.2890969
O	21.0804139	11.7453982	7.0494651	C	19.4034557	18.0639998	7.2121179
O	20.5720333	11.9547171	4.5027014	H	20.4981528	18.2084736	7.1066572
O	21.9675985	10.0263906	5.5496781	H	18.9716070	19.0454737	7.4916784
O	24.4931187	8.6469130	5.8775225	H	18.9906946	17.7952975	6.2182675
O	27.1129424	9.9006453	6.2828189	C	19.6410469	17.4913937	9.6441652
O	27.4400076	12.3444216	7.8008847	H	19.2387880	18.4912385	9.9049498
O	25.3379076	14.2118978	8.4542847	H	20.7462228	17.5728273	9.5982390
C	20.5539408	13.0239524	7.3662451	H	19.3839165	16.8057760	10.4760713
C	19.8647498	13.2240531	8.5911973	C	17.5128974	16.9162012	8.3982121
C	19.4146821	14.5388507	8.8281427	H	17.0812732	17.9066750	8.6484655
H	18.8657022	14.7320274	9.7577923	H	17.1954211	16.2077177	9.1892983
C	19.6269081	15.6232087	7.9475946	H	17.0647744	16.5831263	7.4398788
C	20.3749499	15.3706823	6.7872752	C	24.6441451	15.9831469	3.7128893
H	20.5848730	16.1798015	6.0759622	C	24.0606245	17.3950946	3.9725924
C	20.8659717	14.0798071	6.4801516	H	24.8434369	18.1652562	3.8200522
C	21.7494487	13.9280246	5.2806243	H	23.6837660	17.5145031	5.0083102
C	22.7566819	14.8961394	5.0623525	H	23.2268911	17.6181033	3.2768673
H	22.9094620	15.6589273	5.8394026	C	25.7759213	15.6985589	4.7348999
C	23.5393830	14.9182387	3.8924791	H	26.5664158	16.4741724	4.6642069
C	23.2499411	13.9513656	2.9080005	H	26.2569539	14.7180605	4.5286398
H	23.8061832	13.9865671	1.9660426	H	25.4035007	15.6885526	5.7797647
C	22.2618584	12.9487683	3.0480574	C	25.2488409	15.9622904	2.2937720
C	21.5734080	12.9321345	4.2872605	H	26.0229043	16.7502707	2.2050968
C	19.6595113	12.1130119	9.6541493	H	24.4860594	16.1626722	1.5147532
C	21.0361189	11.5485555	10.0958103	H	25.7406742	14.9964223	2.0584412
H	20.8947955	10.7737361	10.8768246	C	21.9040908	12.0272174	1.8506629
H	21.6676662	12.3492038	10.5321645	C	20.4163670	12.2528296	1.4683752
H	21.5879261	11.0862219	9.2550834	H	20.1567994	11.6278863	0.5892137
C	18.9579598	12.6544107	10.9208493	H	20.2369736	13.3109289	1.1905302
H	18.8503123	11.8339832	11.6580213	H	19.7251770	11.9919877	2.2910999
H	17.9397590	13.0364561	10.7081577	C	22.1462467	10.5350199	2.1845107
H	19.5387832	13.4605408	11.4116428	H	21.9228236	9.9131304	1.2937819
C	18.7709561	10.9756552	9.0951991	H	21.5091510	10.1787339	3.0129402
H	18.6024410	10.2043812	9.8742559	H	23.2065843	10.3561318	2.4593547
H	19.2314108	10.4688839	8.2240441	C	22.7566446	12.3570222	0.6044589

H	22.4523484	11.6933114	−0.2287088
H	23.8400955	12.1913109	0.7734893
H	22.6124986	13.3996846	0.2587351
C	22.0886504	8.6165479	5.8724020
H	21.2115292	8.0608928	5.4762909
H	22.1217379	8.4940228	6.9757192
C	23.3573966	8.0749299	5.2471426
H	23.3530288	6.9644474	5.3757278
H	23.3545889	8.2832125	4.1504595
C	25.7229810	8.1514072	5.3392029
H	25.8922569	8.5603111	4.3143280
H	25.6807277	7.0404558	5.2520250
C	26.8873547	8.4947198	6.2451025
H	26.6962166	8.1011192	7.2725907
H	27.7891971	7.9678586	5.8511127
C	28.2864037	10.2279945	7.0310365
H	29.1842327	9.7560178	6.5659254
H	28.2009378	9.8357812	8.0723012
C	28.4969477	11.7274162	7.0708487
H	29.4787626	11.9233894	7.5633878
H	28.5606860	12.1408656	6.0342921
C	27.6782963	13.7210213	8.0895675
H	27.6739844	14.3277438	7.1518532
H	28.6803529	13.8491724	8.5629435
C	26.6319910	14.2392203	9.0547971
H	26.6400979	13.6250415	9.9868929
H	26.9057200	15.2831946	9.3384814
C	24.3442353	14.7902928	9.2943552
H	23.3755806	14.7351113	8.7611861
H	24.5696194	15.8588565	9.5142319
H	24.2566855	14.2467610	10.2634786
C	13.6084076	8.4921786	7.6095444
C	14.3833998	8.7359541	6.4643968
C	15.7890932	8.6186635	6.5214990
C	16.4015913	8.2508759	7.7374883
C	15.6204821	7.9926798	8.8754615
C	14.2222126	8.1158959	8.8157842
H	12.5140292	8.5915237	7.5535562
H	13.8951398	9.0205122	5.5212835
H	17.4984150	8.1654931	7.7972425
H	16.1090264	7.7022050	9.8176942
H	13.6113309	7.9229458	9.7101779
C	16.6044571	8.8205045	5.2490720
C	16.9788100	7.5581511	4.5774341
O	16.8603753	7.4678582	3.2840562
O	17.3930239	6.5326274	5.2512819
C	17.6853260	5.2826479	4.5547058
H	17.9565469	4.5703470	5.3503366
H	16.7856311	4.9403153	4.0108495
H	18.5246479	5.4329004	3.8502445
C	15.7627343	13.0988520	5.2363646
C	15.4537768	13.6900888	4.0023779
C	15.3039857	12.8805072	2.8621048
C	15.4720217	11.4908640	2.9508662
C	15.7882120	10.9146505	4.1932878
C	15.9269219	11.7045780	5.3475280
H	15.8600675	13.7206835	6.1385699
H	15.0524738	13.3318252	1.8907598
H	15.3508934	10.8497661	2.0649881
H	16.1061819	11.2459401	6.3297057
O	15.9115697	9.5219195	4.2013798
H	15.3157665	14.7785142	3.9284199
H	16.4117683	8.3415772	3.0386331
Cs	24.6771208	11.8567820	6.4797141

INT-C (no RA):

Au	19.3175335	10.1982483	5.7677838	H	20.0751851	11.0053914	8.3324730
P	20.9852510	11.7816384	5.5939483	C	17.8563657	17.3489445	7.9344129
O	21.2735525	12.8246103	6.8193279	C	17.8991801	18.4198942	6.8254477
O	20.5695123	12.7391248	4.3222952	H	18.9174982	18.8375671	6.6894599
O	22.5096126	11.2848215	5.3879982	H	17.2320366	19.2637879	7.0928615
O	22.1604985	9.0075642	7.1713015	H	17.5539533	18.0233091	5.8489432
O	24.5158373	8.6024430	8.9808435	C	18.3221613	18.0005098	9.2615927
O	26.5003733	10.4463479	8.0482536	H	17.6800970	18.8705743	9.5103220
O	29.0011795	8.9394500	7.1980035	H	19.3687517	18.3592594	9.1858362
C	20.3864139	13.8833718	7.1006187	H	18.2682023	17.2945448	10.1146735
C	19.6494035	13.9135877	8.3105272	C	16.3930344	16.8602074	8.0840299
C	18.8544900	15.0645577	8.5122416	H	15.7234778	17.7122990	8.3226540
H	18.2742371	15.1206540	9.4445070	H	16.2836382	16.1145001	8.8974445
C	18.7664488	16.1440028	7.6123812	H	16.0300650	16.3945039	7.1447216
C	19.5439951	16.0660250	6.4452319	C	23.4651783	17.5938916	3.1266799
H	19.5206412	16.8763871	5.7051461	C	23.4167207	18.6265473	4.2709681
C	20.3665827	14.9525847	6.1717657	H	24.0272974	19.5121522	4.0029480
C	21.2169417	14.9869608	4.9443827	H	23.8249993	18.2185258	5.2177870
C	21.9299253	16.1718508	4.6487648	H	22.3854388	18.9857905	4.4648257
H	21.9199868	16.9712225	5.4012150	C	24.9439535	17.1896444	2.8962876
C	22.6418116	16.3297631	3.4514103	H	25.5555694	18.0840960	2.6570320
C	22.5664483	15.2768393	2.5127698	H	25.0542437	16.4768577	2.0542669
H	23.0737340	15.4091462	1.5493936	H	25.3741321	16.7138635	3.8010728
C	21.8765577	14.0680830	2.7335547	C	22.9040286	18.2589867	1.8439845
C	21.2622467	13.9322842	4.0062040	H	23.4872715	19.1695845	1.5951266
C	19.6763845	12.8714429	9.4628849	H	21.8447574	18.5588340	1.9786928
C	20.3051620	13.5528349	10.7085738	H	22.9555399	17.5836333	0.9664444
H	20.3204874	12.8458881	11.5638490	C	21.7319771	13.0226086	1.5966347
H	19.7399649	14.4512679	11.0257862	C	20.2262738	12.8476521	1.2628799
H	21.3492664	13.8650646	10.5051083	H	20.1014337	12.1150003	0.4381278
C	18.2241321	12.4356093	9.7907773	H	19.7830040	13.8077544	0.9292956
H	18.2282326	11.6971848	10.6191251	H	19.6485739	12.4870910	2.1353180
H	17.7413849	11.9628118	8.9102677	C	22.3454155	11.6579719	1.9929102
H	17.5821513	13.2794698	10.1103744	H	22.3108289	10.9643413	1.1272099
C	20.4846216	11.5881692	9.1840286	H	21.7922623	11.1856034	2.8230924
H	20.4256857	10.9339025	10.0777380	H	23.4057767	11.7687215	2.2974580
H	21.5510403	11.7877048	8.9755167	C	22.4436728	13.4821735	0.3042556

H	22.2907537	12.7203421	−0.4863739
H	23.5378397	13.5965506	0.4431341
H	22.0394380	14.4393053	−0.0802462
C	22.8820698	9.9102612	5.0946777
H	23.7234252	9.9777613	4.3784400
H	22.0338357	9.3850470	4.6036941
C	23.3056121	9.1722670	6.3446858
H	23.7151715	8.1803793	6.0303738
H	24.1280349	9.7073610	6.8676772
C	22.3014003	8.0753872	8.2418881
H	22.7177413	7.1122647	7.8602121
H	21.2740363	7.8831153	8.6113757
C	23.1660145	8.5689053	9.3947621
H	22.8195133	9.5841336	9.7086013
H	23.0220384	7.8876762	10.2734519
C	25.3834586	9.3243438	9.8400606
H	25.5640547	8.7651867	10.7918843
H	24.9332408	10.3112755	10.1088527
C	26.7067872	9.5527452	9.1369780
H	27.4292502	9.9893368	9.8694033
H	27.1348426	8.5859649	8.7920626
C	27.6817154	10.9439315	7.4426656
H	28.4192704	11.2646509	8.2186214
H	27.3779643	11.8458031	6.8702297
C	28.3718874	9.9820537	6.4807365
H	27.6194702	9.5748292	5.7570702
H	29.1213701	10.5593415	5.8786013
C	29.6759347	8.0191254	6.3666683
H	30.1400380	7.2539872	7.0180985
H	30.4802343	8.5109907	5.7674181
H	28.9833076	7.5080067	5.6537575
C	18.8478405	5.6045173	7.8804633
C	18.5015967	6.4363938	6.8022500
C	18.1175753	7.7791686	7.0207691
C	18.0973882	8.2553841	8.3559316
C	18.4423725	7.4228319	9.4292594
C	18.8204823	6.0888999	9.1973664
H	19.1331300	4.5597883	7.6831937
H	18.5273345	6.0240600	5.7862145
H	17.7884390	9.2930962	8.5536173
H	18.4087268	7.8187477	10.4555910
H	19.0869509	5.4308186	10.0379921
C	17.6476140	8.7286541	5.9315159
C	17.7523575	8.3789996	4.5315165
O	16.9438772	8.8952311	3.6212818
O	18.6331130	7.5136344	4.0760827
C	18.7594327	7.3100423	2.6448157
H	19.5395198	6.5387402	2.5325403
H	17.8008957	6.9602887	2.2184246
H	19.0696362	8.2521714	2.1535616
C	15.2363598	8.6678794	6.7408571
C	16.3163582	9.4256224	6.2154922
C	16.0685554	10.7841866	5.9043037
C	14.8019588	11.3628127	6.0965226
C	13.7446133	10.5928388	6.6226502
C	13.9781117	9.2346384	6.9453748
H	15.3951284	7.6096949	6.9985062
H	16.8909503	11.4175892	5.5298461
H	14.6456878	12.4266686	5.8551059
H	13.1485750	8.6407156	7.3557281
O	12.5031252	11.0820435	6.8452485
H	12.4668064	12.0237995	6.5893915
H	16.2818009	9.4603430	4.1086417

INT-C (Li^+):

Au	19.0352215	10.0771716	5.7164458	H	21.9113284	11.2654856	9.0795454
P	21.0420381	11.2077778	5.5834410	H	20.4508671	10.4916207	8.3637564
O	21.5937561	12.1750925	6.7854433	C	18.6143401	17.0017507	7.9046113
O	20.9366504	12.1746288	4.2741790	C	18.7637791	18.0662764	6.7989425
O	22.4158632	10.3092616	5.4764195	H	19.8146797	18.3999468	6.6807376
O	24.1808784	8.5603318	6.8329708	H	18.1652730	18.9620324	7.0582851
O	25.3645892	9.1433329	9.1242750	H	18.4008461	17.7029055	5.8160472
O	24.8357714	11.7065494	9.2334098	C	19.1105059	17.6091892	9.2418874
O	25.3741941	11.9439009	6.6401552	H	18.5388252	18.5291110	9.4802699
Li	24.7063423	10.3871853	7.6702693	H	20.1836826	17.8824823	9.1852371
C	20.8340931	13.3353682	7.0916479	H	18.9812905	16.9114480	10.0936285
C	20.1083762	13.4283743	8.3032405	C	17.1135634	16.6326855	8.0287448
C	19.4148283	14.6444187	8.4982995	H	16.5143195	17.5375333	8.2575241
H	18.8337162	14.7528524	9.4255335	H	16.9296635	15.9001156	8.8406808
C	19.4249296	15.7254408	7.5943582	H	16.7286367	16.2014609	7.0817737
C	20.2018112	15.5810858	6.4319345	C	24.2193946	16.7946225	3.1250506
H	20.2505919	16.3917995	5.6935967	C	24.2348665	17.8315875	4.2663036
C	20.9222795	14.3980309	6.1600309	H	24.8897379	18.6818517	3.9909899
C	21.7853451	14.3504357	4.9396411	H	24.6288499	17.4072798	5.2126665
C	22.5940506	15.4755836	4.6479986	H	23.2269945	18.2491138	4.4658573
H	22.6244684	16.2854819	5.3887042	C	25.6731786	16.3193148	2.8739659
C	23.3336087	15.5763187	3.4602792	H	26.3218005	17.1825020	2.6209417
C	23.2097531	14.5173324	2.5327930	H	25.7403540	15.6000714	2.0328973
H	23.7426818	14.6042693	1.5783503	H	26.0985582	15.8317256	3.7756195
C	22.4265352	13.3647706	2.7454398	C	23.6725894	17.4810982	1.8463161
C	21.7667127	13.2926803	4.0011326	H	24.2935245	18.3634339	1.5895192
C	20.0329438	12.3818143	9.4509277	H	22.6300347	17.8294508	1.9920383
C	20.5984235	13.0364896	10.7408305	H	23.6845034	16.8029115	0.9696636
H	20.5342736	12.3245623	11.5892278	C	22.2362431	12.3217342	1.6117533
H	20.0418830	13.9477669	11.0325980	C	20.7341916	12.2632118	1.2242375
H	21.6624586	13.3198989	10.6094627	H	20.5875497	11.5463159	0.3901146
C	18.5512668	11.9869978	9.6801560	H	20.3784101	13.2548547	0.8796136
H	18.4722122	11.2637514	10.5177536	H	20.0957770	11.9456494	2.0703310
H	18.1179274	11.5123979	8.7753329	C	22.7298208	10.9202904	2.0456756
H	17.9162832	12.8568301	9.9374465	H	22.6111584	10.2028152	1.2079934
C	20.8302654	11.0774104	9.2263332	H	22.1620987	10.5316999	2.9089072
H	20.7137578	10.4390360	10.1257141	H	23.8048914	10.9434766	2.3181208

C	23.0258726	12.7064179	0.3404330
H	22.8490763	11.9429973	−0.4431434
H	24.1199774	12.7471229	0.5158753
H	22.7027645	13.6805293	−0.0760492
C	22.3859416	8.8796313	5.2485984
H	22.0848695	8.6631908	4.2017958
H	21.6590176	8.4007196	5.9385465
C	23.7780391	8.3248810	5.4787201
H	23.7440378	7.2326245	5.2711560
H	24.5065345	8.7805450	4.7704496
C	25.0329164	7.5517831	7.4109657
H	26.0651432	7.6372575	7.0009070
H	24.6493469	6.5343266	7.1778619
C	25.0201682	7.7731160	8.9125718
H	24.0042204	7.5678563	9.3230460
H	25.7442494	7.0899699	9.4107786
C	25.0801622	9.6642651	10.4284913
H	25.6696996	9.1390543	11.2125057
H	23.9972770	9.5303007	10.6593229
C	25.4590241	11.1341038	10.3923055
H	25.1294999	11.6432267	11.3249623
H	26.5643576	11.2422761	10.3083102
C	25.4071429	12.9502562	8.8016832
H	26.5150016	12.8991036	8.9046621
H	25.0385449	13.8000182	9.4186229
C	25.0301532	13.1496034	7.3450617
H	23.9444178	13.3592365	7.2199900
H	25.5991515	14.0138823	6.9380043
C	25.5310674	12.1306390	5.2290505
H	25.7921817	11.1484486	4.7933294
H	26.3577590	12.8429734	5.0200804
H	24.5961346	12.5081515	4.7617287
C	17.8566692	5.1950197	6.5390867
C	17.4915285	6.3612690	5.8446050
C	17.6001509	7.6298322	6.4569232
C	18.0787326	7.6862798	7.7908733
C	18.4409046	6.5213944	8.4819002
C	18.3340660	5.2667943	7.8569229
H	17.7508571	4.2180904	6.0434634
H	17.1097398	6.2667293	4.8202328
H	18.1364247	8.6605126	8.3013472
H	18.7961444	6.5932459	9.5211033
H	18.6083182	4.3492881	8.3986589
C	17.1494832	8.9350461	5.8087105
C	16.8739604	8.9675397	4.3764089
O	15.9957544	9.7959200	3.8573187
O	17.4805032	8.1734877	3.5288955
C	17.2125933	8.3029575	2.1027369
H	17.8066546	7.5053928	1.6272226
H	16.1346640	8.1610760	1.9023689
H	17.5363971	9.2998238	1.7486549
C	15.0552137	8.9843432	7.2686790
C	16.0676676	9.6982437	6.5759665
C	15.9626374	11.1115925	6.5419309
C	14.8904388	11.7849367	7.1528276
C	13.8934237	11.0552331	7.8348303
C	13.9944730	9.6436902	7.8900414
H	15.1036074	7.8864327	7.3184463
H	16.7515749	11.7103363	6.0535833
H	14.8431318	12.8847963	7.1144840
H	13.2141779	9.0823799	8.4242445
O	12.8382984	11.6249282	8.4528835
H	12.8598425	12.5950910	8.3413982
H	15.5586911	10.2792986	4.6185654

INT-C (Cs^+):

Au	18.3557300	9.9585897	5.7982775	H	19.1298684	10.6821886	8.5163160
P	20.3917906	11.0365873	5.8559332	C	18.7379616	17.3754546	7.5443700
O	20.8522522	12.0133138	7.0986371	C	19.2617196	18.3136671	6.4380296
O	20.5419149	11.9618514	4.5202065	H	20.3643204	18.4288287	6.4752375
O	21.7164065	10.0739269	5.8590495	H	18.8253952	19.3238853	6.5667397
O	24.1122114	8.5489032	6.4511470	H	18.9810182	17.9623203	5.4245053
O	26.8196957	9.6093021	6.7077315	C	19.1426323	17.9647713	8.9200732
O	27.3332739	12.2090631	7.8675600	H	18.7374816	18.9910546	9.0310861
O	25.3626501	14.2665466	8.2768236	H	20.2452739	18.0227944	9.0238946
C	20.2749068	13.3021495	7.2333778	H	18.7529391	17.3636175	9.7660543
C	19.4080350	13.6135283	8.3073676	C	17.1923984	17.3115076	7.4420673
C	18.9511545	14.9517766	8.3417312	H	16.7598720	18.3282234	7.5378699
H	18.2689821	15.2309623	9.1571732	H	16.7468381	16.6862945	8.2419431
C	19.3129826	15.9488935	7.4140479	H	16.8714808	16.8973109	6.4645245
C	20.2112832	15.5806909	6.3964123	C	24.8750329	15.7185983	3.7559646
H	20.5311366	16.3152405	5.6458619	C	25.0466968	16.6873458	4.9446504
C	20.7095668	14.2652176	6.2900079	H	25.9169308	17.3490559	4.7657099
C	21.7177404	13.9647376	5.2255110	H	25.2266594	16.1432991	5.8953215
C	22.7924114	14.8689612	5.0382181	H	24.1654695	17.3463016	5.0803247
H	22.8883593	15.6989136	5.7499150	C	26.1994673	14.9360419	3.5723352
C	23.7078700	14.7327281	3.9818897	H	27.0382747	15.6394234	3.3972767
C	23.4825266	13.6783287	3.0669246	H	26.1689482	14.2449460	2.7065138
H	24.1479230	13.5977968	2.1991187	H	26.4465536	14.3425313	4.4786251
C	22.4357531	12.7381372	3.1791336	C	24.5860847	16.5435469	2.4741172
C	21.6059373	12.8775114	4.3253810	H	25.4075860	17.2647002	2.2875063
C	18.9471127	12.6797868	9.4620368	H	23.6431076	17.1180818	2.5721511
C	19.4266132	13.2950647	10.8052944	H	24.4975370	15.8980356	1.5771884
H	19.0955076	12.6619337	11.6534411	C	22.1658621	11.7188220	2.0389145
H	19.0220521	14.3118946	10.9746122	C	20.7474549	11.9793490	1.4640948
H	20.5329453	13.3616417	10.8424007	H	20.5512444	11.2847089	0.6218615
C	17.3984729	12.5981888	9.4559573	H	20.6637455	13.0128296	1.0718785
H	17.0478135	11.9634033	10.2951543	H	19.9556341	11.8338060	2.2226137
H	17.0233019	12.1521555	8.5119129	C	22.2769424	10.2564052	2.5338814
H	16.9218065	13.5909707	9.5717523	H	22.1252919	9.5620011	1.6822957
C	19.4869119	11.2339433	9.4112032	H	21.5262948	10.0134709	3.3054269
H	19.1131076	10.6860503	10.2997820	H	23.2843464	10.0521295	2.9529186
H	20.5924328	11.1905448	9.4319804	C	23.1738753	11.8836851	0.8790028

H	22.9333085	11.1520376	0.0826729
H	24.2195435	11.6883158	1.1934257
H	23.1286811	12.8907087	0.4191555
C	21.7145260	8.7298036	6.4197270
H	20.7891755	8.1946405	6.1154341
H	21.7384079	8.7998714	7.5270727
C	22.9272074	7.9799281	5.9133677
H	22.8221289	6.9141884	6.2324245
H	22.9422476	7.9928709	4.7975959
C	25.2908951	7.8501193	6.0390175
H	25.5056627	8.0523024	4.9624951
H	25.1419152	6.7503416	6.1487605
C	26.4758150	8.2398158	6.8980104
H	26.2472025	8.0413246	7.9728072
H	27.3310508	7.5810887	6.6138959
C	28.0217582	9.9533842	7.4008669
H	28.8788142	9.3569406	7.0071246
H	27.9195200	9.7214713	8.4872251
C	28.3362038	11.4245163	7.2271088
H	29.3361019	11.6206953	7.6816647
H	28.4122628	11.6817837	6.1419132
C	27.6617555	13.5937712	7.9522123
H	27.6736022	14.0613326	6.9367971
H	28.6806425	13.7254643	8.3871992
C	26.6699966	14.3079097	8.8476387
H	26.6659284	13.8350635	9.8587038
H	27.0067332	15.3645679	8.9717858
C	24.4172988	15.0018997	9.0479431
H	23.4332011	14.9147477	8.5485912
H	24.6916525	16.0795688	9.1096351
H	24.3346069	14.6024203	10.0850046
C	17.2407938	5.0953766	6.7190582
C	16.9025599	6.2153279	5.9400373
C	16.9233394	7.5138499	6.4961103
C	17.2827808	7.6477010	7.8617326
C	17.6190369	6.5287380	8.6366787
C	17.6032184	5.2441063	8.0666890
H	17.2061773	4.0935399	6.2647208
H	16.6127107	6.0600094	4.8928857
H	17.2691293	8.6454706	8.3284862
H	17.8850994	6.6605691	9.6964912
H	17.8604882	4.3630475	8.6732347
C	16.4972676	8.7721506	5.7450598
C	16.3658350	8.7269010	4.2926813
O	15.5131866	9.4911018	3.6480936
O	17.0847986	7.9205502	3.5512812
C	16.9520150	7.9646307	2.1015534
H	17.6251070	7.1749900	1.7293770
H	15.9062299	7.7585412	1.8078252
H	17.2633465	8.9572805	1.7249100
C	14.2849154	8.8181405	7.0183280
C	15.3239048	9.5310824	6.3658002
C	15.1674769	10.9336407	6.2292635
C	14.0216749	11.5961323	6.7032472
C	12.9991787	10.8670195	7.3473613
C	13.1501407	9.4677072	7.5042268
H	14.3717060	7.7289351	7.1449461
H	15.9716768	11.5345345	5.7695960
H	13.9348628	12.6883872	6.5886699
H	12.3495696	8.9070380	8.0083133
O	11.8733956	11.4261974	7.8365207
H	11.8670127	12.3880054	7.6659464
H	14.9826808	9.9898685	4.3373426
Cs	24.5515790	11.7694545	6.5565749

3.5.11. Collection of spectra

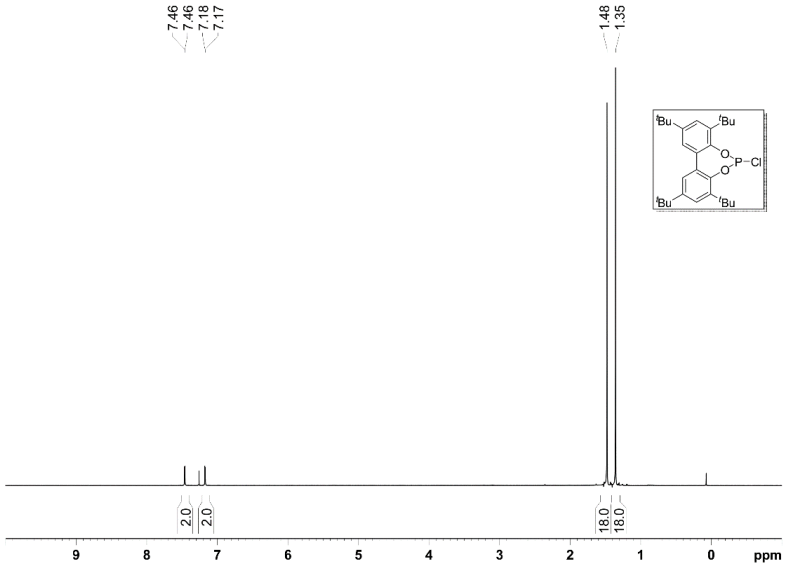

Figure 183. ^{1}H NMR spectrum (400 MHz, $CDCl_3$) for 3,3',5,5'-tetra-*tert*-butylbiphenyl-2,2'-diyl chlorophosphite.

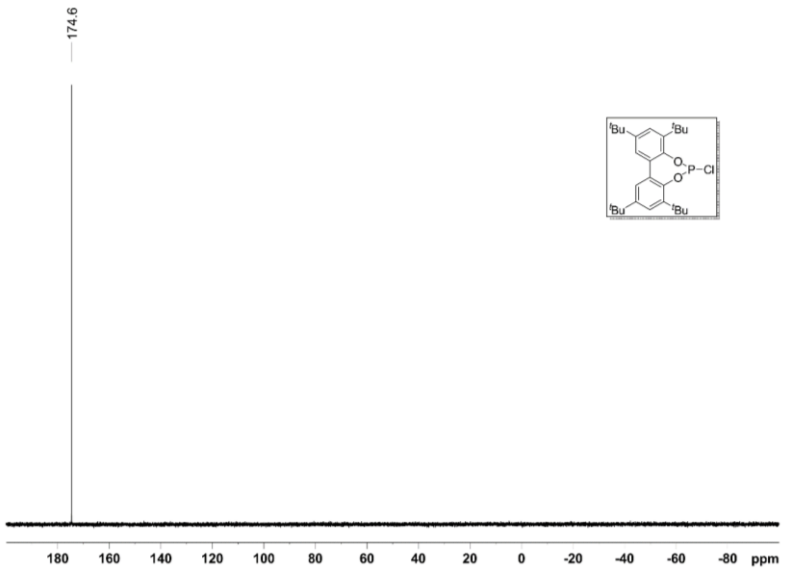

Figure 184. $^{31}P\{1H\}$ NMR spectrum (162 MHz, $CDCl_3$) for 3,3',5,5'-tetra-*tert*-butylbiphenyl-2,2'-diyl chlorophosphite.

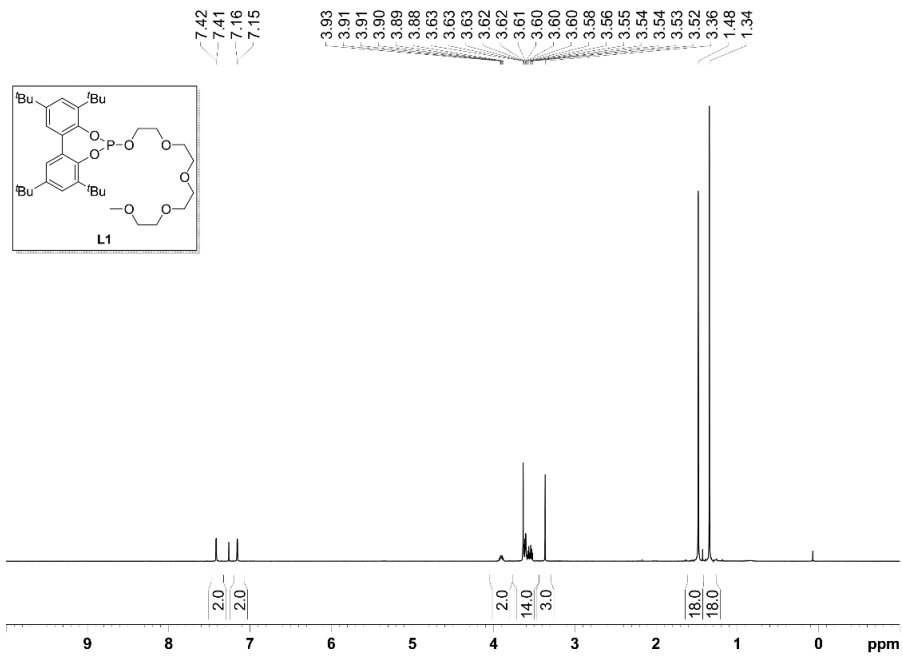

Figure 185. ^{1}H NMR spectrum (400 MHz, $CDCl_3$) for ligand **L1**.

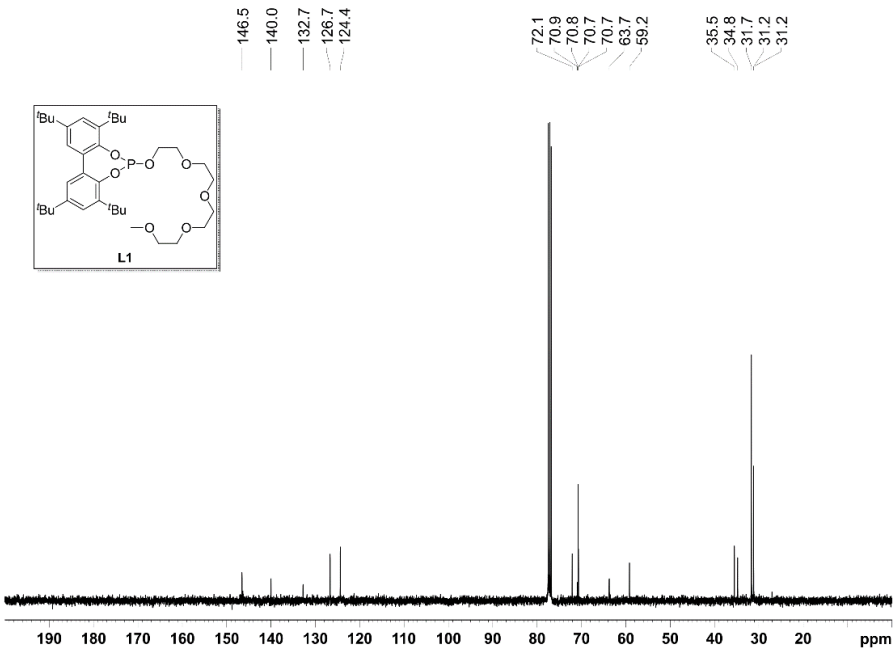

Figure 186. $^{13}C\{^{1}H\}$ NMR spectrum (100 MHz, $CDCl_3$) for ligand **L1**.

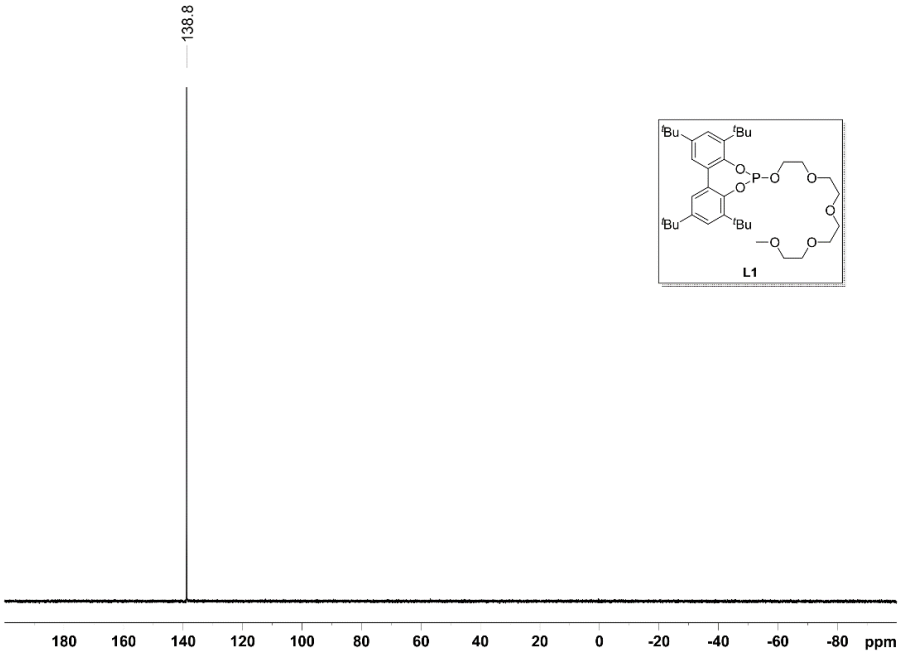

Figure 187. $^{31}P\{^{1}H\}$ NMR spectrum (162 MHz, $CDCl_3$) for ligand **L1**.

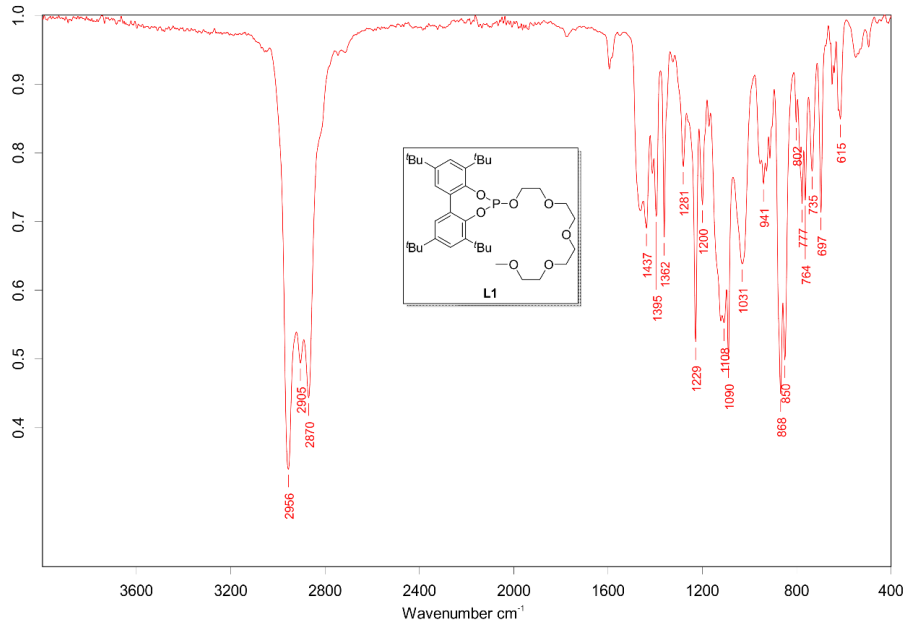

Figure 188. IR spectrum for ligand **L1**.

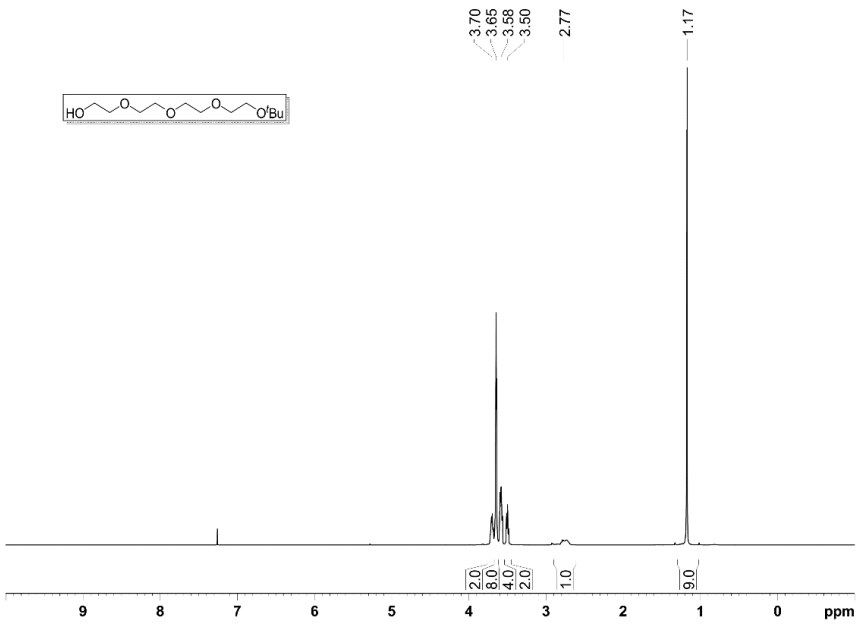

Figure 189. ^{1}H NMR spectrum (400 MHz, $CDCl_3$) for tetraethyleneglycol mono-*tert*-butyl ether.

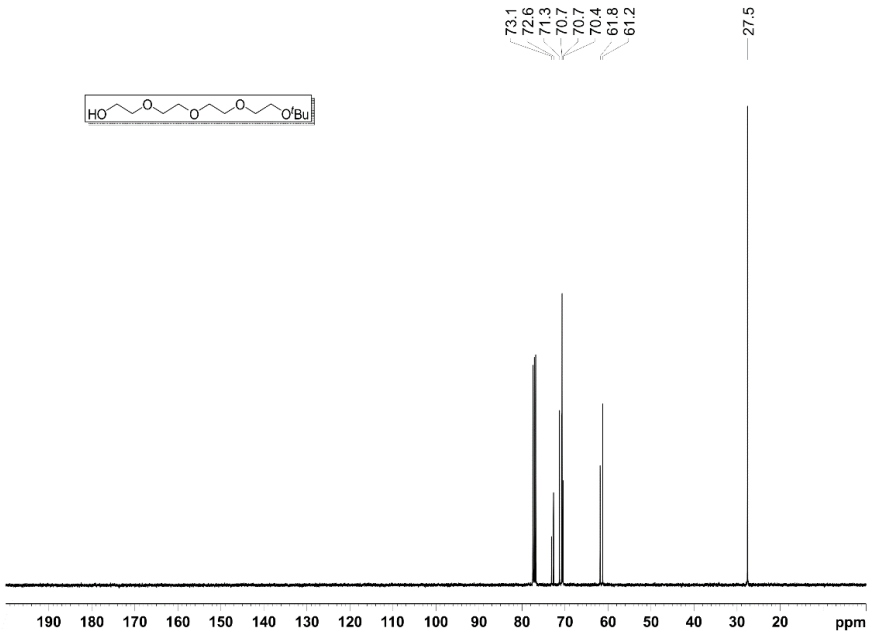

Figure 190. $^{13}C\{^{1}H\}$ NMR spectrum (100 MHz, $CDCl_3$) for tetraethyleneglycol mono-*tert*-butyl ether.

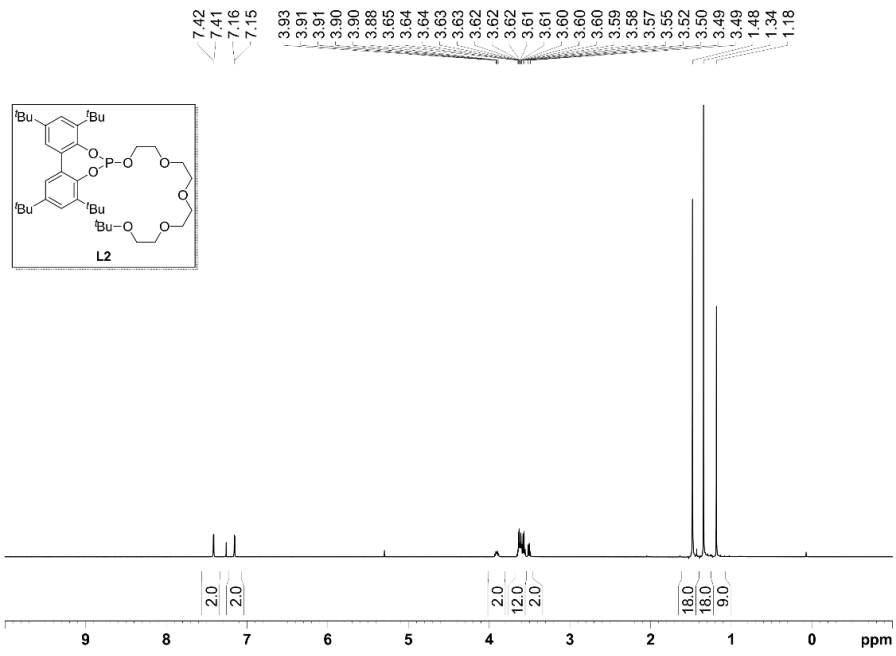

Figure 191. ^{1}H NMR spectrum (400 MHz, $CDCl_3$) for ligand **L2**.

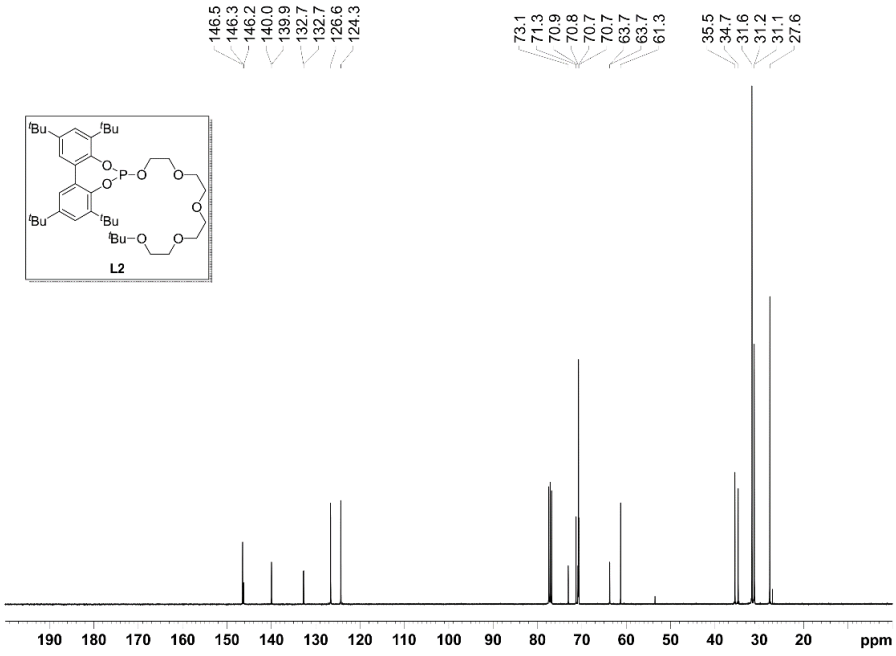

Figure 192. $^{13}C\{^{1}H\}$ NMR spectrum (100 MHz, $CDCl_3$) for ligand **L2**.

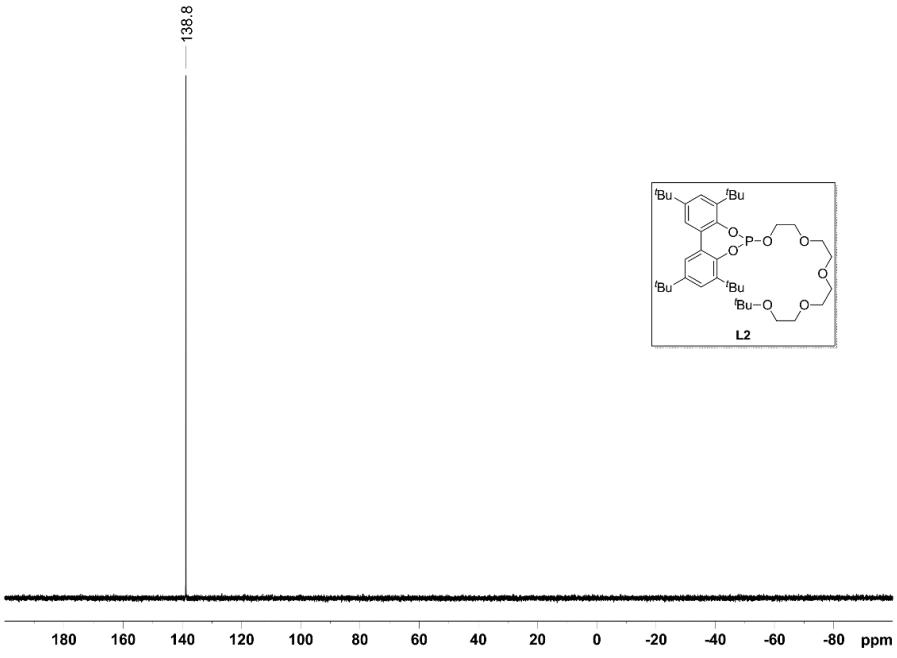

Figure 193. $^{31}P\{^{1}H\}$ NMR spectrum (162 MHz, $CDCl_3$) for ligand **L2**.

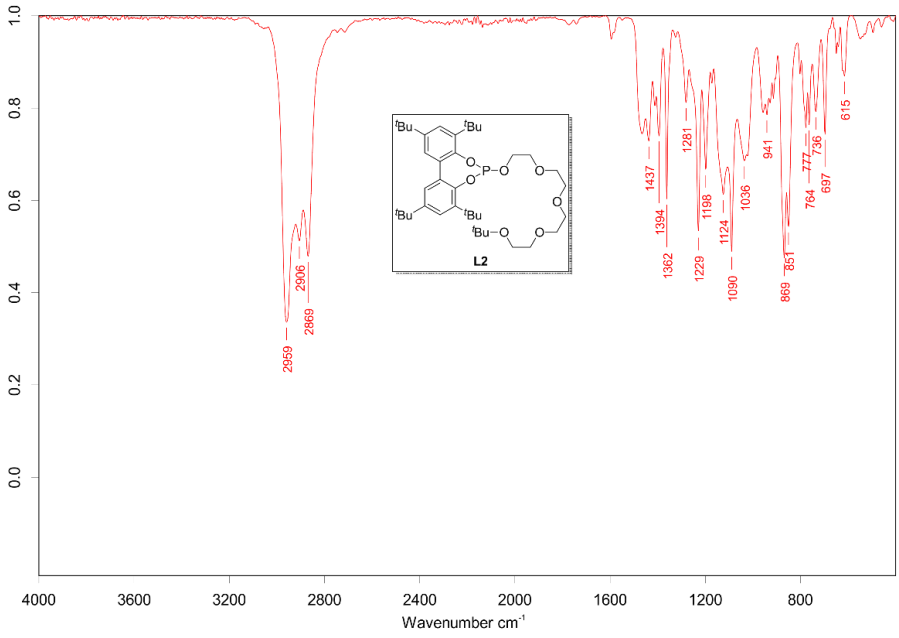

Figure 194. IR spectrum for ligand **L2**.

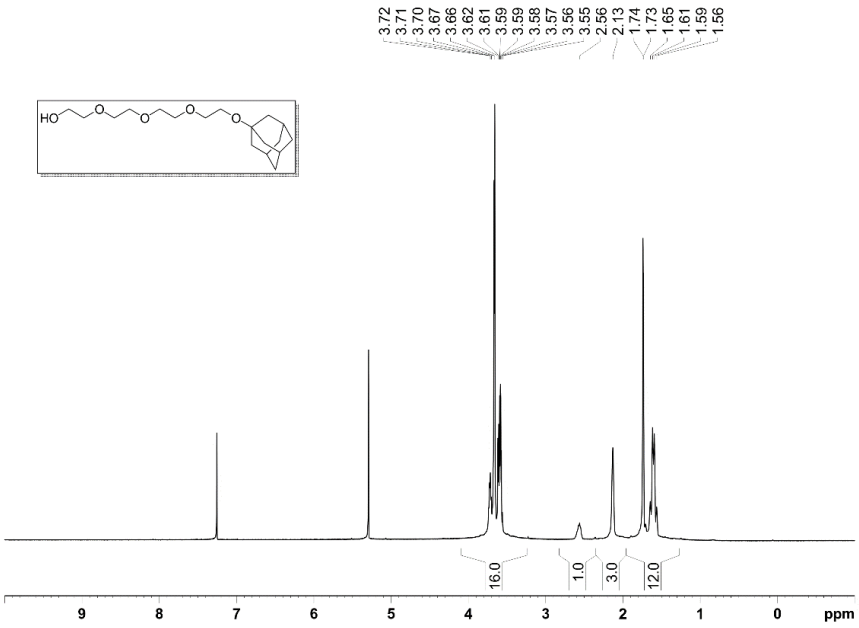

Figure 195. ^{1}H NMR spectrum (400 MHz, $CDCl_3$) for tetraethyleneglycol mono-1-adamantyl ether.

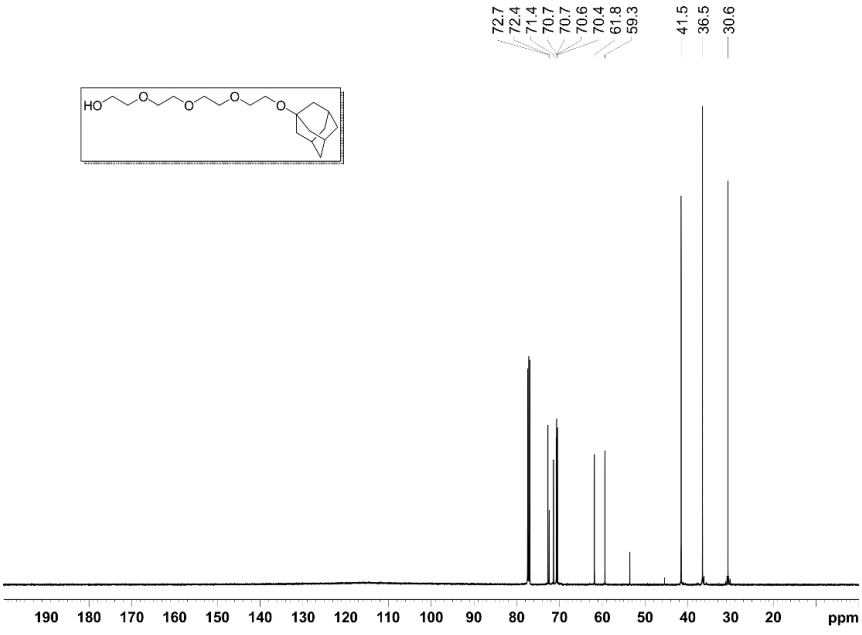

Figure 196. $^{13}C\{^{1}H\}$ NMR spectrum (100 MHz, $CDCl_3$) for tetraethyleneglycol mono-1-adamantyl ether.

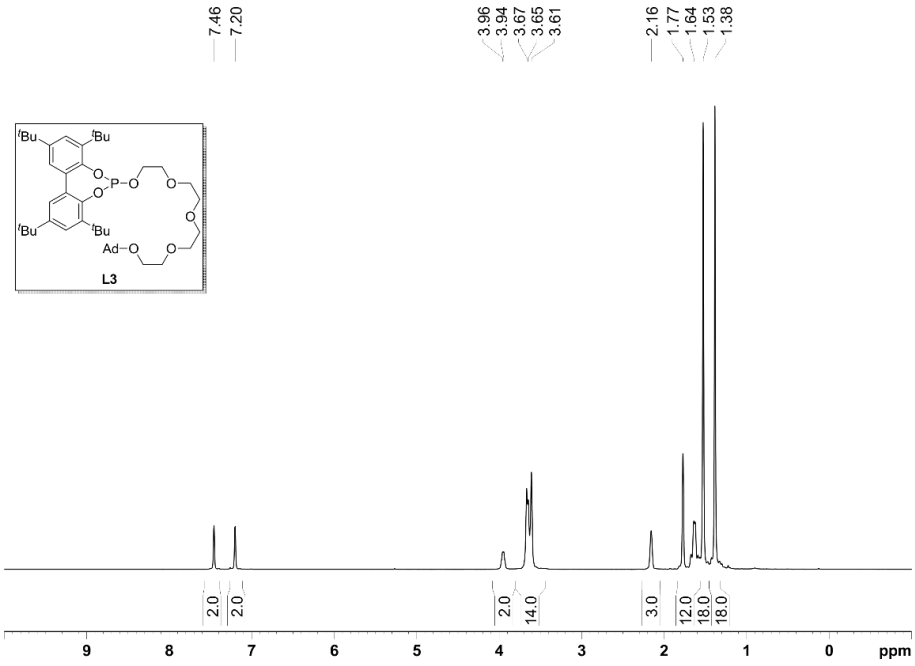

Figure 197. ^{1}H NMR spectrum (400 MHz, $CDCl_3$) for ligand **L3**.

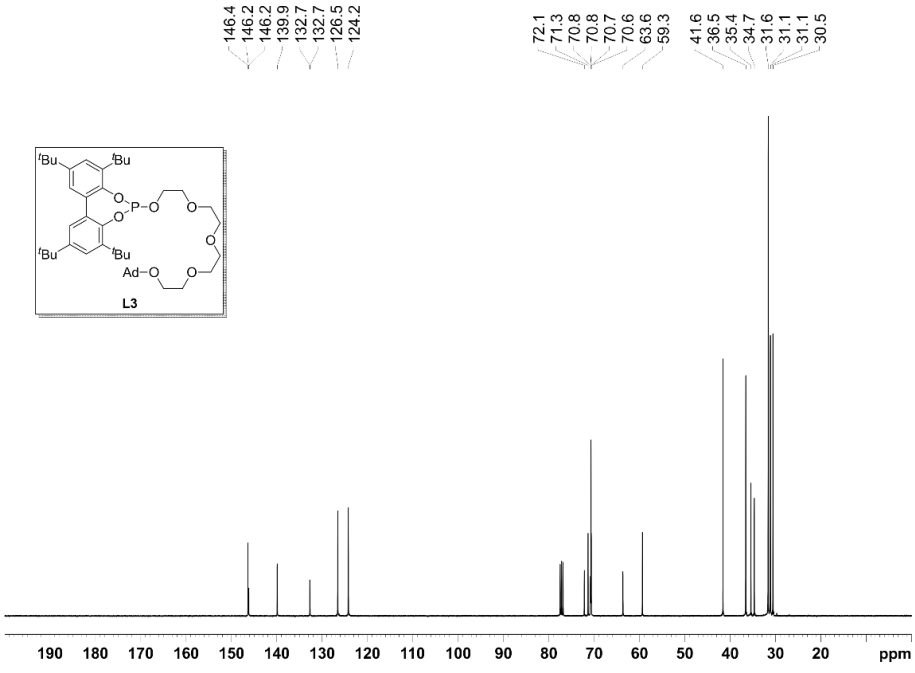

Figure 198. $^{13}C\{^{1}H\}$ NMR spectrum (100 MHz, $CDCl_3$) for ligand **L3**.

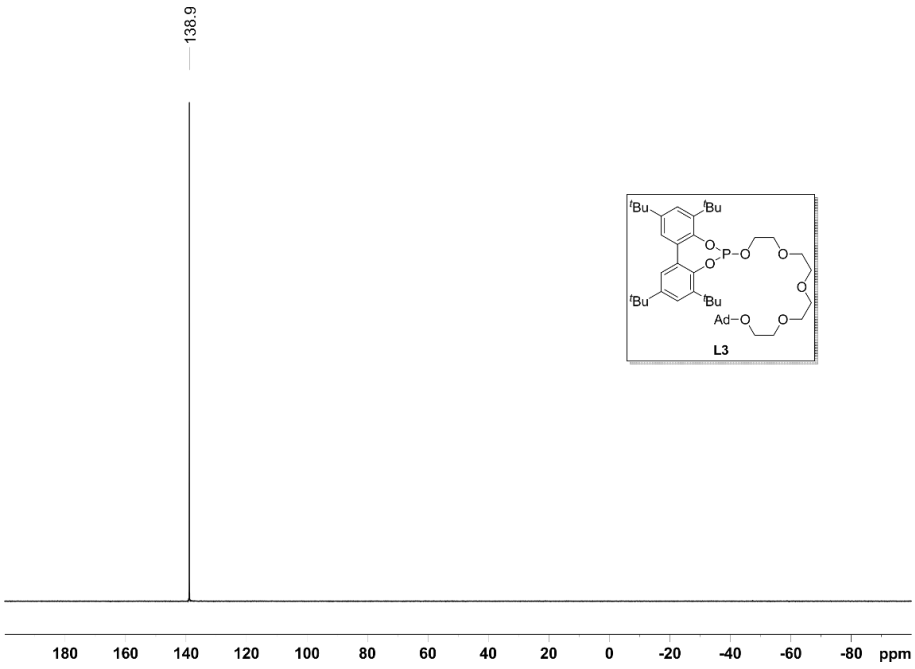

Figure 199. $^{31}P\{^{1}H\}$ NMR spectrum (162 MHz, $CDCl_3$) for ligand **L3**.

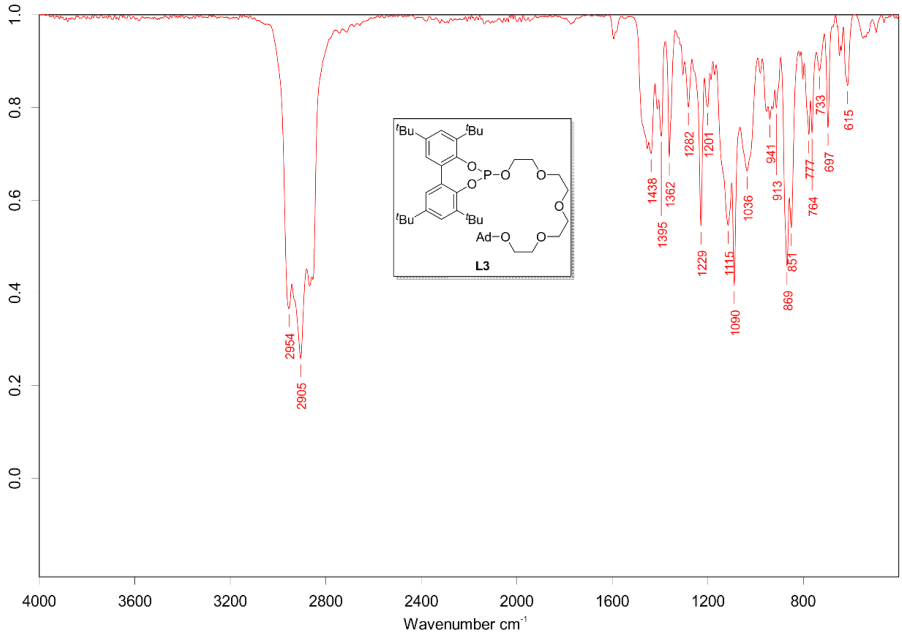

Figure 200. IR spectrum for ligand **L3**.

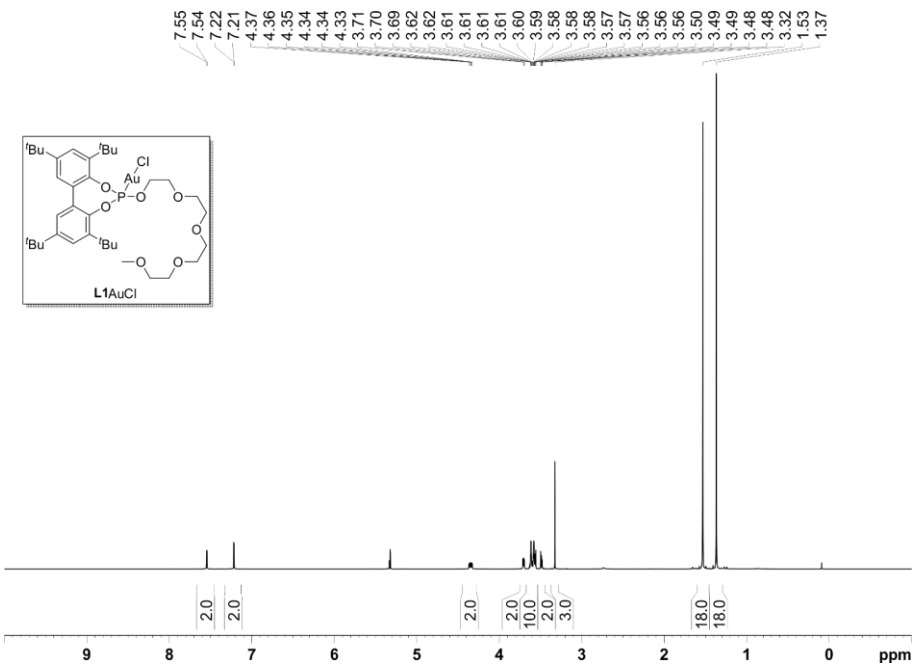

Figure 201. ^{1}H NMR spectrum (500 MHz, CD_2Cl_2) for complex **L1**AuCl.

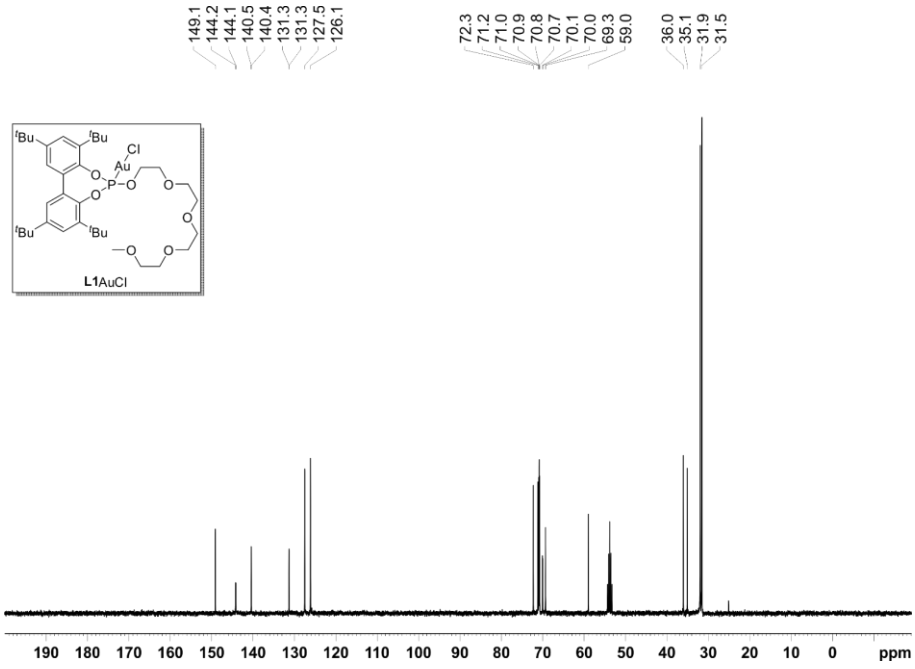

Figure 202. $^{13}C\{^{1}H\}$ NMR spectrum (100 MHz, CD_2Cl_2) for complex **L1**AuCl.

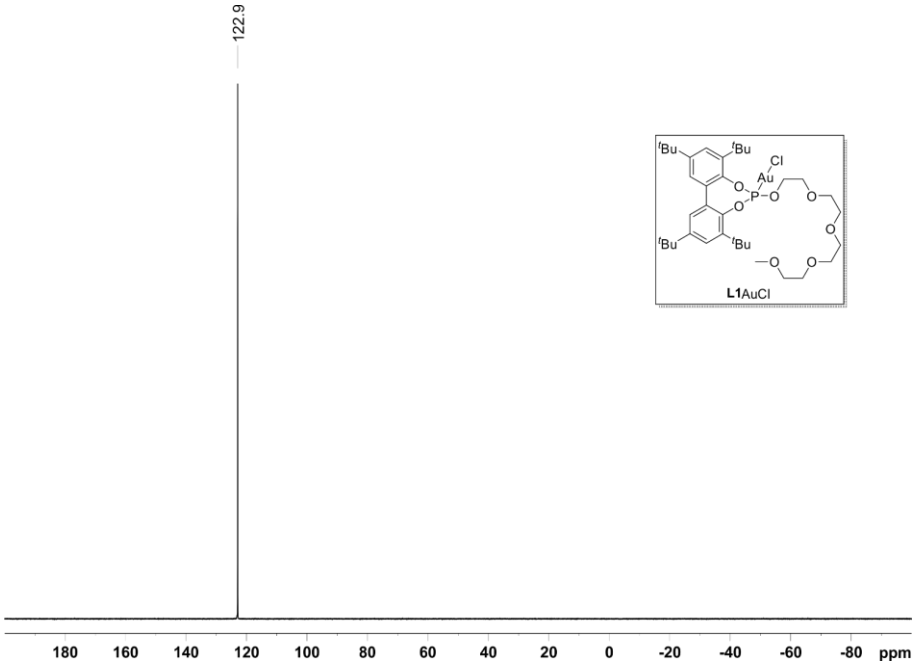

Figure 203. $^{31}P\{^{1}H\}$ NMR spectrum (202 MHz, CD_2Cl_2) for complex **L1**AuCl.

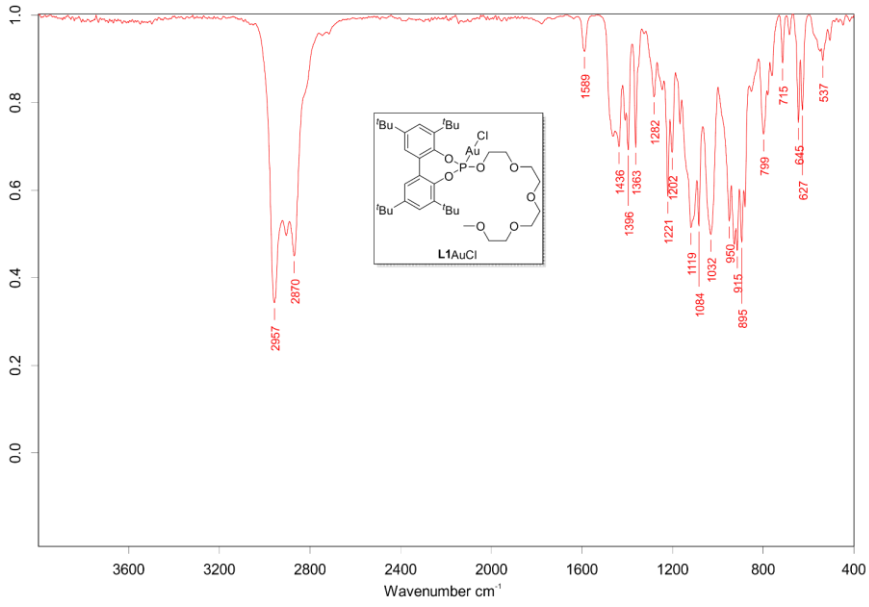

Figure 204. IR spectrum for complex **L1**AuCl.

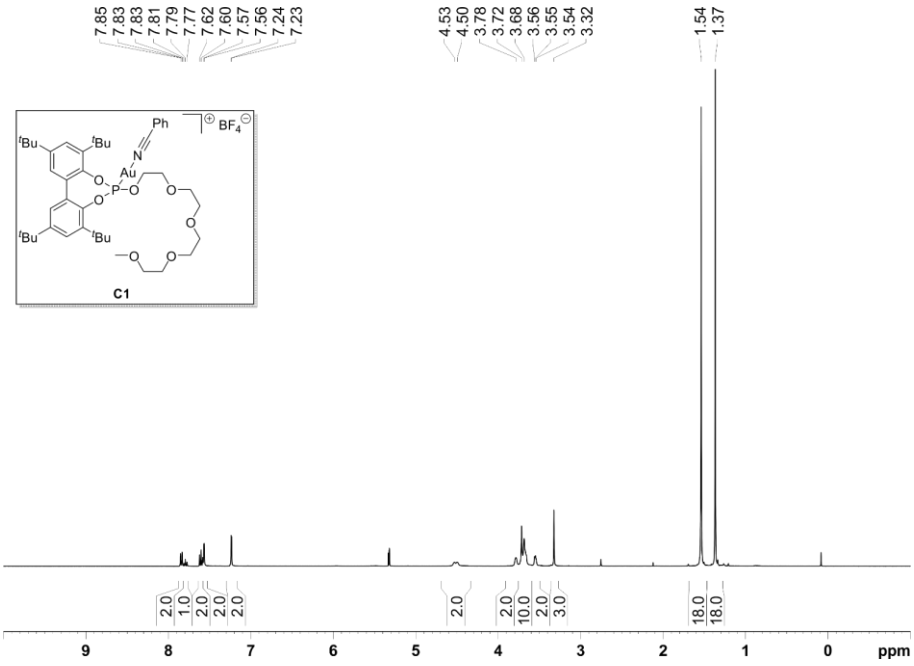

Figure 205. ^{1}H NMR spectrum (400 MHz, CD_2Cl_2) for complex **C1**.

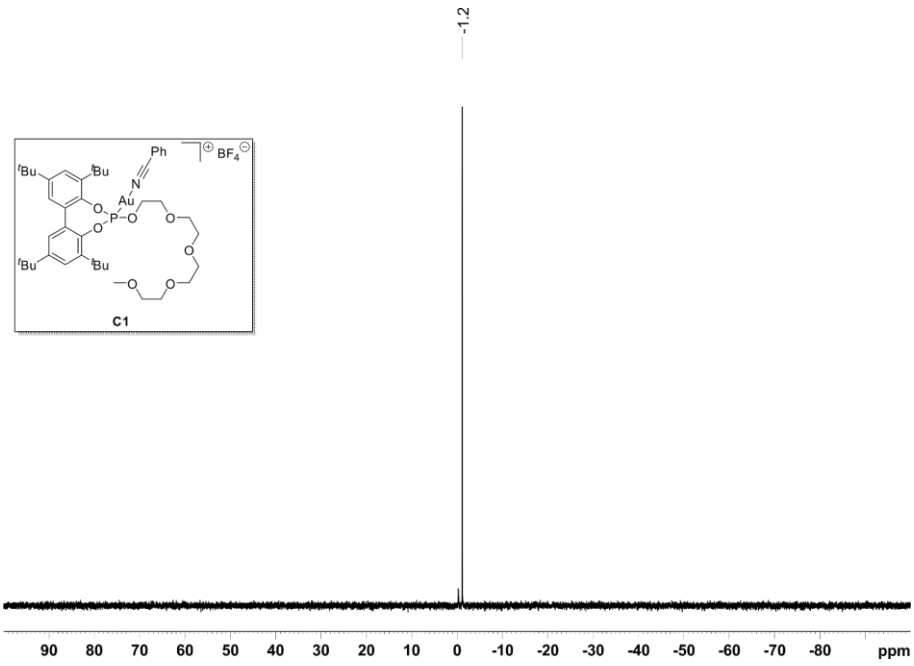

Figure 206. $^{11}B\{^{1}H\}$ NMR spectrum (128 MHz, CD_2Cl_2) for complex **C1**.

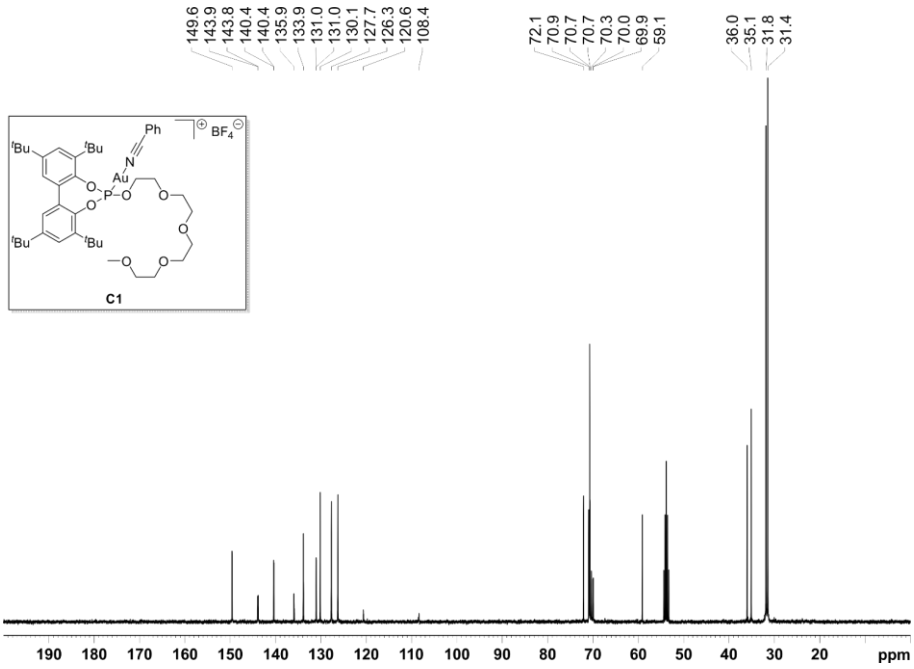

Figure 207. $^{13}C\{^{1}H\}$ NMR spectrum (126 MHz, CD_2Cl_2) for complex **C1**.

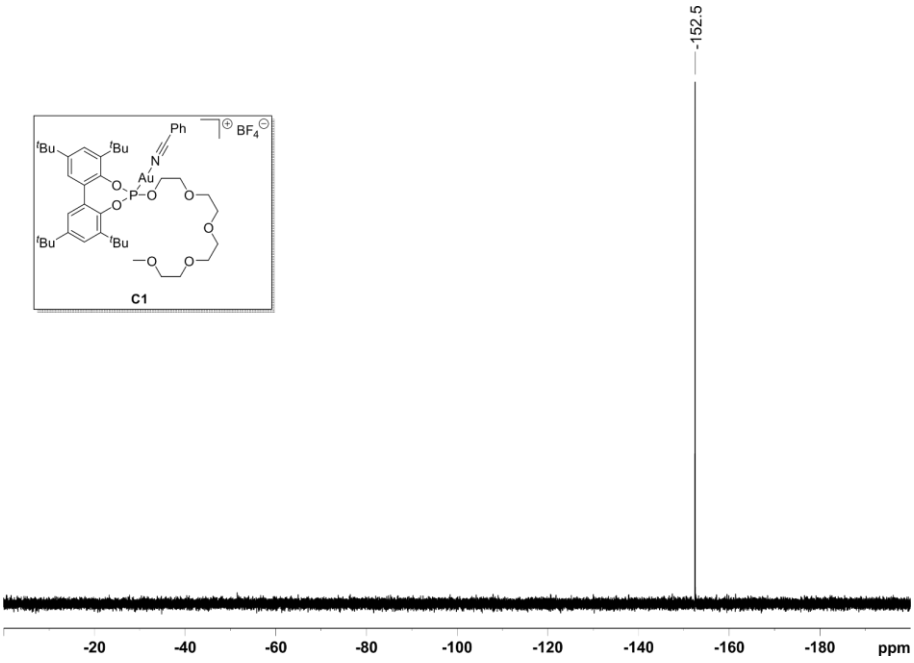

Figure 208. $^{19}F\{^{1}H\}$ NMR spectrum (376 MHz, CD_2Cl_2) for complex **C1**.

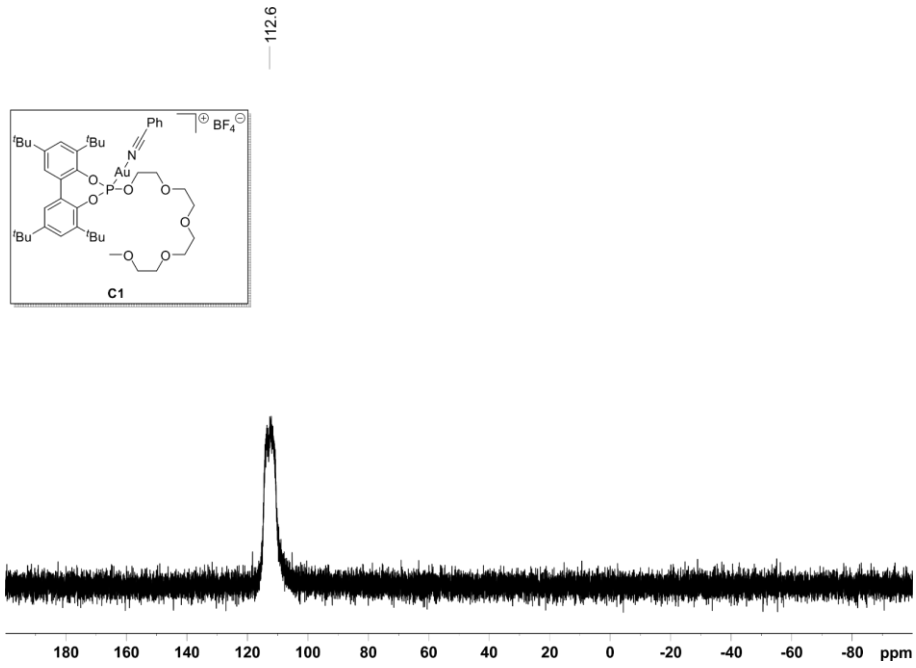

Figure 209. $^{31}P\{^{1}H\}$ NMR spectrum (162 MHz, CD_2Cl_2) for complex **C1**.

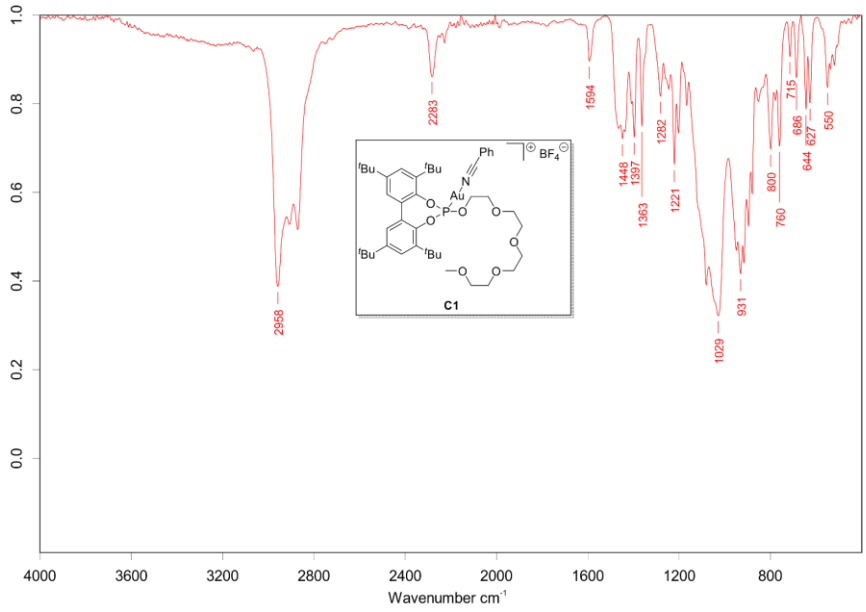

Figure 210. IR spectrum for complex **C1**.

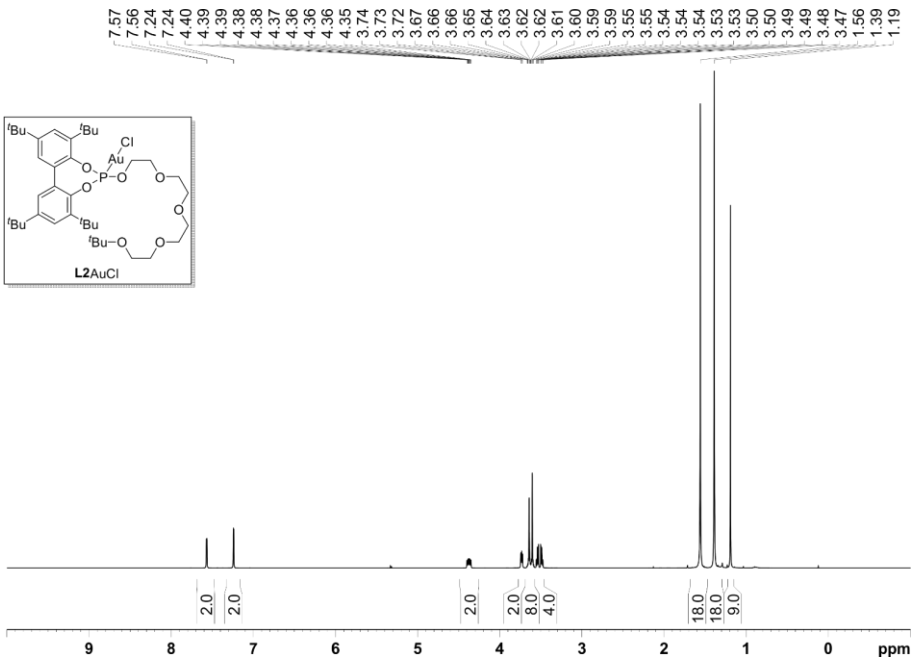

Figure 211. ^{1}H NMR spectrum (400 MHz, CD_2Cl_2) for complex **L2**AuCl.

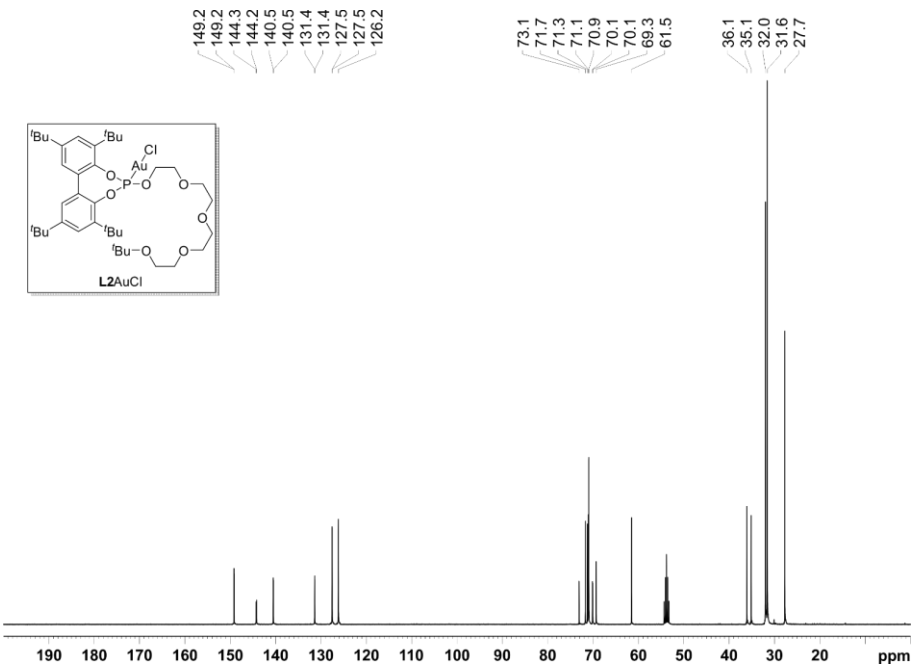

Figure 212. $^{13}C\{^{1}H\}$ NMR spectrum (100 MHz, CD_2Cl_2) for complex **L2**AuCl.

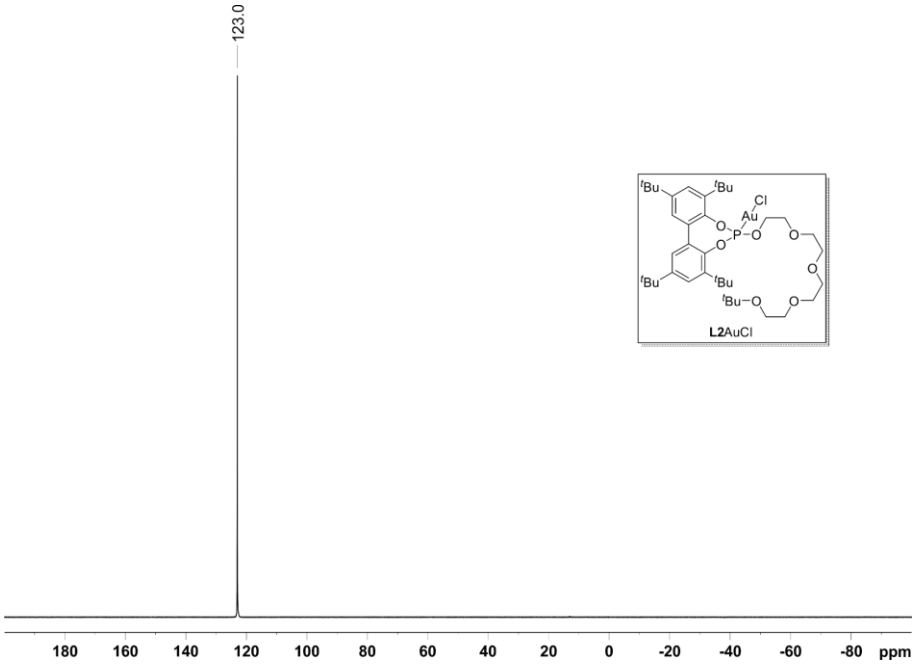

Figure 213. $^{31}P\{^{1}H\}$ NMR spectrum (162 MHz, CD_2Cl_2) for complex **L2**AuCl.

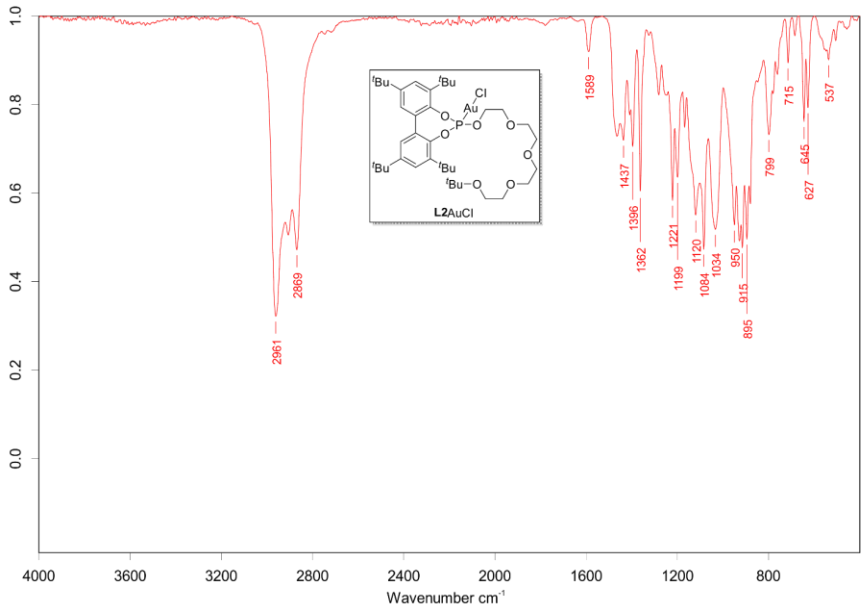

Figure 214. IR spectrum for complex **L2**AuCl.

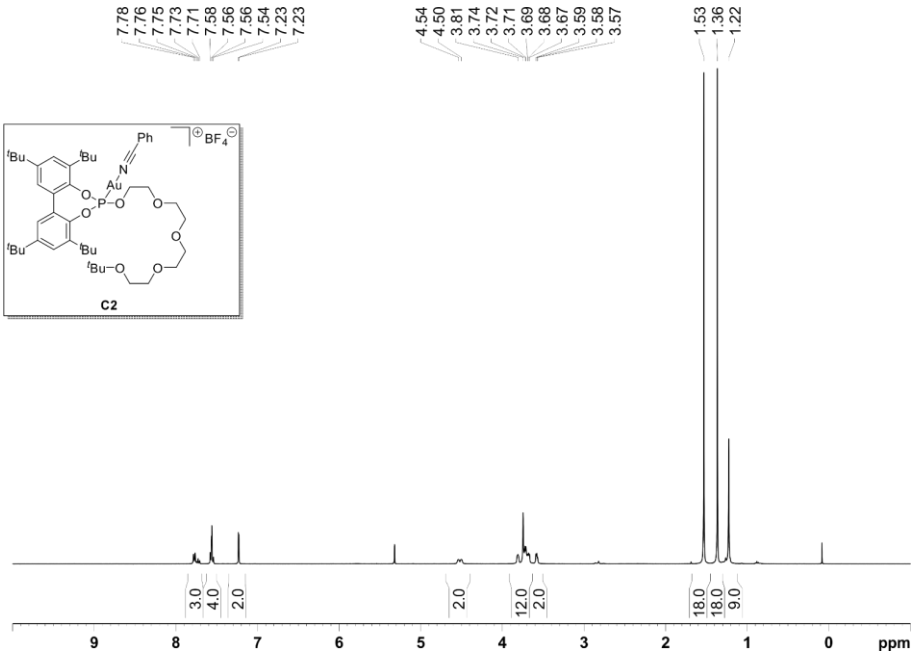

Figure 215. ^{1}H NMR spectrum (400 MHz, CD_2Cl_2) for complex **C2**.

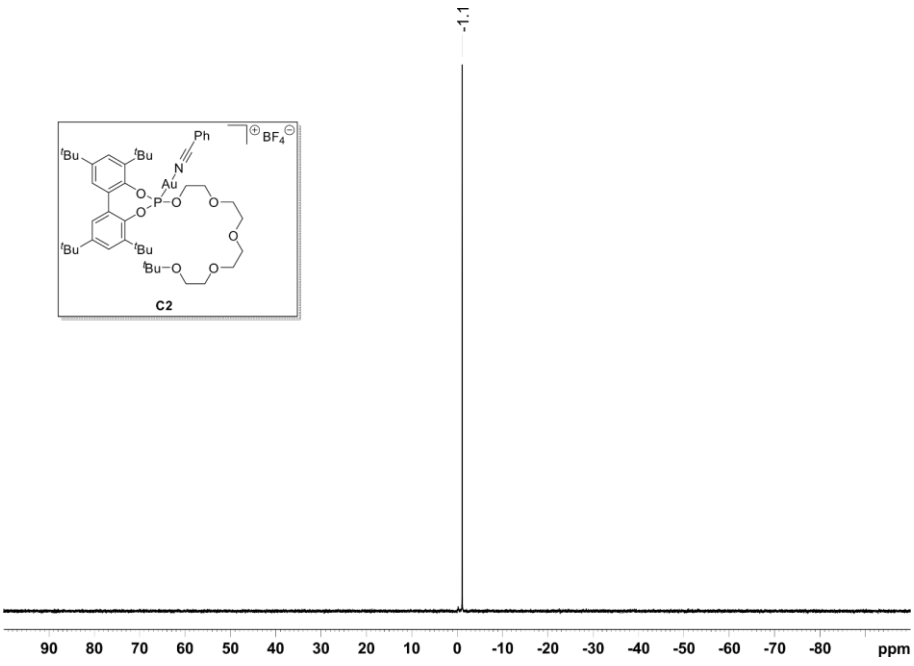

Figure 216. $^{11}B\{^{1}H\}$ NMR spectrum (128 MHz, CD_2Cl_2) for complex **C2**.

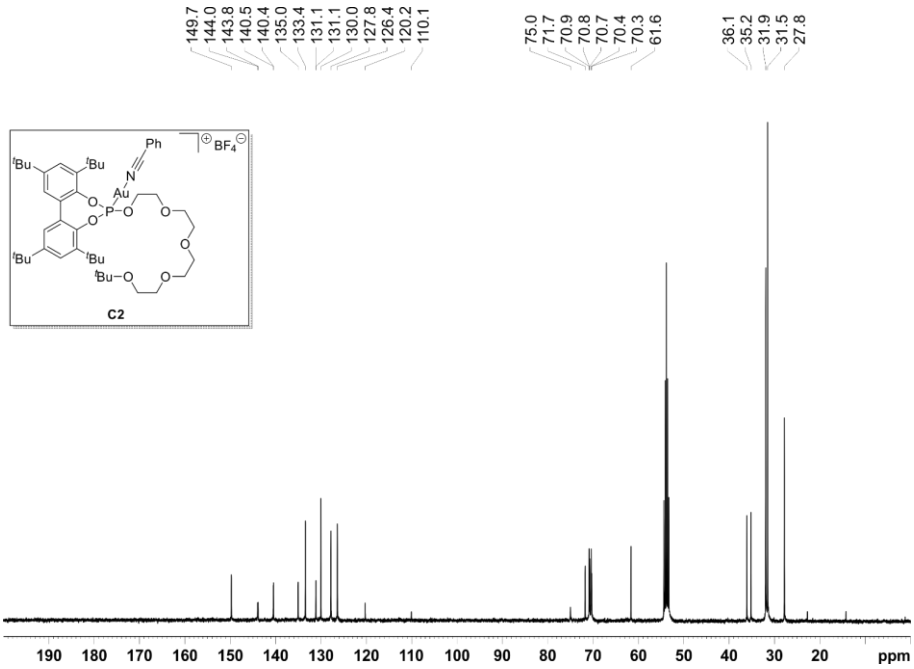

Figure 217. $^{13}C\{^{1}H\}$ NMR spectrum (126 MHz, CD_2Cl_2) for complex **C2**.

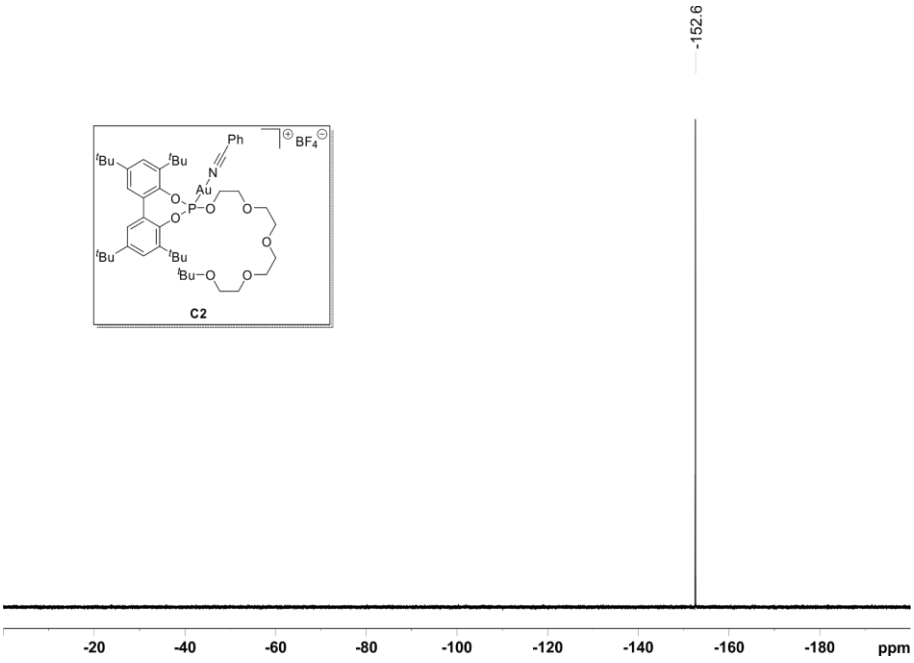

Figure 218. $^{19}F\{^{1}H\}$ NMR spectrum (376 MHz, CD_2Cl_2) for complex **C2**.

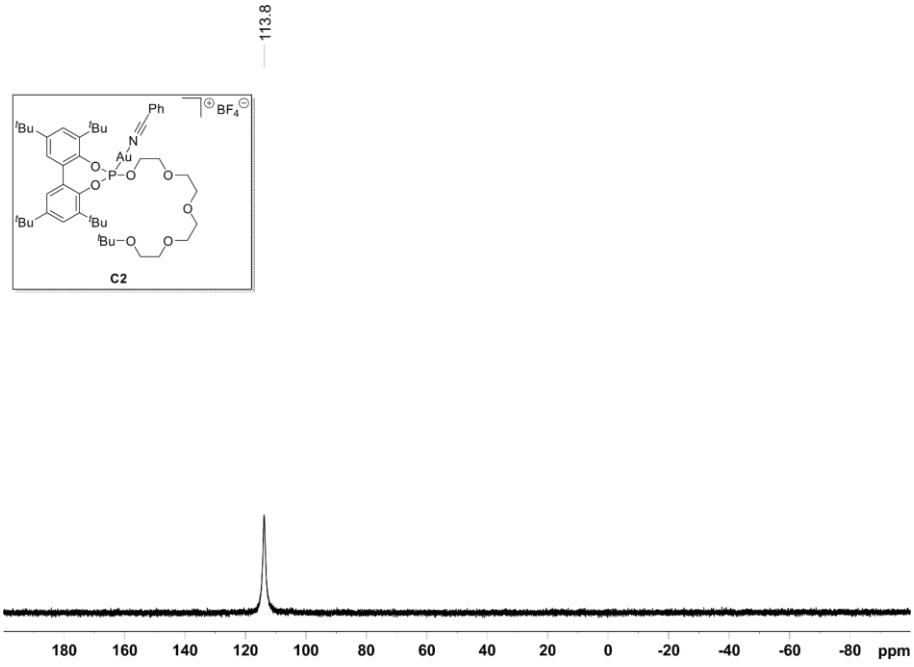

Figure 219. $^{31}P\{^{1}H\}$ NMR spectrum (162 MHz, CD_2Cl_2) for complex **C2**.

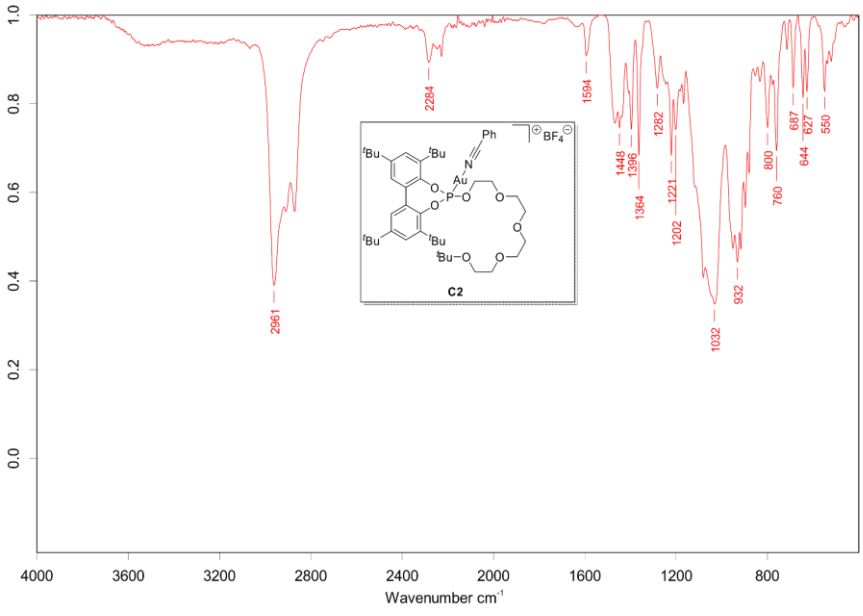

Figure 220. IR spectrum for complex **C2**.

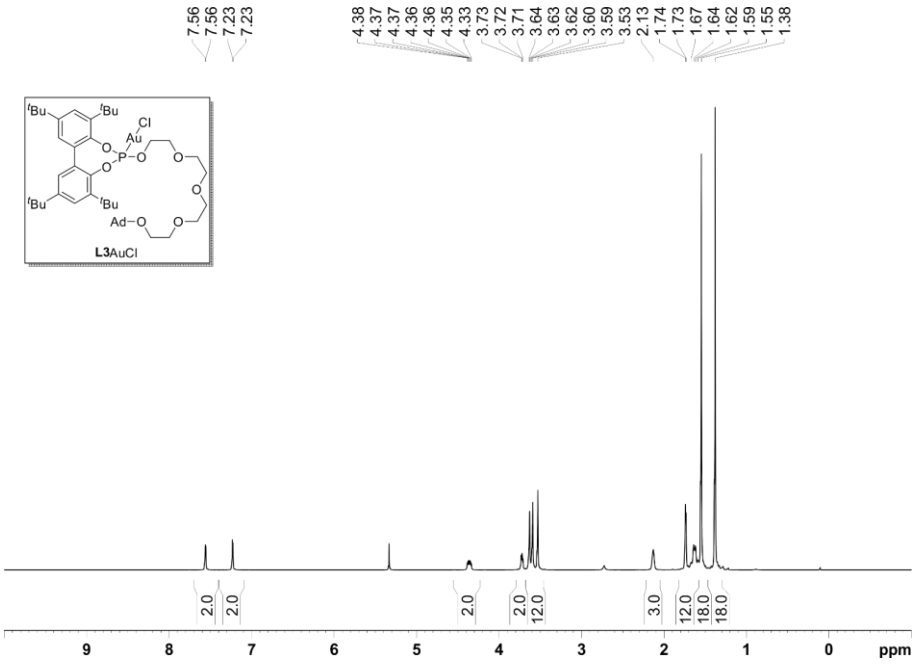

Figure 221. ^{1}H NMR spectrum (400 MHz, CD_2Cl_2) for complex **L3**AuCl.

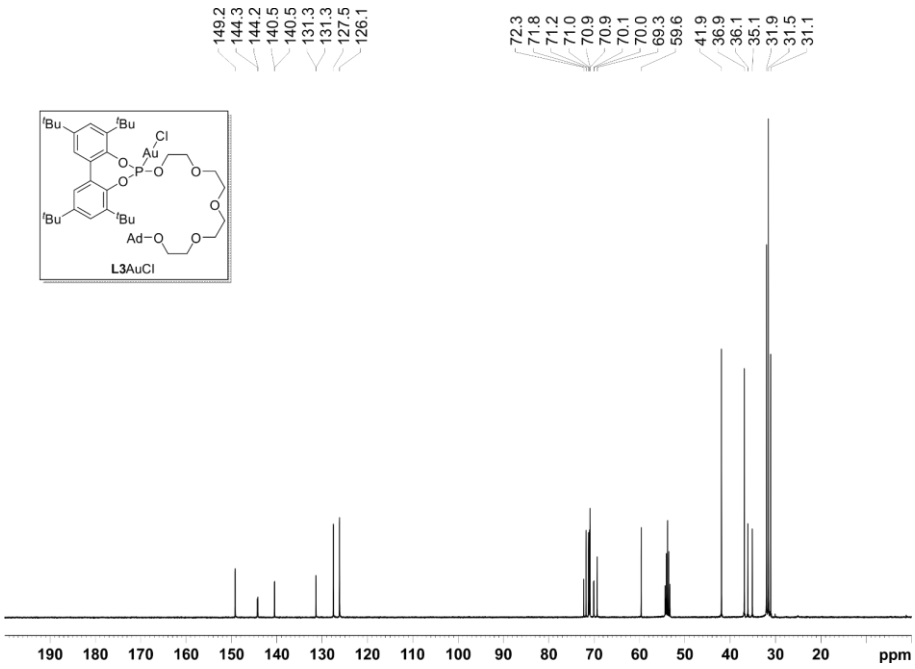

Figure 222. $^{13}C\{^{1}H\}$ NMR spectrum (100 MHz, CD_2Cl_2) for complex **L3**AuCl.

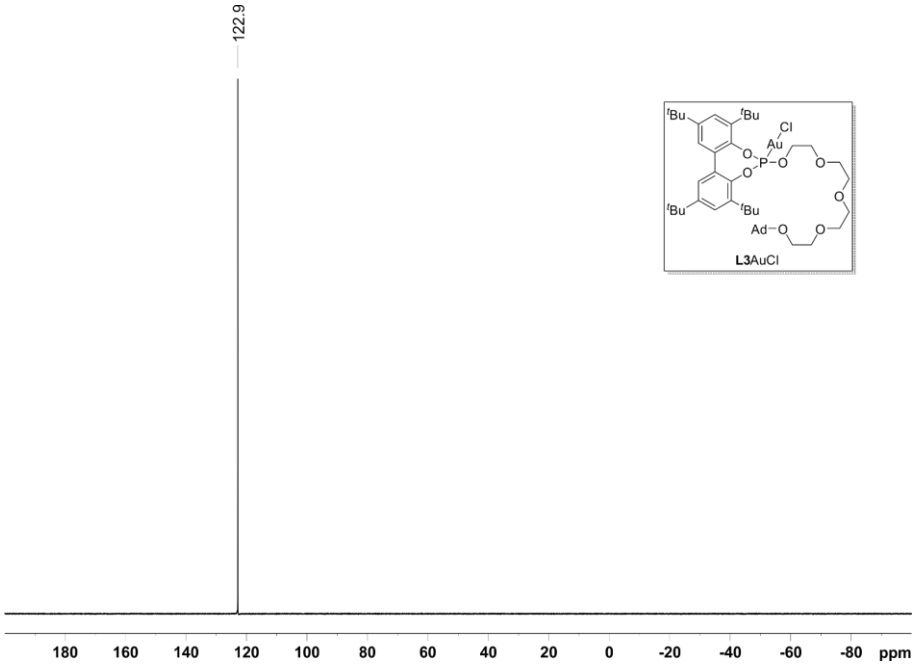

Figure 223. $^{31}P\{^{1}H\}$ NMR spectrum (162 MHz, CD_2Cl_2) for complex **L3**AuCl.

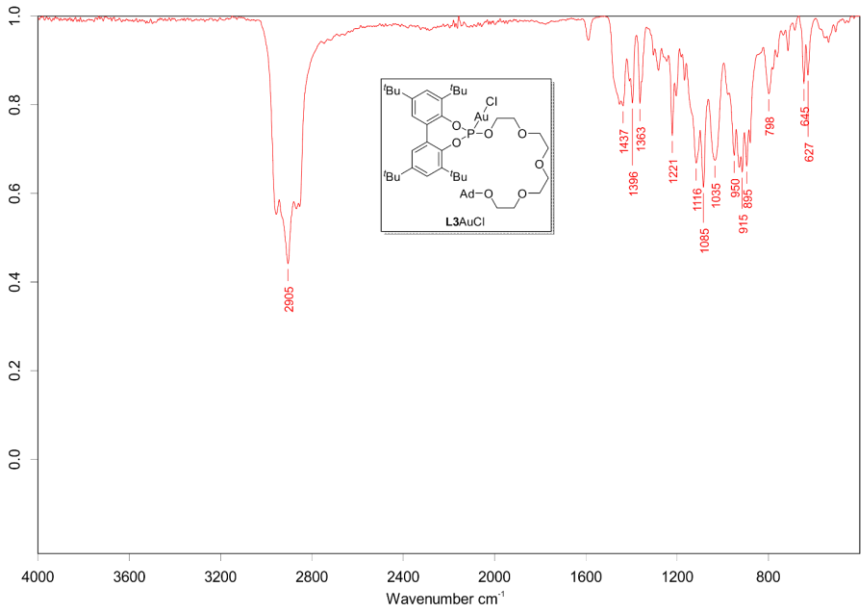

Figure 224. IR spectrum for complex **L3**AuCl.

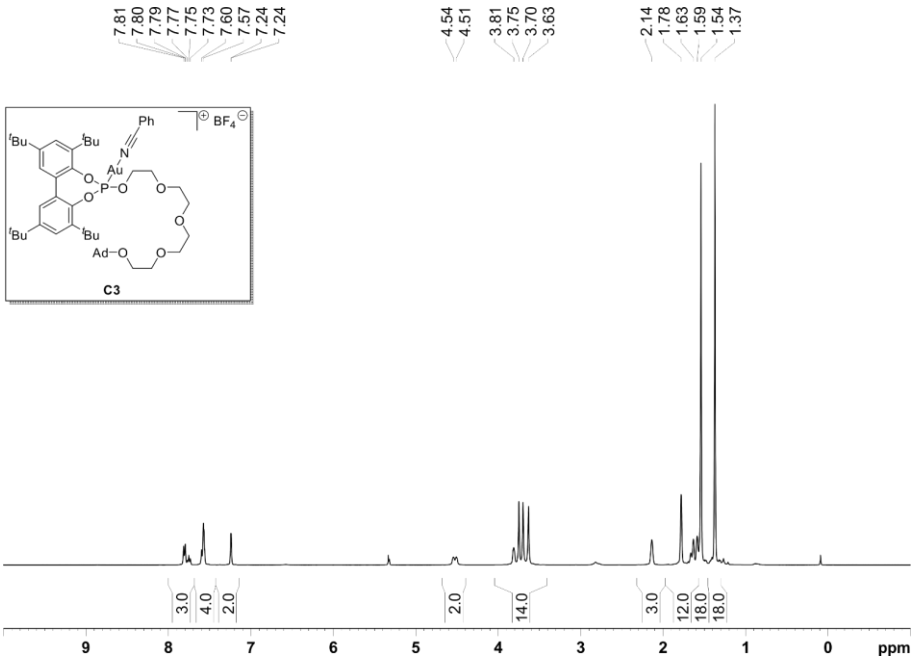

Figure 225. ^{1}H NMR spectrum (400 MHz, CD_2Cl_2) for complex **C3**.

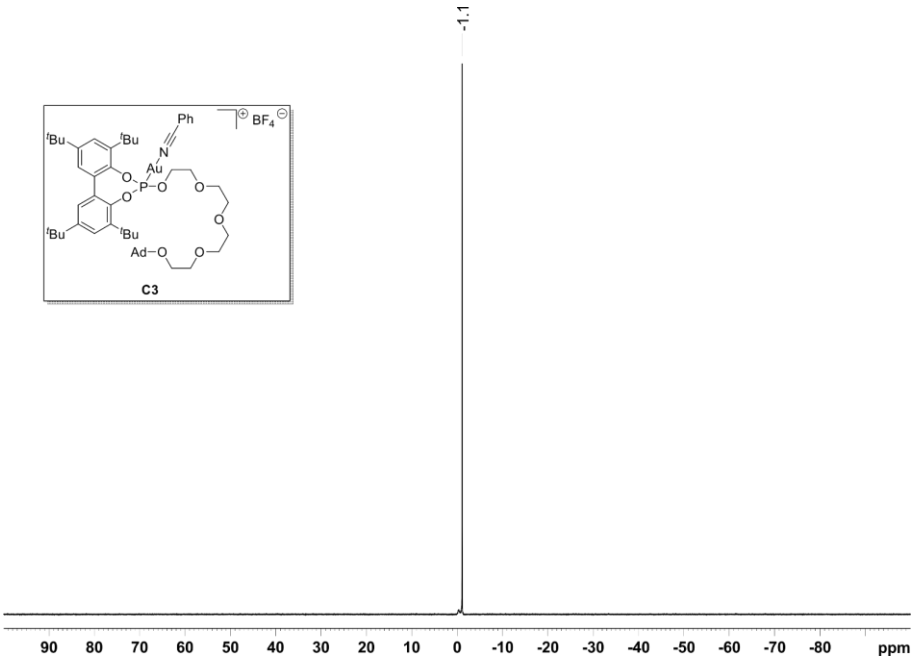

Figure 226. $^{11}B\{^{1}H\}$ NMR spectrum (128 MHz, CD_2Cl_2) for complex **C3**.

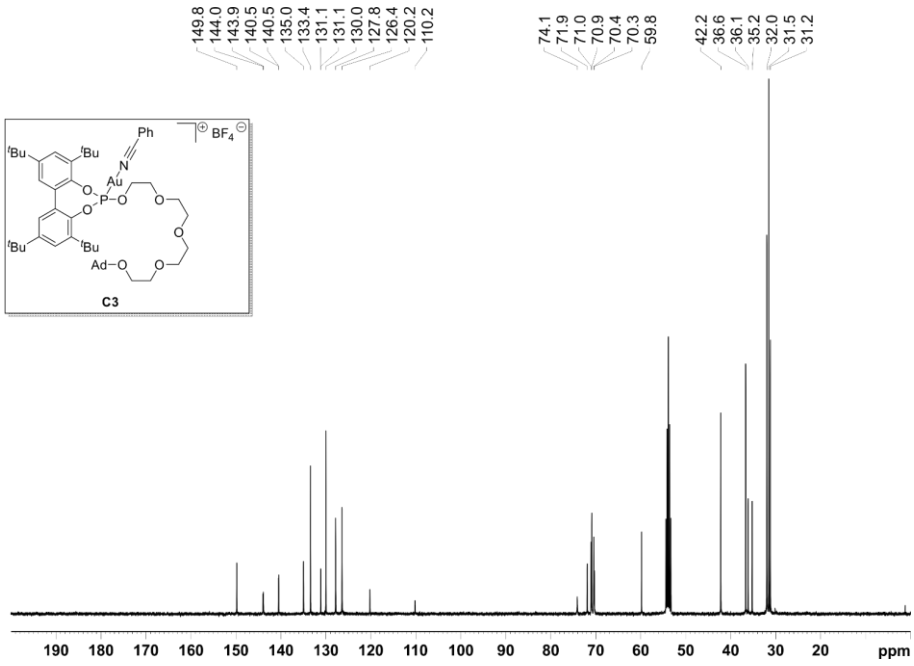

Figure 227. $^{13}C\{^{1}H\}$ NMR spectrum (126 MHz, CD_2Cl_2) for complex **C3**.

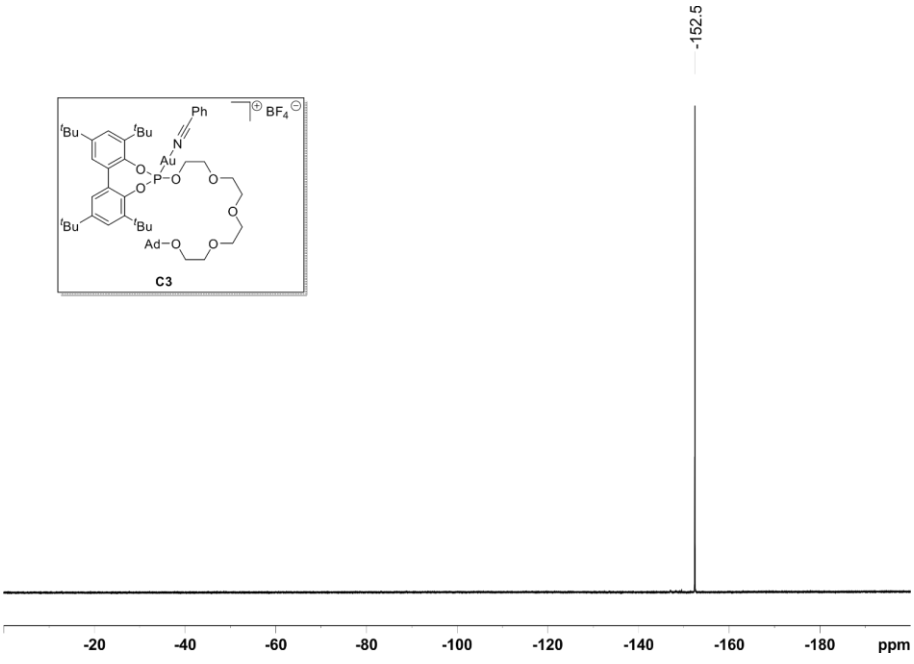

Figure 228. $^{19}F\{^{1}H\}$ NMR spectrum (376 MHz, CD_2Cl_2) for complex **C3**.

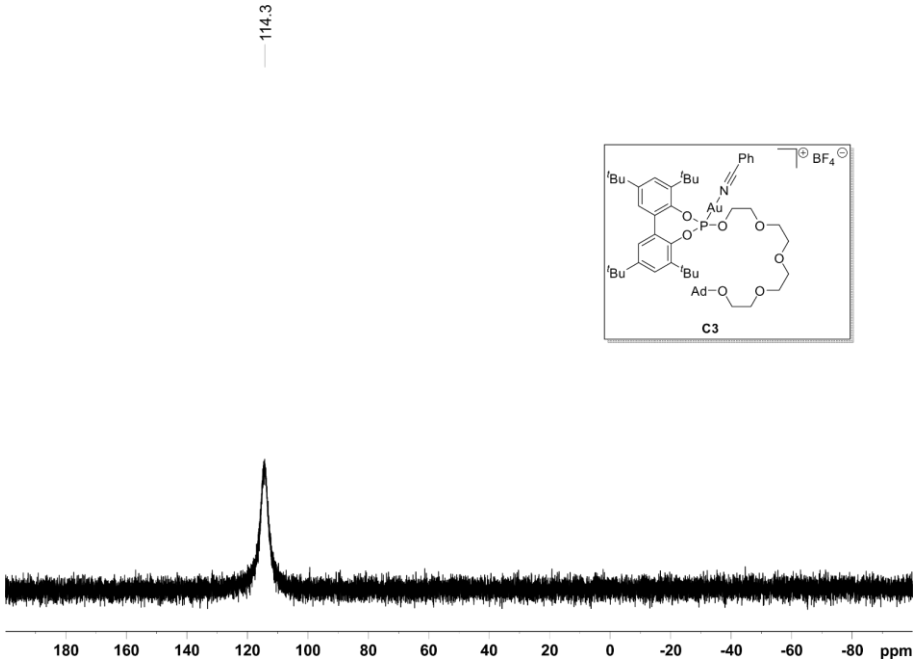

Figure 229. $^{31}P\{^{1}H\}$ NMR spectrum (162 MHz, CD_2Cl_2) for complex **C3**.

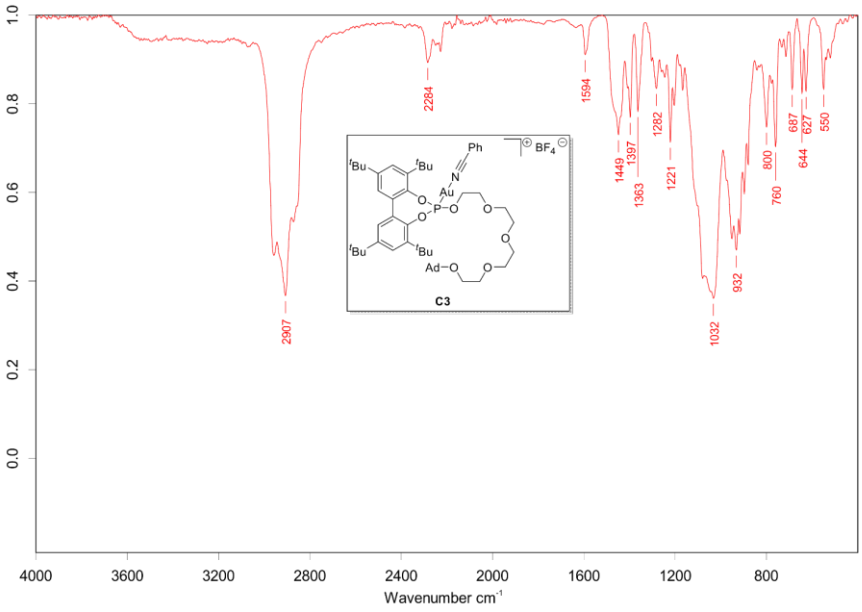

Figure 230. IR spectrum for complex **C3**.

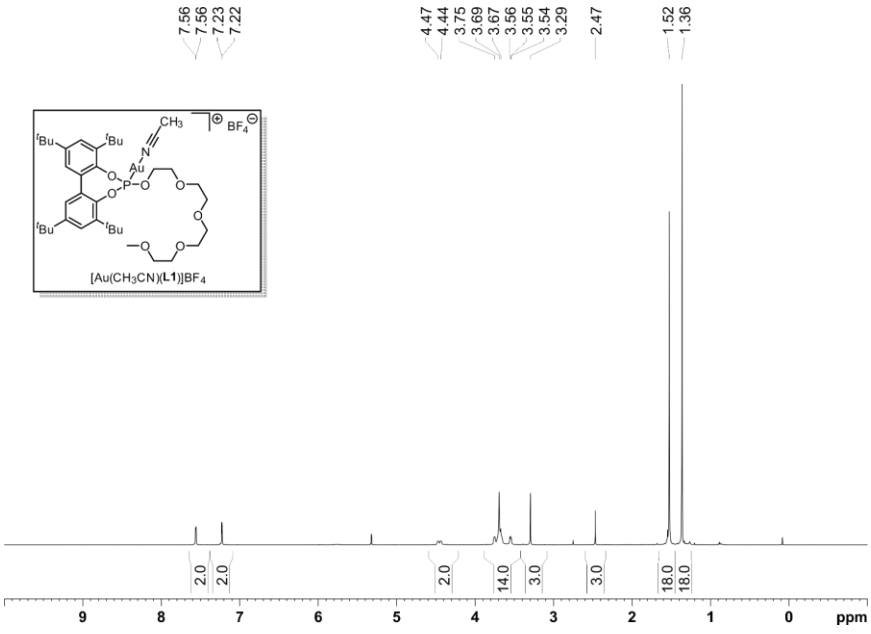

Figure 231. ^{1}H NMR spectrum (400 MHz, CD_2Cl_2) for complex $[Au(CH_3CN)(\mathbf{L1})]BF_4$.

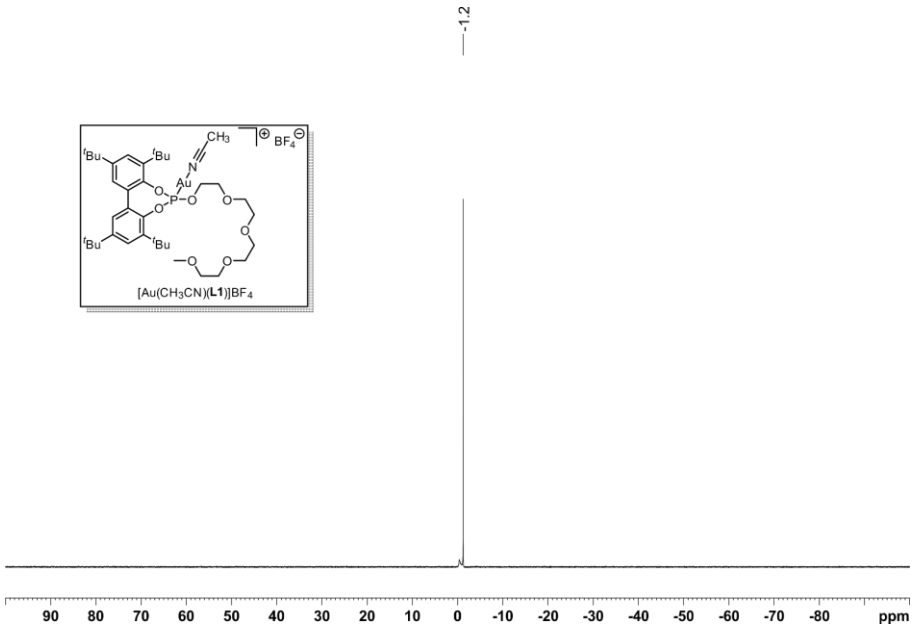

Figure 232. $^{11}B\{^{1}H\}$ NMR spectrum (128 MHz, CD_2Cl_2) for complex $[Au(CH_3CN)(\mathbf{L1})]BF_4$.

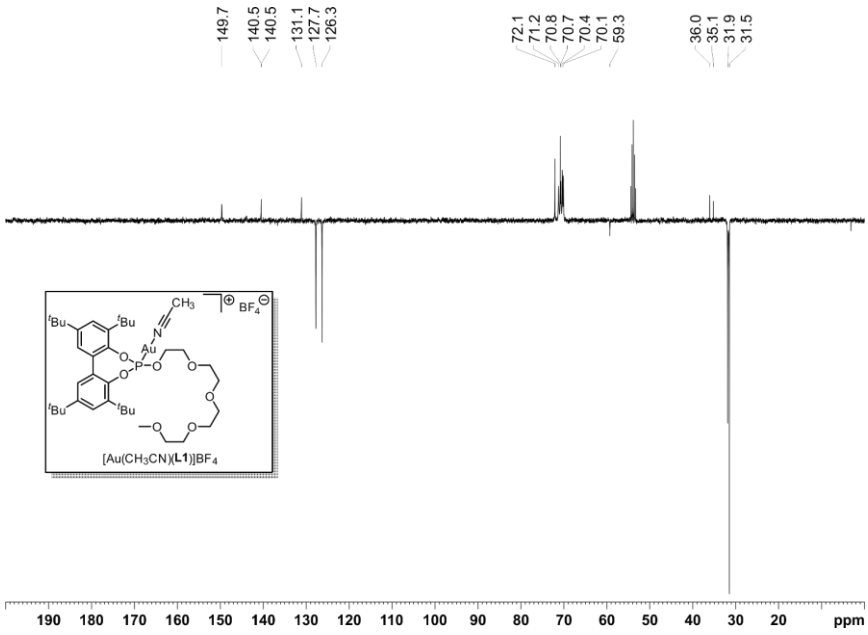

Figure 233. $^{13}C\{^{1}H\}$ DEPTQ135 NMR spectrum (126 MHz, CD_2Cl_2) for complex $[Au(CH_3CN)(\mathbf{L1})]BF_4$.

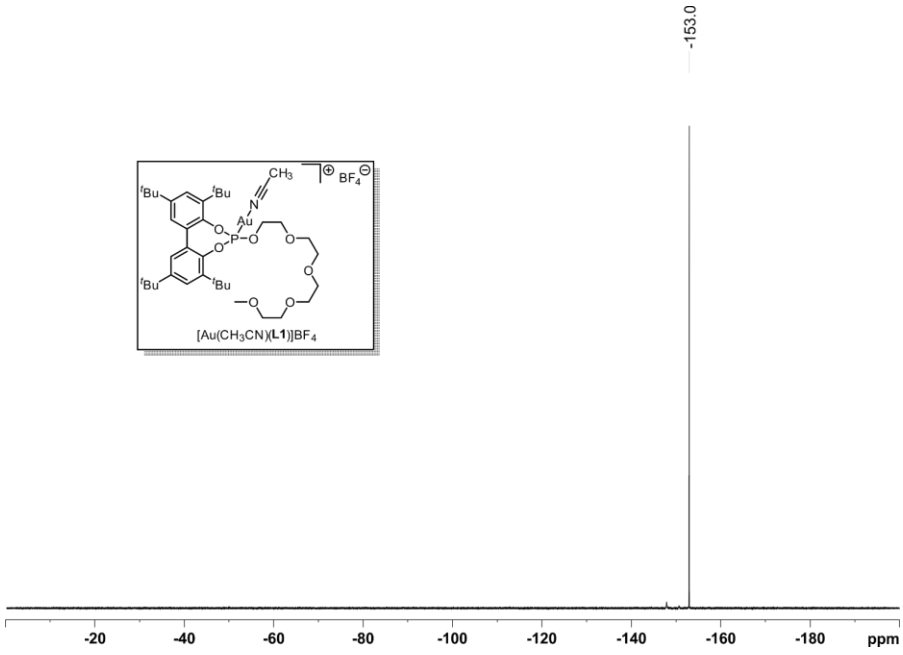

Figure 234. $^{19}F\{^{1}H\}$ NMR spectrum (376 MHz, CD_2Cl_2) for complex $[Au(CH_3CN)(\mathbf{L1})]BF_4$.

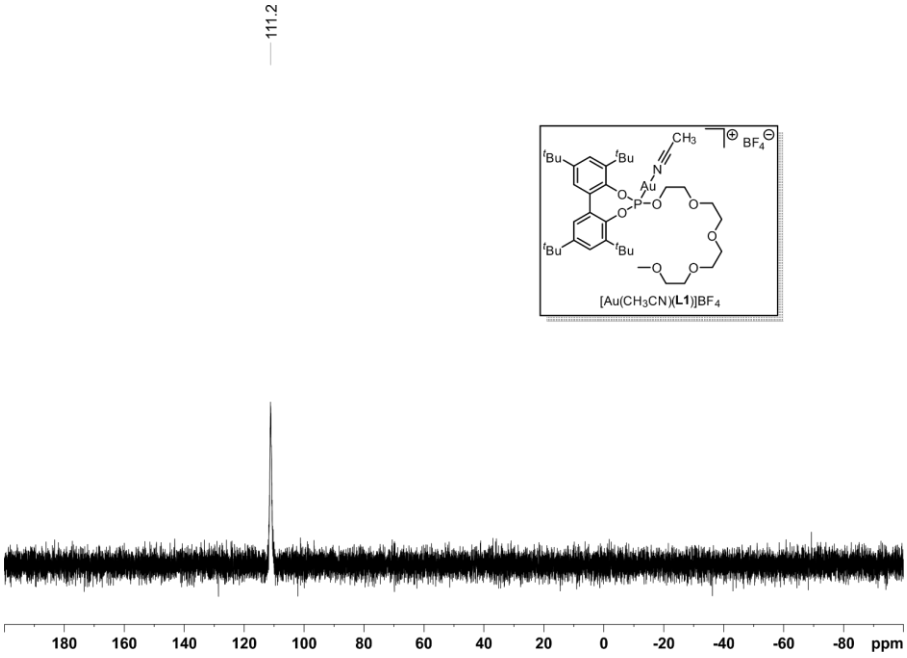

Figure 235. $^{31}P\{^{1}H\}$ NMR spectrum (162 MHz, CD_2Cl_2) for complex $[Au(CH_3CN)(\mathbf{L1})]BF_4$.

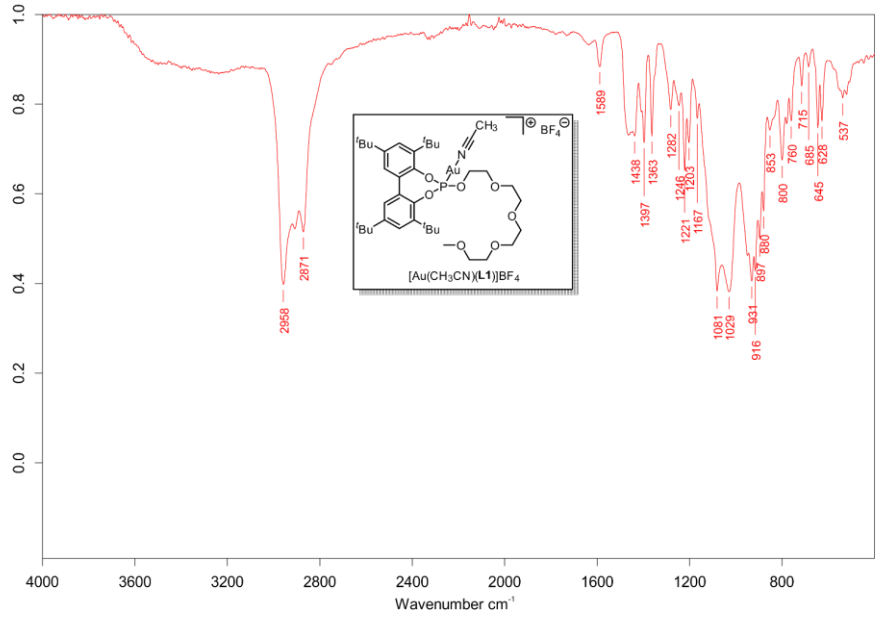

Figure 236. IR spectrum for complex $[Au(CH_3CN)(\mathbf{L1})]BF_4$.

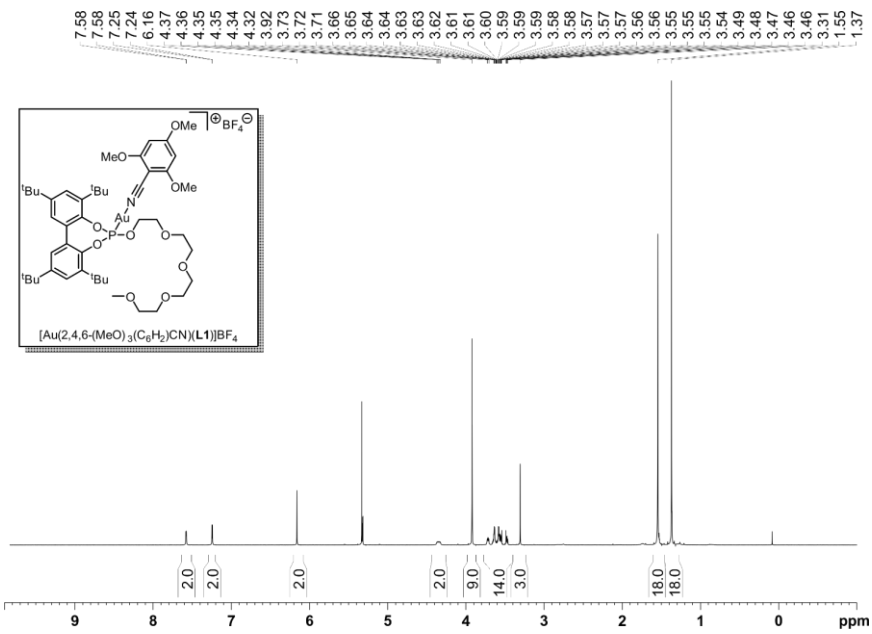

Figure 237. ^{1}H NMR spectrum (400 MHz, CD_2Cl_2) for complex [Au(2,4,6-$(MeO)_3(C_6H_2)CN$(**L1**)]BF_4.

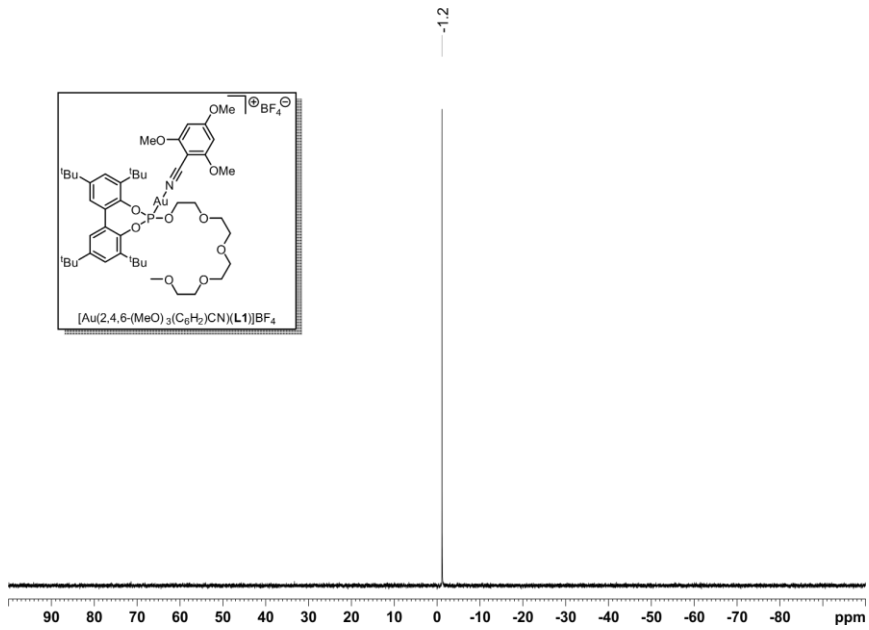

Figure 238. $^{11}B\{^{1}H\}$ NMR spectrum (128 MHz, CD_2Cl_2) for complex [Au(2,4,6-$(MeO)_3(C_6H_2)CN$(**L1**)]BF_4.

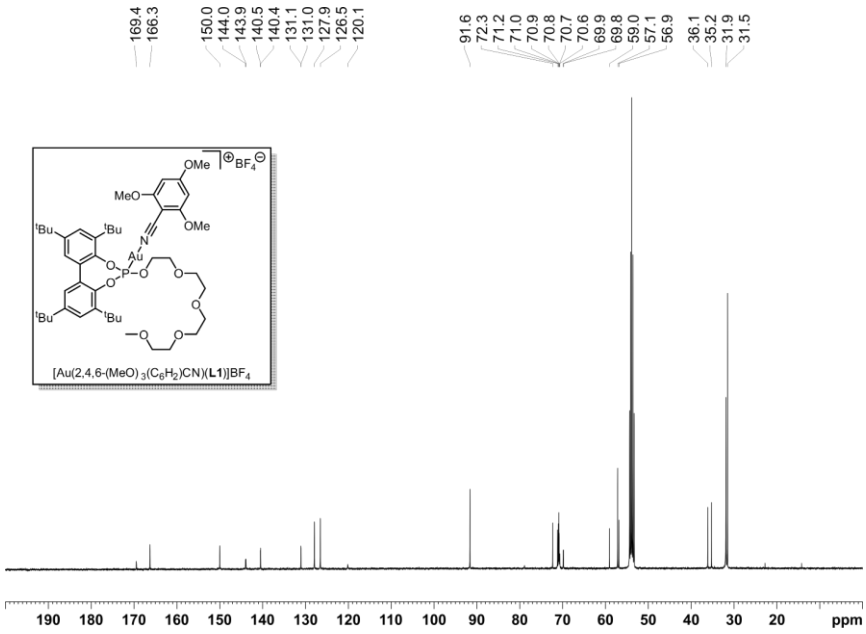

Figure 239. $^{13}C\{^{1}H\}$ NMR spectrum (126 MHz, CD_2Cl_2) for complex [Au(2,4,6-$(MeO)_3(C_6H_2)CN$)(**L1**)]BF_4.

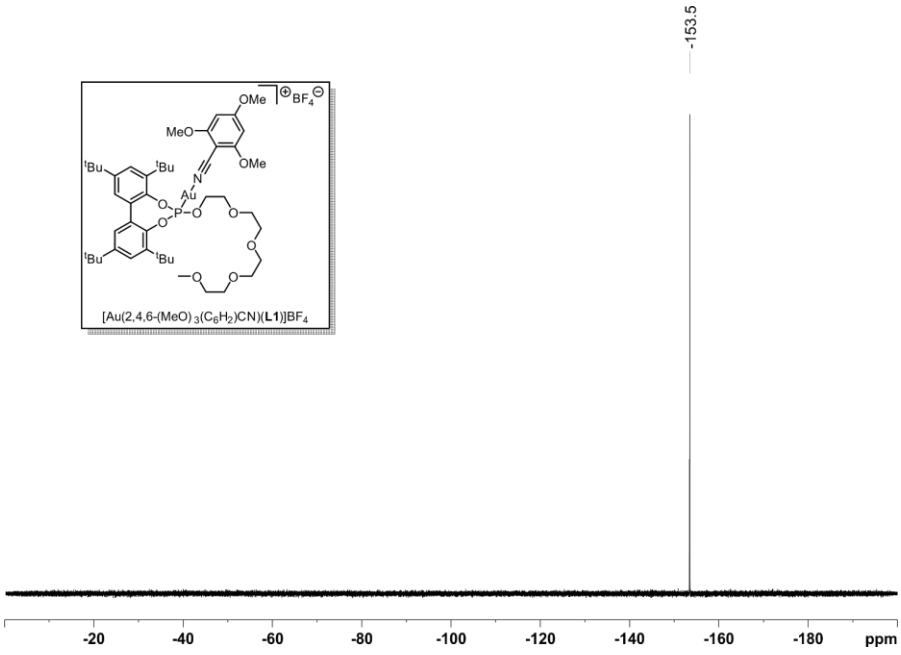

Figure 240. $^{19}F\{^{1}H\}$ NMR spectrum (376 MHz, CD_2Cl_2) for complex [Au(2,4,6-$(MeO)_3(C_6H_2)CN$)(**L1**)]BF_4.

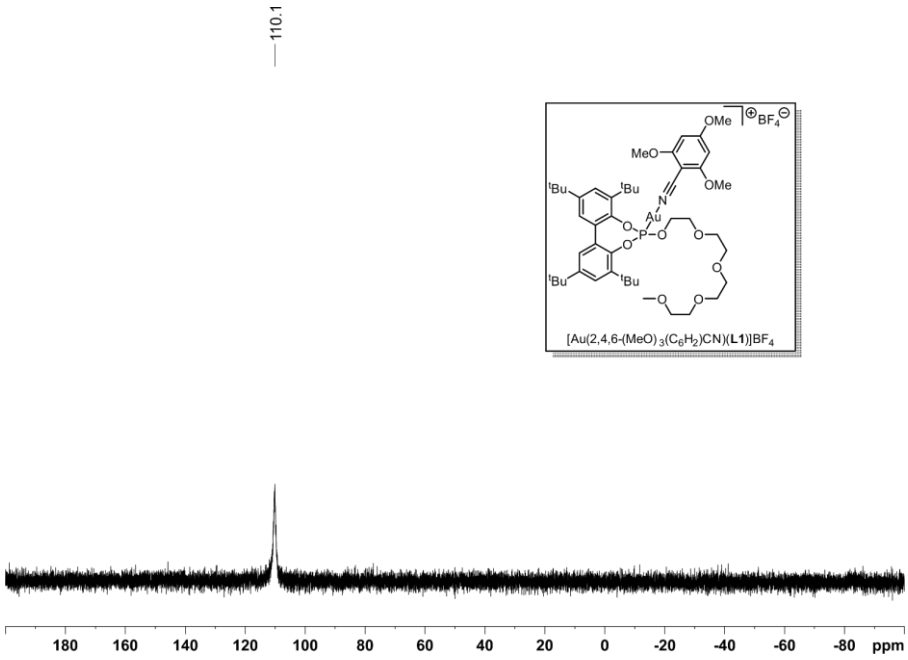

Figure 241. $^{31}P\{^{1}H\}$ NMR spectrum (162 MHz, CD_2Cl_2) for complex [Au(2,4,6-(MeO)$_3$(C_6H_2)CN)(**L1**)]BF_4.

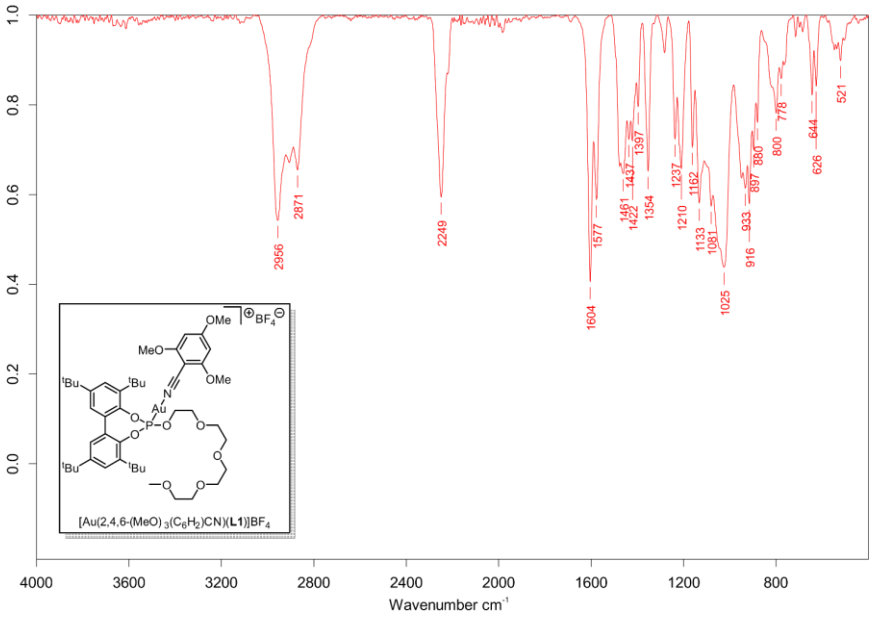

Figure 242. IR spectrum for complex [Au(2,4,6-(MeO)$_3$(C_6H_2)CN)(**L1**)]BF_4.

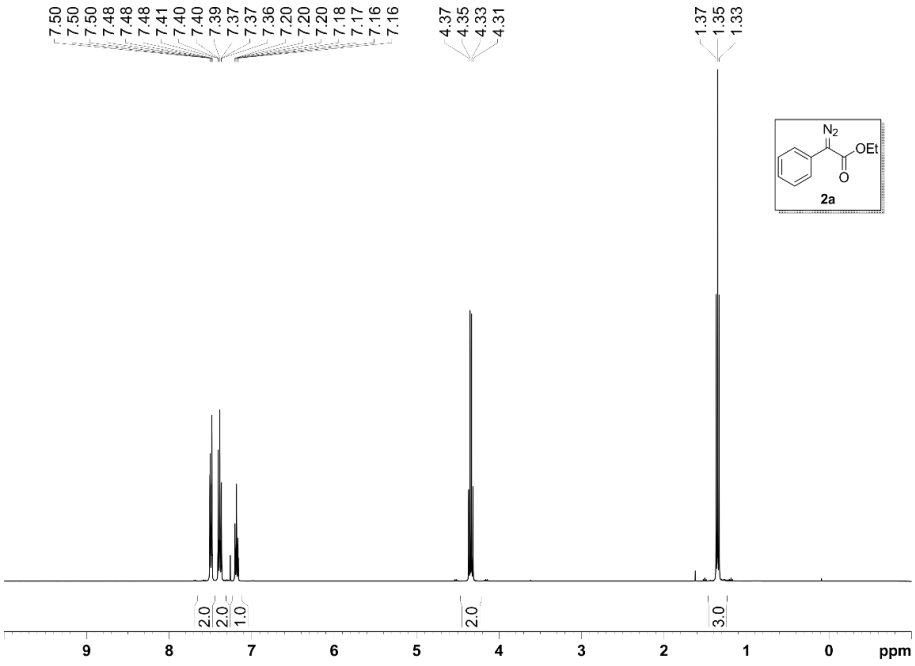

Figure 243. ^{1}H NMR spectrum (400 MHz, $CDCl_3$) for **2a**.

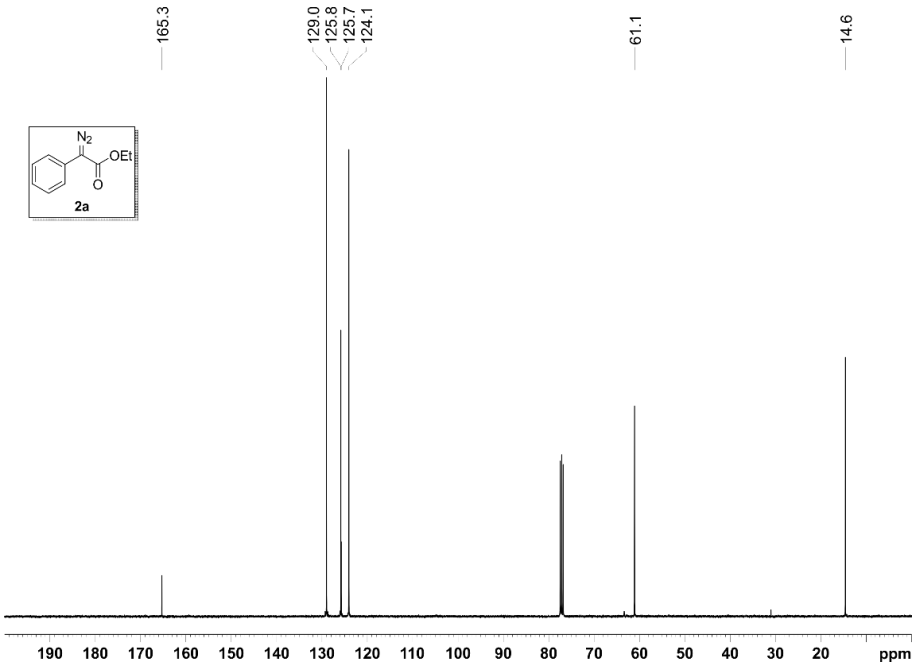

Figure 244. $^{13}C\{^{1}H\}$ NMR spectrum (100 MHz, $CDCl_3$) for **2a**.

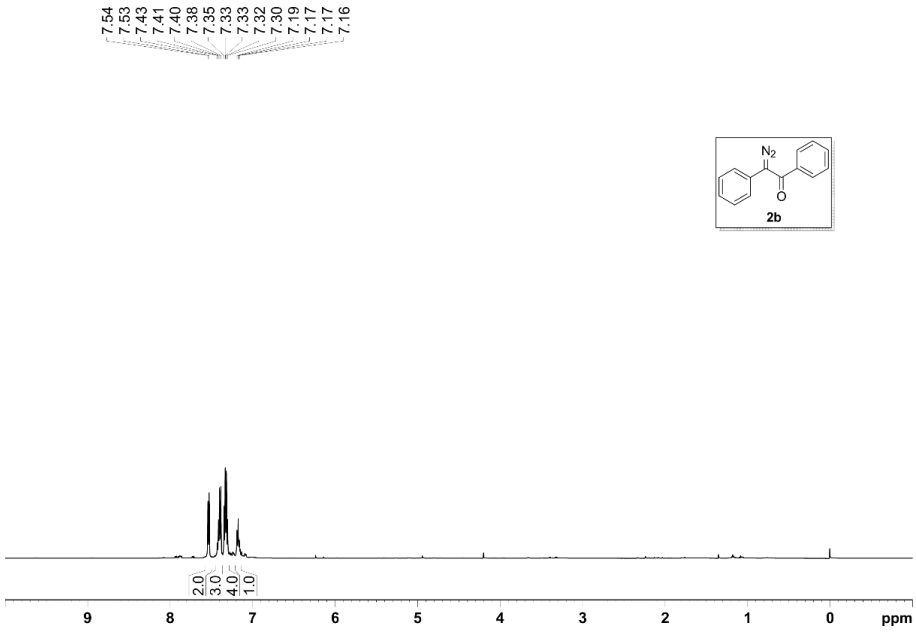

Figure 245. ^{1}H NMR spectrum (500 MHz, $CDCl_3$) for **2b**.

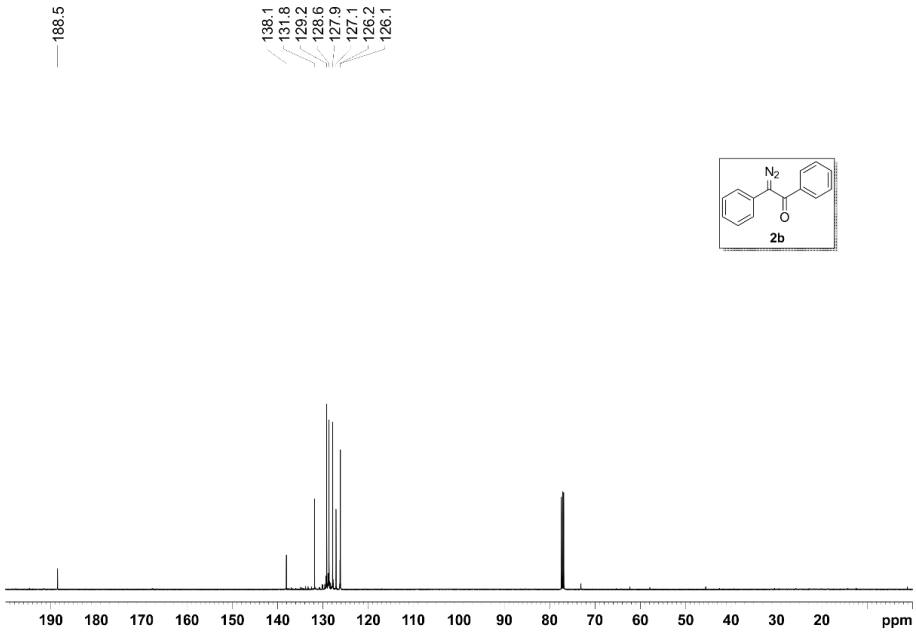

Figure 246. $^{13}C\{^{1}H\}$ NMR spectrum (126 MHz, $CDCl_3$) for **2b**.

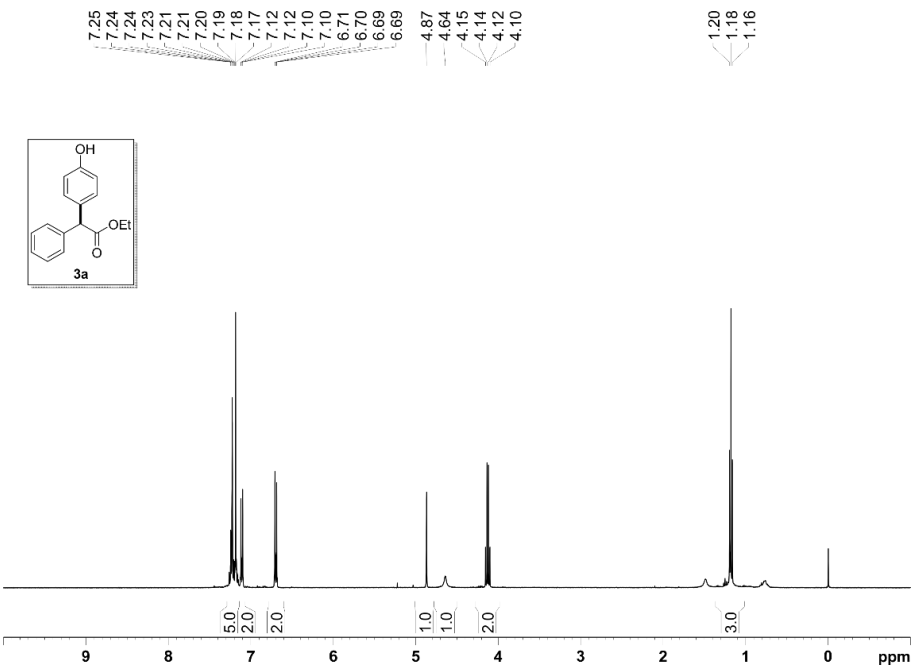

Figure 247. ^{1}H NMR spectrum (400 MHz, $CDCl_3$) for **3a**.

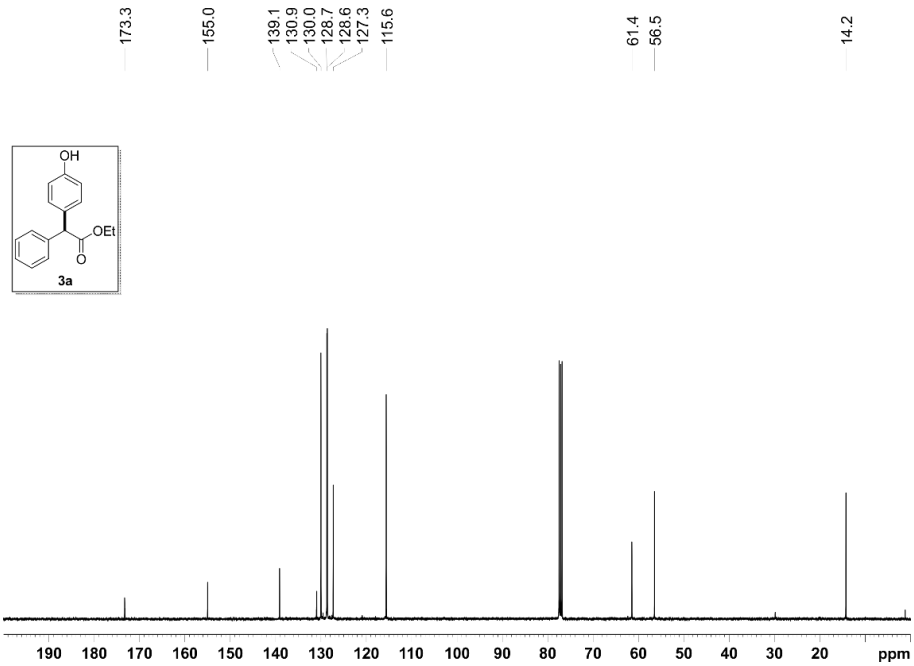

Figure 248. $^{13}C\{^{1}H\}$ NMR spectrum (100 MHz, $CDCl_3$) for **3a**.

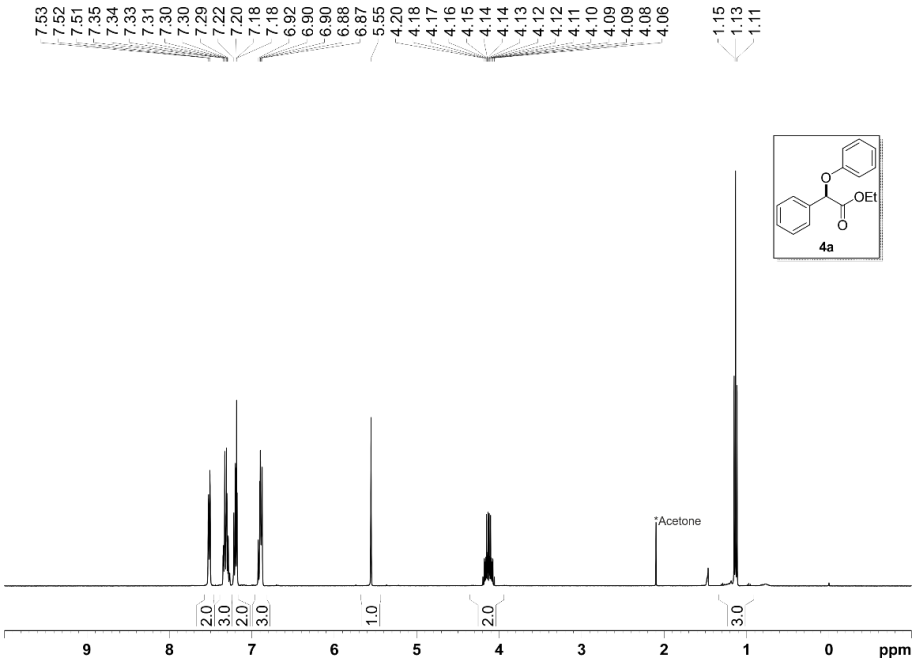

Figure 249. ^{1}H NMR spectrum (400 MHz, $CDCl_3$) for **4a**.

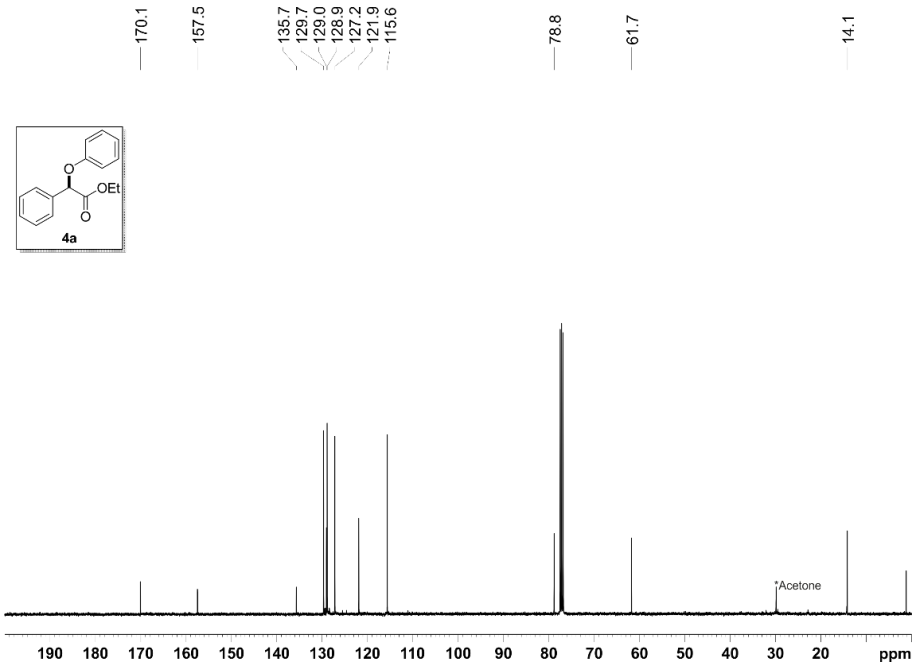

Figure 250. $^{13}C\{^{1}H\}$ NMR spectrum (100 MHz, $CDCl_3$) for **4a**.

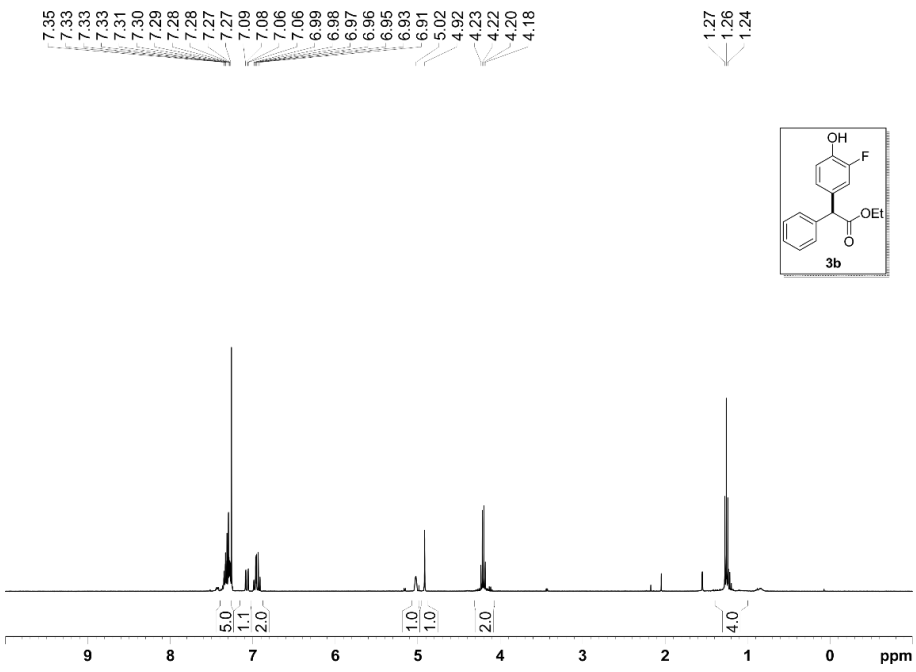

Figure 251. ^{1}H NMR spectrum (400 MHz, $CDCl_3$) for **3b**.

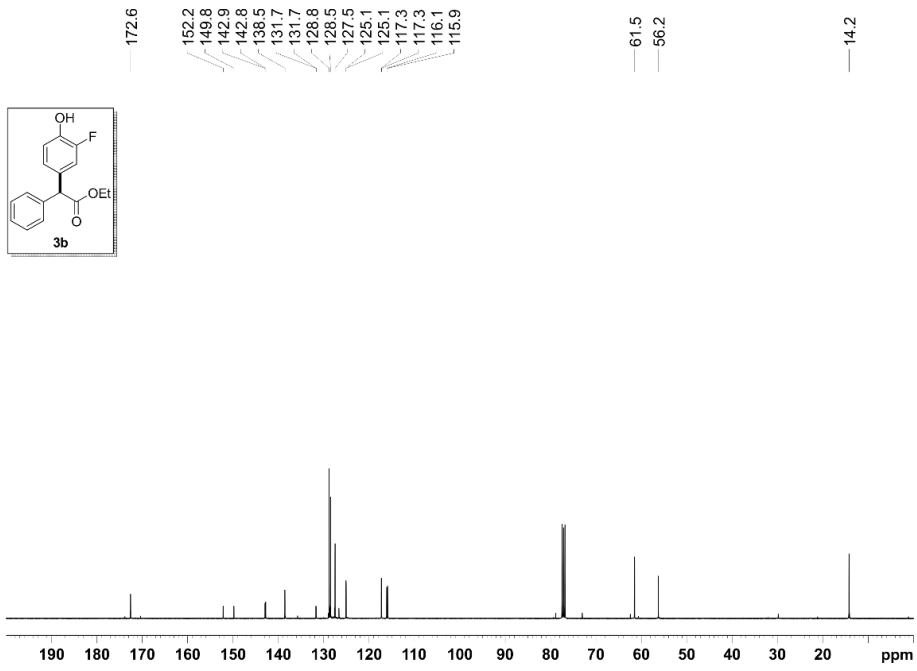

Figure 252. $^{13}C\{^{1}H\}$ NMR spectrum (100 MHz, $CDCl_3$) for **3b**.

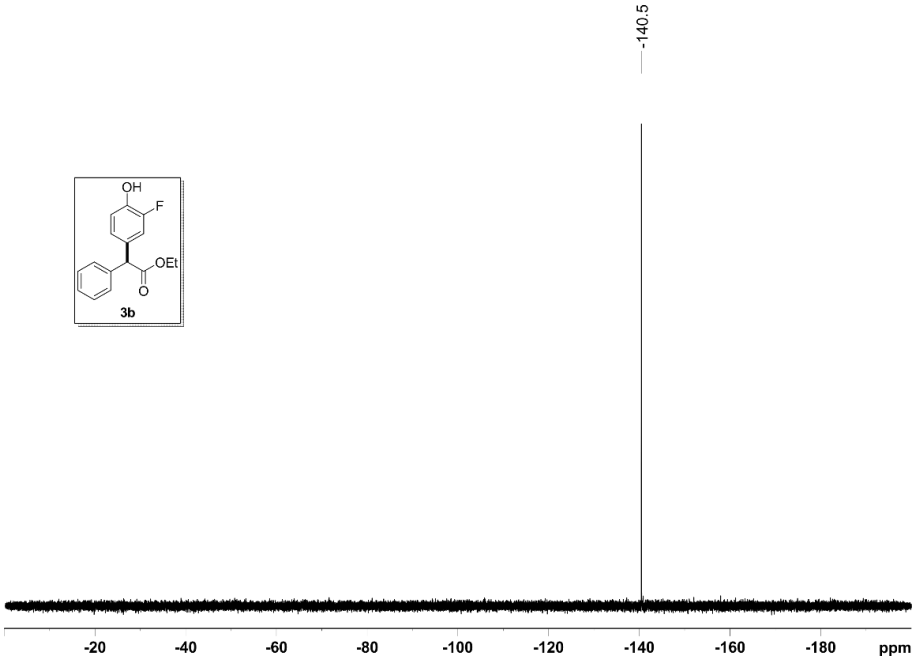

Figure 253. $^{19}F\{^{1}H\}$ NMR spectrum (376 MHz, $CDCl_3$) for **3b**.

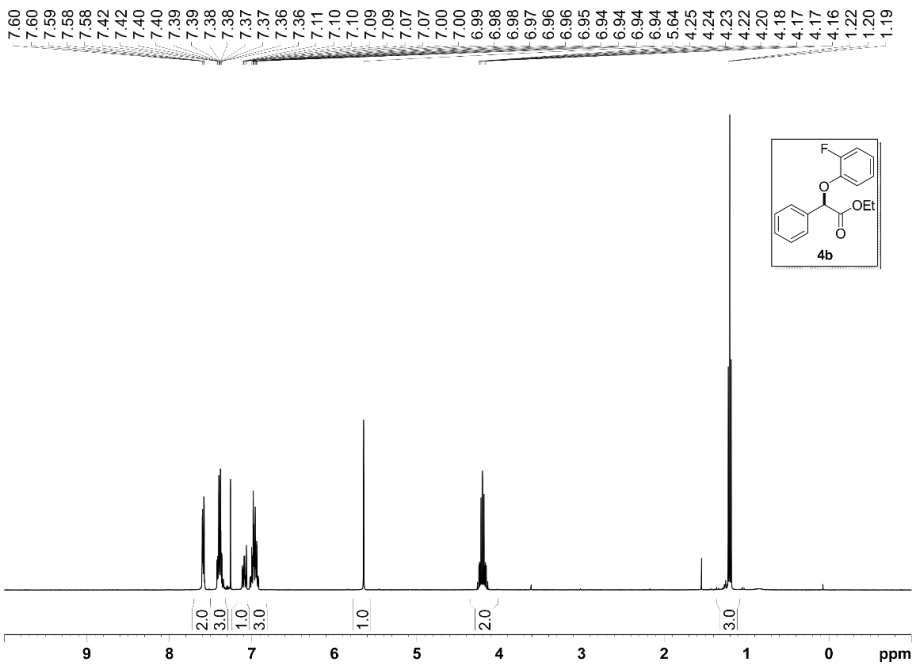

Figure 254. ^{1}H NMR spectrum (400 MHz, $CDCl_3$) for **4b**.

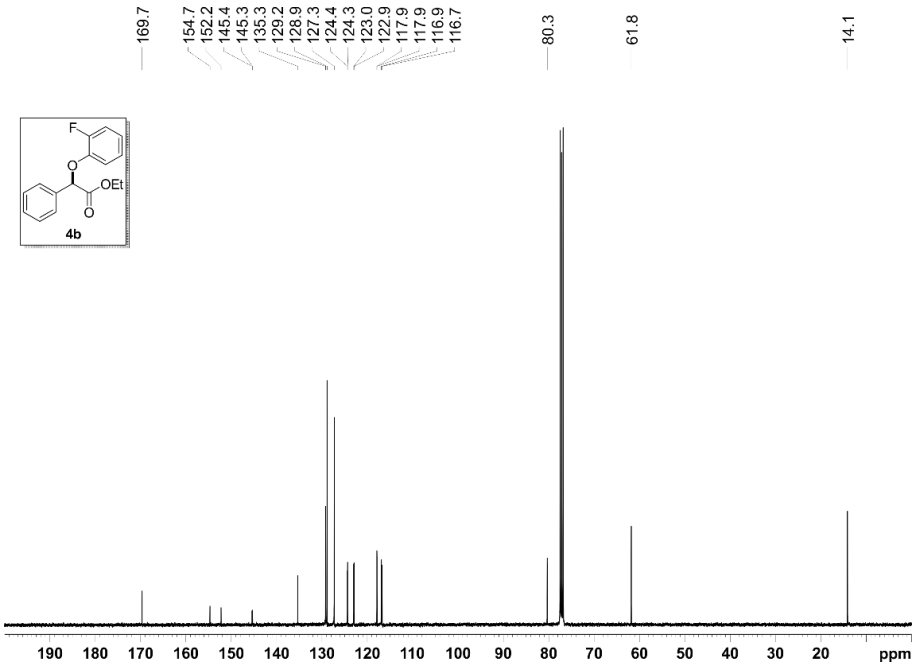

Figure 255. $^{13}C\{^{1}H\}$ NMR spectrum (100 MHz, $CDCl_3$) for **4b**.

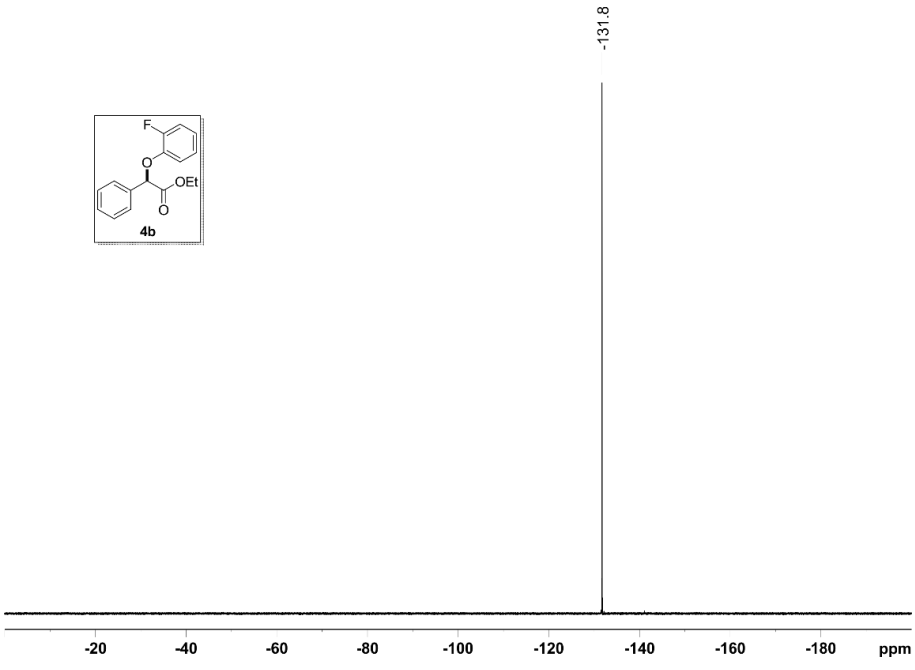

Figure 256. $^{19}F\{^{1}H\}$ NMR spectrum (376 MHz, $CDCl_3$) for **4b**.

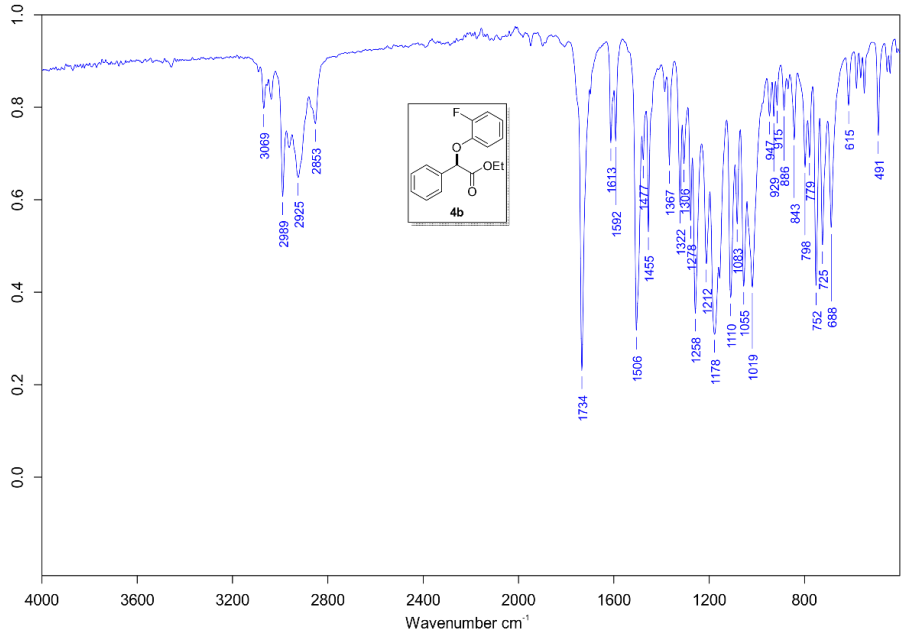

Figure 257. IR spectrum for **4b**.

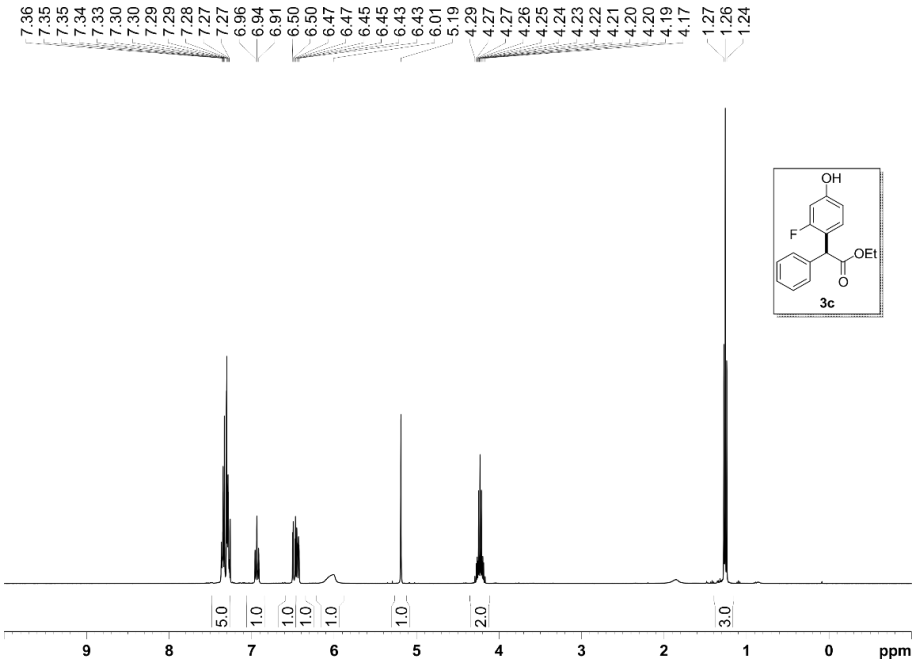

Figure 258. ^{1}H NMR spectrum (400 MHz, $CDCl_3$) for **3c**.

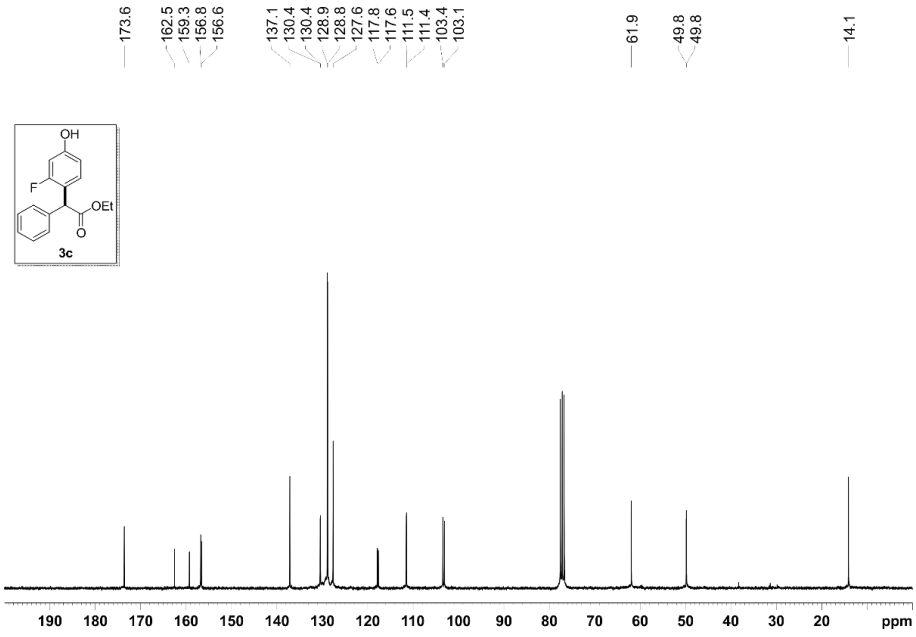

Figure 259. $^{13}C\{^{1}H\}$ NMR spectrum (76 MHz, $CDCl_3$) for **3c**.

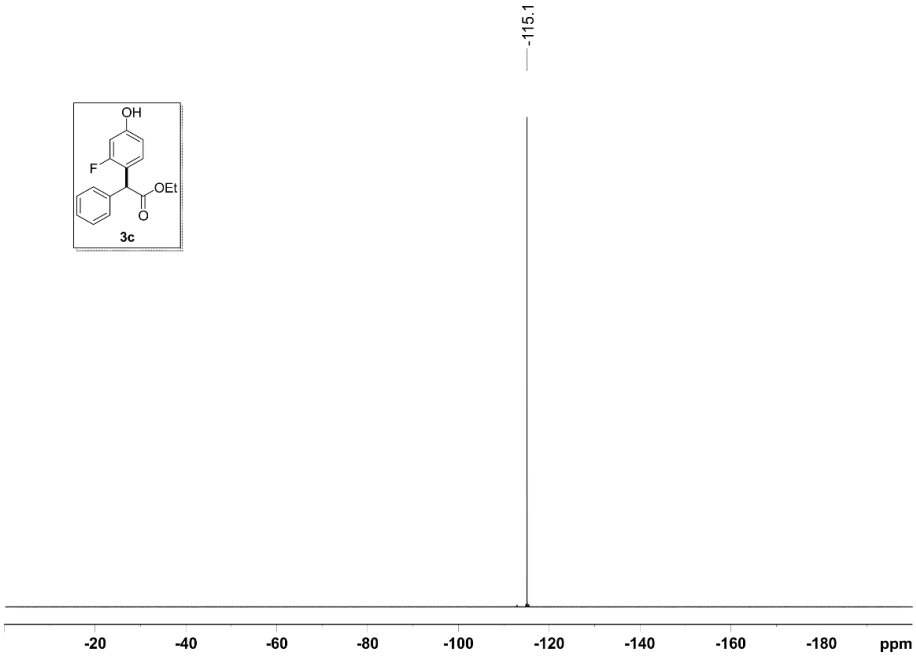

Figure 260. $^{19}F\{^{1}H\}$ NMR spectrum (376 MHz, $CDCl_3$) for **3c**.

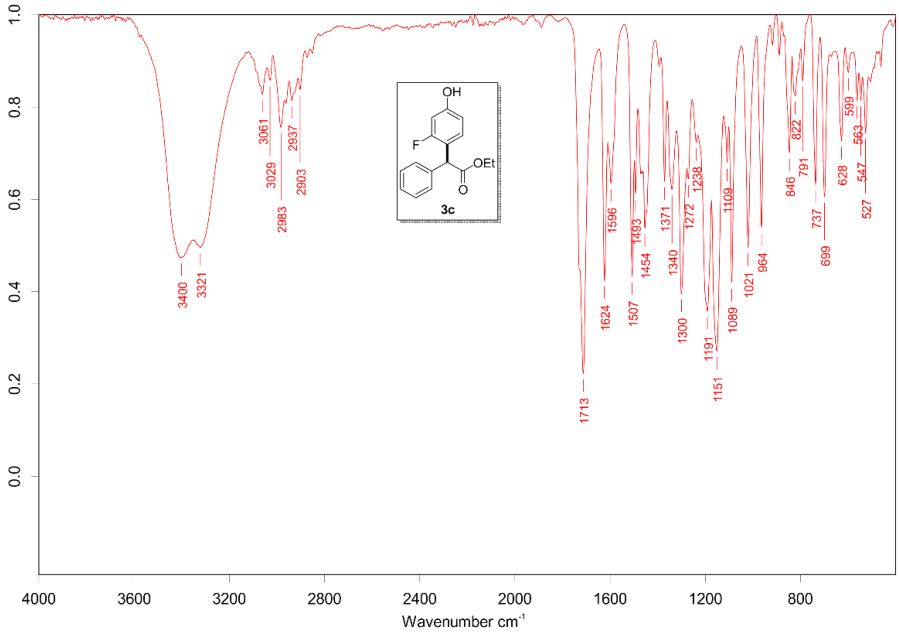

Figure 261. IR spectrum for **3c**.

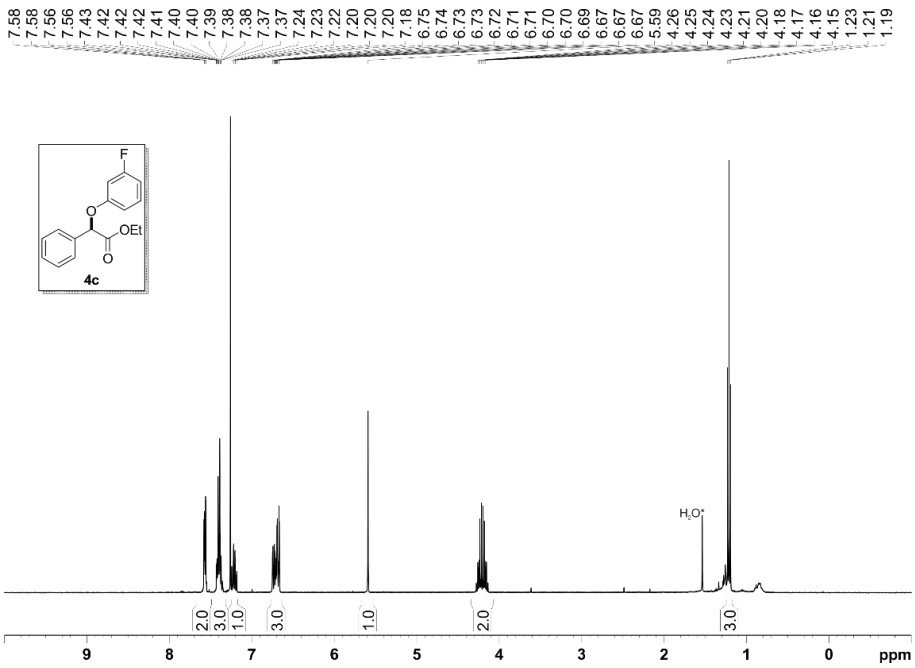

Figure 262. ^{1}H NMR spectrum (400 MHz, $CDCl_3$) for **4c**.

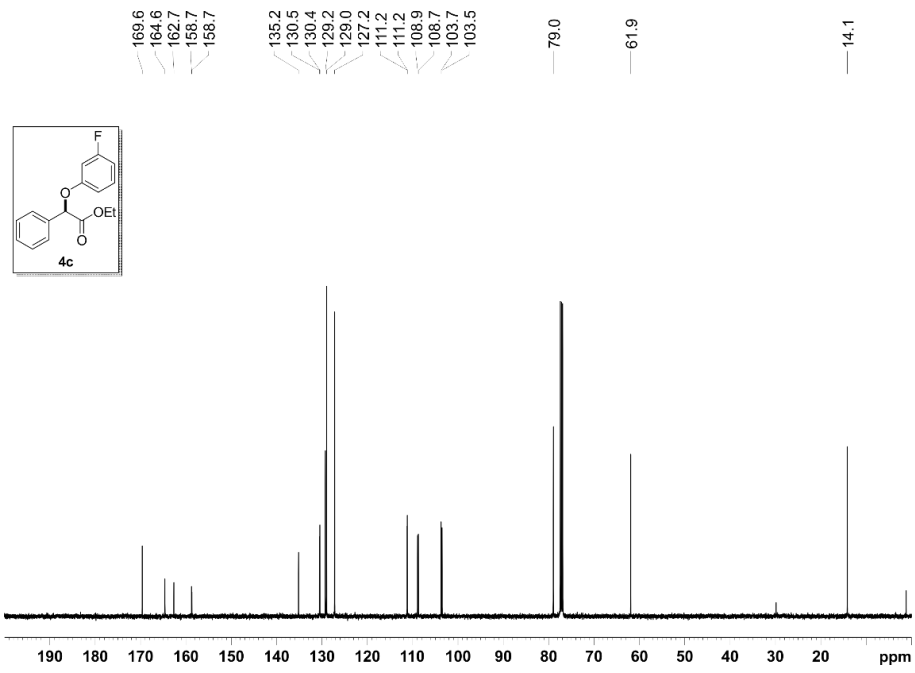

Figure 263. $^{13}C\{^{1}H\}$ NMR spectrum (126 MHz, $CDCl_3$) for **4c**.

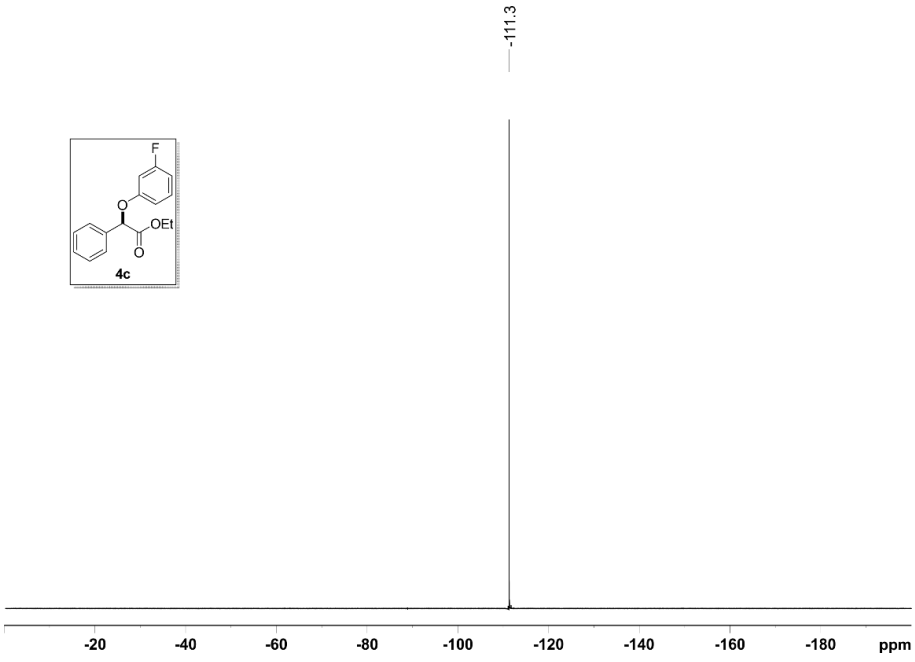

Figure 264. $^{19}F\{^{1}H\}$ NMR spectrum (376 MHz, $CDCl_3$) for **4c**.

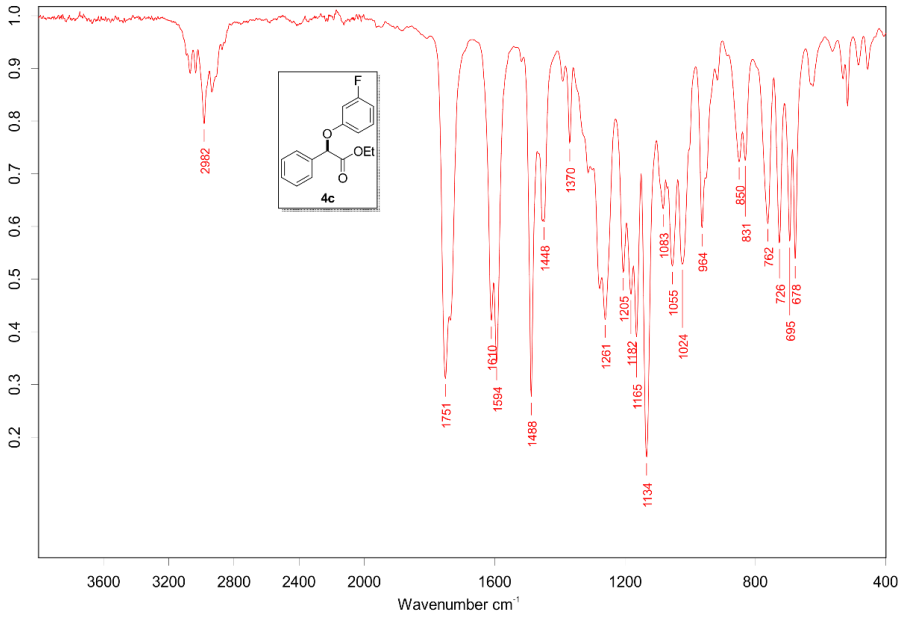

Figure 265. IR spectrum for **4c**.

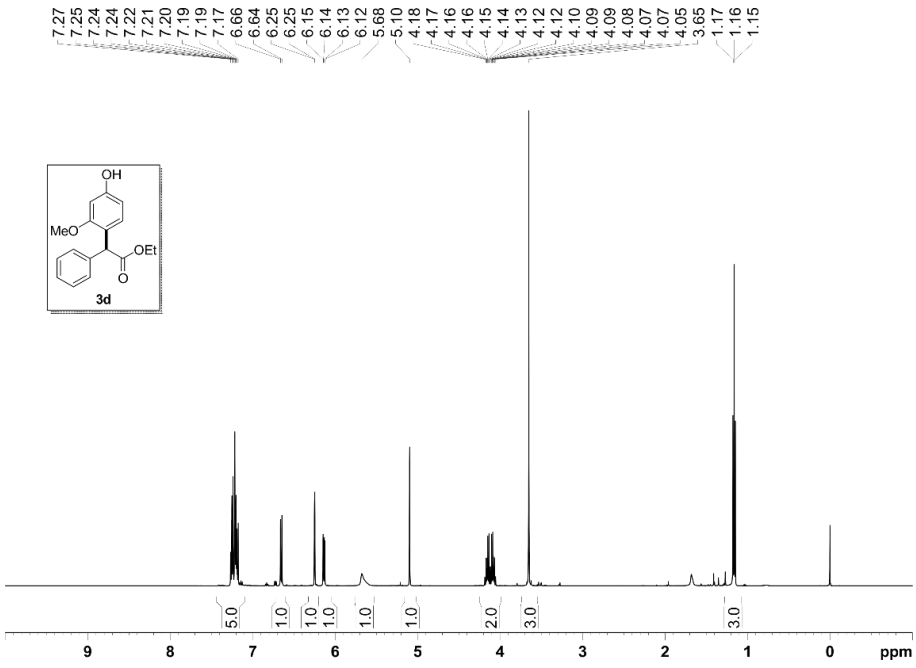

Figure 266. ^{1}H NMR spectrum (500 MHz, $CDCl_3$) for **3d**.

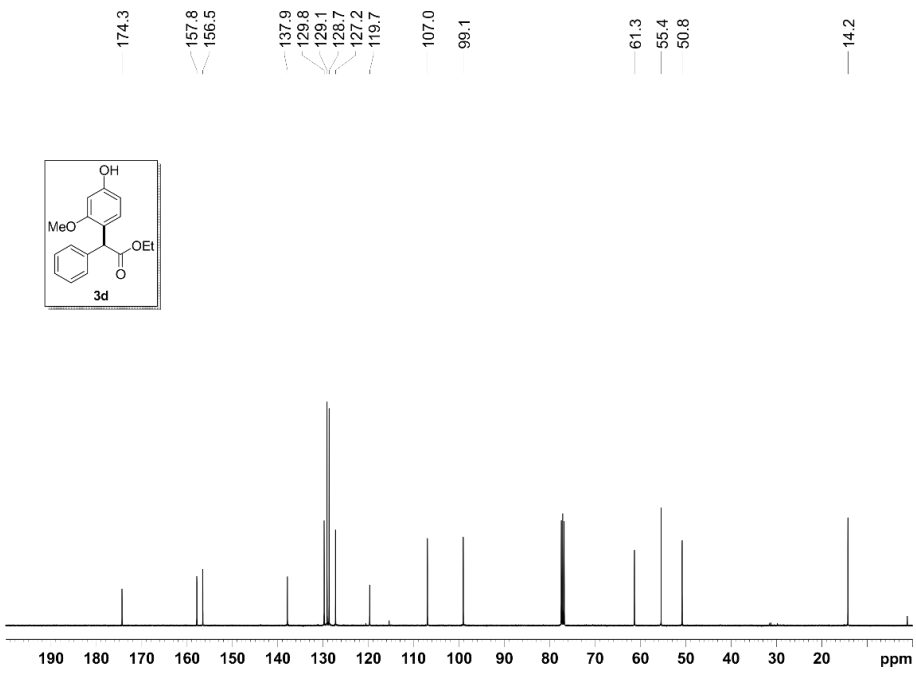

Figure 267. $^{13}C\{^{1}H\}$ NMR spectrum (100 MHz, $CDCl_3$) for **3d**.

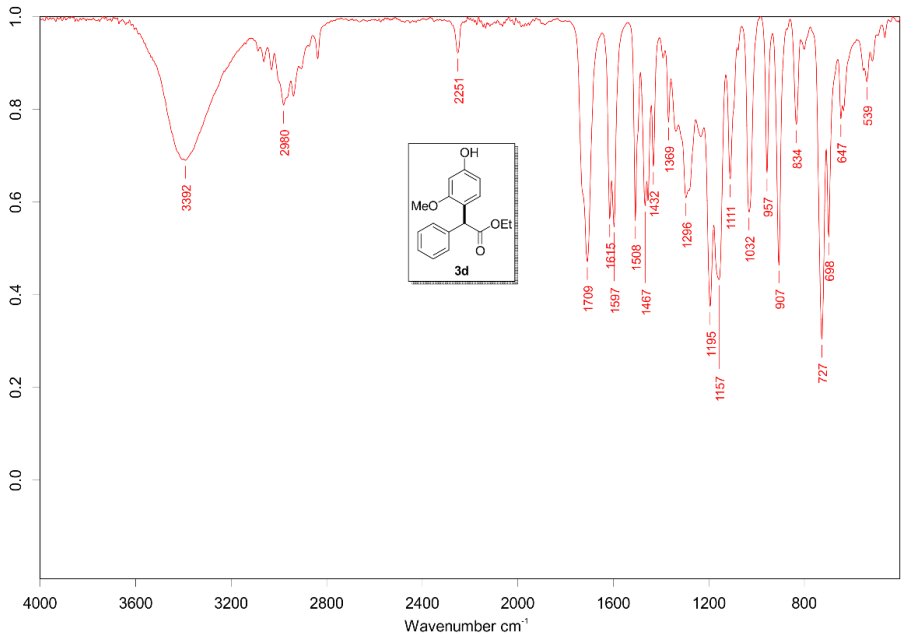

Figure 268. IR spectrum for **3d**.

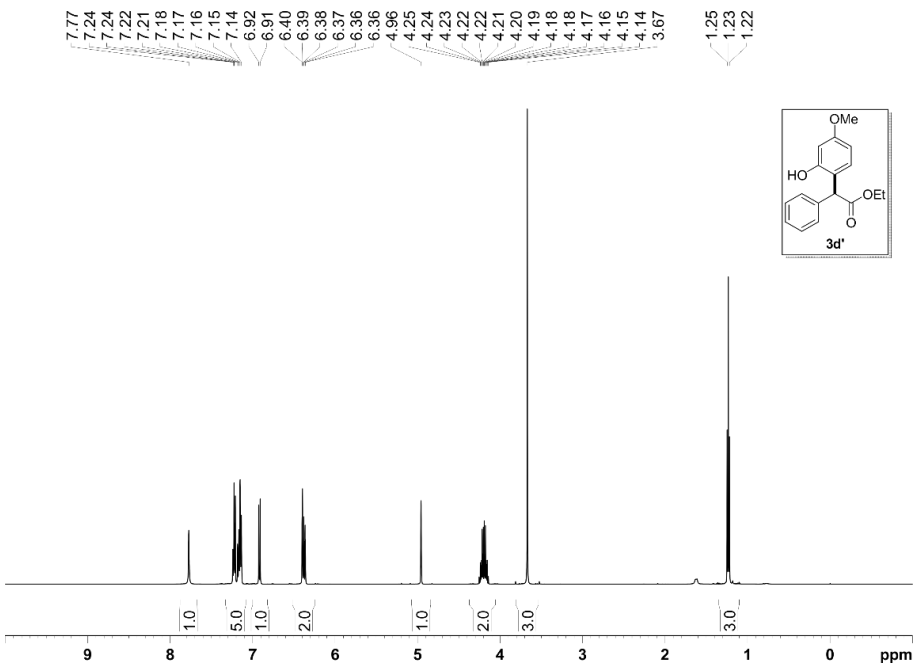

Figure 269. ^{1}H NMR spectrum (500 MHz, $CDCl_3$) for **3d'**.

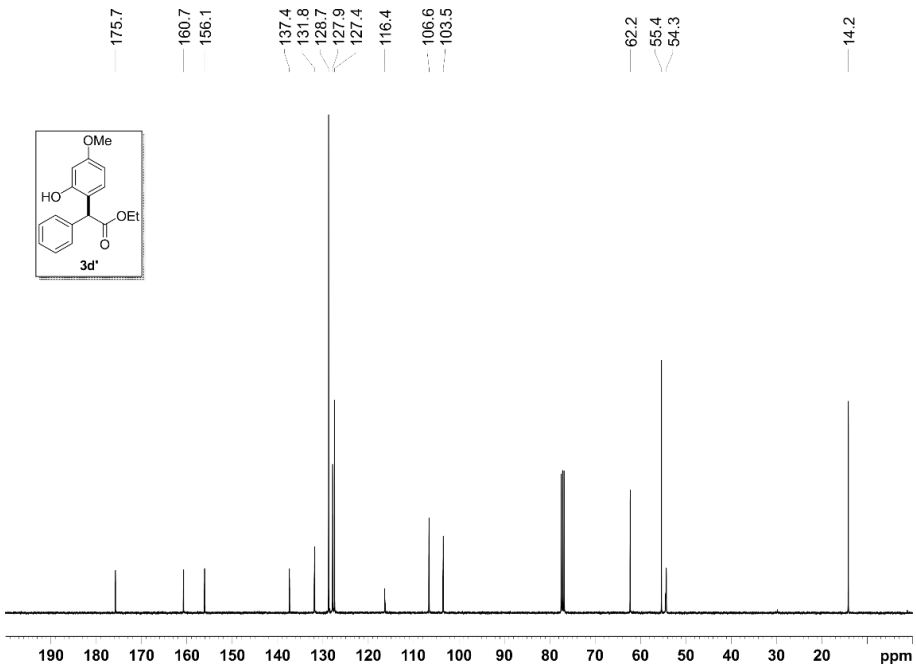

Figure 270. $^{13}C\{^{1}H\}$ NMR spectrum (100 MHz, $CDCl_3$) for **3d'**.

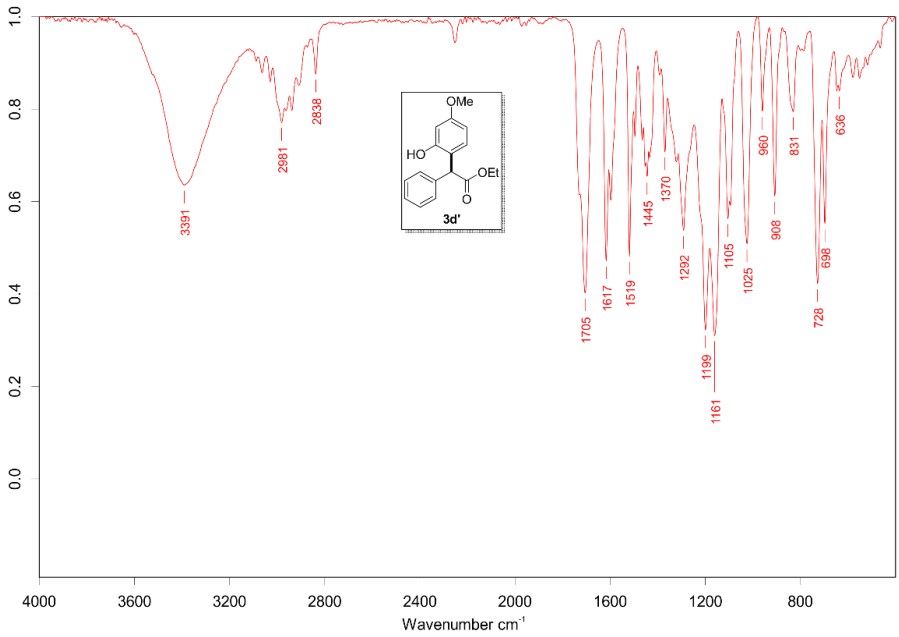

Figure 271. IR spectrum for **3d'**.

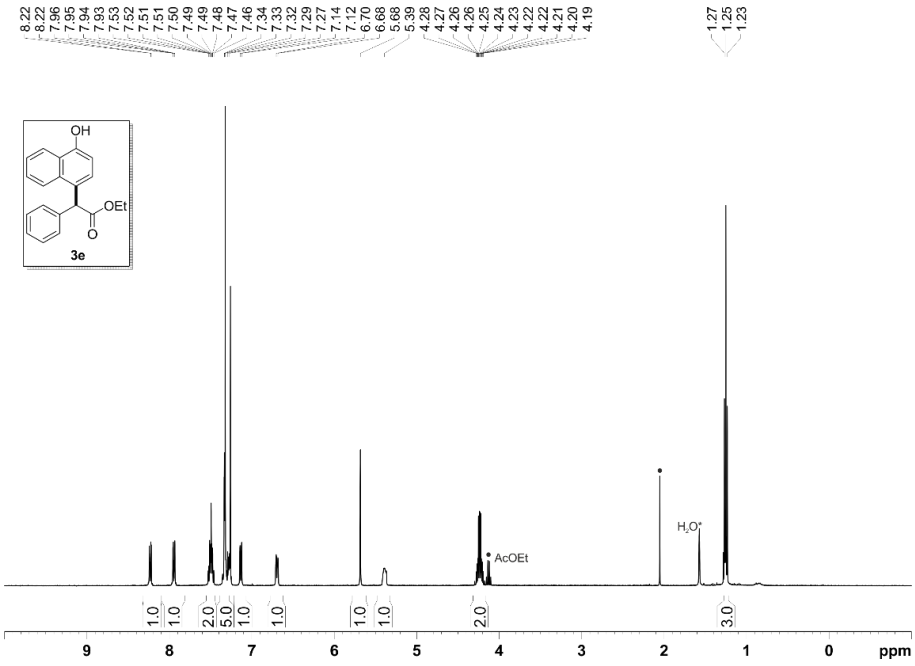

Figure 272. ^{1}H NMR spectrum (400 MHz, $CDCl_3$) for **3e**.

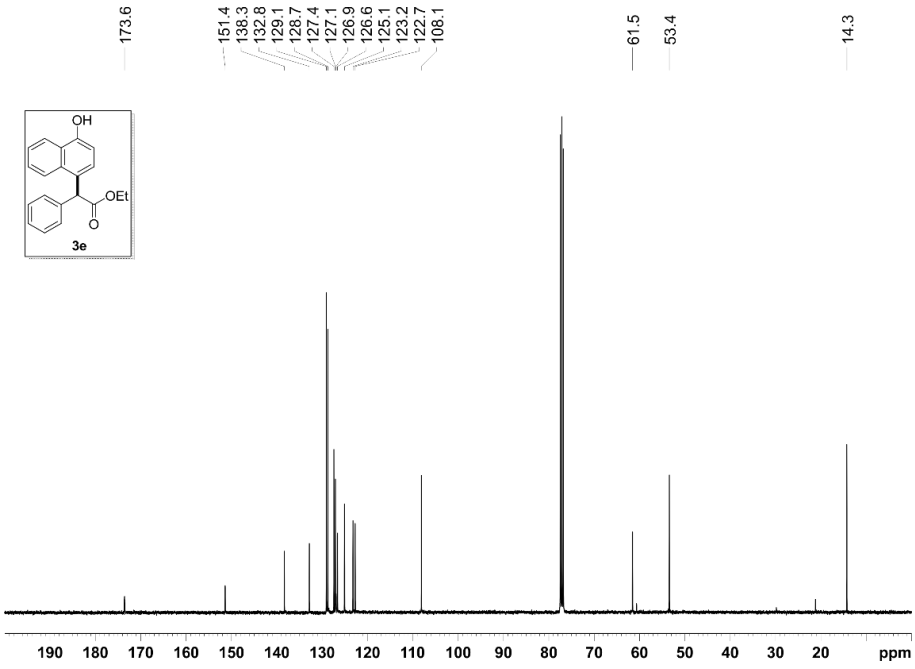

Figure 273. $^{13}C\{^{1}H\}$ NMR spectrum (100 MHz, $CDCl_3$) for **3e**.

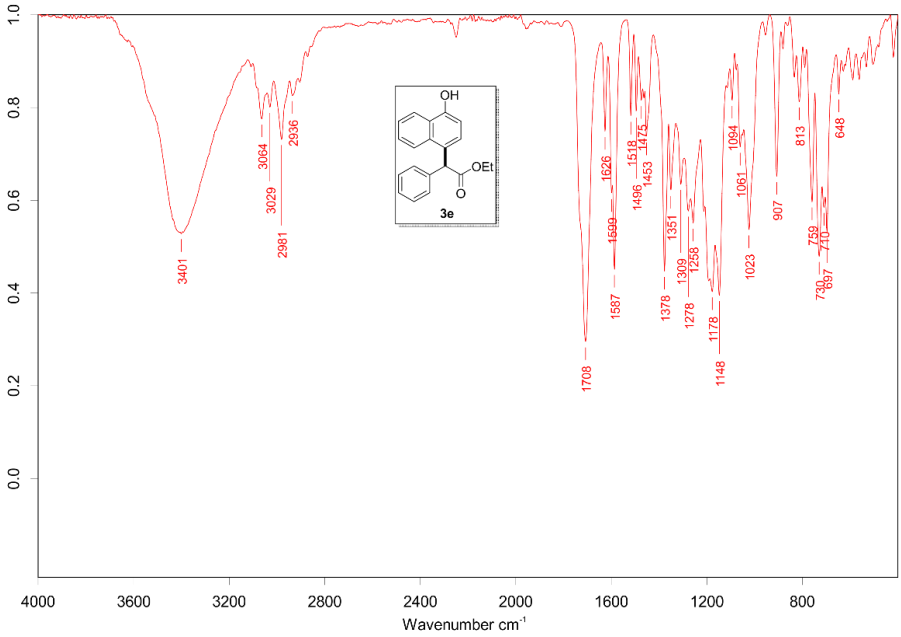

Figure 274. IR spectrum for **3e**.

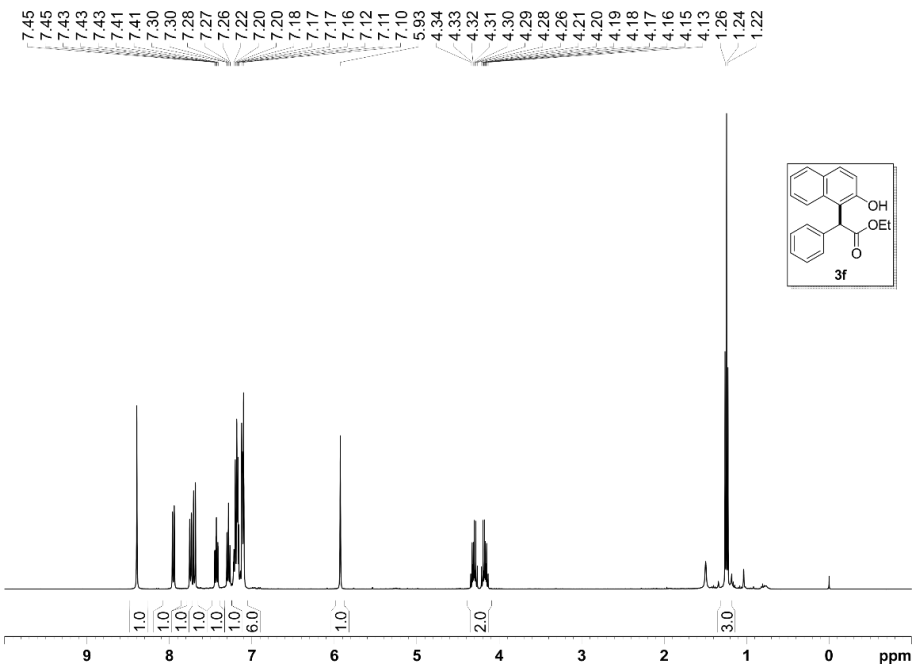

Figure 275. ^{1}H NMR spectrum (400 MHz, $CDCl_3$) for **3f**.

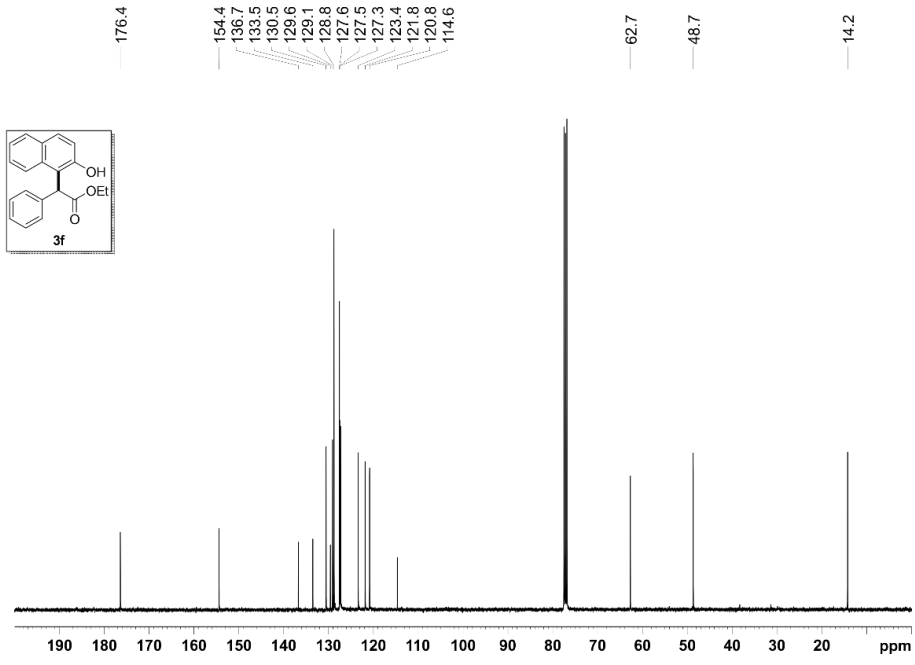

Figure 276. $^{13}C\{^{1}H\}$ NMR spectrum (100 MHz, $CDCl_3$) for **3f**.

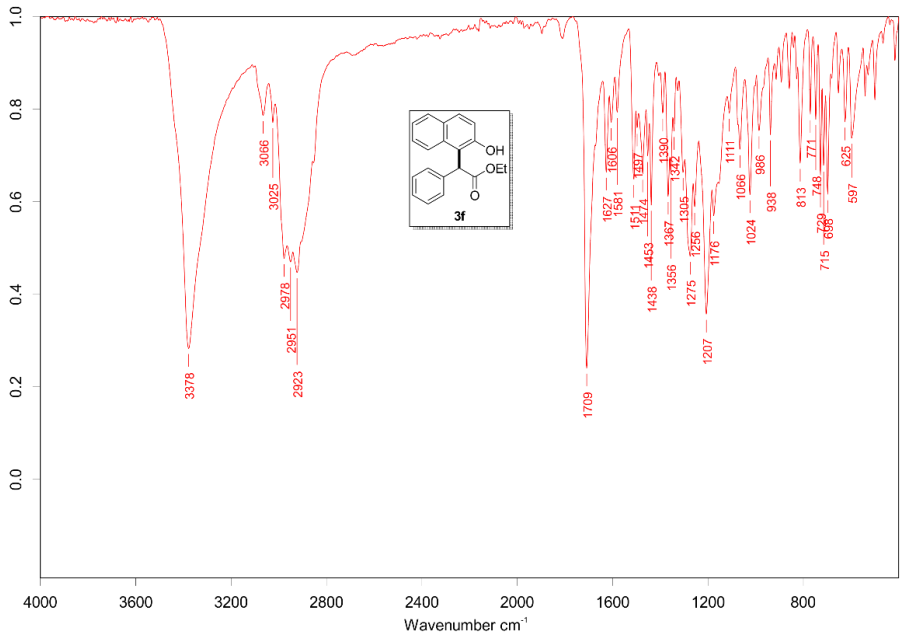

Figure 277. IR spectrum for **3f**.

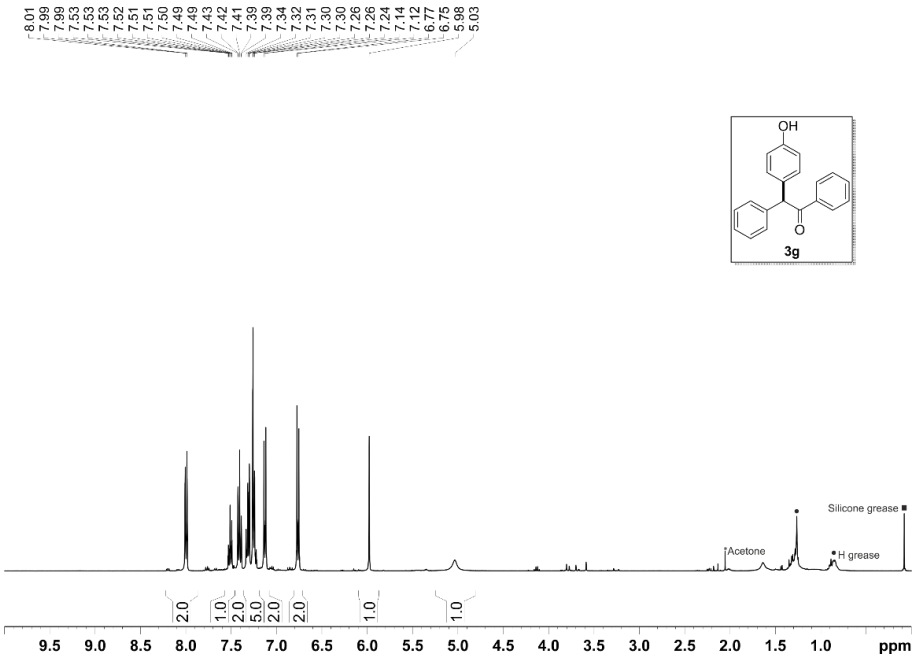

Figure 278. ^{1}H NMR spectrum (400 MHz, $CDCl_3$) for **3g**.

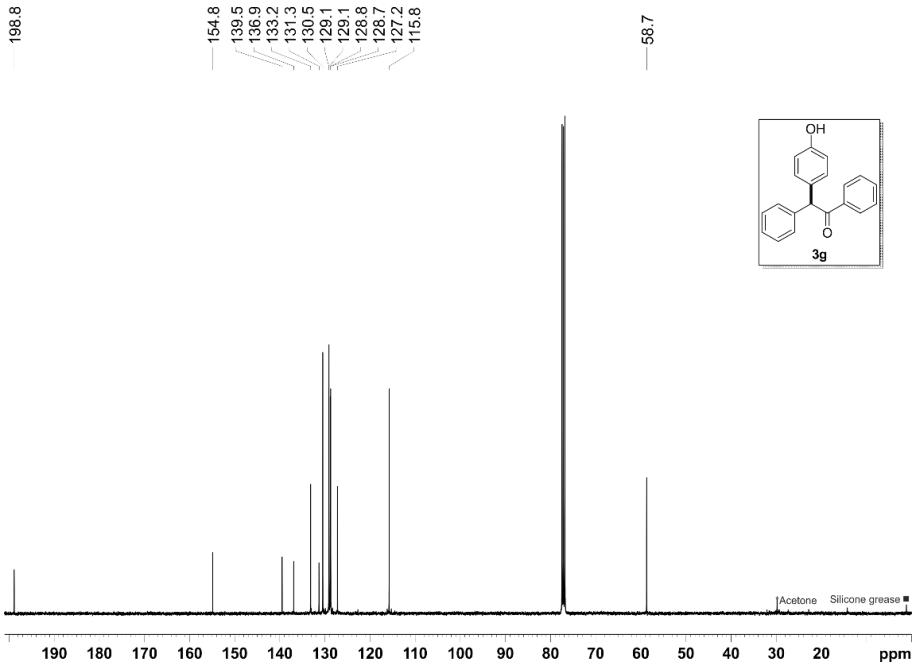

Figure 279. $^{13}C\{^{1}H\}$ NMR spectrum (100 MHz, $CDCl_3$) for **3g**.

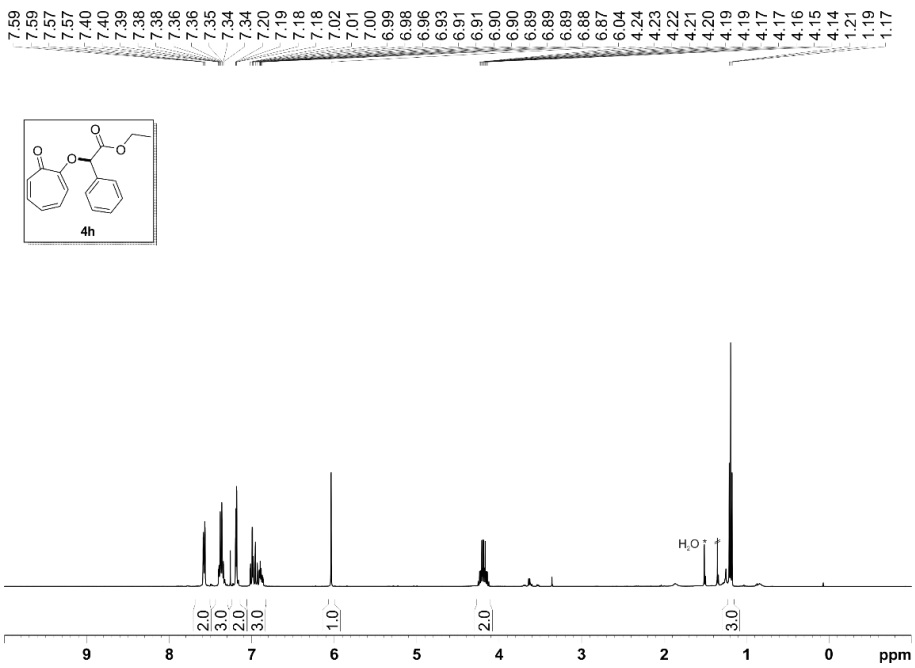

Figure 280. ^{1}H NMR spectrum (400 MHz, $CDCl_3$) for **4h**.

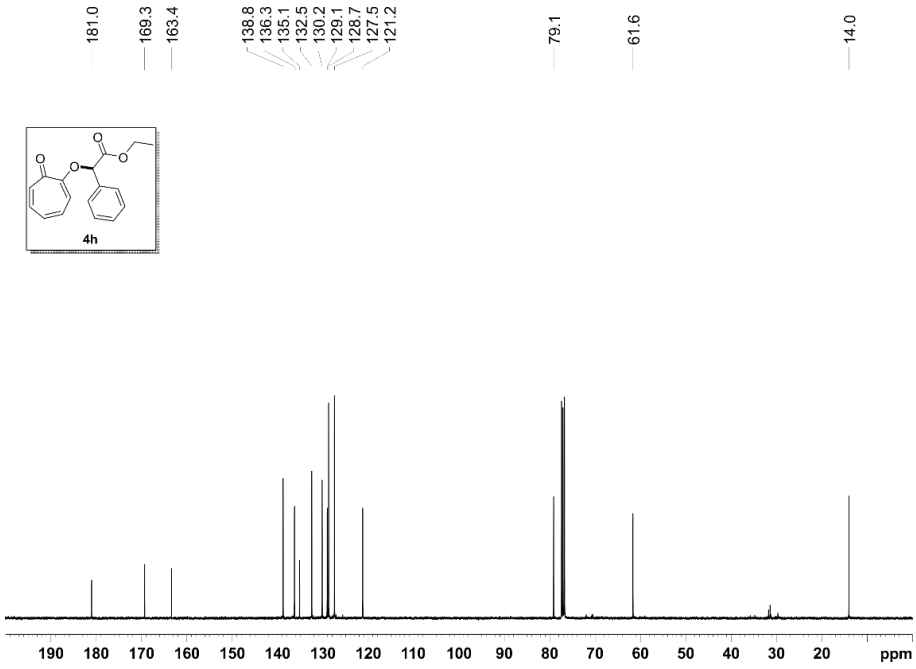

Figure 281. $^{13}C\{^{1}H\}$ NMR spectrum (100 MHz, $CDCl_3$) for **4h**.

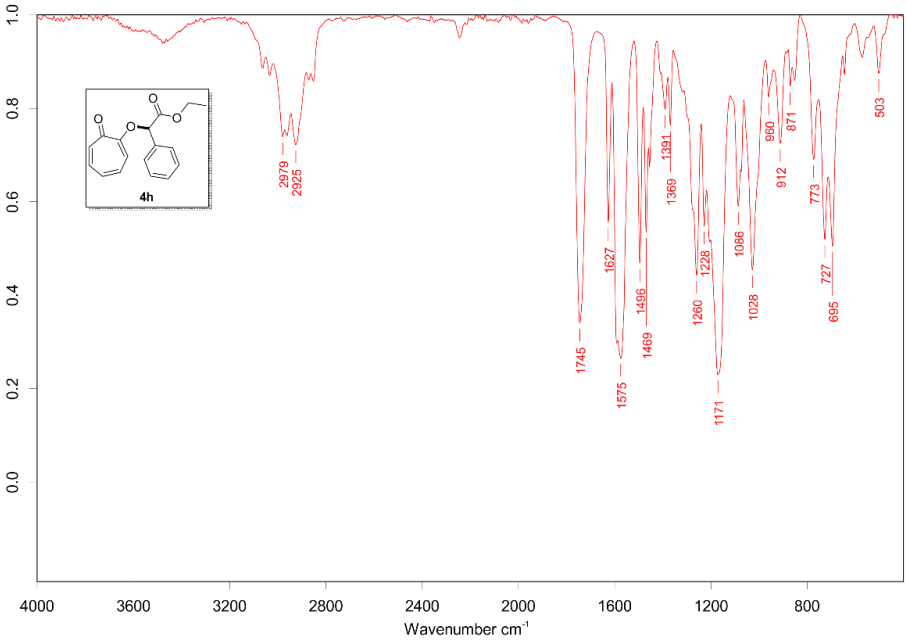

Figure 282. IR spectrum for **4h**.

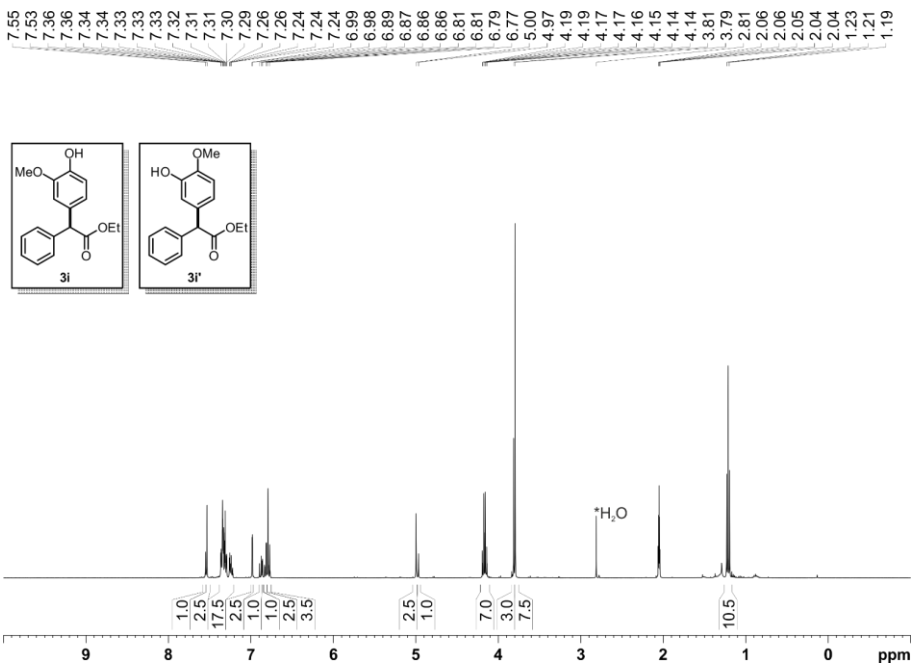

Figure 283. ^{1}H NMR spectrum (400 MHz, acetone-d6) for **3i**+**3i'** isomeric mixture (ratio **3i**:**3i'** 1.0 : 2.5).

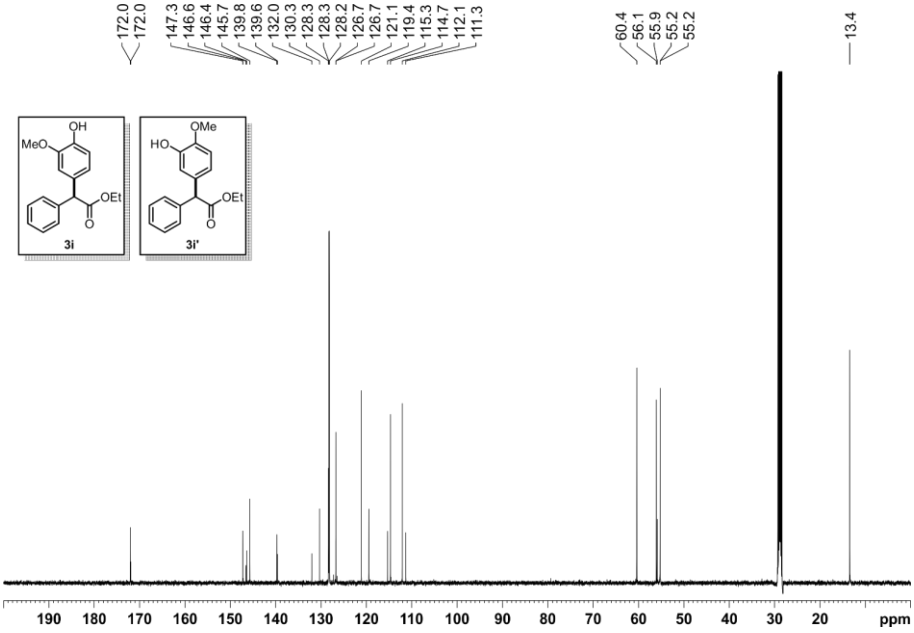

Figure 284. ^{13}C{^{1}H} NMR spectrum (126 MHz, acetone-d6) for **3i**+**3i'** isomeric mixture.

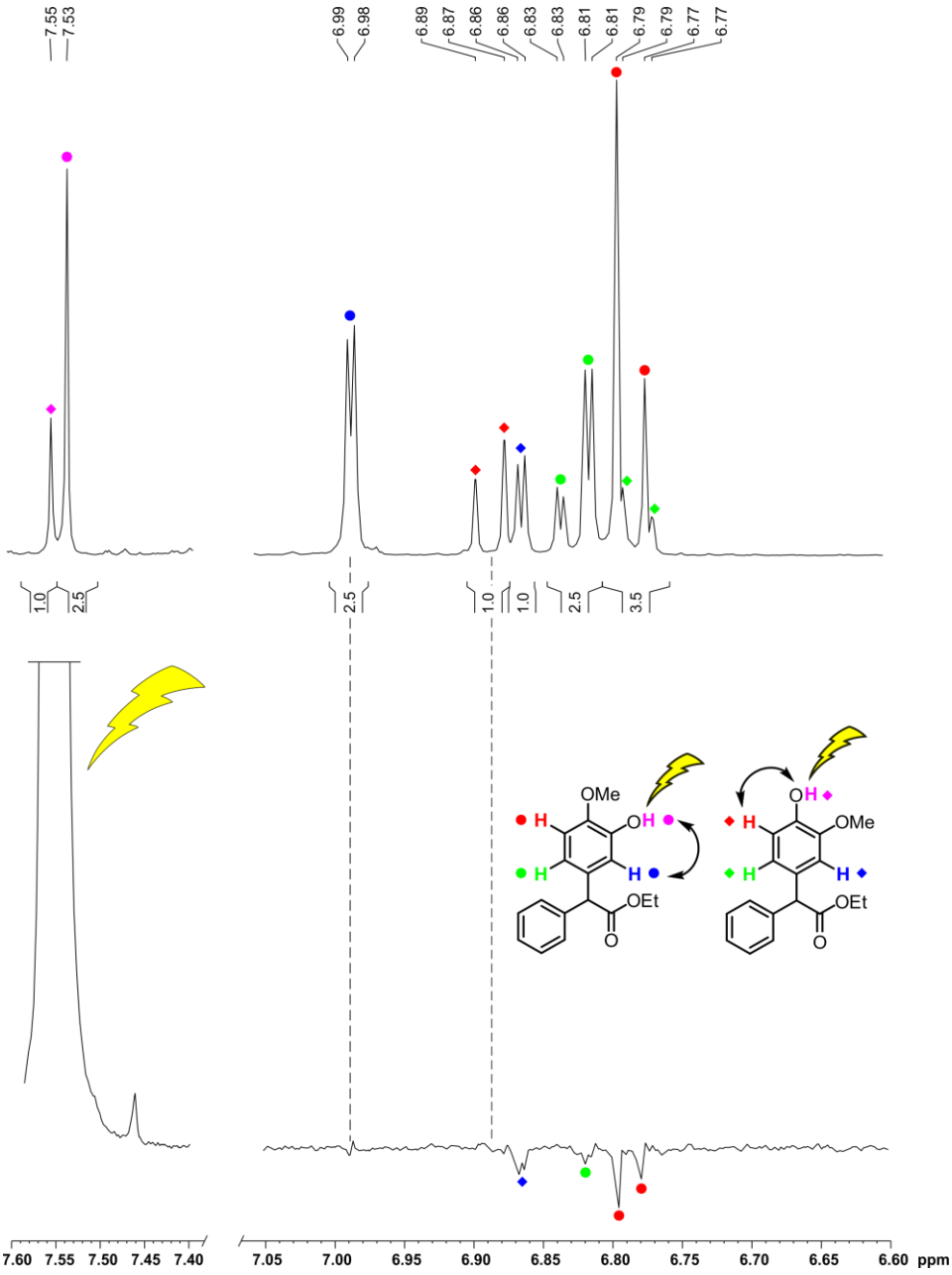

Figure 285. *Up*: Detail of the aromatic region of the ^{1}H NMR spectrum (400 MHz, acetone-d6) for the **3i**+**3i'** mixture (ratio **3i**:**3i'** 1.0 : 2.5). *Down*: GOESY spectrum (500 MHz, acetone-d6) upon irradiation of the –OH signals (δ: 7.54 ppm).

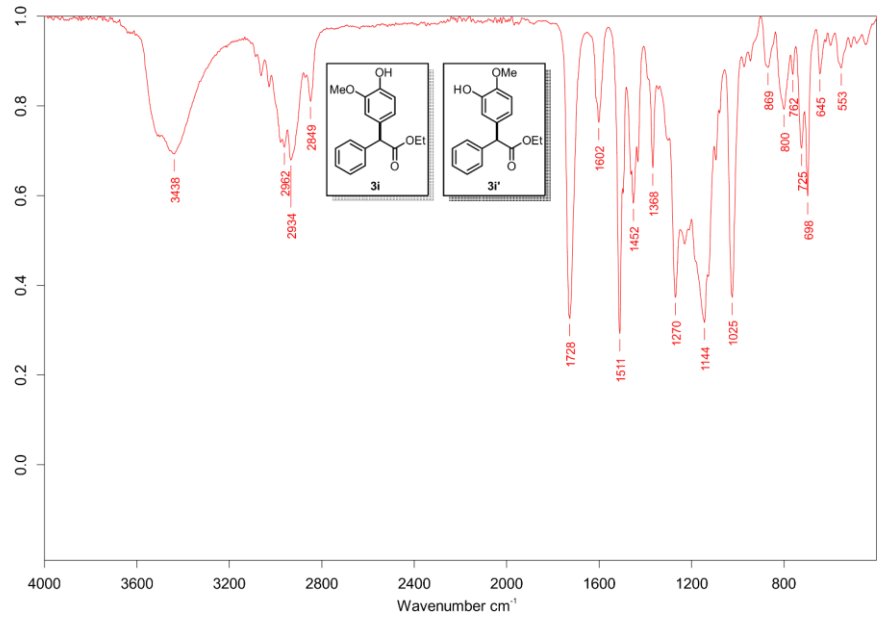

Figure 286. IR spectrum for **3i**+**3i'** isomeric mixture.

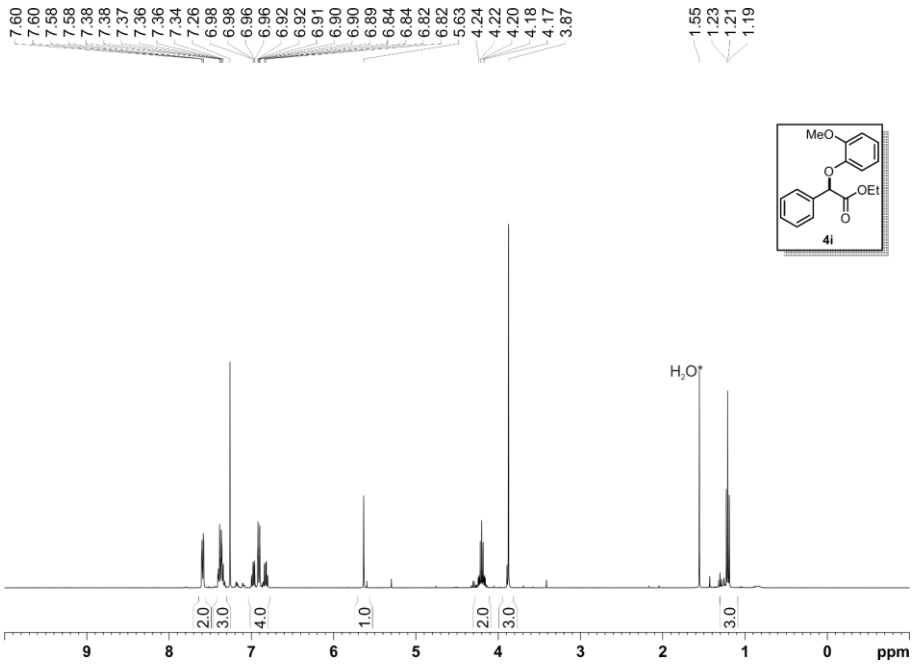

Figure 287. ^{1}H NMR spectrum (400 MHz, $CDCl_3$) for **4i**.

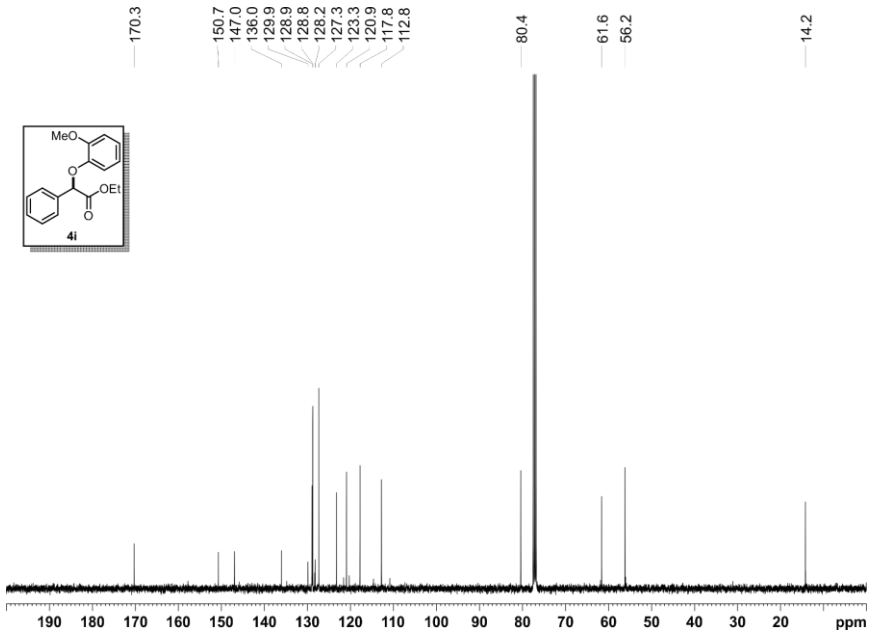

Figure 288. $^{13}C\{^{1}H\}$ NMR spectrum (100 MHz, $CDCl_3$) for **4i**.

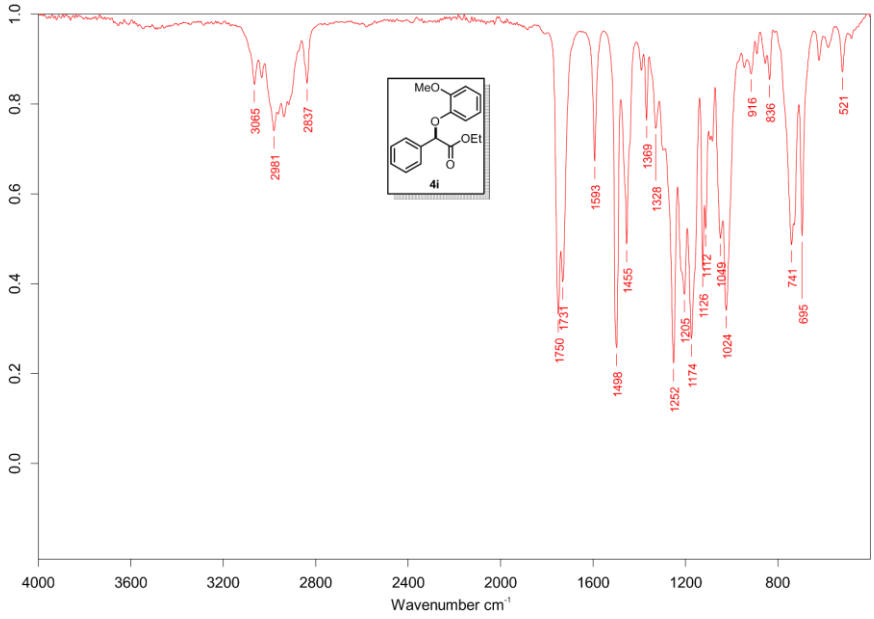

Figure 289. IR spectrum for **4i**.

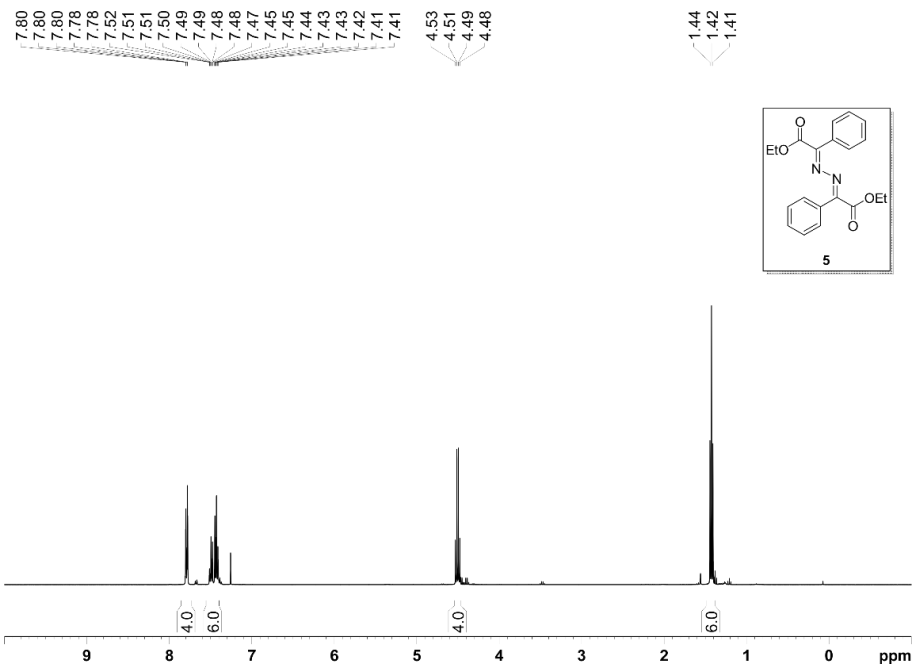

Figure 290. ^{1}H NMR spectrum (400 MHz, $CDCl_3$) for **5**.

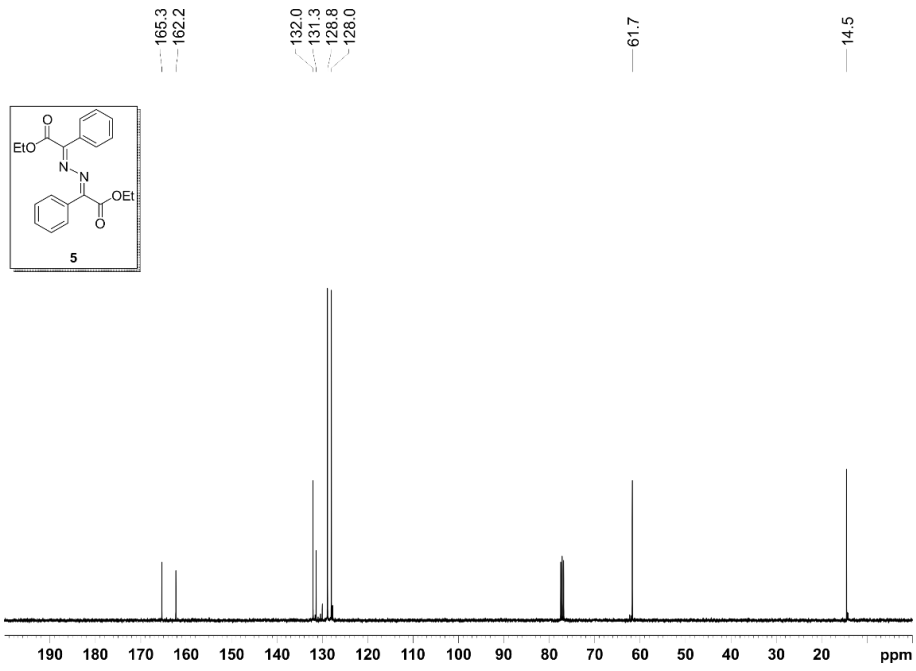

Figure 291. $^{13}C\{^{1}H\}$ NMR spectrum (100 MHz, $CDCl_3$) for **5**.

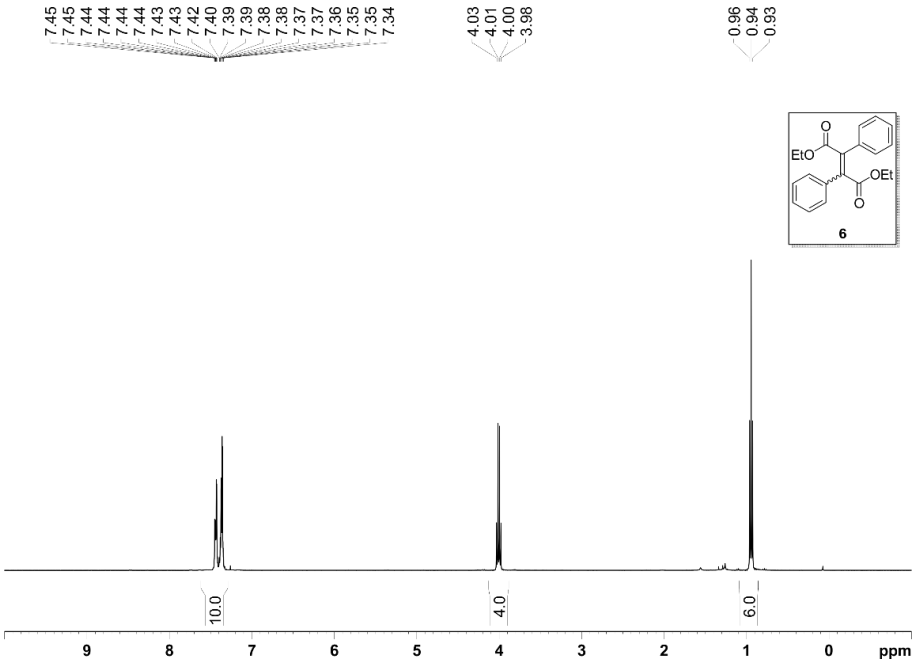

Figure 292. ^{1}H NMR spectrum (400 MHz, $CDCl_3$) for **6**.

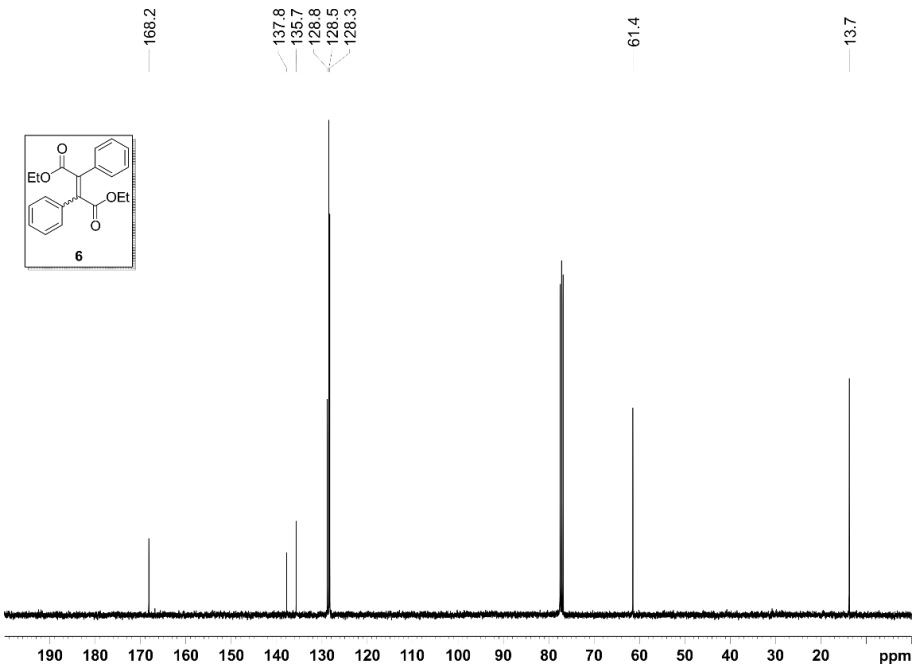

Figure 293. $^{13}C\{^{1}H\}$ NMR spectrum (100 MHz, $CDCl_3$) for **6**.

CONCLUSIONS

1. The first halogen-bonded supramolecular rhodium(I) complexes have been successfully prepared and fully characterized. To the best of our knowledge, these are the only examples where halogen bonding is the driving force for the assembly of the catalyst backbone. Furthermore, it has been demonstrated that the presence of fluorine groups at the iodo-containing supramolecular motif is not necessary for efficient halogen bonding due to the favorable template effect exerted by the rhodium center. Nonetheless, evidences arising from solid-state studies and DFT calculations indicate that the halogen bond interaction is stronger in those systems incorporating a perfluorinated motif. The two newly prepared rhodium complexes are active in the hydroboration of terminal alkynes, with the catalytic activity of **XBphos-Rh** outperforming other catalysts screened. Moreover, halogen-bonded catalysts favored enhanced ratios of the branched alkenyl boronic acid products, providing in some cases the highest reported yield for those branched derivatives.

2. Metal complex diversity has been exploited using halogen bonding for efficiently preparing rhodium(I) and rhodium(III) complexes. The results obtained illustrate how the careful selection of the rhodium precursor and the geometry of the halogen-bond donor and acceptor ligands determines the outcome of the Rh–P complexation chemistry. Thus, either P–I–P pincer-like Rh(I) complexes with a permanent halogen bonding interaction (**XBphos-Rh**, Chapter I) or the P–P Rh(III) cyclometallated complexes described in Chapter II of this thesis were obtained. The latter complexes arise from an unprecedented halogen-bond-driven C_{α}–I oxidative addition process to the rhodium(I) centers. It has been demonstrated, both experimentally and computationally, that the N···I-halogen-bond interaction and the inner coordination sphere at the metal center are key factors that control the reactivity towards oxidative addition processes as observed in the complexes obtained. Selectivity in the complexation process has also been controlled by halogen bonding: Ligand preorganization by *in situ* formation of halogen-bonded

complexes translates into a selective formation of a rhodium(I) norbornadiene complex.

3. An array of supramolecularly regulated phosphite-based Au(I) catalytic systems containing a polyether-based regulation site and steric effectors of different sizes has been described. The polyether-containing phosphite ligands proved to have a high affinity for alkali metal salts according to binding studies carried out with NMR techniques. These Au(I) complexes have been successfully used as catalysts in the catalytic C–H selective functionalization of phenol and related derivatives with metal-carbenoids derived from diazo compounds. The regulation of the steric congestion around the catalytic Au(I) center by the choice of the suitable external regulation agent provided an enhancement in the activity (up to 20%) and selectivity (from 28:1 to >50:1 in terms of C–H *vs.* O–H functionalization products) of the reaction. The catalytic performance of the supramolecularly regulated catalysts has been rationalized using DFT calculations. These studies demonstrated that regulation agents of large size (*i.e.*, $CsBF_4$ and $RbBF_4$) favor the *para*-C_{sp2}–H insertion process. This new approach in supramolecular gold(I) catalysis has been applied to the derivatization of an array of substituted phenols, naphthols, tropolone and to the preparation of an advanced synthetic intermediate of anticancer agent Tamoxifen.

SUMMARY / RESUM / RESUMEN

Summary in English

The present doctoral thesis encompasses the design and synthesis of new supramolecular catalysts based on halogen bonding interactions and the design and preparation of supramolecular catalytic systems based on regulation strategies. These approaches have been applied to transformations of interest such as hydroboration of terminal alkynes, leading to vinylboronates, and also to selective *para*-C_{sp2}–H functionalization of phenols and related compounds that could be used for the preparation of molecules with pharmaceutical interest.

Research efforts were initially directed to the preparation of halogen-bonded supramolecular catalysts (Chapter I). Preliminary models revealed that 2-pyridyldiphenylphosphine, containing the halogen bond acceptor motif, and 2-iodo-3,4,5,6-tetrafluorophenyldiphenylphosphine, incorporating the halogen bond donor moiety, respectively, were adequate for the formation of halogen-bonded rhodium(I) complexes. The preparation of the supramolecular complex, referred to as **XBphos-Rh** throughout this thesis, was successfully achieved starting from the above-mentioned ligands. The corresponding complex was fully characterized in solution and in the solid-state, with the halogen bond interaction being observed in the solid-state. Further exploration of the architecture of the halogen-bonded complexes pointed to the fact that non-perfluorinated halogen bond donors were also compatible with the approach, as subsequently proven both experimentally and computationally. **XBphos-Rh** has been applied to the catalytic hydroboration of terminal alkynes, providing enhanced ratios of the branched vinylboronates, and exhibiting a higher catalytic activity for terminal aryl-substituted alkynes, when compared with reported mono- and bidentate phosphorus-rhodium catalysts (Figure 294).

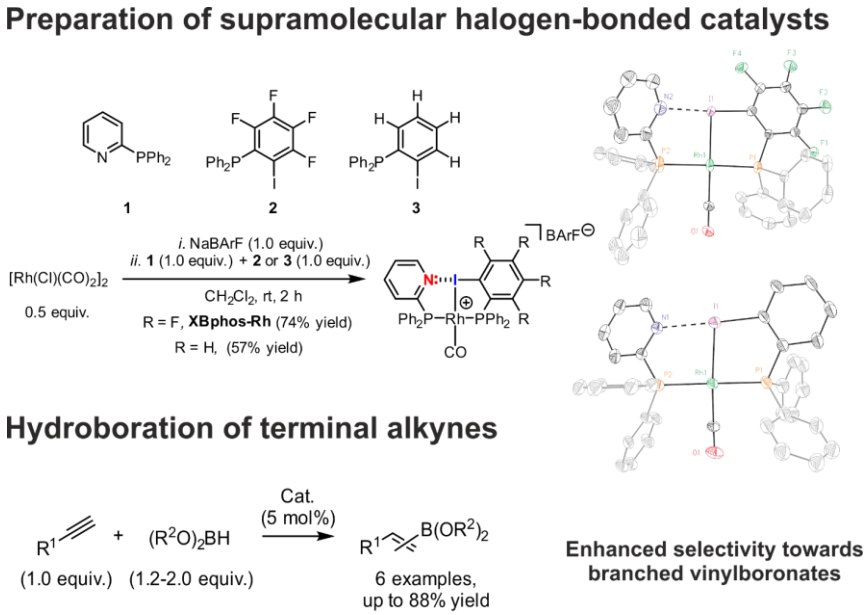

Figure 294. Summary of Chapter I.

Aiming to broaden the applicability of the previous approach, the influence of halogen-bonded bisphosphine ligands was subsequently studied on other rhodium(I) precursors (Chapter II). It was observed that rhodium(I) bisnorbornadiene tetrafluoroborate, $[Rh(nbd)_2]BF_4$, a common precursor in hydrogenation, rendered the corresponding *cis* heterocomplex incorporating 2-pyridyldiphenylphosphine and 2-iodo-3,4,5,6-tetrafluorophenyldiphenylphosphine as ligands in high yields (90% yield) and in a selective manner (the formation of homocomplexes was not observed). The influence of halogen bonding in this selective process was further supported by diffusion ordered spectroscopy (DOSY). In addition, complexation of the above-mentioned ligands with $[Rh(acac)(CO)_2]$, a widely used rhodium(I) precursor in hydroformylations, rendered the corresponding monodentate acetylacetonate carbonylrhodium(I) complexes. Useful stereoelectronic parameters of the ligands used in our studies, such as the Tolman electronic parameter and the percent buried volume of the ligands, were determined. [Rh(acac)(cod)], a precursor used as catalyst for asymmetric hydrogenations, isomerization, or hydroformylation reactions among other transformations, displayed a different reactivity when used in combination with the above-mentioned

ligands, leading to the selective formation of cyclometallated rhodium(III) complexes by oxidative addition of the metal center to the C–I bond. Experimental and DFT computational data pointed that this reactivity at the metal center was mediated by halogen bonding interactions. To the date, this is the first reported halogen-bond-mediated oxidative addition process to a metal center. The formation of Rh(III) rhodacycles, compounds with therapeutic potential, could be extended to other rhodium precursors (Figure 295).

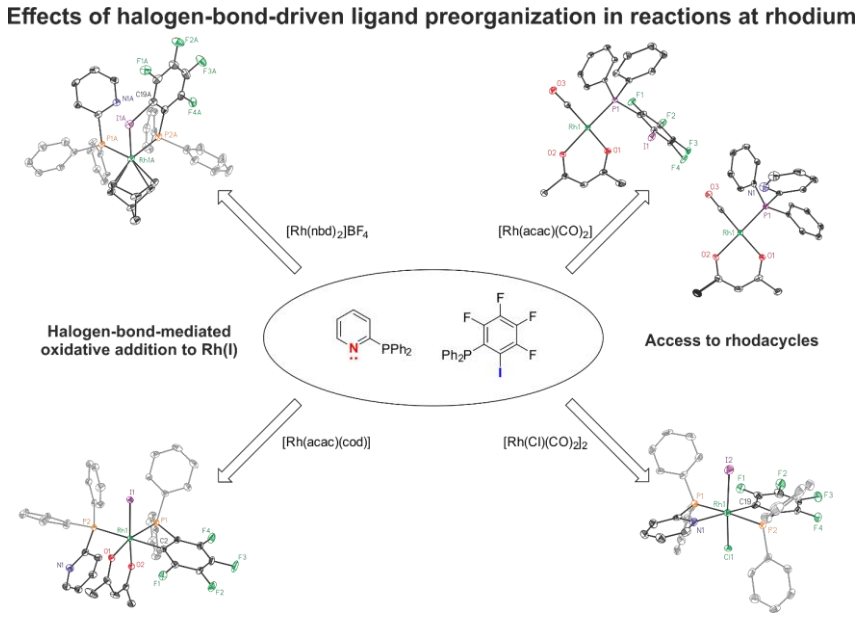

Figure 295. Summary of Chapter II.

Research efforts have also been directed towards the development of new gold(I) supramolecularly regulated catalysts. The modular design was based on a phosphite incorporating a 3,3',5,5'-tetra-*tert*-butyl-(1,1'-biphenyl) motif and a mono-functionalized tetraethyleneglycol fragment, with a steric effector appended at the end of the tetraethyleneglycol chain. The underlying principle is a supramolecularly regulated catalytic system, whose steric congestion around the metal center can be modified by the choice of an external regulation agent (RA). After successfully preparing an array of ligands, binding between the ligand and alkali metal salts was studied, proving that ion-dipole interactions between the salt and the polyether chain are thermodynamically favorable in standard organic

solvents. With the ligands in hand, cationic gold(I) catalysts were prepared and assayed in the selective *para*-functionalization of phenols. It was observed that bulkier steric effectors were detrimental for the activity of the catalyst. Therefore, further studies were performed with catalysts derived from the ligand with a methyl group as steric effector. Gold(I) complexes derived from this ligand showed enhanced activities and selectivities when using large alkali metal salts such as cesium tetrafluoroborate. The effectiveness of the approach was tested by screening an array of electronically diverse phenols and naphthols. Enhancements of the catalytic activity upon using a suitable regulation agent (up to 20% increase in yield) were observed in all cases. The utility of the approach was demonstrated by extending the use of the supramolecularly regulated catalysts to challenging substrates, such as tropolone, which displayed a different reactivity, and by preparing an advanced synthetic intermediate of the world's largest selling drug for the hormonal therapy of breast cancer (*i.e.*, Tamoxifen). DFT calculations were performed in order to gain insight into the regulation mechanism. It was computationally demonstrated that complexes incorporating large alkali metal salts lead to a more energetically favorable pathway for the *para*-C_{sp2}–H insertion reaction (Figure 296).

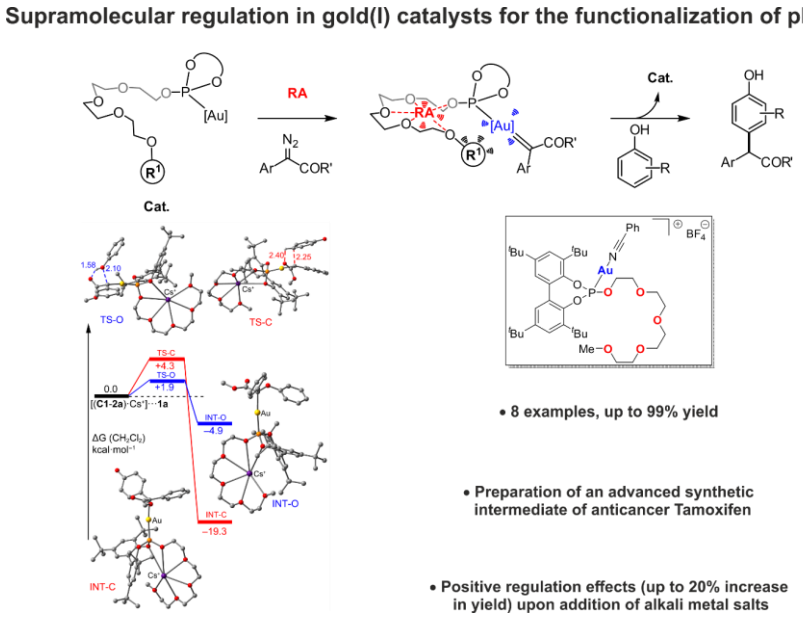

Figure 296. Summary of Chapter III.

Resum en català

Aquesta tesi doctoral combina el disseny i la síntesi de nous catalitzadors supramoleculars basats en interaccions d'enllaç d'halogen, així com el disseny i preparació de sistemes catalítics basats en estratègies de regulació. Aquestes aproximacions s'han aplicat a transformacions d'interès com són la hidroboració d'alquins terminals, generant els corresponents vinilboronats ramificats, i també a la funcionalització selectiva d'alcohols aromàtics a la posició *para*-C_{sp2}–H, generant productes que es poden utilitzar per a la síntesi de molècules rellevants en l'àmbit farmacèutic.

En aquest context, les activitats d'investigació es van dirigir primer a la preparació de catalitzadors supramoleculars d'enllaç d'halogen (Capítol I). Models preliminars van revelar que la disposició relativa dels substituents als lligands 2-piridildifenilfosfina, que conté la subunitat acceptora d'enllaç d'halogen, i la 2-iodo-3,4,5,6-tetrafluorofenil-difenilfosfina, que incorpora el residu donador d'enllaç d'halogen, eren adequats per a la formació del complex desitjat de rodi(I) amb enllaç d'halogen. La preparació del complex supramolecular, anomenat **XBphos-Rh** al llarg de la present tesi, es va assolir exitosament amb els lligands anteriorment esmentats. El complex de rodi resultant es va caracteritzar en dissolució així com en estat sòlid, observant la interacció d'enllaç d'halogen per raigs-X. L'exploració addicional de l'estructura del complex va apuntar que donadors d'enllaç d'halogen no-perfluorats també podrien ser compatibles amb l'aproximació d'assemblatge supramolecular, tal i com es va poder demostrar posteriorment tant a nivell experimental com computacional. El catalitzador **XBphos-Rh** es va aplicar a la hidroboració catalítica d'alquins terminals, afavorint la formació dels vinilboronats ramificats, així com exhibint una major activitat catalítica pels alquins terminals aril substituïts quan es va comparar amb catalitzadors mono- i bidentats de fòsfor de rodi ja descrits (Figura 297).

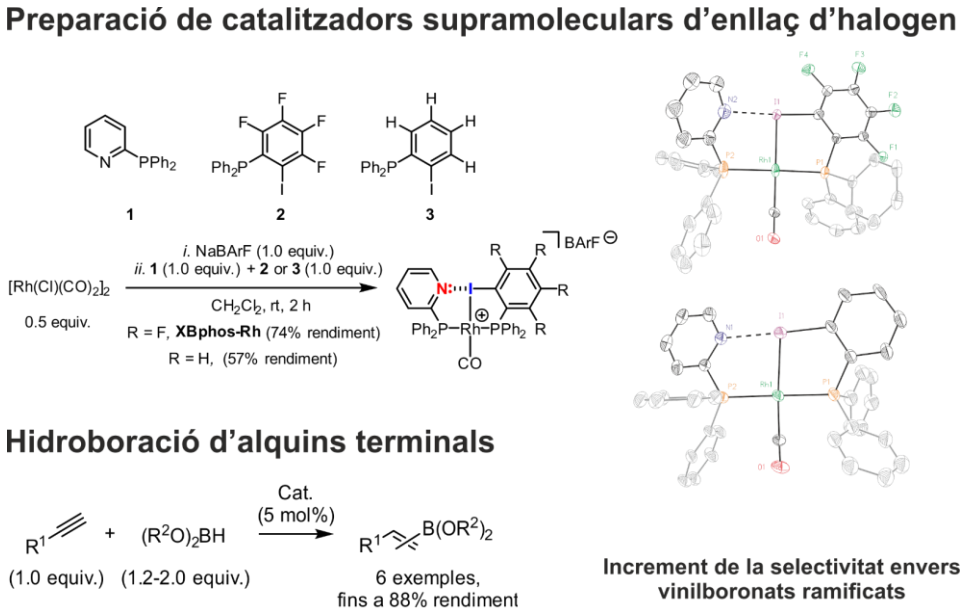

Figura 297. Resum del Capítol I.

Amb l'objectiu d'ampliar l'aplicabilitat de l'anterior aproximació, es va estudiar subseqüentment la influència del sistema supramolecular d'enllaç d'halogen sobre altres precursors de rodi(I) (Capítol II). Es va observar que amb el tetrafluoroborat de rodi(I) bisnorbornadiè, $[Rh(nbd)_2]BF_4$, un precursor habitual a processos d'hidrogenació, es formava el corresponent heterocomplex *cis* derivat de la 2-piridil-difenilfosfina i la 2-iodo-3,4,5,6-tetrafluorofenildifenilfosfina com lligands, amb rendiments alts (90% rendiment) i d'una manera selectiva, sense observar la formació d'homocomplexes. La influència de l'enllaç d'halogen en aquest procés selectiu estava d'acord amb els resultats obtinguts en estudis d'espectroscòpia difusional (DOSY). D'altra banda, la complexació amb $[Rh(acac)(CO)_2]$, un pre-catalitzador comunament utilitzat a hidroformilació, va resultar en la formació dels corresponents complexes acetilacetonat de carbonilrodi(I) monodentats, la qual cosa va permetre extreure paràmetres estereoelectrònics d'utilitat dels lligands utilitzats al sistema supramolecular, com són el paràmetre electrònic de Tolman o el percentatge de volum enterrat dels lligands. El [Rh(acac)(cod)], un precursor emprat com a catalitzador per a hidrogenacions asimètriques, isomeritzacions o hidroformilacions entre

d'altres reaccions, va mostrar una reactivitat diferent quan es va utilitzar juntament amb els lligands supramoleculars assemblats mitjançant enllaç d'halogen, observant la formació selectiva de complexes de rodi(III) ciclometal·lats per addició oxidativa de l'enllaç C–I al centre metàl·lic. Observacions experimentals i computacionals amb càlculs DFT van demostrar que aquesta reactivitat al centre metàl·lic venia donada per les interaccions d'enllaç d'halogen. A dia d'avui, es tracta de la primera ressenya d'una addició oxidativa a un centre metàl·lic mediada per enllaç d'halogen. La formació de rodacicles de Rh(III), compostos amb potencial terapèutic, es va poder estendre a altres precursors de rodi (Figura 298).

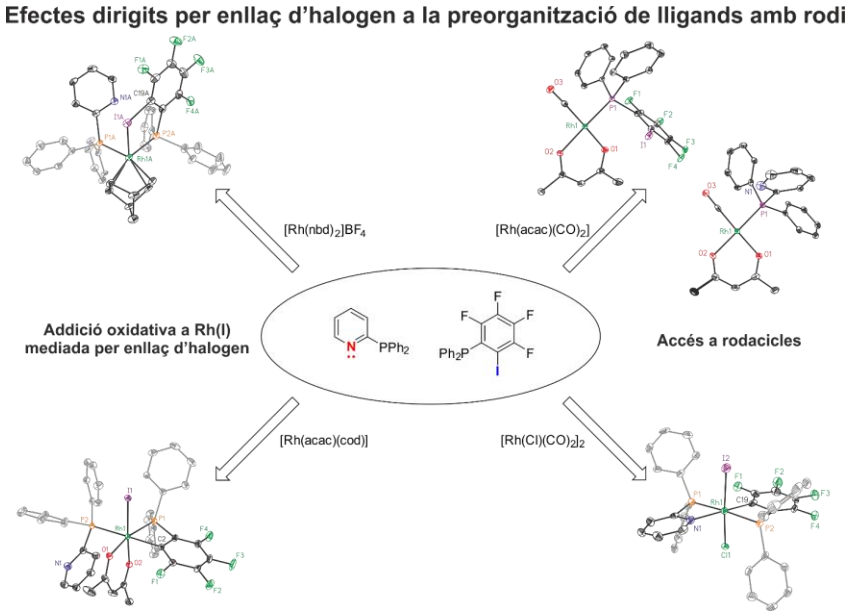

Figura 298. Resum del Capítol II.

Altres activitats d'investigació es van enfocar cap al desenvolupament de nous sistemes catalítics d'or(I) regulables supramolecularment. El disseny modular es va basar en fosfits que incorporen un esquelet de 3,3',5,5'-tetra-*terc*-butil-(1,1'-bifenil) i una cadena de tetraetilenglicol mono-funcionalitzada, amb un efector estèric al final d'aquesta cadena. El principi subjacent és el de preparar un sistema catalític sobre el que la congestió estèrica al voltant del centre metàl·lic pugui ser regulada mitjançant un agent de regulació (RA). Després de preparar una sèrie de lligands amb les característiques anteriorment esmentades, es va estudiar

el procés supramolecular de complexació via interaccions ió-dipol entre els lligands i les sals metàl·liques. Aquests estudis van permetre concloure que la interacció supramolecular està afavorida termodinàmicament en dissolvents orgànics d'ús habitual. Amb els lligands en mà, els complexes catiònics d'or(I) es van preparar i assajar en la funcionalització selectiva de l'enllaç C–H en *para* en derivats tipus fenol. Es va observar que els efectors estèrics més voluminosos eren perjudicials per a l'activitat del catalitzador. Així doncs, els estudis subseqüents es van realitzar sobre el lligand que contenia un grup metil com a efector estèric. L'eficiència d'aquesta aproximació es va demostrar estudiant la reacció sobre fenols electrònicament diversos i naftols. En tots els casos es va observar un increment de l'activitat catalítica amb l'ús de l'agent de regulació adient (fins a un 20% d'increment en el rendiment). La utilitat de l'aproximació es va demostrar estenent l'ús dels catalitzadors regulats supramolecularment a nous substrats com la tropolona, que va mostrar una activitat diferenciada respecte a la resta de compostos estudiats, i també preparant un intermedi sintètic avançat del fàrmac més venut mundialment per al tractament hormonal de càncer de mama, el Tamoxifè. Es van realitzar càlculs DFT per entendre millor el mecanisme de regulació. Es va demostrar computacionalment que els complexes que incorporen sals alcalines voluminoses proporcionen un camí de baixa energia per a les reaccions d'inserció a la posició *para*-C_{sp2}–H (Figura 299).

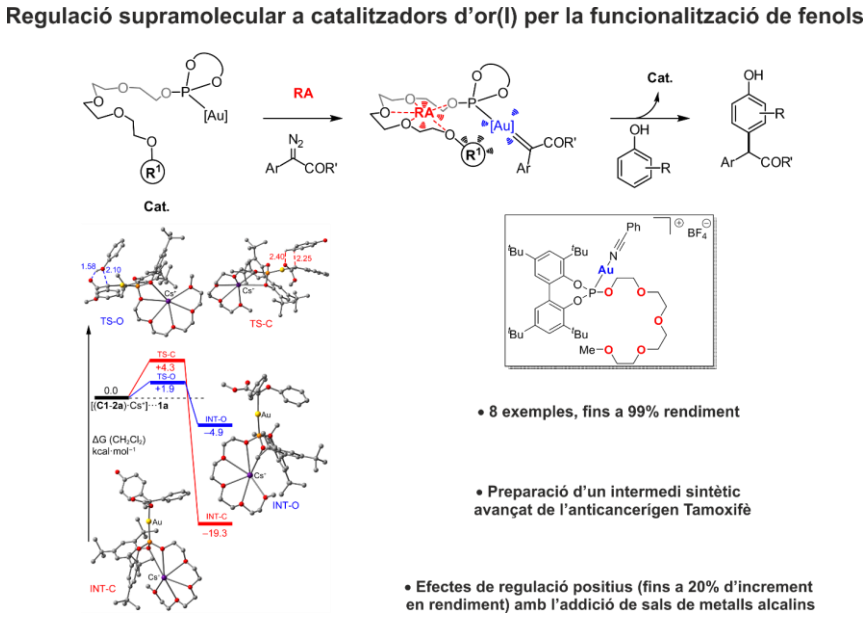

Figura 299. Resum del Capítol III.

Resumen en castellano

Esta tesis doctoral combina el diseño y la síntesis de nuevos catalizadores supramoleculares basados en interacciones por enlace de halógeno, así como el diseño y preparación de sistemas catalíticos basados en estrategias de regulación. Estas aproximaciones se han aplicado a transformaciones de interés como son la hidroboración de alquinos terminales, generando los correspondientes vinilboronatos ramificados, y la funcionalización selectiva de alcoholes aromáticos en la posición *para*-C_{sp2}–H, generando productos que se pueden utilizar para la síntesis de moléculas relevantes en el ámbito farmacéutico.

En este contexto, las actividades de investigación iniciales se dirigieron en primer lugar a la preparación de catalizadores supramoleculares por enlace de halógeno (Capítulo I). Modelos preliminares revelaron que la disposición relativa de los sustituyentes en los ligandos 2-piridil-difenilfosfina, que contiene la subunidad aceptora de enlace de halógeno, y la 2-iodo-3,4,5,6-tetrafluorofenildifenilfosfina, que incorpora el residuo dador de enlace de halógeno, eran adecuados para la formación del complejo de enlace de halógeno de rodio(I) deseado. La preparación del complejo supramolecular, llamado **XBphos-Rh** a lo largo de la presente tesis, se consiguió exitosamente con los ligandos anteriormente mencionados. El complejo de rodio resultante se caracterizó en disolución, así como en estado sólido, observando la interacción por enlace de halógeno por rayos-X. Estudios adicionales sobre la estructura del complejo apuntaron a que dadores de enlace de halógeno no-perfluorados también podrían ser compatibles con la aproximación de ensamblaje supramolecular, tal y como se pudo demostrar posteriormente tanto a nivel experimental como computacional. El catalizador **XBphos-Rh** se aplicó a la hidroboración catalítica de alquinos terminales, favoreciendo la formación de vinilboronatos ramificados, y exhibiendo una mayor actividad catalítica para los alquinos terminales aril sustituidos al compararla con catalizadores mono- y bidentados de fósforo de rodio ya descritos (Figura 300).

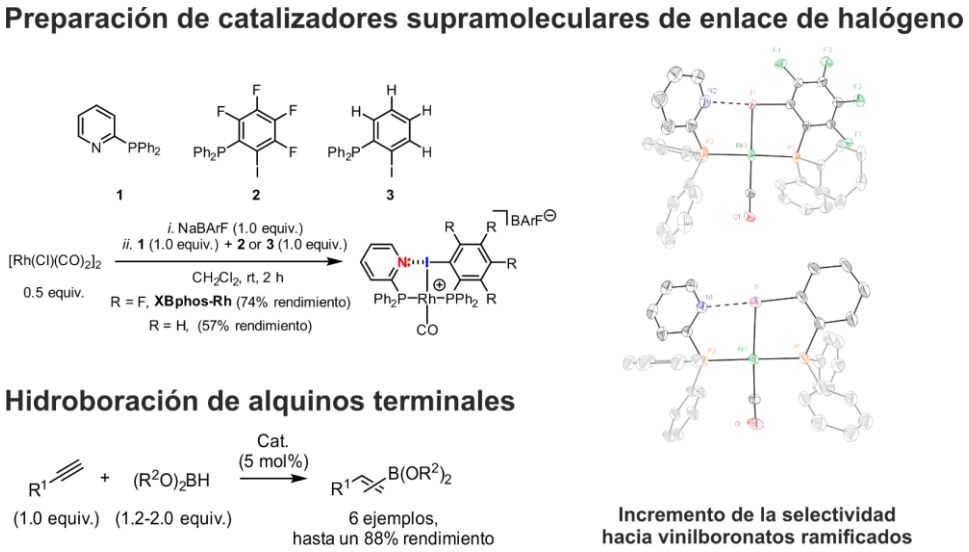

Figura 300. Resumen del Capítulo I.

Con el objetivo de ampliar la aplicabilidad de la anterior aproximación, se estudió subsiguientemente la influencia del sistema supramolecular por enlace de halógeno sobre otros precursores de rodio(I) (Capítulo II). Se observó que con el tetrafluoroborato de rodio(I) bisnorbornadieno, $[Rh(nbd)_2]BF_4$, un precursor habitual en procesos de hidrogenación, se formaba el correspondiente heterocomplejo *cis* derivado de la 2-piridil-difenilfosfina y la 2-iodo-3,4,5,6-tetrafluorofenildifenilfosfina como ligandos, con rendimientos altos (90% rendimiento) y de una manera selectiva, sin observar la formación de homocomplejos. La influencia del enlace de halógeno en este proceso selectivo pudo confirmarse con los resultados obtenidos en estudios de espectroscopía difusional (DOSY). Por otra parte, la complejación con $[Rh(acac)(CO)_2]$, un pre-catalizador comúnmente utilizado en hidroformilación, condujo a la formación de los correspondientes complejos de acetilacetonato de carbonilrodio(I) monodentados, lo que permitió extraer parámetros estereoelectrónicos de utilidad para los ligandos utilizados en el sistema supramolecular, como son el parámetro electrónico de Tolman o el porcentaje de volumen enterrado de los ligandos. El [Rh(acac)(cod)], un precursor utilizado como catalizador para hidrogenaciones asimétricas, isomerizaciones o hidroformilaciones, entre otras reacciones, mostró una reactividad diferente cuando se utilizó conjuntamente con los ligandos supramoleculares ensamblados por enlace de halógeno, observando la

formación selectiva de complejos de rodio(III) ciclometalados por adición oxidativa del enlace C–I al centro metálico. Observaciones experimentales y computacionales mediante cálculos DFT demostraron que esta reactividad en el centro metálico venía dada por las interacciones de enlace de halógeno. A día de hoy, se trata del primer caso descrito de una adición oxidativa a un centro metálico mediada por enlace de halógeno. La formación de rodaciclos de Rh(III), compuestos con potencial terapéutico, se pudo extender a otros precursores de rodio (Figura 301).

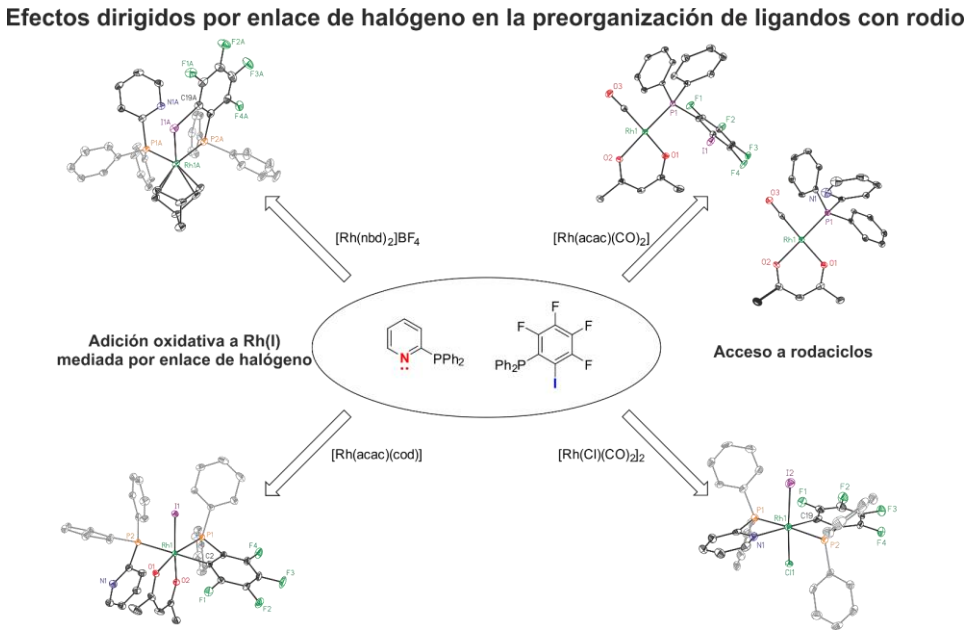

Figura 301. Resumen del Capítulo II.

Otras actividades de investigación se enfocaron hacia el desarrollo de nuevos sistemas catalíticos de oro(I) regulables supramolecularmente. El diseño modular se basó en fosfitos que incorporan un esqueleto de 3,3',5,5'-tetra-*terc*-butilo-(1,1'-bifenilo) y una cadena de tetraetilenglicol mono-funcionalizada, con un efector estérico al final de esta cadena. El principio subyacente es el de preparar un sistema catalítico cuya congestión estérica alrededor del centro metálico pueda ser regulada mediante un agente de regulación (RA). Después de preparar una serie de ligandos con las características anteriormente mencionadas, se estudió el

proceso supramolecular de complejación vía interacciones ion-dipolo entre los ligandos y las sales metálicas. Estos estudios permitieron concluir que la interacción supramolecular está favorecida termodinámicamente en disolventes orgánicos de uso habitual. Con los ligandos en mano, se prepararon los complejos catiónicos de oro(I) y éstos se ensayaron en la funcionalización selectiva del enlace C–H en *para* en derivados de tipo fenol. Se observó que los efectores estéricos más voluminosos eran perjudiciales para la actividad del catalizador. Así pues, los estudios subsiguientes se realizaron sobre el ligando que contenía el grupo metilo como efector estérico. La eficiencia de esta aproximación se demostró estudiando la reacción sobre fenoles electrónicamente diversos y naftoles. En todos los casos se observó un incremento en la actividad catalítica con el uso del agente de regulación adecuado (hasta un 20% de incremento en el rendimiento). La utilidad de la aproximación se demostró extendiendo el uso de los catalizadores regulados supramolecularmente a nuevos sustratos como la tropolona, que mostró una actividad diferenciada respecto al resto de compuestos estudiados, y también preparando un intermedio sintético avanzado del fármaco más vendido mundialmente para el tratamiento hormonal del cáncer de mama, el Tamoxifeno. Se realizaron cálculos DFT para entender mejor el mecanismo de regulación. Se demostró computacionalmente que los complejos que incorporan sales alcalinas voluminosas proporcionan un camino de baja energía para las reacciones de inserción en la posición *para*-C_{sp2}–H (Figura 302).

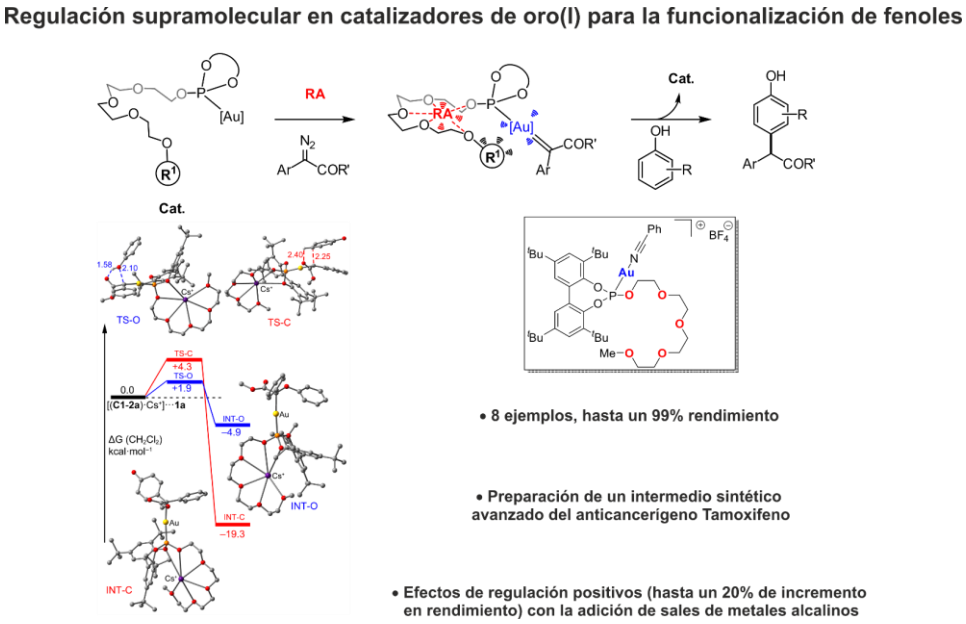

Figura 302. Resumen del Capítulo III.

UNIVERSITAT
ROVIRA i VIRGILI